PB80-175102

Modeling of Simulated Photochemical Smog with Kinetic Mechanisms
Volume 1. Final Report

Systems Applications, Inc.
San Rafael, CA

Prepared for

Environmental Sciences Research Lab.
Research Triangle Park, NC

Feb 80

U.S. Department of Commerce
National Technical Information Service
NTIS

United States
Environmental Protection
Agency

Environmental Sciences Research
Laboratory
Research Triangle Park NC 27711

EPA-600/3-80-028a
February 1980

PB80-175102

Research and Development

EPA

Modeling of Simulated Photochemical Smog with Kinetic Mechanisms

Volume 1.
Final Report

REPRODUCED BY
NATIONAL TECHNICAL
INFORMATION SERVICE
U. S. DEPARTMENT OF COMMERCE
SPRINGFIELD, VA. 22161

RESEARCH REPORTING SERIES

Research reports of the Office of Research and Development, U.S. Environmental Protection Agency, have been grouped into nine series. These nine broad categories were established to facilitate further development and application of environmental technology. Elimination of traditional grouping was consciously planned to foster technology transfer and a maximum interface in related fields. The nine series are:

1. Environmental Health Effects Research
2. Environmental Protection Technology
3. Ecological Research
4. Environmental Monitoring
5. Socioeconomic Environmental Studies
6. Scientific and Technical Assessment Reports (STAR)
7. Interagency Energy-Environment Research and Development
8. "Special" Reports
9. Miscellaneous Reports

This report has been assigned to the ECOLOGICAL RESEARCH series. This series describes research on the effects of pollution on humans, plant and animal species, and materials. Problems are assessed for their long- and short-term influences. Investigations include formation, transport, and pathway studies to determine the fate of pollutants and their effects. This work provides the technical basis for setting standards to minimize undesirable changes in living organisms in the aquatic, terrestrial, and atmospheric environments.

This document is available to the public through the National Technical Information Service, Springfield, Virginia 22161.

TECHNICAL REPORT DATA

(Please read Instructions on the reverse before completing)

1. REPORT NO. EPA-600/3-80-028a	2.	3. RECIPIENT'S ACCESSION NO. PB80-175102
4. TITLE AND SUBTITLE MODELING OF SIMULATED PHOTOCHEMICAL SMOG WITH KINETIC MECHANISMS Volume 1. Final Report		5. REPORT DATE February 1980
		6. PERFORMING ORGANIZATION CODE
7. AUTHOR(S) G. Z. Whitten, J.P. Killus, and H. Hogo		8. PERFORMING ORGANIZATION REPORT NO. EF79-124
9. PERFORMING ORGANIZATION NAME AND ADDRESS Systems Applications, Incorporated 950 Northgate Drive San Rafael, California 94903		10. PROGRAM ELEMENT NO. 1AA603 AC-054 (FY-79)
		11. CONTRACT/GRANT NO. Contract No. 68-02-2428
12. SPONSORING AGENCY NAME AND ADDRESS Environmental Sciences Research Laboratory-RTP, NC Office of Research and Development U.S. Environmental Protection Agency Research Triangle Park, North Carolina 27711		13. TYPE OF REPORT AND PERIOD COVERED Final 7/78-9/79
		14. SPONSORING AGENCY CODE EPA/600/09
15. SUPPLEMENTARY NOTES		

16. ABSTRACT

Mechanisms that describe the formation of photochemical smog are developed using a computer modeling technique directed toward the simulation of data collected in two smog chambers: an indoor chamber and a dual outdoor chamber. The results of simulating 164 different experiments are presented in Vol. 1. Individual compounds for which specific experiments were simulated and mechanisms developed include the following: formaldehyde, acetaldehyde, ethylene, propylene, butane, and toluene. Experiments in both chambers were simulated for all these compounds. The mechanisms reported describe the decay of the precursor organic compound, formation and decay of secondary organic compounds, conversion of nitrogen oxides, formation of nitrates, and the appearance and decay of ozone. Special emphasis is given to the chemistry of toluene. Also included is a study of a generalized smog-based or carbon-bond mechanism developed in a previous study. Volume 2 contains the user's manual and coding for a chemical kinetics computer program, CHEMK.

17. KEY WORDS AND DOCUMENT ANALYSIS

a. DESCRIPTORS	b. IDENTIFIERS/OPEN ENDED TERMS	c. COSATI Field/Group
* Air Pollution * Reaction kinetics * Photochemical reactions * Test chambers * Mathematical models * Computerized simulation		13B 07D 07E 14B 12A 09B

18. DISTRIBUTION STATEMENT RELEASE TO PUBLIC	19. SECURITY CLASS *(This Report)* UNCLASSIFIED	21. NO. OF PAGES
	20. SECURITY CLASS *(This page)* UNCLASSIFIED	22. PRICE

EPA Form 2220-1 (9-73)

EPA-600/3-80-028a
February 1980

MODELING OF SIMULATED PHOTOCHEMICAL SMOG WITH KINETIC MECHANISMS
Volume 1. Final Report

by

G. Z. Whitten
J. P. Killus
H. Hogo

Systems Applications, Incorporated
950 Northgate Drive
San Rafael, California 94903

Contract No. 68-02-2428

Project Officer

Marcia C. Dodge
Atmospheric Chemistry and Physics Division
Environmental Sciences Research Laboratory
Research Triangle Park, North Carolina 27711

ENVIRONMENTAL SCIENCES RESEARCH LABORATORY
OFFICE OF RESEARCH AND DEVELOPMENT
U.S. ENVIRONMENTAL PROTECTION AGENCY
RESEARCH TRIANGLE PARK, NORTH CAROLINA 27711

1a

DISCLAIMER

This report has been reviewed by the Environmental Sciences Research Laboratory, U.S. Environmental Protection Agency, and approved for publication. Approval does not signify that the contents necessarily reflect the views and policies of the U.S. Environmental Protection Agency, nor does mention of trade names or commercial products constitute endorsement or recommendation for use.

ABSTRACT

Mechanisms that describe the formation of photochemical smog are developed using a computer modeling technique directed toward the simulation of data collected in two smog chambers: an indoor chamber and a dual outdoor chamber. The results of simulating 164 different experiemnts are presented in Vol. I. Individual compounds for which specific experiments were simulated and mechanisms developed include the following: formaldehyde, acetaldehyde, ethylene, propylene, butane, and toluene. Experiments in both chambers were simulated for all these compounds. The mechanisms reported describe the decay of the precursor organic compound, formation and decay of secondary organics, conversion of nitrogen oxides, formation of nitrates, and the appearance and decay of ozone. Special emphasis is given to the chemistry of toluene. Also included is a study of a generalized smog-based or carbon-bond mechanism developed in a previous study. Vol. II contains the user's manual and coding for a chemical kinetics computer program, CHEMK.

This report was submitted to the U.S. Environmental Protection Agency in fulfillment of Contract No. 68-02-2428 by Systems Applications, Incorporated. This report covers the period 23 August 1978 to 23 August 1979, and work was completed as of 23 August 1979.

CONTENTS

Abstract iii
Figures vii
Tables xii

1. Introduction 1
2. Summary of Results, Conclusions, and Recommendations . . . 7
    General conclusions 7
    Mechanism refinement 9
3. Treatment of Inorganic Reactions 19
    Photolysis reactions 22
    HO_2 chemistry 25
    Peroxynitric acid chemistry 26
4. Development and Application of the Explicit Mechanisms . . 28
    Formaldehyde 29
    Acetaldehyde 52
    Ethylene 58
    Ethylene/acetaldehyde 100
    Propylene 120
    Propylene/acetaldehyde 195
    Butane 202
5. The Toluene Mechanism 233
    Empirical features of aromatics oxidation 233
    The explicit photochemistry of aromatic compounds . 241
    Mass balance in the toluene mechanism 248
    Description of toluene simulations for UCR 248
    Description of toluene simulations for UNC 255
    The propylene toluene experiment (6/21/79) 256
6. Carbon-Bond Chemistry 277
    Comparison of old and new mechanisms 277

Preceding page blank

A compendium of isopleth diagrams 325
References 342

FIGURES

Number Page

1 Mechanism development and refinement activities 3

UCR formaldehyde experiments

2 Simulation results for EC-250 31
3 Simulation results for EC-251 32
4 Simulation results for EC-252 33
5 Simulation results for EC-253 34

UNC formaldehyde experiments

6 Simulation results for UNCR 5/18/77 35
7 Simulation results for UNCR 7/18/77 36
8 Simulation results for UNCR 9/14/77 37
9 Simulation results for UNCB 9/14/79 38
10 Simulation results for UNCR 9/08/78 39
11 Simulation results for UNCB 9/08/79 40
12 Simulation results for UNCB 9/15/78 41
13 Simulation results for UNCB 9/19/78 42
14 Simulation results for UNCB 9/21/78 44

UCR acetaldehyde experiments

15 Simulation results for EC-253 53
16 Simulation results for EC-254 55

UNC acetaldehyde experiments

17 Simulation results for UNCR 5/18/77 61
18 Simulation results for UNCB 7/18/77 62
19 Simulation results for UNCB 11/12/77 63
20 Simulation results for UNCB 11/20/77 64
21 Simulation results for UNCB 12/26/77 66
22 Simulation results for UNCB 2/27/78 67
23 Simulation results for UNCB 3/06/78 68
24 Simulation results for UNCB 3/31/78 69
25 Simulation results for UNCR 8/08/78 70
26 Simulation results for UNCB 8/08/78 71
27 Simulation results for UNCR 10/13/78 72
28 Simulation results for UNCB 10/13/78 73

UNC ethylene experiments

29 Simulation results for UNCR 10/18/77 77
30 Simulation results for UNCB 10/18/77 78
31 Simulation results for UNCR 11/12/77 79
32 Simulation results for UNCR 11/20/77 80

Number Page

33 Simulation results for UNCB 1/10/78 81
34 Simulation results for UNCR 6/16/78 82
35 Simulation results for UNCB 6/30/78 83
36 Simulation results for UNCR 7/01/78 84
37 Simulation results for UNCR 7/30/78 85
38 Simulation results for UNCB 8/06/78 86
39 Simulation results for UNCR 8/10/78 86
40 Simulation results for UNCB 8/10/78 87
41 Simulation results for UNCB 8/15/78 88
42 Simulation results for UNCR 8/21/78 89
43 Simulation results for UNCR 9/15/78 90
44 Simulation results for UNCR 9/19/78 91
45 Simulation results for UNCR 9/21/78 92
46 Simulation results for UNCB 10/02/78 93
47 Simulation results for UNCR 10/03/78 95
48 Simulation results for UNCB 10/17/78 96
49 Simulation results for UNCR 10/18/78 97
50 Simulation results for UNCB 11/07/78 99

UCR ethylene experiments

51 Simulation results for EC-142 102
52 Simulation results for EC-143 103
53 Simulation results for EC-156 105
54 Simulation results for EC-285 107
55 Simulation results for EC-286 109
56 Simulation results for EC-287 111

UNC ethylene/acetaldehyde experiments

57 Simulation results for UNCR 10/12/78 114
58 Simulation results for UNCB 10/12/78 115
59 Simulation results for UNCR 10/25/78 116
60 Simulation results for UNCB 10/25/78 118

UCR propylene experiments

61 Simulation results for EC-230 129
62 Simulation results for EC-256 131
63 Simulation results for EC-257 133
64 Simulation results for EC-276 135
65 Simulation results for EC-277 136
66 Simulation results for EC-278 138
67 Simulation results for EC-279 139
68 Simulation results for EC-314 141
69 Simulation results for EC-315 143
70 Simulation results for EC-316 144
71 Simulation results for EC-317 145
72 Simulation results for EC-318 147
73 Simulation results for EC-319 149
74 Simulation results for EC-320 151

Number Page

UNC propylene experiments

75 Simulation results for UNCR 10/24/77 153
76 Simulation results for UNCR 12/26/77 155
77 Simulation results for UNCR 1/10/78 156
78 Simulation results for UNCR 2/27/78 157
79 Simulation results for UNCR 3/06/78 158
80 Simulation results for UNCR 3/31/78 159
81 Simulation results for UNCB 6/16/78 160
82 Simulation results for UNCR 6/30/78 161
83 Simulation results for UNCB 7/01/78 163
84 Simulation results for UNCR 7/24/78 165
85 Simulation results for UNCB 7/24/78 167
86 Simulation results for UNCB 7/30/78 169
87 Simulation results for UNCR 8/05/78 170
88 Simulation results for UNCB 8/05/78 171
89 Simulation results for UNCR 8/06/78 172
90 Simulation results for UNCR 8/15/78 173
91 Simulation results for UNCB 8/21/78 174
92 Simulation results for UNCR 10/17/78 176
93 Simulation results for UNCB 10/18/78 178
94 Simulation results for UNCR 10/20/78 180
95 Simulation results for UNCB 10/20/78 182
96 Simulation results for UNCR 10/21/78 184
97 Simulation results for UNCB 10/21/78 186
98 Simulation results for UNCR 10/22/78 188
99 Simulation results for UNCB 10/22/78 190
100 Simulation results for UNCR 10/29/78 192
101 Simulation results for UNCB 10/29/78 193
102 Simulation results for UNCR 11/07/78 194

UCR propylene/acetaldehyde experiments

103 Simulation results for EC-216 197
104 Simulation results for EC-217 199

UNC propylene/acetaldehyde experiments

105 Simulation results for UNCR 6/12/79 200
106 Simulation results for UNCB 6/12/79 201

UCR butane experiments

107 Simulation results for EC-304 208
108 Simulation results for EC-304 (with NO_3 conversion) 210
109 Simulation results for EC-305 211
110 Simulation results for EC-306 214
111 Simulation results for EC-307 217
112 Simulation results for EC-308 220
113 Simulation results for EC-309 223

UNC butane experiments

114 Simulation results for UNCB 10/24/77 225
115 Simulation results for UNCR 7/21/78 226

Number Page

116 Simulation results for UNCB 7/21/78 227
117 Simulation results for UNCR 7/22/78 228
118 Simulation results for UNCB 7/22/78 228
119 Simulation results for UNCR 7/27/78 229
120 Simulation results for UNCB 7/27/78 229

UCR toluene experiments

121 Simulation results for EC-266 235
122 Simulation results for EC-269 236
123 Simulation results for EC-270 237
124 Simulation results for EC-271 237
125 Simulation results for EC-272 238
126 Simulation results for EC-273 239

UCR benzaldehyde experiments

127 Simulation results for EC-327 257
128 Simulation results for EC-336 258
129 Simulation results for EC-337 259
130 Simulation results for EC-339 260
131 Simulation results for EC-340 261

UNC toluene experiments

132 Simulation results for UNCB toluene 9/18/78 263
133 Simulation results for UNCR ethylene 9/18/78 263
134 Simulation results for UNCR ethylene 9/18/78 264
135 Simulation results for UNCB toluene 9/18/78 264
136 Simulation results for UNCR 9/14/78 265
137 Simulation results for UNCB 9/14/78 266
138 Simulation results for UNCR 8/16/78 267
139 Simulation results for UNCB 8/16/78 268

UNC propylene/toluene experiments

140 Simulation results for UNCB tol-pro 6/21/79 273
141 Simulation results for UNCR propene 6/21/79 274
142 Simulation results for UNCB tol-pro without NO_3 loss 275

UCR experiments using the original Carbon-Bond Mechanism

143 Simulation results for EC-231 289
144 Simulation results for EC-232 290
145 Simulation results for EC-233 291
146 Simulation results for EC-237 292
147 Simulation results for EC-238 293
148 Simulation results for EC-241 294
149 Simulation results for EC-242 295
150 Simulation results for EC-243 296
151 Simulation results for EC-245 297
152 Simulation results for EC-246 298
153 Simulation results for EC-247 299

Number Page

UCR experiments using the new Carbon-Bond Mechanism (CBM-II)

154 Simulation results for EC-231 300
155 Simulation results for EC-232 302
156 Simulation results for EC-233 304
157 Simulation results for EC-237 306
158 Simulation results for EC-238 308
159 Simulation results for EC-241 310
160 Simulation results for EC-242 312
161 Simulation results for EC-243 314
162 Simulation results for EC-245 316
163 Simulation results for EC-246 318
164 Simulation results for EC-247 320
165 Standard ozone isopleth conditions 327
166 Ozone isopleth used in EKMA 328
167 Ozone produced by a 10/90 propylene butane mix 329
168 PAN isopleth 330
169 Ozone and PAN at HC/NO_x = 6.7 331
170 NO_2 isopleth 332
171 HNO_3 isopleth 334
172 NO_3 isopleth (10000 X ppm) 335
173 HCHO isopleth 336
174 HO_2 isopleth (10000 X ppm) 337
175 H_2O_2 isopleth 338
176 OH isopleth (1×10^6 X ppm) 340
177 Ratio of organic nitrate to total nitrate after 10 hours . . 341

TABLES

Number Page

1 Inorganic Reactions and Rate Constants in the Explicit Mechanisms . 20

2 Aldehyde Photolysis Ratios to NO_2 as a Function of Solar Zenith Angle 24

3 Initial Conditions and Photolysis Rate Constants for the UCR Formaldehyde/NO_x Smog Chamber Experiments 45

4 Initial Conditions and Aldehyde Photolysis Constants for the UNC Formaldehyde/NO_x Smog Chamber Experiments 46

5 Reactions of Formaldehyde and Acetaldehyde 48

6 UCR Formaldehyde Experiments--Simulations and Measurements 50

7 UNC Formaldehyde Experiments--Simulations and Measurements 51

8 Initial Conditions and Photolysis Rate Constants for UCR Acetaldehyde/NO_x Smog Chamber Experiments 57

9 UCR Acetaldehyde Experiments--Simulations and Measurements 57

10 Initial Conditions and Aldehyde Photolysis Constants for the UNC Acetaldehyde Smog Chamber Experiments 59

11 UNC Acetaldehyde Experiments--Simulations and Measurements 60

12 Reactions of Ethylene 74

13 Initial Conditions and Aldehyde Photolysis Constants for UNC Ethylene/NO_x Smog Chamber Experiments 75

14 UNC Ethylene Experiments--Simulations and Measurements 76

15 Initial Conditions and Photolysis Rate Constants for the UCR Ethylene/NO_x Smog Chamber Experiments 101

16 UCR Ethylene Experiments--Simulations and Measurements 101

17 Initial Conditions for UNC Ethylene/Acetaldehyde Experiments and Other Side Propylene/NO_x Experiment 113

Number Page

18 UNC Ethylene/Acetaldehyde and Propylene Experiments--Simulations and Measurements 113

19 Reactions of Propylene 121

20 Initial Conditions for UCR Propylene/NO_x Experiments 125

21 UCR Propylene Experiments--Simulations and Measurements 126

22 Initial Conditions for UNC Propylene/NO_x Experiments 127

23 UNC Propylene Experiment--Simulation Results and Measurements . 128

24 Initial Conditions for UCR Propylene/Acetaldehyde and Propylene/NO_x Experiments 196

25 Initial Conditions for UNC Propylene/Acetaldehyde and Propylene/NO_x Experiments 196

26 Reactions of Butane 203

27 Initial Conditions for UCR Butane/NO_x Experiments 206

28 Initial Conditions for UNC Butane/NO_x Experiments 206

29 UCR Butane Experiments--Simulations and Measurements 207

30 UNC Butane Experiments--Simulations and Measurements 207

31 The Developmental Toluene Mechanism 249

32 UCR Simulation Conditions 254

33 UNC Simulation Conditions 262

34 The Carbon-Bond Mechanism 269

35 The Original Formulation of the Carbon-Bond Mechanism 278

36 The New Carbon-Bond Mechanism (CBM-II) 280

37 Initial Conditions for the Seven-Hydrocarbon/NO_x Experiments . 322

38 Normalized Initial Conditions for the Seven-Hydrocarbon/NO_x Experiments (ppmC) Used for Carbon-Bond I 323

39 Normalized Initial Conditions for the Seven-Hydrocarbon/NO_x Experiments (ppmC) Used for Carbon-Bond II 324

Number Page

40 Statistical Analysis of the Original CBM and CBM-II Ozone Predictions Compared with Measured Data 325

SECTION 1

INTRODUCTION

This report describes the final year of a three-year study, sponsored by the Environmental Protection Agency (EPA), to model the formation and evolution of photochemical oxidants. The study has three basic parts:

1. Development and refinement of explicit chemical kinetic mechanisms* for simulating smog chamber experiments that were initiated with a few simple hydrocarbon species and NO_x. This effort is intended to assist in developing a greater understanding of the formation of photochemical oxidants, to point out specific chemical reactions most in need of further study, and to provide a basis for the second part of this study.
2. Refinement of a generalized mechanism for describing the chemical aspects of photochemical oxidant formation in the atmosphere. This mechanism, known as the Carbon-Bond Mechanism (CBM) is incorporated in large air-quality simulation models used for predicting spatial and temporal pollutant distributions in the atmosphere. Consequently, the mechanism must be able to treat complex mixtures of hydrocarbons yet have modest computing requirements.
3. Analysis of the effects of the physical and chemical characteristics of smog chambers on smog formation and evolution. Knowledge of these chamber effects is valuable for validating kinetic mechanisms with smog chamber data and for applying mechanisms in atmospheric studies.

---

* A chemical kinetic mechanism is a set of chemical reactions and rate constants. From a kinetic mechanism one can derive a set of coupled differential equations, which when integrated using a computer, can yield concentration/time profiles for the chemical species in the mechanism. Explicit mechanisms describe individual species, whereas generalized mechanisms include surrogate species that represent an entire group of similar species.

These portions were nearly completed during the first two years of this study, and the results have been released in an interim report (Whitten et al., 1979). During the past year, our efforts have primarily concentrated on extensions of the first two parts of the study. The work on the first part centered on the development of a mechanism for aromatic hydrocarbons and a careful adaptation of the previously developed smog chemistry to outdoor conditions of lighting, temperature, and humidity. Efforts on the second part describe the behavior of the generalized chemistry over a range of precursor concentrations. The number of smog chamber experiments in our inventory has increased substantially during this past year so that the statistical validity of the mechanism can now be based on nearly 300 experiments with time-dependent data.

A graphic illustration of the technical approach used in this study is displayed in Figure 1. Mechanism development in the present context is based primarily on simulating smog chamber experiments with explicit kinetic mechanisms. An explicit mechanism for a given chemical system individually treats each species and reaction thought to be important in that system. To simulate a smog chamber experiment, one must have data from the smog chamber experiment, a kinetic mechanism, and a computer program that simulates gas-phase chemistry by integrating the differential equations developed from the chemical mechanism.

The explicit mechanism work provided the framework for the second part of this study--refinement of the Carbon-Bond Mechanism (CBM). Developed in an earlier SAI study for the EPA (Whitten and Hogo, 1977), the CBM is a generalized mechanism--it treats generalized species rather than individual compounds, primarily for the purpose of reducing computing requirements. Many generalized mechanisms treat chemically similar molecules in groups, but the CBM treats chemically similar carbon atoms in groups, regardless of the compounds in which they occur. Our approach to refining the CBM involved condensing the essential features of the revised or newly developed explicit mechanisms from the first part of this study. For aromatics the procedure was reversed. Several alternate pathways or splits in the explicit chemistry were unresolved a year ago; therefore, an empirical, condensed scheme was developed. As new information on aromatics chemistry became available to us during this past year, we have begun filling in the condensed steps with

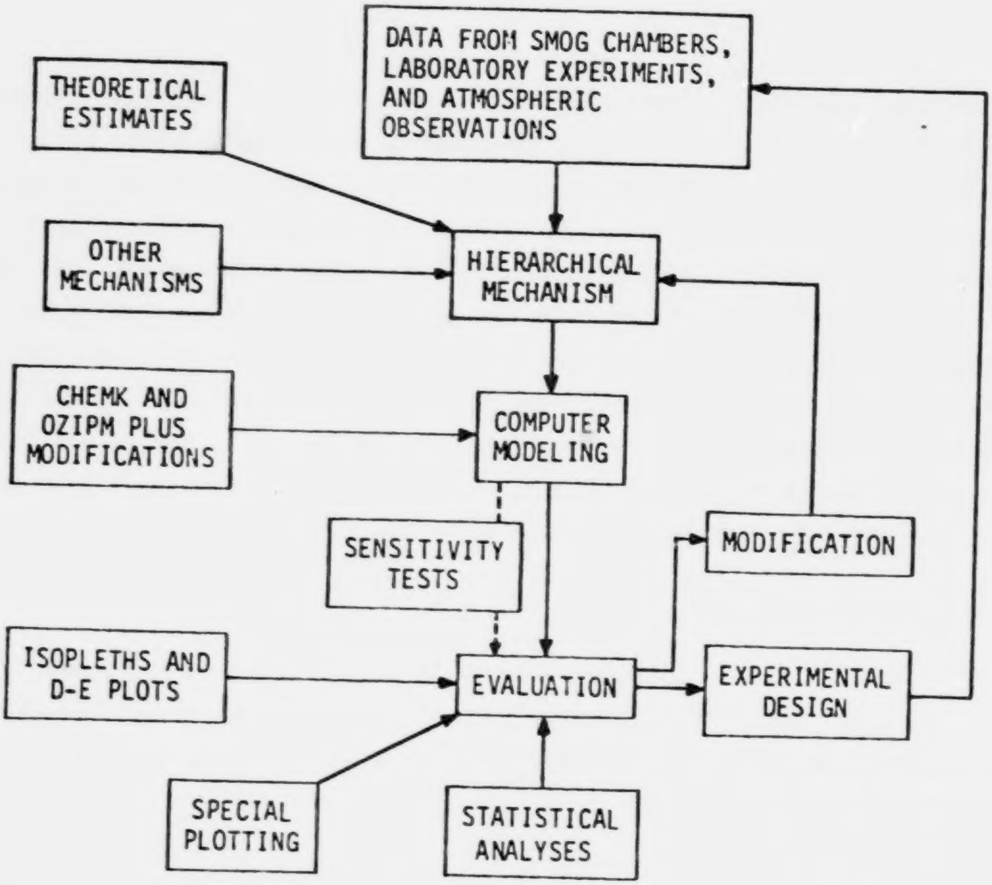
DATA FROM SMOG CHAMBERS, LABORATORY EXPERIMENTS, AND ATMOSPHERIC OBSERVATIONS
THEORETICAL ESTIMATES
OTHER MECHANISMS
HIERARCHICAL MECHANISM
CHEMK AND OZIPM PLUS MODIFICATIONS
COMPUTER MODELING
SENSITIVITY TESTS
MODIFICATION
ISOPLETHS AND D-E PLOTS
EVALUATION
EXPERIMENTAL DESIGN
SPECIAL PLOTTING
STATISTICAL ANALYSES

FIGURE 1. MECHANISM DEVELOPMENT AND REFINEMENT ACTIVITIES

appropriate explicit chemistry. The revised Carbon-Bond Mechanism (CBM-II) was validated using smog chamber data and was incorporated in the current SAI Airshed Model, which is now being used to model air quality in Los Angeles, Sacramento, and St. Louis.

For the study of chamber effects we used an explicit propylene mechanism to simulate data from propylene/NO_x experiments performed in eight smog chambers. We also analyzed the relative speeds of reaction and diffusion to the chamber walls to determine which are rate limiting for various species. The simulation results and that analysis were used to evaluate the effects of different wall materials, light sources, surface/volume ratios, and other characteristics. Differences in the spectral distribution of irradiation between chambers appear to account for most of the observed differences in photochemical oxidant formation. Wall effects appear to be small, and they are often within the uncertainty of the spectral distribution of the light source. The results of this study were presented in the interim report (Whitten et al., 1979).

A principal goal in computer modeling of smog chemistry is to develop a set of reactions and rate constants that provides the closest possible agreement between simulations and measurements for a series of experiments. This development is carried out by:

> Using measurements or estimates for all important reactions, products, and rate constants known or expected to occur in the system of interest, within their limits of uncertainty, to formulate a kinetic mechanism.
> Estimating the physical conditions appropriate for the experiments performed (e.g., the initial HONO concentrations, the temperature during each experiment, and other parameters).
> Simulating the smog chamber experiments using a computer.
> Modifying or adding reactions, products, and rate constants until satisfactory agreement between simulations and measurements is achieved. However, there are many constraints that must be met:
    - Common reactions must have the same rate constants in all experiments.

- Chamber-dependent effects should be consistent.
- Precursor decay must be simulated correctly.

Published data on reactions and rate constants were used where possible in constructing the mechanisms, but, because of gaps in the data, all mechanisms contained hypothetical reactions or estimated rate constants. Simulated time profiles of precursor decay and secondary product appearance and decay were compared with the profiles using smog chamber data to evaluate the hypotheses and estimates and, thus, to develop a deeper understanding of the formation of photochemical oxidants.

In constructing mechanisms, we followed the concept of a hierarchy of chemical species that has been described in detail elsewhere (Whitten et al., 1979). Essentially, each species can be assigned to a hierarchical level on the basis of the number of photochemical-oxidant-forming systems in which it occurs. NO, NO_2, CO, ozone, and some other inorganic species, for example, occur in every photochemical-oxidant-forming system, and they are thus assigned to the lowest level. Formaldehyde, which occurs in every system except the CO/NO_x system, occupies a higher level in the hierarchy. Acetaldehyde occurs in most systems, but not in formaldehyde/NO_x or CO/NO_x, and so it is at a still higher level. This description of the hierarchical concept, although ambiguous, suggests an order for development of explicit kinetic mechanisms. After constructing and evaluating a mechanism for CO, one can develop a formaldehyde mechanism by adding a few reactions and rate constants to the CO mechanism. The same procedure can be used for acetaldehyde. In validating each successive mechanism, one can focus attention on the added reactions and rate constants because the other reactions and rate constants have already been validated. Following this procedure reduces the probability that a complex mechanism, such as that for propylene, contains errors that compensate for each other in simulations of a set of smog chamber experiments.

During this study we used an approach for validating each mechanism that is intended to minimize the possibility of fortuitous agreement between simulations and measurements. A valid kinetic mechanism, unlike a mere curve-fitting exercise, should give reasonable predictions when used in applications such as atmospheric modeling that are outside the range of conditions and smog chamber experiments for which it was developed. Our approach is based on the following principles:

> The first measurements that must be reproduced with acceptable accuracy are those related to the consumption of the initial precursors. A mechanism for propylene/NO_x systems, for example, should describe the disappearance of propylene and NO_x. Ozone development and other manifestations of the experiment must depend on the products that result from decay of the precursor hydrocarbons and NO_x. Good agreement between measured and simulated ozone concentrations, coupled with poor agreement for hydrocarbon decay, is indicative of compensating errors in the kinetic mechanism. Errors that compensate one another under the conditions of a particular smog chamber experiment are not likely to do so for other experiments or atmospheric applications. For example, if a new experiment were to be initiated at the point at which a previous experiment reached half the decay of a key precursor, then the same mechanism would simulate both experiments correctly only if the decay of that key precursor were simulated correctly in the original experiment.

> In simulating a series of experiments in the same smog chamber, chamber-dependent effects must be treated consistently. If ozone is assumed to react with the walls of the chamber, for example, the same rate constant for that reaction should be used in all simulations of experiments in that chamber unless some characteristic of the chamber has been changed. If a light source is assumed to emit progressively lower amounts of short-wavelength radiation over a period of several months, the photolysis rate constants for the series of experiments must diminish in accordance with the order of performance of the experiments. Arbitrary adjustments for such effects must be avoided.

The results of applying these procedures and principles is summarized in Section 2, which also presents the conclusions and recommendations. Sections 3, 4, and 5 each present detailed discussions on the developmental work in the areas of inorganic chemistry, explicit mechanisms, and the chemistry of toluene. Section 6 describes some studies using the generalized chemistry of the CBM.

SECTION 2

SUMMARY OF RESULTS, CONCLUSIONS, AND RECOMMENDATIONS

This section of the report presents general conclusions based on the final year of this study. The three main topics summarized are (1) the development of aromatics chemistry; (2) the adaptation of smog chemistry to the changing atmospheric effects caused by natural variations in ultraviolet light, temperature, and humidity; and (3) the precursor dependence of various species in smog chemistry.

In computer modeling studies such as this one, many ideas are tried, and large quantities of computer output are produced. In the descriptions of the activity that produced the current closest agreement between simulations and observational data, the implicit conclusion is that the steps taken were both unique and necessary. However, experience has shown that equally close agreement is possible from several combinations of adjustments to physical conditions and mechanisms. Hence, the conclusions presented here must be qualified with the caveat that the results are subject to change in accordance with new data and further modeling efforts.

GENERAL CONCLUSIONS

During the past year, significant progress in mechanism development has occurred, particularly in aromatics chemistry and inorganic chemistry. Important discoveries in aromatics chemistry indicate that many of the carbon atoms react with few conversions of NO to NO_2, that some carbon atoms are very reactive, and that considerable NO_x, apparently via NO_3, is converted to organic nitrates. Olefin and paraffin chemistries, which were developed in earlier studies, tended to have nearly all carbon atoms equally reactive, and the major portion of NO_x was converted to nitric acid with little invlovement of the NO_3 radical.

The atmospheric lighting effects from intermittent clouds or overcast conditions are difficult to characterize quantitatively. A single measure of light intensity, such as total solar radiation, appears to be inadequate for completely simulating observed smog chamber data. The changes produced by clouds in the ultraviolet spectrum have yet to be adequately characterized in our simulations as a function of wavelength. The major effect of temperature on smog chemistry, in our current mechanism, is connected with the chemistry of peroxynitric acid (PNA). At low temperatures the formation of PNA is enhanced because of a negative activation energy, and at the same time, the decomposition of PNA is retarded because of a large positive activation energy. This compound acts as a temporary sink for radicals that would otherwise be available to drive the smog chemistry. Since PNA is formed from both a radical (HO_2) and NO_2, the temperature effects on experiments with low HO_2 and NO_2 concentrations are minimal.

It is likely that PNA chemistry also explains the effect of humidity on smog chemistry, but more experiments comparing wet and dry atmospheres need to be studied. The involvement of water vapor on many important individual reactions also needs further study.

Various species produced by the generalized chemistry of the CBM have been plotted as isopleths, which are functions of the smog precursor concentrations of hydrocarbons and nitrogen oxides. The shapes and locations of these isopleths are useful for predicting measurement and experimental programs designed to verify the CBM. These diagrams should also be useful for predicting the conditions most affected by the reactions that could be added to the CBM. For instance, the reaction of OH· with SO_2 might be added to simulate sulfate formation. In this case, the isopleth diagram for OH· generated by the CBM suggests that maximum OH· occurs at a specific HC/NO_x ratio and is virtually independent of concentration of the HC and NO_x precursors if their ratio is held constant.

MECHANISM REFINEMENT

The initial conditions and mechanisms are provided for all of the UCR simulations reported in this study. However, a satisfactory method of presenting the time-dependent temperature and light flux data used to simulate the UNC experiments is not available at this time and, therefore, they are not included in this report. Adjustments were made from the reported data only as follows:

> A small initial concentration of HONO was assumed in each simulation to help reproduce the measured rate of consumption of the initial hydrocarbon(s) early in each experiment. The amount of HONO assumed was always less than the equilibrium concentration calculated for the initial NO and NO_2 concentrations using the equation (Durbin, Hecht, and Whitten, 1975):

$$[HNO_2]_{eq} = (4.18 \times 10^{-7}) \exp 2365/T \, ([NO][NO_2][H_2O])^{1/2}$$

> In simulations, primarily of UCR data, small adjustments were made in the photolysis constants. These adjustments, like those of the initial HONO concentration, helped to simulate accurately the measured consumption of the initial hydrocarbon(s). The adjustments were within the range of reported intensity variations and the main justification for their use is that they ensured hydrocarbon decay products were being used in the mechanisms at the observed rates.

> In a few simulations, the initial HC or NO_x concentration was changed slightly from the measured value. The adjustments were generally within the observed scatter in the data. The reported initial value is merely one data point in a series; adjustments were made to obtain the closest overall agreement between all the simulated and measured concentrations of HC and NO_x.

> In some UCR experiments, for which the reported initial NO_x concentration was zero, PAN was detected. The presence of PAN, which contains nitrogen, indicates the presence of NO_x at some time during the experiment. To simulate these experiments we had to assume limited degassing of NO_x from the chamber walls. The assumed input of NO_x was so small that including it in simulations of smog chamber experiments with nonzero initial NO_x concentrations had no discernible effects. In fact, there seemed to be an unexplained loss of NO_x in many UCR experiments, which may be the result of trapping of NO_x on the walls of the chamber.

We used these methods to adjust the simulated hydrocarbon consumption rate to fit the measurements so that the simulation results would reflect the generation of secondary products in the chamber from the decay products of the primary precursors. Future research on photolysis constants, for example, may show that the adjustments used in this report are in error. Other sources of radicals and radical sinks may be discovered that our current mechanisms do not properly describe. Nevertheless, the present approach uses carbonyl compounds as surrogates for the compounds produced during an experiment, and these in turn generate radicals. In this approach, the rate of production of radicals varies during the simulations. This variation produces different simulations than a constant rate of radical production would (e.g., if radicals are assumed to be supplied by the walls of the chamber, the radical production would be constant).

The assumption that radicals are supplied by the photolysis of products formed from the decay of the precursors is directly applicable to atmospheric modeling. The range of photolysis rate constants used to simulate UCR experiments provides an indication of the sensitivity of radical production and subsequent ozone formation to light intensity. The average value of 0.004 for the ratio of the formaldehyde radical production photolysis rate constant to the NO_2 photolysis rate constant, used in simulations of UCR experiments, is close to the 0.003 average value used in simulations of experiments in the outdoor smog chamber at UNC. Thus, the solar simulator used at UCR produces a spectrum that is consistent with the actual solar spectrum in terms of the aldehyde photolysis required in our mechanisms.

All the explicit mechanisms were tested in two different smog chambers. The only changes made between chambers were the following:

> Photolysis constants were adjusted and maintained for each UCR experiment. Adjustments were almost never made for the UNC experiments except on an experimental basis on cloudy days. However, the photolysis rates for the UNC simulations were varied continously according to the measured solar radiation.

> Ozone decay on the chamber walls was simulated in all UCR runs with a first-order rate constant of 0.001 min^{-1}, and in all UNC runs with a rate constant of 0.00022 min^{-1}.

> The rate constant used for $N_2O_5 + H_2O$ was 5×10^{-6} $\text{ppm}^{-1}\text{min}^{-1}$ for all UCR runs with an EC number between 121 and 279, and 1.5×10^{-5} $\text{ppm}^{-1}\text{min}^{-1}$ was used for all others. (The chamber was apparently altered after EC-279.) A value of 5.5×10^{-7} $\text{ppm}^{-1}\text{min}^{-1}$ was used for all UNC experiments.

> Two reactions were used to simulate formaldehyde adsorption and desorption from the walls in all UNC experiments. In some UNC formaldehyde experiments, the amounts of formaldehyde initially assumed to be on the chamber walls were adjusted to simulate the observed formaldehyde behavior. No wall interactions were considered for formaldehyde in the UCR simulations because these experiments were performed with the walls heated to 303K.

Conclusions that can be drawn from the formaldehyde simulations are clouded by problems with the measurement of formaldehyde and its tendency to adhere to surfaces. However, the present chemistry used to simulate the experiments in both chambers shows no gross inadequacies. The UCR experiments utilized trace levels of butane which could be used to monitor OH levels. In two experiments, without added NO_x, the simulated butane decay was too fast. Thus, the mechanism appears to lack a sink reaction for radicals that becomes important at very low NO_x levels. There is no evidence in these formaldehyde simulations to indicate a need for reactions which would suppress ozone or lower the efficiency of ozone production from the conversion of NO to NO_2. The agreement between simulated and observed concentrations of CO in the UNC experiments confirms that the peroxyformyl radical, HCO_3, is probably not important since CO_2 would be expected from the reaction of this radical with NO.

The chemistry of acetaldehyde adds the chemistries of the CH_3O_2 radical and PAN to the formaldehyde mechanism in addition to the acetaldehyde itself. Section 4 presents evidence to support the use of a low overall quantum yield for radical production from the photolysis of acetaldehyde. The acetaldehyde simulations themselves are basically consistent with the observations, but the PAN predictions are uncertain. In early 1978, the PAN analyzer at UNC was recalibrated downward; therefore, most of our simulations of UNC experiments prior to this recalibration underpredict PAN while those after the recalibration overpredict PAN. Acetaldehyde experiments without added NO_x appear to be a useful means of monitoring the offgassing of NO_x from smog chamber walls by monitoring PAN production.

From the study of several simulations of ethylene chemistry, we have concluded that further characterization of the formaldehyde and inorganic chemistry will be necessary before any major changes to the ethylene chemistry can be tested adequately.

The combination of the ethylene and acetaldehyde mechanisms was tested in the dual UNC chamber against the chemistry of propylene. Although more experiments will be needed for confirmation, it appears that too much PAN is generated by the present acetaldehyde mechanism. The same instrument is used to monitor PAN from both sides of the dual chamber; however, using the present chemistry, PAN in the ethylene/acetaldehyde side was overpredicted while PAN in the propylene side was underpredicted. The only organic precursor for PAN in both mechanisms is acetaldehyde. Hence, an error in the acetaldehyde mechanism causing the production of too much PAN infers that a pathway to PAN formation is missing from the propylene mechanism.

The discrepancies between the observations and the computer simulations, like those in the ethylene chemistry, are often masked by the light flux, temperature, and humidity effects; these discrepancies are due to inaccuracies in the formaldehyde and inorganic mechanisms. These problems show up in the ethylene and propylene simulations more often than in the formaldehyde experiments because of the limited number of formaldehyde experiments. A significant change made in the propylene chemistry was the reduction in radical yield resulting from oxygen atom attack on propylene. We conclude that our current yield of two radicals 25 percent of the time represents an upper limit since higher yields tend to initiate the oxidation chemistry too early in simulations of UNC experiments.

From these propylene simulations, we tentatively conclude that some form of suppression is needed for either ozone itself or the NO_x conversion efficiency. That is, the number of NO-to-NO_2 conversions per reaction of propylene appears to be too high, especially for simulations of the UCR data. The problem with this conclusion is that the UNC simulations often result in the reverse effect. Hence, there may be a chamber-dependent effect that is specific to propylene. Indeed, the performance of similar propylene/acetaldehyde experiments indicates that some factor is missing since the current mechanisms do not successfully simulate the results from both chambers.

From the present study of butane chemistry, we conclude that the assumption of close competition between alternate pathways for the sec-butoxyl radical has finally been verified. For several years, modelers have found that this assumption was a convenient way to tune the predictions of butane simulations to observed product distributions. However, the competition between thermal decomposition and reaction with oxygen could not be measured in laboratory studies at conditions relevant to the smog chamber experiments. The results of the present simulations of experiments conducted at three different temperatures show that the variance in product distribution between acetaldehyde and MEK is explained by the activation energy of the decomposition pathway.

Other conclusions based on the butane study are that an ozone suppression reaction is needed and that nitrate production is an important but limited sink for both radicals and NO_x. A major source for radicals, in general, and PAN, in particular, is the photolysis of MEK in our mechanism, but this conclusion needs the further verification that will be possible when the smog chamber experiments using only this organic are modeled.

Our simulations of toluene/NO_x systems lead us to conclude that the α-dicarbonyl compounds, formed in the photooxidation of aromatics systems, photolyze very rapidly, yielding a high overall radical concentration. However, compared with other hydrocarbons, aromatics systems are relatively inefficient producers of peroxy radicals. The net result of these two factors is a high rate of hydrocarbon and NO_x decay in aromatics systems but an inefficient production of ozone.

In the aromatics system, there also appears to be a major sink for NO_x, in addition to the formation of PAN and nitric acid. Unlike the NO_x sink represented by alkylnitrate formation in paraffinic systems, the aromatics NO_x sink dominates after the NO_2 peak and seems to be associated with the NO_3 radical.

The overall mass balance is very poor for both nitrogen and carbon in the smog chamber data available to us.

RECOMMENDATIONS

In this section, we offer specific recommendations that focus on using modeling to highlight needs for future studies. In many cases, the discussions in the rest of this report explain thoroughly the reasons for these recommendations. The recommendations are divided into three categories: laboratory measurements of reaction products and rate constants, smog chamber experiments, and analytical techniques. In addition to these specific recommendations, we wish to emphasize the need for continued research to reduce the uncertainties in reaction rate constants and product distributions for individual reactions associated with, and under experimental conditions relevant to, smog chemistry. We also wish to stress the need for continued chamber and modeling studies and analytical improvements to provide carbon and nitrogen mass balances for smog chamber experiments.

The specific recommendations regarding smog chamber experiments to be used with modeling studies are:

> A series of experiments using individual hydrocarbons from a homologous series should be performed. In the paraffin series, only butane and 2,3-dimethylbutane have been carefully studied. Such molecules as pentane, hexane, and others found in the atmosphere should be studied so that the schemes used in generalized mechanisms to generate average rate constants can be evaluated. Developmental work on butane chemistry itself should be enhanced because the chemistry of nitrate production and alkyl radical reactions would require that the reactions pertinent to butane be treated as part of a similar series.

> Experiments using molecules with various ring structures should be performed so that explicit mechanisms for them can be developed. Cyclohexane and cyclohexene are observed in the atmosphere, as are the various ring structures of natural hydrocarbons such as α-pinene. However, the details of the smog chemistry of such compounds are not known well enough to justify using generalized mechanisms to evaluate the importance of those compounds in photochemical oxidant formation in the atmosphere.

- Smog chamber experiments should be performed, similar to the formaldehyde and acetaldehyde series reported here, for the other photolytically active species utilized in this study such as MEK, acetone, glyoxal, methylglyoxal, and biacetyl. Trace quantities of butane should be present in these experiments to monitor the hydroxyl concentration.
- Experiments at high HC/NO_x ratios are needed, along with nitrate measurements, for long chain paraffins and aromatics in order to verify the predictions of the carbon bond chemistry.
- Experiments in an aerosol chamber should be utilized so that organic and nitrate aerosol production can be simulated using the aromatics mechanism.
- Experiments designed to determine the threshold of importance of $O(^1D)$ should be performed. Ozone should be a significant initial reactant so that the hydroxyl radicals generated from $O(^1D)$ dominate other sources of radicals such as formaldehyde.
- Experiments using H_2O_2, or some other suitable radical source, should be conducted with CO at various temperatures and humidities to verify the inorganic chemistry.

Experiments commonly performed in laboratory vessels can also be performed in smog chambers (at night if photochemistry is to be avoided).

The recommendations concerning laboratory experiments of specific reactions are:

- Reactions and rate constants of alkylperoxy radicals at typical atmospheric concentrations should be studied. The reactions of alkylperoxy radicals with NO, NO_2, O_3, and other radicals (particularly $HO_2^{\cdot}$) are most appropriate for study. In addition to the rate of reaction with NO, the pathway to nitrate formation needs to be determined as a function of the structure of the alkyl group.

- The fate of the addition products when hydroxyl radicals react with olefins under atmospheric conditions should be determined. In particular, the peroxy radical that apparently forms when oxygen adds to the addition product may react with ozone; this possibility may still warrant consideration. The upper limit to formation of hydroxy substituted products should also be determined.
- The photolysis of ketones and aldehydes under typical atmospheric conditions should be studied to determine possible radical products. Modern kinetic mechanisms generally rely on the photolysis of carbonyl compounds (which are intermediate products in the atmospheric oxidation of hydrocarbons) to supply the majority of the radicals necessary to sustain the overall smog formation process in simulations.
- The competitive chemistry for Criegee intermediates needs to be determined between NO, NO_2, SO_2, aldehydes, and other possible reactions. The products of these reactions also need verification, especially the reactions with NO_2.
- The effects of water concentration on virtually all smog reactions are uncertain. However, the chemistry of HO_2 and peroxynitric acid requires immediate verification since current modeling studies are assuming that the chemistry of these compounds is strongly influenced by water.
- The influence of ammonia on smog chemistry may parallel that of water so that the studies using H_2O might include this compound as well.
- The yield of various products from the attack of oxygen atoms on olefins should be studied at atmospheric conditions to verify the assumed yields given in this report.
- Significant involvement of the NO_3 radical is implicated in many cases. The products and rate constants for the

many possible reactions of NO_3 need to be determined. In particular, the various intermediates in aromatics chemistry, as well as butane chemistry, warrant special attention for study with NO_3.

> The compound 2-butene-dial is the logical product of the aromatics mechanism. However, the chemistry of this species is very uncertain. Photolysis, hydroxyl attack, and reaction with ozone and NO_3 all require investigation.

Our recommendations for improved measurements are as follows:

> Data at 300 nm [for $O(^1D)$ chemistry], 320 nm (for aldehyde photolysis), and 380 nm (for NO_2 photolysis) need to be continuously monitored relative to each other with at least one determined absolutely. The shape and level of the solar spectra appear to be the most important data needed to model smog photochemistry, especially on partially cloudy days.

> The measurement of the following compounds is needed: organic nitrates, 2-butene-dial, MEK, acetone, glyoxals, and H_2O_2.

> The accuracy of aldehyde measurements, especially formaldehyde, must be improved.

> The temperature and water effects on the formaldehyde adsorption/desorption problem should be characterized.

SECTION 3

TREATMENT OF INORGANIC REACTIONS

The inorganic reaction set forms the basis of all smog chemistry. In practical terms, the nearly 300 smog chamber experiments now in our data inventory all need to be modeled using the same set of inorganic reactions. Recent significant changes to this set of reactions have led to questions concerning the reliability of previous simulations as well as those currently being performed. The following examples indicate important recent developments:

> The discovery of peroxynitric acid and related compounds having strong temperature-dependent chemistries.

> Drastic changes in rate constant estimates for important reactions such as HO_2 plus NO.

> The discovery of a significant water effect in the UNC chamber and the consequent need for further laboratory studies of many individual reactions.

Smog chamber experiments that emphasize the inorganic set of reactions are becoming more available. In the present study, the experiments using formaldehyde were intended for the purpose of emphasizing inorganic reactions, but complications have arisen involving the measurement and physical adsorption-desorption of this compound onto and off the chamber walls. In the near future, experiments using hydrogen peroxide as a radical source together with carbon monoxide to convert hydroxyl radicals to HO_2 will be carried out. By that time, we hope that the temperature and water dependence of the basic inorganic reaction set will have been established more firmly.

Before the writing of the interim report for this contract (Whitten et al., 1979) the National Bureau of Standards (NBS) evaluation of atmospheric chemistry was released (Hampson and Garvin, 1978). This year the NASA evaluation (DeMore et al., 1979) has been released. For the most part, we have used the latest recommended set of rate constants. The remainder of this section discusses our reasons for using alternative reaction rate estimates and our particular implementation of the NASA recommendations. If a reaction appeared in the 1978 NBS evaluation, but not in the recent NASA evaluation, the NBS recommendation was used. The inorganic reaction set used in this report is presented in Table 1.

TABLE 1. INORGANIC REACTIONS AND RATE CONSTANTS IN THE EXPLICIT MECHANISMS

Reaction	Rate constant at 298K ($ppm^{-1}min^{-1}$)	Activation energy (K)
$NO_2 + h\nu \rightarrow NO + O(^3P)$	Experimental*	--
$O(^3P) + O_2 + M \rightarrow O_3 + M$	$2.08 \times 10^{-5\dagger}$	-510.0
$O(^3P) + NO_2 \rightarrow NO + O_2$	1.38×10^4	--
$O_3 + NO \rightarrow NO_2 + O_2$	2.66×10^1	1450.0
$O(^1D) + M \rightarrow O(^3P) + M$	4.45×10^4	-97.3
$O(^1D) + H_2O \rightarrow 2OH\cdot$	3.4×10^5	--
$O_3 + OH\cdot \rightarrow HO_2\cdot + O_2$	1.0×10^2	940
$O_3 + HO_2\cdot \rightarrow OH\cdot + 2O_2$	2.4	580
$O_3 + NO_2 \rightarrow NO_3 + O_2$	4.75×10^{-2}	2450
$O_3 + h\nu \rightarrow O(^1D) + O_2$	Experimental*	--
$O_3 + h\nu \rightarrow O(^3P) + O_2$	Experimental*	--
$2HONO \rightarrow NO + NO_2 + H_2O$	1.5×10^{-5}	--
$HONO + h\nu \rightarrow OH\cdot + NO$	Experimental*	--

TABLE 1 (Concluded)

Reaction	Rate constant at 298K ($ppm^{-1}min^{-1}$)	Activation energy (K)
$NO_2 + OH\cdot + M \rightarrow HONO_2 + M$	1.4×10^4	--
$NO + OH\cdot \rightarrow HONO$	1.4×10^4	--
$CO + OH\cdot \xrightarrow{O_2} HO_2^{\cdot} + CO_2$	4.0×10^2	--
$HO_2^{\cdot} + NO \rightarrow OH\cdot + NO_2$	1.2×10^4	--
$2HO_2^{\cdot} \rightarrow H_2O_2 + O_2$	3.37×10^3	-1930
$2HO_2^{\cdot} + H_2O \rightarrow H_2O_2 + H_2O$	1.16×10^{-1}	-6020
$H_2O_2 + h\nu \rightarrow 2OH\cdot$	Experimental*	--
$O_3 \rightarrow$ wall	1×10^{-3}**	--
$NO_3 + h\nu \rightarrow NO_2 + O(^3P)$	5.94	--
$NO_3 + h\nu \rightarrow NO + O_2$	2.4	--
$NO_3 + NO \rightarrow 2NO_2$	2.8×10^4	--
$NO_3 + NO_2 \rightarrow N_2O_5$	3.8×10^3	--
$N_2O_5 (+M) \rightarrow NO_3 + NO_2 (+M)$	1.22×10^1*	10600
$NO + NO_2 + H_2O \rightarrow 2HONO$	1.6×10^{-11}†	--
$NO + NO + O_2 \rightarrow NO_2 + NO_2$	7.14×10^{-10}†	--
$N_2O_5 + H_2O \rightarrow 2HONO_2$	5×10^{-6}§,**	--
$HO_2^{\cdot} + NO_2 \rightarrow HO_2NO_2$	1.7×10^3	-1400
$HO_2^{\cdot} + NO_2 + H_2O \rightarrow HO_2NO_2\cdot H_2O$	5.0×10^{-2}†	-2000
$HO_2NO_2 \rightarrow HO_2^{\cdot} + NO_2$	4.6	10000
$HO_2NO_2\cdot H_2O \rightarrow HO_2^{\cdot} + NO_2 + H_2O$	2.0	10000
$HO_2NO_2\cdot H_2O + H_2O \rightarrow$ wall	5.0×10^{-6}	--

* Rate constant in min^{-1}.

† Rate constant in $ppm^{-2}min^{-1}$.

§ In simulations of runs prior to UCR EC-121 and after EC-279, a value of $K = 1.5 \times 10^{-5}$ $ppm^{-1}min^{-1}$ was used.

** Varies according to different chambers.

PHOTOLYSIS REACTIONS

As in previous studies we have used NO_2 photolysis rates, k_1, as reported for simulating UCR and Battelle smog chamber experiments. For experiments in the UNC chamber we have used 0.4 times the value reported for total solar radiation (TSR) as recommended by Jeffries (private communication, 1978) unless ultraviolet (UV) data were available. Evidently the presence of reflective clouds and overcast conditions alters the ratio of ultraviolet radiation to total radiation in a manner that not only can change rapidly with time but also is impractical to characterize in any general way (Demerjian, Schere, and Peterson, 1979). Hence, the UNC experiments on cloudy days without UV data are often poorly simulated. The constant we have used to convert the UNC data from UV into values for k_1 is $12 cm^2/cal$; this value corresponds to 0.4 times the TSR data on very clear days. Jeffries, Fox, and Kamens (1976) have shown that the value of k_1 inside the chamber is higher than the values reported outside because of the reflective bottom of the chamber. To account for the reflective bottom, we have further adjusted the k_1 values using a correction factor recommended by Jeffries (private communication, 1979), which varies linearly with time: At 0900 and 1600 hours the factor equals 1.0, and at noon the value is 1.15.

The photolysis constants for O_3, HONO, H_2O_2, and the aldehydes are determined, as a rule, relative to the NO_2 photolysis. As discussed in our interim report (Whitten et al., 1979), the photolysis constant for each of these species tends to have a region of the ultraviolet spectra (290 to 420 nm) that is particularly sensitive to the determination of each photolysis constant. In particular, the photolysis of O_3 to form $O(^1D)$ is most sensitive to the photon flux near 290 nm; the photolysis of most aldehydes appears to be most sensitive at about 320 nm; the HONO photolysis is mostly determined near 370 nm; and the NO_2 photolysis constant is mostly determined by the photon flux near 390 nm.

Our procedure was to use the published information on absorption cross sections and quantum yields in conjunction with the data taken at the smog chamber facility on light intensity and the k_1 in our computer simulation scheme.

Outdoor Simulations

For outdoor simulations the solar flux data for various zenith angles recommended by Schere and Demerjian (1977) were used with cross-section and quantum yield information for each species (including NO_2) in order to determine the matrix of photolysis ratios relative to NO_2 for each species at the various zenith angles. During each simulation, the NO_2 photolysis is determined directly from the UV or TSR data as discussed previously. From the location, date, and time at any moment in the simulation a zenith angle is determined using the subroutine called SOLAR, which was developed by Busse (1971). A series of cubic spline functions is then used to interpolate among the various zenith angle values of the photolysis constants relative to NO_2, which were determined earlier for carbonyl species. Other species such as H_2O_2 and HONO are unchanged relative to NO_2. Table 2 shows the matrix of photolysis ratios to NO_2 as a function of the zenith angles for formaldehyde and acetaldehyde. Higher aldehydes are treated as acetaldehyde. These are the photolysis ratios to NO_2 photolysis used in the UNC simulations:

$O_3 + h\nu \rightarrow O(^3P) + O_2$	.042
$O_3 + h\nu \rightarrow O(^1D) + O_2$	.001
$HONO + h\nu \rightarrow NO + OH$	.30
$HOOH + h\nu \rightarrow 2\ OH$	.0014 .

Smog Chamber Simulations

For a discussion of the procedures for conducting simulations of experiments in the UCR smog chamber or other chambers in which artificial light is used, as well as some of the problems encountered, see Whitten et al. (1979). Basically, our simulations have employed the reported NO_2 photolysis constant. All other photolysis constants are then determined relative to NO_2 using the same cross-section and quantum yield data that were employed in the outdoor simulations and relative spectra information appropriate to the light source used in the chamber experiment. However, we have arbitrarily varied the aldehyde and ozone [to form $O(^1D)$] constants to improve the agreement between the simulations and the observed data.

TABLE 2. ALDEHYDE PHOTOLYSIS RATIOS TO NO_2 AS A FUNCTION OF SOLAR ZENITH ANGLE

Solar zenith angle (deg)	$HCHO + h\nu \rightarrow H_2 + CO$ ratio to NO_2	$HCHO + h\nu \rightarrow 2H\cdot + CO$ ratio to NO_2	$CH_3CHO + h\nu \rightarrow$ ratio to NO_2
0	6.22×10^{-3}	4.05×10^{-3}	9.16×10^{-4}
10	6.2×10^{-3}	4.03×10^{-3}	9.08×10^{-4}
20	6.12×10^{-3}	3.91×10^{-3}	8.74×10^{-4}
30	5.98×10^{-3}	3.71×10^{-3}	8.16×10^{-4}
40	5.76×10^{-3}	3.42×10^{-3}	7.34×10^{-4}
50	5.44×10^{-3}	3.01×10^{-3}	6.26×10^{-4}
60	5.05×10^{-3}	2.46×10^{-3}	4.88×10^{-4}
70	4.39×10^{-3}	1.87×10^{-3}	3.48×10^{-4}
78	3.90×10^{-3}	1.35×10^{-3}	2.34×10^{-4}
86	3.76×10^{-3}	9.99×10^{-4}	1.63×10^{-4}

As demonstrated in Whitten et al. (1979), the published relative spectra obtained for the UCR chamber showed considerable scatter at the wavelengths to which these two types of photolysis processes are sensitive. The range over which we varied the photolysis constants is less than the range of the observed scatter for aldelydes. For example, the average aldehyde photolysis value for formaldehyde photolysis to radical products approximates the average value calculated from the reported relative spectra. The calculated ozone photolysis, on the other hand, exhibits a wide range of fluctuations. In general, we have arbitrarily lowered this rate, which produces $O(^1D)$, if the reported spectra indicate high levels of radiation in the 290 to 300 nm wavelength range. Using large production rates for $O(^1D)$ tends to produce results that are typical of simulations involving too many radicals. Our experience in modeling smog chamber experiments indicates that $O(^1D)$ chemistry is not important.

However, the chemistry of $O(^1D)$ in the unpolluted atmosphere must be important because the ratios of ozone to precursor concentrations are much higher than in typical smog chamber experiments. Thus, an area for future research is the definition of the transition zone at which $O(^1D)$ chemistry becomes important.

HO_2 CHEMISTRY

During the past year, we have attempted to incorporate some of the recent information on the chemistry of this species into our inorganic set of reactions. Hamilton and Naleway (1976) have demonstrated the theoretical bases for the formation of a strong complex between HO_2 and water. The involvement of such a complex has been used to explain an observed enhancement of the apparent rate constant for the self reaction of HO_2 (Hamilton and Lii, 1978). Cox (1978) has studied the pressure, water, and temperature dependence of this reaction and derived the following relationship for the rate constant:

$$k = \left(8[M] + 4.08 \times 10^{20}\right)^{-1} \left(3.25 \times 10^{8} + 4 \times 10^{-10}[M]\, A^{-1}\right) + 1.1 \times 10^{-34}[H_2O] \exp\left(+ 3730/T\right) A^{-1} \quad ,$$

where $A = 1 + 3.5 \times 10^{-16}[M] \exp\left(- 2060/T\right)$, and the units of k are in $\text{molecules}^{-1}\ \text{cm}^{3}\text{sec}^{-1}$. We have converted this relationship to $\text{ppm}^{-1}\text{min}^{-1}$ units in two terms with two activation energies; at 298K, $k = 3370 + 0.116[H_2O]$, and the activation energies of the two terms are -1930K and -6020K, respectively. The two activation energies were obtained by fitting an Arrhenius form to the original relationship at 298K and 260K. The rate constant at 298K without water is close to the 3750 value recommended in the latest NASA review.

Other reactions of HO_2 may be influenced by water, though a recent study by DeMore (1979) indicates that such is not the case for the reaction with O_3. Jeffries (private communication, 1979) has suggested that the reaction of HO_2 with NO_2 to form PNA is influenced by water vapor. This suggestion explains, at least partially, the humidity effect observed in the UNC chamber. Our approach has involved modeling the humidity effect by modifying the chemistry of PNA. Analogous to the rate expression for the HO_2 self-reaction, we use the following expression for the HO_2 reaction rate constant with NO_2 at 298K: $k = 1700 + 0.05\ [H_2O]$. The activation energies we use for the two terms are -1400K and -2000K, respectively. The first term is close to the value of -1500K suggested recently by Cox and Patrick (1979). The negative activation energy of -1400K is obtained by fitting an Arrhenius expression to the temperature dependence factor--$(T/300)^{-5}$--suggested in the NASA review by DeMore et al. (1979). For the activation energy of the water-dependent term, we tried values near -4400K that would be analogous to the ratio used for the two terms in the HO_2 self-reaction. However, we have lowered the value to -2000K because use of the higher value tended to result in too much PNA in cold smog chamber experiments, such as the propylene run of 10 January 1978 in the UNC chamber.

PEROXYNITRIC ACID CHEMISTRY

The PNA formed without water unimolecularly decomposes back to the HO_2 and NO_2 precursors. For this reaction, we used the rate constant and activation energy estimated by Graham, Winer, and Pitts (1978). In our attempts to model the substantial humidity effect observed in the UNC smog chamber on 21 October 1978, we treated the PNA formed by means of the $HO_2 \cdot H_2O$ complex differently from the "dry" PNA. We assumed that (1) the water molecule attached to the PNA lowers the decomposition rate by stabilizing the peroxy bond, and that (2) whereas the rate of dry PNA removal by the chamber walls is not important, the "wet" PNA can add yet another water molecule and then be removed at the walls. Hence, the main features of our current model of the substantial humidity effect are the enhancement of PNA production combined with slower PNA decomposition and water-dependent removal of the wet PNA. Obviously, we expect this scheme to be modified in the near future as additional dual smog chamber experiments verify the humidity effect and map the dependence of the effect on temperature and water concentrations. In addition, the dark removal rate of PNA to the UNC chamber walls and the possible influence of water vapor on that rate must be determined. The removal rate of PNA has been observed to be rapid in laboratory vessels (Levine et al., 1977). Independent laboratory measurements of any effects of H_2O on the formation and decomposition rates of PNA must also be taken. The influence of NH_3 might also be studied since Hamilton and Naleway (1976) have shown that the formation of ammonia complexes with HO_2 are similar to those that are formed with water.

SECTION 4

DEVELOPMENT AND APPLICATION OF THE EXPLICIT MECHANISMS

The interim report described the major developmental effort of the first two years of this contract (Whitten et al., 1979). It reflected the split of developmental work from the traditional propylene and butane mechanisms to the more fundamental mechanisms, such as formaldehyde and acetaldehyde, on the one hand, and to expansions of the traditional mechanisms to include ethylene, 1-butene, trans-2-butene, and 2-3 dimethylbutane, on the other hand. The concept of hierarchical levels was developed and used to help build mechanisms which contained common, independently validated subsets of reactions.

This year the split of developmental work was even more pronounced because the basic inorganic chemistry received special attention while explicit (or at least semi-explicit) aromatics chemistry was developed simultaneously. The work on aromatics chemistry represents a reversal of our traditional approach based on hierarchical levels that would normally lead to a condensed version of aromatics chemistry for use in the carbon-bond atmospheric mechanism. To develop explicit aromatics chemistry, we began with a condensed empirical mechanism and are now developing the overall explicit chemistry by filling in the fundamental chemistry responsible for the empirical pathways we had been using. We have reformulated the condensed chemistry, where necessary, as our knowledge and the data base have expanded.

A key facet of our efforts this past year has been the use of an expanded data base from smog chamber experiments primarily from the outdoor chamber at UNC. Hence the remainder of this section illustrates the present state of modeling a large data base, but does not detail mechanism development (aromatics chemistry is described in Section 5). The developmental discussions on inorganic chemistry were given previously.

FORMALDEHYDE

The basic parts of smog chemistry are found in the simple system of formaldehyde and NO_x irradiated in air. Furthermore, the set of chemical reactions that describe this system is common to virtually any smog chamber experiment and is common to all smog chemistry in the troposphere. Hence, the establishment of a reliable and well-founded mechanism for this system acts as a cornerstone to the knowledge of smog chemistry.

The basic parts of smog chemistry consist of NO_x chemistry in air and hydrocarbon chemistry. The buildup of oxidants, primarily ozone, occurs when NO is converted to NO_2 by reactions other than the reaction of ozone itself with nitric oxide. The hydrocarbon chemistry supplies this independent NO_x conversion; hydroxyl attack produces the required peroxy radicals; the subsequent NO_x conversions regenerate the hydroxyls. Carbonyl side products, such as aldehydes, photolyze to maintain the balance of the hydroxyl-peroxy radical pool with the radical sink reactions (e.g., nitrate formation). Formaldehyde is subject to hydroxyl attack yet it can also photolyze to generate the radicals necessary to sustain the oxidation chemistry. There appear to be three primary reactions of formaldehyde in photochemical smog: photolysis (two reactions) and reaction with $OH\cdot$:

$$HCHO + h\nu \rightarrow H\cdot + HCO\cdot \quad , \qquad (1)$$
$$HCHO + h\nu \rightarrow H_2 + CO \quad , \qquad (2)$$
$$HCHO + OH\cdot \rightarrow H_2O + HCO\cdot \quad . \qquad (3)$$

Note that formaldehyde photolysis can produce both radical and nonradical products. The former is a major source of radicals important to smog chemistry:

$$H\cdot + O_2 + M \rightarrow HO_2^{\cdot} + M \quad , \qquad (4)$$
$$HCO\cdot + O_2 \rightarrow HO_2^{\cdot} + CO \quad . \qquad (5)$$

In air at atmospheric pressure, Reactions (4) and (5) are very fast, and so Reactions (1) and (3) are normally written as:

$$HCHO + h\nu \xrightarrow{2O_2} 2HO_2\cdot + CO \quad , \qquad (6)$$

$$HCHO + OH\cdot \xrightarrow{O_2} H_2O + HO_2\cdot + CO \quad . \qquad (7)$$

This formaldehyde mechanism was tested using smog chamber data from the UCR and UNC facilities. Figures 2 through 5 present four simulations of formaldehyde experiments in the UCR chamber and Figures 6 through 14 illustrate nine in the UNC chamber. The initial conditions used are given in Tables 3 and 4. The UCR experiments contained trace quantities of butane that could be used to check the hydroxyl levels. This check was useful for these experiments because the decay of formaldehyde occurs through a combination of photolysis and hydroxyl attack.

The data on formaldehyde in both chambers was difficult to obtain and is probably not very accurate. For the UCR experiments, we have ignored the initial concentrations measured and have derived initial concentrations that correspond to the actual carefully measured amounts of formaldehyde injected into the chamber for each experiment. Two of the UCR experiments, EC-250 and EC-255, ostensibly contained no nitrogen oxides. However, the data indicate low levels of NO_x (<0.02 ppm) and we assumed that the walls were emitting low levels at the constant rate of 8×10^{-5} ppm min^{-1}. This level of NO_x release profoundly changes the ozone produced in these experiments, but such low levels barely affect the more normal experiments when NO_x is added intentionally. Moreover, we feel that, when high levels of NO_x are added to the chamber, some NO_x is probably lost to the walls rather than gained from them. Analysis of and experimentation with various release rates of NO_2 and NO show that the hydroxyl level (as monitored by butane decay) and ozone production could best be simulated by assuming only NO was released. A sensitive test of our assumptions on NO_x release, in addition to parts of the mechanism itself, would have been possible, however, if accurate H_2O_2 data has existed. Very low levels of NO allow HO_2 radicals to build up until the self-

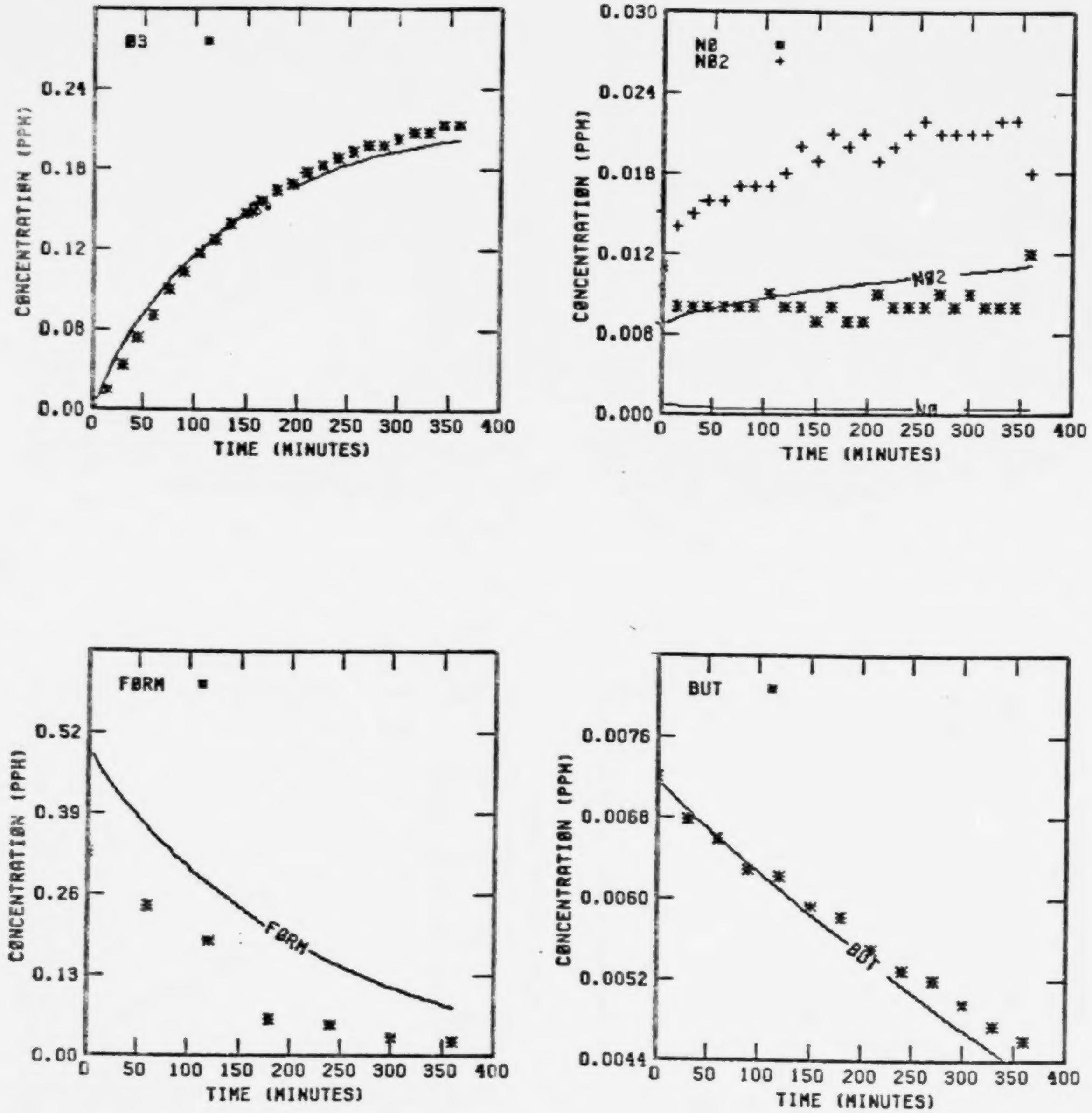

FIGURE 2 . SIMULATION RESULTS FOR
EC-250

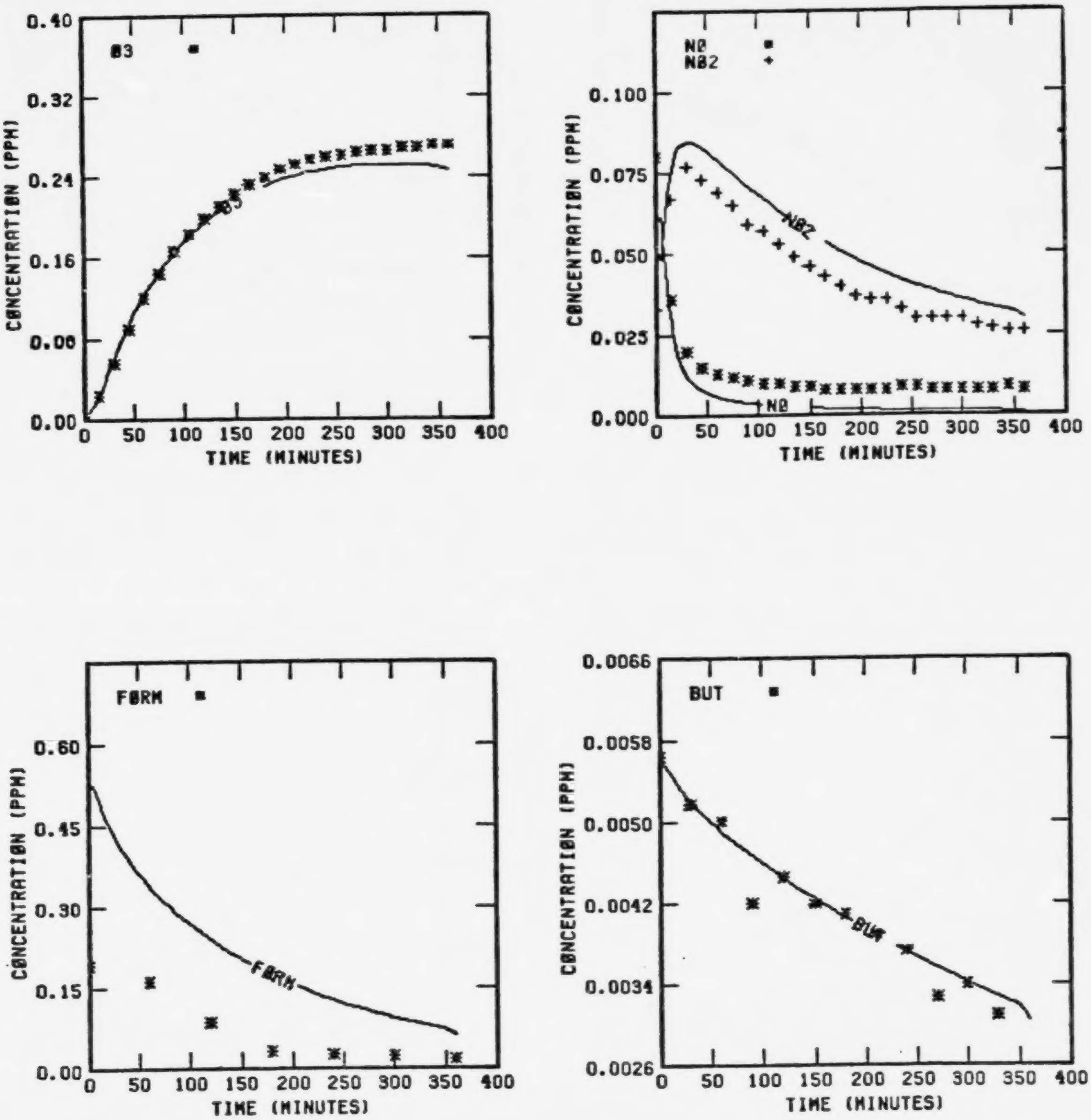

FIGURE 3 . SIMULATIØN RESULTS FØR
EC-251

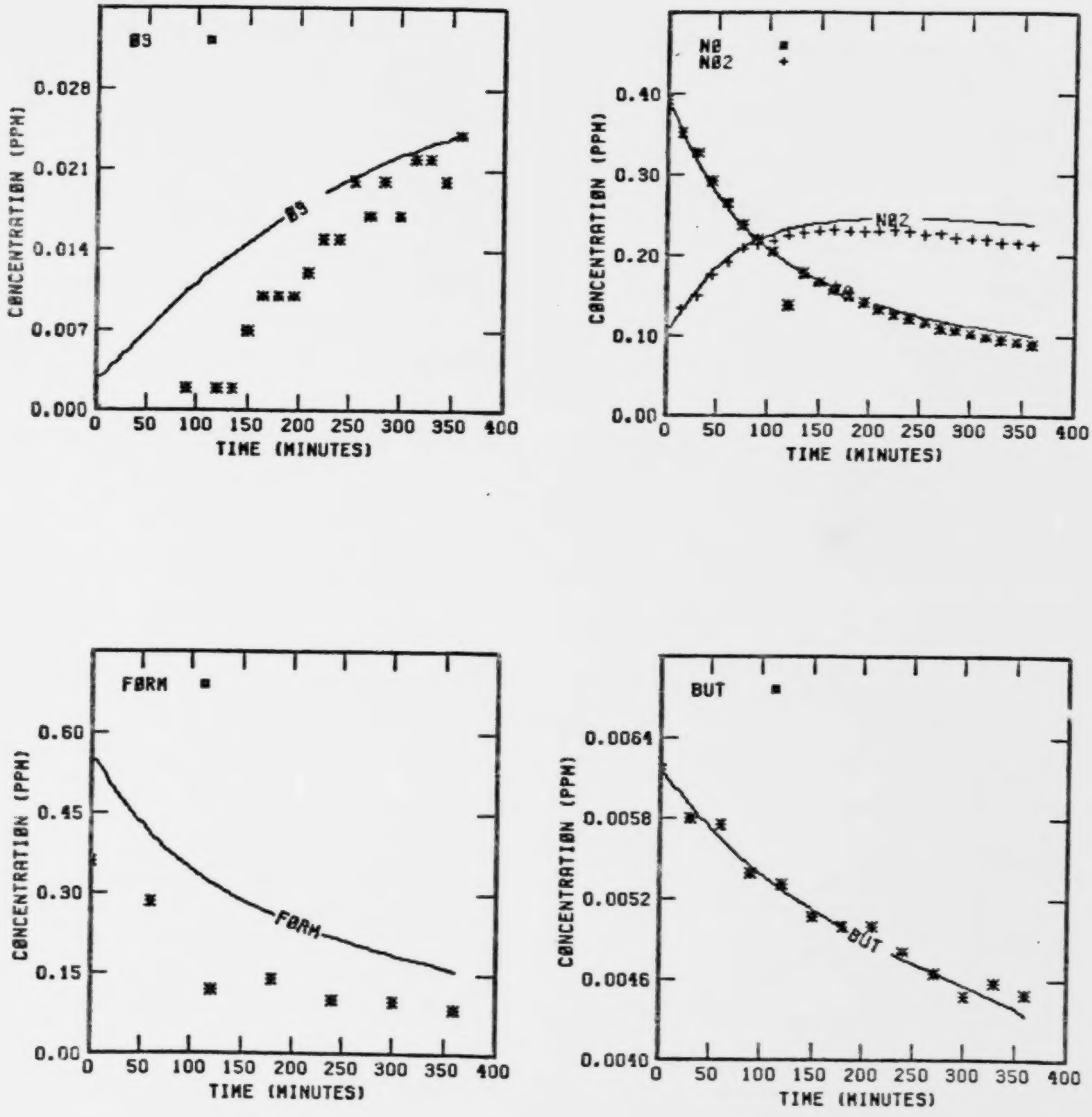

FIGURE 4 . SIMULATION RESULTS FOR
EC-252

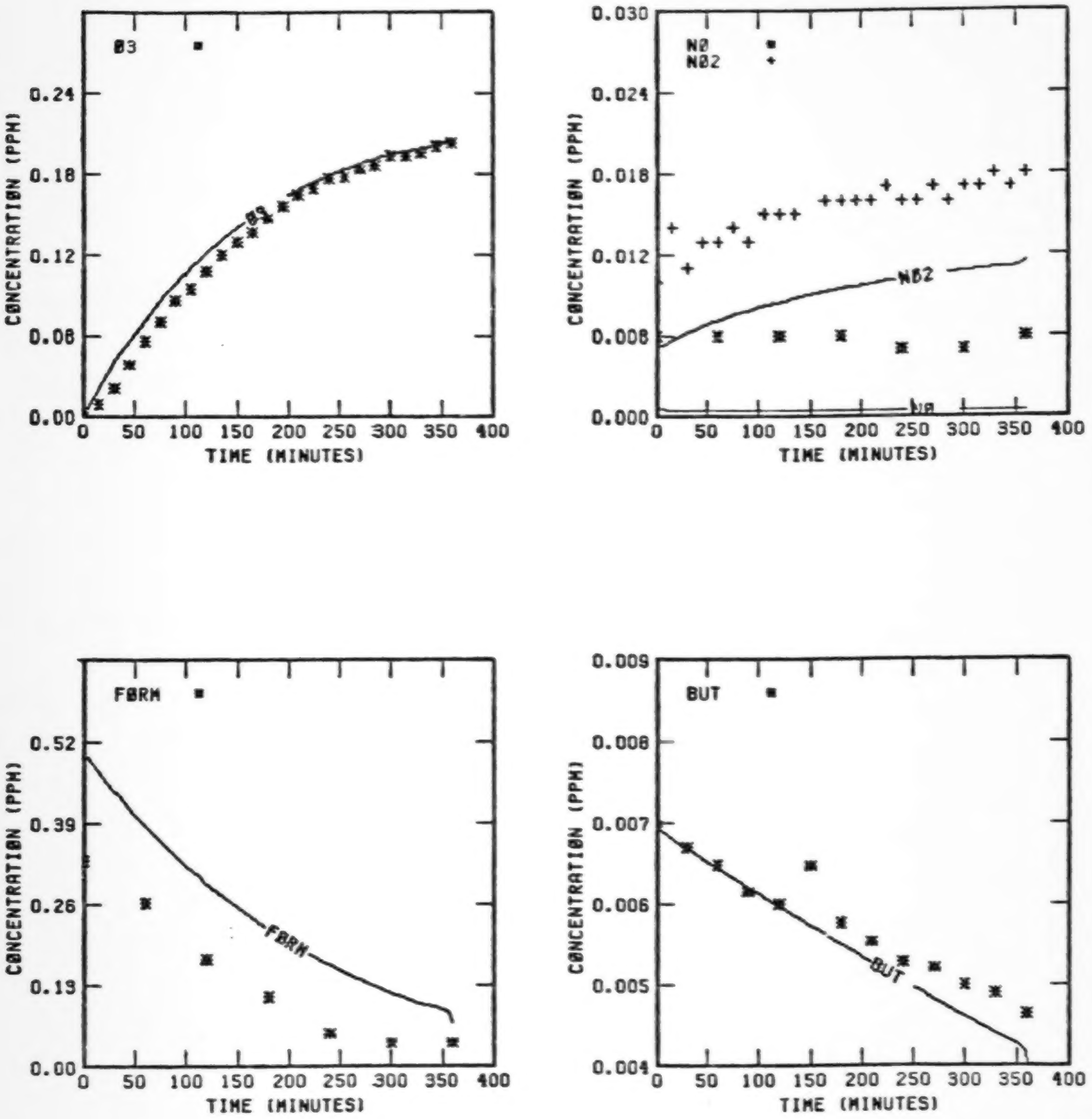

FIGURE 5 . SIMULATIØN RESULTS FØR
EC-255

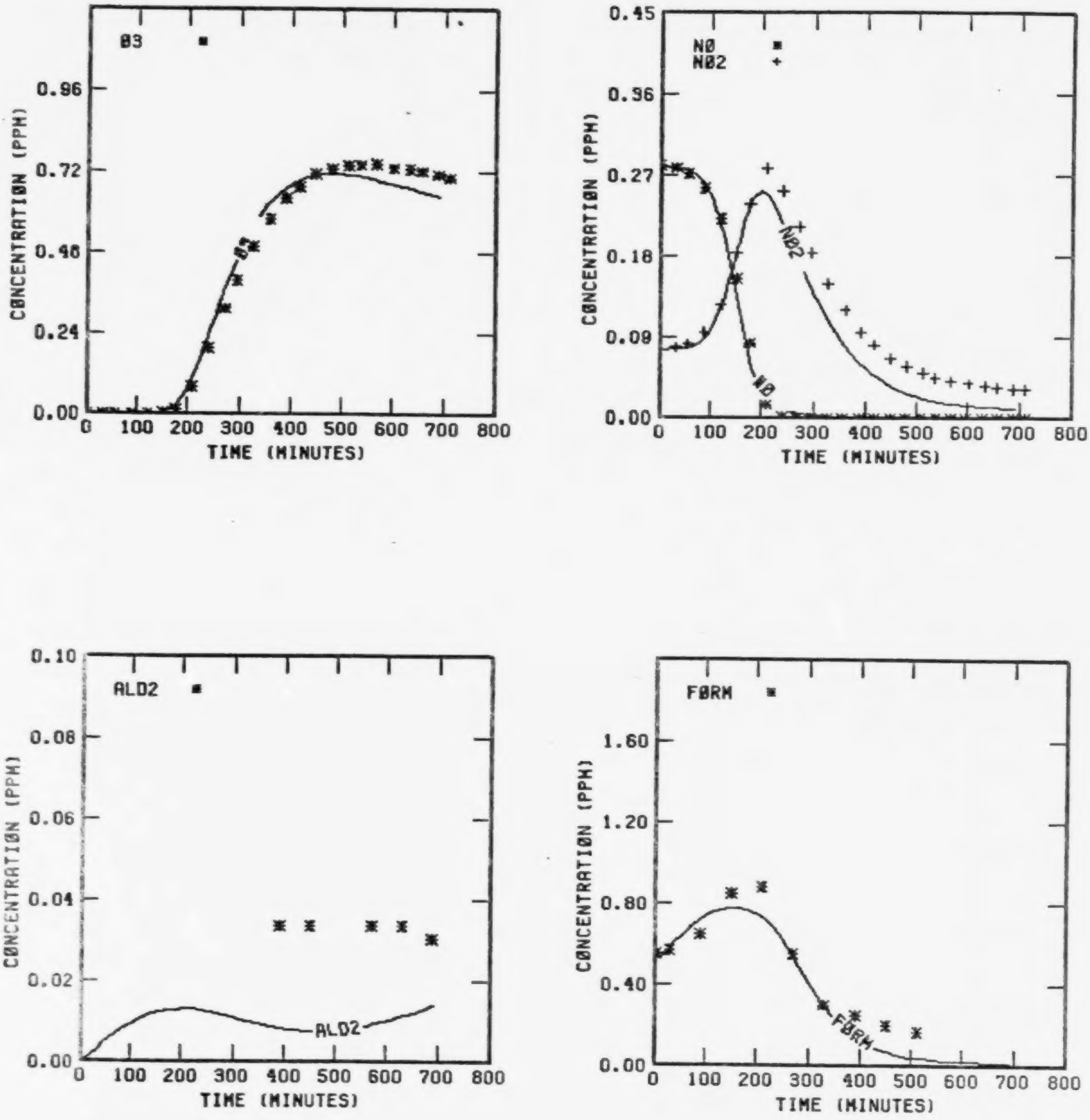

FIGURE 6 . SIMULATION RESULTS FOR
UNCB 51877

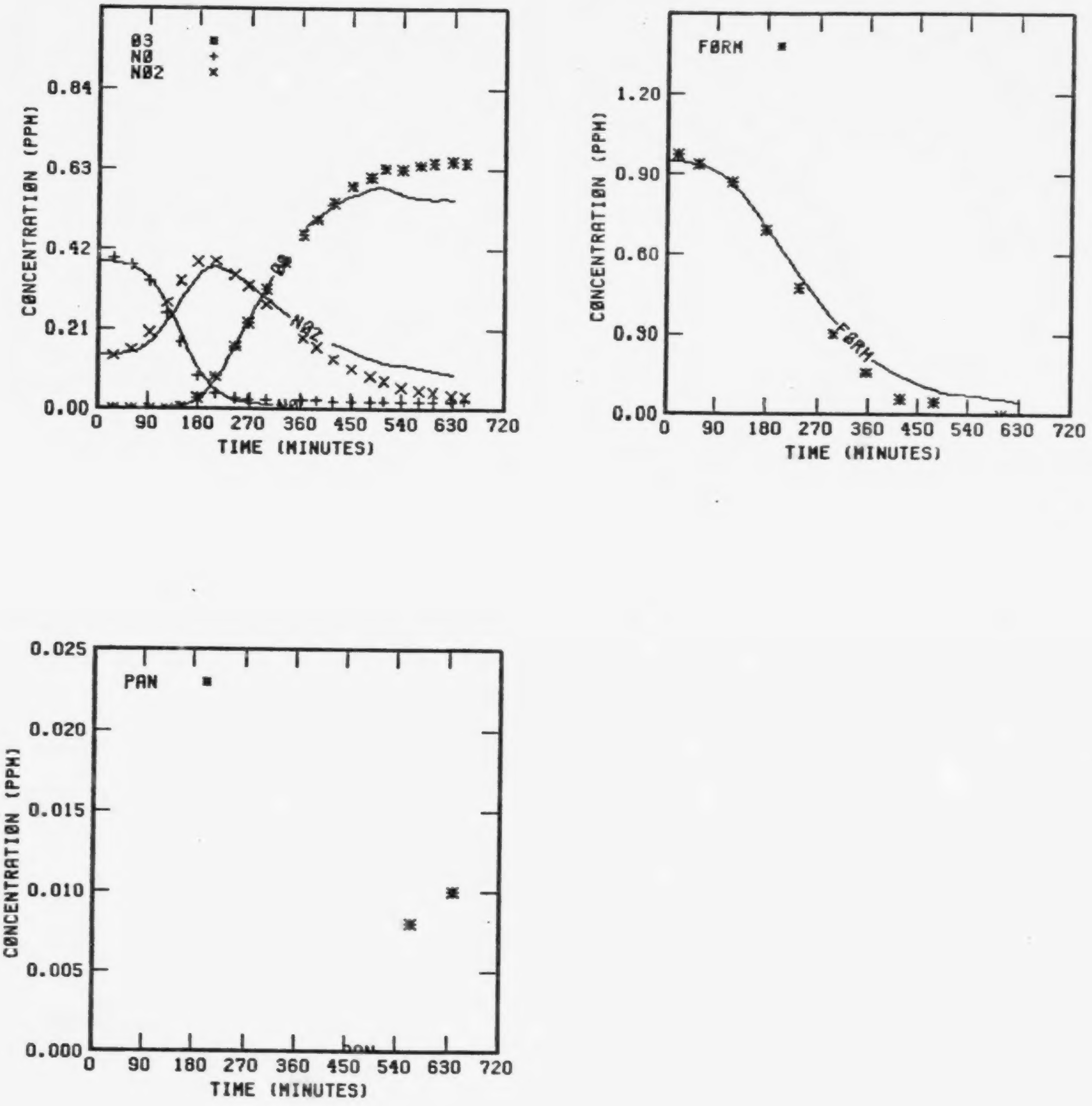

FIGURE 7 . SIMULATI0N RESULTS F0R
UNCR 71877

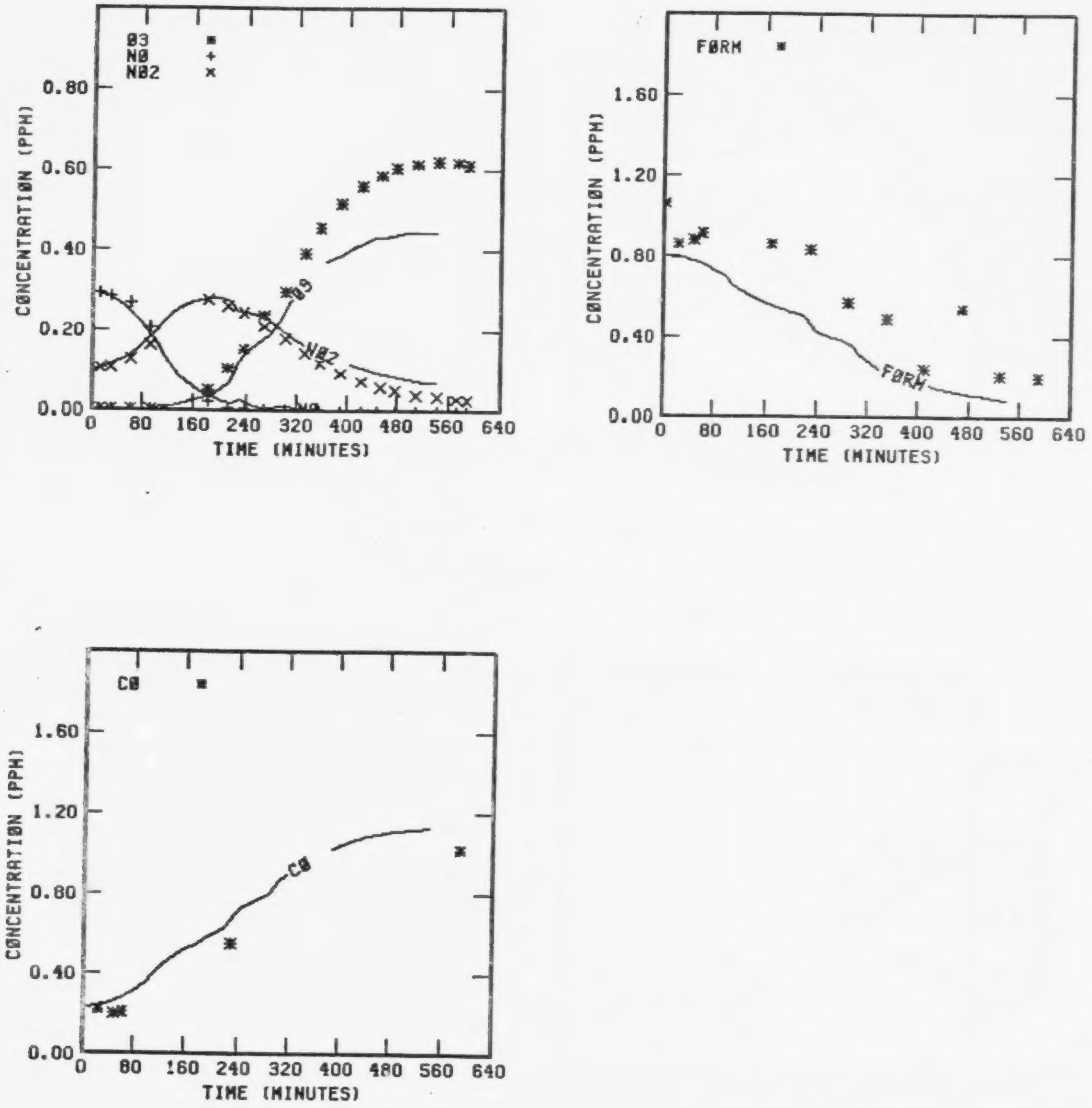

FIGURE 8 . SIMULATION RESULTS FOR
UNCR 91477

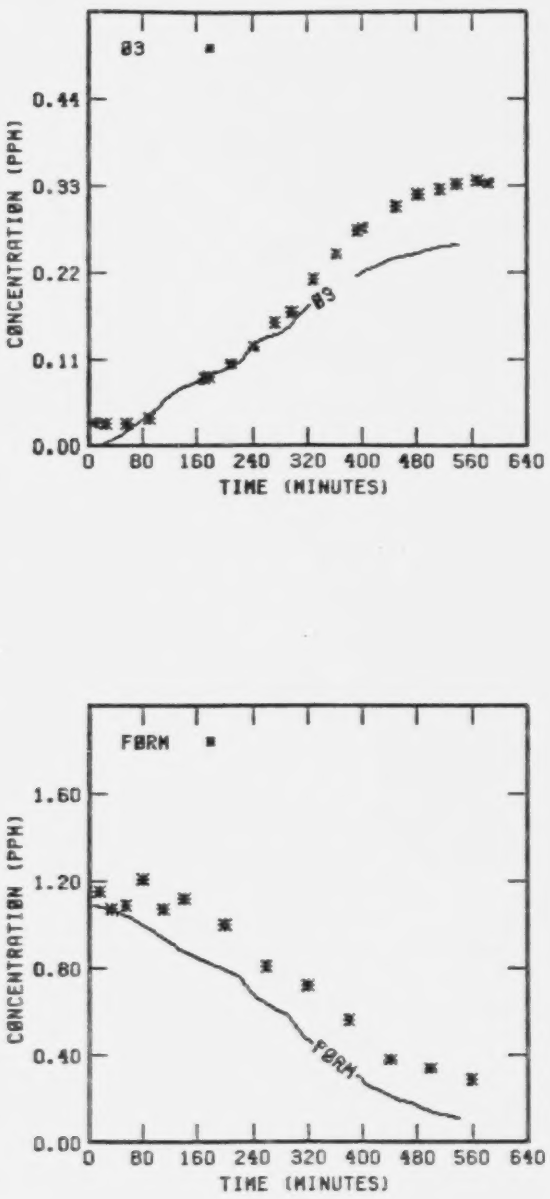

FIGURE 9 . SIMULATIØN RESULTS FØR
UNCB 91477

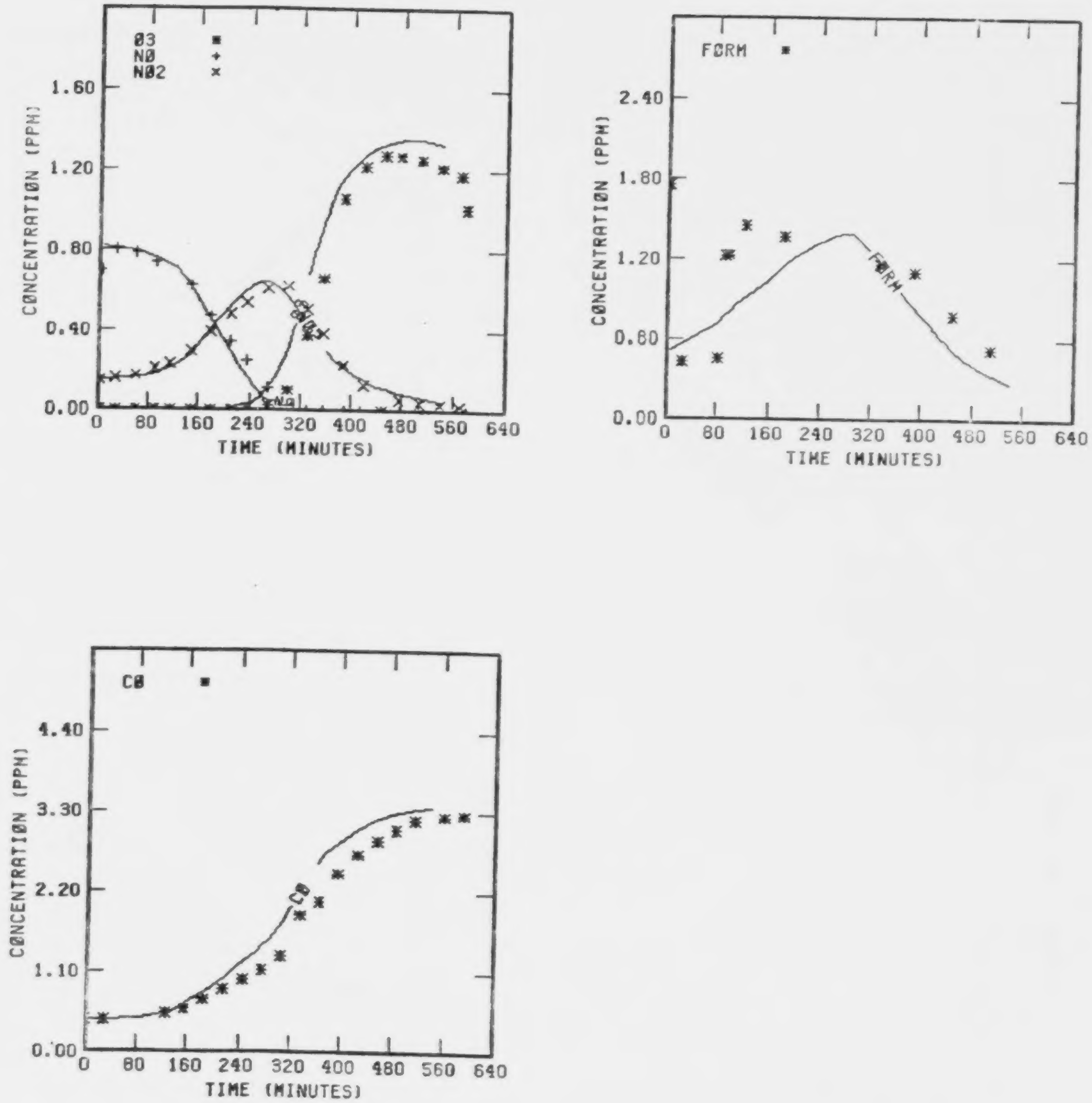

FIGURE 10 . SIMULATION RESULTS FOR
UNCR 90878

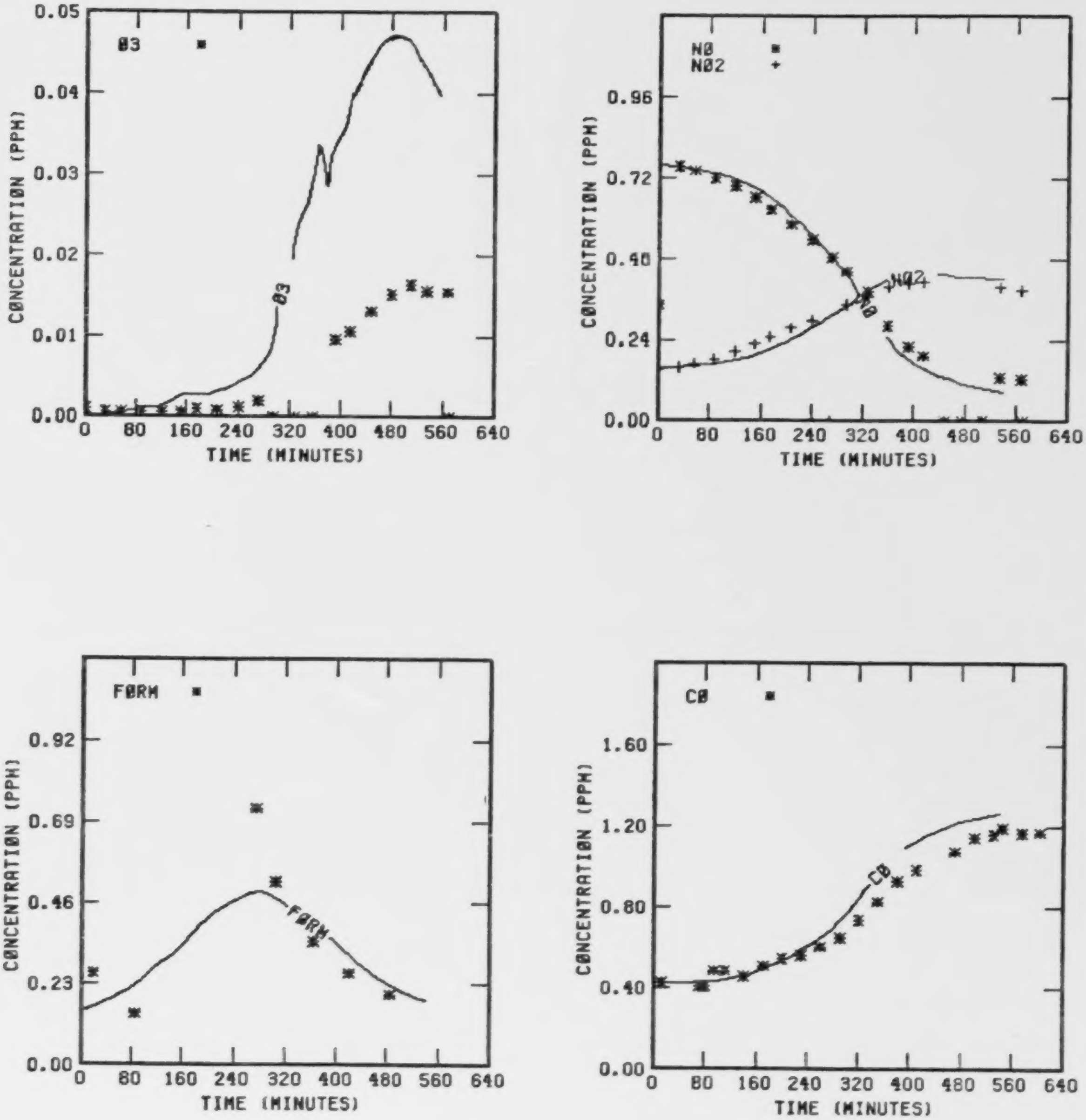

FIGURE 11 . SIMULATION RESULTS FOR
UNCB 90878

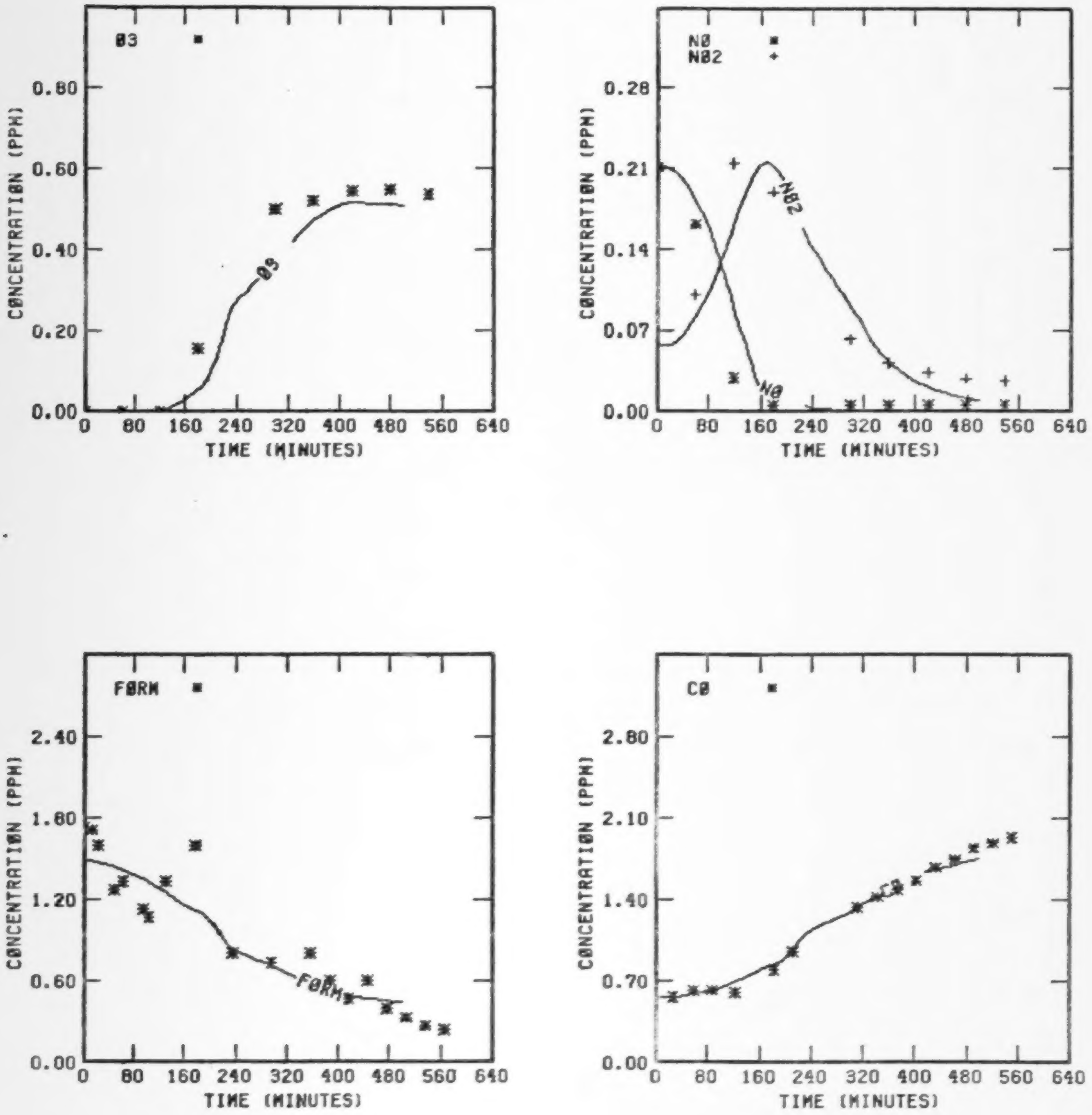

FIGURE 12 . SIMULATIØN RESULTS FØR
UNCB 91578

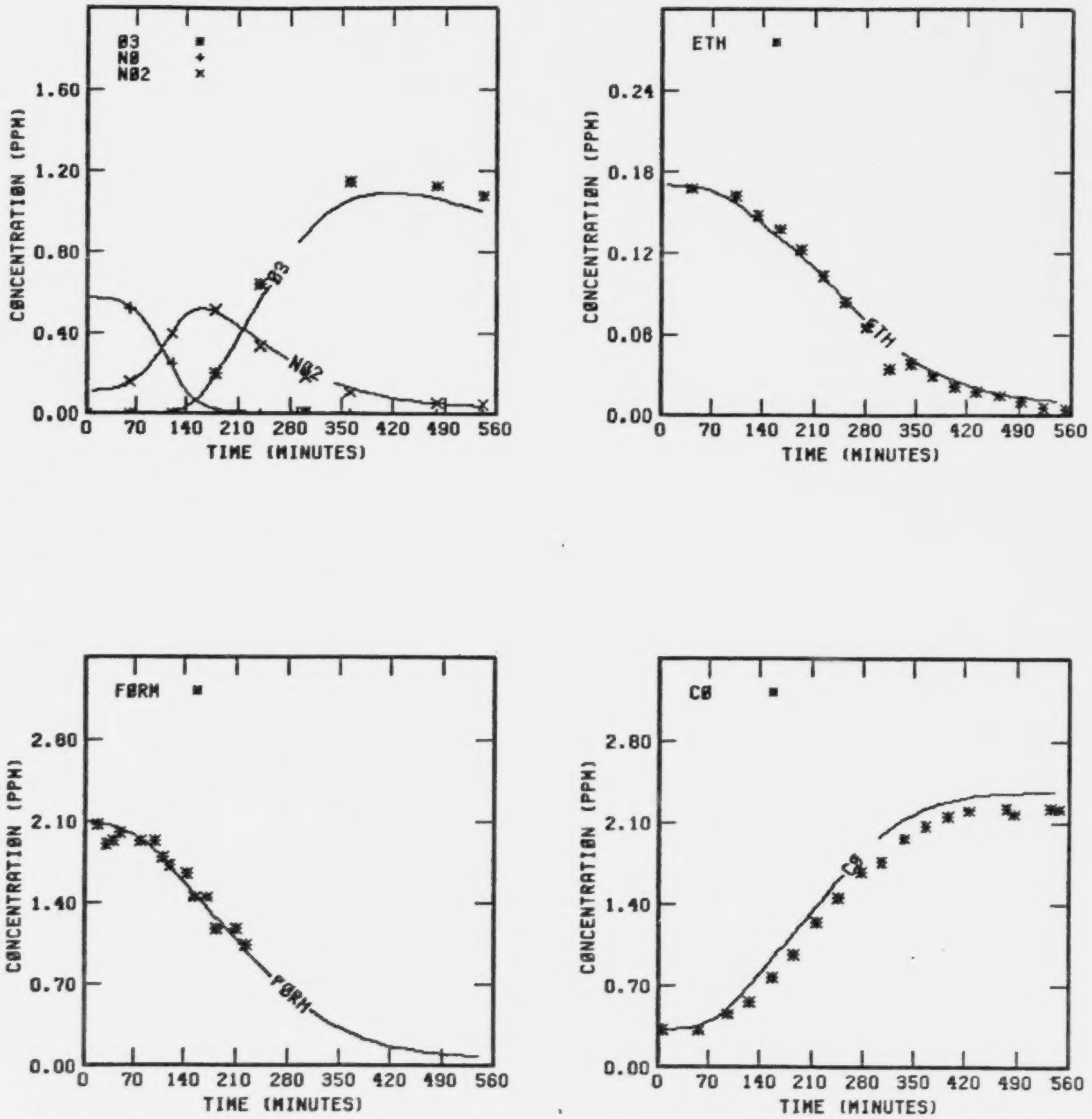

FIGURE 13 . SIMULATION RESULTS FOR
UNCB 91978

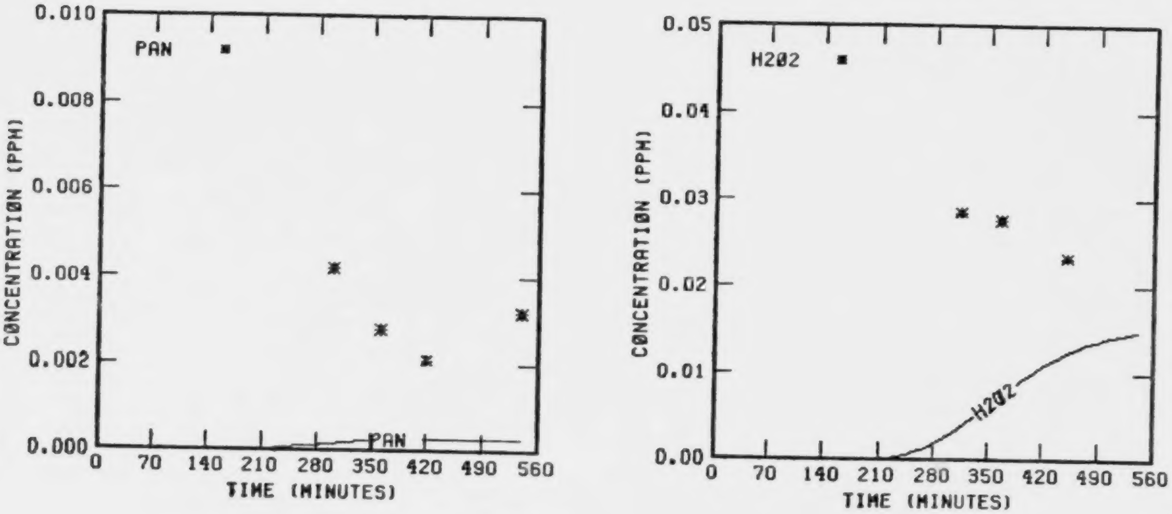

FIGURE 13. (Concluded)

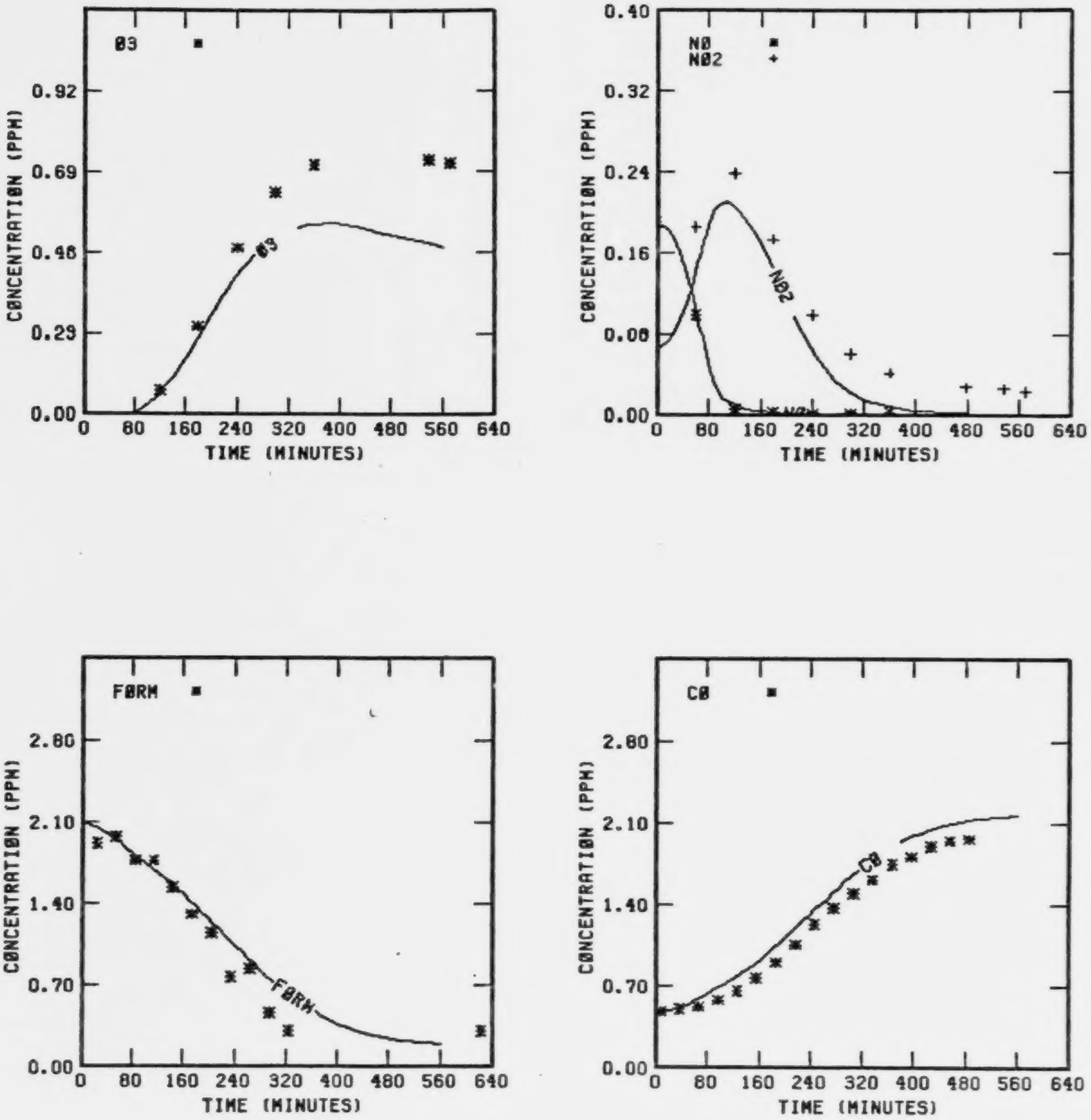

FIGURE 14 . SIMULATION RESULTS FOR
UNCB 92178

TABLE 3. INITIAL CONDITIONS AND PHOTOLYSIS RATE CONSTANTS FOR THE UCR FORMALDEHYDE/NO_x SMOG CHAMBER EXPERIMENTS

Run	Initial concentration (ppm)					Photolysis rate constant (x 10^4 min^{-1})*						
Number	Light Source	HCHO	NO	NO_2	HONO	$NO_2 \rightarrow NO+O$	$O_3 \rightarrow O(^1D)$	$O_3 \rightarrow O(^3P)$	$HONO \rightarrow NO+OH\cdot$	$H_2O_2 \rightarrow 2OH\cdot$	$HCHO \rightarrow H_2+CO$	$HCHO \rightarrow 2HO_2\cdot+CO$
EC-250	Xenon arc	0.50	0.008	0.0	0.0005	0.3	6.9	90	830	5.9	6	6
EC-251	Xenon arc	0.55	0.08	0.033	0.002	0.3	6.9	90	830	5.9	6	6
EC-252	Xenon arc	0.56	0.392	0.103	0.009	0.3	6.9	90	830	5.9	6	6
EC-255	Xenon arc	0.51	0.006	0.00	0.0004	0.3	6.9	90	830	5.9	6	6

* Rate constant in min^{-1} for NO_2.

TABLE 4. INITIAL CONDITIONS AND ALDEHYDE PHOTOLYSIS CONSTANT FOR THE UNC FORMALDEHYDE/NO_x SMOG CHAMBER EXPERIMENTS

				Initial concentrations (ppm)					
Date	Chamber side	Sky conditions	Sunrise	FORM	NO	NO_2	HONO	H_2O	ALD + $h\nu$ constant
5/18/77	Blue	Clear	6:00	1.20	.287	.07	0.0	2×10^4	1.0
7/18/77	Red	Clear	6:08	1.21*	.398	.141	.005	2×10^4	1.0
9/14/77	Red	Variable cloudiness	7:10	1.05	.293	.104	.008	1.6×10^4	1.2
9/14/77	Blue	Variable cloudiness	7:10	1.20	.007	.002	.00022	1.6×10^4	1.2
9/08/78	Red	Variable cloudiness	6:56	3.25	.817	.151	.009	1.6×10^4	1.0§
9/08/78	Blue	Variable cloudiness	6:56	0.90	.761	.155	.022	1.6×10^4	1.0§
9/15/78	Blue	Overcast	6:52	2.0	.211	.057	.008	1×10^4	1.0§
9/19/78	Blue	Clear	7:00	2.0†	.576	.114	.006	1.6×10^4	1.0
9/21/78	Blue	Variable cloudiness	7:06	1.97	.19	.067	.002	1.6×10^4	1.2§

* Ethylene leak into chamber (0.1 ppm assumed initially).

† 0.17 ppm ethylene added initially.

§ UV data are used to calculate the NO_2 photolysis rate constant, instead of TRS.

reaction produces H_2O_2. In such cases, this H_2O_2 production reaction becomes an important radical sink, whereas the hydroxyl attack on NO_2 dominates the sink reactions for most other simulations.

The other two formaldehyde experiments simulated using UCR data were at a moderate NO_x level, 0.1 ppm, and a rather high NO_x level, 0.5 ppm. Both of these experiments are simulated by the current inorganic chemistry (Table 1) combined with the three reactions of formaldehyde (Table 5). The apparent overprediction of ozone in the early part of Experiment EC-252 can be rationalized by the sample tube effect which occurs when NO concentrations are large enough to deplete ozone significantly between the time the sample leaves the ultraviolet light of the chamber and the time it is finally measured.

The nine experiments from the UNC chamber could be simulated with the current chemistry, but the modeling of these experiments is complicated by many factors:

- The lighting under overcast conditions or variable clouds has yet to be satisfactorily determined. The UV data gave better simulations than the TSR data. The data were enhanced by 20 percent in three of the experiments as indicated in Table 4. The last of these three, the experiment performed on 21 September 1978 in the blue side, has UV data, yet the simulation still seems to be low in radicals, as indicated by the inadequate decay of formaldehyde shown in Figure 14.
- Cool temperatures apparently lead to formaldehyde condensation on the walls of the chamber. We have attempted to model this complication by using the following two reactions in all nine experiments at UNC. For each individual experiment we adjusted the ratio of initial formaldehyde on the walls to the initial formaldehyde in the gas phase, in order to reproduce the observed overall experiment:

TABLE 5. REACTIONS OF FORMALDEHYDE AND ACETALDEHYDE*

Reaction	Rate constant ($ppm^{-1}min^{-1}$)
$HCHO + h\nu \rightarrow H_2 + CO$	Experimental†
$HCHO + h\nu \xrightarrow{2O_2} 2HO_2^{\cdot} + CO$	Experimental†
$HCHO + OH\cdot \xrightarrow{O_2} HO_2^{\cdot} + CO + H_2O$	1.4×10^4
$CH_3CHO + h\nu \xrightarrow{2O_2} CH_3O_2^{\cdot} + HO_2^{\cdot} + CO$	Experimental†
$CH_3CHO + OH\cdot \xrightarrow{O_2} CH_3C(O)O_2^{\cdot} + H_2O$	2.4×10^4
$CH_3C(O)O_2^{\cdot} + NO \xrightarrow{O_2} CH_3O_2^{\cdot} + NO_2 + CO_2$	3.8×10^3
$CH_3O_2^{\cdot} + NO \rightarrow CH_3O\cdot + NO_2$	1.2×10^4
$CH_3O\cdot + O_2 \rightarrow HCHO + HO_2^{\cdot}$	1.2
$CH_3C(O)O_2^{\cdot} + HO_2^{\cdot} \rightarrow CH_3C(O)O_2H + O_2$	1.5×10^3
$CH_3O_2^{\cdot} + HO_2^{\cdot} \rightarrow CH_3O_2H + O_2$	1.5×10^3
$CH_3C(O)O_2^{\cdot} + NO_2 \rightarrow CH_3C(O)O_2NO_2$	2×10^3
$CH_3C(O)O_2NO_2 \rightarrow CH_3C(O)O_2^{\cdot} + NO_2$	2.8×10^{-2}†§
$CH_3O\cdot + NO_2 \rightarrow CH_3ONO_2$	1.5×10^4
$CH_3O\cdot + NO_2 \rightarrow HCHO + HONO$	4.4×10^3
$CH_3O_2^{\cdot} + O_3 \rightarrow CH_3O\cdot + 2O_2$	4×10

* The first three reactions in this table and the inorganic reactions listed earlier constitute the explicit formaldehyde mechanism. The reactions in this table and the inorganic reactions listed earlier constitute the explicit acetaldehyde mechanism.

† Rate constant in min^{-1}.

§ Activation energy is 12,500K; rate constant is given at 298K.

$$HCHO \rightarrow HCHO\ (wall) \quad k=(7.9 \times 10^{-25})\ \exp(14000/T)\ \min^{-1}$$
$$HCHO\ (wall) \rightarrow HCHO \quad k=(7.02 \times 10^{26})\ \exp(-20000/T)\ \min^{-1}$$

- Butane was not added to the UNC experiments but CO data was often available. A small quantity of ethylene was present in the experiment of 19 September 1978, on the blue side, which was useful for monitoring the hydroxyl level. The success of the current mechanism for monitoring CO seems to indicate that the peroxyformyl radical, HCO_3, is probably not important since CO_2 would be expected from the reaction of this radical with NO.

In future experiments with formaldehyde we recommend the following:

- Dual UV data at 320 nm and at 390 nm so that the ratio of formaldehyde photolysis to NO_2 photolysis can be determined.
- Addition of trace levels of butane to monitor hydroxyl levels.
- Characterization of the temperature and humidity effects associated with the problem of formaldehyde condensation on, or evaporation from, the chamber walls.
- Improved formaldehyde data.

All of these recommendations are currently being considered at UNC. In summary, we are encouraged by the ability of the present chemistry to predict the drastic range of reactivity shown in the dual chamber experiment of 8 September 1978. Both sides of the smog chamber had essentially equal loadings of NO_x near 1 ppm, yet the side with over 3 ppm of formaldehyde showed an ozone level near 1.3 ppm while the side with about 1 ppm of formaldehyde showed an ozone peak less than 0.05 ppm. As discussed previously, the low ozone observed in the low formaldehyde side is partially due to titration of O_3 by NO in the sample tube. Tables 6 and 7 present a summary of the results for the formaldehyde simulations.

TABLE 6. UCR FORMALDEHYDE EXPERIMENTS--SIMULATIONS AND MEASUREMENTS

Exp. no.	Initial $[NO_x]$ (ppm)	Initial NO_2/NO_x ratio	Initial HC/NO_x ratio (ppmC/ppm)	Maximum $[O_3]$ (ppm)*		Difference in O_3 maxima (percent)†	Time to maximum $[O_3]$ (minutes)§		Difference in times to O_3 maxima (percent)†	Maximum $[NO_2]$ (ppm)		Difference in NO_2 maxima (percent)†	Time to maximum $[NO_2]$ (minutes)§		Difference in times to NO_2 maxima (percent)†
				Sim.	Meas.		Sim.	Meas.		Sim.	Meas.		Sim.	Meas.	
EC-250	0.008	0.0	62.5	0.20	0.204	-2	>360	>360	--	0.011	0.021	-49	>360	>360	--
EC-251	0.11	0.29	4.9	0.248	0.264	-6	220	220	0	0.084	0.077	9	30	30	0
EC-252	0.495	0.21	1.1	0.023	0.020	14	>360	>360	--	0.243	0.22	9.1	100	100	0
EC-255	0.006	0.0	85.0	0.198	0.198	0	>360	>360	--	0.011	0.017	-37	>360	>360	--

O_3 maxima: average difference = 2 percent; standard deviation = ±9 percent.

NO_2 maxima: average difference = -17 percent; standard deviation = ±30 percent.

* Maximum one-hour-average concentration.

† [(Simulated Value - Measured Value) ÷ Measured Value] x 100.

§ Time from beginning of irradiation to beginning of the period during which the maximum one-hour-average concentration occurred.

TABLE 7. UNC FORMALDEHYDE EXPERIMENTS--SIMULATIONS AND MEASUREMENTS

Date	Chamber side	Initial $[NO_x]$ (ppm)	Initial NO_2/NO_x ratio	Initial HC/NO_x (ppmC/ppm)	Maximum $[O_3]$ (ppm)*		Difference in O_3 maxima (percent)	Time to maximum $[O_3]$ (minutes)		Difference in times to O_3 maxima (percent)	Maximum $[NO_2]$ (ppm)		Difference in $[NO_2]$ maximum (percent)	Time to maximum $[NO_2]$ (min)		Difference in times NO_2 maxima (percent)
					Sim.	Meas.		Sim.	Meas.		Sim.	Meas.		Sim.	Meas.	
5/18/77	Blue	.351	.20	3.36	.71	.74	-4	400	450	-11	.25	.28	-11	200	225	-11
7/18/77	Red	.539	.26	2.24	.56	.63	-11	420	450	-7	.38	.4	-5	190	180	6
9/14/77	Red	.397	.26	2.64	.44	.60	-27	-	-	0	.28	.28	0	170	170	0
9/14/77	Blue	.009	.22	133.3	.253	.33	-23	480	480	0	.008	.01	-20	>560	>560	-
9/08/78	Red	.968	.15	3.36	1.32	1.26	5	400	400	0	.64	.64	0	260	280	7
9/08/78	Blue	.916	.16	0.98	.045	.015	200	>560	480	-	.39	.42	-7	420	180	6
9/15/78	Blue	.268	.21	7.46	.50	.54	-7	280	370	-24	.21	.21	0	180	120	33
9/19/78	Blue	.690	.17	3.15	1.08	1.12	-4	320	320	0	.52	.52	0	160	160	0
9/21/78	Blue	.257	.26	7.67	.53	.69	-23	250	330	-24	.208	.24	-13	120	120	0

* O_3 average = -12 percent, Standard deviation = 11.4 percent.

NO_2 average = -6 percent, Standard deviation = 7.7 percent.

† O_3 and NO_2 averages do not include runs performed on 9/08/78.

ACETALDEHYDE

The chemistry of acetaldehyde (Table 5) has not changed significantly within the last year except for the photolysis reaction of acetaldehyde itself. Once the formaldehyde photolysis reactions and chemistry were established for the UNC experiments, it was apparent that experiments with NO_x and pure acetaldehyde needed less radicals than our former mechanism had predicted. Surprisingly, we found that using the lower limit quantum yields recommended by Dermerjian, Schere, and Peterson (1979) provided ratios of acetaldehyde photolysis to NO_2 photolysis, which produced good simulations of the UNC experiments. As shown in Table 2, the new values are about 15 percent of the formaldehyde photolysis rate constant which produces radicals. Last year we had used a value of 50 percent which was based on a general impression from several UCR experiments. One important exception to the use of the higher acetaldehyde photolysis had been UCR experiment EC-217, a mixture of propylene and acetaldehyde with NO_x. For the results presented in the interim report (Whitten et al., 1979), we had arbitrarily varied the photolysis rates for each experiment to optimize each simulation, keeping the constants for formaldehyde to acetaldehyde radical producing photolysis fixed at a 2:1 ratio. In general, we tried to keep the range of adjustment within the range of observed fluctuations in the spectra reported. We also attempted to keep similar photolysis constants for a series of consecutive experiments. However, EC-216 and EC-217 seemed to require an "adjustment" of nearly a 40 percent reduction for EC-217 compared with EC-216. With the lower acetaldehyde photolysis, both of these experiments can be simulated with identical photolysis constants.

The two acetaldehyde experiments presented in this report from UCR data are shown in Figures 15 and 16. The initial conditions and results are given in Tables 8 and 9. Aldehyde photolysis rate constants are presented as HCHO → Radicals. The experiment without NO_x intentionally added, EC-253, illustrates a sensitive method to measure NO_x release from the chamber walls. During the experiment, PAN built up to 40 ppb in six hours, yet NO_2 and NO remained below the detection limit of 10 ppb. Most NO_x leaving the chamber walls is evidently held in the gas phase as PAN, which can be readily monitored with the PAN analyzer. Without acetaldehyde as the dominant organic species, the NO_x would typically be converted to HNO_3, a species which is not only

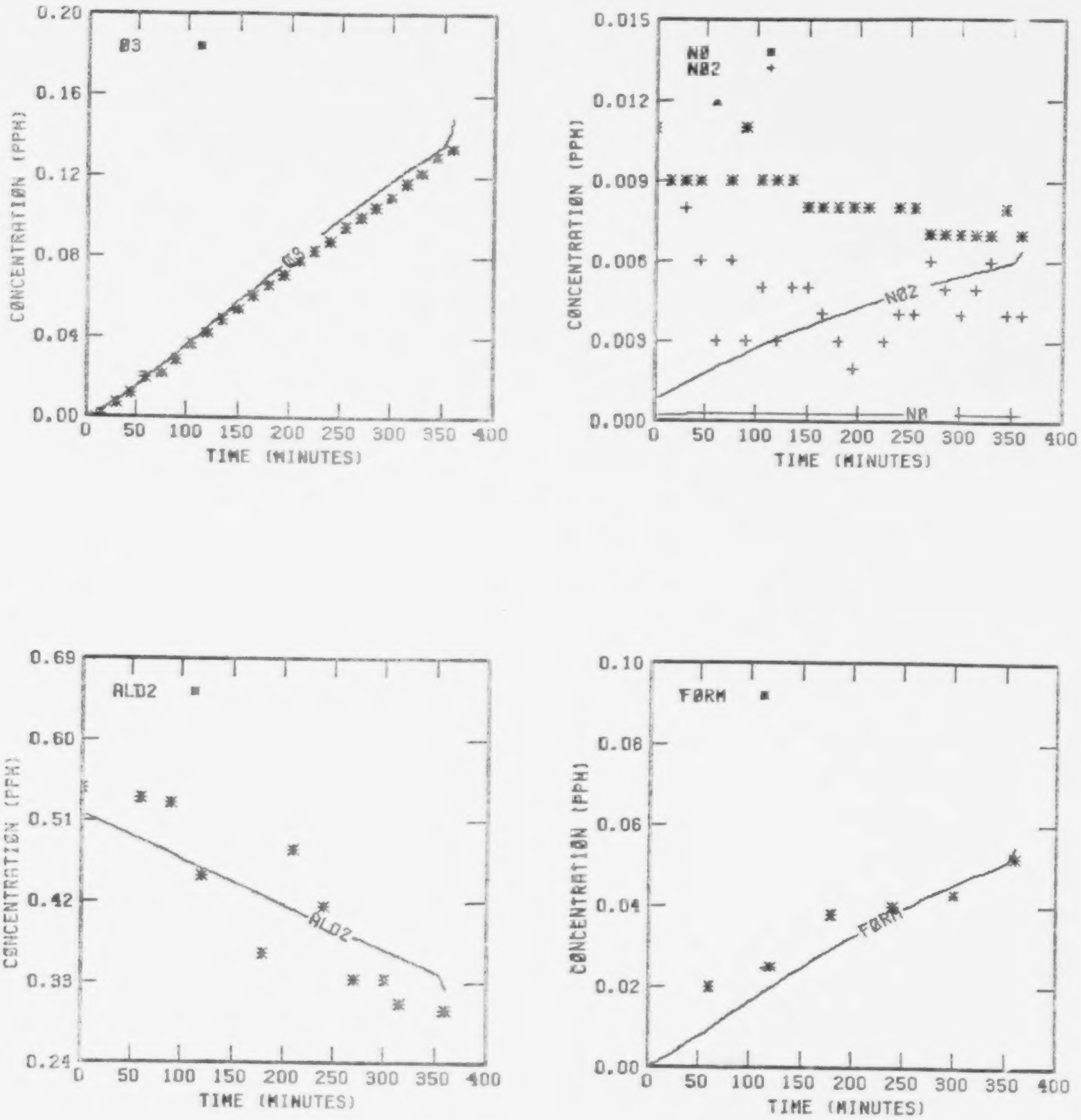

FIGURE 15. SIMULATION RESULTS FOR EC-253

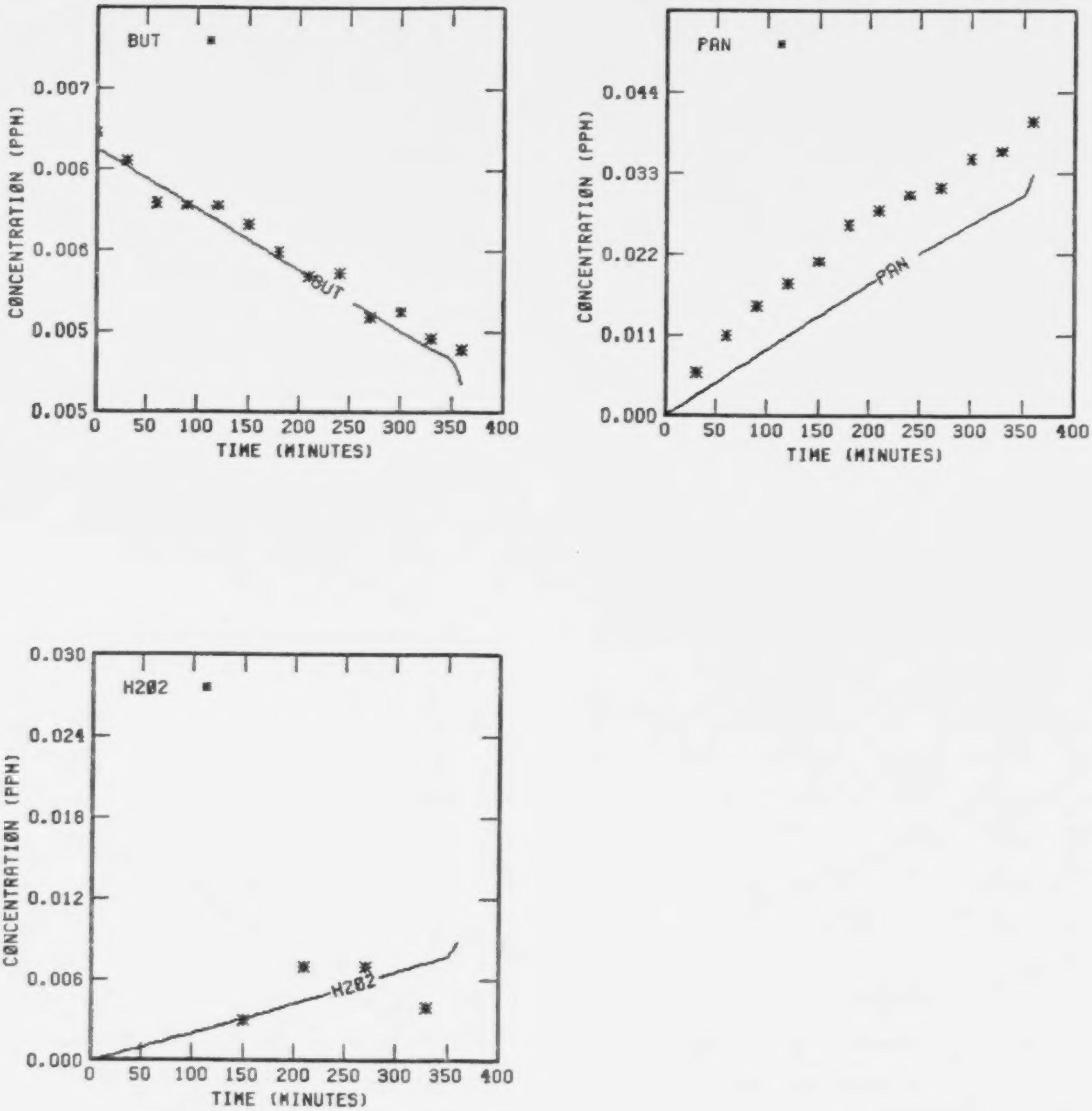

FIGURE 15 . (Concluded)

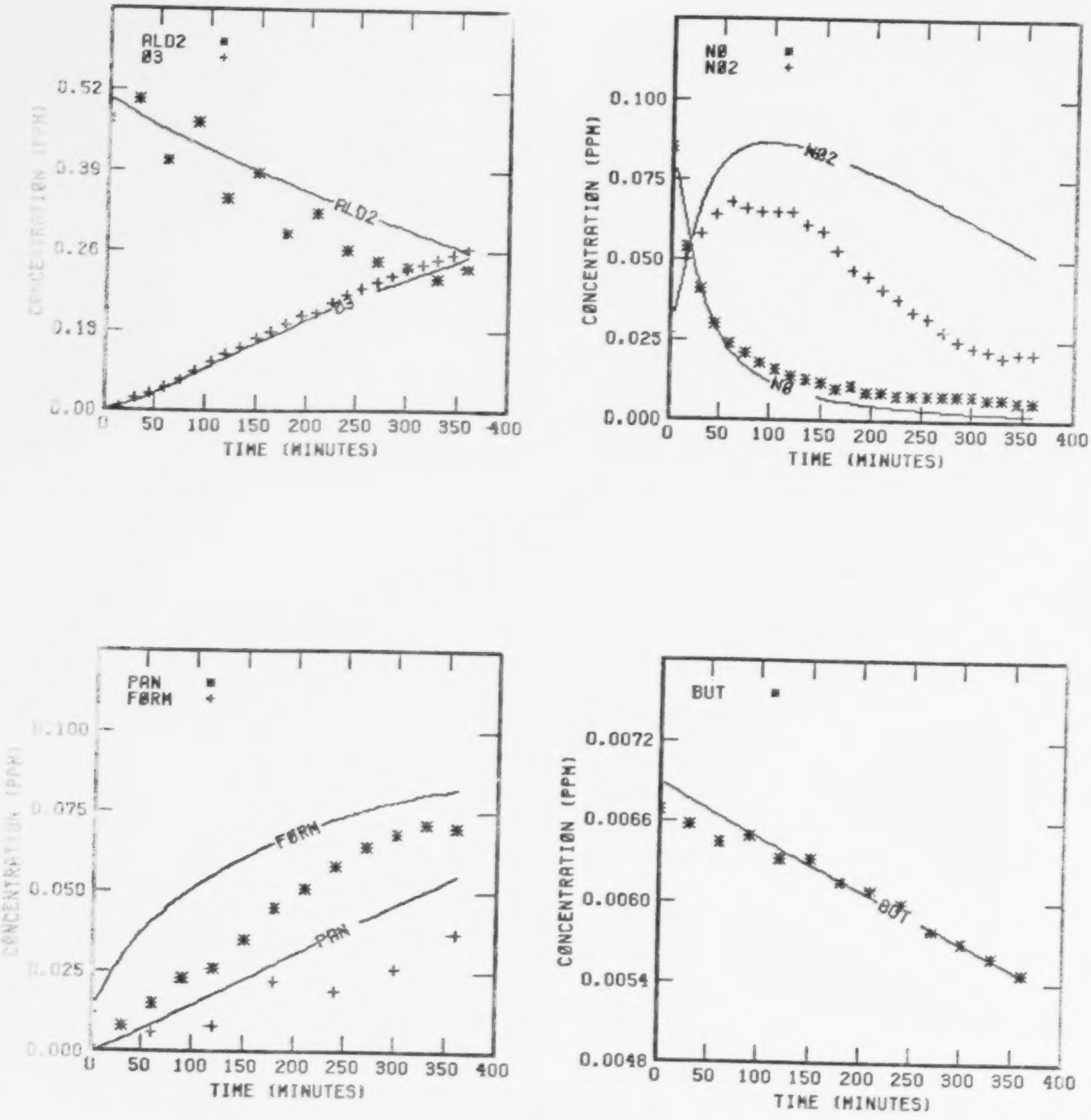

FIGURE 16 . SIMULATION RESULTS FOR
EC-254

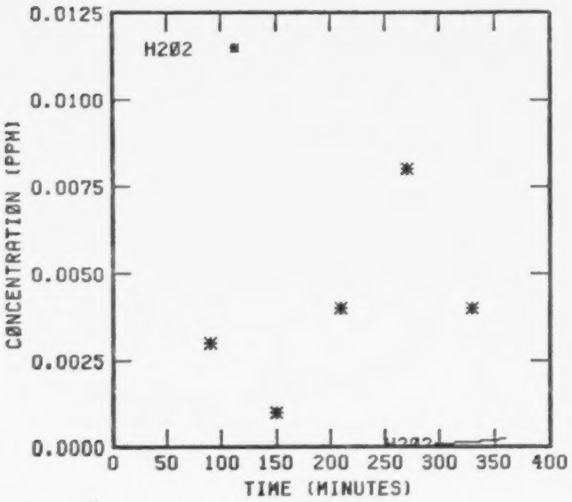

FIGURE 16 . (Concluded)

TABLE 8. INITIAL CONDITIONS AND PHOTOLYSIS RATE CONSTANTS FOR UCR ACETALDEHYDE/NO_x SMOG CHAMBER EXPERIMENTS

Run number	Initial concentration (ppm)				Photolysis rate constant (x 10^4 min^{-1})*†					
	Acetaldehyde	NO	NO_2	HONO	NO_2→NO+O	O_3→O(^{1}D)	O_3→O(^{3}P)	HONO→NO+OH·	H_2O_2→2OH·	FORM→Products
EC-253	.517	0.001	0.0	0.0	0.30	6.9	90	830	5.9	8
EC-254	.508	0.085	0.027	0.0	0.30	6.9	90	830	5.9	8

* Rate constant in min^{-1} for NO_2.

† The relationship between FORM→Products and carbony photolysis rate constants is discussed in Section 4.

TABLE 9. UCR ACETALDEHYDE EXPERIMENTS-SIMULATIONS AND MEASUREMENTS

Exp. no.	Initial [NO_x] (ppm)	Initial NO_2/NO_x ratio	Initial HC/NO_x ratio (ppmC/ppm)	Maximum [O_3] (ppm)*		Difference in O_3 maxima (percent)†	Time to maximum [O_3] (minutes)‡		Difference in times to O_3 maxima (percent)†	Maximum [NO_2] (ppm)		Difference in NO_2 maxima (percent)†	Time to maximum [NO_2] (minutes)‡		Difference in times to NO_2 maxima (percent)†
				Sim.	Meas.		Sim.	Meas.		Sim.	Meas.		Sim.	Meas.	
EC-253	0.0	0.0	--	0.13	0.124	5	>360	>360	--	0.006	0.009	-37	>360	30	--
EC-254	0.11	0.24	9.2	0.234	0.24	-3	>360	>360	--	0.085	0.064	33	60	60	0

O_3 maxima: average difference = 1 percent; standard deviation = ±6 percent.

NO_2 maxima: average difference = -2 percent; standard deviation = ±49 percent.

* Maximum one-hour-average concentration.

† [(Simulated Value - Measured Value) ÷ Measured Value] x 100.

‡ Time from beginning of irradiation to beginning of the period during which the maximum one-hour-average concentration occurred.

difficult to measure but also is subject to absorption by the walls. The NO_x "off gassing" from the walls was modeled for experiment EC-253 by a simple zero-order reaction producing NO at the rate of 1.0×10^{-4} ppm min^{-1}.

Twelve acetaldehyde experiments were simulated for the UNC chamber. Tables 10 and 11 present the tabulated initial conditions and results while Figures 17 through 28 show the results graphically. The NO_2 data are not corrected for PAN because the PAN data were not always available and when the data were available, before February 1978, the PAN calibration was about 40 percent too high. As with the formaldehyde experiments, on overcast days or under partial cloud cover, the photolysis constants are poorly represented. However, more developmental work is needed on both the acetaldehyde and propylene mechanisms to account for temperature effects. This is demonstrated by the dual run performed on 26 December 1977 (see Figures 21 and 76). The blue side simulation for acetaldehyde shows too many radicals yet the red side simulation for propylene appears to be well simulated.

ETHYLENE

The ethylene chemistry itself is essentially unchanged from the mechanism reported last year (Whitten et al., 1979). The reaction of the hydroxyethylperoxy radical with ozone was eliminated and the rate constant for the reaction of the Criegee intermediate with NO_2 was lowered to 3000 $ppm^{-1}min^{-1}$. Both changes are analogous to reactions changed in the propylene mechanism discussed later. The new inorganic and formaldehyde chemistry is central to the overall chemistry of experiments involving ethylene. During this past year, we have simulated 22 experiments from the UNC chamber. Without the UV data for photolysis constants and without the temperature dependent PNA and formaldehyde-wall reactions, the simulations for this series of UNC were very poor. However, these modifications have considerably improved the agreement between observation data and the computer simulations. Table 12 shows the present ethylene mechanism. Tables 13 and 14 present the initial conditions and results for the 22 experiments while Figures 29 through 50 show the time-dependent results. The most sensitive uncertainties

TABLE 10. INITIAL CONDITIONS AND ALDEHYDE PHOTOLYSIS CONSTANTS FOR THE UNC ACETALDEHYDE SMOG CHAMBER EXPERIMENTS

Date	Chamber Side	Sky Conditions	Beginning Time of Simulation	Initial Concentrations (ppm)					Ald + hν Constant
				Acetaldehyde	NO	NO_2	HONO	H_2O	
5/18/77	Red	Clear	6:00	0.94	.287	.072	.001	2×10^4	1.0
7/18/77	Blue	Clear	6:08	0.49	.394	.141	.023	2×10^4	1.0
11/12/77	Blue	Overcast	7:44	0.86	.358	.113	0.	3×10^3	1.1
11/20/77	Blue	Clear	7:30	1.96	.837	.044	.002	6×10^3	1.0
12/26/77	Blue	Clear	8:08	1.91	.290	.117	0.	4×10^3	1.0
2/27/78	Blue	Clear	8:00	0.95	.268	.086	0.	4×10^3	1.0
3/06/78	Blue	Overcast in morning	7:36	0.90	.291	.083	.004	1.4×10^4	1.1
3/31/78	Blue	Overcast	6:48	1.00	.327	.066	.004	2×10^4	1.1
8/08/78	Red	Overcast	6:20	0.46	.421	.095	.020	2.4×10^4	1.0*
8/08/78	Blue	Overcast	6:20	2.00	.424	.103	.012	2.4×10^4	1.0*
10/13/78	Red	Overcast	7:13	0.46	.378	.115	.004	1.6×10^4	1.0*
10/13/78	Blue	Overcast	7:13	1.01	.770	.136	.005	1.6×10^4	1.0*

* UV data was used for the calculation of the NO_2 photolysis rate constant, instead of TSR.

TABLE 11. UNC ACETALDEHYDE EXPERIMENTS--SIMULATIONS AND MEASUREMENTS*

Date	Chamber side	Initial $[NO_x]$ (ppm)	Initial NO_2/NO_x Ratio	Initial HC/NO_x (ppmc/ppm)	Maximum $[O_3]$ (ppm)†		Difference in O_3 maxima § (percent)	Time to maximum $[O_3]$ (minutes)		Difference in time to O_3 maxima (percent)
					Sim.	Meas.		Sim.	Meas.	
5/18/77	Red	.359	.20	5.24	.89	.93	-4	500	500	0
7/18/77	Blue	.535	.26	1.83	.45	.64	-30	>630	>630	-
11/12/77	Blue	.471	.24	3.65	.092	.025	268	330	360	-8
11/20/77	Blue	.881	.05	4.45	.086	.056	54	450	450	0
12/26/77	Blue	.407	.29	9.39	.16	.036	344	300	420	-29
2/27/78	Blue	.354	.24	5.37	.23	.14	-61	480	520	-8
3/06/78	Blue	.374	.22	4.81	.28	.25	10	540	540	0
3/31/78	Blue	.393	.17	5.09	.48	.45	8	>600	>600	-
8/08/78	Red	.516	.18	1.78	.38	.48	-21	560	>640	-
8/08/78	Blue	.527	.20	7.59	1.16	1.08	7	440	440	0
10/13/78	Red	.493	.23	1.87	.051	.075	-32	400	450	-11
10/13/78	Blue	.906	.15	2.23	.11	.14	-21	480	480	0

* NO_2 maxima were not tabulated because the reported NO_2 data contain PAN and other nitrates.

† O_3 average = -9, Standard deviation = 31 percent.

§ O_3 and NO_2 averages do not include runs performed on 11/12/77 and 12/26/77.

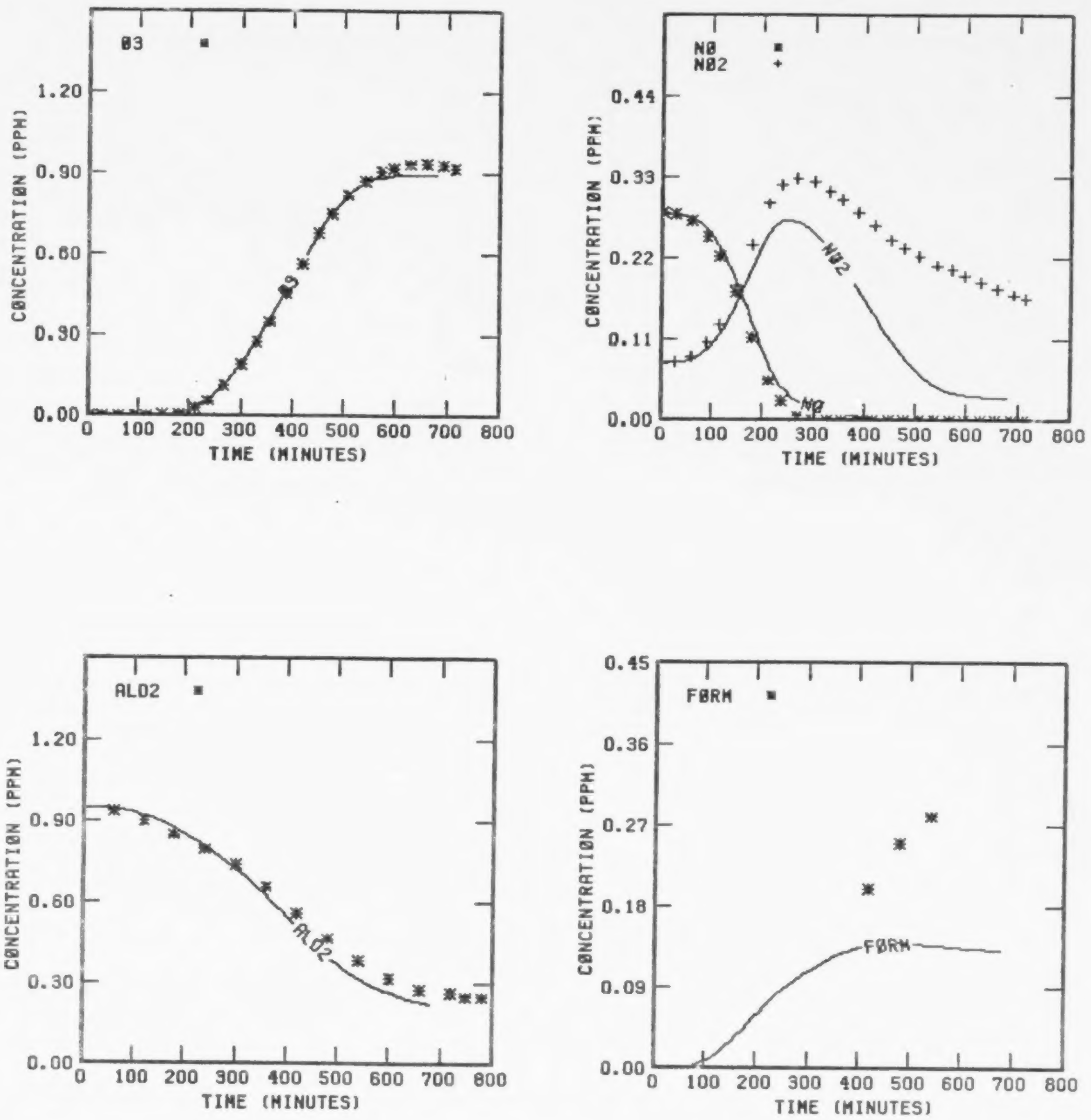

FIGURE 17 . SIMULATION RESULTS FOR
UNCR 51877

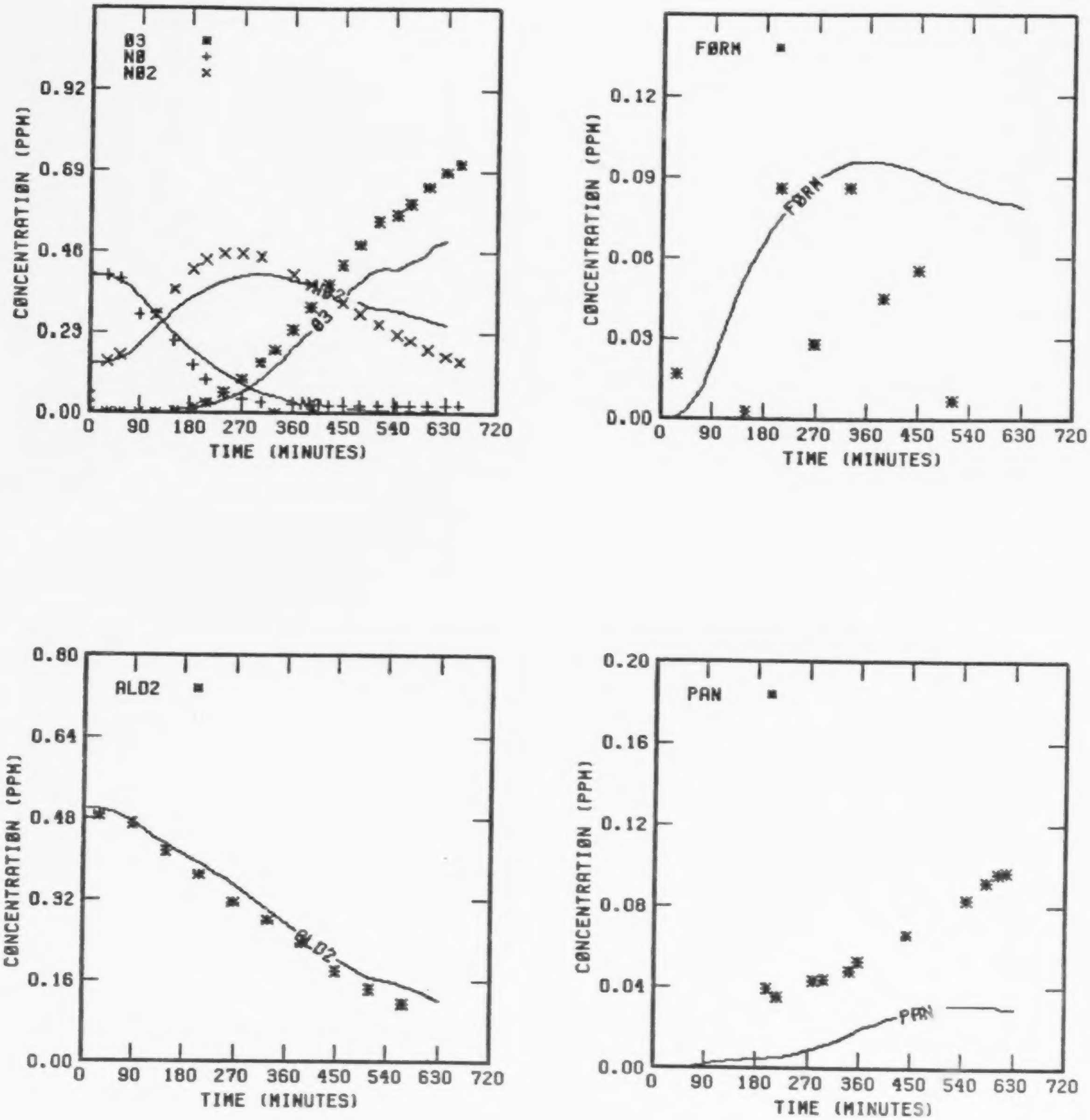

FIGURE 18. SIMULATION RESULTS FOR
UNCB 71877

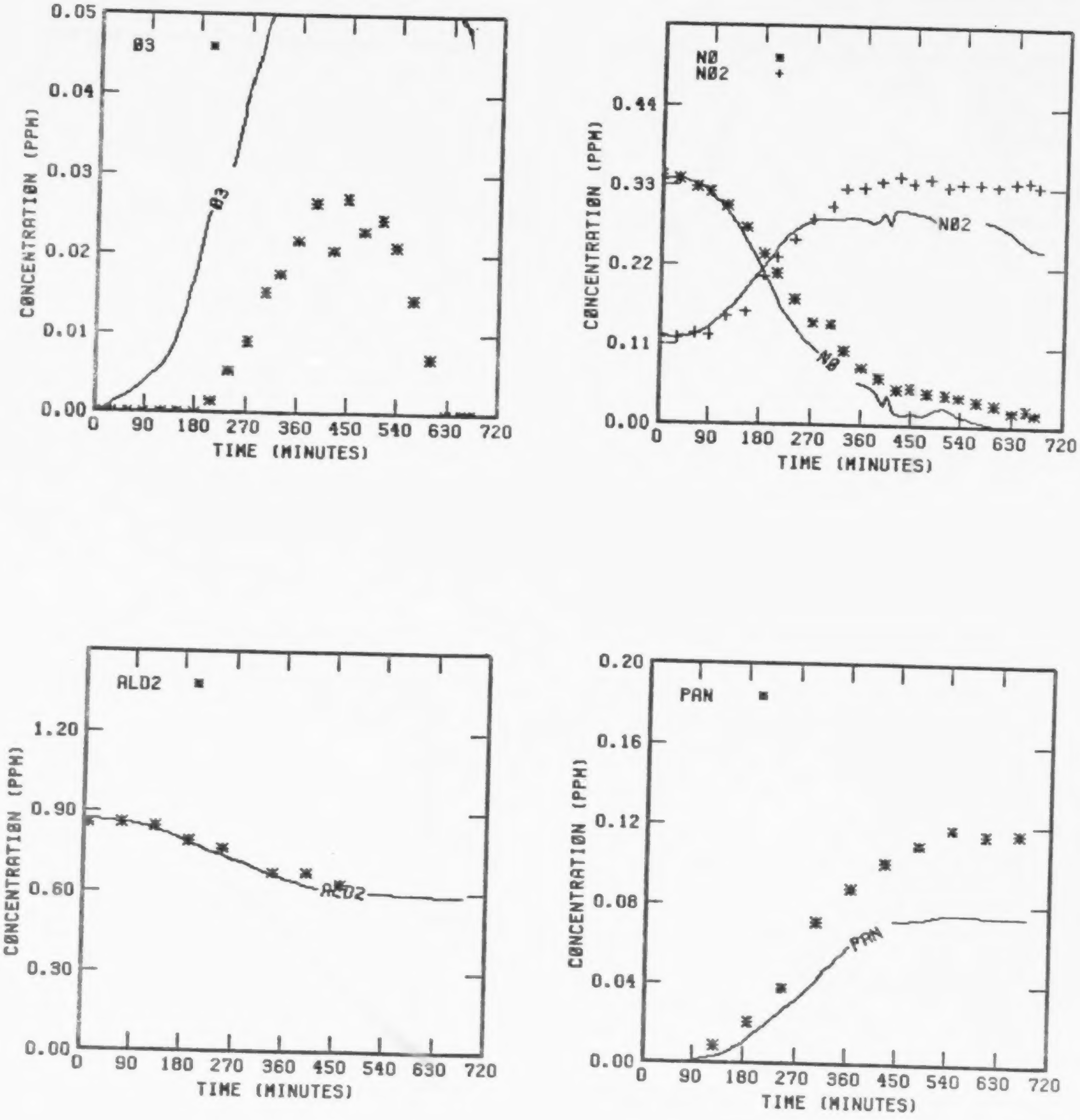

FIGURE 19 . SIMULATIØN RESULTS FØR
UNCB 111277

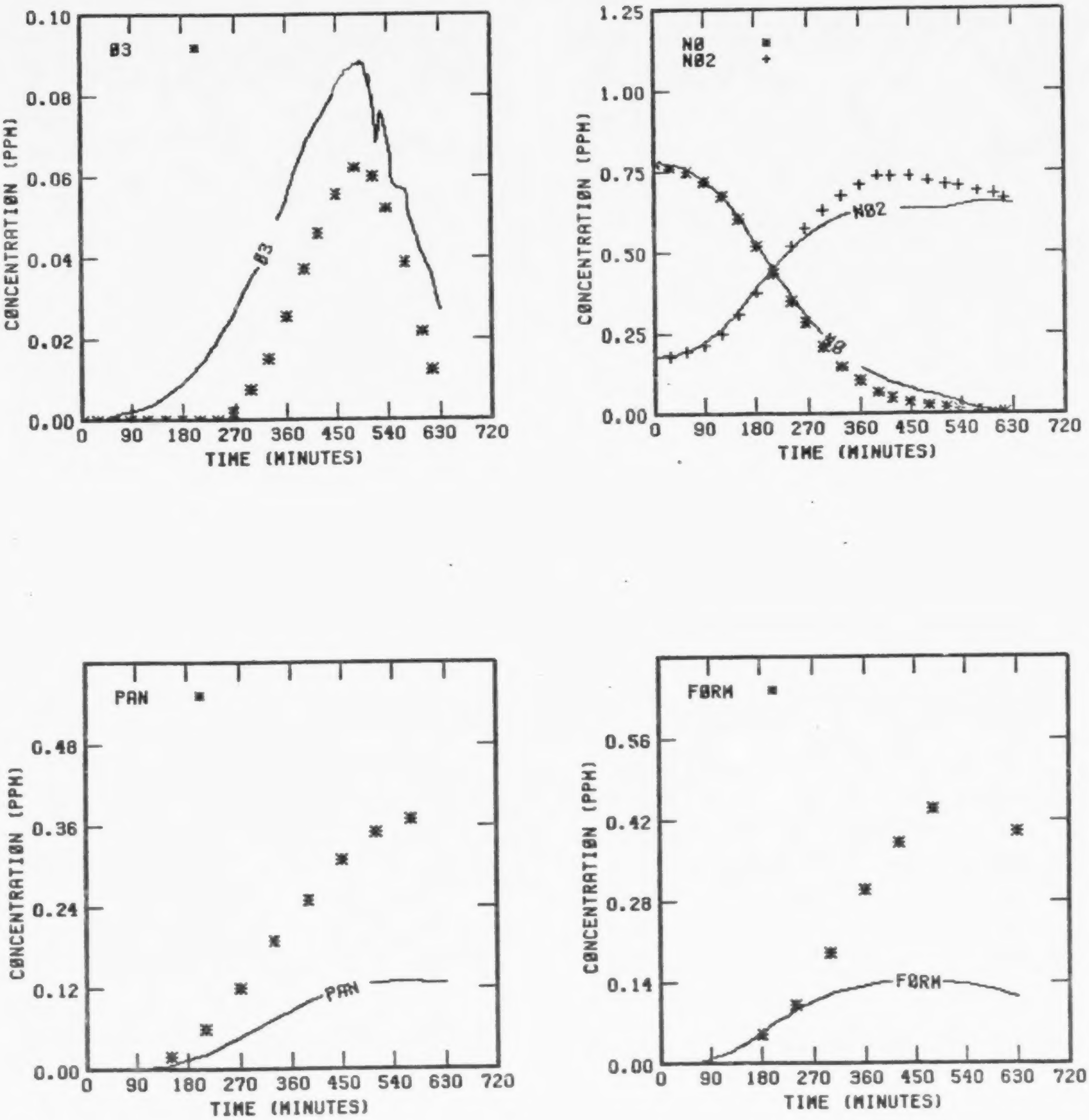

FIGURE 20. SIMULATION RESULTS FOR
UNCB 112077

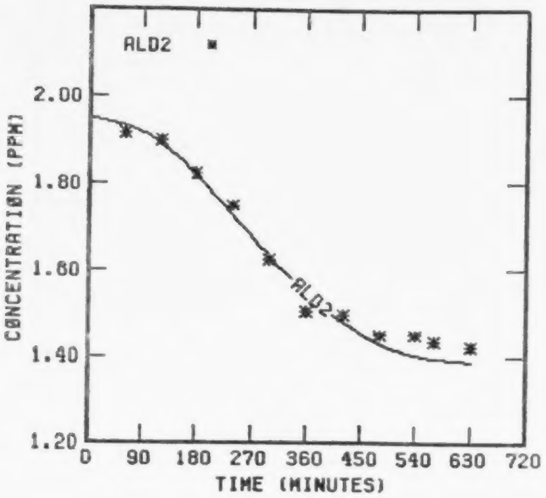

FIGURE 20 . (Concluded)

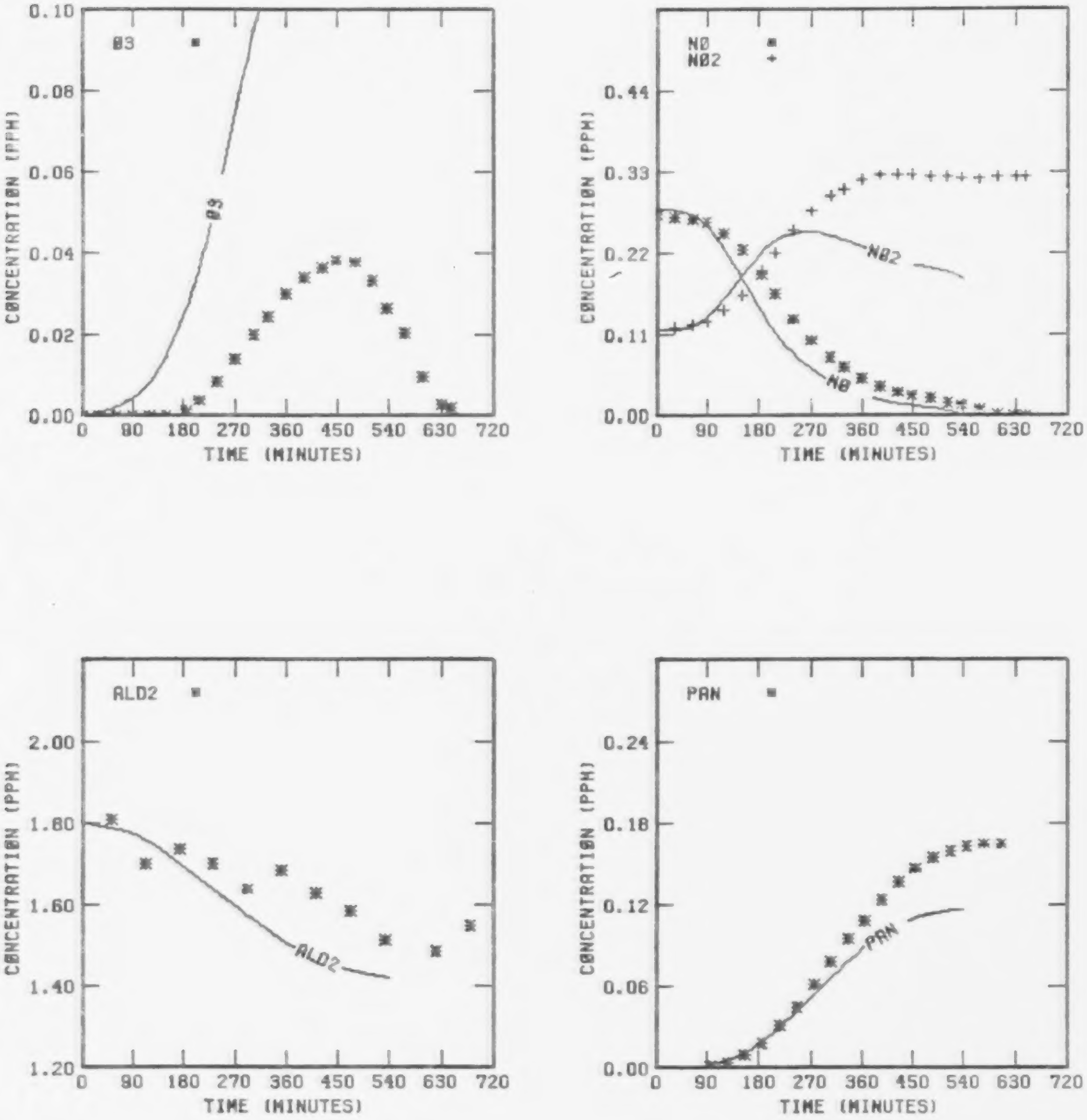

FIGURE 21. SIMULATIØN RESULTS FØR UNCB 122677

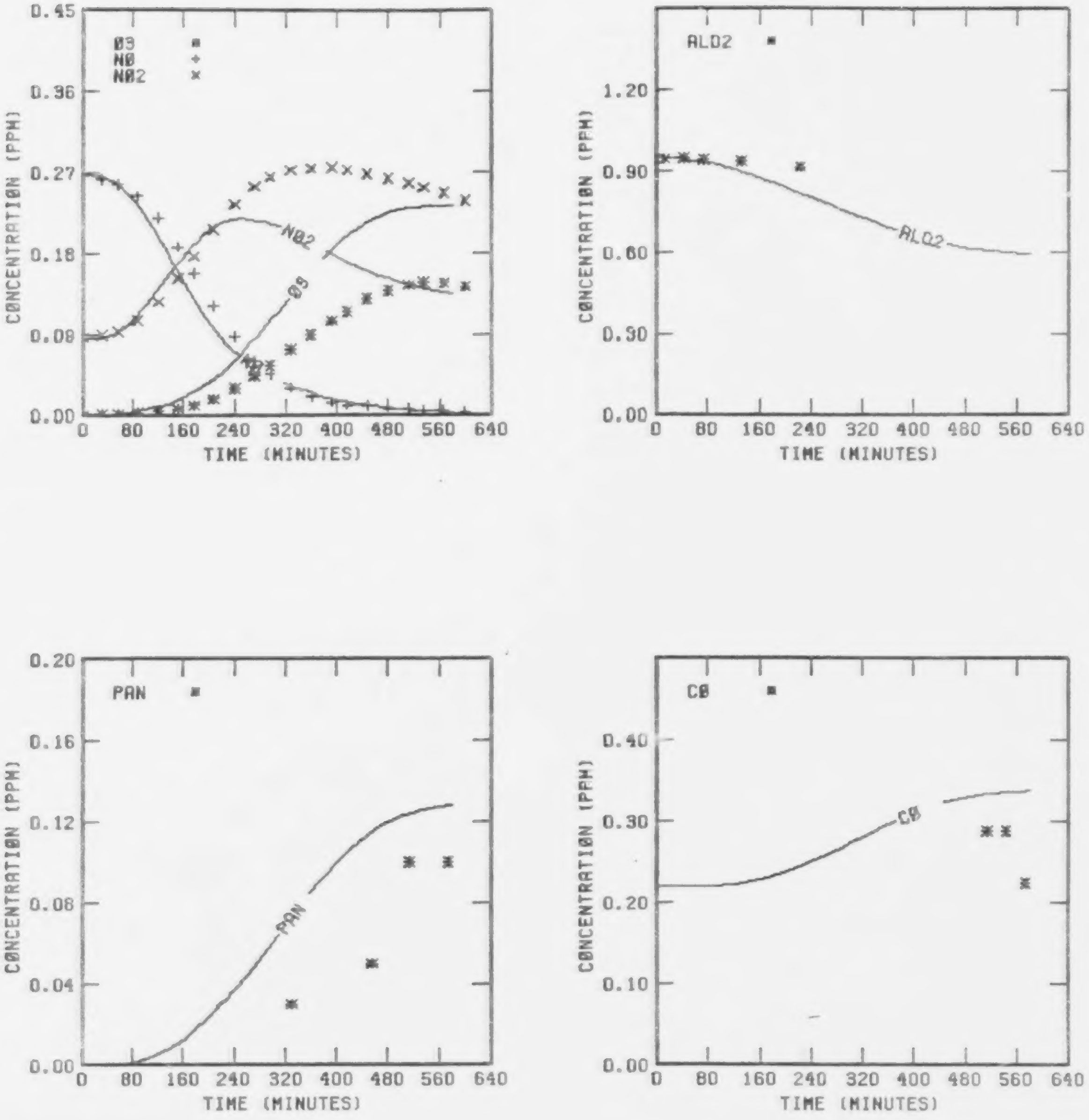

FIGURE 22 . SIMULATION RESULTS FOR
UNCB 22778

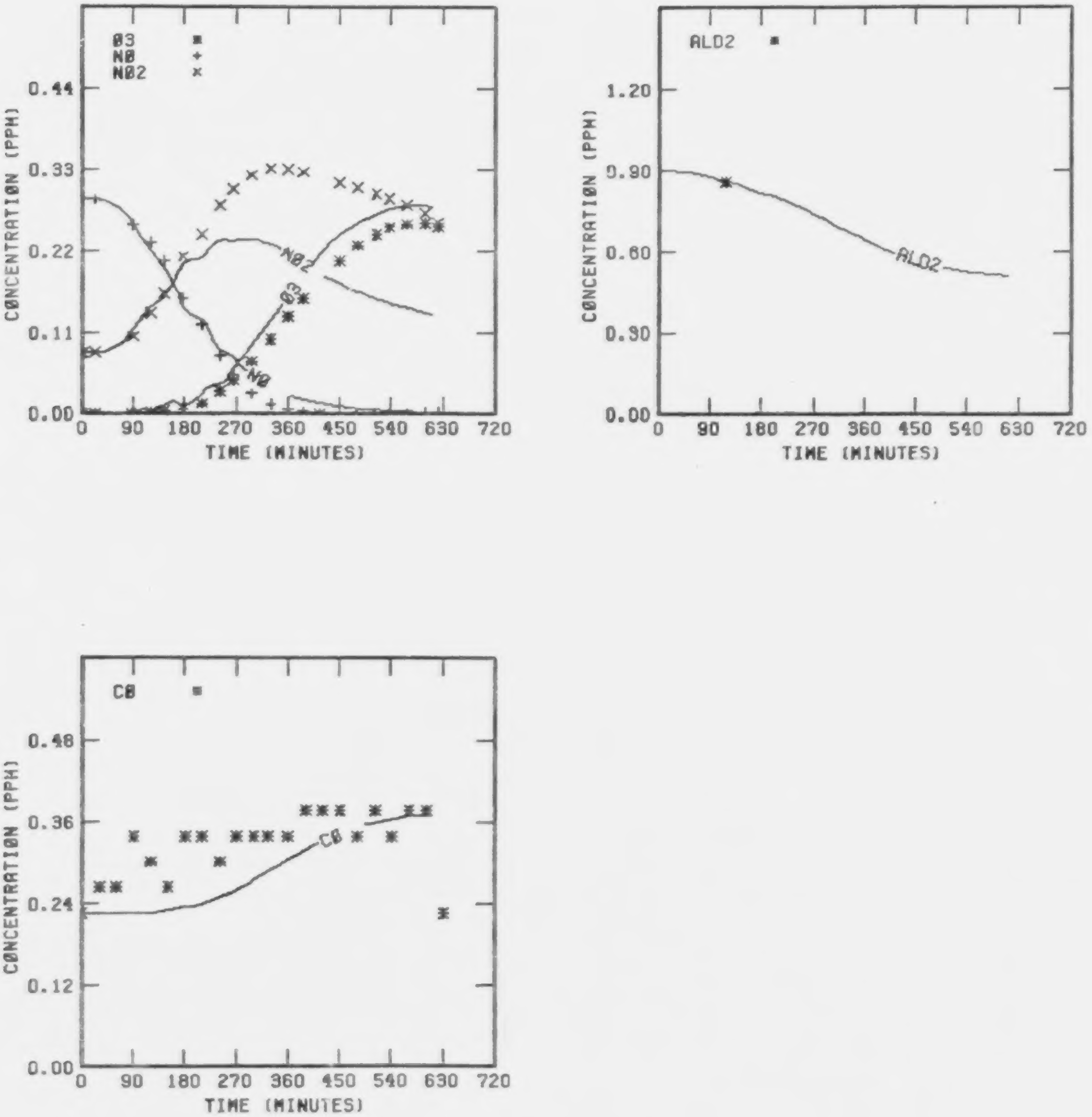

FIGURE 23. SIMULATION RESULTS FOR
UNCB 30678

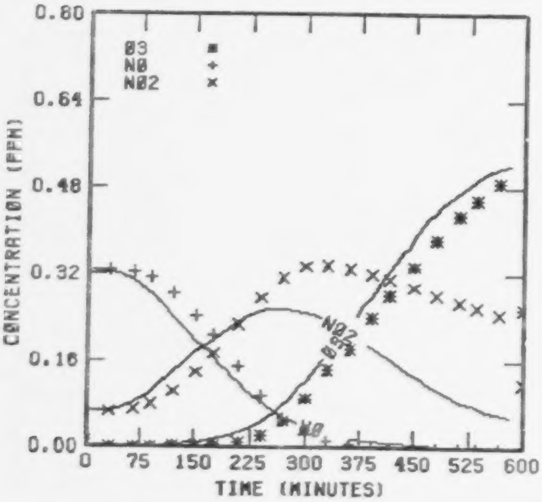

FIGURE 24 . SIMULATION RESULTS FOR
UNCB 33178

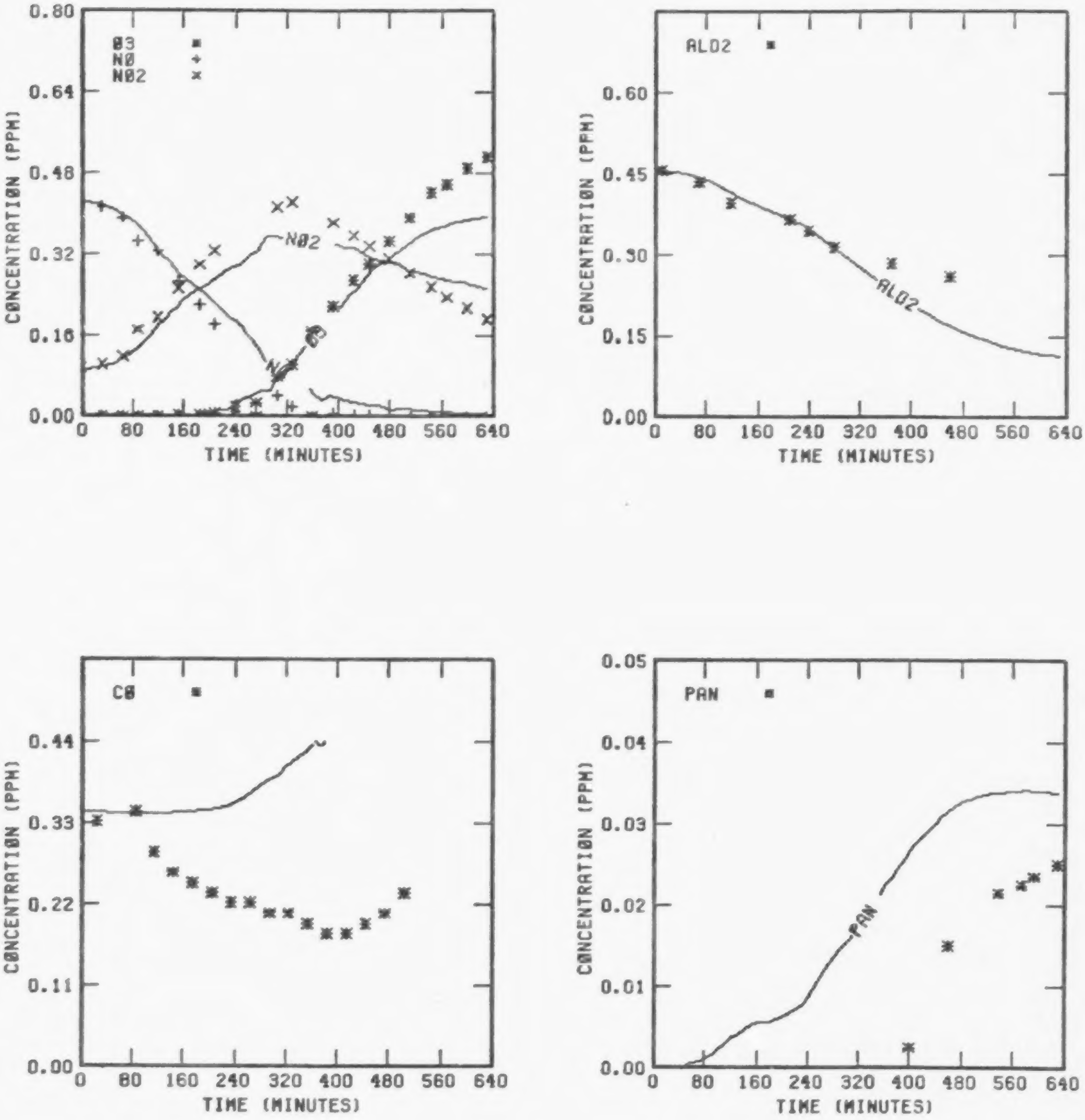

FIGURE 25 . SIMULATION RESULTS FOR UNCR 80878

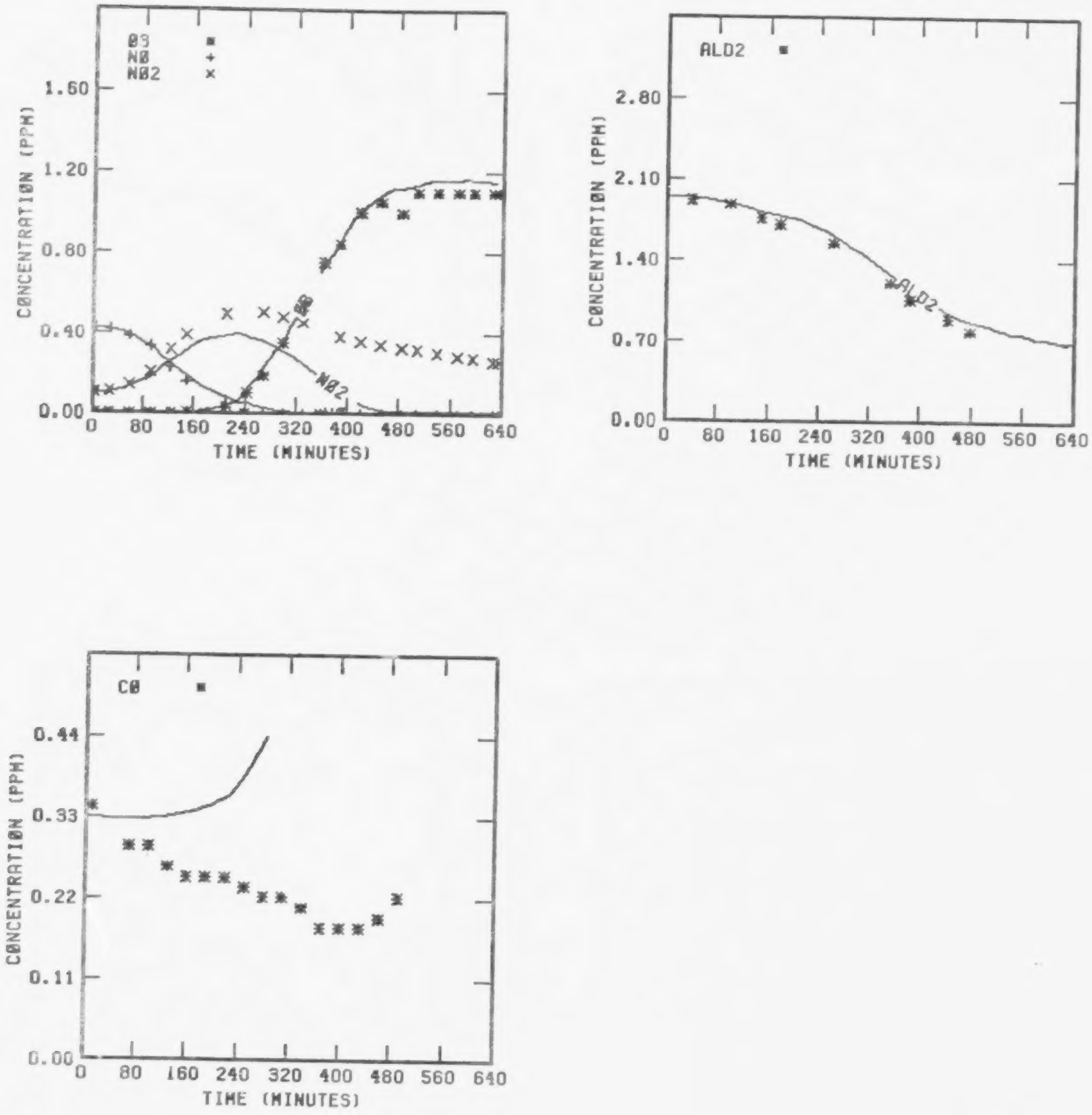

FIGURE 26 . SIMULATION RESULTS FOR
UNCB 80878

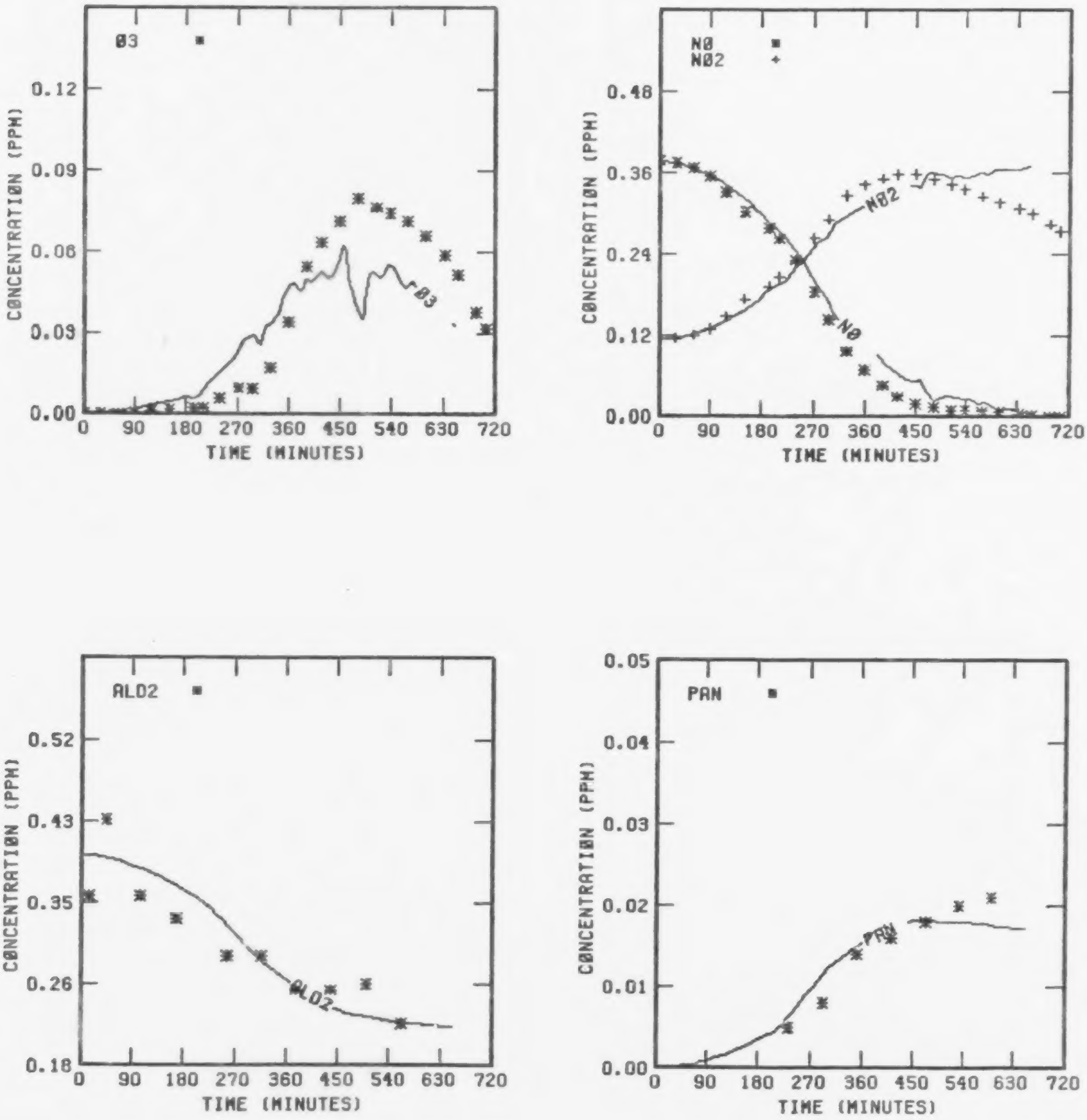

FIGURE 27 . SIMULATION RESULTS FOR
UNCR 101378

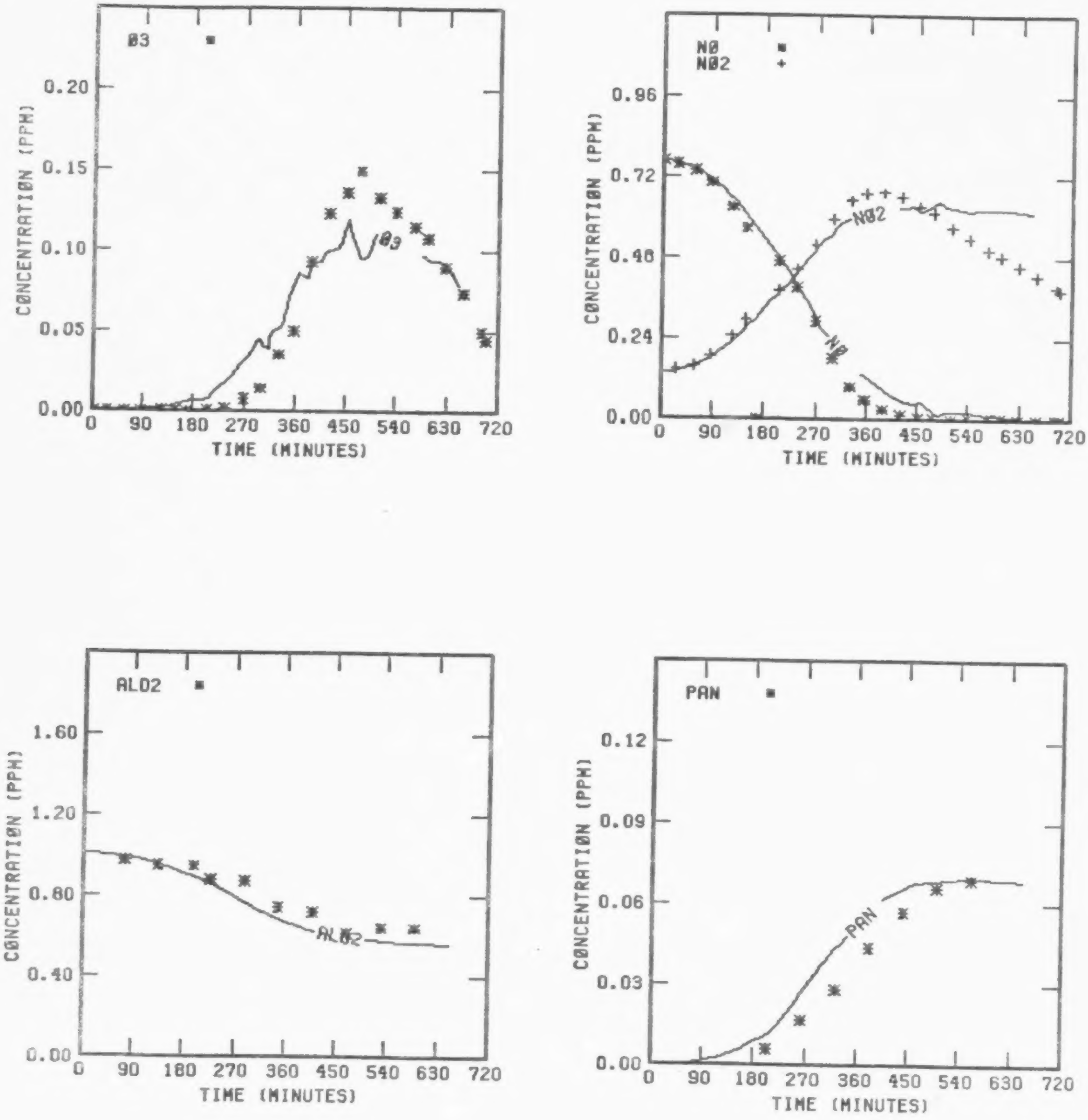

FIGURE 28. SIMULATION RESULTS FOR
UNCB 101378

TABLE 12. REACTIONS OF ETHYLENE*

Reaction	Rate constant ($ppm^{-1}min^{-1}$)
$CH_2{=}CH_2 + O \xrightarrow{2O_2} CH_3O_2^{\cdot} + HO_2^{\cdot} + CO$	6×10^2
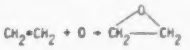	6×10^2
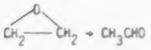	1×10^{-1}†
$CH_2{=}CH_2 + OH\cdot \xrightarrow{O_2} HOCH_2CH_2O_2^{\cdot}$	1.2×10^4
$CH_2{=}CH_2 + NO_3^{\cdot} \rightarrow NO_2 +$ Product	1.1
$CH_2{=}CH_2 + O_3 \rightarrow HCHO + CH_2O_2^{\cdot}$	2.4×10^{-3}
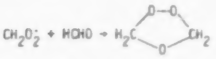	2×10^3
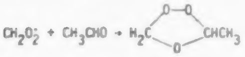	2×10^3
$CH_2O_2^{\cdot} + NO \rightarrow NO_2 + HCHO$	1.2×10^4
$CH_2O_2^{\cdot} + NO_2 \rightarrow NO_3 + HCHO$	3×10^3§
$CH_2O_2^{\cdot} \rightarrow CO + H_2 + O_2$	6.7×10^2†
$CH_2O_2^{\cdot} \rightarrow CO_2 + H_2$	1.8×10^2†
$CH_2O_2^{\cdot} \rightarrow 2HO_2^{\cdot} + CO_2$	9×10^1†
$CH_2O_2^{\cdot} \rightarrow HC(O)OH$	6×10^1†
$HOCH_2CH_2O_2^{\cdot} + NO \rightarrow NO_2 + HOCH_2CH_2O\cdot$	1.2×10^4
$HOCH_2CH_2O\cdot \xrightarrow{O_2} 2HCHO + HO_2^{\cdot}$	3×10^5†
$HOCH_2CH_2O_2^{\cdot} + HO_2^{\cdot} \rightarrow HOCH_2CH_2O_2H + O_2$	4×10^3
$2HOCH_2CH_2O_2^{\cdot} \rightarrow 2HOCH_2CH_2O\cdot + O_2$	5.0×10^2

* The inorganic, formaldehyde, and acetaldehyde reactions listed earlier must be added to construct the explicit ethylene mechanism.

† Rate constant in min^{-1}.

§ Activation energy = -1400 K, rate constant is given at 298 K.

TABLE 13. INITIAL CONDITIONS AND ALDEHYDE PHOTOLYSIS CONSTANTS FOR UNC ETHYLENE/NO_x SMOG CHAMBER EXPERIMENTS

Date	Chamber side	Sky conditions	Beginning time of simulation	Initial concentrations (ppm)					ALD + hν constant
				Ethylene	NO	NO_2	HONO	H_2O	
10/18/77	Red	Partly cloudy afternoon	7:24	1.92	.383	.111	0	2×10^4	1.0
10/18/77	Blue	Partly cloudy afternoon	7:24	0.94	.375	.109	.001	2×10^4	1.0
11/12/77	Red	Overcast afternoon	7:44	1.00	.39	.113	.004	2×10^4	1.0
11/20/77	Red	Overcast	7:30	2.19	.416	.030	.008	2×10^4	1.2
1/10/78	Blue	Clear	8:15	2.18	.344	.138	.001	1.5×10^3	1.0
6/16/78	Red	Scattered clouds in afternoon	6:16	1.98	.423	.211	.002	2×10^4	1.0
6/30/78	Blue	Clear	6:12	0.77	.384	.097	.024	2×10^4	1.0
7/01/78	Red	Mostly clear, sparse clouds	5:52	0.73	.679	.208	.029	2×10^4	1.0
7/30/78	Red	Scattered clouds in morning	6:28	0.66	.396	.078	.017	2×10^4	1.0*
8/06/78	Blue	Scattered clouds all day	6:20	1.30	.418	.151	.028	2×10^4	1.0*
8/10/78	Blue	Scattered clouds all day	6:36	0.52	.415	.113	.024	2×10^4	1.0*
8/10/78	Blue	Scattered clouds all day	6:36	1.51	.408	.114	.018	2×10^4	1.0*
8/15/78	Blue	Scattered clouds in afternoon	6:23	0.79	.430	.133	.025	2×10^4	1.0
8/21/78	Red	Clear	6:31	0.70	.797	.181	.005	1.6×10^4	1.0*
9/15/78	Red	Overcast	6:52	1.49	.407	.119	.010	1.6×10^4	1.0*
9/19/78	Red	Clear	7:00	0.94	.568	.120	.028	1.6×10^4	1.0
9/21/78	Red	Overcast	7:06	0.97	.192	.065	.010	1.6×10^4	1.0*
10/02/78	Blue	Variable cloudiness in afternoon	7:12	1.49	.383	.107	.008	1.6×10^4	1.0*
10/03/78	Red	Variable cloudiness in afternoon	7:16	0.49	.359	.135	.005	1.6×10^4	1.0*
10/17/78	Blue	Variable cloudiness in afternoon	7:22	1.37	.366	.125	.004	1×10^4	1.0*
10/18/78	Red	Clear	7:28	1.56	.343	.113	.001	1×10^4	1.0*
11/07/78	Blue	Overcast most of the day	7:40	1.34	.295	.146	.007	1×10^4	1.0*

*UV data used in computer simulations, instead of TSR.

TABLE 14. UNC ETHYLENE EXPERIMENTS--SIMULATIONS AND MEASUREMENTS

Date	Chamber side	Initial $[NO_x]$ (ppm)	Initial NO_2/NO_x ratio	Initial HC/NO_x (ppmC/ppm)	Maximum O_3 (ppm) Sim.	Maximum O_3 (ppm) Meas.	Difference in O_3 maxima	Time to maximum O_3 (minutes) Sim.	Time to maximum O_3 (minutes) Meas.	Difference in times to O_3 maximum	Maximum $[NO_2]$ (ppm) Sim.	Maximum $[NO_2]$ (ppm) Meas.	Difference in NO_2 maximum (percent)	Time to maximum $[NO_2]$ (min) Sim.	Time to maximum $[NO_2]$ (min) Meas.	Difference in times NO_2 maxima
10/18/77	Red	.494	.22	7.8	1.21	.93	30	420	420	0	.4	.4	0	260	260	0
10/18/77	Blue	.484	.23	3.9	.44	.44	0	>560	>560	--	.39	.41	5	360	360	0
11/12/77	Red	.503	.22	4.0	.06	.054	11	370	420	-12	.36	.36	0	390	390	0
11/20/77	Red	.446	.07	9.8	.38	.72	47	450	420	7	.40	.44	-9	270	270	0
1/10/78	Blue	.482	.29	9.1	.125	.042	198		455	--	.37	.34	9	350	350	0
6/16/78	Red	.634	.33	6.3	1.48	1.12	32	400	380	5	.48	.48	0	240	240	0
6/30/78	Blue	.481	.20	3.2	.96	.96	10	490	440	11	.36	.37	-3	280	250	12
7/01/78	Red	.887	.23	1.7	.12	.24	-50	630	700	9	.52	.54	-4	450	450	0
7/30/78	Red	.474	.16	2.8	.83	.75	-11	540	540	0	.33	.38	-13	300	300	0
8/06/78	Blue	.569	.27	4.6	.87	1.08	-19	350	300	17	.48	.54	-11	240	180	33
8/10/78	Red	.528	.21	2.0	.21	.17	24	>560	>560	--	.34	.37	-9	[illegible]	360	0
8/10/78	Blue	.522	.22	5.8	1.40	1.12	25	380	360	6	.42	.45	-7	[illegible]	210	0
8/15/78	Blue	.563	.24	2.8	.68	.83	-18	>480	>480	--	.65	.70	-7	320	240	33
8/21/78	Red	.978	.19	1.4	.036	.03	20	500	>780	--	.51	.36	42	460	400	15
9/15/78	Red	.526	.23	5.7	.46	.56	-20	500	500	--	.40	.42	-5	300	300	0
9/19/78	Red	.688	.17	2.7	.56	.90	-38	500	500	--	.49	.50	-2	300	240	25
9/21/78	Red	.268	.25	7.2	.88	.78	13	360	360	0	.22	.25	-12	180	180	0
10/02/78	Blue	.490	.22	6.1	1.17	.87	35	390	360	8	.38	.39	-3	260	260	0
10/03/78	Red	.494	.27	2.0	.030	.024	25	450	480	-6	.31	.31	0	>560	>560	--
10/17/78	Blue	.491	.25	[illegible]	.55	.41	34	>400	>400	--	.38	.39	-3	350	350	0
10/18/78	Red	.456	.25	6.8	1.00	.7	43	400	455	-12	.35	.30	17	280	280	0
11/07/78	Blue	.441	.33	6.1	.65	.74	-12	240	400	5	.34	.34	0	240	240	0

O_3 maxima average difference = 8 percent, standard deviation = ±27 percent

NO_2 maxima average difference = 1 percent, standard deviation = ±12 percent.

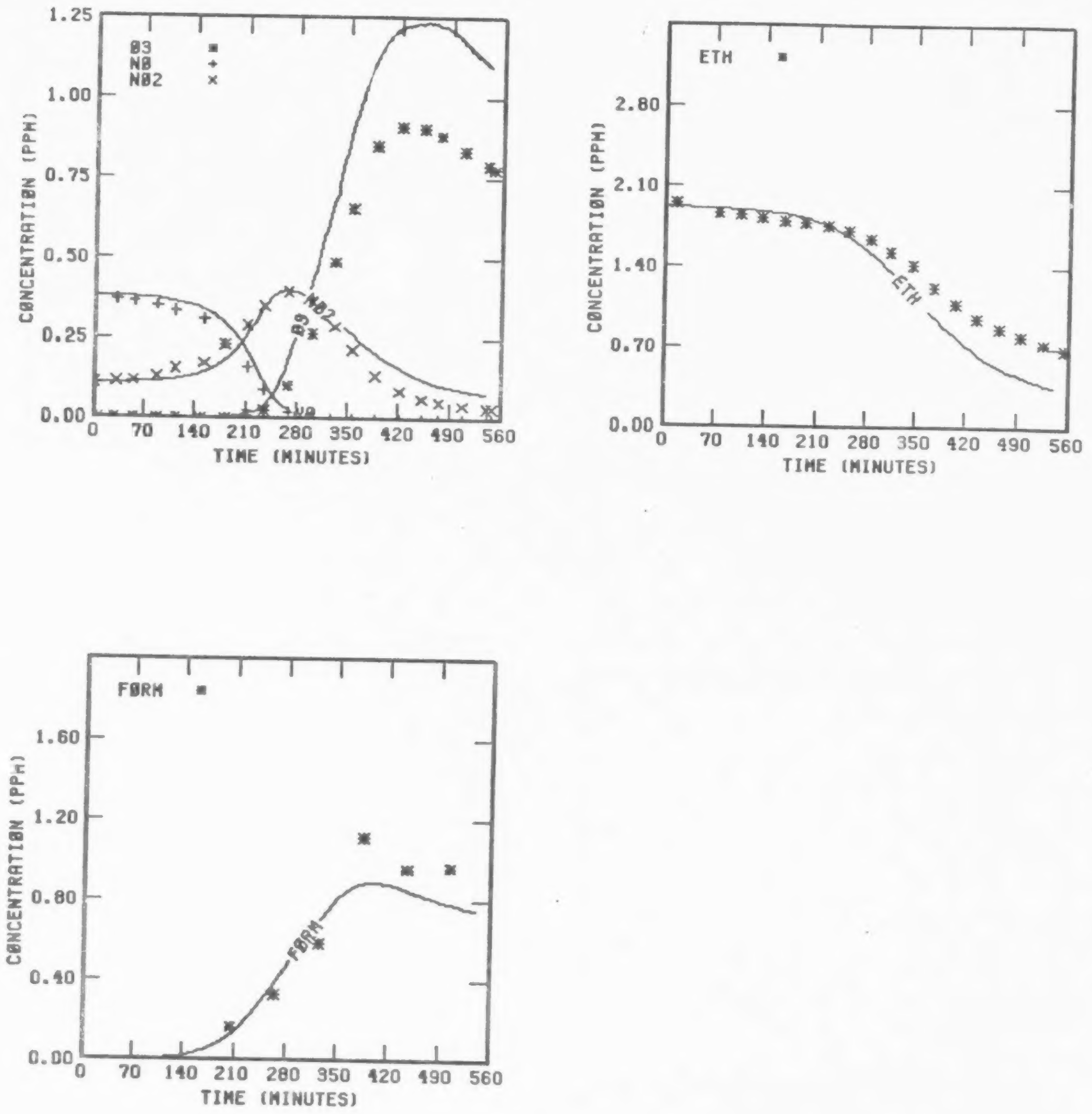

FIGURE 29. SIMULATION RESULTS FOR UNCR 101877

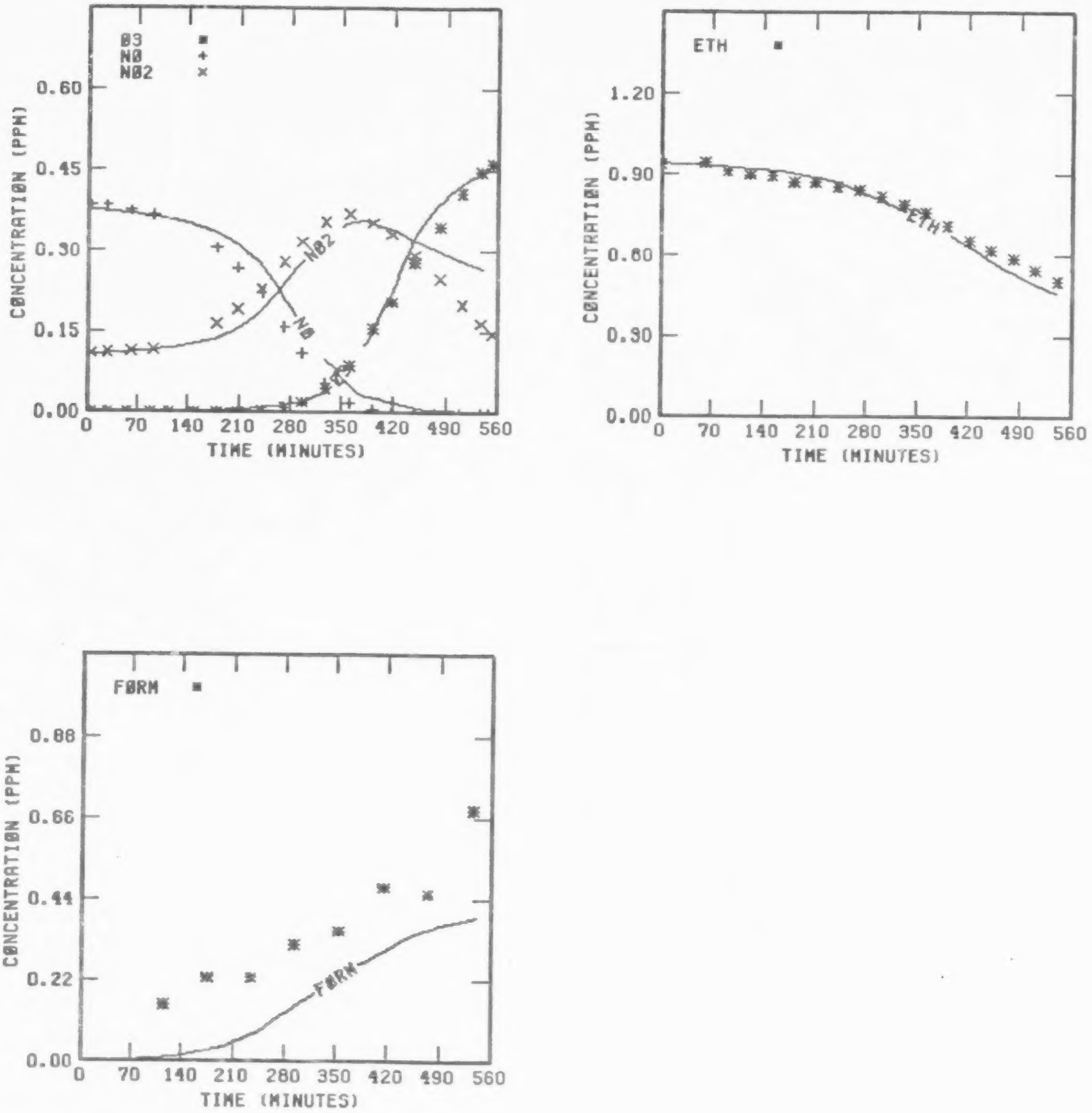

FIGURE 30 . SIMULATION RESULTS FOR
UNCB 101877

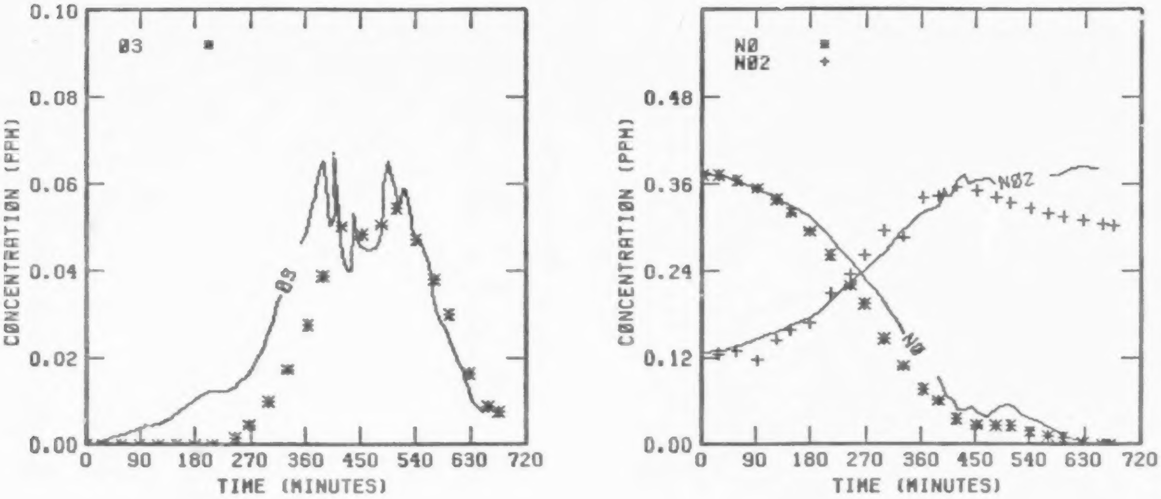

FIGURE 31 . SIMULATIØN RESULTS FØR
UNCR 111277

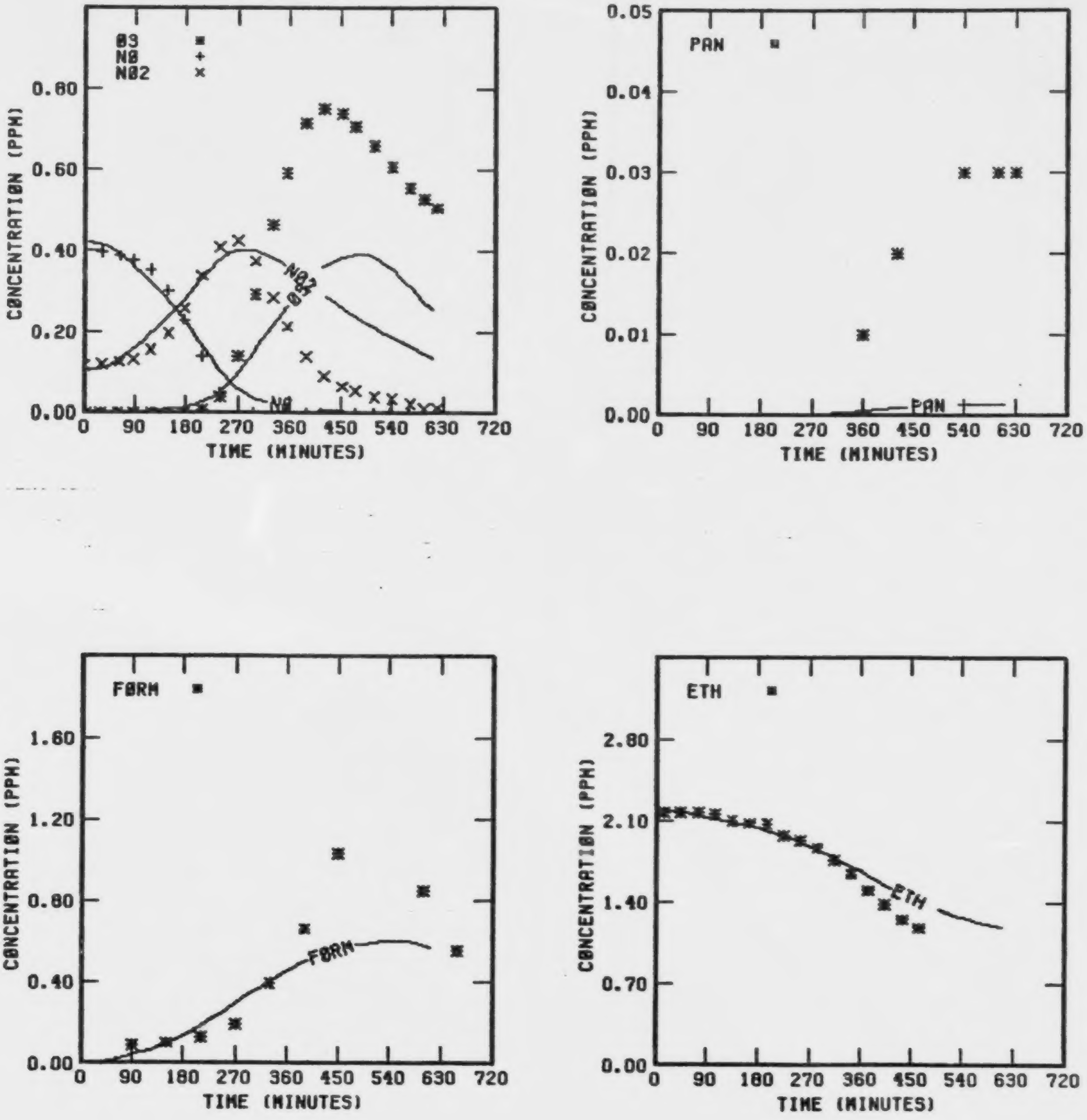

FIGURE 32 . SIMULATION RESULTS FOR
UNCR 112077

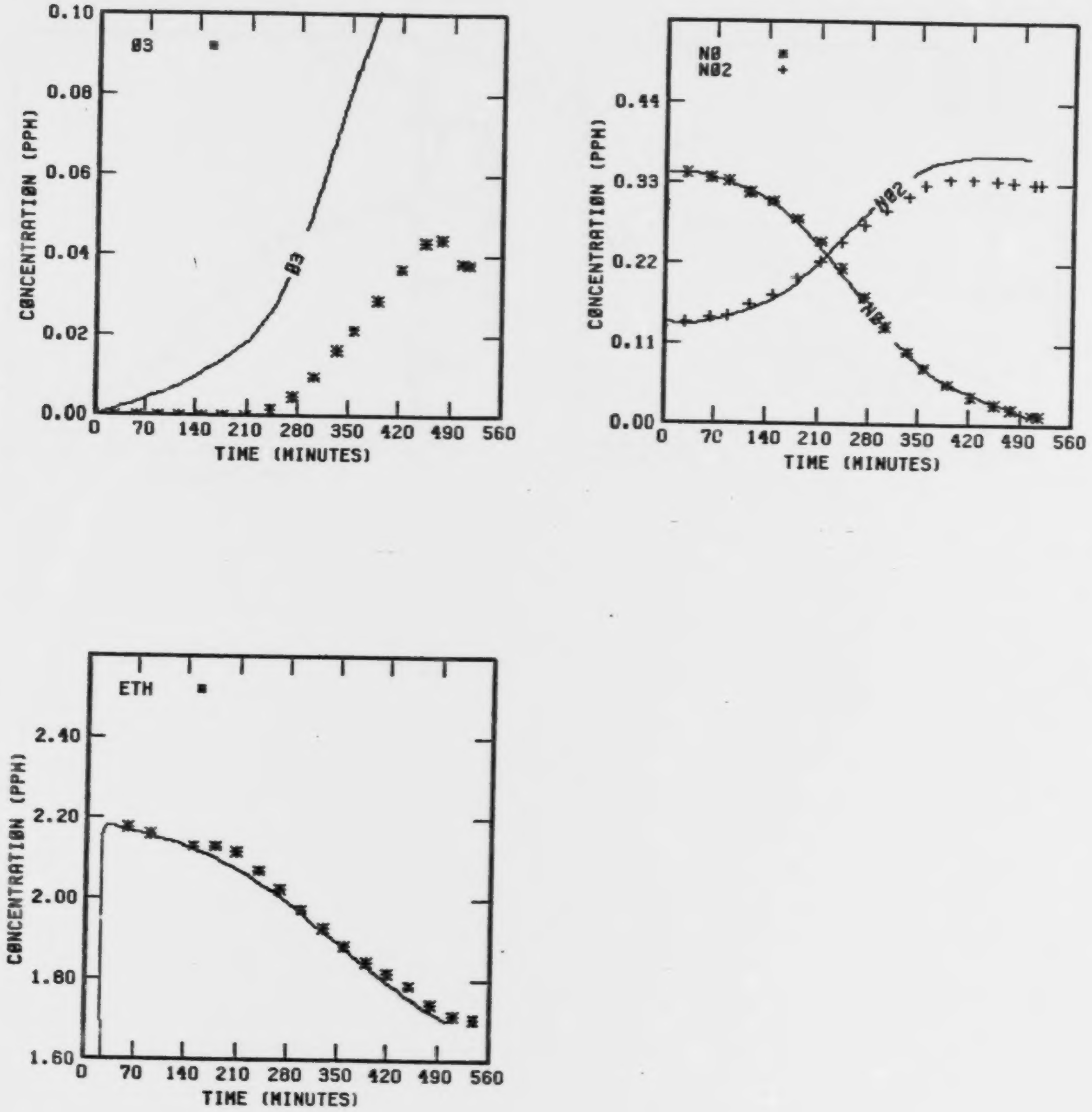

FIGURE 33. SIMULATION RESULTS FOR
UNCB 11078

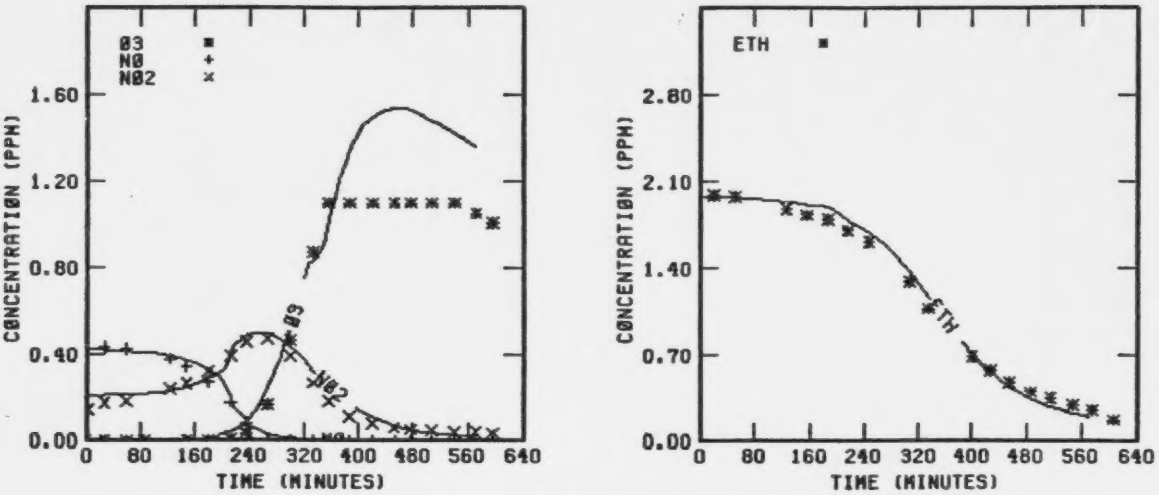

FIGURE 34. SIMULATION RESULTS FOR
UNCR 61678

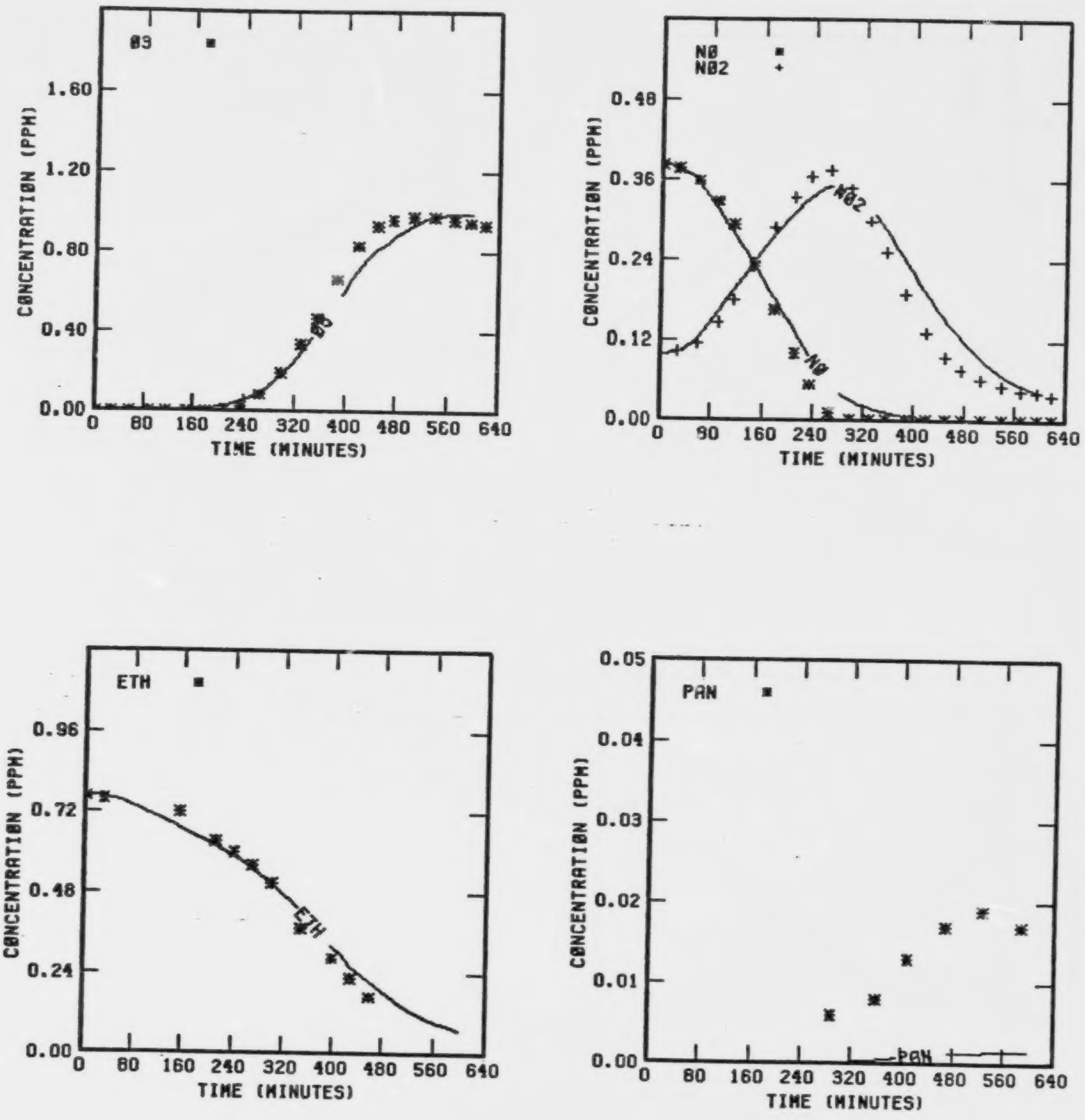

FIGURE 35. SIMULATION RESULTS FOR
UNCB 63078

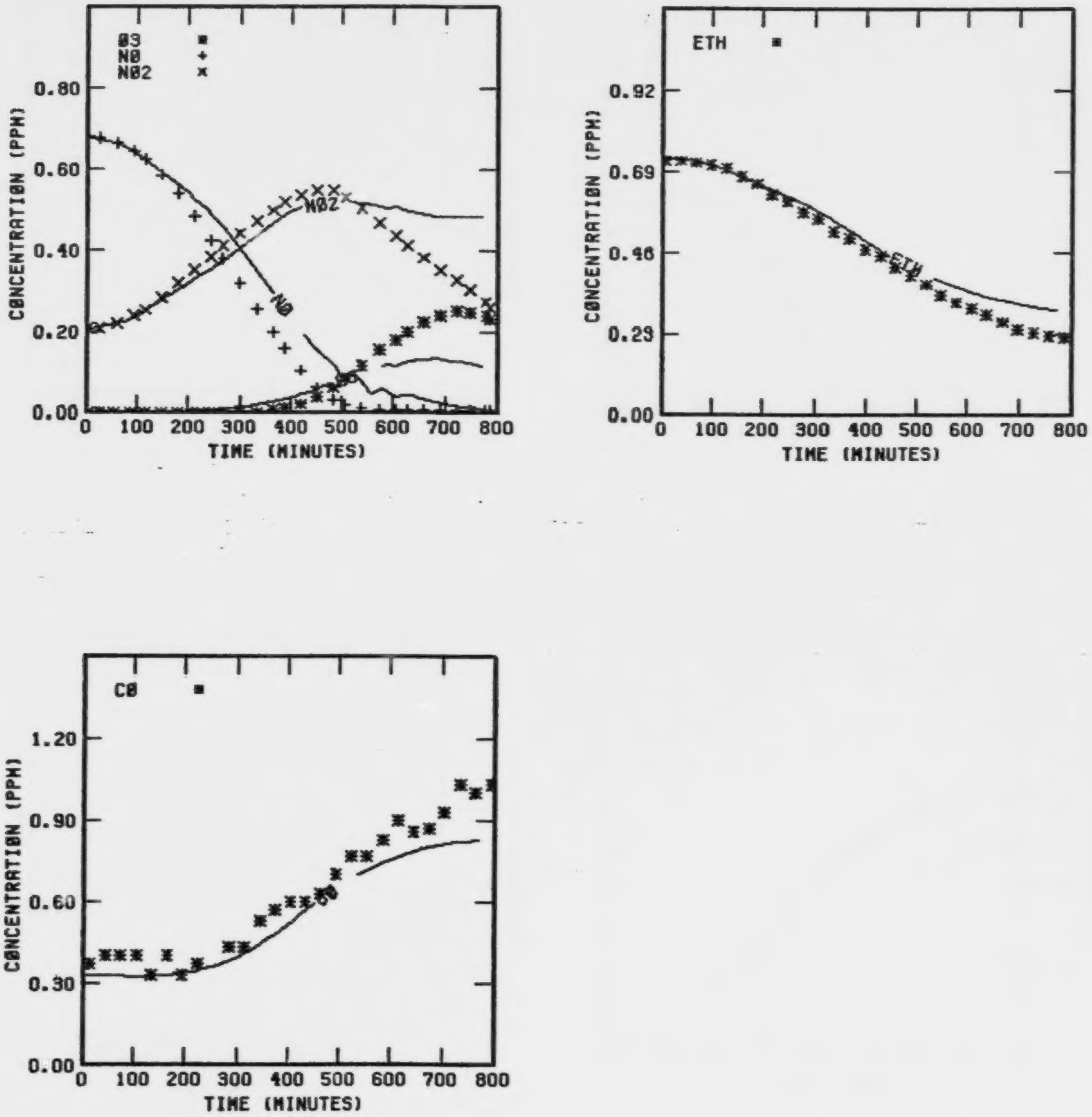

FIGURE 36 . SIMULATION RESULTS FOR
UNCR 70178

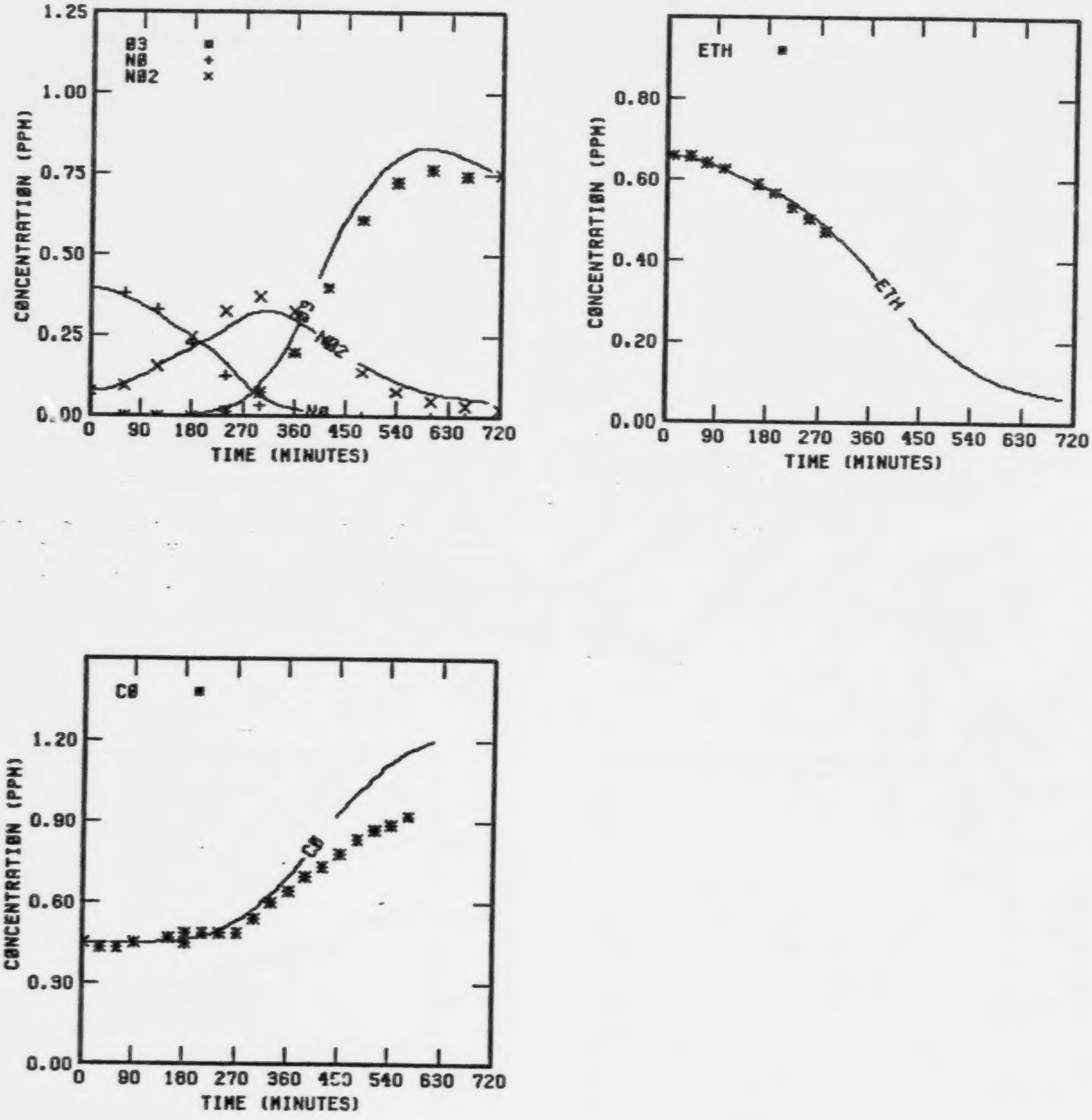

FIGURE 37 . SIMULATION RESULTS FOR
UNCR 73078

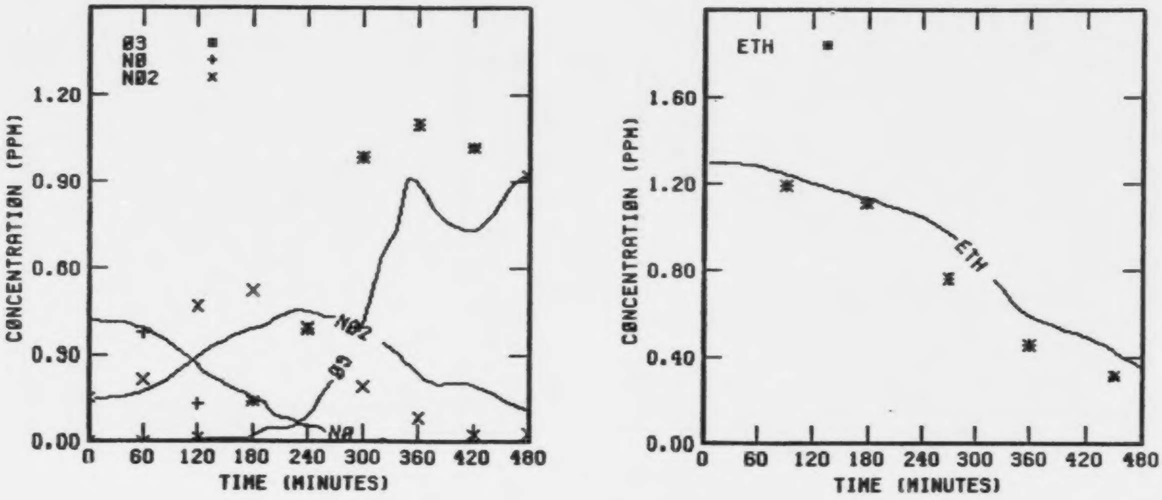

FIGURE 38 . SIMULATIØN RESULTS FØR
UNCB 80678

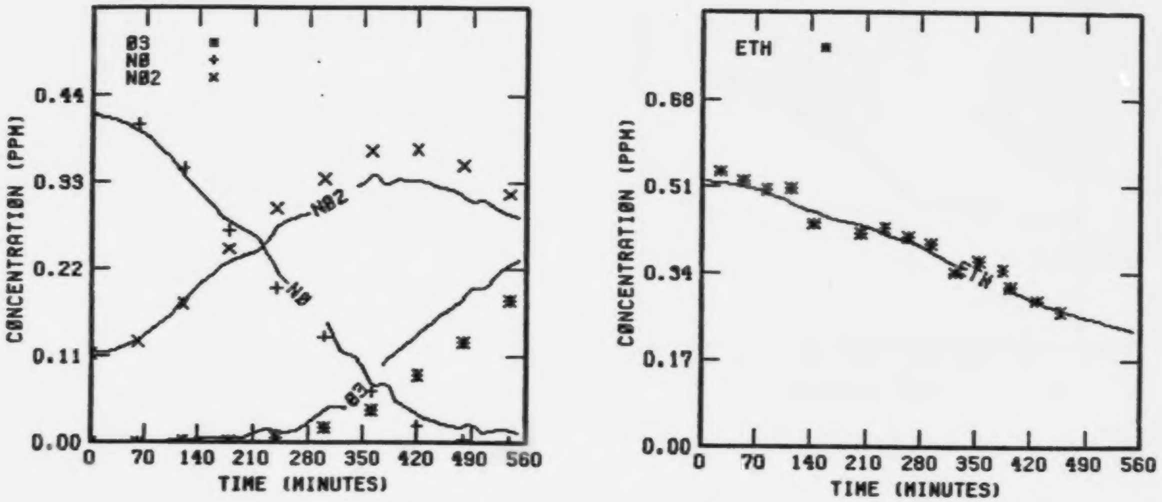

FIGURE 39 . SIMULATIØN RESULTS FØR
UNCR 81078

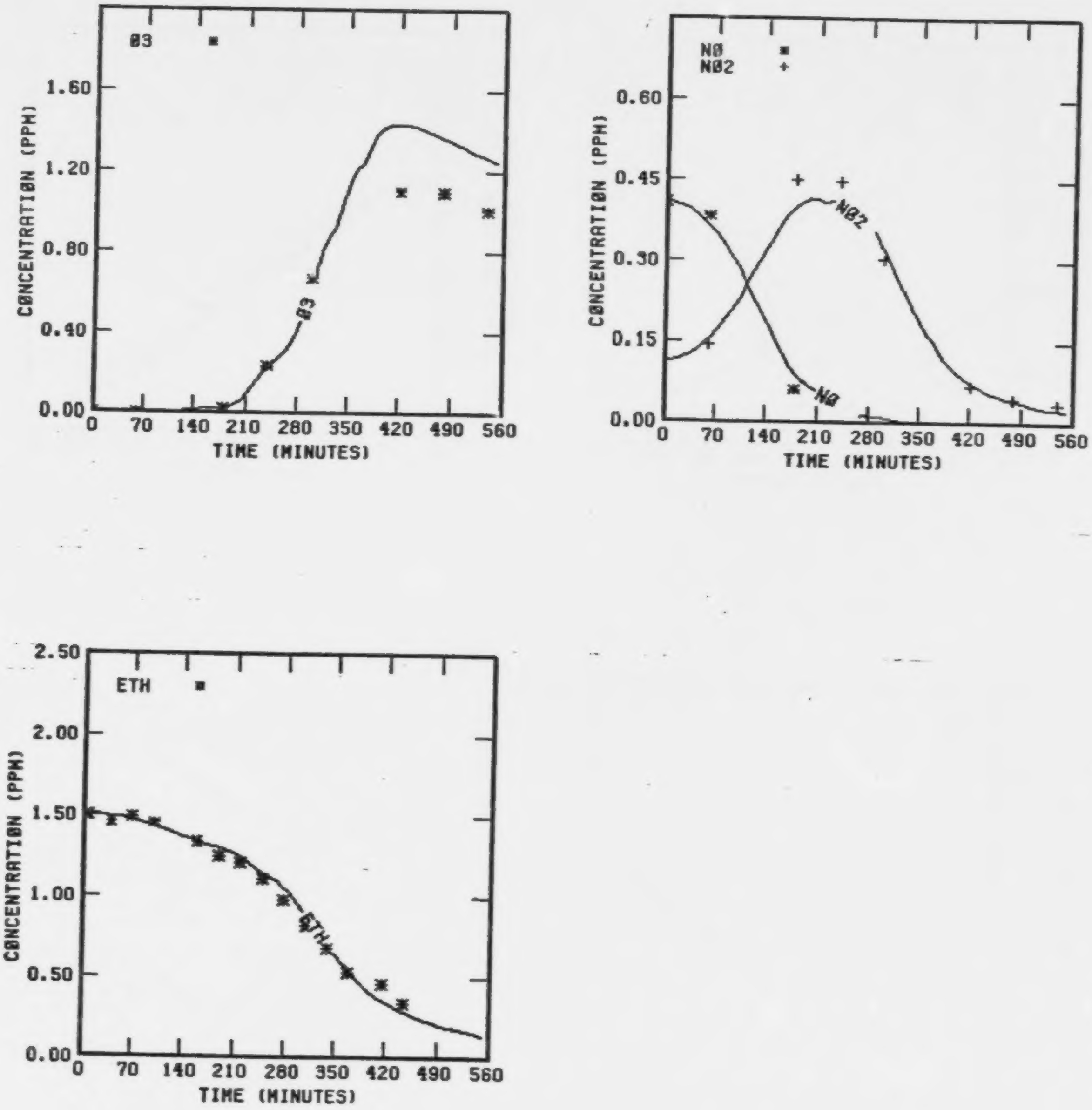

FIGURE 40 . SIMULATIØN RESULTS FØR
UNCB 81078

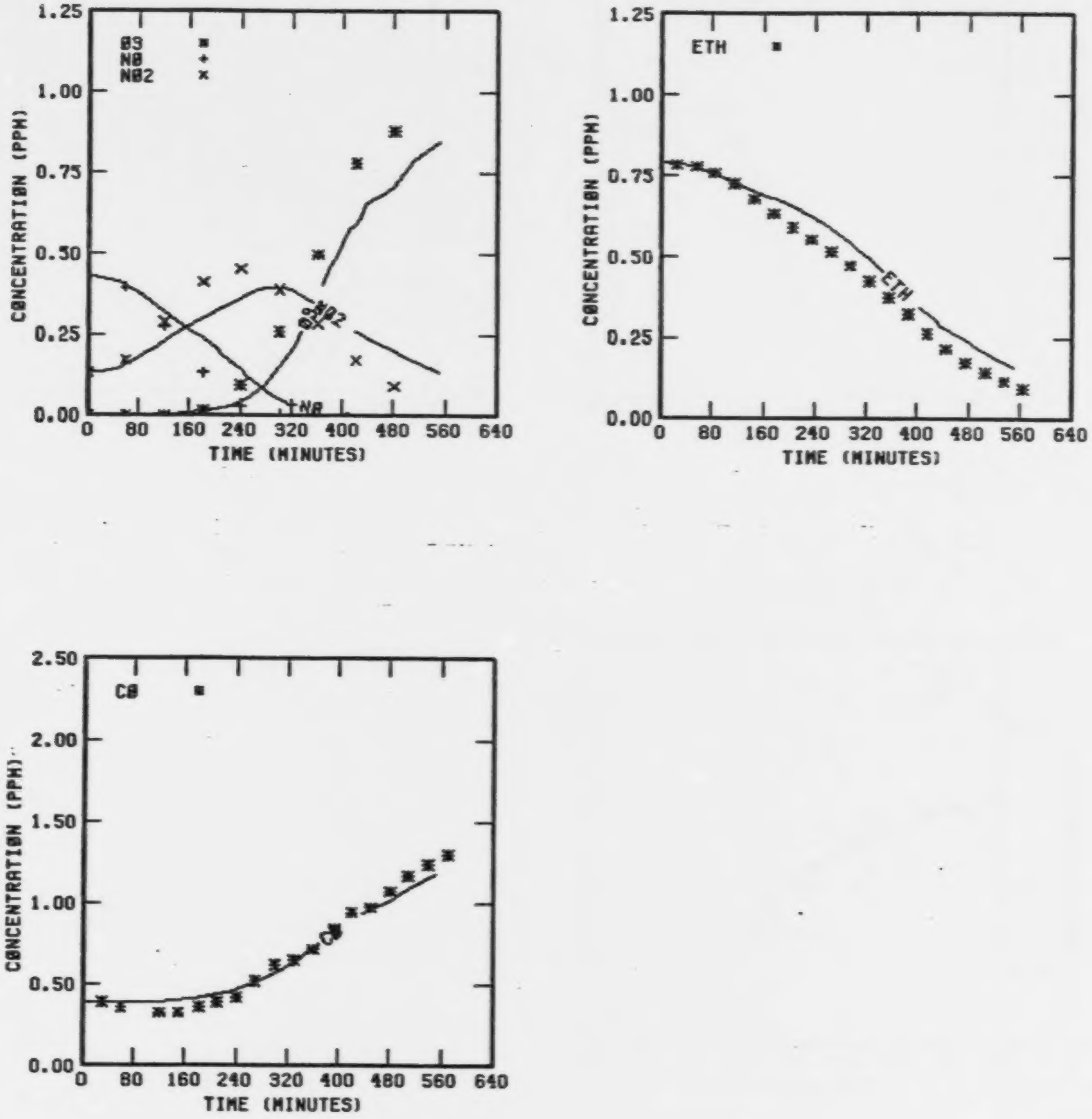

FIGURE 41 . SIMULATION RESULTS FOR
UNCB 81578

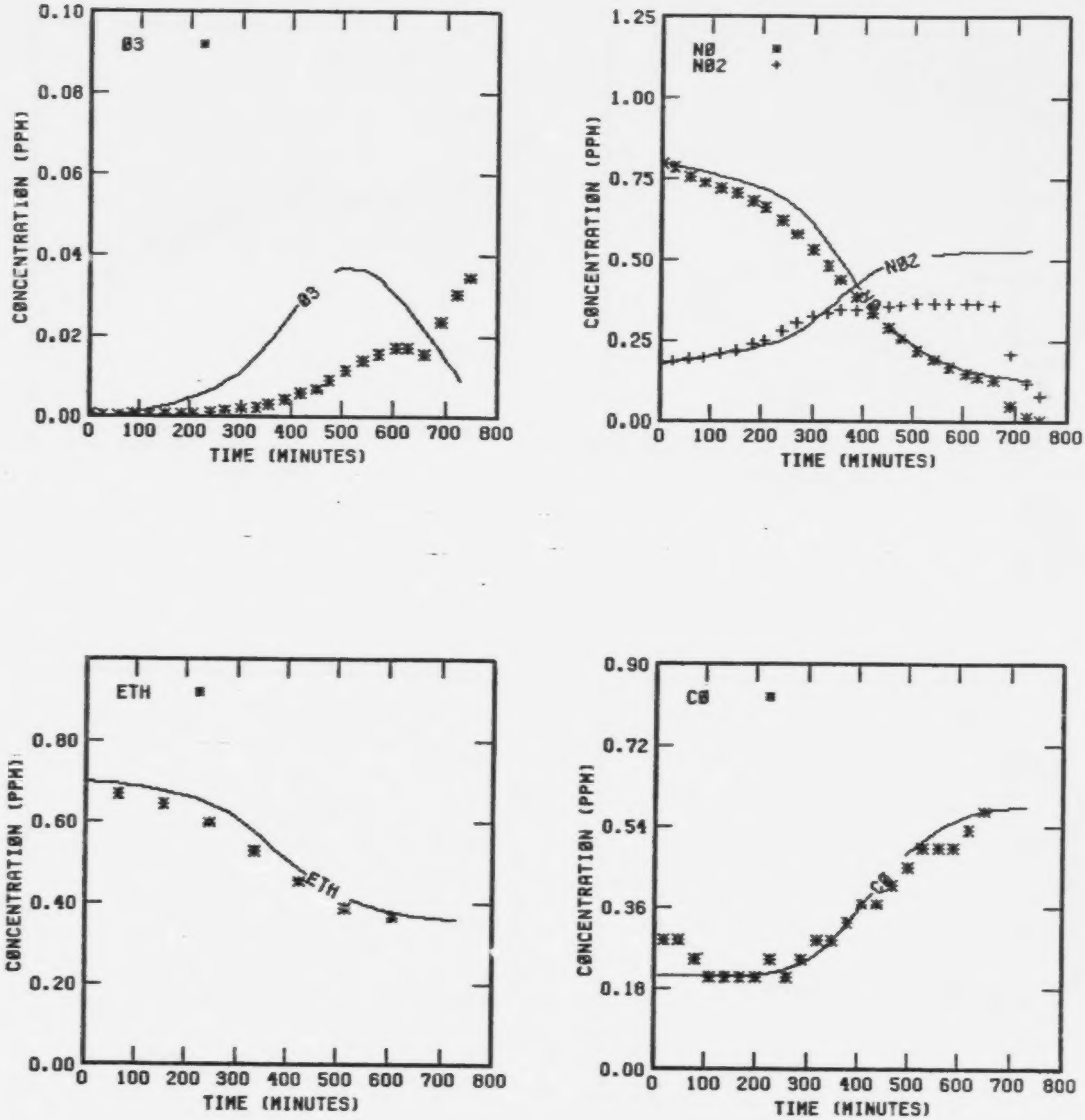

FIGURE 42 . SIMULATIØN RESULTS FØR UNCR 82178

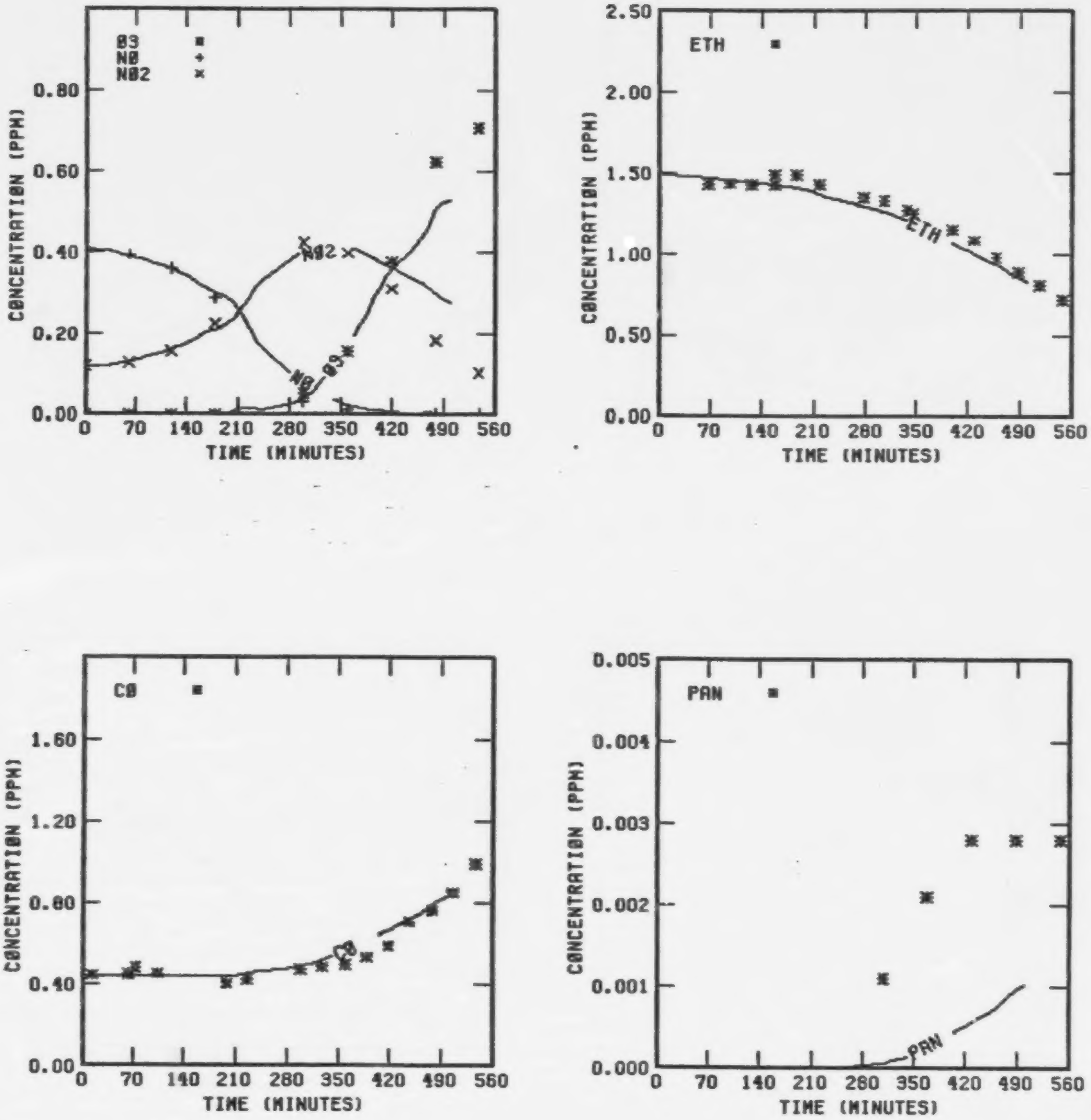

FIGURE 43 . SIMULATION RESULTS FOR UNCR 91578

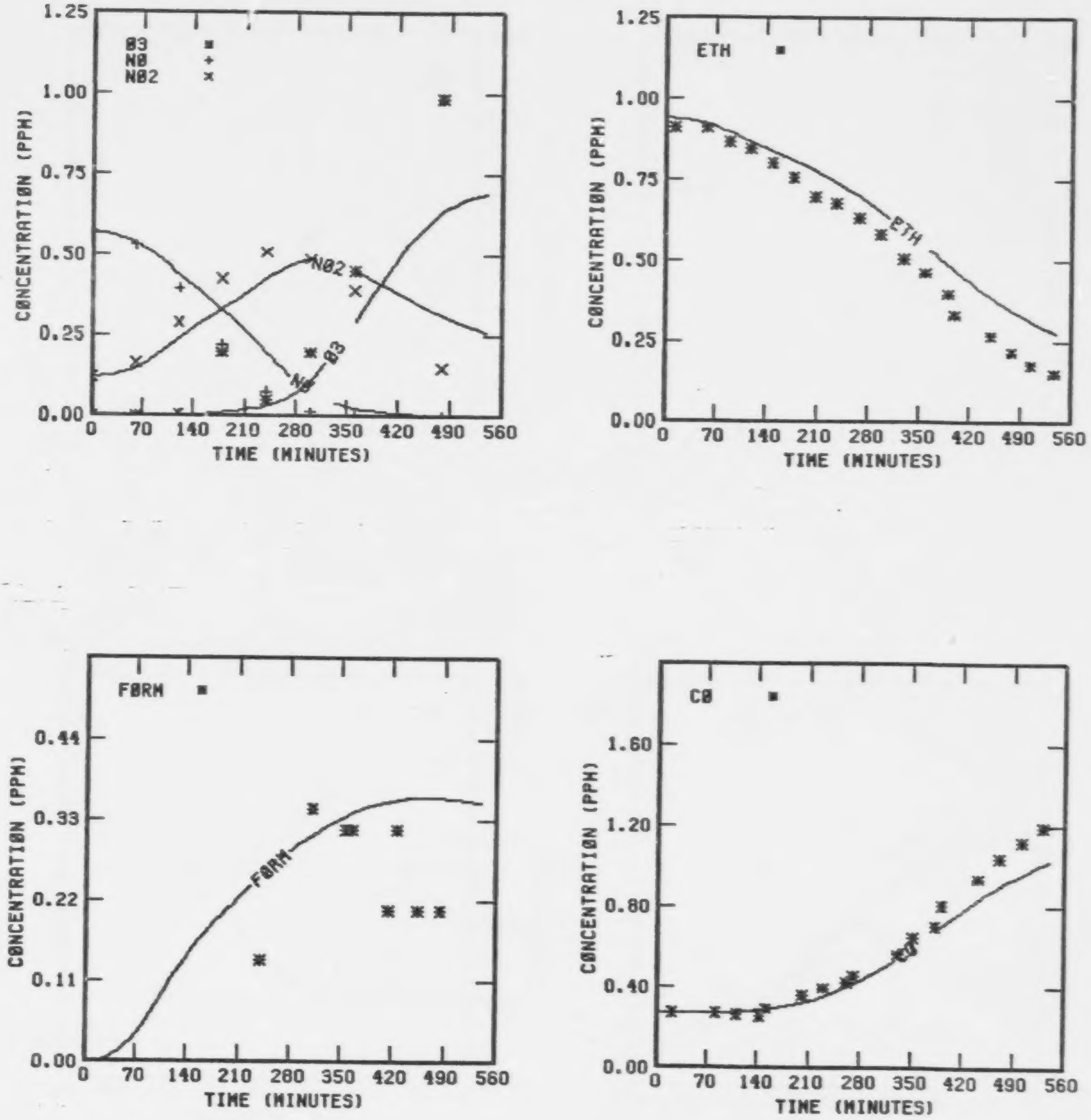

FIGURE 44 . SIMULATION RESULTS FOR
UNCR 91978

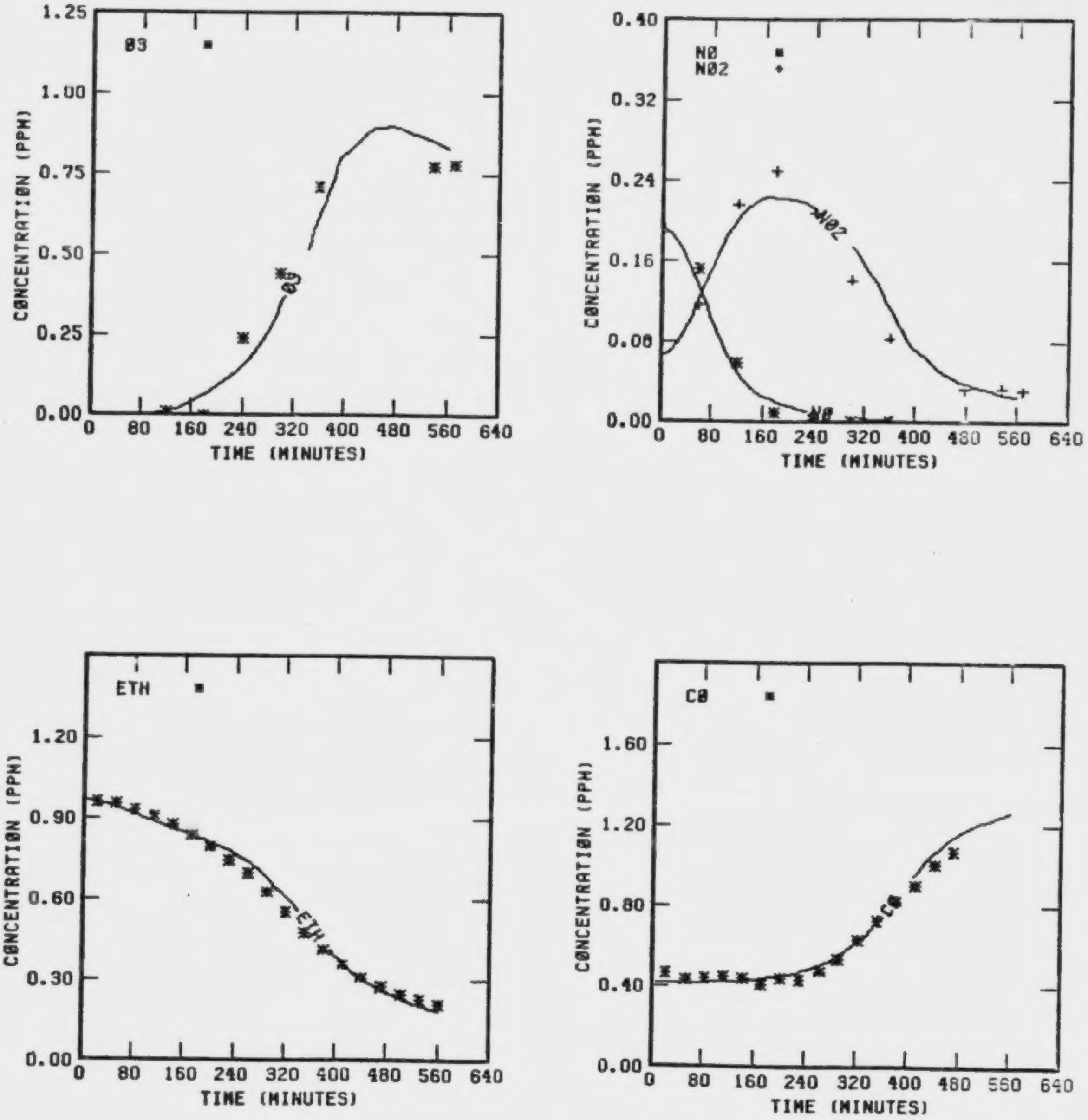

FIGURE 45 . SIMULATIØN RESULTS FØR
UNCR 92178

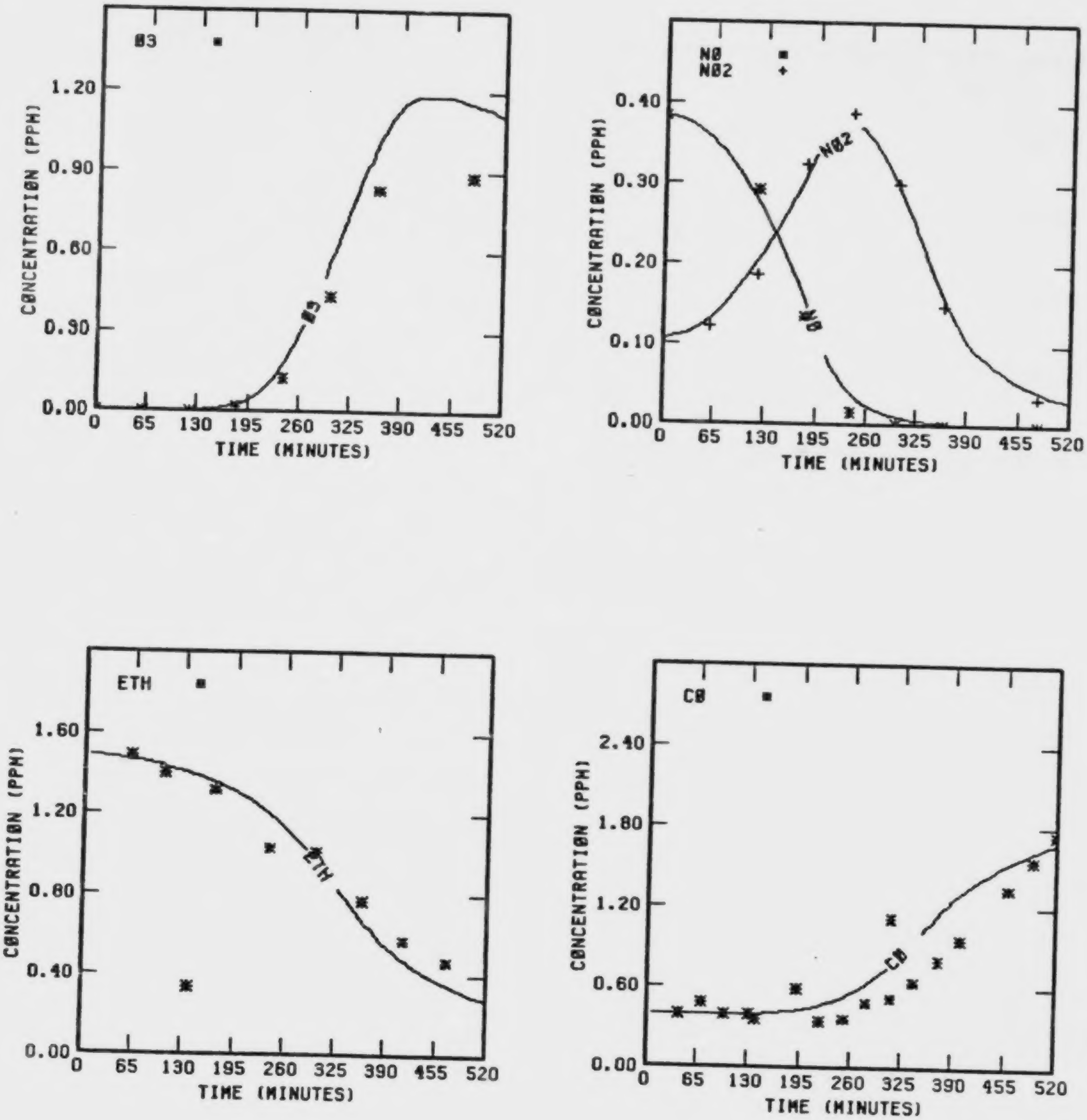

FIGURE 46 . SIMULATION RESULTS FOR UNCB 100278

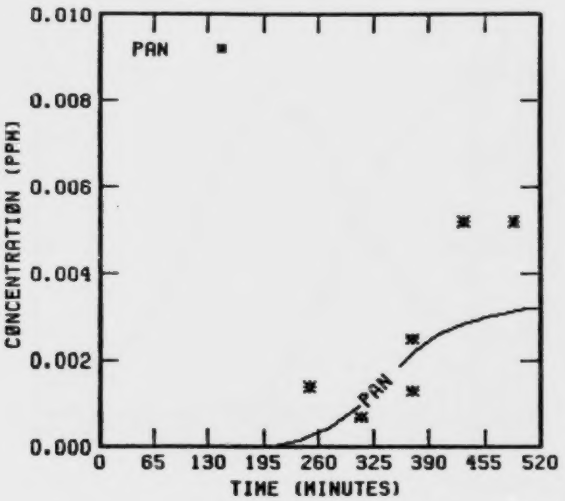

FIGURE 46 . (Concluded)

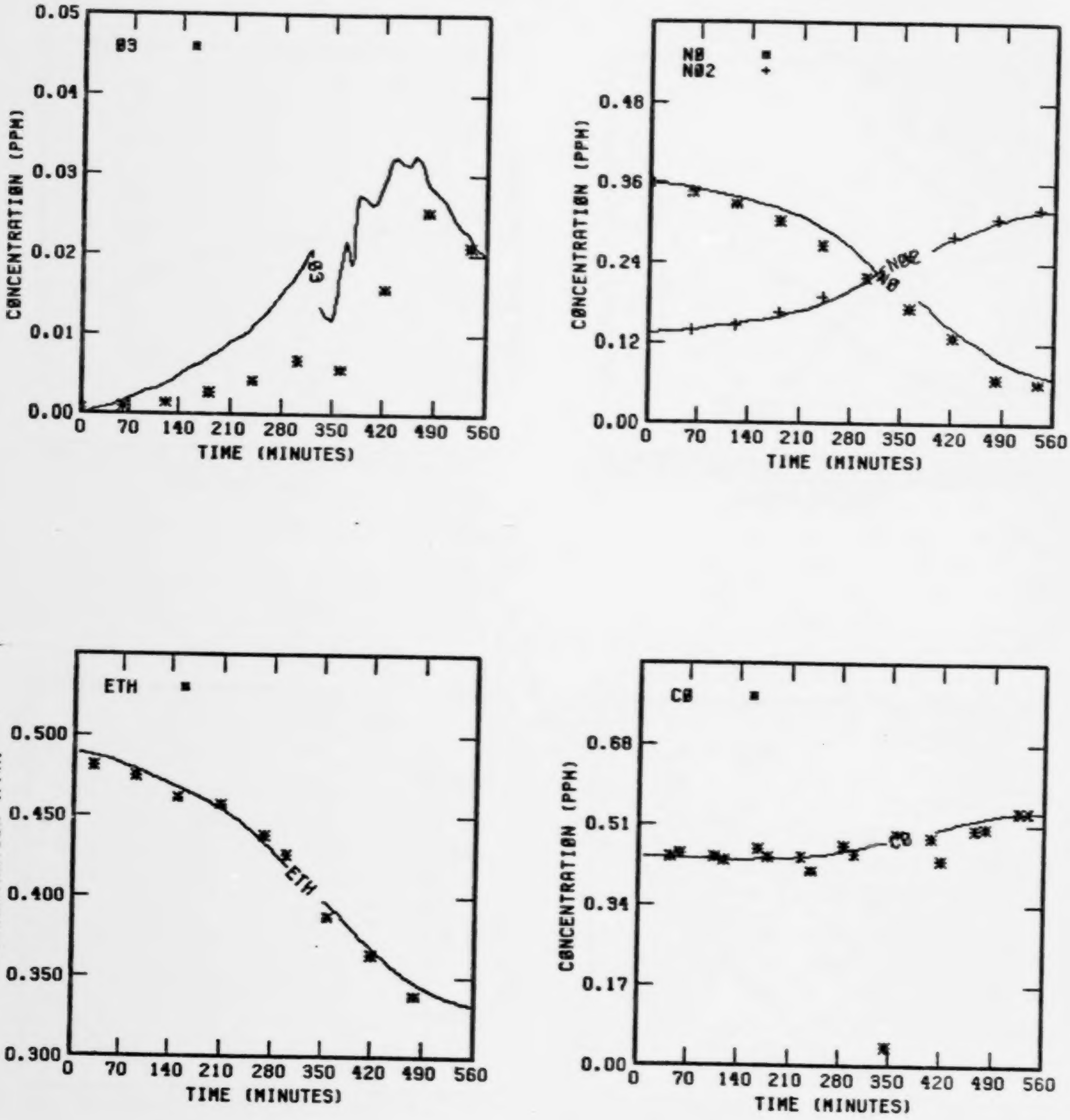

FIGURE 47 . SIMULATION RESULTS FOR
UNCR 100378

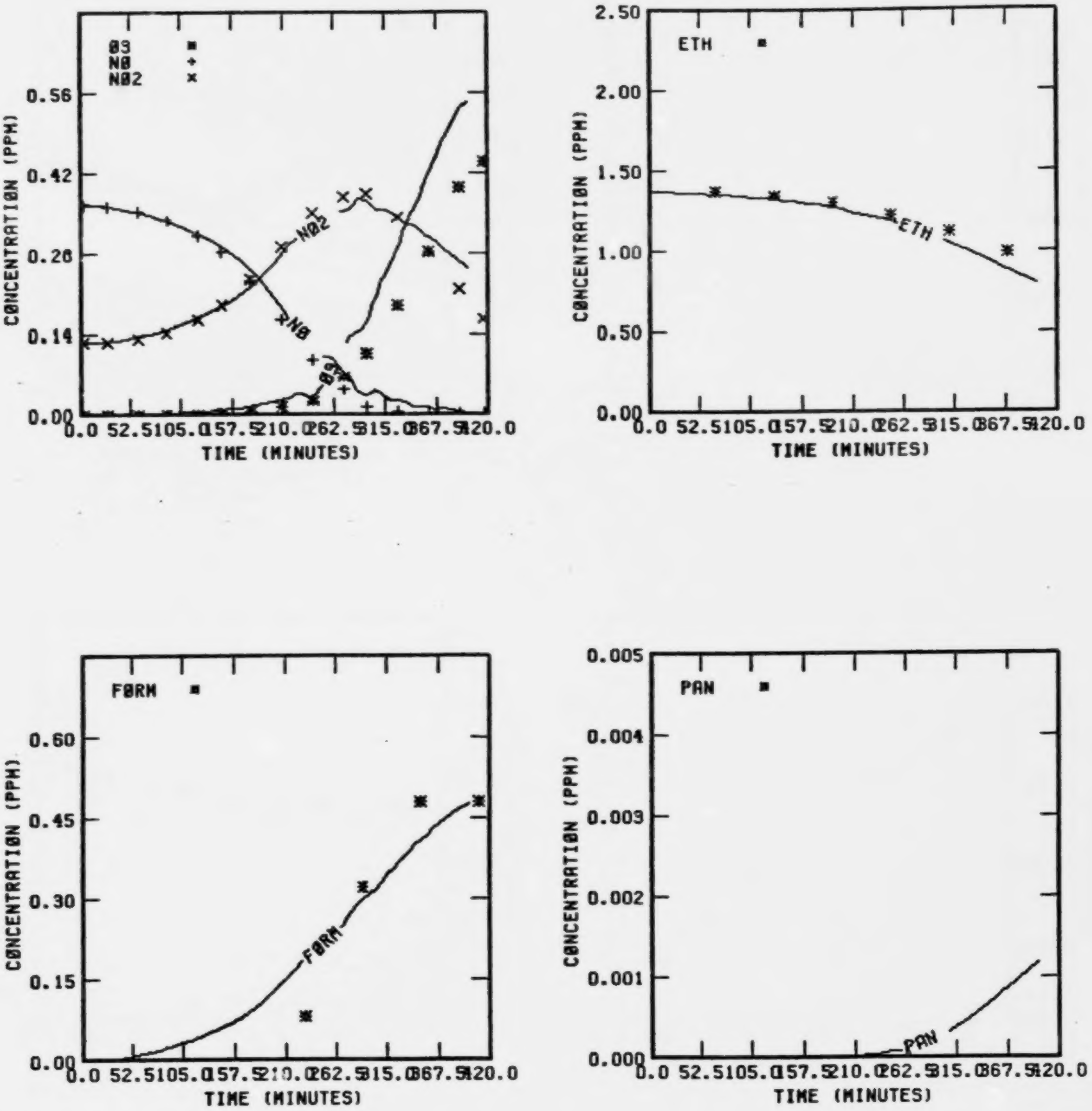

FIGURE 48 . SIMULATIØN RESULTS FØR
UNCB 101778

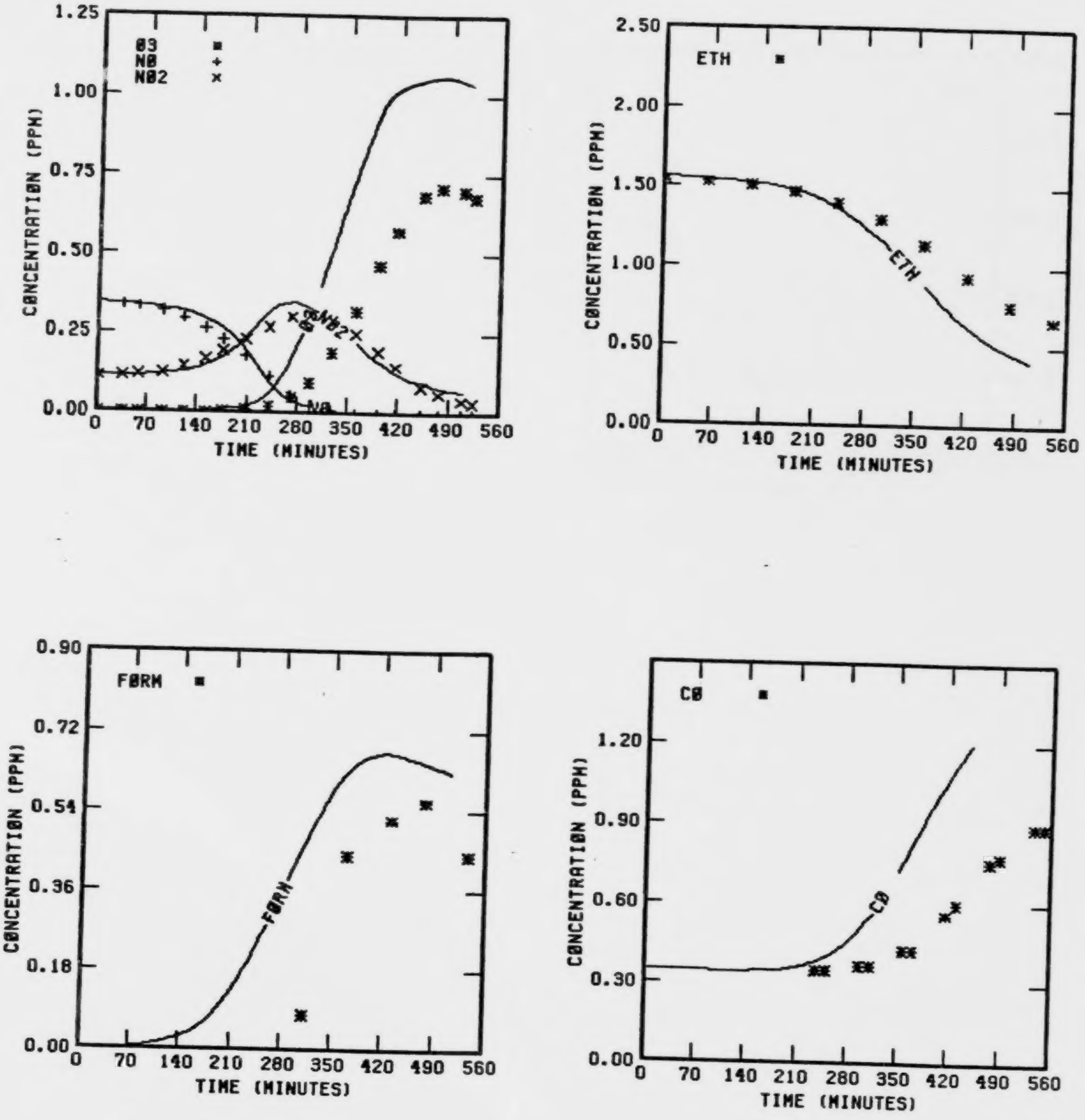

FIGURE 49 . SIMULATION RESULTS FOR
UNCR 101878

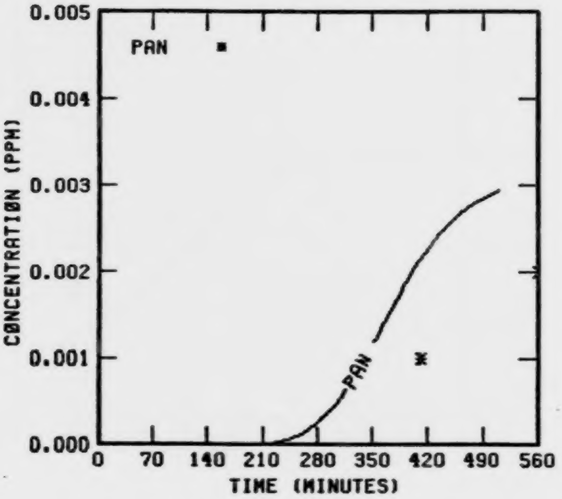

FIGURE 49 . (Concluded)

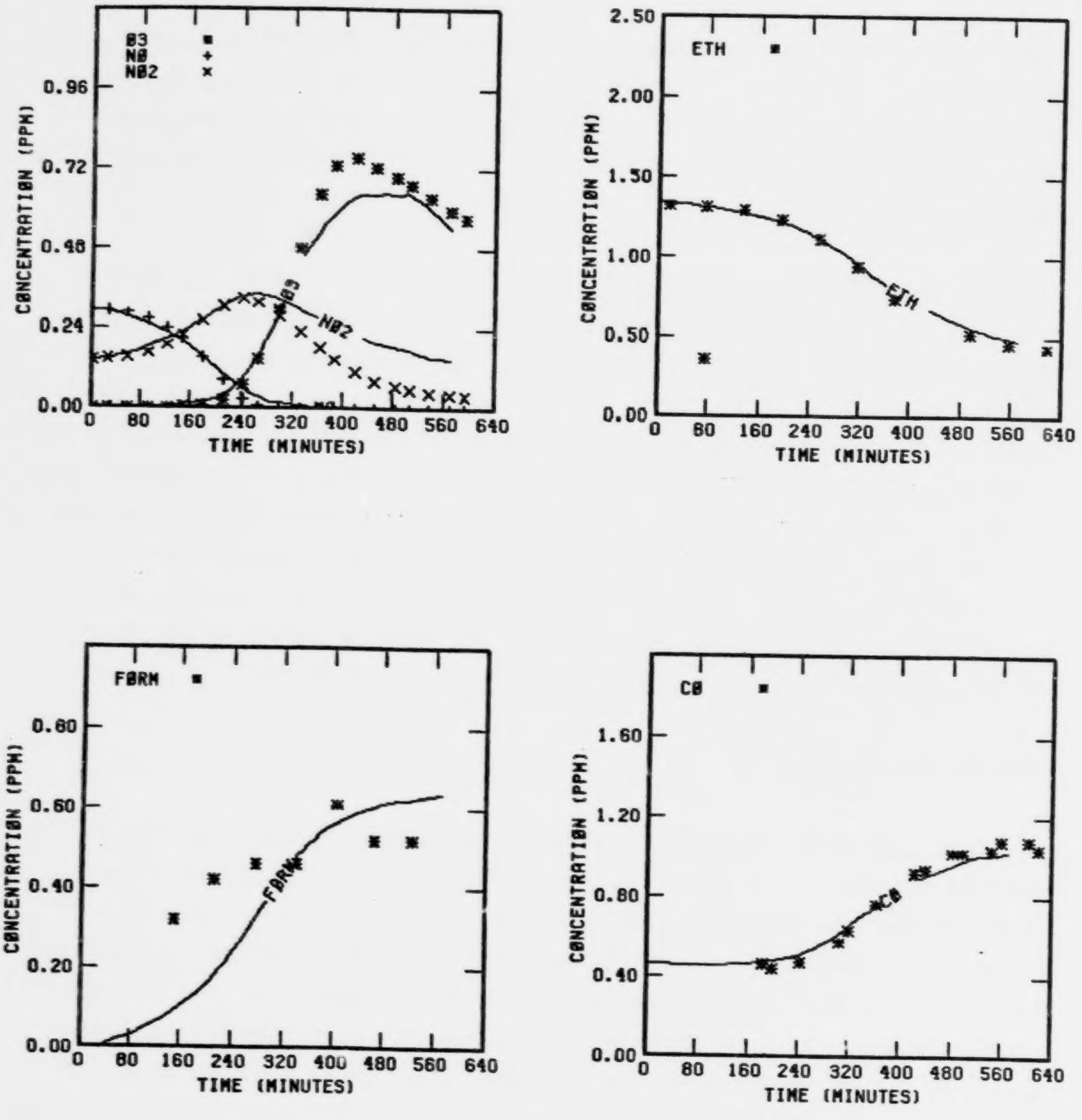

FIGURE 50 . SIMULATION RESULTS FOR
UNCB 110778

appear to be the UV data and the initial reactivity. Thus there are clear days that have low photolysis rates (e.g., 30 June 1978) and clear days that have high photolysis rates (e.g., 18 October 1978). Then there are days that have high initial reactivity (e.g., 1 July 1978) and days showing a low initial reactivity (e.g., 18 October 1977).

For the interim report of last year (Whitten et al., 1979), we had simulated six ethylene experiments in the UCR chamber. The same six experiments were included this year, but the new chemistry has reversed the problems we reported previously. Two sets of three experiments were performed; the second set used about twice the concentration of precursors as the first set, yet similar ozone maxima resulted. Last year the simulations showed too much ethylene decay in the second set but correct decay in the first set of experiments. Tables 15 and 16 show the initial conditions and results for this year while Figures 51 through 56 present the graphical results. Note that the simulations are now somewhat slow for ethylene decay in the first set and agree closely with the measurements in the second set.

ETHYLENE/ACETALDEHYDE

This combination of precursors requires essentially the same set of chemical reactions as a simulation of propylene, except for the numerical values of the rate constants involving the olefin. The proper choice of organic concentrations can control the rate of the smog chemistry so that the two sides of a dual chamber experiment have equal reactivity. Two such dual chamber experiments comparing propylene with ethylene/acetaldehyde were performed at the UNC chamber; we then simulated these experiments using our current chemical mechanisms. The initial conditions are provided in Table 17. The results are given in Table 18 and are illustrated by Figures 57 through 60. (The mechanism used for propylene will be reported in the following segment.) The results show that PAN chemistry will require further developmental work. The dual chamber experiment of 25 October 1978 shows that the acetaldehyde mechanism simulates too much PAN and, therefore, an additional pathway to PAN production is probably needed in the propylene mechanism, since the

TABLE 15. INITIAL CONDITIONS AND PHOTOLYSIS RATE CONSTANTS FOR THE UCR ETHYLENE/NO_x SMOG CHAMBER EXPERIMENTS

Run number	Initial concentration (ppm)				Photolysis rate constant (x 10^4 min^{-1})*					
	Ethylene	NO	NO_2	HONO	NO_2→NO+O	O_3→$O(^1D)$	O_3→$O(^3P)$	HONO→NO+OH·	H_2O_2→2OH·	FORM→Products†
EC-142	0.92	0.322	0.158	0.010	0.33	10	107	990	4	16
EC-143	1.95	0.39	0.11	0.012	0.33	10	107	990	4	16
EC-156	1:95	0.376	0.124	0.018	0.32	5	104	600	5	16
EC-285	1.9	0.791	0.215	0.02	0.39	5	120	1100	5	1.1
EC-286	3.758	0.708	0.237	0.02	0.39	5	120	1100	5	1.1
EC-287	3.995	0.404	0.124	0.008	0.39	5	120	1100	5	1.1

* Rate constant in min^{-1} for NO_2.

† The relationship between FORM→Products and carbonyl photolysis rate constants is discussed elsewhere.

TABLE 16. UCR ETHYLENE EXPERIMENTS--SIMULATIONS AND MEASUREMENTS

Exp. no.	Initial [NO_x] (ppm)	Initial NO_2/NO_x ratio	Initial HC/NO_x ratio (ppmC/ppm)	Maximum [O_3] (ppm)*		Difference in O_3 maxima (percent)†	Time to maximum [O_3] (minutes)§		Difference in times to O_3 maxima (percent)†	Maximum [NO_2] (ppm)*		Difference in NO_2 maxima (percent)†	Time to maximum [NO_2] (minutes)§		Difference in times to NO_2 maxima (percent)†
				Sim.	Meas.		Sim.	Meas.		Sim.	Meas.		Sim.	Meas.	
EC-142	0.48	0.33	3.8	0.71	0.77	-8	>300	>330	9	0.38	0.30	27	100	100	0
EC-143	0.50	0.22	7.8	0.87	1.07	-19	170	170	0	0.42	0.38	11	65	60	8
EC-156	0.50	0.25	7.8	0.78	1.03	-24	170	150	13	0.41	0.36	14	50	50	0
EC-285	1.0	0.21	3.8	0.86	0.75	17	>360	>360	--	0.75	0.70	7	150	150	0
EC-286	0.95	0.25	7.95	1.17	1.06	10	190	160	19	0.80	0.75	7	60	60	0
EC-287	0.53	0.24	15.1	1.07	0.92	11	120	100	20	0.46	0.45	3	45	45	0

O_3 maxima: average difference = -2 percent, standard deviation = ±17 percent.

NO_2 maxima: average difference = 12 percent, standard deviation = ±8 percent

* Maximum one-hour-average concentration.

† [(Simulated value - Measured value)/Measured value] x 100.

§ Time from beginning of irradiation to beginning of the period during which the maximum one-hour-average concentration occurred.

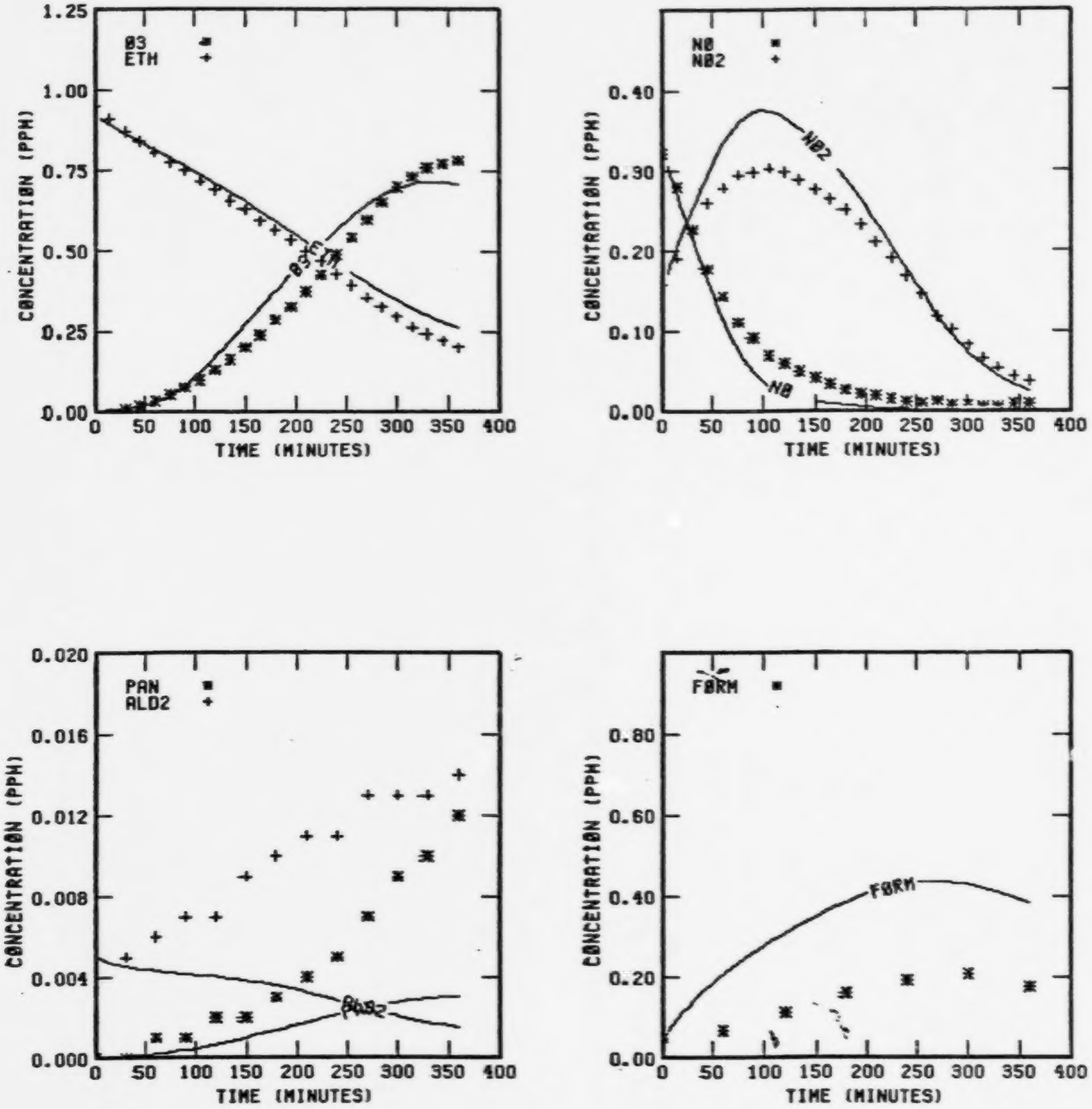

FIGURE 51 . SIMULATION RESULTS FOR
EC-142

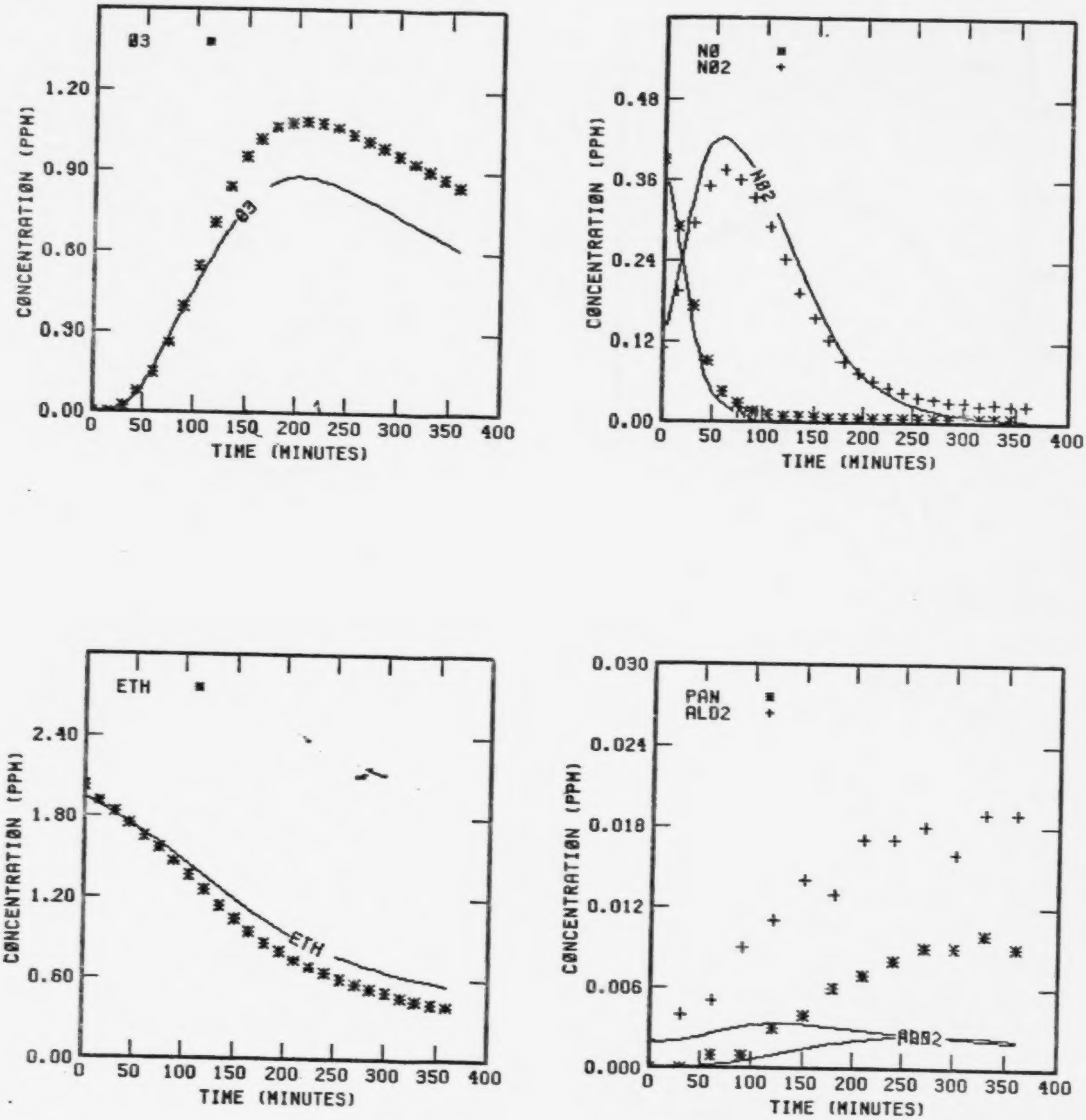

FIGURE 52 . SIMULATION RESULTS FOR
EC-143

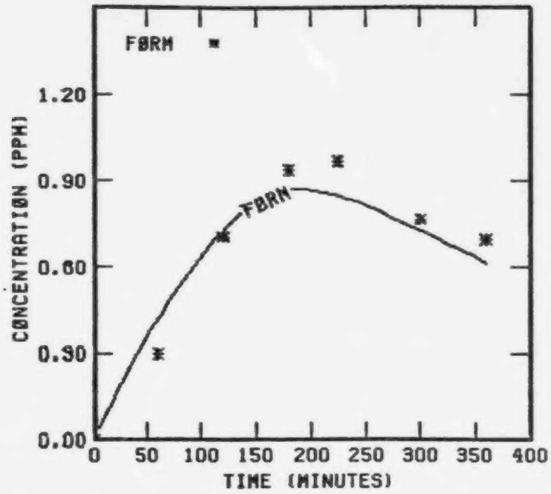

FIGURE 52 (Concluded)

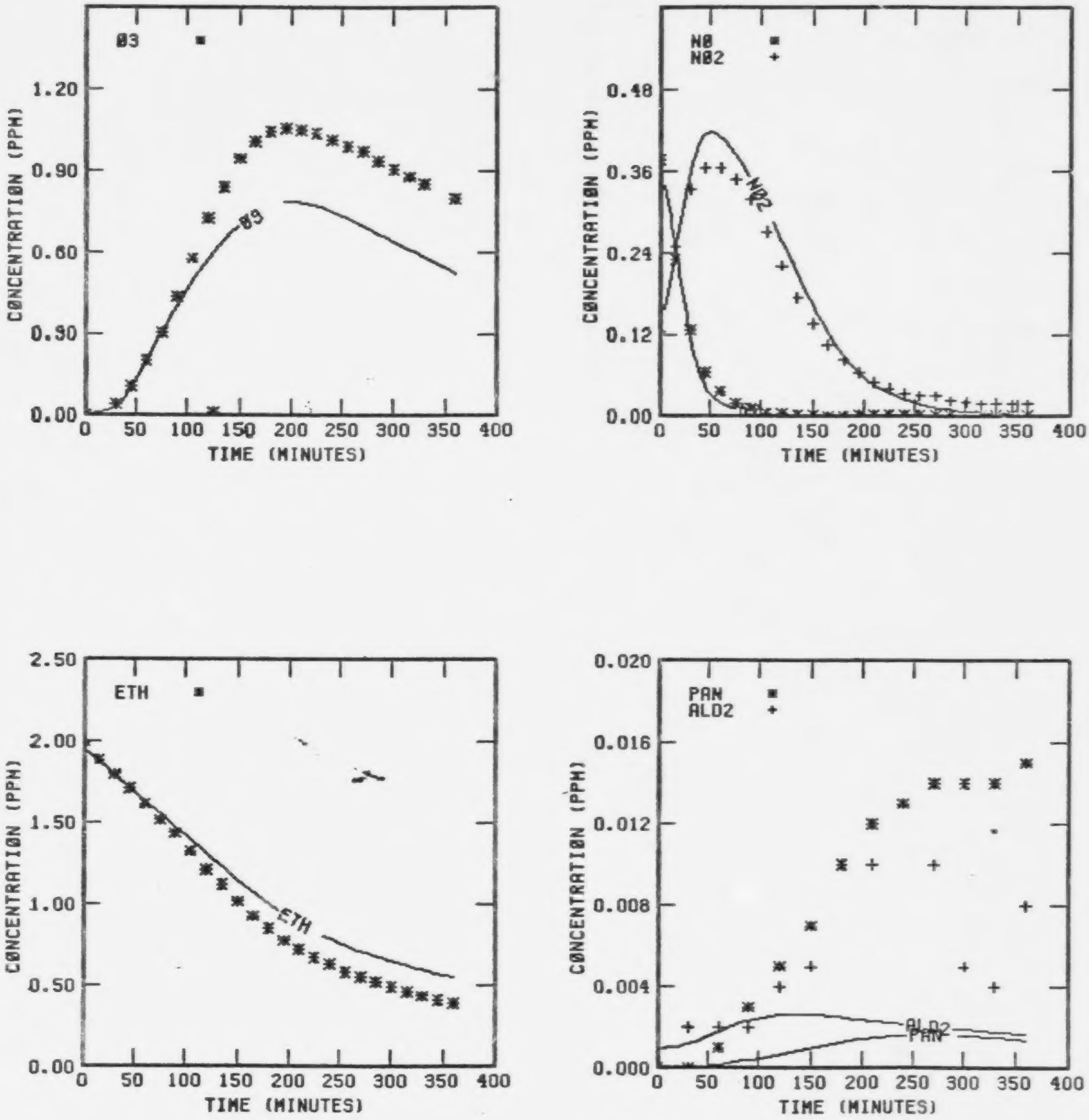

FIGURE 53 . SIMULATION RESULTS FOR EC-156

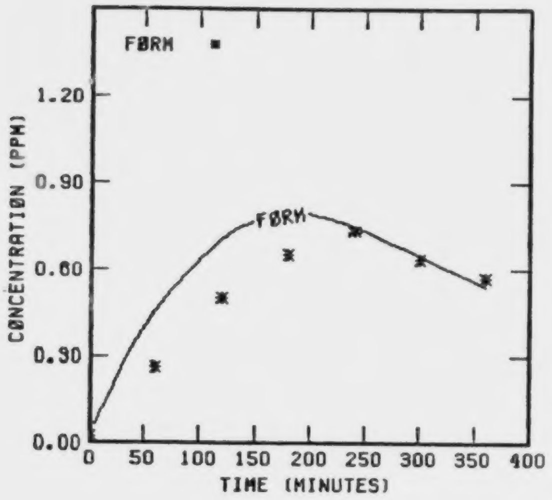

FIGURE 53 . (Concluded)

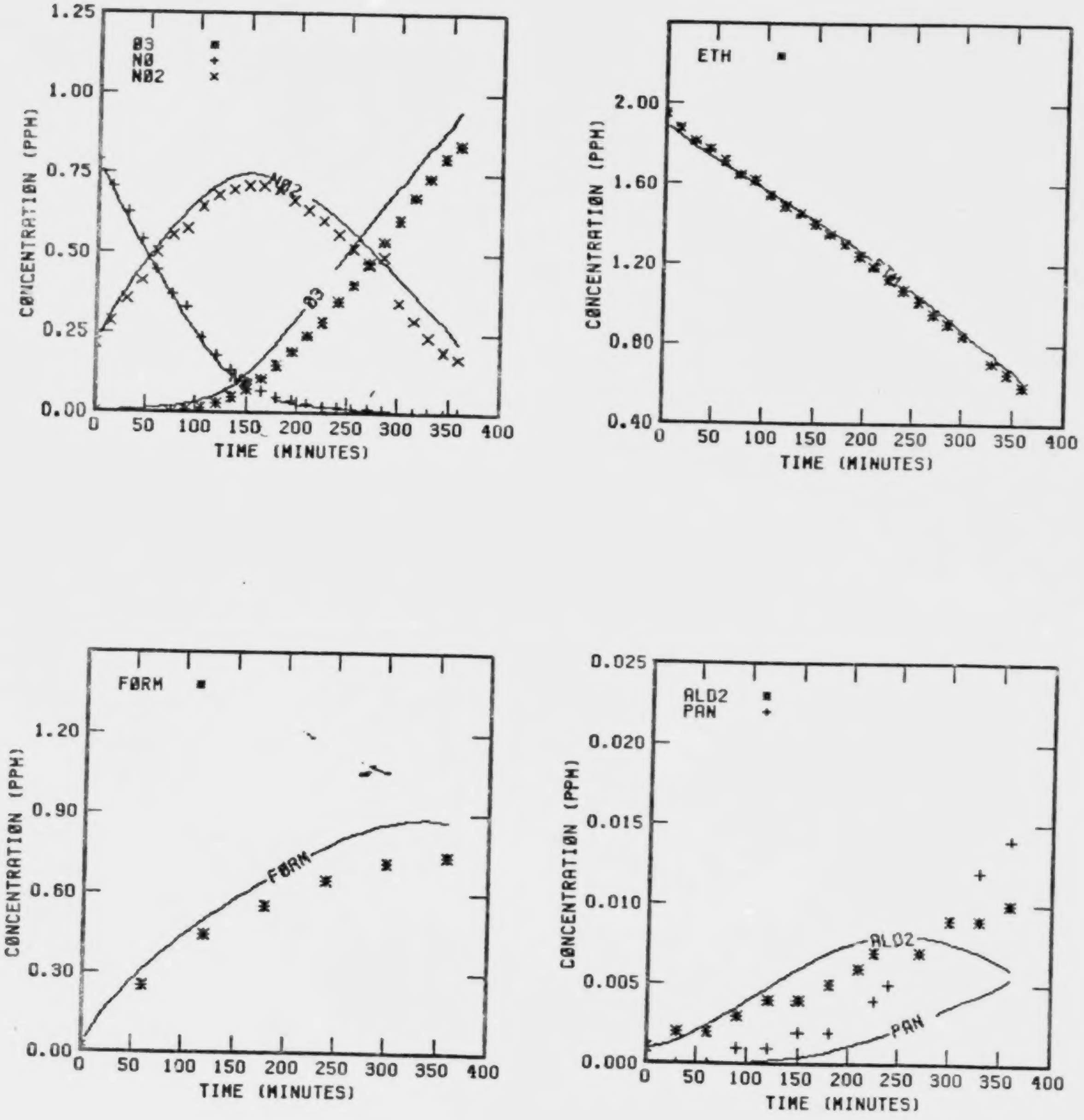

FIGURE 54 . SIMULATION RESULTS FOR
EC-285

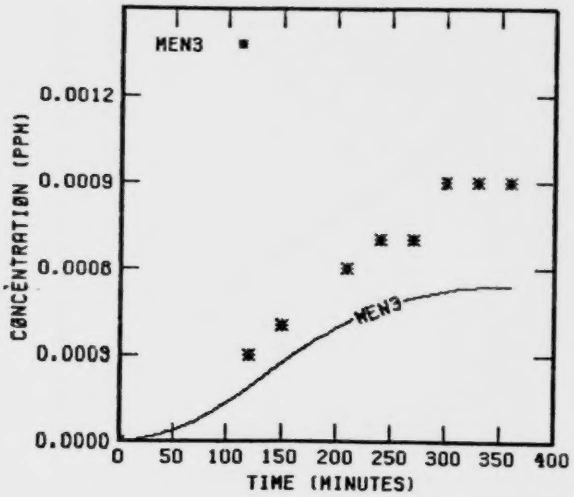

FIGURE 54. (Concluded)

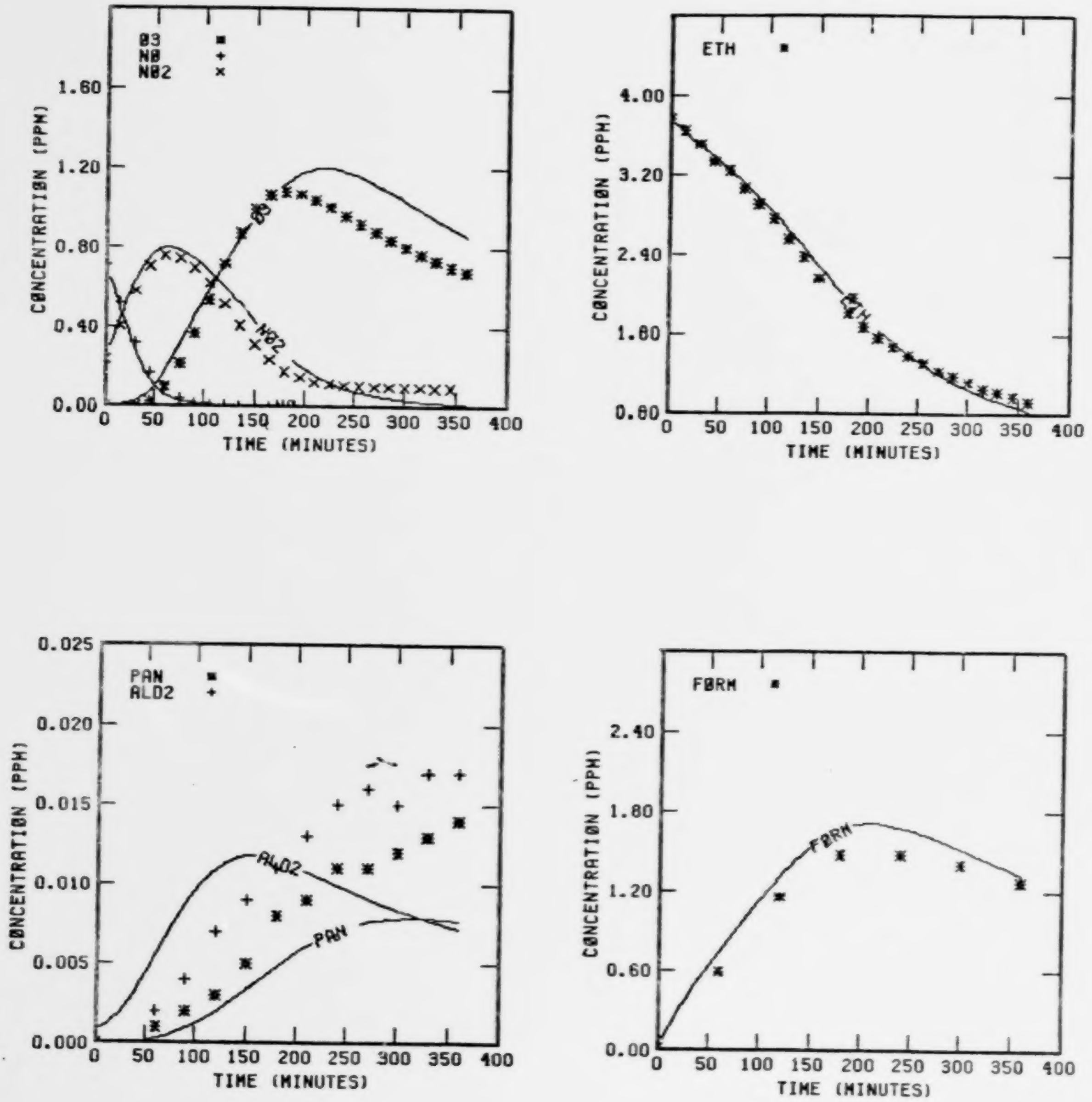

FIGURE 55 . SIMULATIØN RESULTS FØR
EC-286

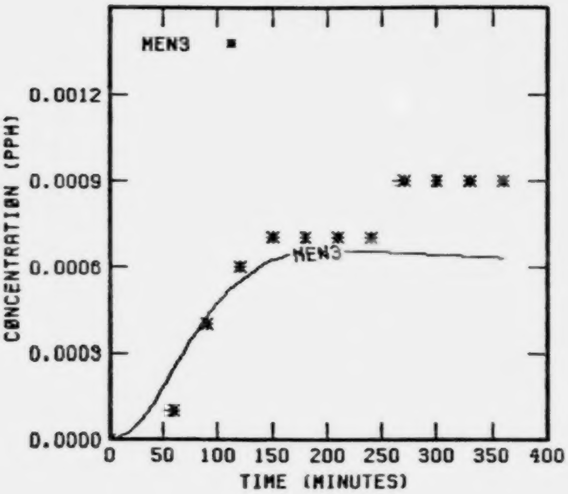

FIGURE 55 . (Concluded)

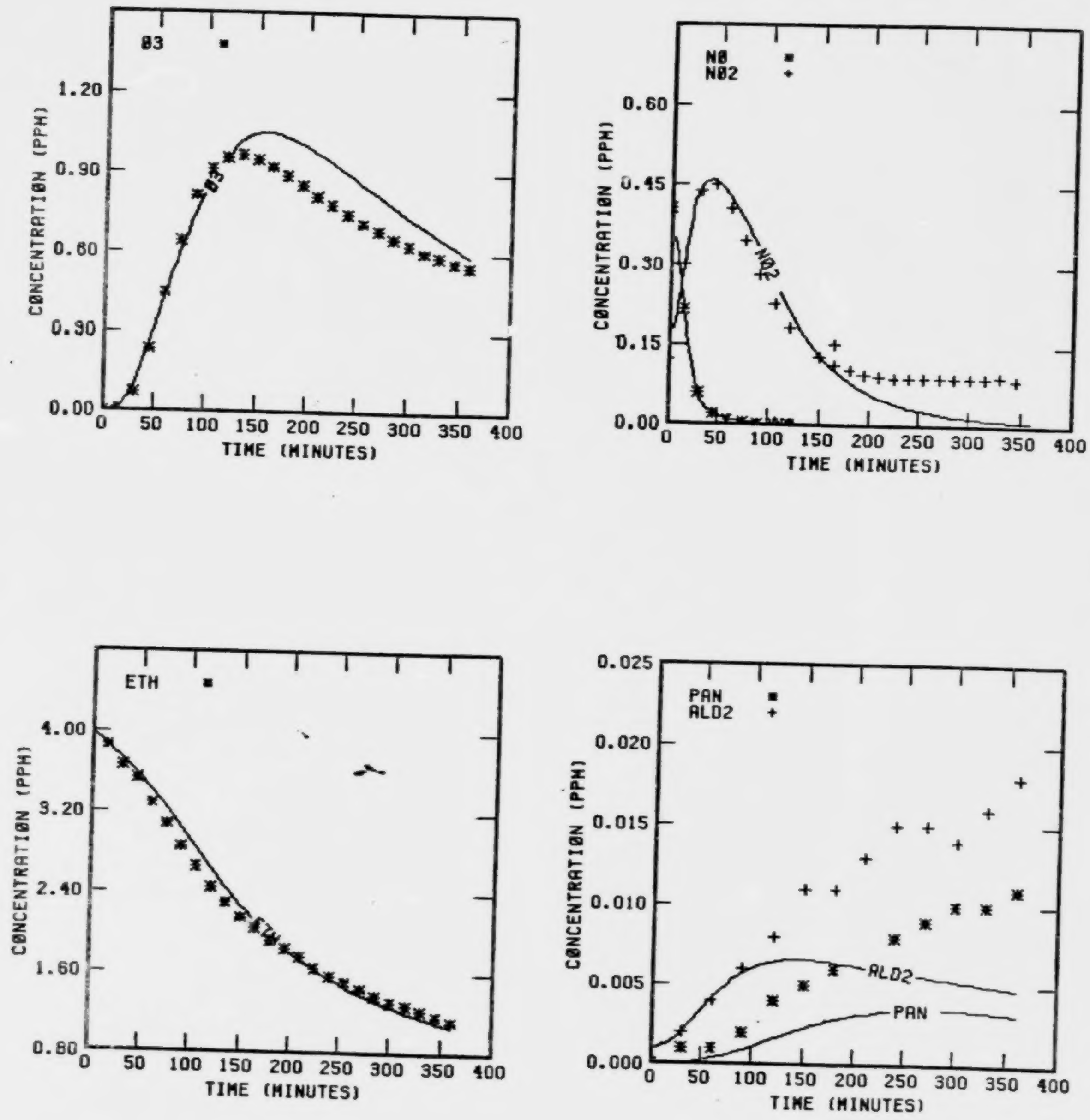

FIGURE 56 . SIMULATIØN RESULTS FØR
EC-287

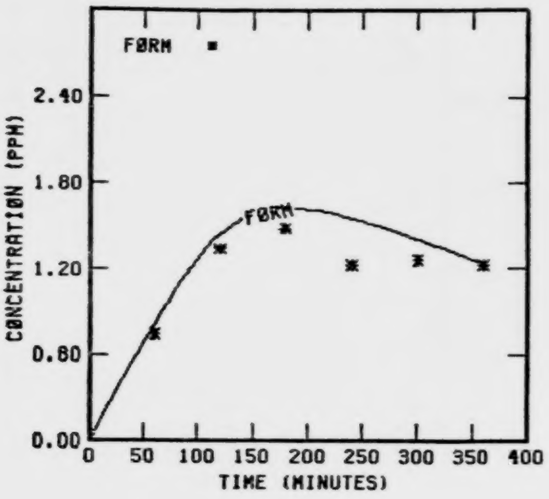

FIGURE 56 . (Concluded)

TABLE 17. INITIAL CONDITIONS FOR UNC ETHYLENE/ACETALDEHYDE EXPERIMENTS AND OTHER SIDE PROPYLENE/NO_x EXPERIMENT

Date	Chamber Side	Sky Conditions	Beginning time of simulation	Initial Concentrations (ppm)							ALD + hν Constant
				CH_3CHO·	Ethylene	Propylene	NO	NO_2	HONO	H_2O	
10/12/78	Red	Clear	7:24	.63	.0985	--	.364	.115	.004	2×10^4	1.0*
10/12/78	Blue	Clear	7:24	--	--	.443	.364	.115	--	1.6×10^4	1.0*
10/25/78	Red	Clear	7:14	.58	.0985	--	.341	.103	.002	2×10^4	1.0*
10/25/78	Blue	Clear	7:14	--	--	.408	.338	.104	.009	1.6×10^4	1.0*

* UV data used in simulations instead of TSR.

TABLE 18. UNC ETHYLENE/ACETALDEHYDE AND PROPYLENE EXPERIMENTS--SIMULATIONS AND MEASUREMENTS

Date	Chamber Side	Initial $[NO_x]$	Initial NO_2/NO_x	Initial HC/NO_x (ppmC/ppm)	Maximum $[O_3]$		Difference in \O_3 maxima	Time to maxima O_3 (min)		Difference in Time to O_3 maxima
					Sim.	Meas.		Sim.	Meas.	
10/12/78	Red	.479	.24	3.04	.25	.24	4	490	490	0
10/12/78	Blue	.479	.24	2.77	.34	.39	-13	450	>490	--
10/25/78	Red	.444	.23	3.06	.15	.14	7	490	490	0
10/25/78	Blue	.442	.24	2.77	.23	.23	0	480	>560	--

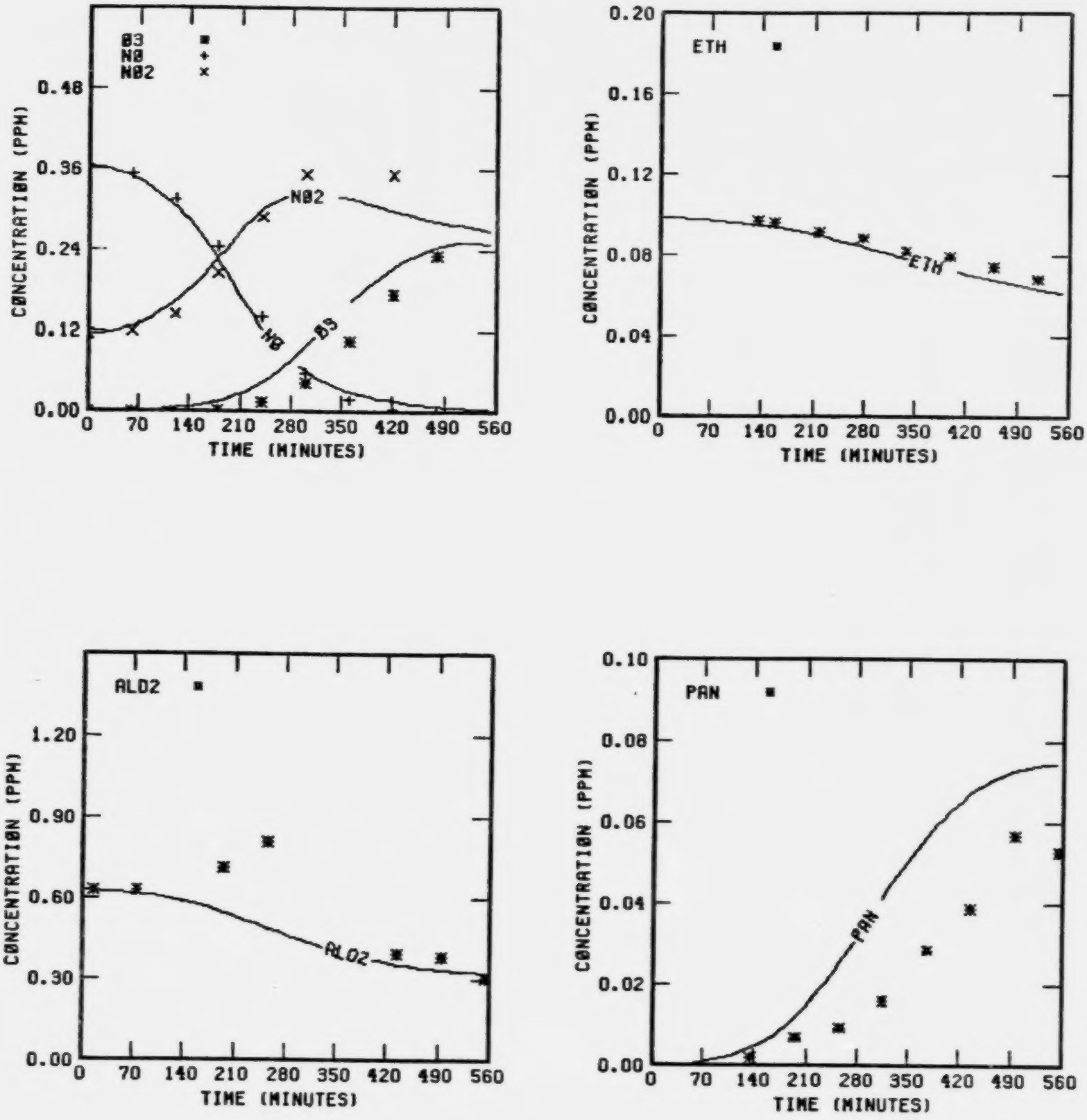

FIGURE 57 . SIMULATION RESULTS FOR
UNCR 101278

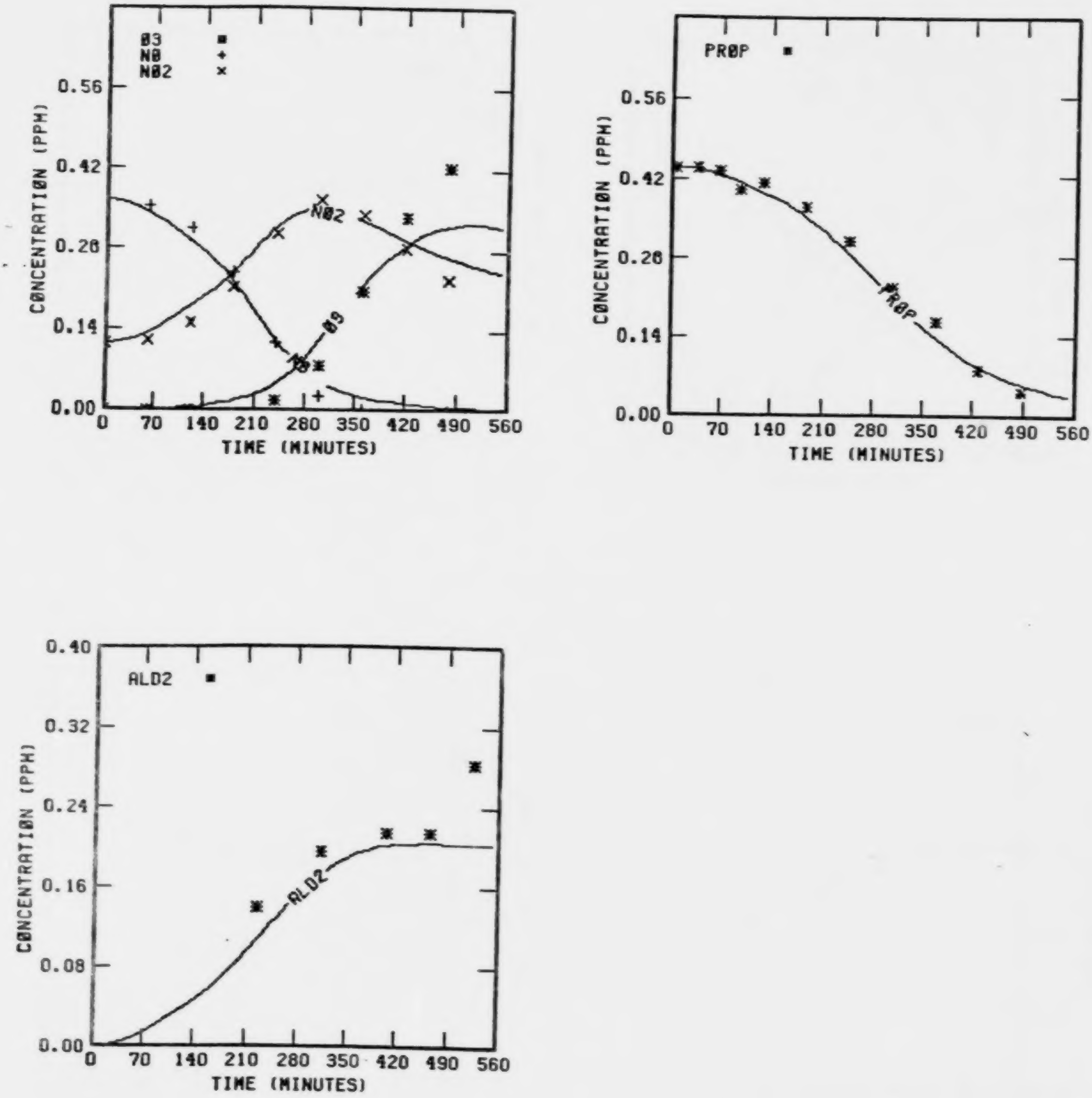

FIGURE 58. SIMULATION RESULTS FOR
UNCB 101278

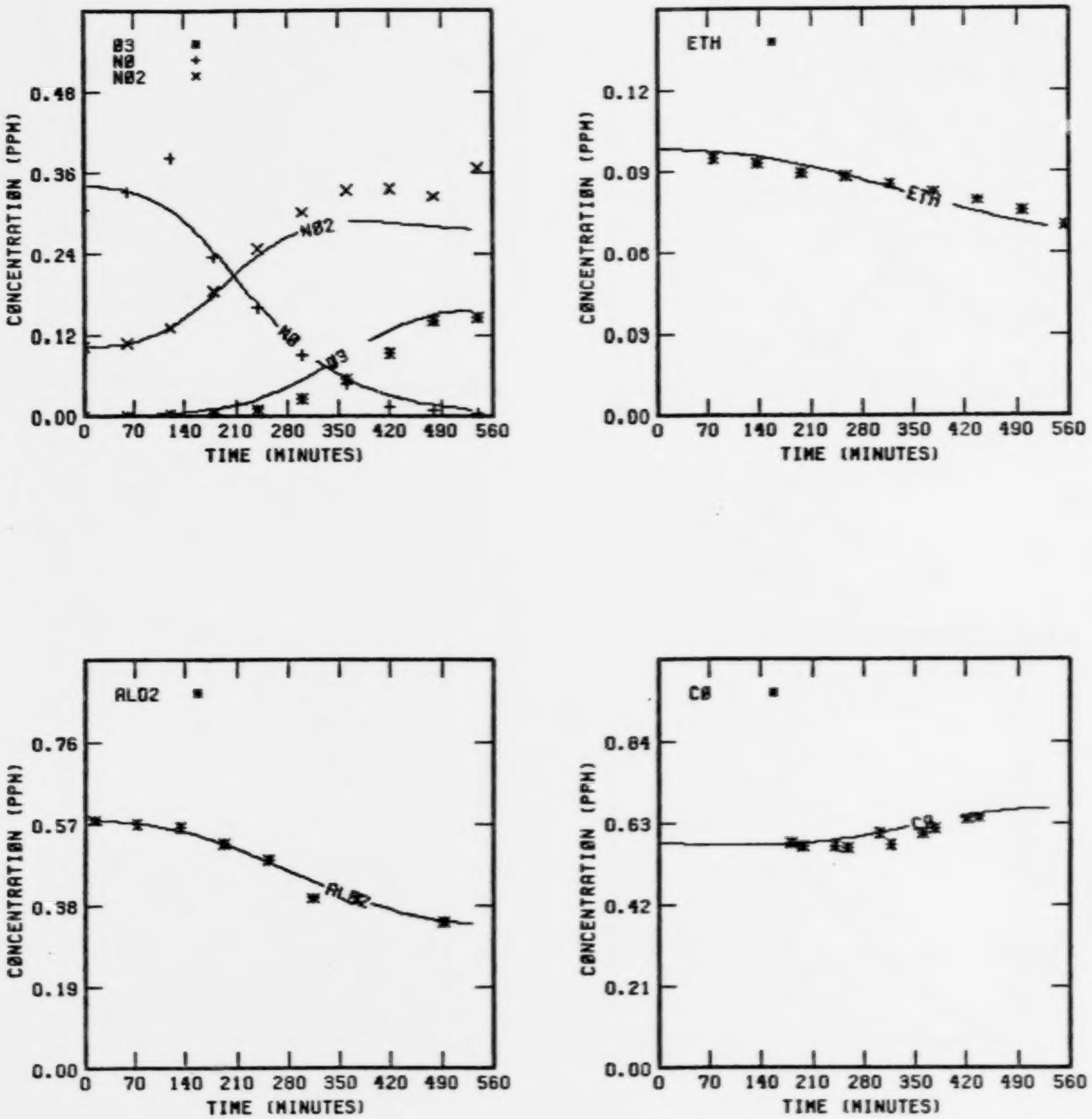

FIGURE 59 . SIMULATION RESULTS FOR UNCR 102578

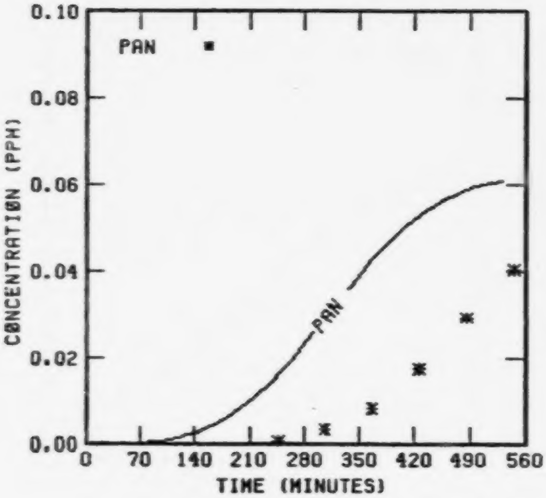

FIGURE 59 . (Concluded)

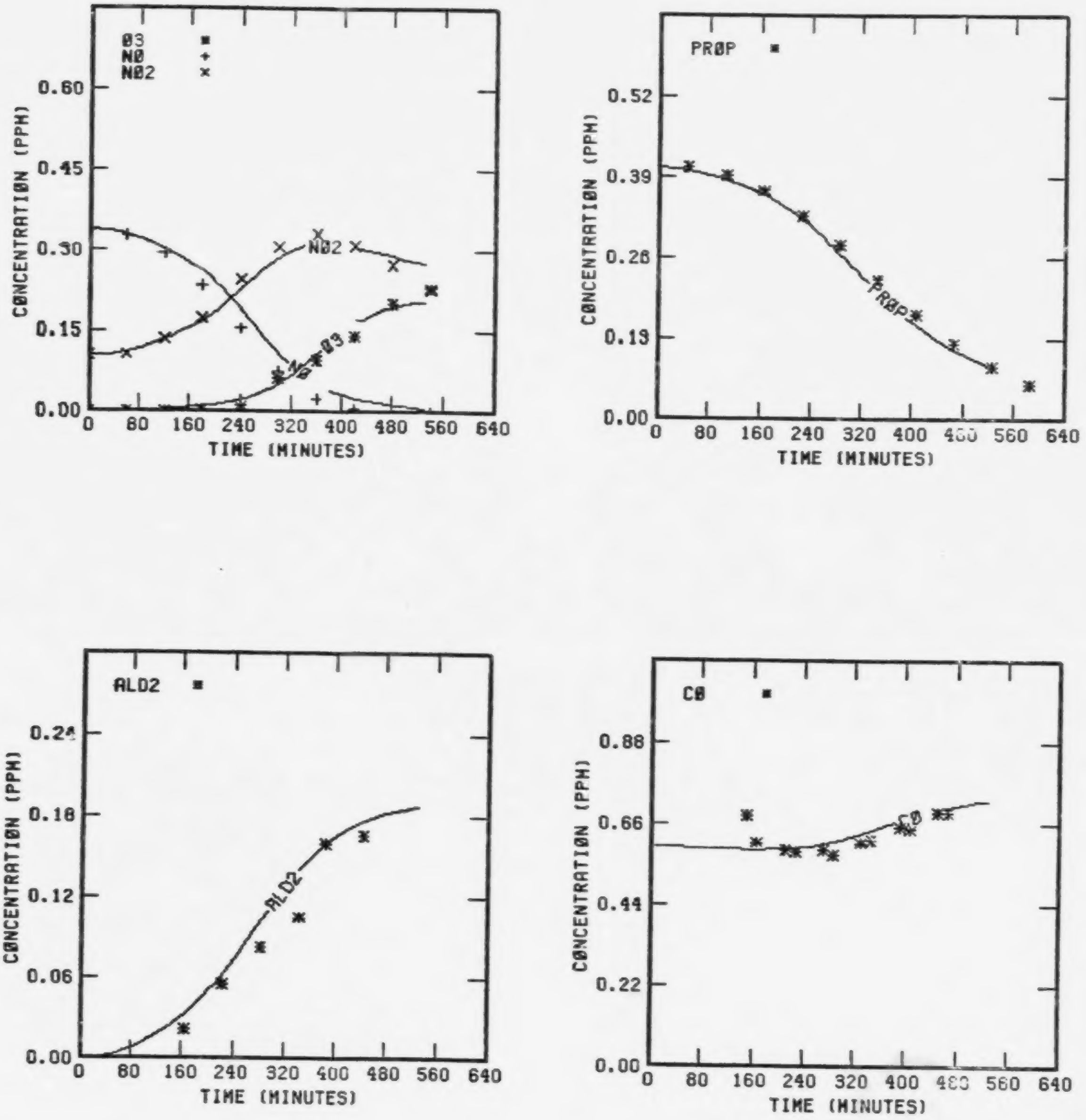

FIGURE 60 . SIMULATION RESULTS FOR
UNCB 102578

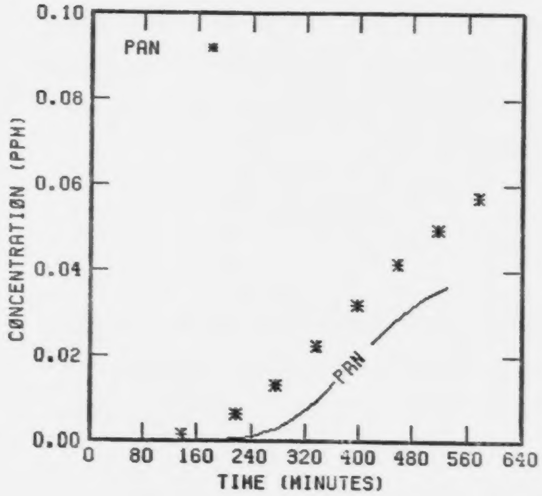

FIGURE 60. (Concluded)

simulated PAN for the propylene side is too low. Involvement of the methyl-substituted Criegee intermediate with NO_x may be implicated, or at least some species must be involved that does not exist in the ethylene/acetaldehyde chemistry.

PROPYLENE

Most of the experiments for which we have smog chamber data have used propylene either exclusively or in mixtures. Traditional mechanism development has, in the recent past, concentrated on this molecule. However, our own recent experience indicates that reactions in the inorganic, formaldehyde, and acetaldehyde parts of the propylene chemistry may require more thorough validation before significant changes in the chemistry particular to propylene can be justified. The present report demonstrates the performance of the current propylene mechanism (Table 19) on 15 experiments in the UCR chamber and 28 experiments in the UNC chamber. In the course of modeling these experiments, four changes were made to the propylene mechanism reported last year (Whitten et al., 1979). However, the main changes in the overall chemistry used in the simulations were produced by the temperature and water dependent PNA reactions. The four reactions that were changed are described in the following subsections.

$O(^3P)$ + Propylene

Previously, this reaction resulted in either radicals or propylene oxide, in equal proportions. Currently, we have changed the ratio of these products, adding proprionaldehyde in a ratio of 1.4:3:1.0. This change reduced the number of radicals produced in the early stages of smog chamber experiments, involving propylene, at the UNC facility. Typically, we use minor amounts of assumed HONO to help initiate the photochemistry in computer simulations of smog chamber experiments. This reduction of radical production from propylene brings the typical HONO required for propylene experiments in line with simulations of other organics. A higher yield of radicals caused the simulation of some propylene experiments in the UNC chamber to show too much early reactivity although zero HONO was used.

TABLE 19. REACTIONS OF PROPYLENE*

Reaction	Rate constant ($ppm^{-1}min^{-1}$)
$CH_3CH{=}CH_2 + O \xrightarrow{2O_2} CH_3O_2^{\cdot} + CH_3C(O)O_2^{\cdot}$	1.4×10^{3}**
$CH_3CH{=}CH_2 + O \rightarrow$ 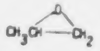	3×10^{3}§§
$CH_3CH = CH_2 + O \rightarrow CH_3CH_2CHO$	1×10^{3}
$CH_3CH{=}CH_2 + OH\cdot \xrightarrow{O_2} CH_3CH(O_2^{\cdot})CH_2OH$	4.2×10^{4}
$CH_3CH{=}CH_2 + NO_3 \rightarrow NO_2 + \text{Products}$	7.82
$CH_3CH{=}CH_2 + O_3 \rightarrow HCHO + CH_3CHO_2^{\cdot}$	7.5×10^{-3}
$CH_3CH{=}CH_2 + O_3 \rightarrow CH_3CHO + CH_2O_2^{\cdot}$	7.5×10^{-3}
$CH_2O_2^{\cdot} + HCHO \rightarrow$ 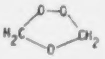	2×10^{3}
$CH_2O_2^{\cdot} + CH_3CHO \rightarrow$ 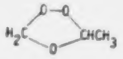	2×10^{3}
$CH_2O_2^{\cdot} + NO \rightarrow NO_2 + HCHO$	1.2×10^{4}
$CH_2O_2^{\cdot} + NO_2 \rightarrow NO_3 + HCHO$	3×10^{3}**
$CH_2O_2^{\cdot} \rightarrow CO + H_2 + O_2$	6.7×10^{2}†
$CH_2O_2^{\cdot} \rightarrow CO_2 + H_2$	1.8×10^{2}†
$CH_2O_2^{\cdot} \rightarrow 2HO_2^{\cdot} + CO_2$	9×10^{1}†
$CH_2O_2^{\cdot} \rightarrow HC(O)OH$	6×10^{1}†
$CH_3CHO_2^{\cdot} + HCHO \rightarrow$ 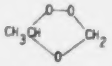	2×10^{3}
$CH_3CHO_2^{\cdot} + CH_3CHO \rightarrow$ 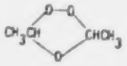	2×10^{3}
$CH_3CHO_2^{\cdot} + NO \rightarrow NO_2 + CH_3CHO$	1.2×10^{4}
$CH_3CHO_2^{\cdot} + NO_2 \rightarrow NO_3 + CH_3CHO$	3×10^{3} **

TABLE 19. (Concluded)

Reaction	Rate constant (ppm^{-1}min^{-1})
$CH_3CHO_2^{\cdot} \rightarrow CO_2 + CH_4$	$1.5 \times 10^{2\dagger}$
$CH_3CHO_2^{\cdot} \xrightarrow{O_2} CH_3O_2^{\cdot} + CO + OH\cdot$	$3.4 \times 10^{2\dagger}$
$CH_3CHO_2^{\cdot} \xrightarrow{2O_2} CH_3O_2^{\cdot} + CO_2 + HO_2^{\cdot}$	$4.25 \times 10^{2\dagger}$
$CH_3CHO_2^{\cdot} \xrightarrow{O_2} CH_3O\cdot + CO + HO_2^{\cdot}$	$8.5 \times 10^{1\dagger}$
$CH_3CH_2CHO + h\nu \xrightarrow{2O_2} CH_3CH_2O_2^{\cdot} + HO_2^{\cdot} + CO$	Experimental†
$CH_3CH_2CHO + OH\cdot \xrightarrow{O_2} CH_3CH_2C(O)O_2^{\cdot} + H_2O$	2.4×10^4
$CH_3CH_2C(O)O_2^{\cdot} + NO \xrightarrow{O_2} NO_2 + CH_3CH_2O_2^{\cdot} + CO_2$	3.8×10^3
$CH_3CH(O_2^{\cdot})CH_2OH + NO \rightarrow NO_2 + CH_3CH(O\cdot)CH_2OH$	1.2×10^4
$CH_3CH_2O_2^{\cdot} + NO \rightarrow NO_2 + CH_3CH_2O\cdot$	1.2×10^4
$CH_3CH_2O_2^{\cdot} + NO \rightarrow CH_3CH_2ONO_2$	1×10^2
$CH_3CH(O\cdot)CH_2OH \xrightarrow{O_2} CH_3CHO + HCHO + HO_2^{\cdot}$	$3 \times 10^{5\dagger}$
$CH_3CH_2O\cdot + O_2 \rightarrow CH_3CHO + HO_2^{\cdot}$	3.3
$CH_3CH_2C(O)O_2^{\cdot} + HO_2^{\cdot} \rightarrow CH_3CH_2C(O)O_2H + O_2$	1.5×10^3
$CH_3CH(O_2^{\cdot})CH_2OH + HO_2^{\cdot} \rightarrow CH_3CH(O_2H)CH_2OH + O_2$	1.5×10^3
$CH_3CH_2O_2^{\cdot} + HO_2^{\cdot} \rightarrow CH_3CH_2O_2H + O_2$	1.5×10^3
$CH_3CH_2C(O)O_2^{\cdot} + NO_2 \rightarrow CH_3CH_2C(O)O_2NO_2$	2×10^3
$CH_3CH_2C(O)O_2NO_2 \rightarrow NO_2 + CH_3CH_2C(O)O_2^{\cdot}$	$2.8 \times 10^{-2\dagger\ddagger}$
$CH_3CH_2O\cdot + NO_2 \rightarrow CH_3CH_2ONO_2$	1.5×10^4
$CH_3CH_2O\cdot + NO_2 \rightarrow CH_3CHO + HNO_2$	2.9×10^3
$CH_3CH(O_2^{\cdot})CH_2OH + CH_3CH(O_2^{\cdot})CH_2OH \rightarrow CH_3CH(O\cdot)CH_2OH + CH_3CH(O\cdot)CH_2OH + O_2$	5.0×10^2

* The inorganic, formaldehyde, and acetaldehyde reactions listed earlier must be added to construct the explicit propylene mechanism.

† Rate constant in min^{-1}.

‡ Activation energy is 12,500K; rate constant is given at 298K.

** Activation energy is -1400K; rate constant is given at 298K.

†† Activation energy is 1000K; rate constant is given at 298K.

‡‡ Activation energy is -1000K; rate constant is given at 298K.

Another change involves the minor products of propylene oxide and proprionaldehyde. Last year the proprionaldehyde was treated as an isomerization product of the propylene oxide but the resulting time profiles did not reflect the data reported from UCR. The present chemistry improves the simulation of these minor products. The reactions of proprionaldehyde were taken to be the same as those of acetaldehyde.

$HORO_2^{\cdot} + O_3$

The hydroxyl attack on propylene produces two additional products (one terminal and one internal), which apparently add an oxygen molecule to produce a peroxy radical with the hydroxyl group still attached ($HORO_2^{\cdot}$). In the interim report (Whitten et al., 1979), we speculated that these special peroxy radicals might react with ozone much faster than the known reaction of $HO_2^{\cdot}$ with ozone. This reaction reduced the NO-to-NO_2 conversions in propylene simulations at the time when ozone increases rapidly. The need for such a reaction stemmed from a tendency to generate too much ozone in simulations of propylene but not in simulations of other species such as formaldehyde, acetaldehyde, and ethylene. The chemistry associated with peroxynitric acid (PNA), particularly the present speculative reactions of PNA in wet atmospheres, accomplishes the same effect even though the reactions have been included in all the explicit studies reported here. Propylene was singled out previously because the problem of overprediction was associated primarily with a very rapid rise in ozone which appeared only in propylene experiments. However, the report last year did show one instance of a steep ozone rise for some formaldehyde experiments at very high concentrations (12 ppm). In this case, PNA chemistry was effective in reducing the ozone in the simulations. Nevertheless, the speculative reaction of $HORO_2^{\cdot}$ with ozone has presently been eliminated from the propylene chemistry.

Criegee Intermediate + NO_2

The original estimates for the rate constants used for these reactions were based on early measurements of the HO_2 reaction with NO_2 at low pressures. Current estimates for this reaction are much slower and we have lower rate constants to reflect this. However, study of the present computer simulations indicates that this reaction is often the major pathway for the Criegee intermediates; we therefore recommend that the products of this reaction and the rate constant be measured in the near future.

$CH_3O_2^{\cdot} + HO_2^{\cdot}$

The rate constant for this reaction was lowered to the value recommended in the 1979 NASA review (DeMore et al., 1979). However, the reaction is not very important in the present simulations and the recommended rate constant is merely the geometric mean of the rate constants for the self reactions of $CH_3O_2^{\cdot}$ and $HO_2^{\cdot}$.

Propylene Simulations

The lighting, temperature, and humidity effects on propylene simulations (like those on ethylene) require further study, but the present chemistry is a substantial improvement over our first attempts to simulate the experiments reported here. Tables 20, 21, 22, and 23 provide the initial conditions and summaries of results for the two sets of simulations. Figures 61 through 102 provide the graphical results.

The simulations of UCR data show a consistant overprediction of ozone when the propylene decay is closely simulated. Likewise, the NO-to-NO_2 conversions per propylene molecule reacted seem to be overpredicted, as demonstrated by the results for EC-256. This experiment had a very low HC/NO_x ratio so that the NO_x crossover point, at which NO and NO_2 become equal, was barely reached by the end of the six-hour experiment. However, the current propylene mechanism appears to generate too much ozone in the UCR simulations, indicating that the efficiency for ozone production should be much lower than the NO-to-NO_2 conversion rate, or that the NO_x conversion rate itself becomes limited when ozone builds up. Unfortunately, the latter effect can not be tested easily because low NO_x concentrations accompany the higher ozone concentration. Under such conditions, accurate NO_x data are difficult

TABLE 20. INITIAL CONDITIONS FOR UCR PROPYLENE/NO_x EXPERIMENTS

Exp. no.	Temperature (Degrees K)	Initial concentrations (ppm)					Photolysis rate constant (x 10^4 min^{-1})*					
		Propylene	NO	NO_2	HONO	H_2O	NO_2 + hν	$O_3 \rightarrow O^1D$	$O_3 \rightarrow O$	HONO →	H_2O_2 →	FORM→radicals†
EC-230	303.	.546	.392	.128	.008	2.1×10^4	.3	13.	92.	870.	4.	14.
EC-256	304.	.109	.52	.044	.009	2.2×10^4	.3	6.9	90.	830.	3.6	10.
EC-257	304.	.112	.53	.032	.008	2.2×10^4	.3	6.9	90.	830.	3.6	10.
EC-276	303.	.510	.410	.106	.008	1.9×10^4	.35	9.9	108.	1000.	5.	13.
EC-277	303.	.564	.098	.010	.001	2×10^4	.35	9.9	108.	1000.	5.	13.
EC-278		1.016	.366	.128	.006	1.97×10^4	.35	9.9	108.	1000.	5.	15.
EC-279		1.10	.73	.244	.008	1.97×10^4	.35	9.9	108.	1000.	5.	15.
EC-314	303.	1.03	.684	.246	.009	2.4×10^4	.48	18.7	150.	1580	6.	18.
EC-315	290.	.967	.664	.276	.009	1.04×10^4	.48	18.7	150.	1580.	6.	11.
EC-316	312.	1.07	.735	.246	.015	4.61×10^4	.51	20.	160.	1680.	6.	24.
EC-317	304.	.493	.256	.281	.016	2.54×10^4	.53	24.	165.	1750.	6.	24.
EC-318§	303.	.509	.172	.331	.014	3.8×10^4	.53	24.	165.	1750	6.	18.
EC-319**	303.	.502	.100	.430	.012	2.4×10^4	.53	24.	165.	1750.	6.	18.
EC-320††		.536	.222	.290	.012	4.1×10^4	.55	25.	171.	1820.	6.2	18.

---

* Rate constant in min^{-1} for NO_2.

† The relationship between HCHO Products and carbonyl photolysis rate constants are discussed in Section 4.

§ Initial PAN added = 0.072 ppm.

** Initial PAN added = 0.149 ppm.

†† Initial PAN added = 0.636 ppm.

TABLE 21. UCR PROPYLENE EXPERIMENTS--SIMULATIONS AND MEASUREMENTS

Exp. no.	Initial $[NO_x]$ (ppm)	Initial NO_2/NO_x ratio	Initial HC/NO_x (ppmC/ppm)	Maximum $[O_3]$ (ppm)		Difference in O_3 maxima (percent)	Time to maximum $[O_3]$ (minutes)		Difference in times to O_3 maxima (percent)	Maximum $[NO_2]$ (ppm)		Difference in time to NO_2	Time to maximum $[NO_2]$ (min)		Difference in times to NO_2 maxima (percent)
				Sim.	Meas.		Sim.	Meas.		Sim.	Meas.		Sim.	Meas.	
EC-230	.520	.25	3.15	.48	.33	45	>420	>420	-	.39	.36	8	120	120	0.
EC-256	.564	.08	.58	.01	.002	400	>360	>360	-	.23	.21	10	>360	>360	-
EC-257	.562	.06	.60	.093	.06	55	>360	>360	-	.35	.30	17	200	200	0.
EC-276	.516	.21	2.97	.43	.35	23	>360	>360	-	.39	.36	8	120	120	0.
EC-277	.108	.09	15.7	.37	.31	19	100	100	0.	.09	.085	6	30	30	0.
EC-278	.494	.26	6.2	.62	.62	0	180	160	13	.40	.38	5	60	60	0.
EC-279	.974	.25	3.39	.67	.67	0	>360	>360	-	.76	.7	9	120	100	20.
EC-314	.930	.27	3.32	.78	.72	8	300	>360	-	.72	.68	6	90	90	0.
EC-315	.940	.29	3.09	.36	.33	9	>360	>360	-	.66	.61	8	180	140	29.
EC-316	.981	.25	3.27	.93	.95	2	230	280	-	.79	.75	5	70	60	17
EC-317	.537	.52	2.75	.68	.60	13	290	330	-12	.42	.39	8	60	60	0.
EC-318	.503	.66	3.04	.64	.68	-6	240	240	0.	.43	.41	5	30	30	0.
EC-319	.530	.81	2.84	.78	.75	4	200	220	-9	.47	.46	2	20	20	0.
EC-320	.512	.57	3.14	.60	.64	-6	250	240	4	.42	.40	5	40	40	0.

O_3 average = 12 percent, standard deviation = ±18 percent (excluding EC-256).

NO_2 average = 7 percent, standard deviation = ± 3 percent.

TABLE 22. INITIAL CONDITIONS FOR UNC PROPYLENE/NO_x EXPERIMENTS

Date	Chamber Side	Sky Conditions	Beginning time of Simulation	Initial concentrations (ppm)					ALD + hν Constant
				Propylene	NO	NO_2	HONO	H_2O	
10/24/77	Red	Variable clouds	7:16	1.23	.338	.129	.005	1.6×10^4	1.2
12/26/77	Red	Clear	8.08	.988	.281	.118	0.	1.5×10^3	1.0
1/10/78	Red	Clear	8:15	1.08	.323	.139	.015	1.5×10^3	1.0
2/27/78	Red	Clear	8:00	1.32	.371	.125	0.	4×10^3	1.0
3/06/78	Red	Variable clouds	7:36	1.26	.394	.117	.007	4×10^3	1.0
3/31/78	Red	Variable clouds	6:48	1.27	.392	.091	0.	1×10^4	1.0
6/16/78	Blue	Clear	6:16	.667	.429	.211	0.	1.6×10^4	1.0
6/30/78	Red	Variable clouds in afternoon	6:12	.503	.382	.082	.011	2.2×10^4	1.0
7/01/78	Blue	Sparse clouds in afternoon	5:52	.503	.612	.323	.020	2.2×10^4	1.0
7/24/78		Variable clouds	6.04	.99	.775	.184	.025	2.4×10^4	1.0*
7/24/78	Blue	Variable clouds	6:04	.49	.778	.174	.022	2.4×10^4	1.0*
7/30/78	Blue	Scattered clouds	6:28	.417	.399	.084	.011	2.4×10^4	1.0*
8/05/78	Red	Scattered clouds	6:16	.277	.196	.052	.008	2.4×10^4	1.0*
8/05/78	Blue	Scattered clouds	6:16	.518	.423	.145	.012	2.4×10^4	1.0*
8/06/78	Red	Scattered clouds	6:20	.563	.420	.141	.027	2.4×10^4	1.0*
8/15/78	Red	Scattered clouds	6:23	.483	.434	.109	.015	2.2×10^4	1.0
8/21/78	Blue	Clear	6:31	.427	.798	.183	.003	1.6×10^4	1.0
10/17/78	Red	Overcast in afternoon	7:22	.450	.371	.125	.002	1.0×10^4	1.0*
10/18/78	Blue	Clear	7:28	.507	.340	.116	.002	1.6×10^4	1.0*
10/20/78	Red	Clear	7:30	.463	.336	.124	.003	1.5×10^4	1.0*
10/20/78	Blue	Clear	7:30	1.217	.329	.128	.004	1.6×10^4	1.0*
10/21/78	Red	Clear	7:27	1.167	.397	.100	.0015	1.6×10^4	1.0*
10/21/78	Blue	Clear	7:27	1.18	.395	.100	.002	8×10^3	1.0*
10/22/78	Red	Clear	7:24	.467	.379	.111	.003	1.6×10^4	1.0*
10/22/78	Blue	Clear	7:24	.467	.373	.114	.002	1.6×10^4	1.0*
10/29/78	Red	Overcast in morning	7:28	.450	.374	.124	.011	1×10^4	1.0*
10/29/78	Blue	Overcast in morning	7:28	1.227	.370	.125	.013	1×10^4	1.0*
11/07/78	Red	Overcast in afternoon	7:40	.457	.301	.140	.005	1×10^4	1.0*

* UV data used in computer simulations, instead of TSR.

TABLE 23. UNC PROPYLENE EXPERIMENT--SIMULATION RESULTS AND MEASUREMENTS

Date	Chamber Side	Initial [NO_x] (ppm)	Initial NO_2/NO_x Ratio	Initial HC/NO_x (ppmC/ppm)	Maximum [O_3] (ppm)		Difference in O_3 Maxima (Percent)	Time to Maximum [O_3] (Minutes)		Difference in time to O_3 Maxima (Percent)
					Sim.	Meas.		Sim.	Meas.	
10/24/77	Red	.467	.28	7.90	.48	.62	-23	>360	300	-
12/26/77	Red	.399	.30	7.43	.36	.38	-5	400	400	0.
1/10/78	Red	.462	.30	7.01	.31	.36	-14	400	400	0.
2/27/78	Red	.496	.25	7.98	.80	.57	40	380	300	27
3/06/78	Red	.511	.23	7.40	.84	.63	33	380	300	27
3/31/78	Red	.483	.19	7.89	.87	.78	12	360	280	29
6/16/78	Blue	.640	.33	3.13	.93	1.08	-14	>560	500	-
6/30/78	Red	.464	.18	3.25	.80	1.00	20	460	420	10
7/01/78	Blue	.935	.35	1.61	.35	.56	-37	600	600	0.
7/24/78	Red	.959	.19	3.10	.92	1.20	-23	>560	470	-
7/24/78	Blue	.952	.18	1.54	.23	.20	15	>560	>560	-
7/30/78	Blue	.483	.17	2.59	.74	.80	-8	530	530	0.
8/05/78	Red	.238	.22	3.49	.50	.62	-19	510	510	0.
8/05/78	Blue	.568	.26	2.74	.64	.76	-16	510	510	0.
8/06/78	Red	.561	.25	3.01	.39	.50	-22	350	350	0.
8/15/78	Red	.543	.20	2.67	.70	.83	-16	460	460	0.
8/21/78	Blue	.981	.19	1.31	.13	.093	40	540	600	-10
10/17/78	Red	.496	.25	2.72	.08	.12	33	>400	330	-
10/18/78	Blue	.456	.25	3.34	.33	.26	27	455	455	0.
10/20/78	Red	.470	.26	2.96	.31	.34	-9	455	455	0.
10/20/78	Blue	.457	.28	7.99	.75	.73	3	350	280	25
10/21/78	Red	.497	.20	7.04	.78	.65	19	385	300	28
10/21/78	Blue	.495	.20	7.15	.90	.73	23	380	280	36
10/22/78	Red	.490	.23	2.86	.30	.35	-14	470	470	0.
10/22/78	Red	.487	.23	2.88	.30	.34	-12	480	480	0.
10/29/78	Red	.498	.25	2.71	.20	.22	-9	510	510	0.
10/29/78	Blue	.595	.21	6.19	.76	.64	19	410	340	21
11/07/78	Red	.441	.32	3.11	.21	.33	-36	450	450	0.

O_3 average = 0.25 percent; Standard deviation = ±23 percent.

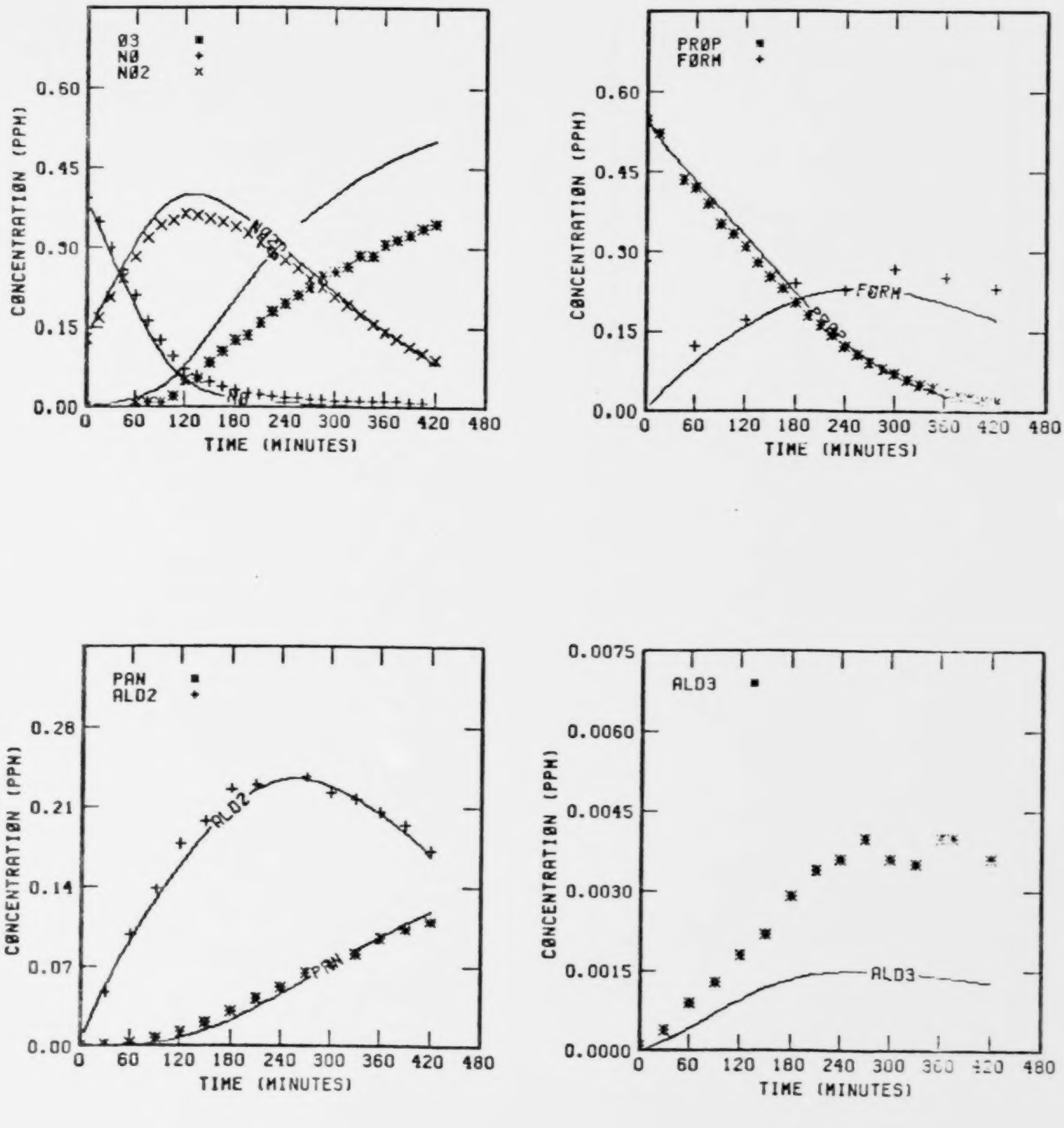

FIGURE 61 . SIMULATIØN RESULTS FØR
EC-230

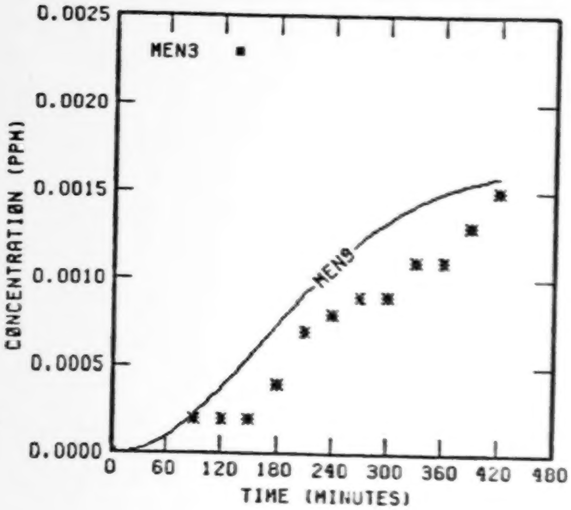

FIGURE 61. (Concluded)

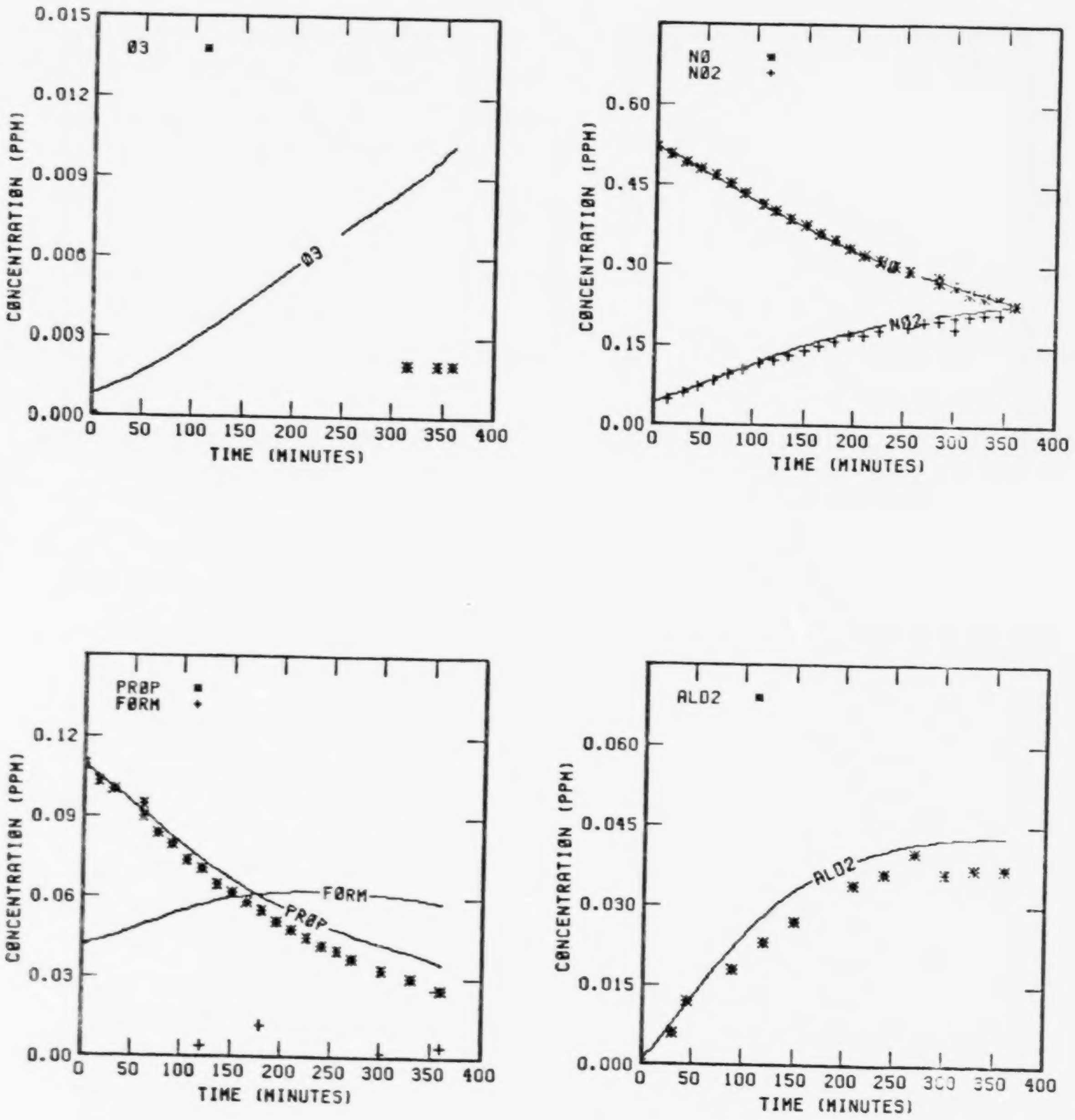

FIGURE 62. SIMULATION RESULTS FOR EC-256

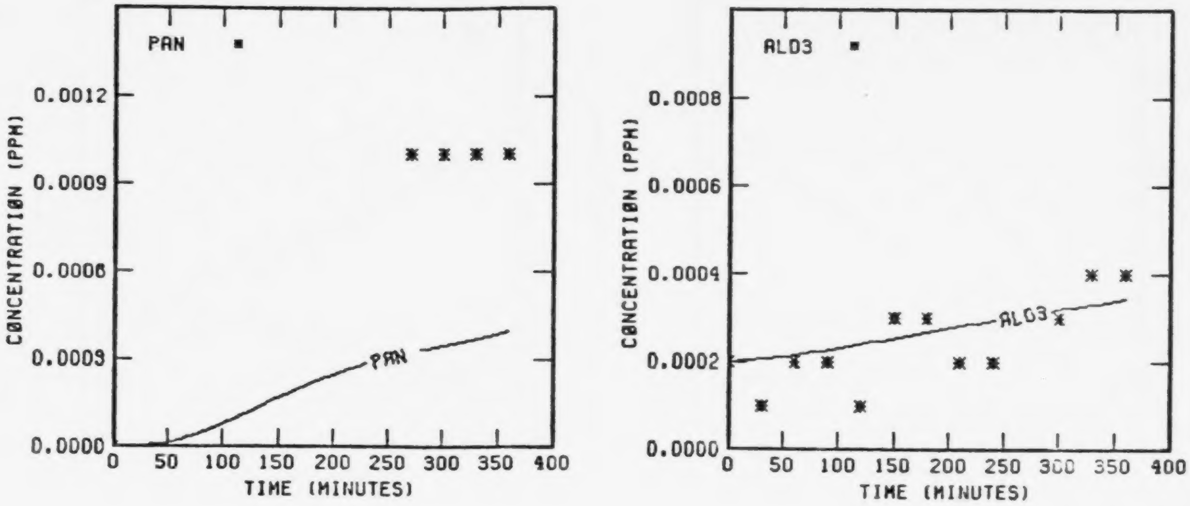

FIGURE 62 . (Concluded)

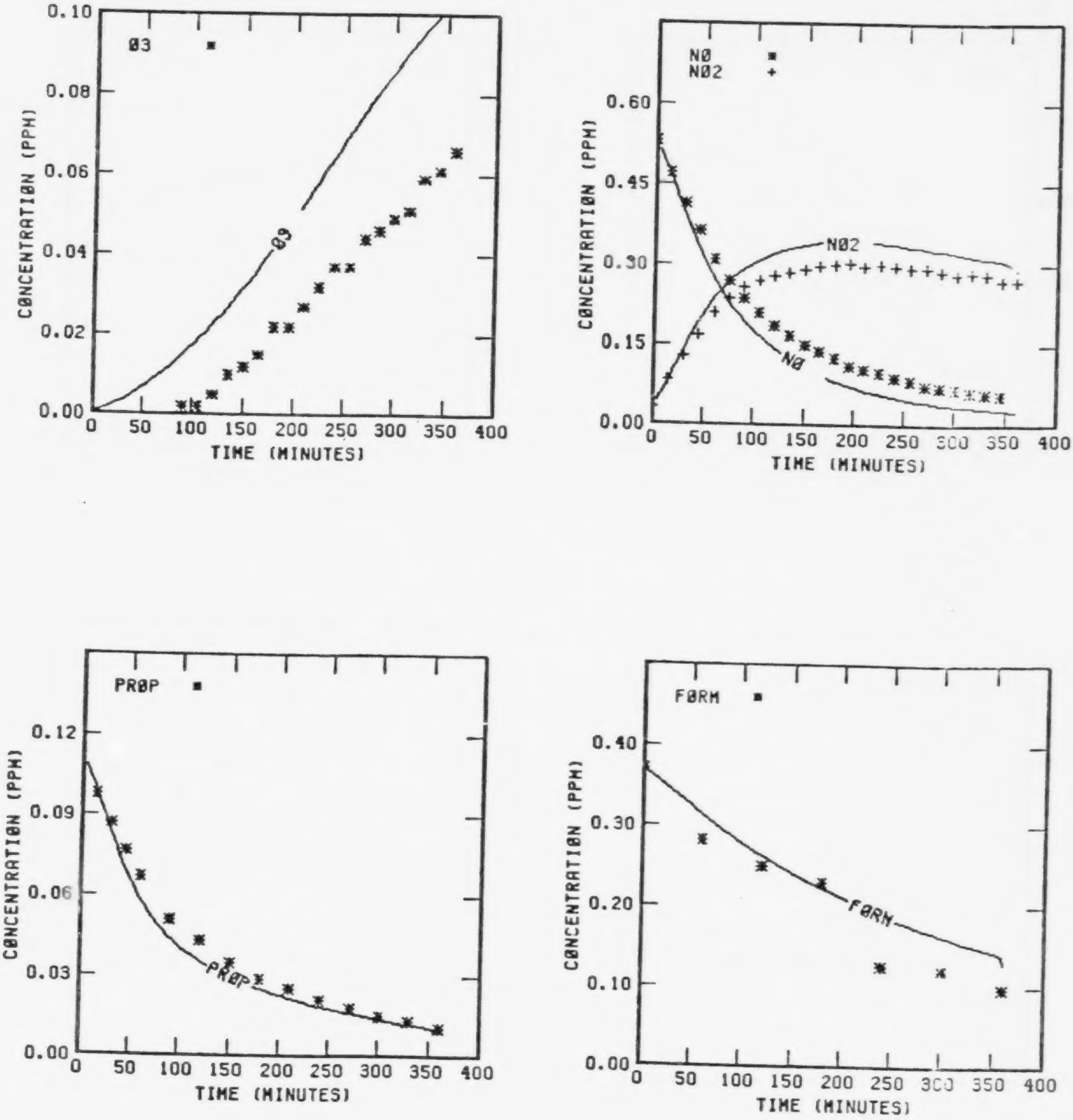

FIGURE 63. SIMULATION RESULTS FOR EC-257

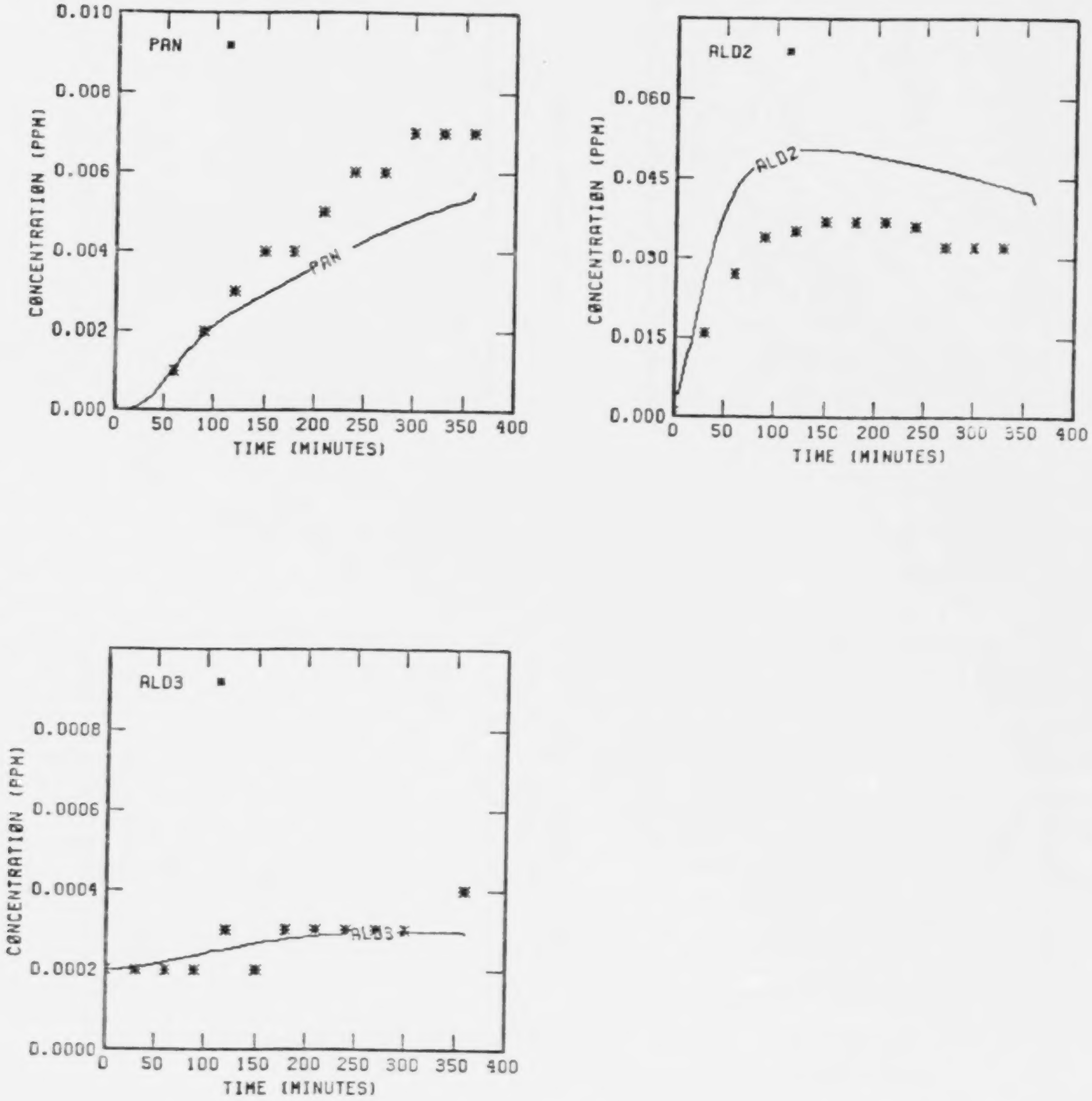

FIGURE 63 . (Concluded)

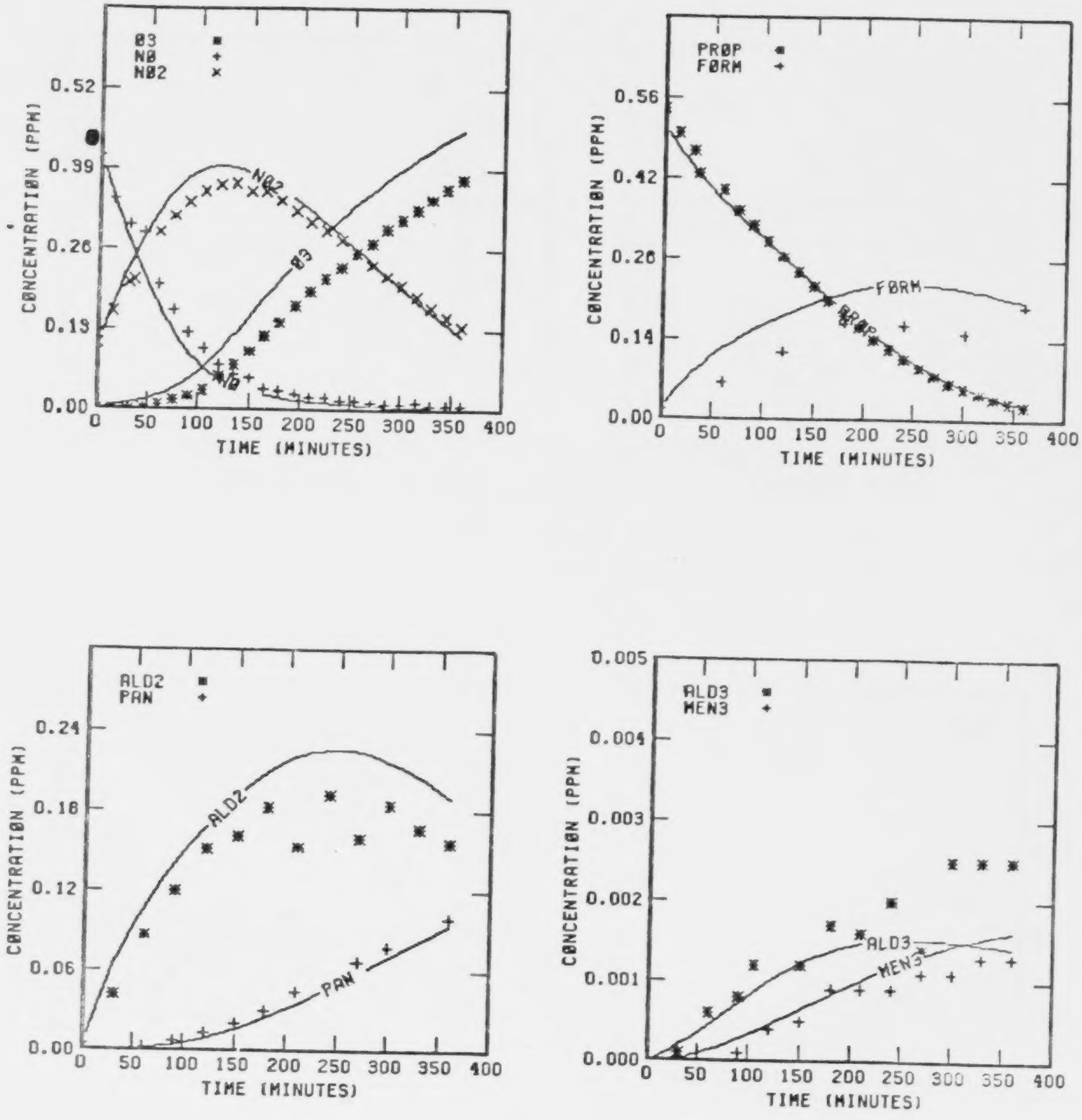

FIGURE 64 . SIMULATIØN RESULTS FØR
EC-276

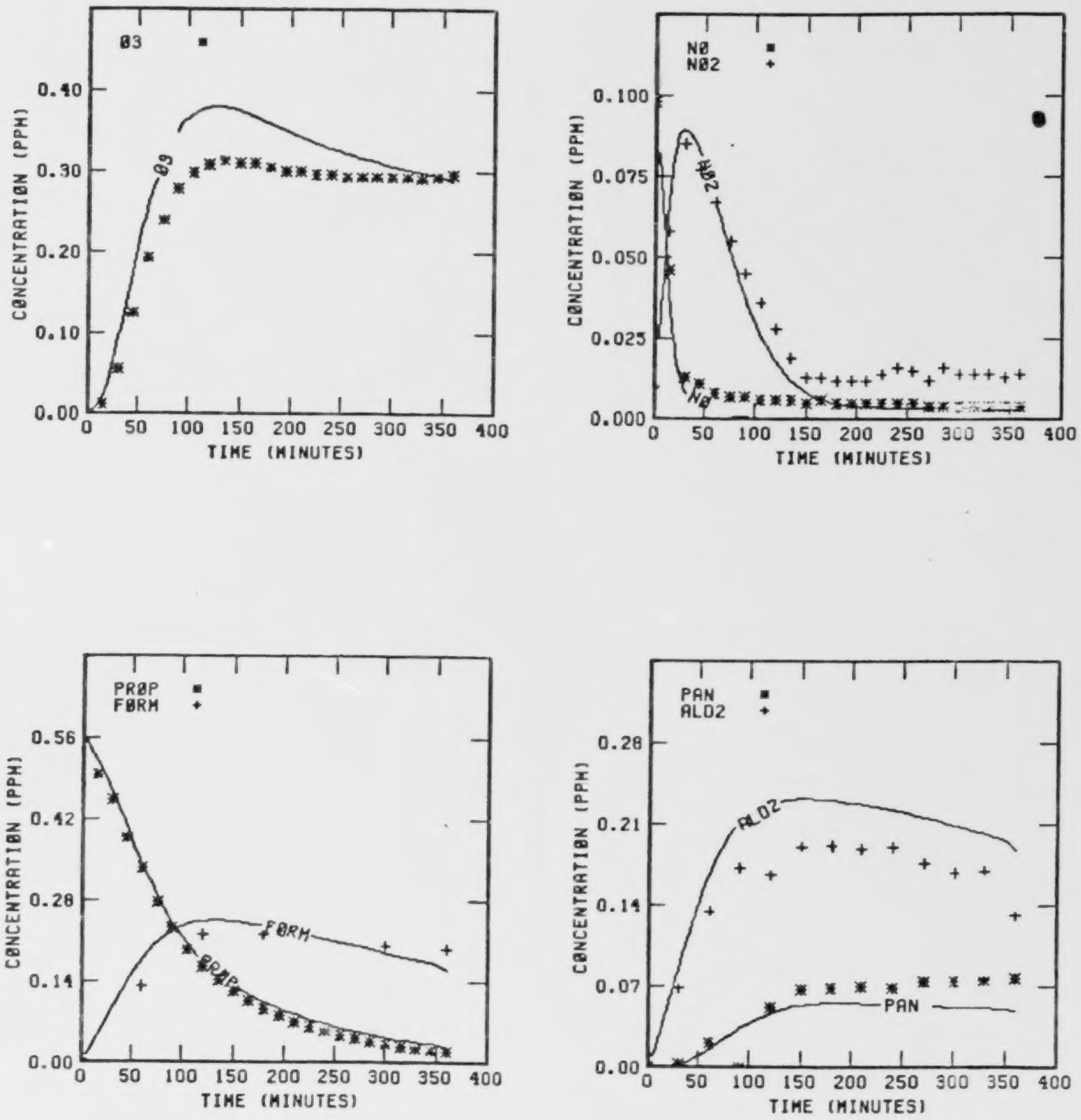

FIGURE 65 . SIMULATION RESULTS FOR
EC-277

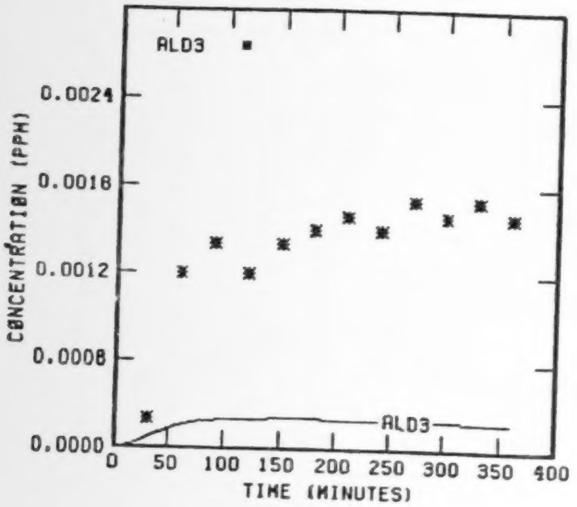

FIGURE 65 . (Concluded)

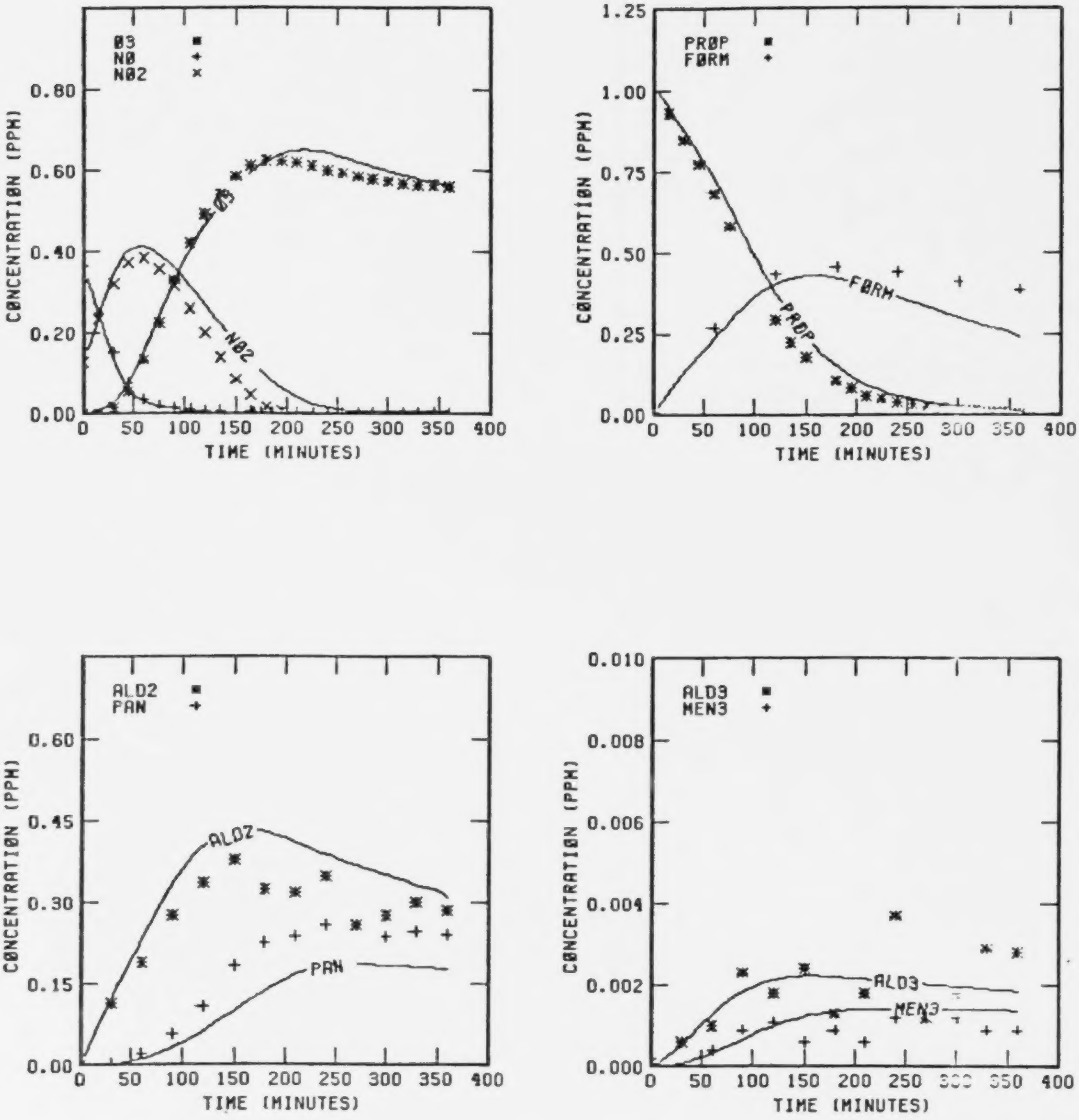

FIGURE 66 . SIMULATIØN RESULTS FØR
EC-278

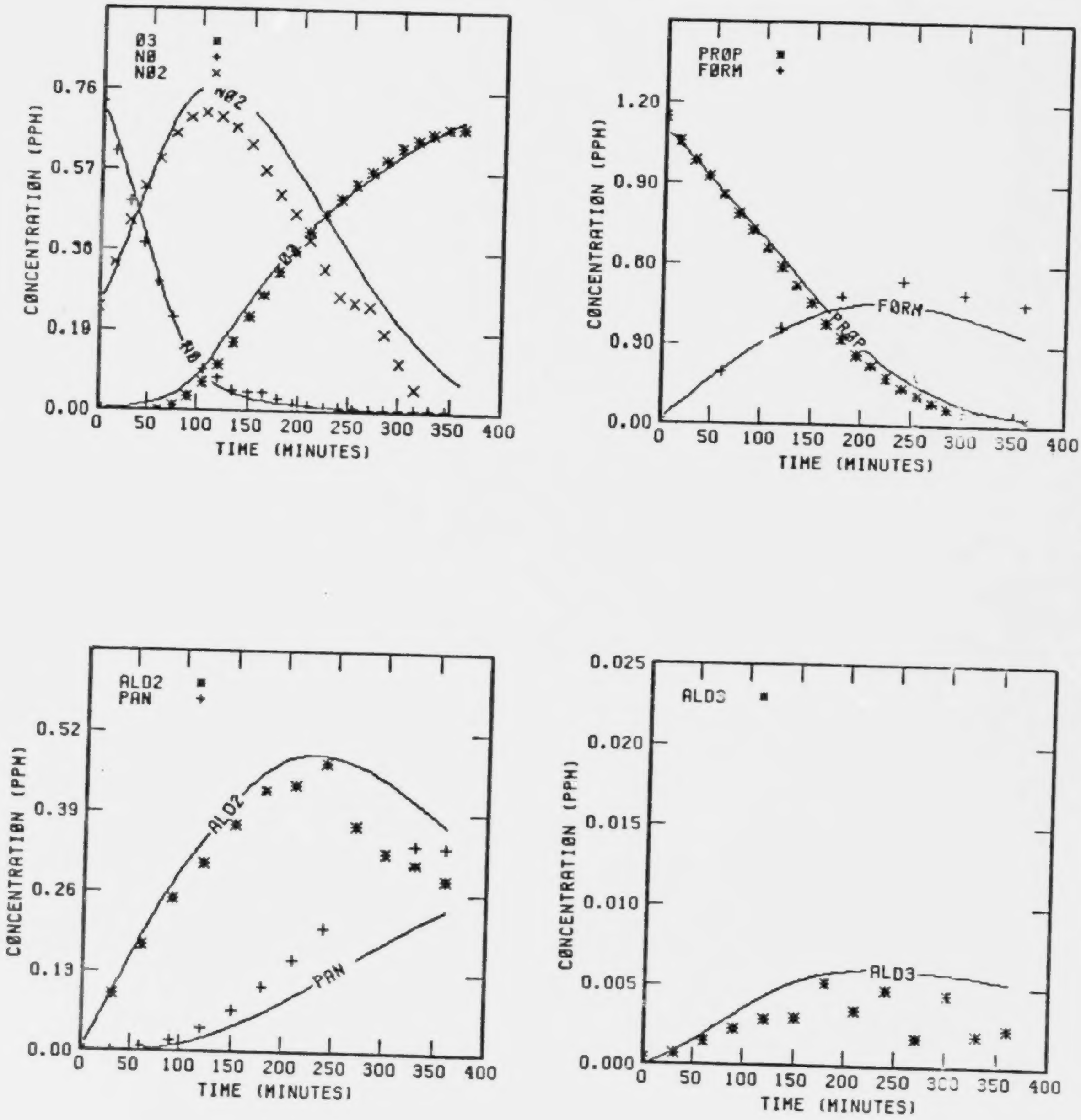

FIGURE 67 . SIMULATIØN RESULTS FØR
EC-279

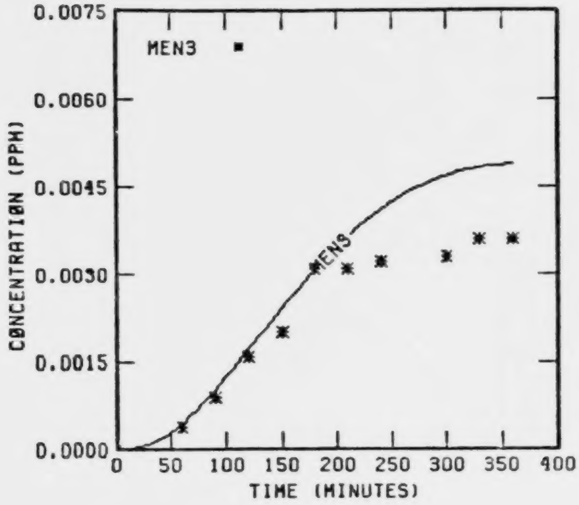

FIGURE 67 . (Concluded)

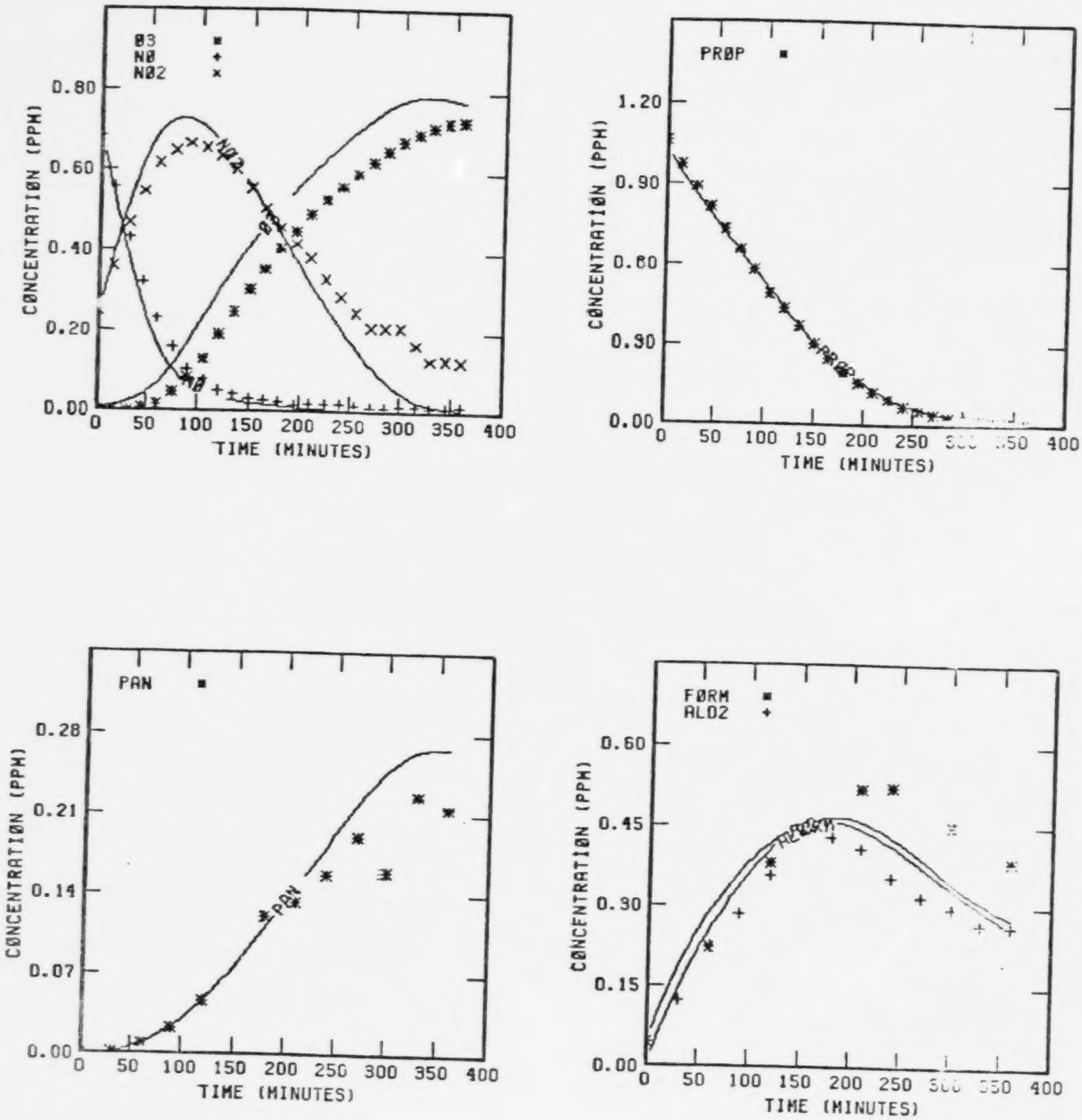

FIGURE 68 . SIMULATIØN RESULTS FØR EC-314

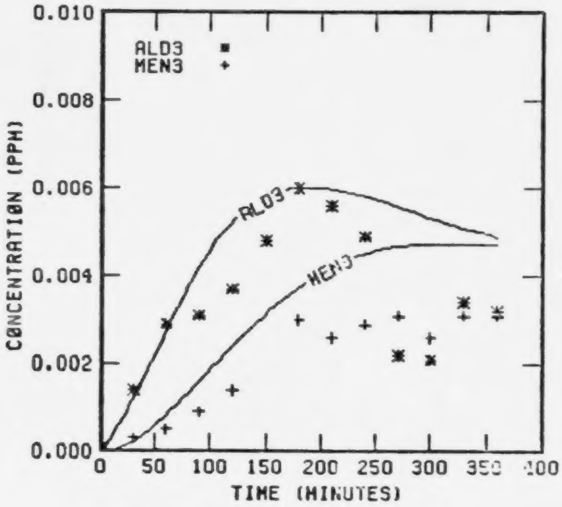

FIGURE 68 . (Concluded)

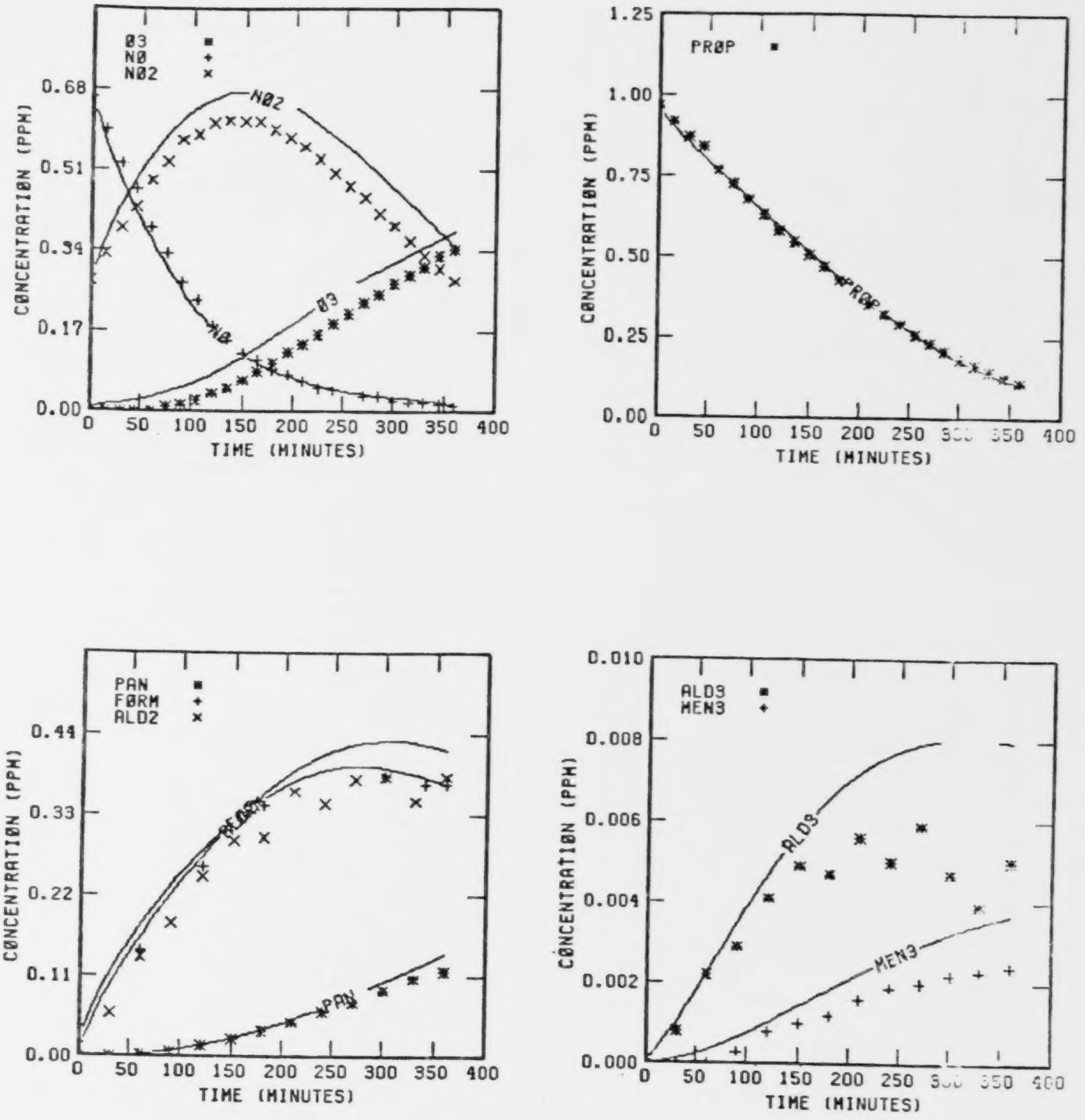

FIGURE 69 . SIMULATION RESULTS FOR
EC-315

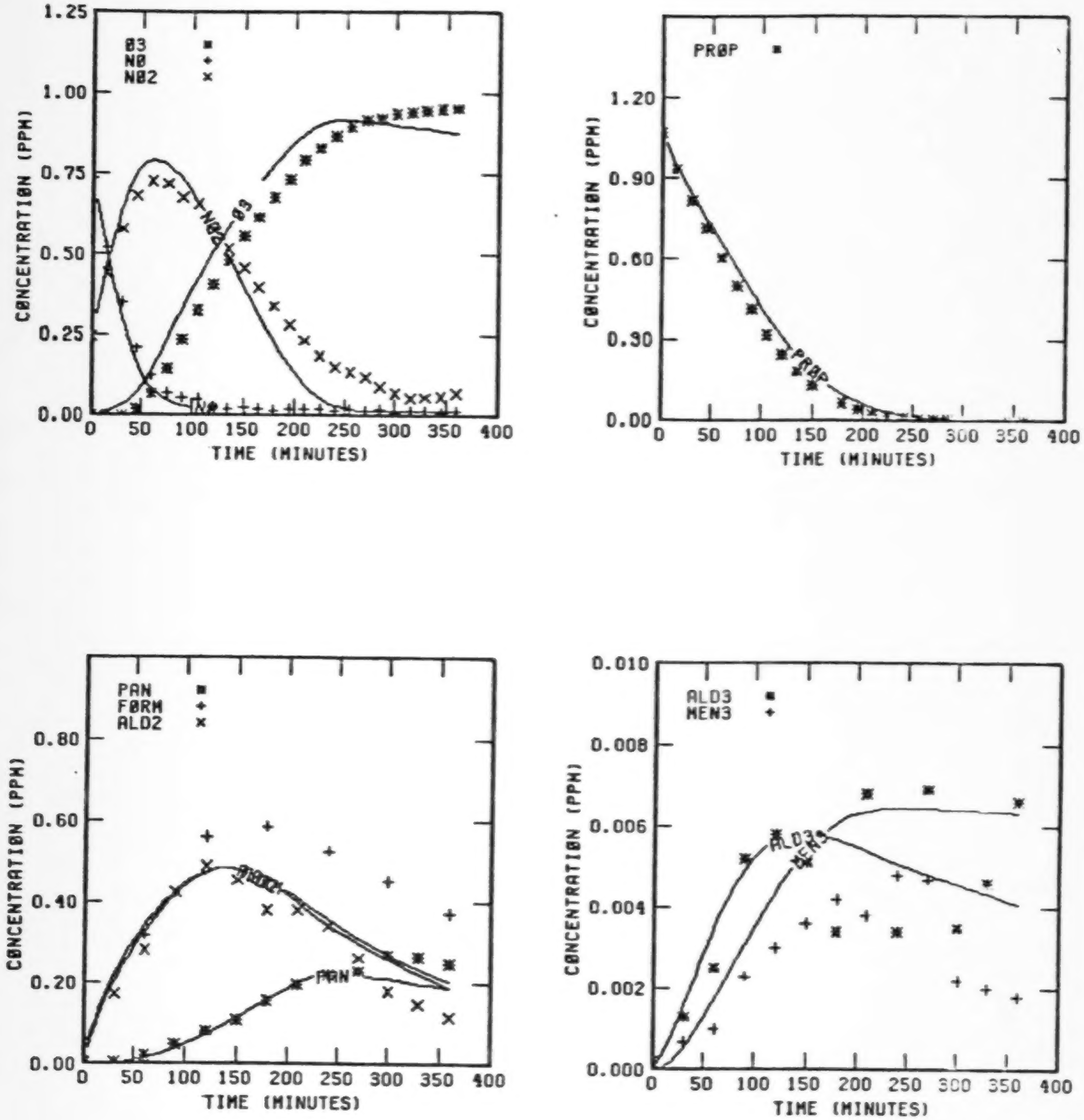

FIGURE 70 . SIMULATION RESULTS FOR EC-316

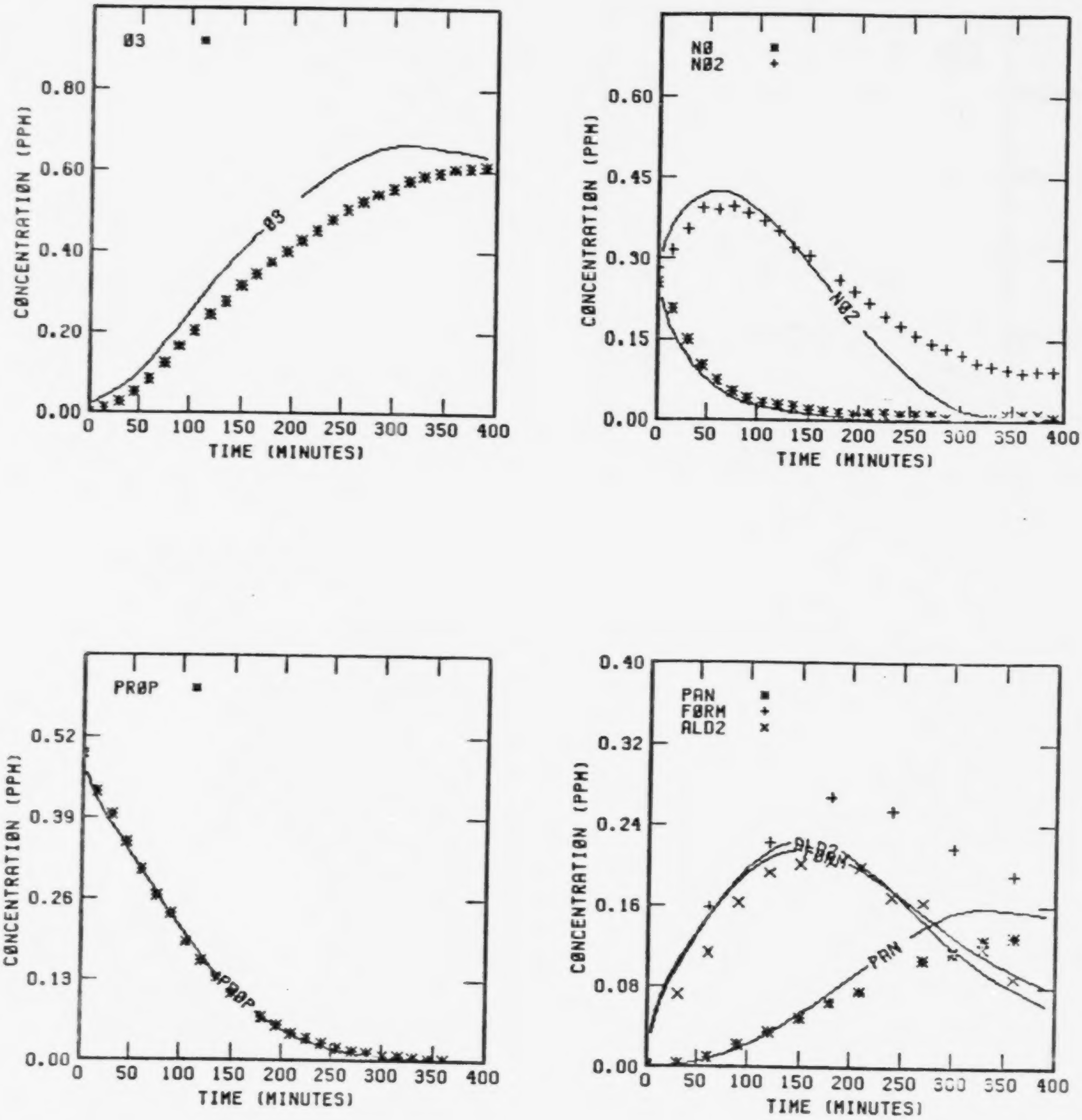

FIGURE 71 . SIMULATION RESULTS FOR EC-317

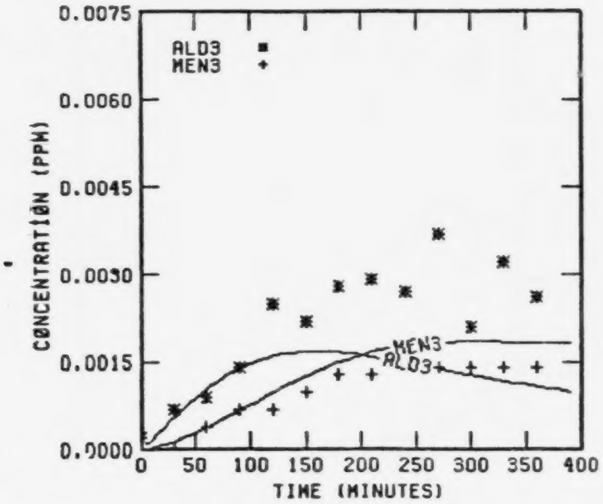

FIGURE 71. (Concluded)

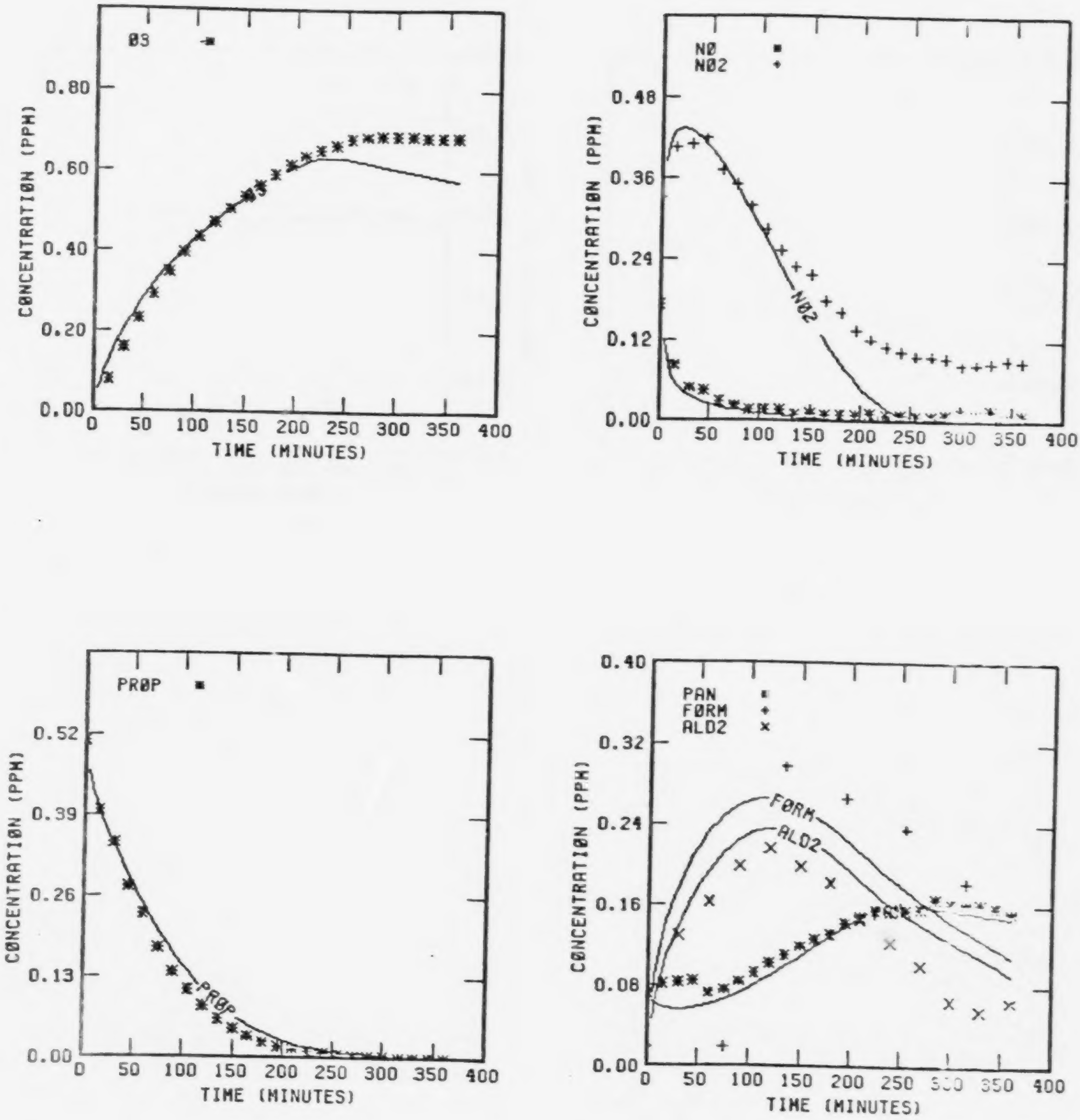

FIGURE 72. SIMULATION RESULTS FOR EC-318

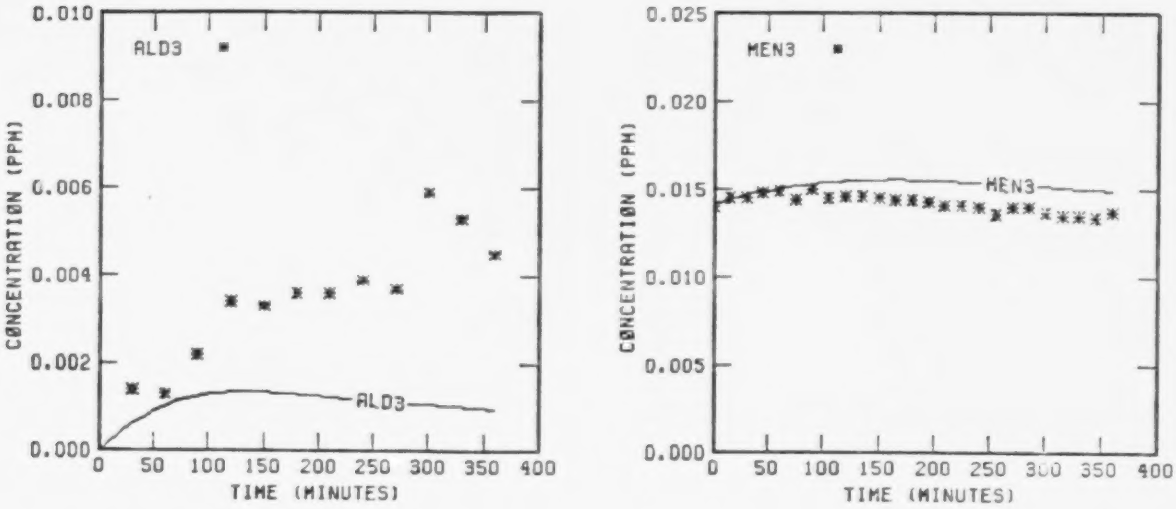

FIGURE 72. (Concluded)

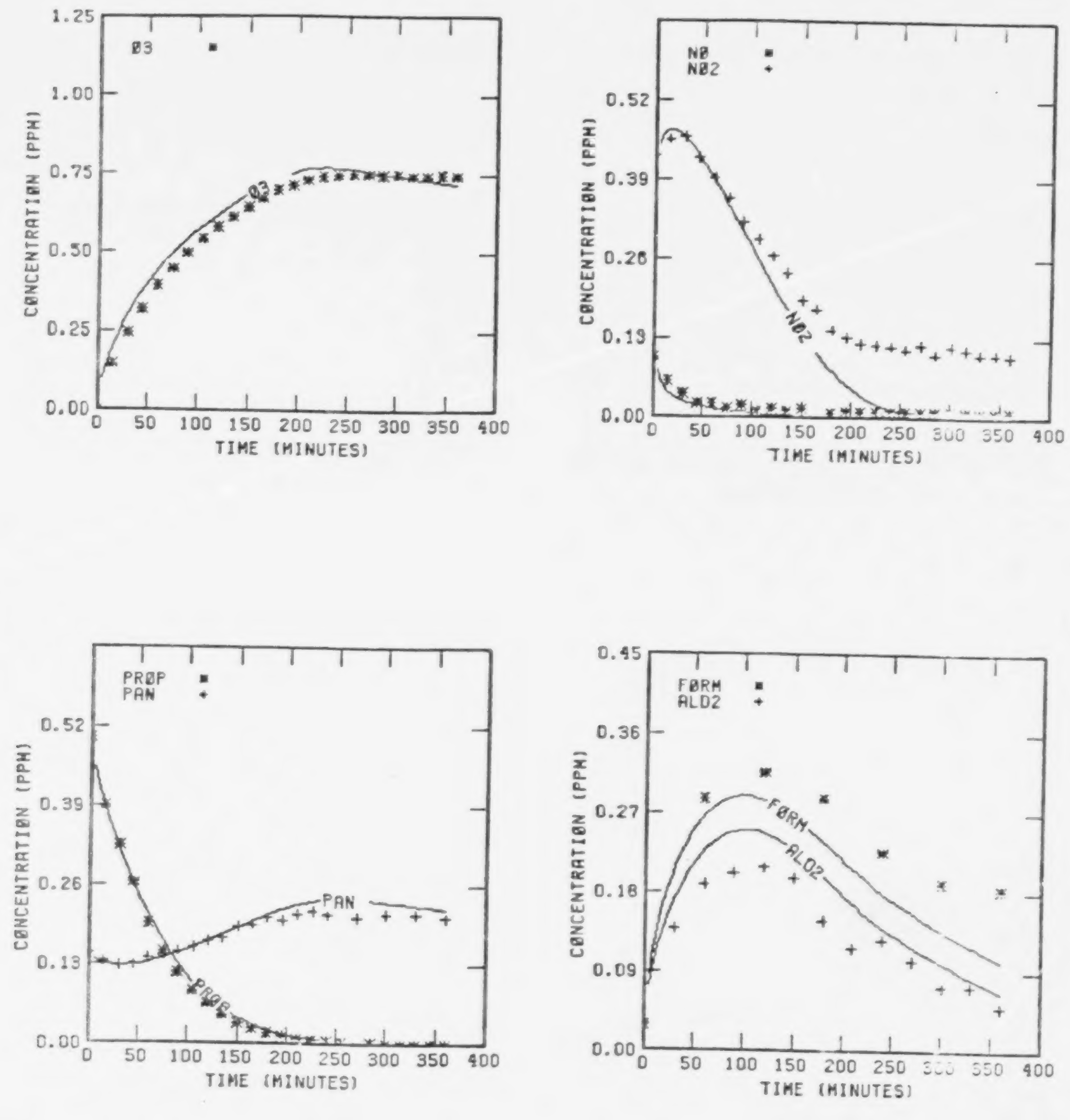

FIGURE 73 . SIMULATIØN RESULTS FØR EC-319

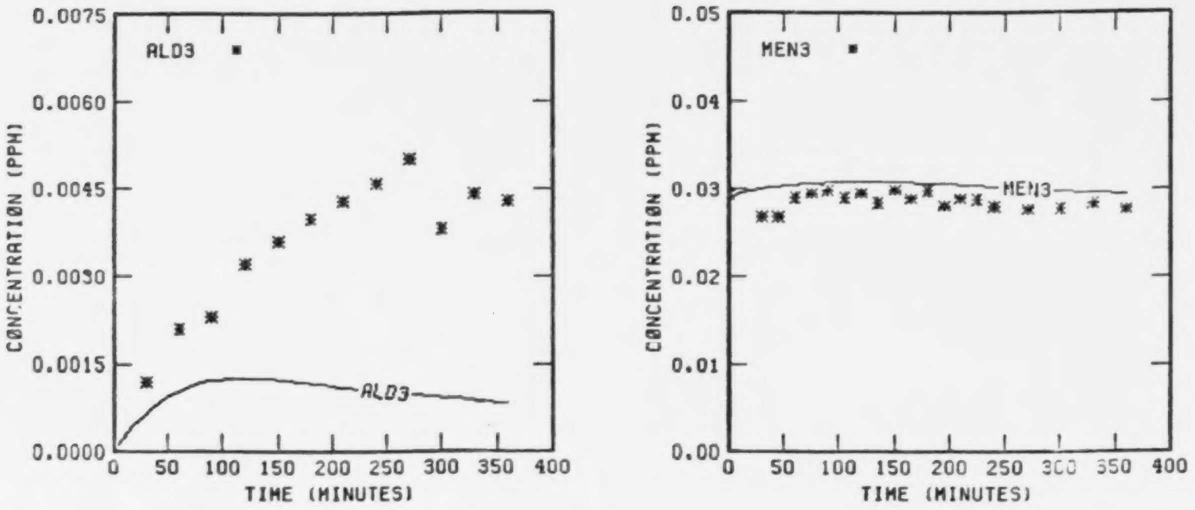

FIGURE 73. (Concluded)

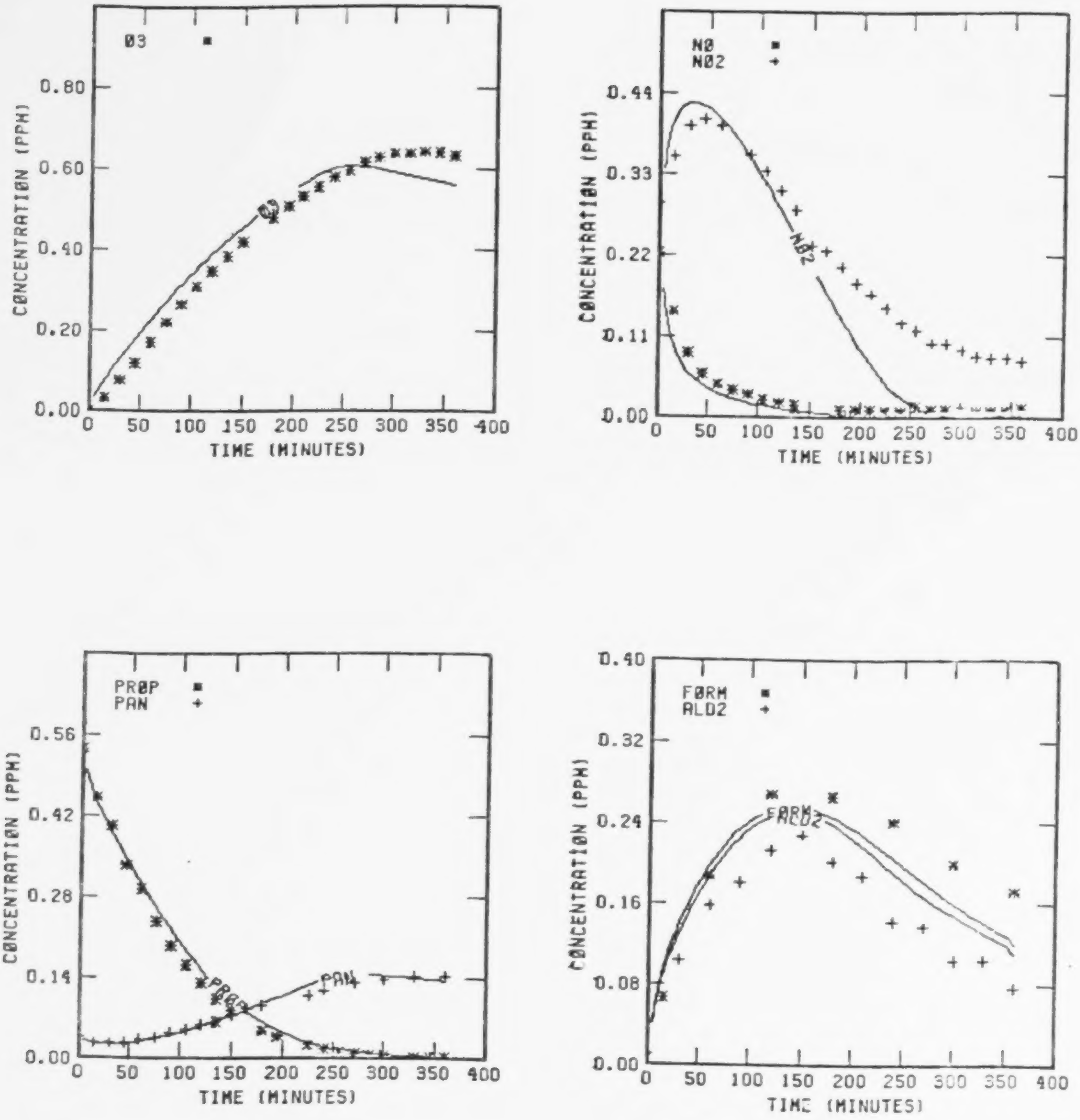

FIGURE 74 . SIMULATION RESULTS FOR
EC-320

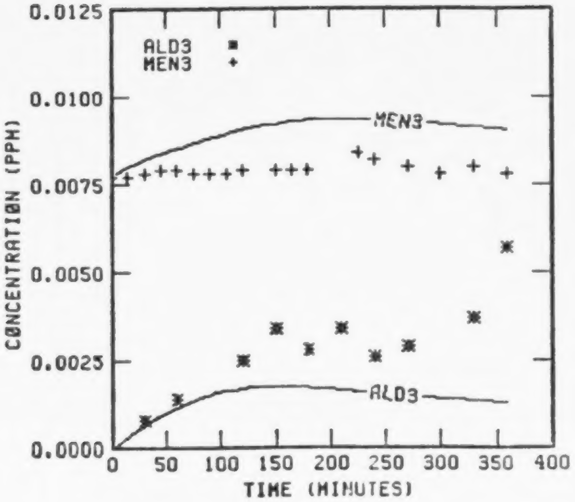

FIGURE 74 . (Concluded)

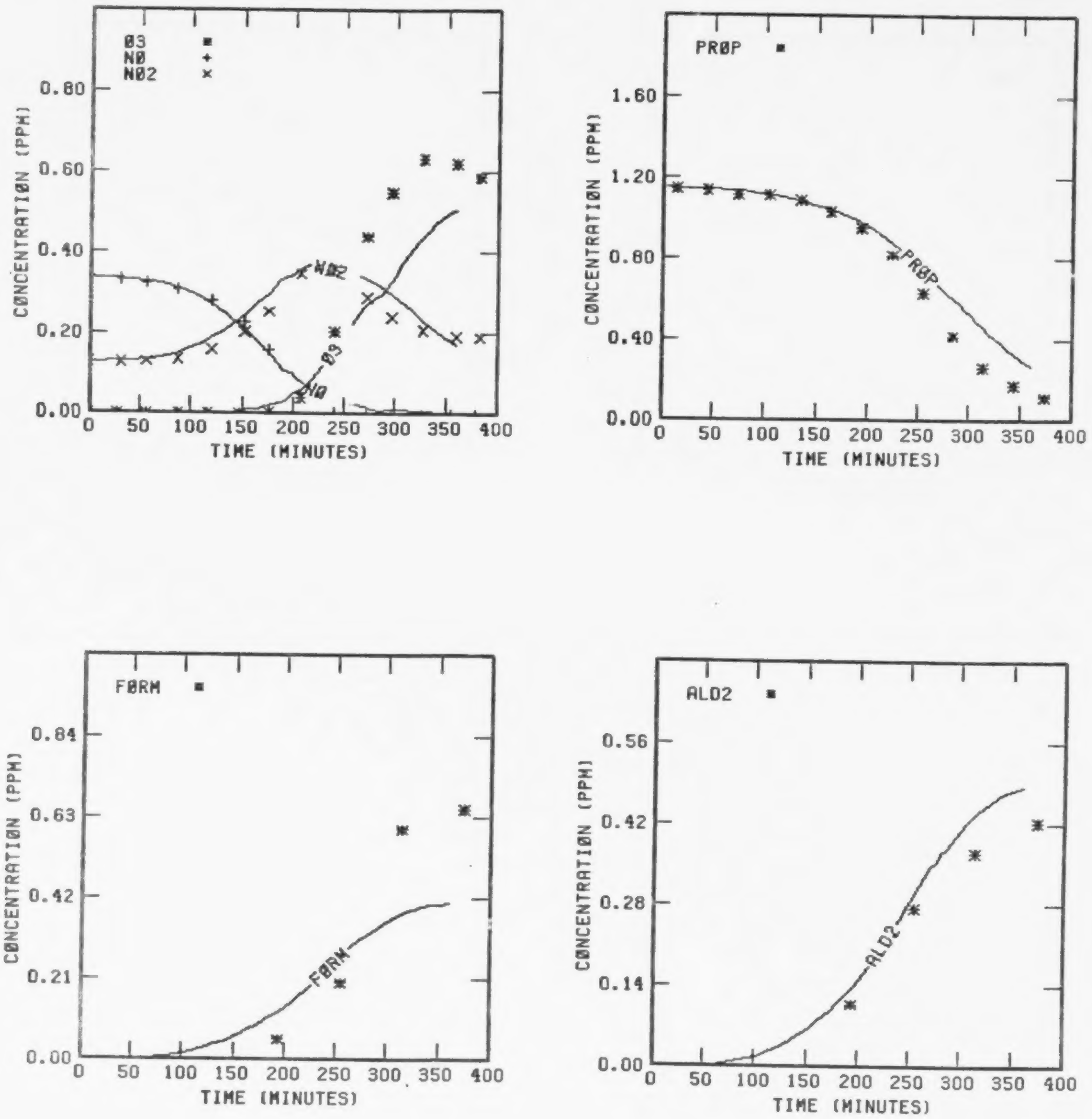

FIGURE 75. SIMULATION RESULTS FOR
UNCR 102477

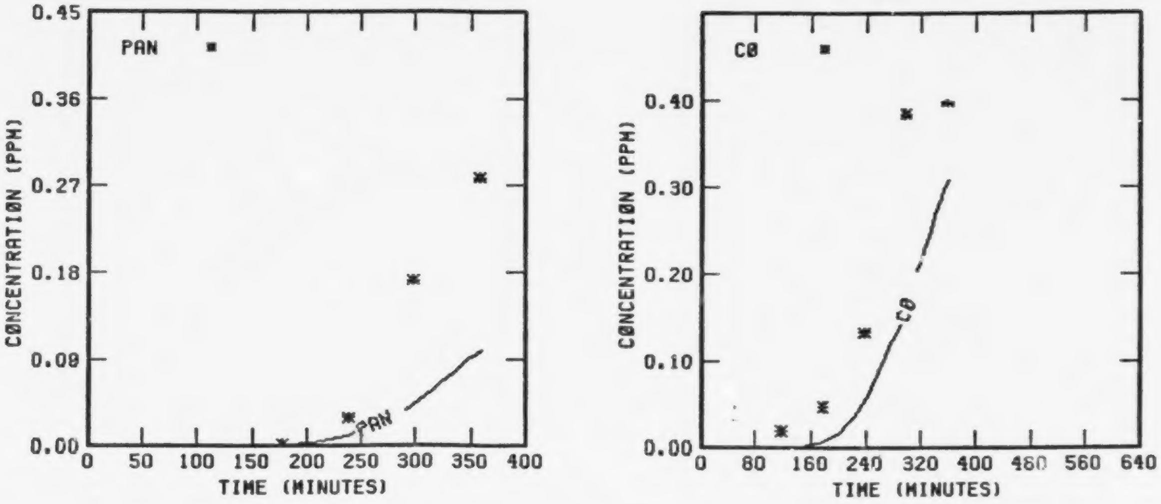

FIGURE 75. (Concluded)

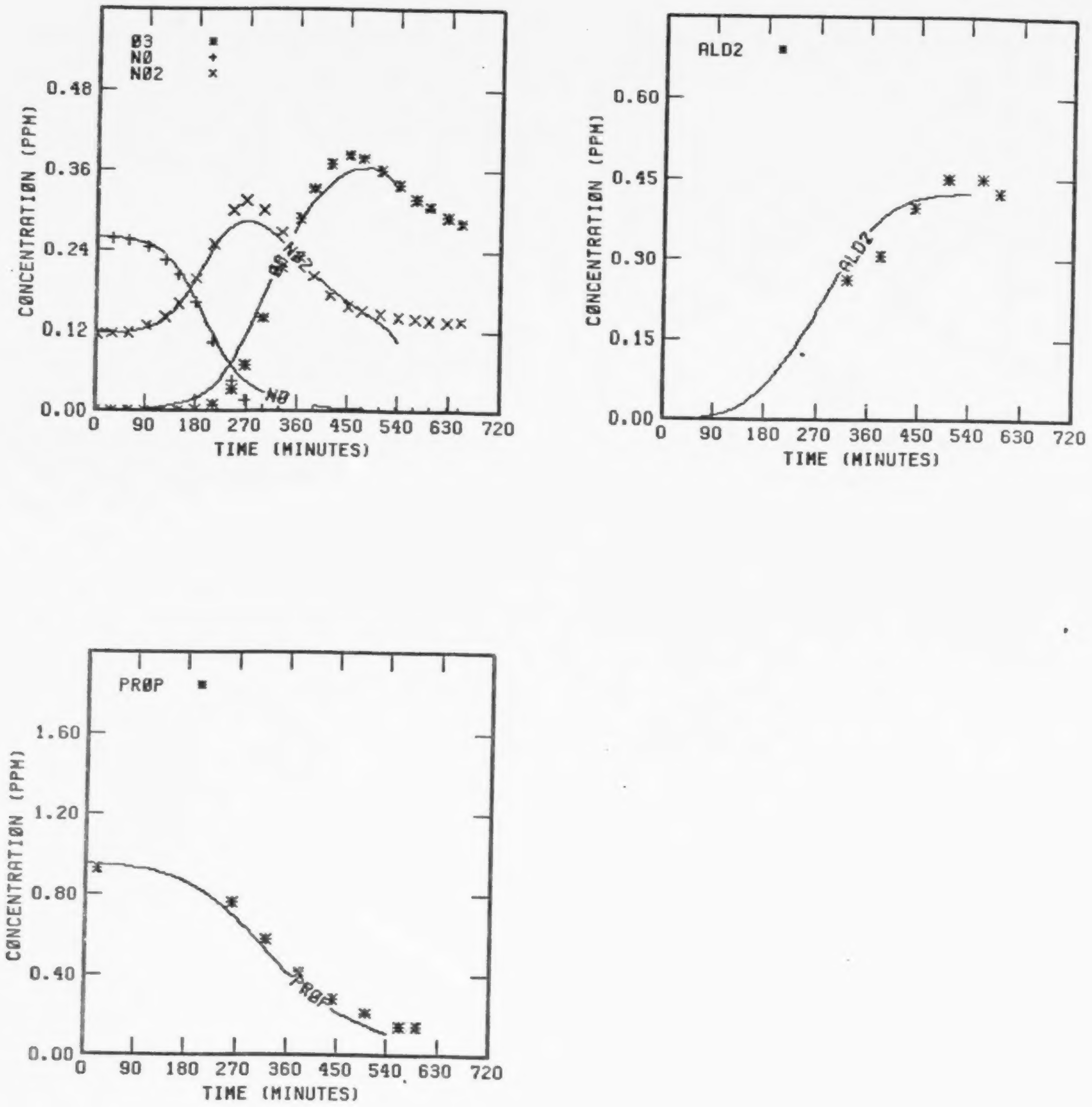

FIGURE 76. SIMULATION RESULTS FOR
UNCR 122677

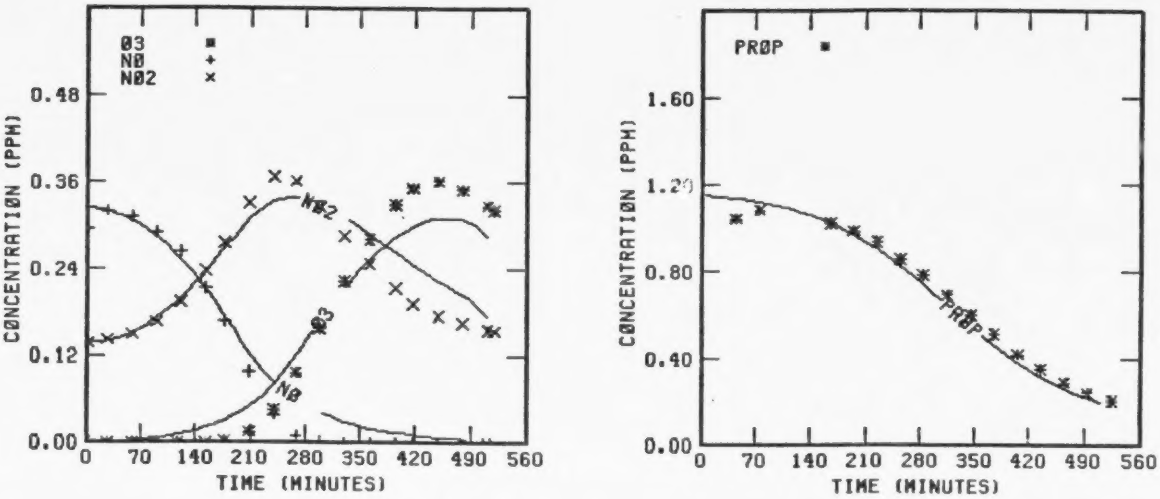

FIGURE 77 . SIMULATION RESULTS FOR
UNCR 11078

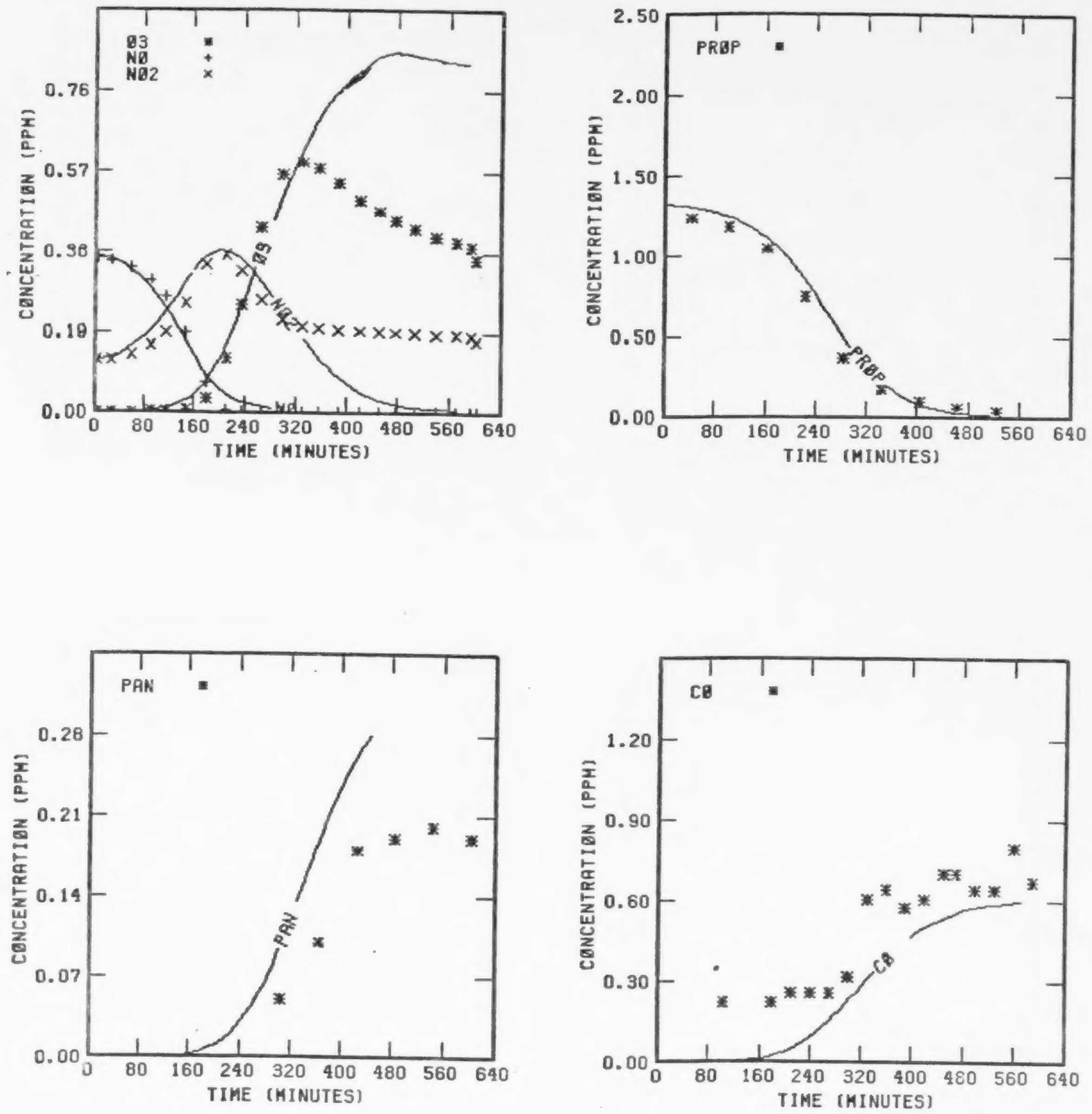

FIGURE 78 . SIMULATION RESULTS FOR
UNCR 22778

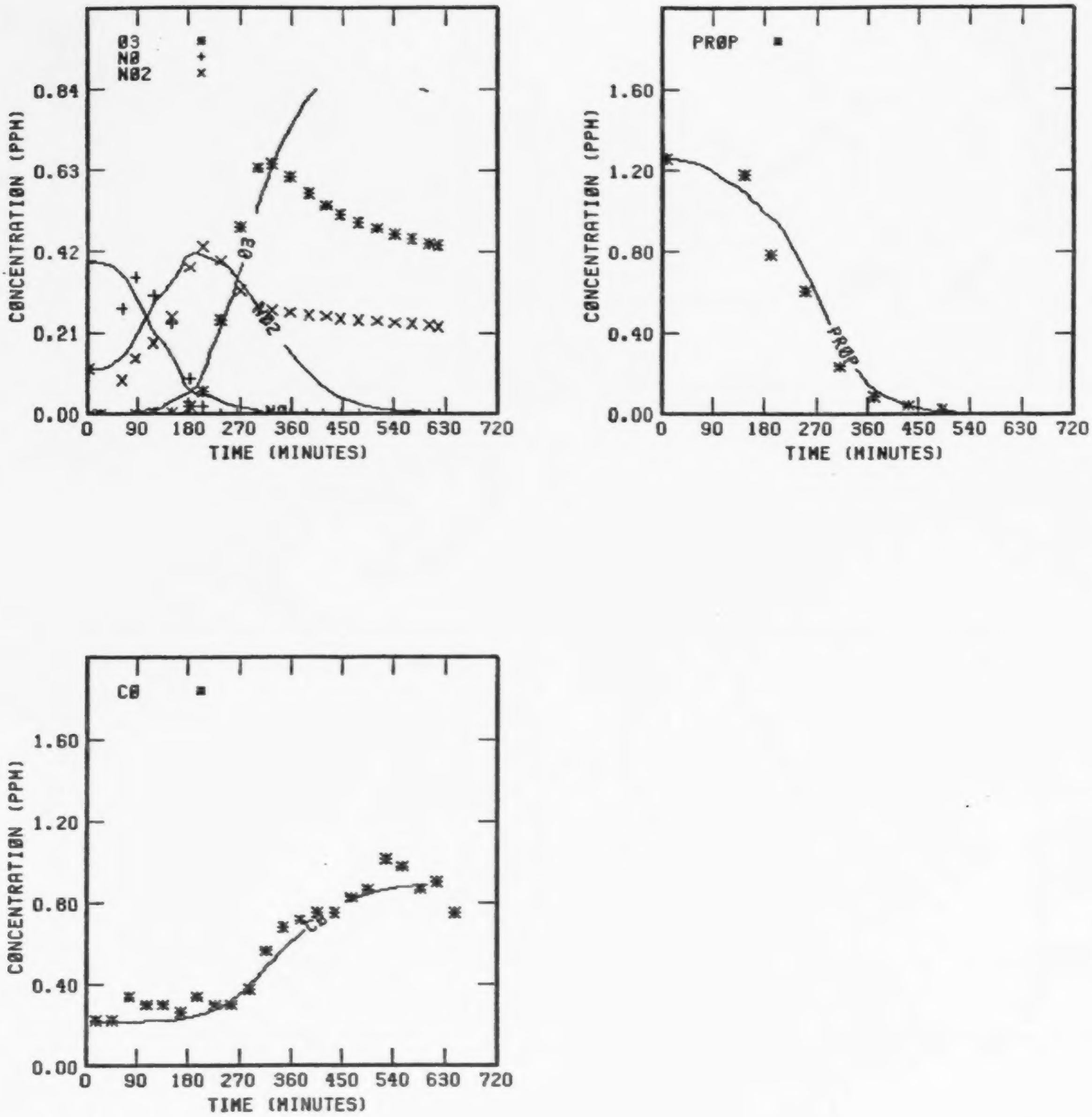

FIGURE 79. SIMULATION RESULTS FOR UNCR 30678

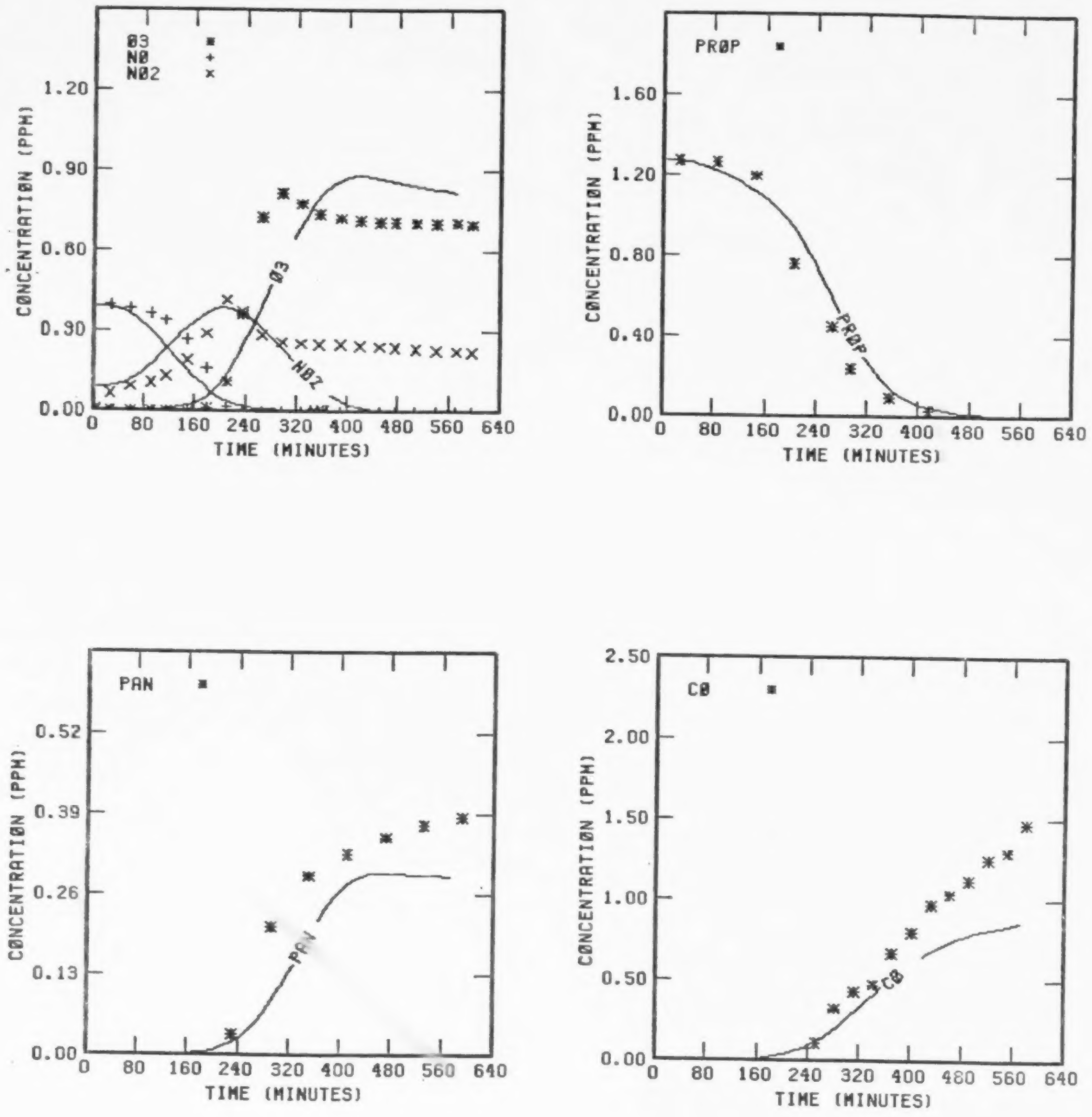

FIGURE 80 . SIMULATION RESULTS FOR
UNCR 33178

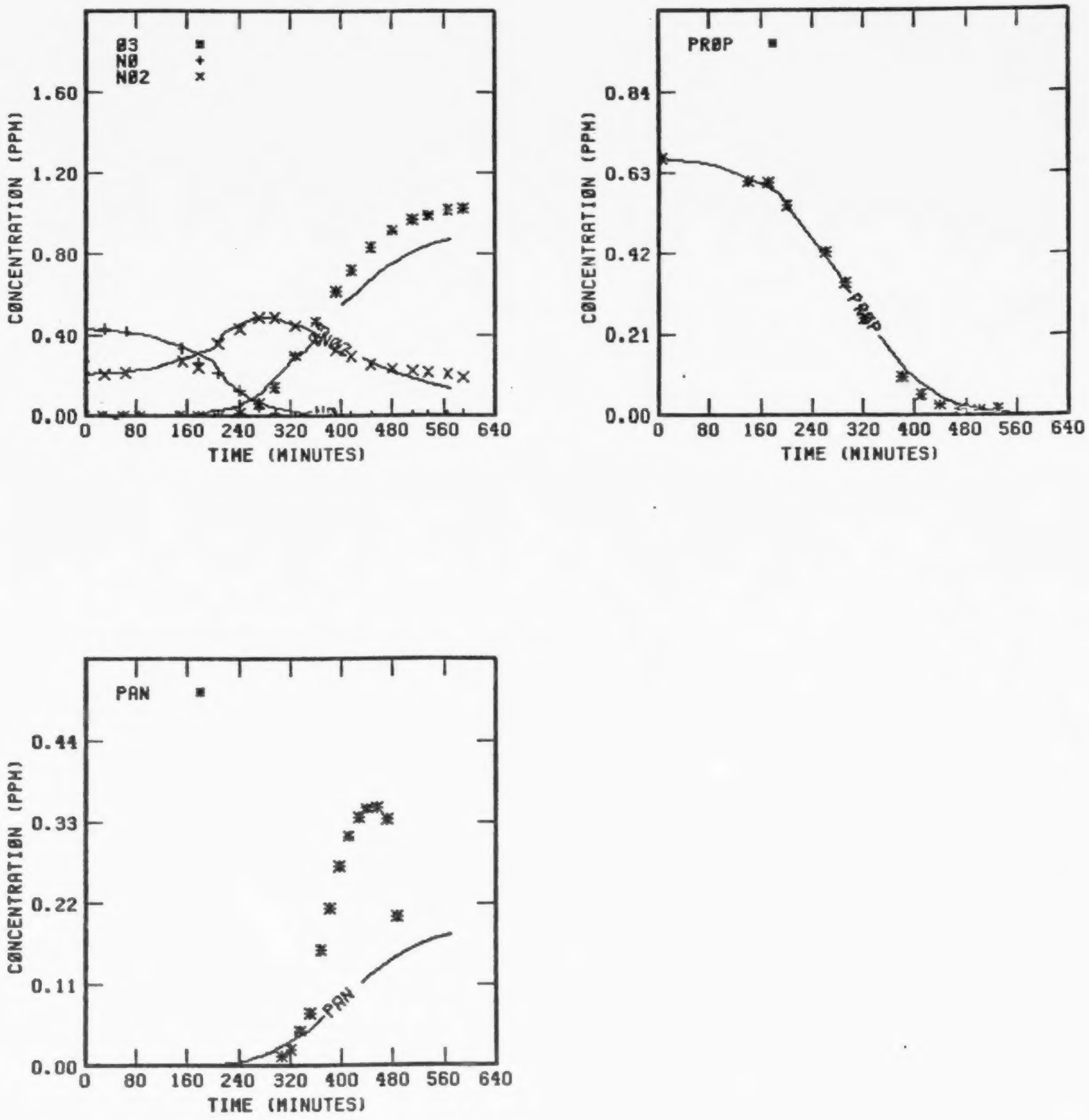

FIGURE 81 . SIMULATIØN RESULTS FØR
UNCB 61678

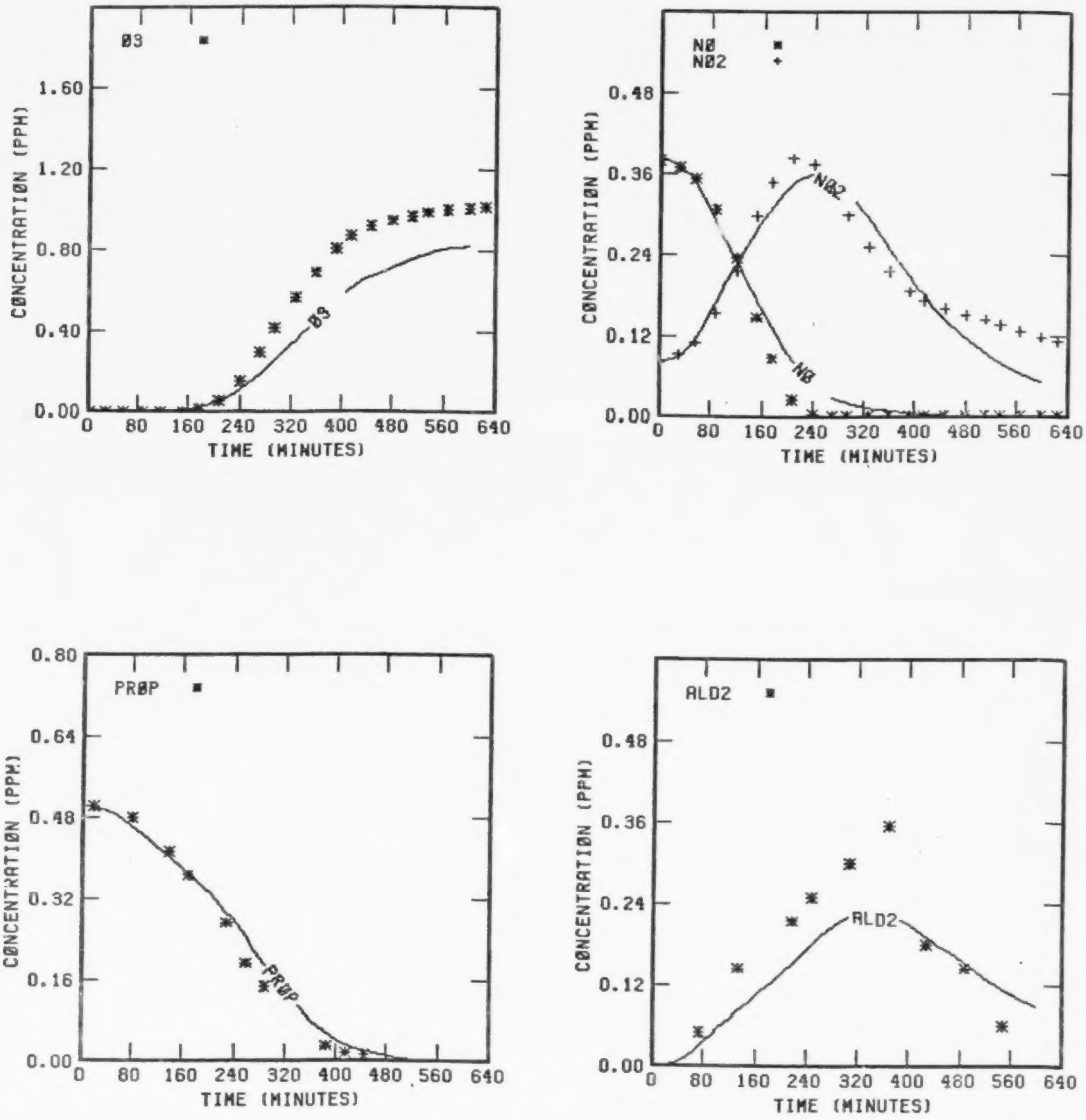

FIGURE 82 . SIMULATIØN RESULTS FØR
UNCR 63078

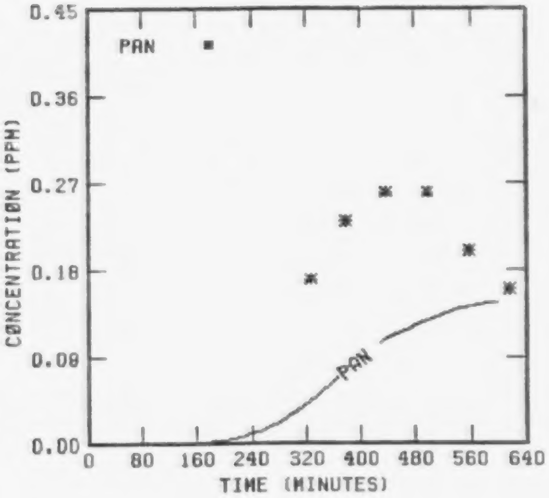

FIGURE 82 . (Concluded)

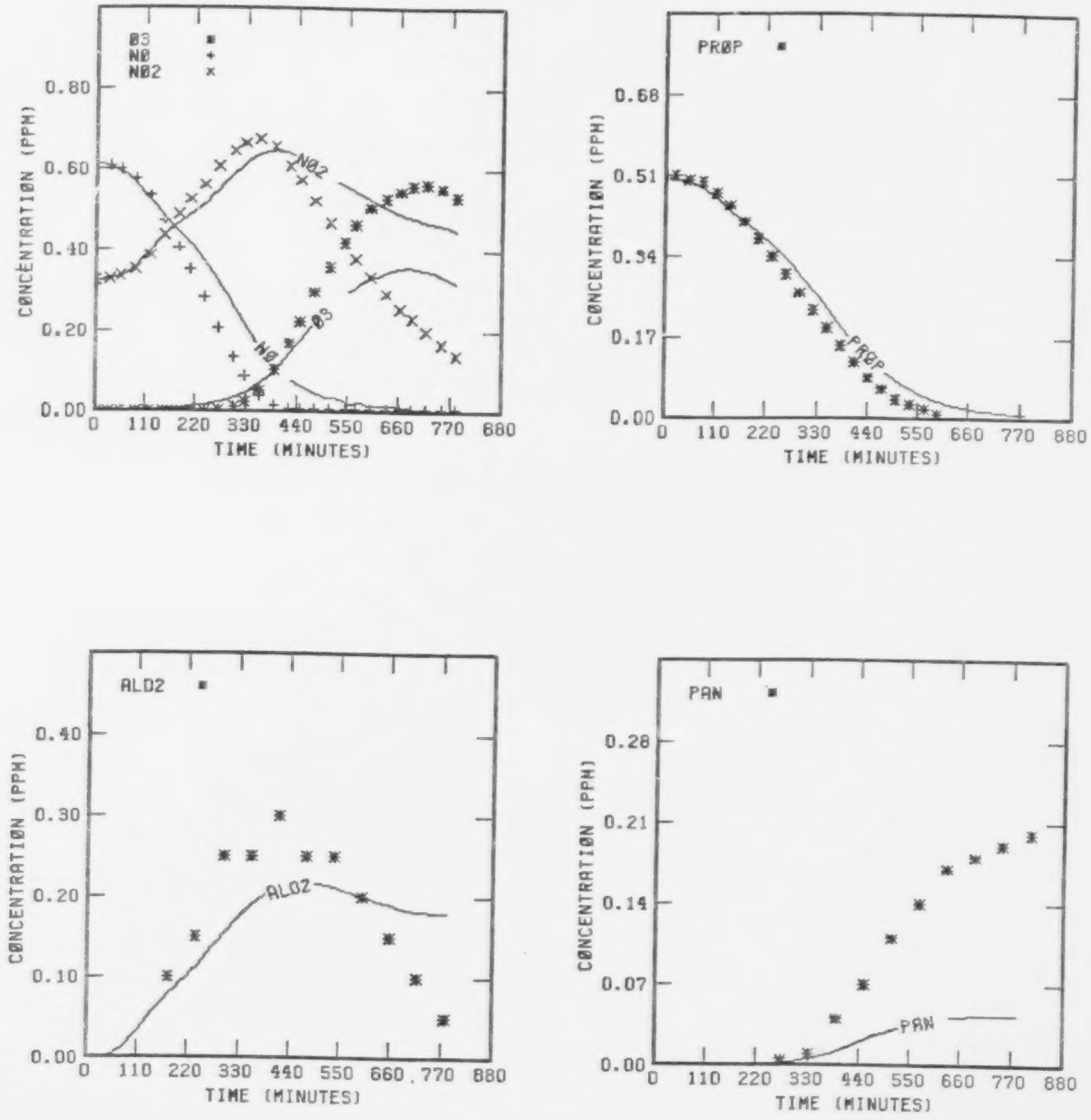

FIGURE 83 . SIMULATIØN RESULTS FØR
UNCB 70178

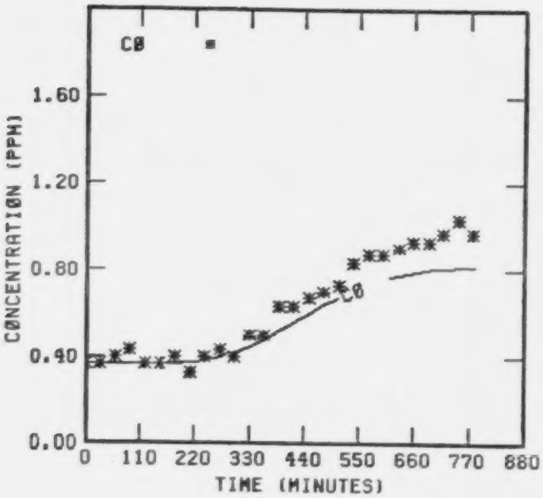

FIGURE 83 . (Concluded)

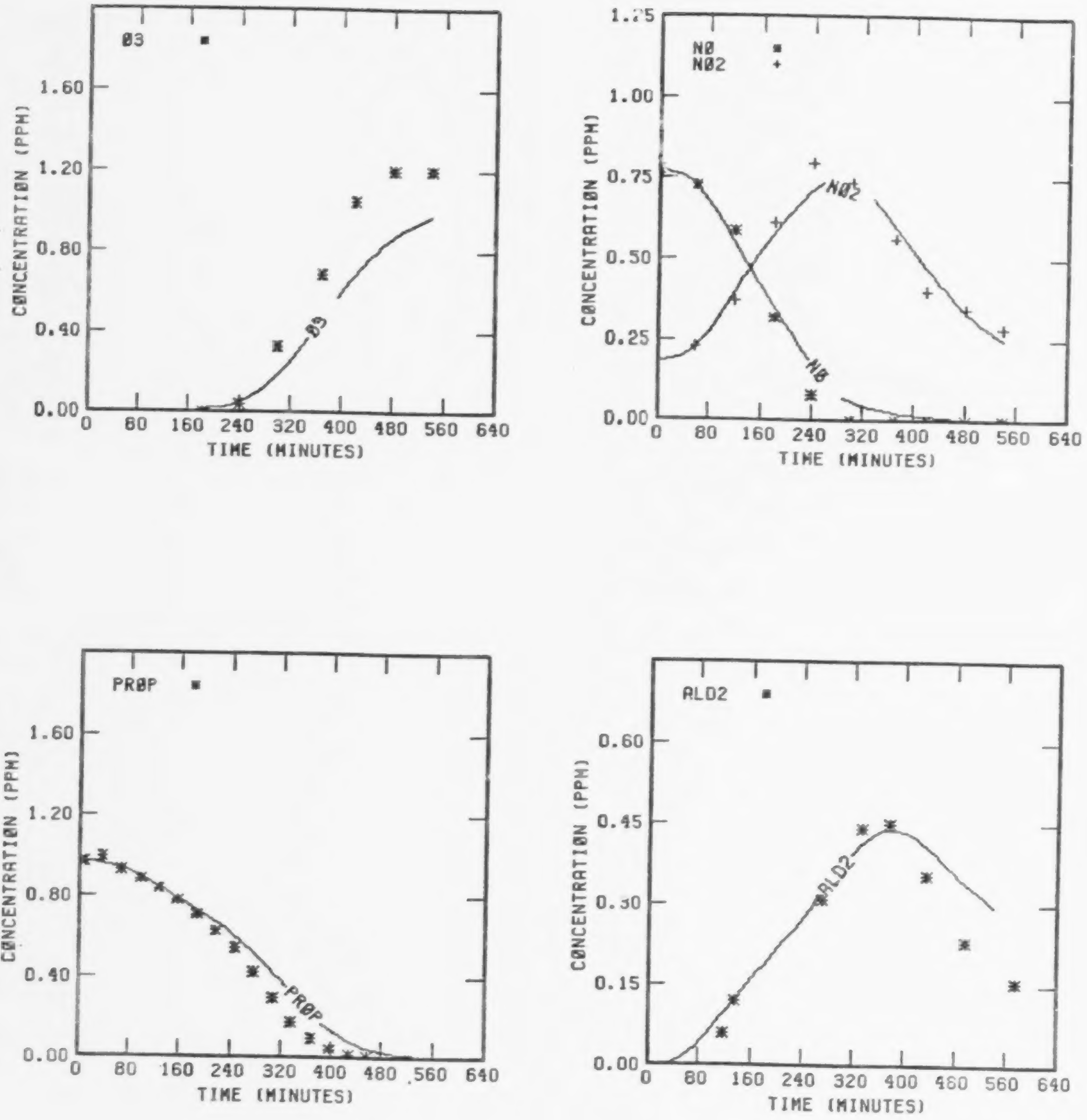

FIGURE 84 . SIMULATIØN RESULTS FØR
UNCR 72478

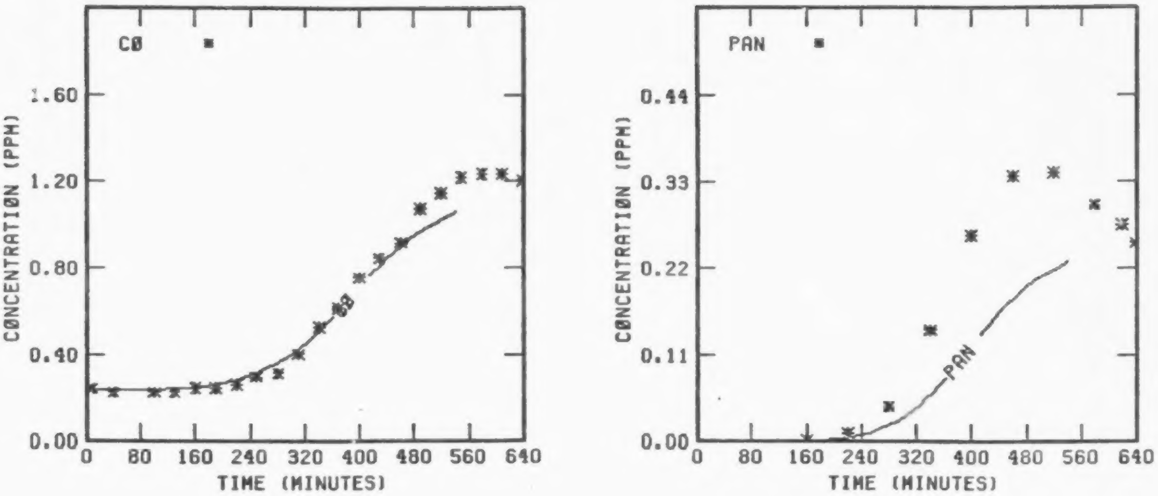

FIGURE 84 . (Concluded)

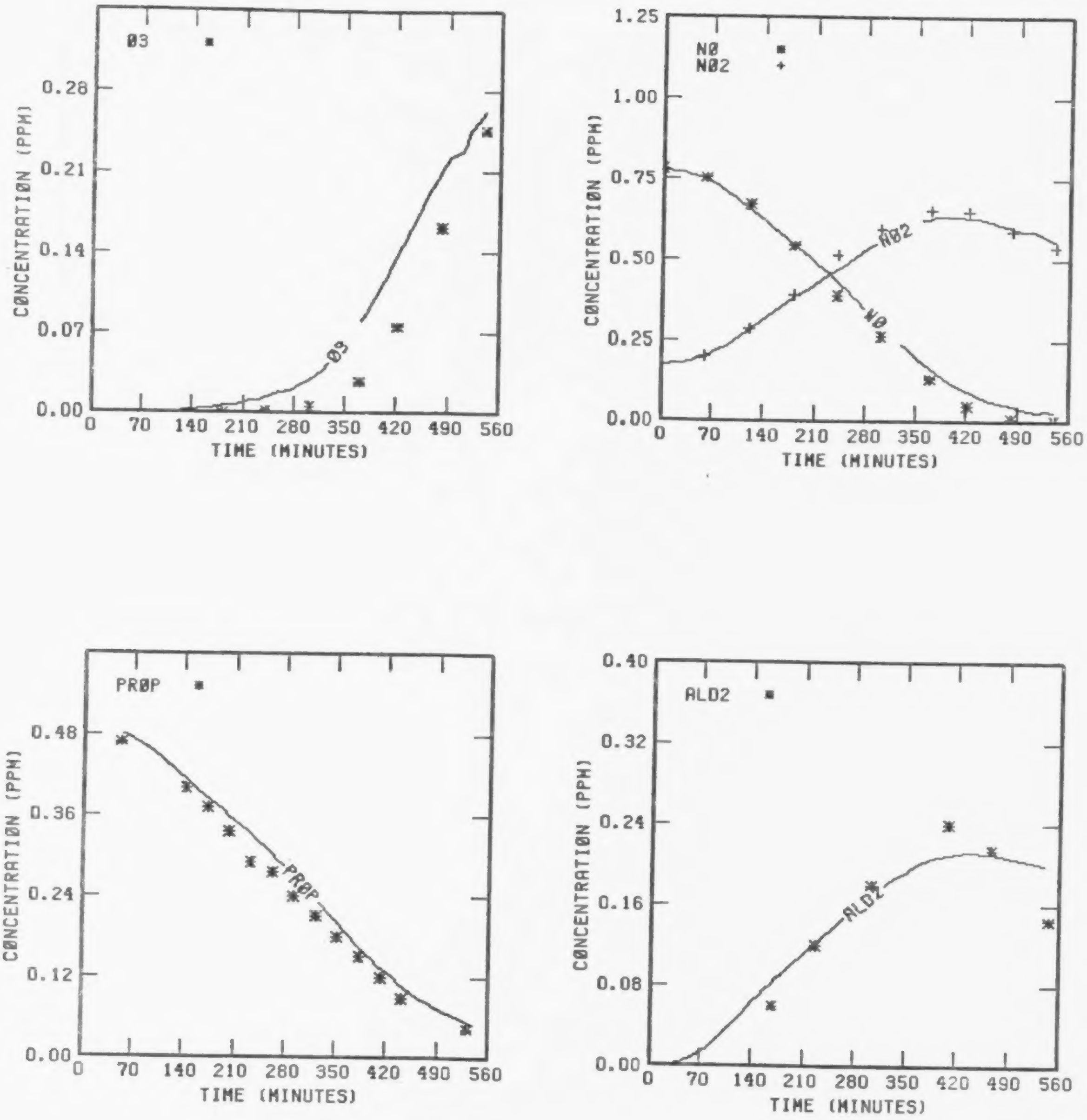

FIGURE 85 . SIMULATIØN RESULTS FØR
UNCB 72478

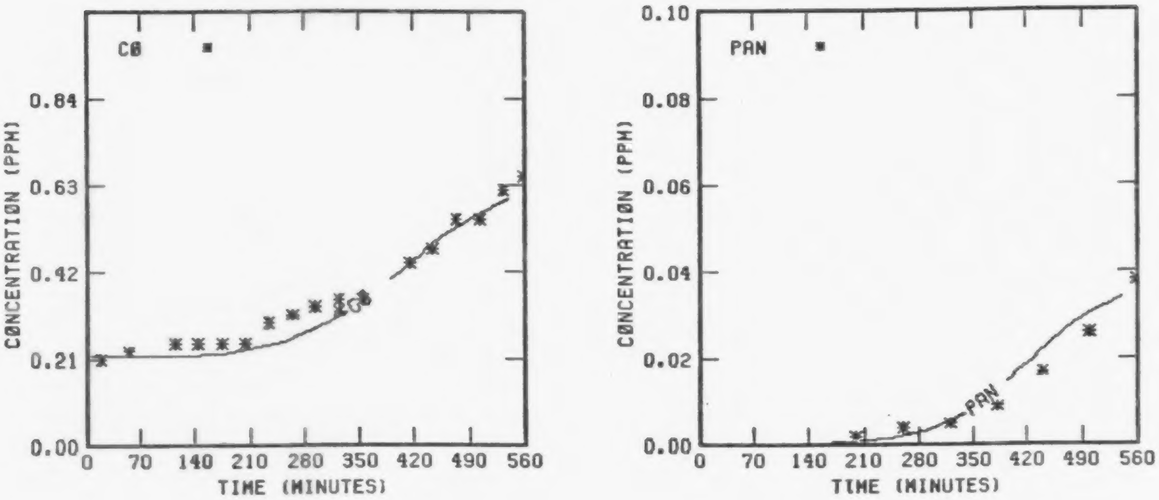

FIGURE 85. (Concluded)

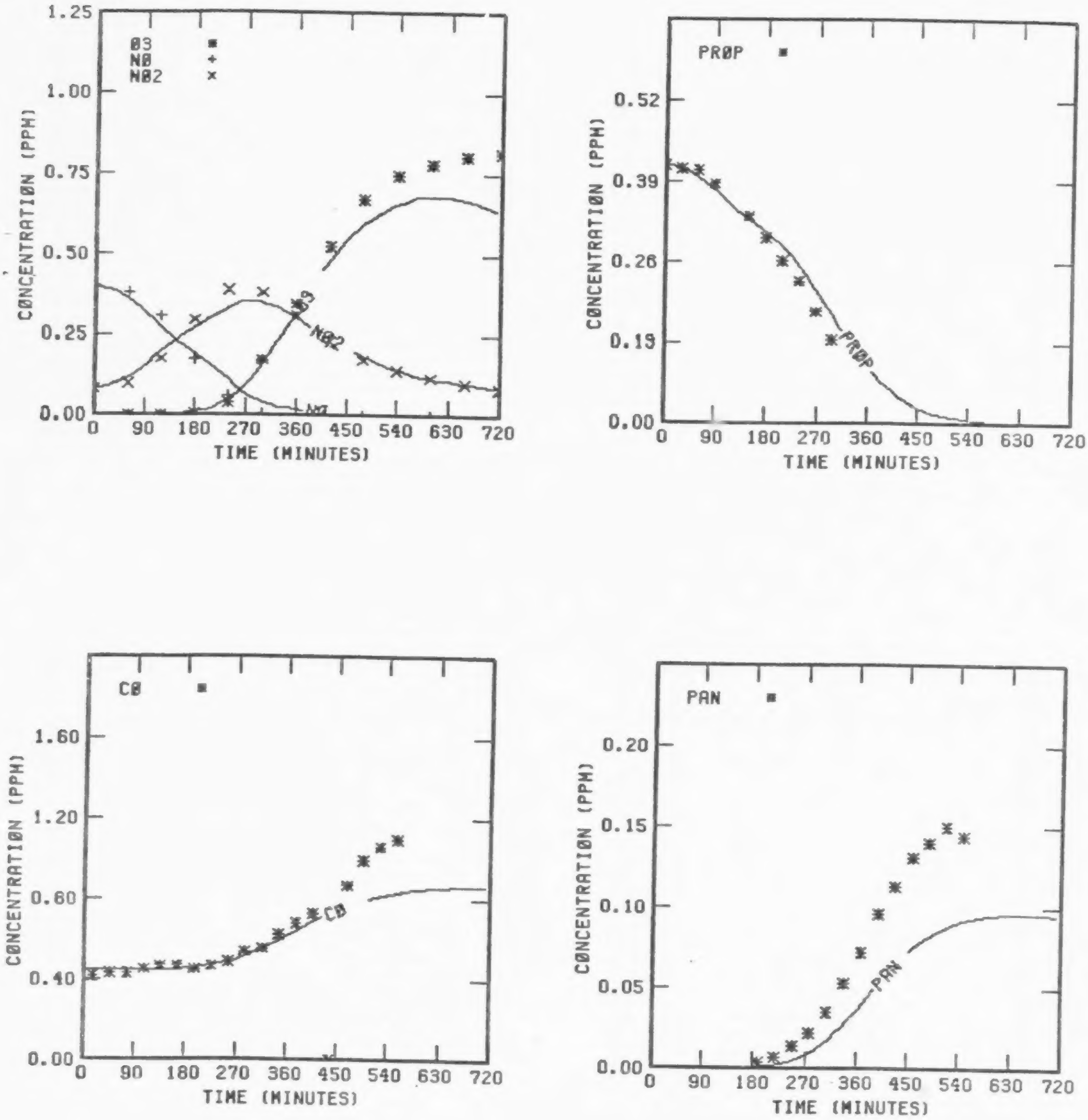

FIGURE 86. SIMULATION RESULTS FOR
UNCB 73078

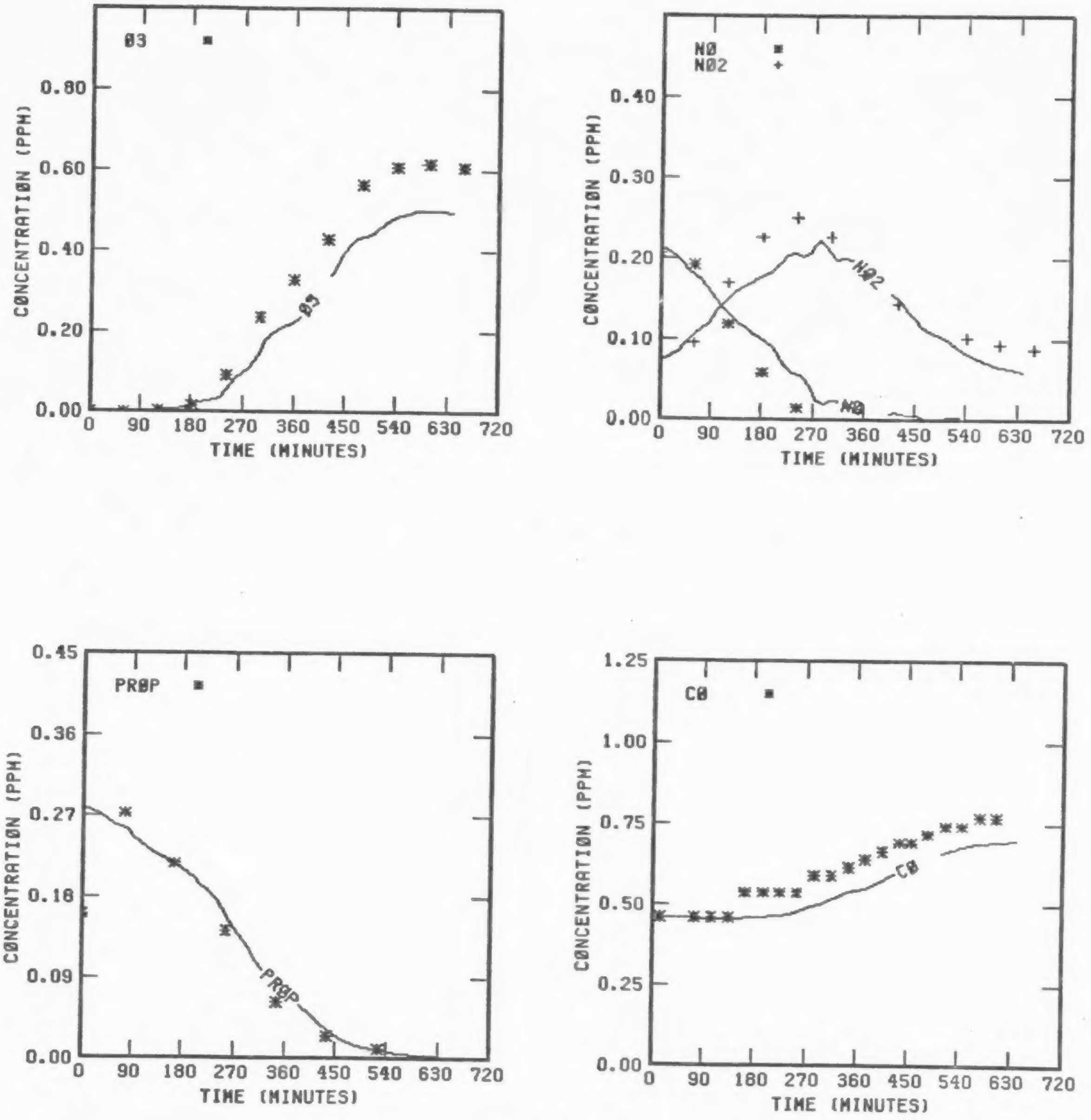

FIGURE 87 . SIMULATION RESULTS FOR
UNCR 80578

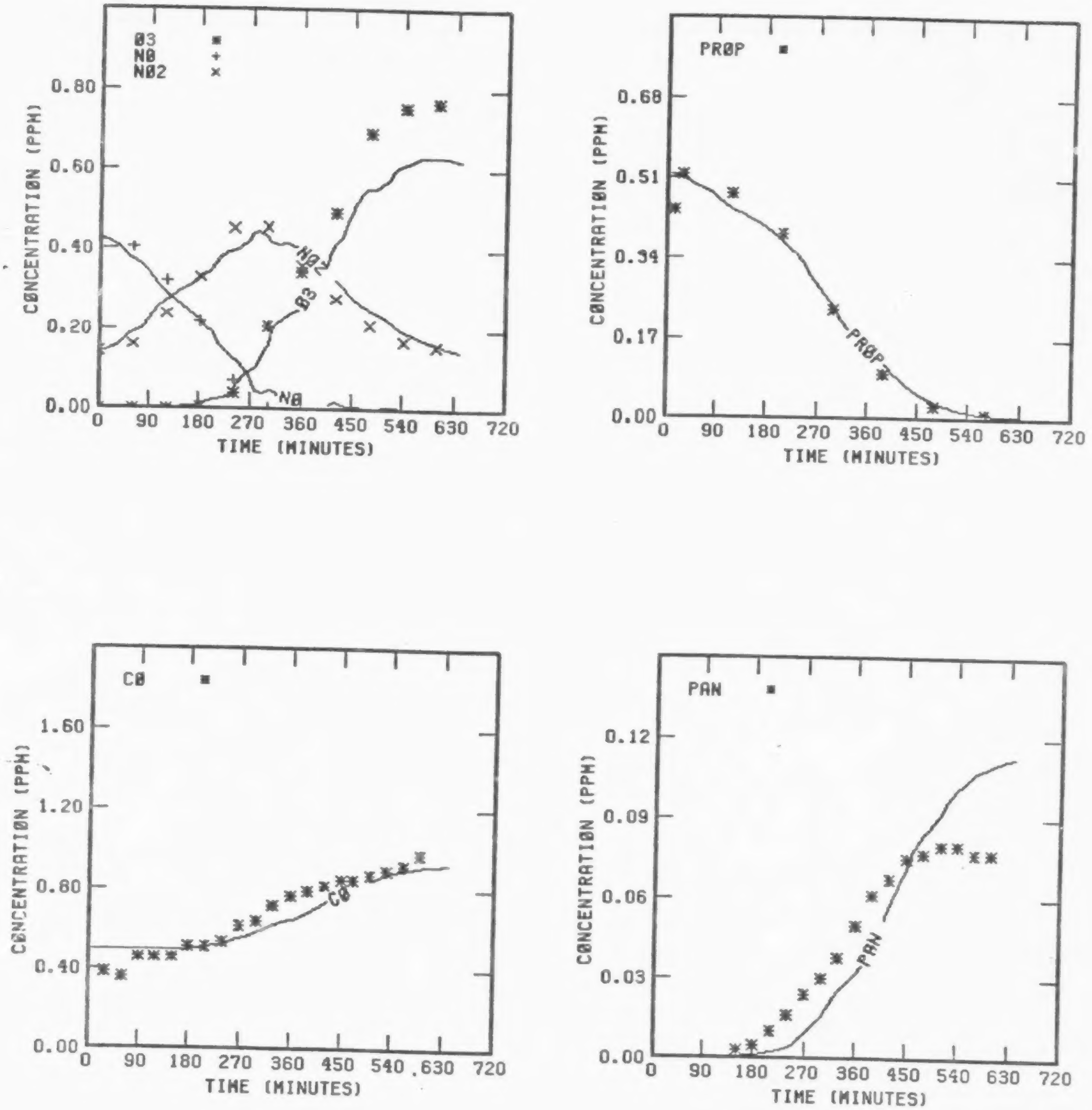

FIGURE 88 . SIMULATION RESULTS FOR
UNCB 80578

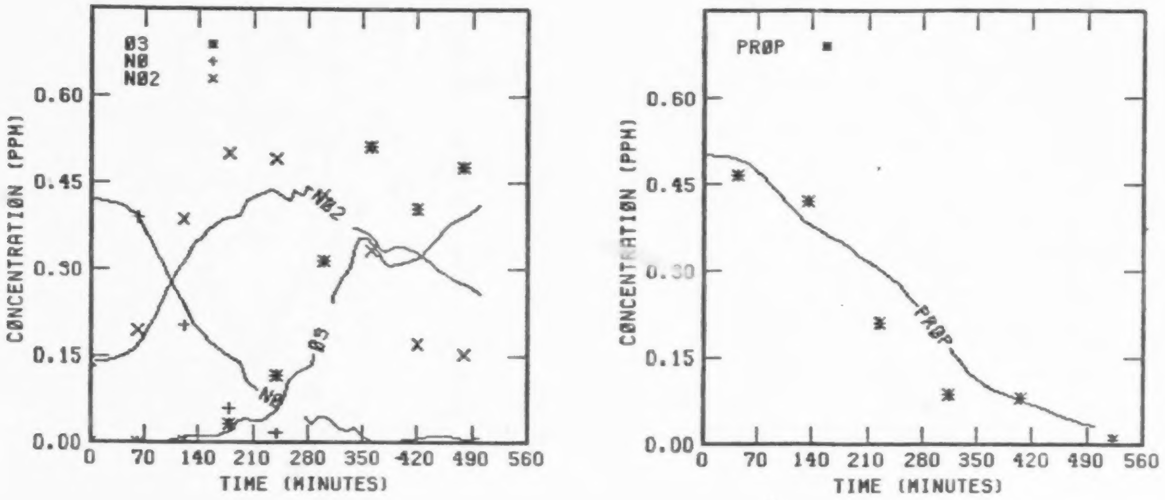

FIGURE 89 . SIMULATION RESULTS FOR
UNCR 80678

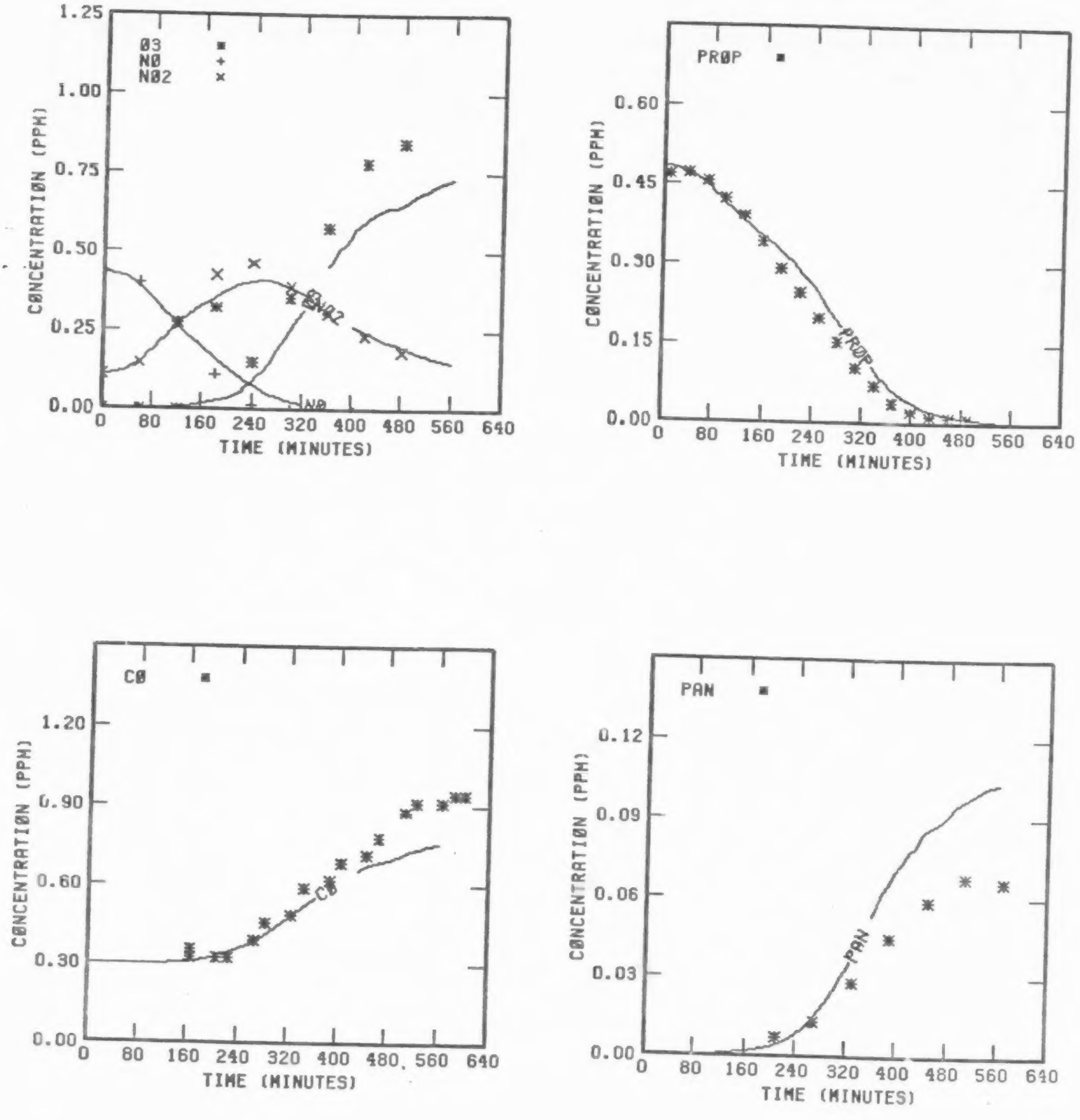

FIGURE 90 . SIMULATION RESULTS FOR UNCR 81578

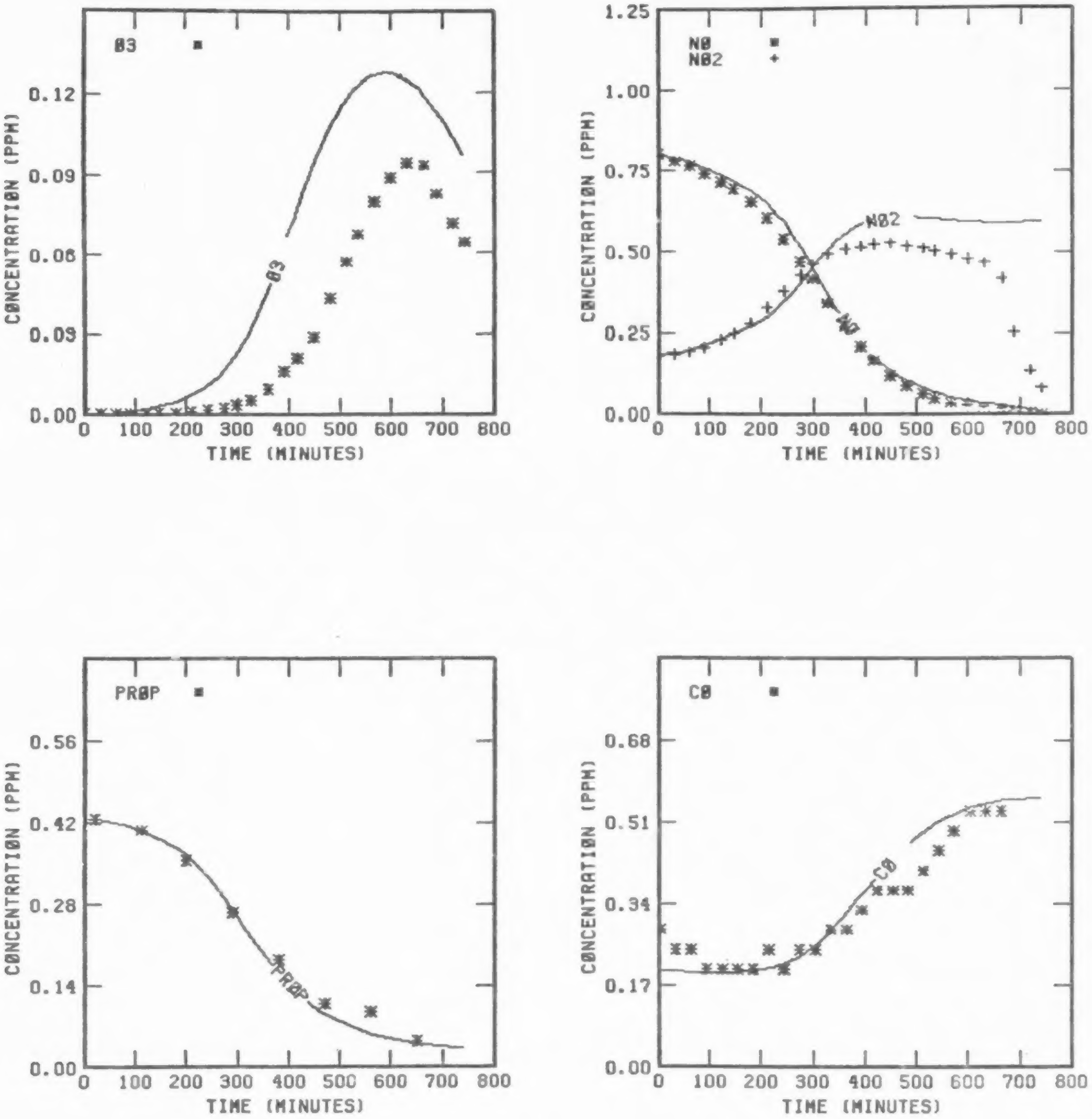

FIGURE 91. SIMULATION RESULTS FOR
UNCB 62178

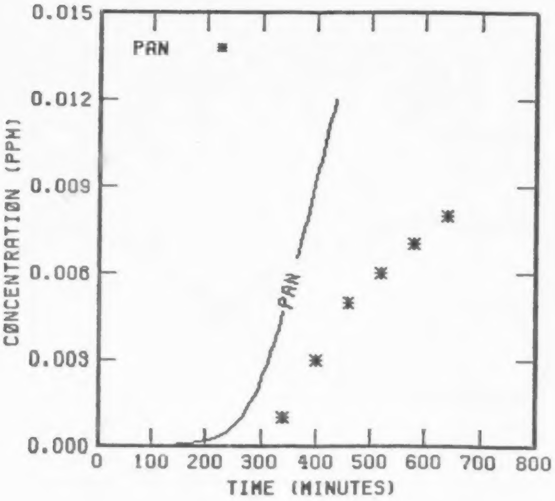

FIGURE 91. (Concluded)

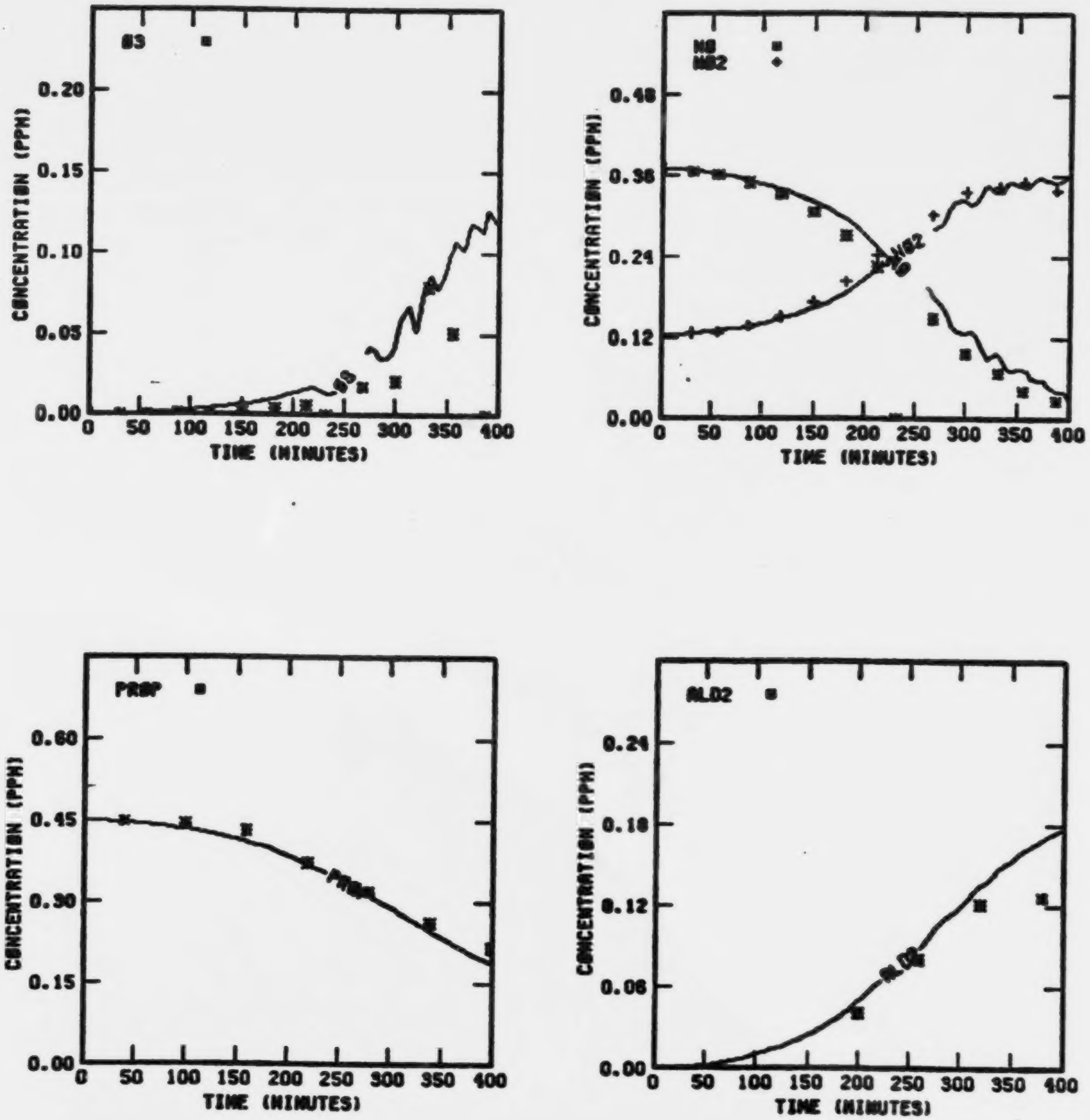

FIGURE 92 . SIMULATION RESULTS FOR
UNCR 101778

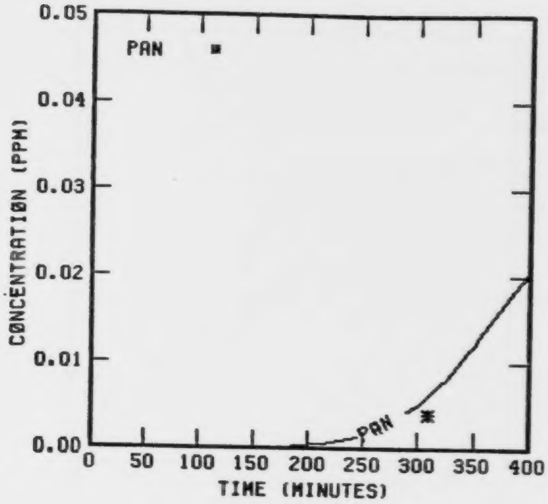

FIGURE 92 . (Concluded)

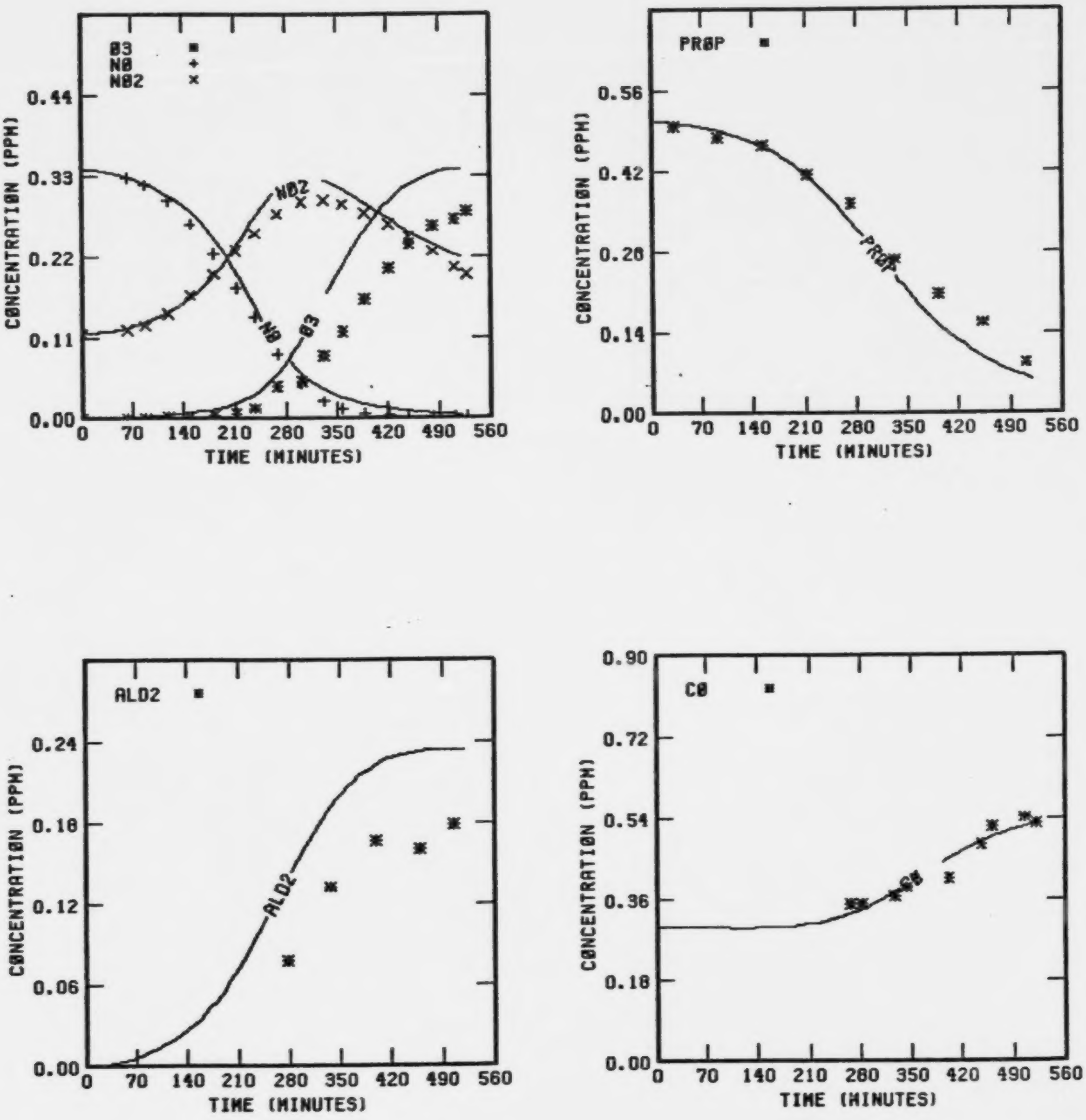

FIGURE 93 . SIMULATIØN RESULTS FØR
UNCB 101878

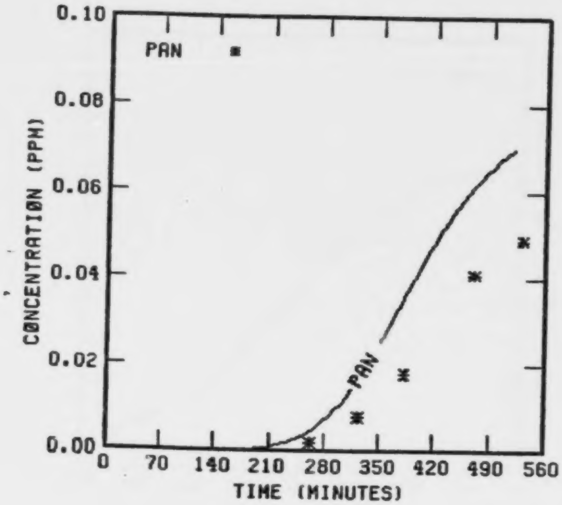

FIGURE 93. (Concluded)

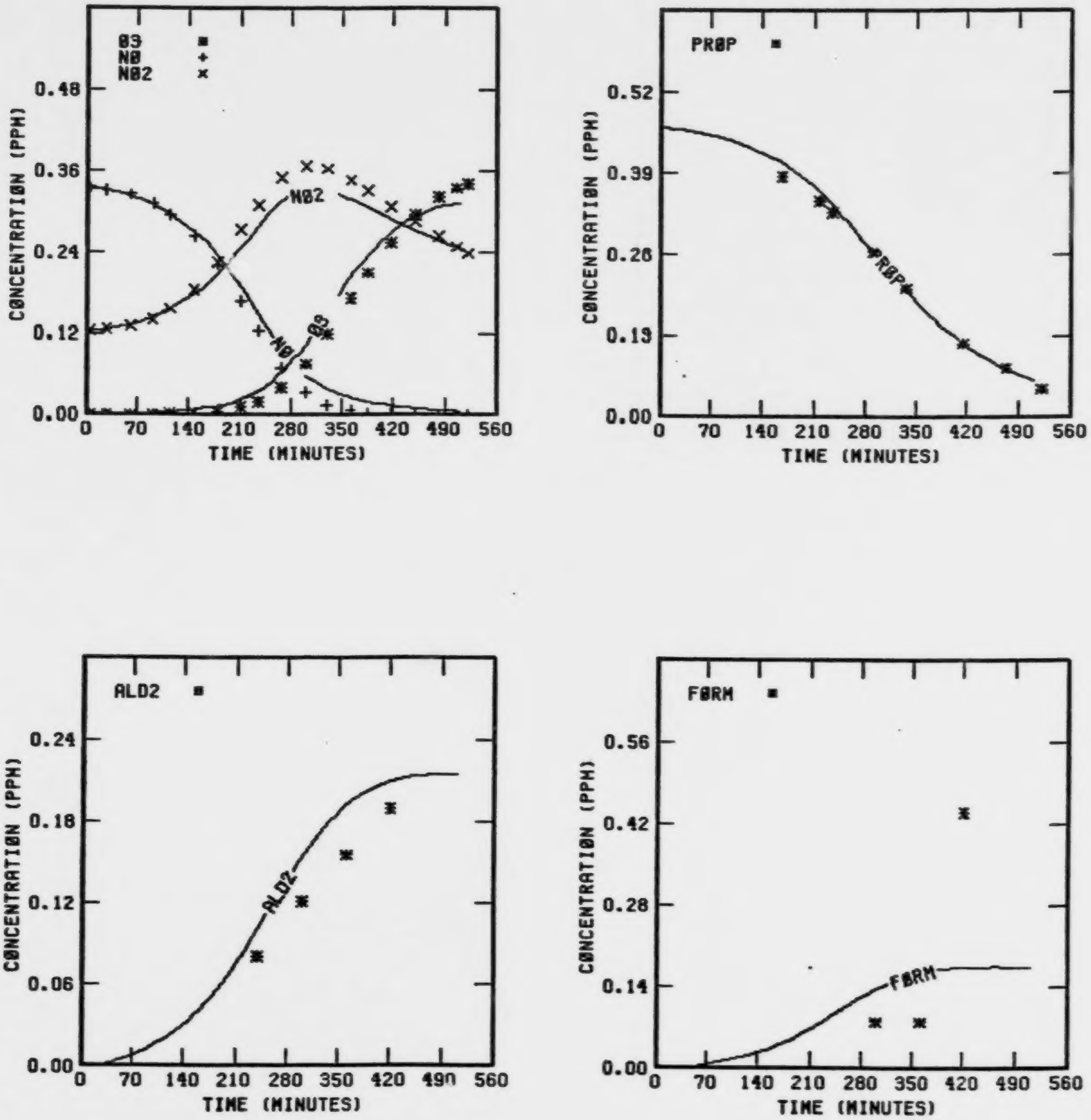

FIGURE 94 . SIMULATION RESULTS FOR
UNCR 102078

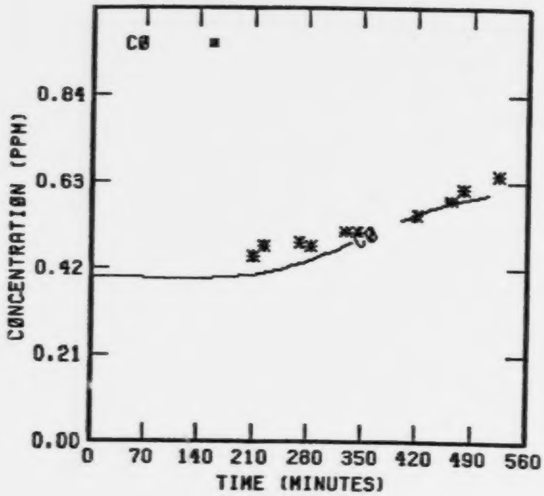

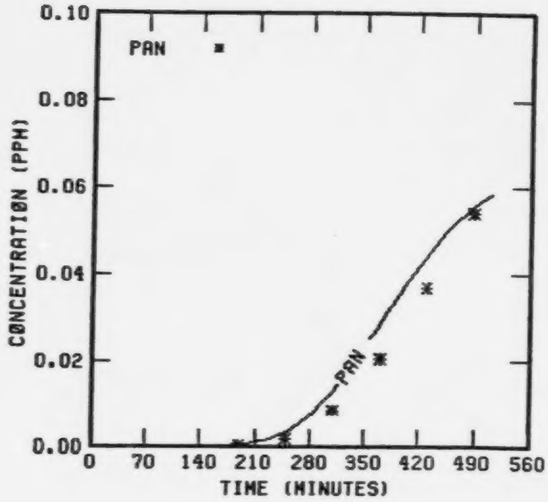

FIGURE 94. (Concluded)

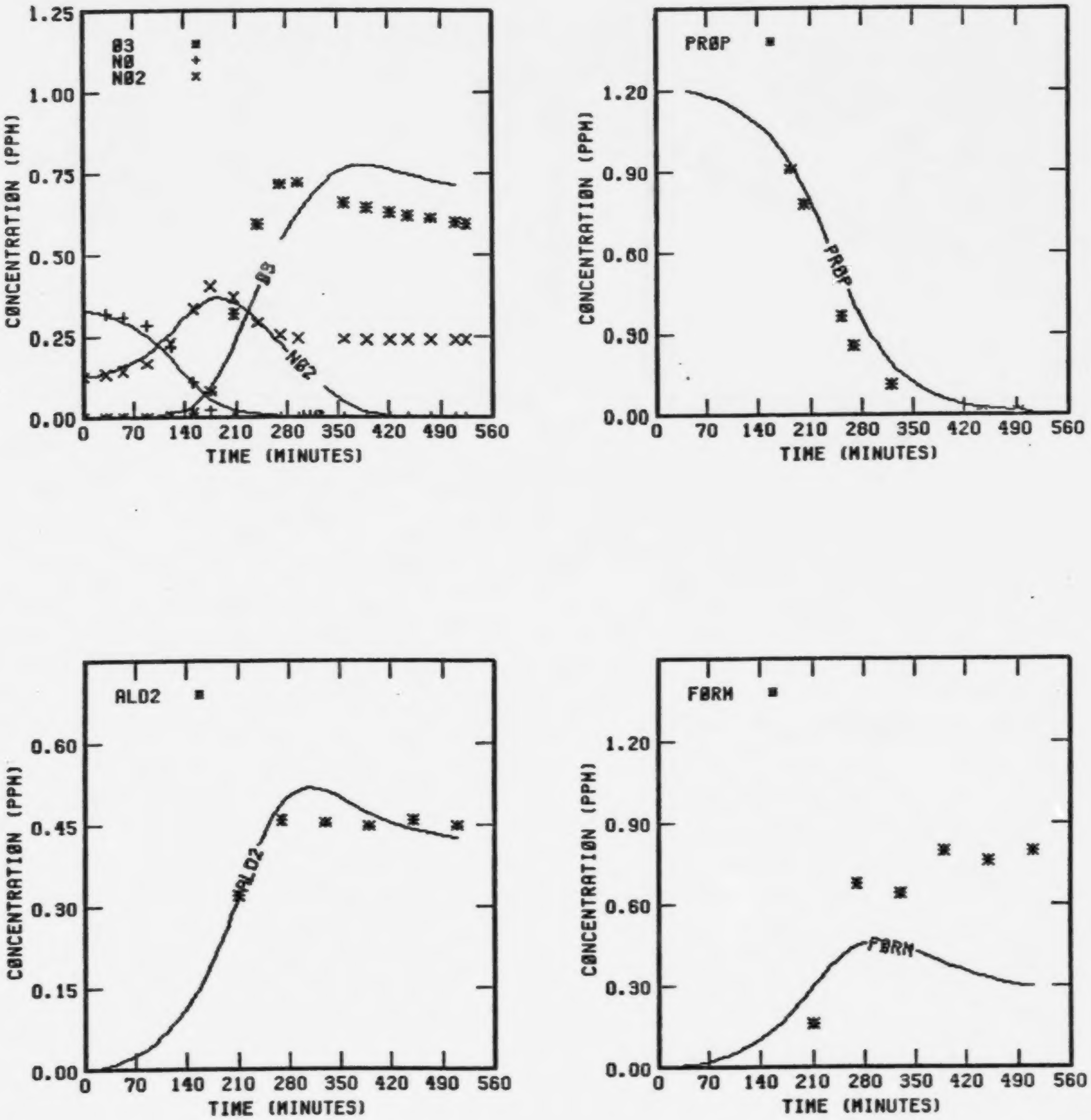

FIGURE 95 . SIMULATION RESULTS FOR
UNCB 102078

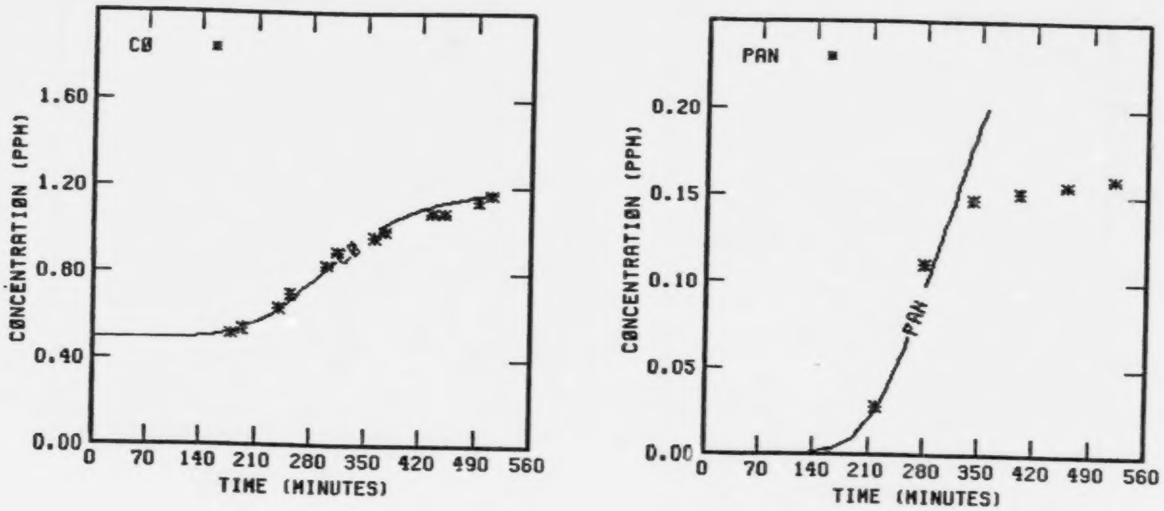

FIGURE 95 . (Concluded)

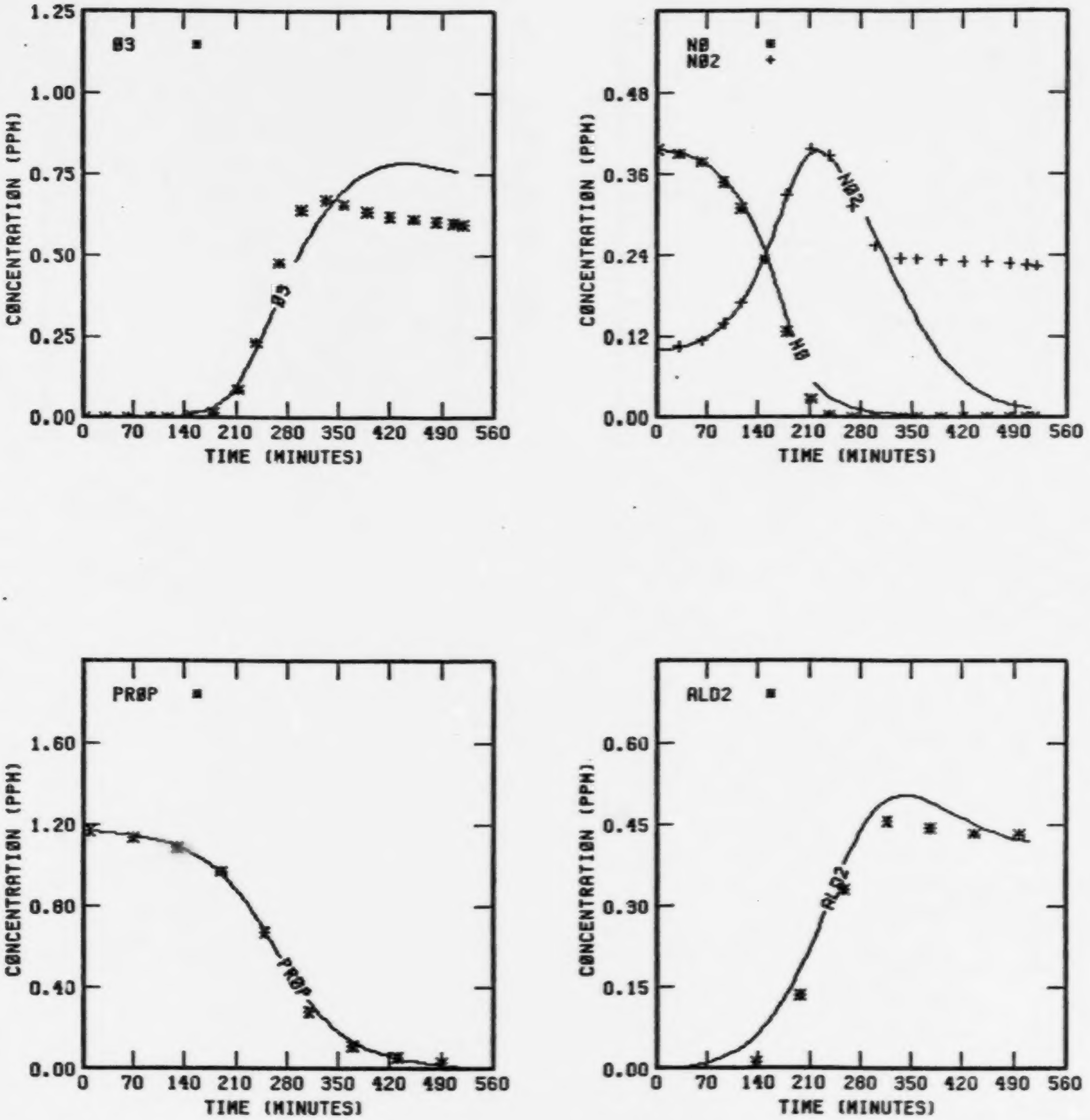

FIGURE 96 . SIMULATION RESULTS FOR
UNCR 10217B

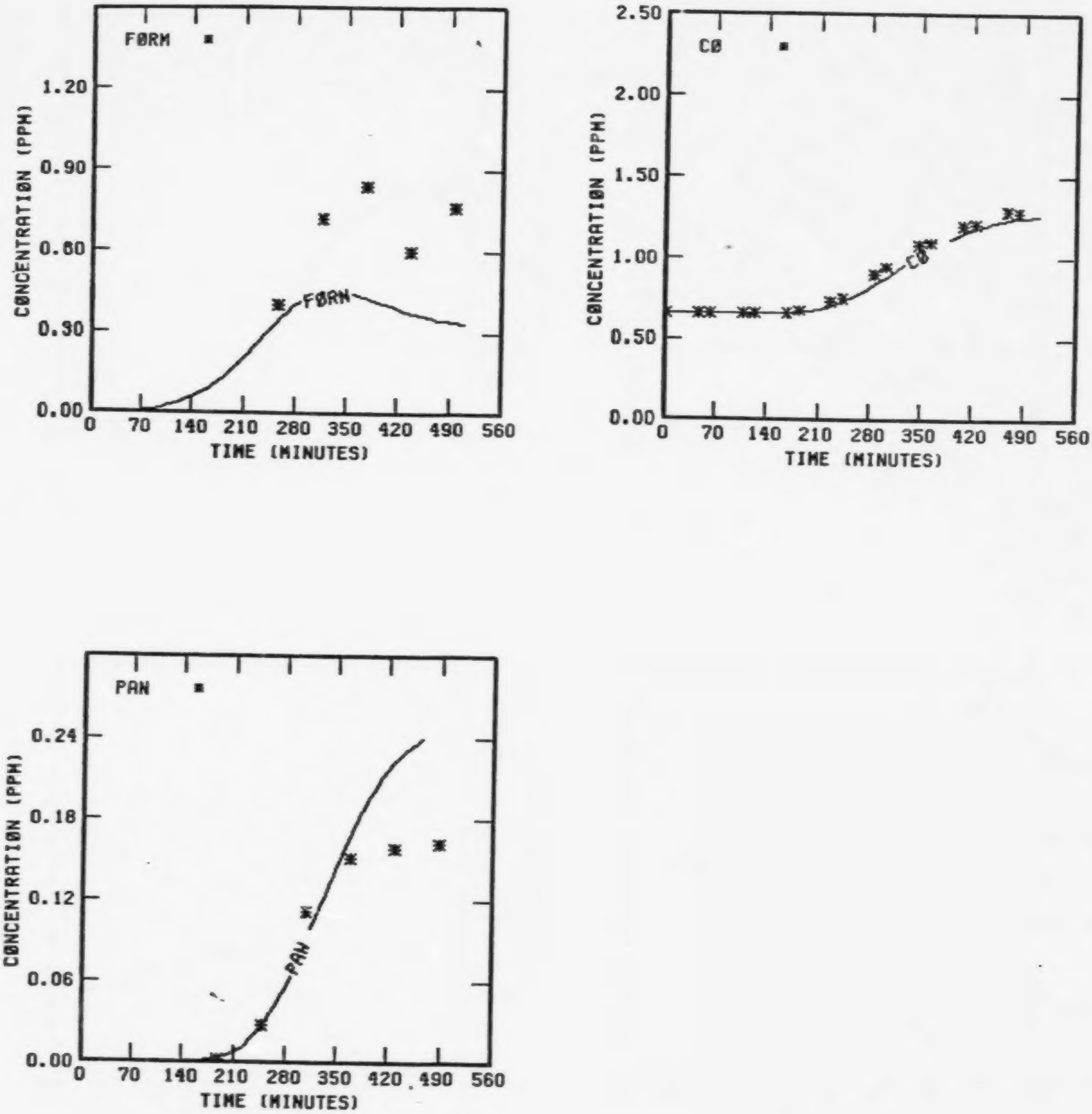

FIGURE 96 . (Concluded)

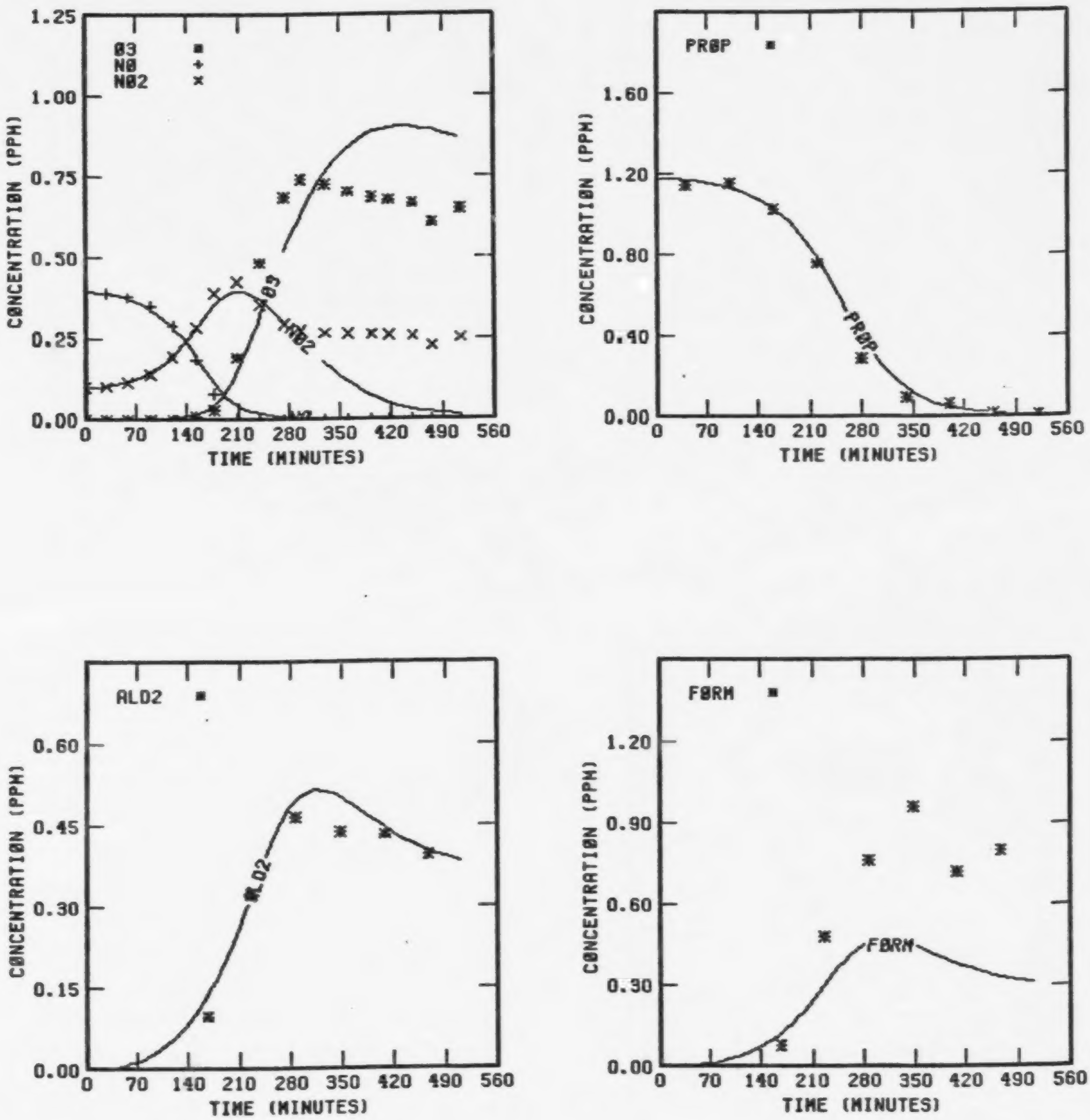

FIGURE 97 . SIMULATIØN RESULTS FØR
UNCB 102178

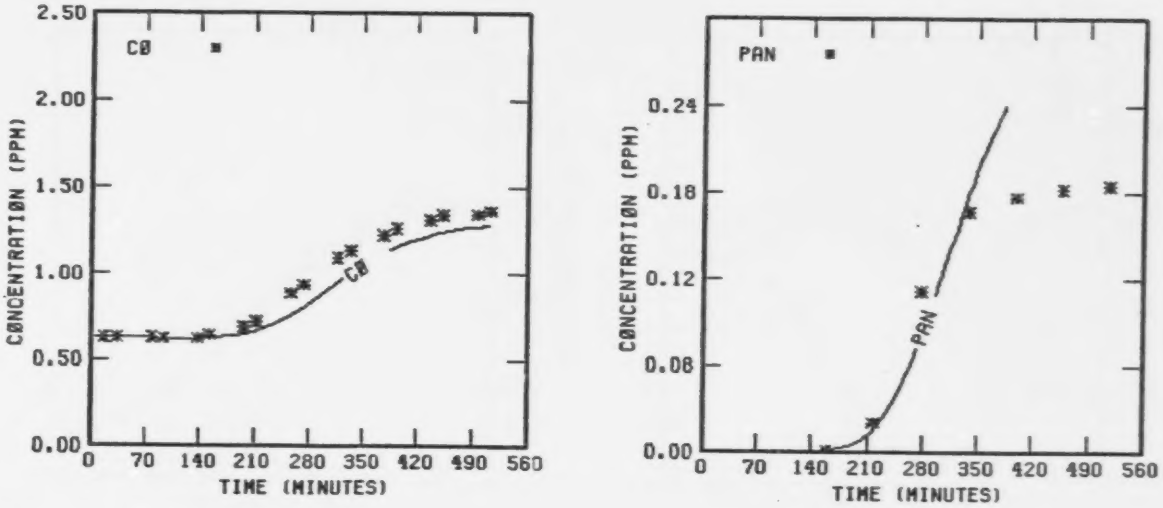

FIGURE 97 . (Concluded)

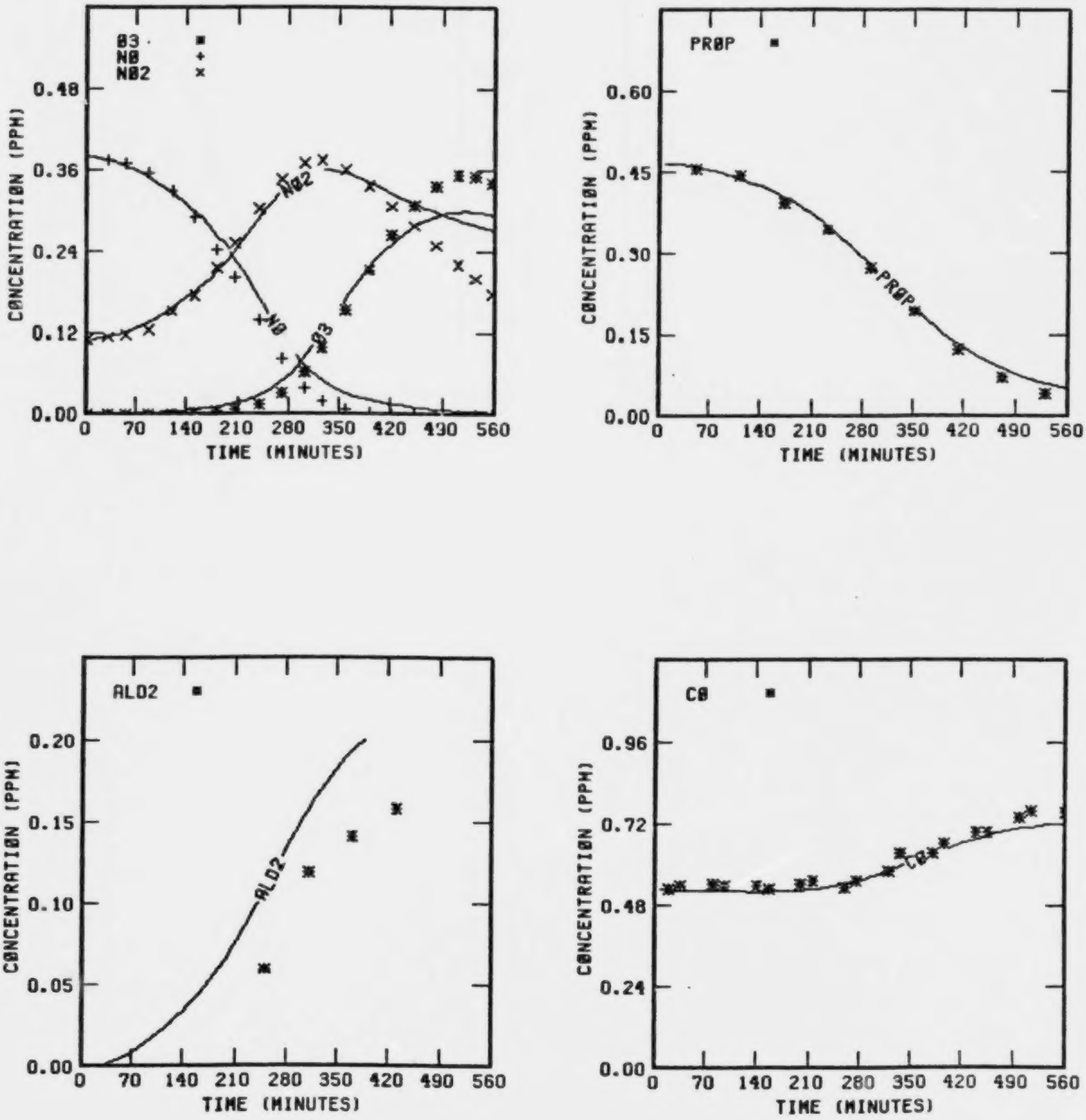

FIGURE 98 . SIMULATION RESULTS FOR
UNCR 102278

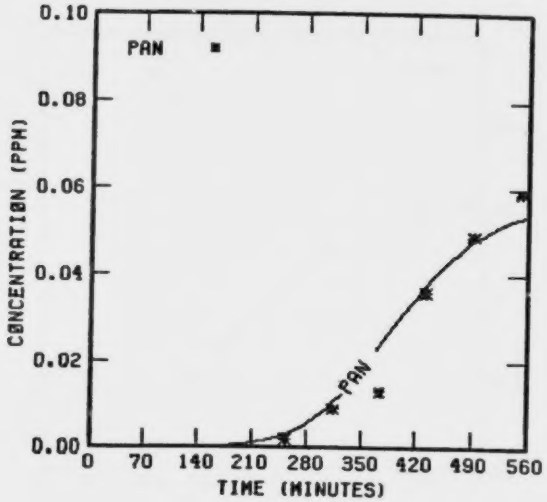

FIGURE 98. (Concluded)

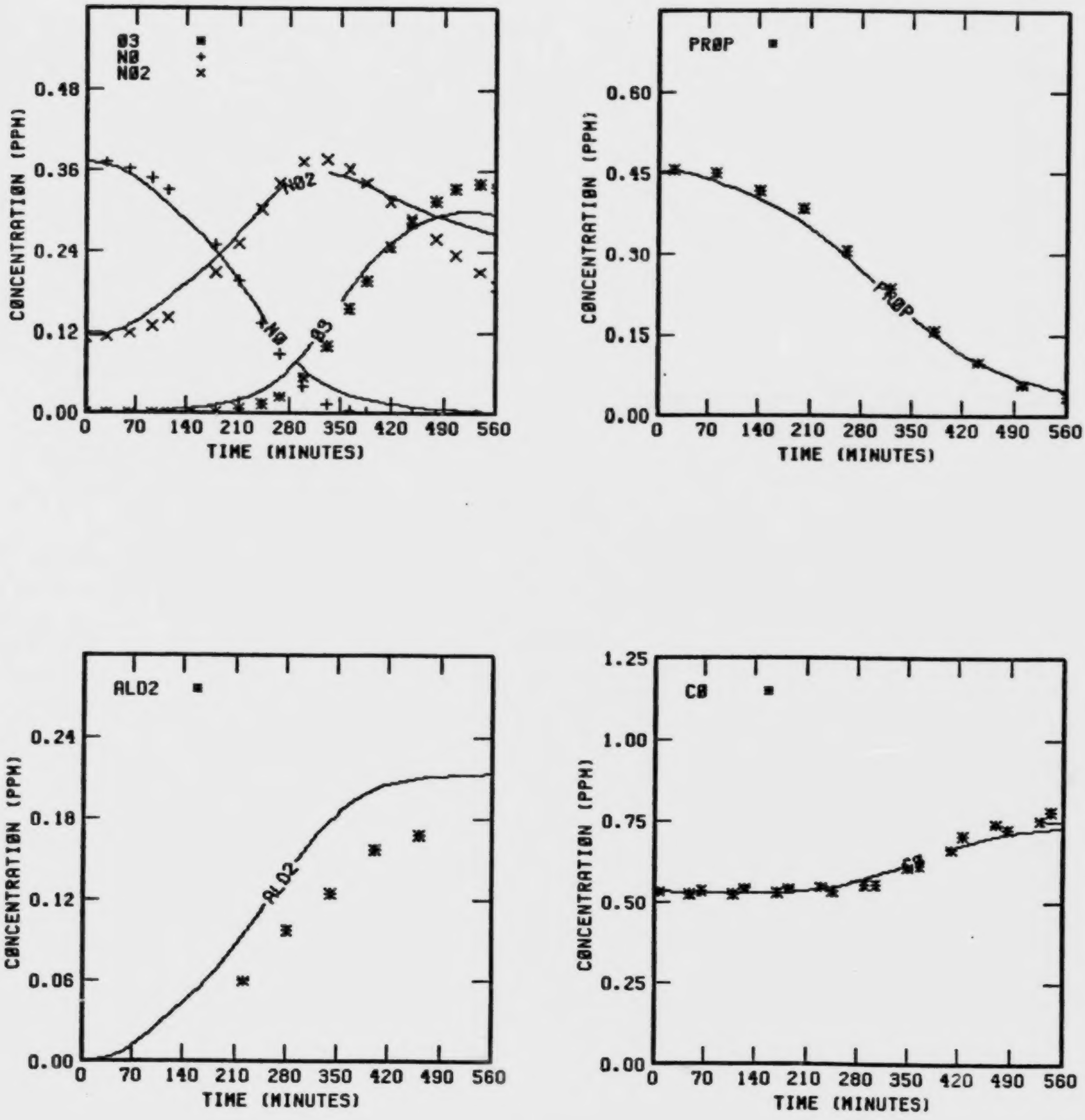

FIGURE 99 . SIMULATION RESULTS FOR
UNCB 10227B

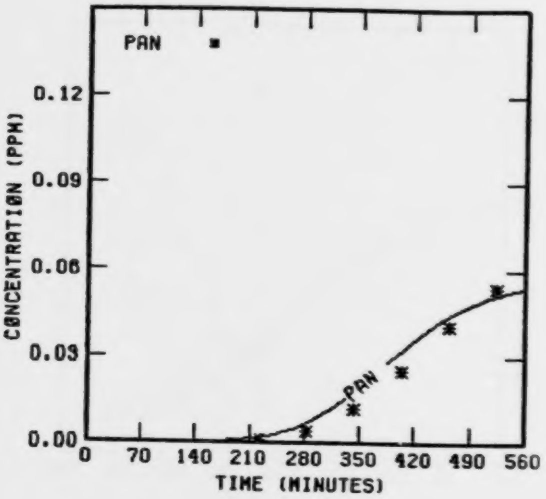

FIGURE 99 . (Concluded)

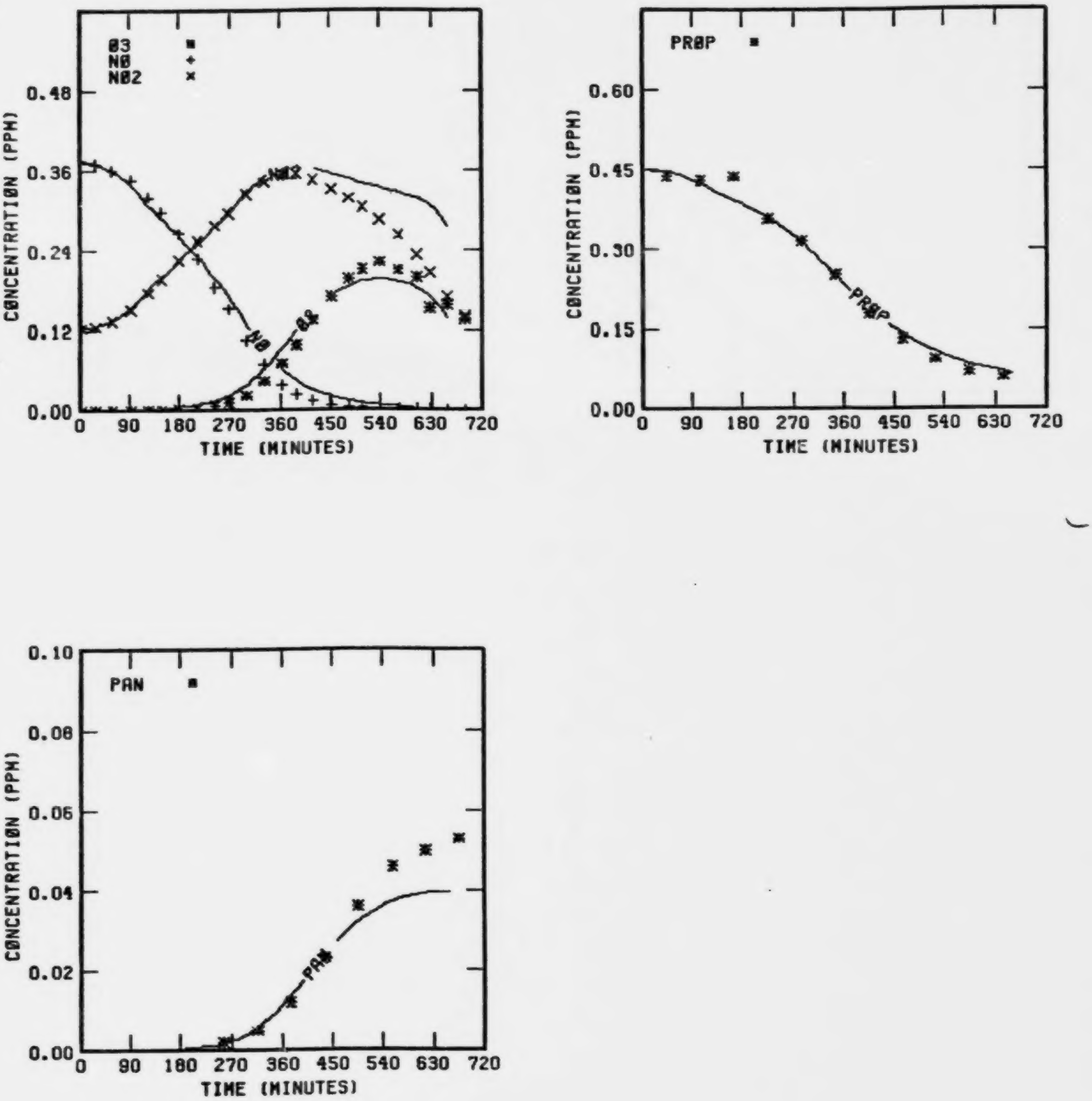

FIGURE 100. SIMULATION RESULTS FOR UNCR 102978

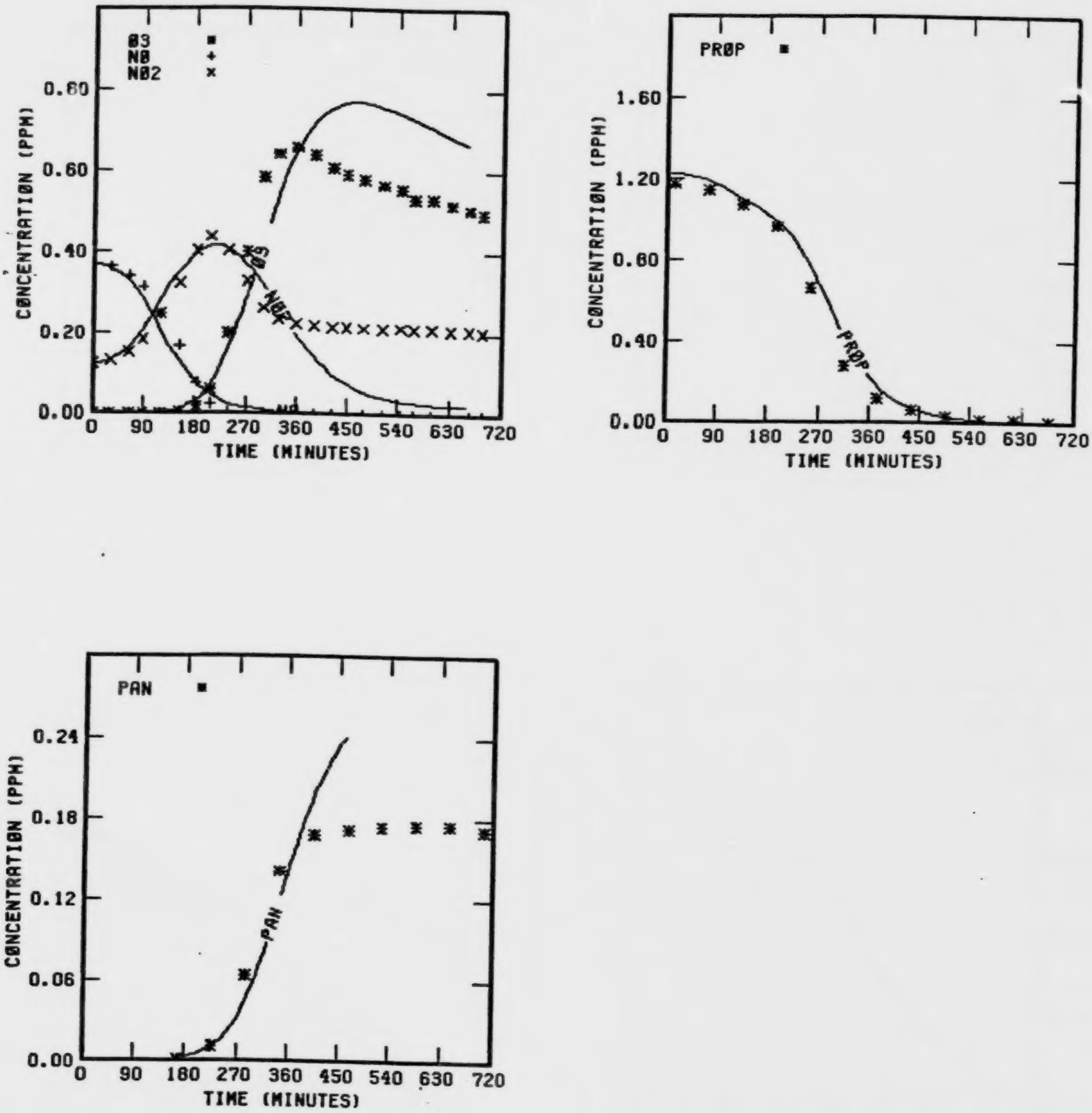

FIGURE 101. SIMULATION RESULTS FOR
UNCB 102978

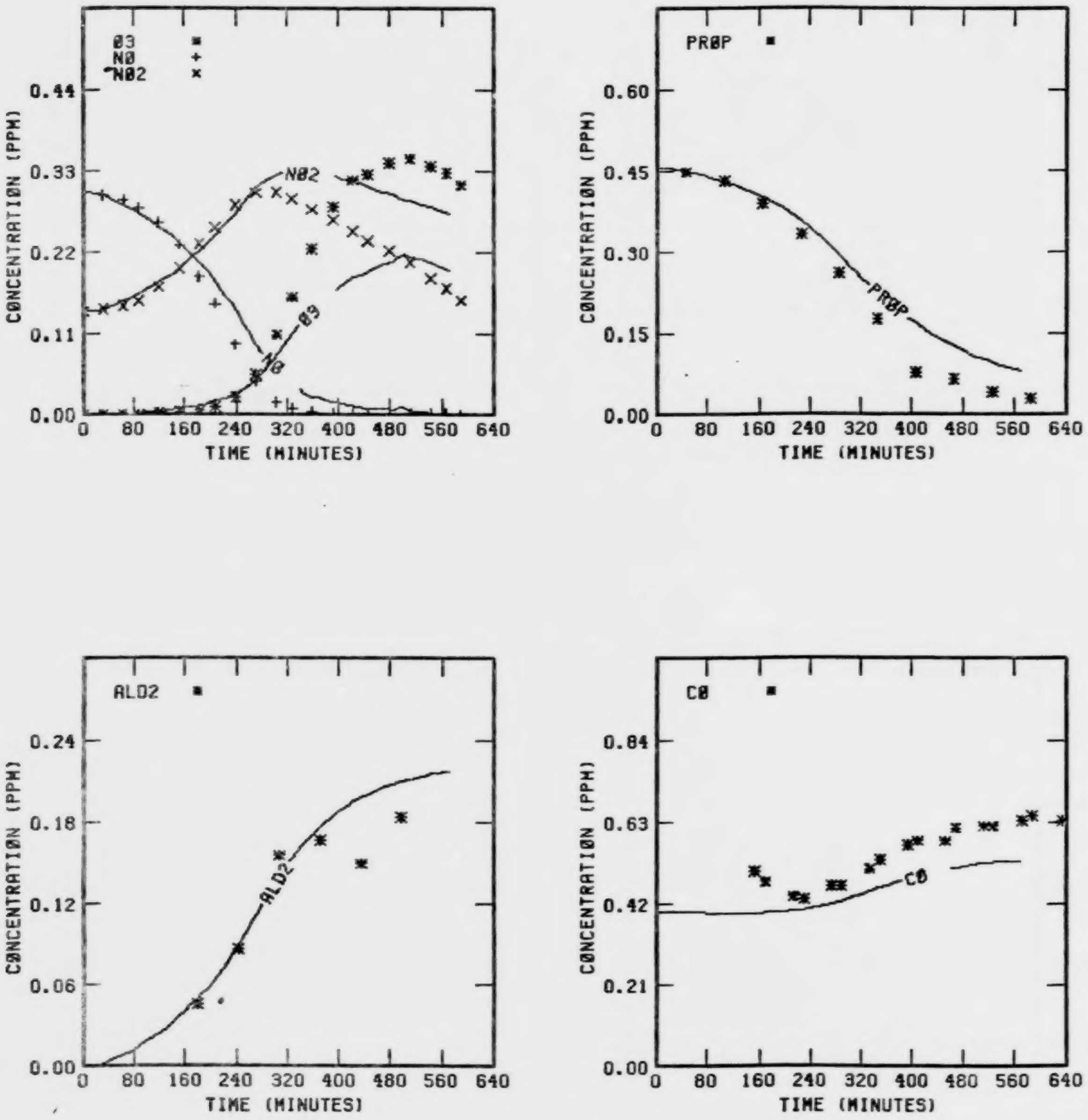

FIGURE 102. SIMULATION RESULTS FOR UNCR 110778

to obtain due to a combination of detection limits, interference from ozone and secondary nitrogen compounds, and sample line problems.

Somewhat different problems appear in the UNC simulations. In these simulations UV data were used rather than arbitrarily varying photolysis constants to simulate propylene decay (as was done in the UCR simulations); therefore, several days appear to have improper radical inputs, especially on cloudy days when only TSR data were available. Nevertheless, several days show rather close simulations of observed propylene decay, yet ozone may be either underpredicted or overpredicted. On many days, a very rapid rise in ozone occurs around 1200 hours which the present simulations cannot follow even if the NO_x crossover is simulated too early. A drastic example of this is seen in Figure 80 for the red side of the experiment performed on 31 March 1978. One explanation for the overprediction/underprediction problem in the UNC set of simulations may be an NO_x loss reaction that changes between experiments and has yet to be properly characterized. Candidates for future study are the N_2O_5 reaction with H_2O and the loss rate of PNA to the walls.

PROPYLENE/ACETALDEHYDE

Differences between the PAN simulations in dual chamber experiments at UNC, which compared ethylene/acetaldehyde on one side of the chamber to propylene on the other, were discussed earlier. Also, to support the use of a low acetaldehyde photolysis rate, we indicated that successive experiments at UCR (EC-216 and EC-217) should use similar photolysis constants; EC-217 contained a large initial concentration of acetaldehyde added to propylene while in EC-216 propylene was the only organic compound. Finally, the mixture of acetaldehyde and propylene represents a means of using the hierarchical concept to further test parts of the propylene and PAN chemistry. However, a key experiment, EC-217, is poorly simulated by our current chemistry in an unusual fashion: the decay of propylene and acetaldehyde cannot be simultaneously simulated as indicated in Figure 104. We requested that a similar pair of experiments be performed in the dual facility at UNC and, on 12 June 1979, these experiments were carried out. Table 24 and 25 show the initial conditions for the two UCR and two UNC experiments. Figures 103 through 106

TABLE 24. INITIAL CONDITIONS FOR UCR PROPYLENE/ACETALDEHYDE AND PROPYLENE/NO_x EXPERIMENTS

	Initial concentrations (ppm)						Photolysis rate constant ($10^4 min^{-1}$)*					
Exp. No.	Propylene	Acetaldehyde	NO	NO_2	HONO	H_2O	$NO_2 + h\nu$	$O_3 + h\nu \rightarrow O'D$	$O_3 + h\nu \rightarrow O$	$HONO + h\nu \rightarrow$	$H_2O_2 + h\nu \rightarrow$	Carbonyl + $h\nu \rightarrow$
EC-216	.48	.002	.412	.104	.008	2.4×10^4	.43	35.3	135.	1280.	6.	15.
EC-217	.076	.16	.210	.238	.005	2.8×10^4	.43	35.3	135.	1280.	6.	15.

* Rate constant in min^{-1} for NO_2.

TABLE 25. INITIAL CONDITIONS FOR UNC PROPYLENE/ACETALDEHYDE AND PROPYLENE/NO_x EXPERIMENTS

			Initial Concentration (ppm)						
Date	Chamber Side	Sky Conditions	Propylene	Acetaldehyde	NO	NO_2	HONO	H_2O	Carbonyl + $h\nu$ Constant
6/12/79	Red	Clear	.278	-	.257	.243	.008	2×10^4	1.0*
6/12/79	Blue	Clear	.178	.04	.254	~.24	0	2×10^4	1.0*

* UV data used in computer simulations instead of TSR data.

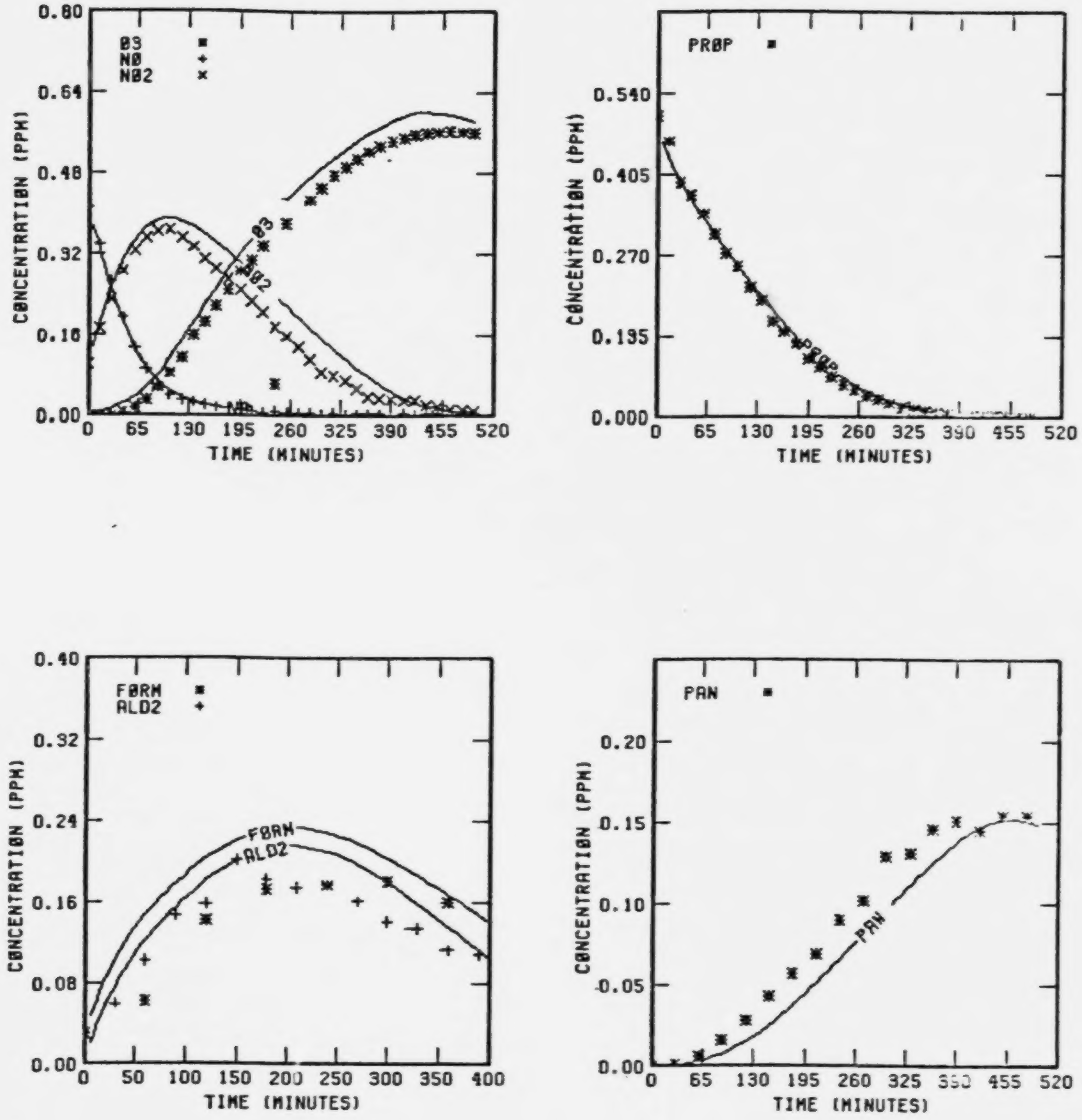

FIGURE 103. SIMULATION RESULTS FOR EC-216

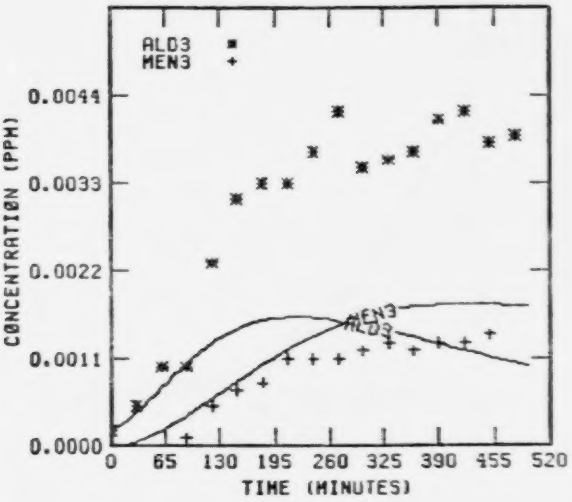

FIGURE 103. (Concluded)

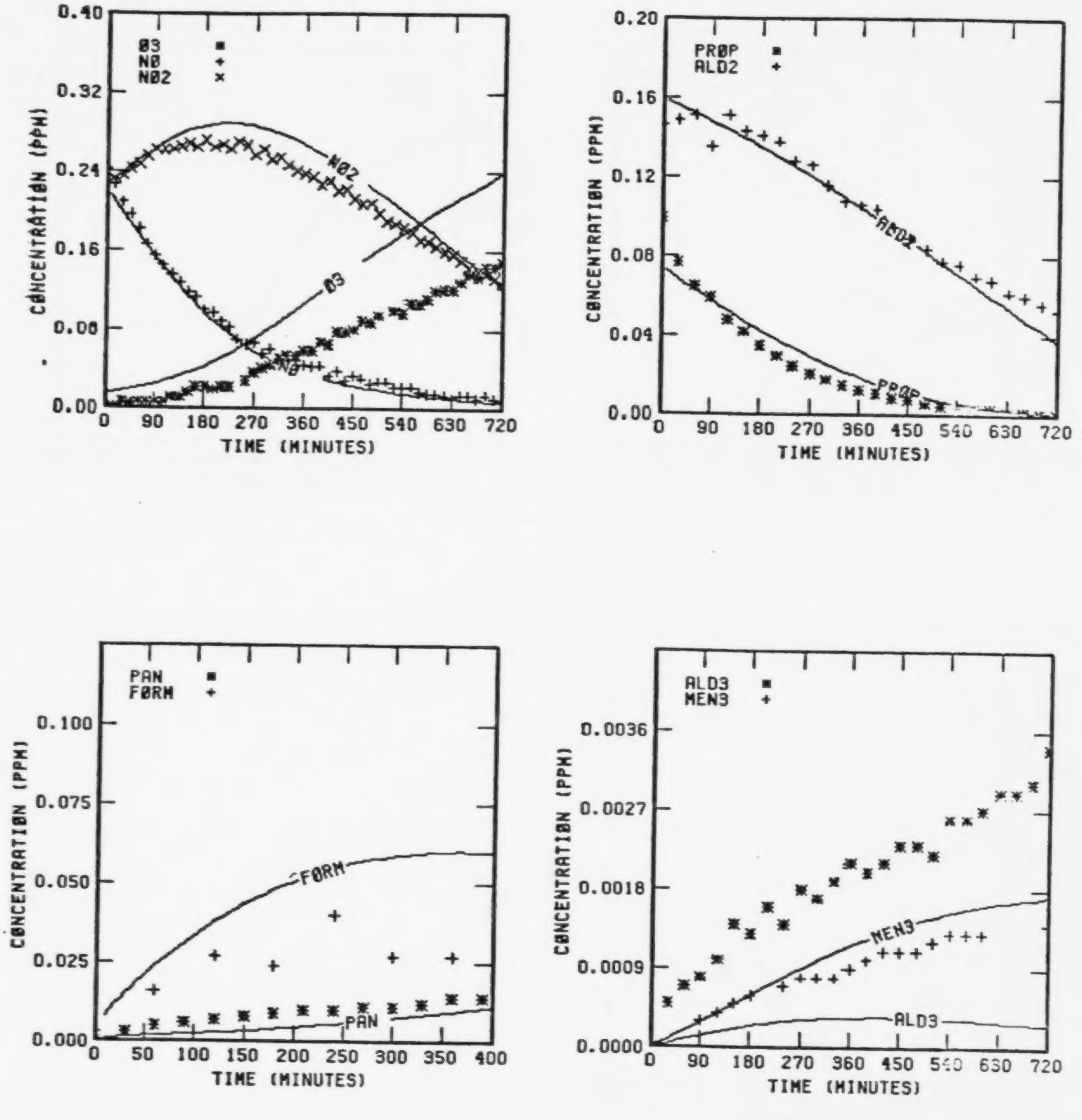

FIGURE 104. SIMULATIØN RESULTS FØR
EC-217

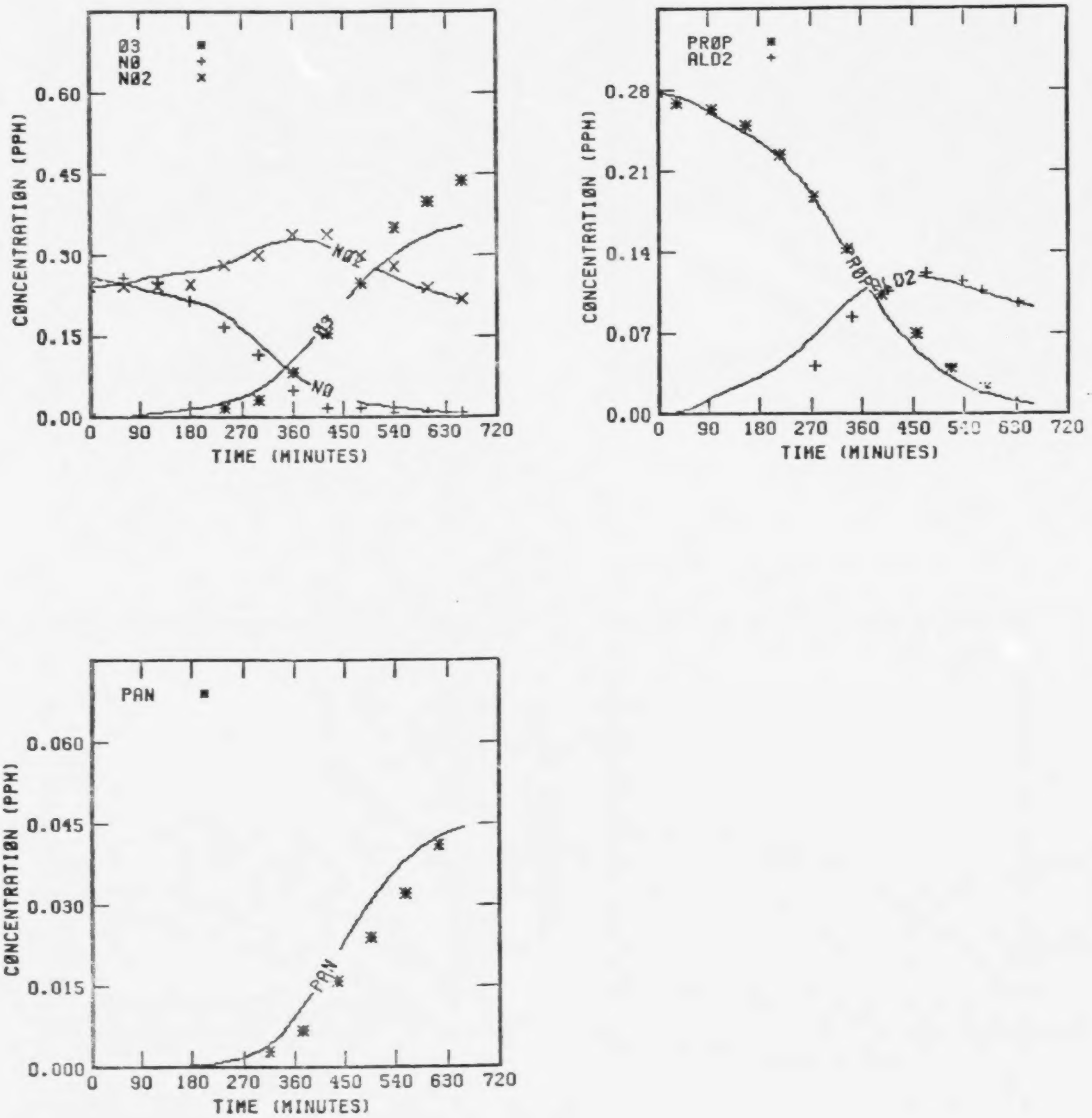

FIGURE 105. SIMULATIØN RESULTS FØR
UNCR 61279

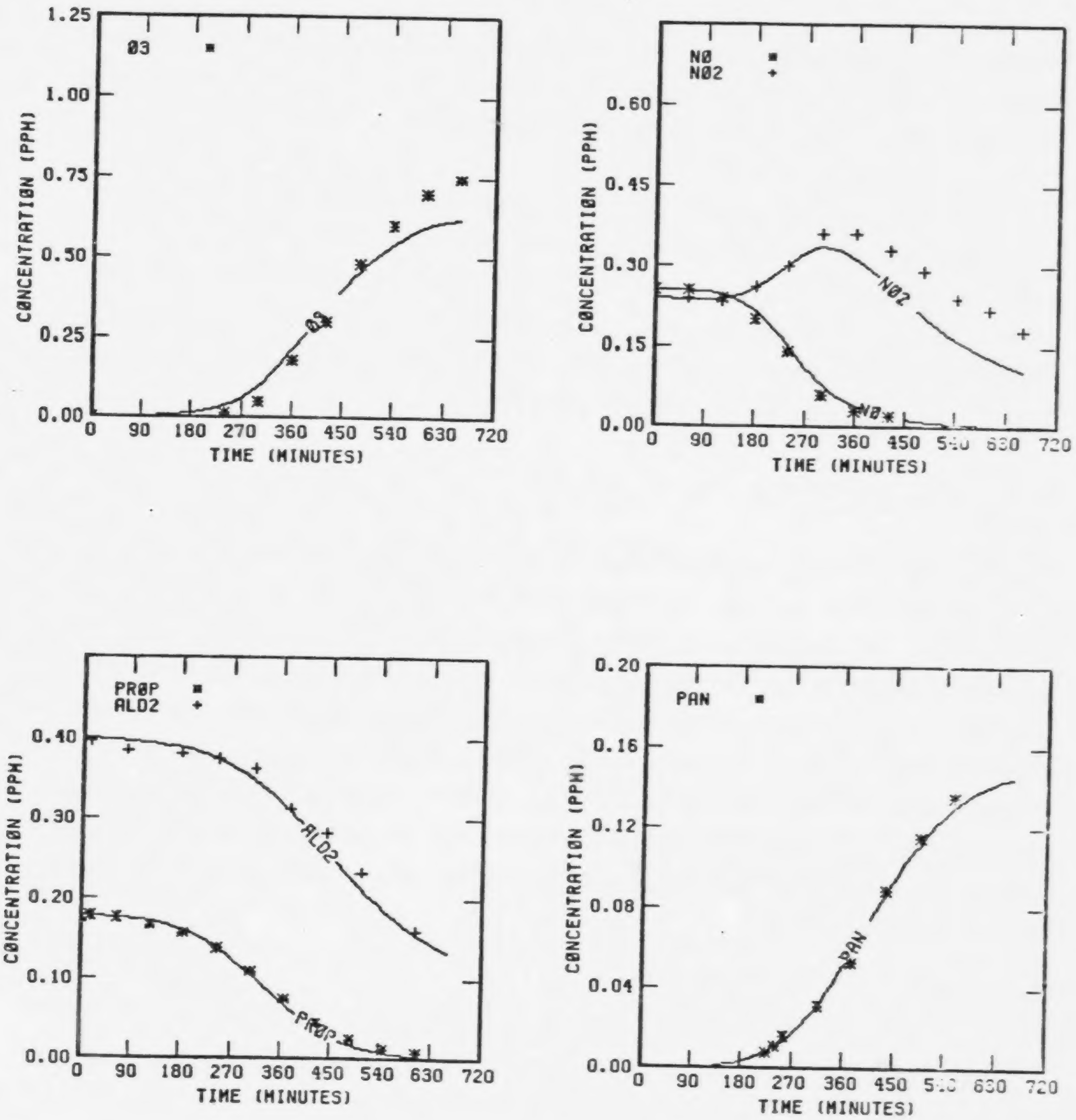

FIGURE 106. SIMULATIØN RESULTS FØR
UNCB 61279

present the graphical results. Surprisingly, the current chemistry appears to predict the decay curves for acetaldehyde and propylene simultaneously in the UNC experiment, but not in the UCR experiment.

A better test of the PAN chemistry would have been possible if the propylene side of the dual chamber experiments had used more propylene so that similar PAN could be predicted for both sides. Since the same instrument is used to measure PAN, by alternating between both sides of the chamber, a prediction and verification of equal PAN on both sides would constitute a sensitive test of the PAN chemistry.

BUTANE

The butane mechanism published in our interim report (Whitten et al., 1979) was modified to model the data from new experiments performed in both the UCR and UNC chambers. Table 26 presents the current version of the butane chemistry. The initial conditions and results from simulations of six experiments in the UCR chamber and seven experiments in the UNC chamber are presented in Tables 27 through 30 and Figures 107 through 120. The minor changes made to the butane chemistry are briefly described in the following subsections. The photolysis rate constants for butyraldehyde and methylethylketone are assumed to be the same as the formaldehyde photolysis rate constant producing radicals.

$RO_2^{\cdot} + HO_2^{\cdot}$

As described earlier for $CH_3O_2^{\cdot}$ in the propylene chemistry, rate constants for these reactions were reduced to the number recommended in the 1979 NASA review (DeMore et al., 1979).

$RO_2^{\cdot} + NO$

We have lowered the rate constant for the pathway to nitrate formation from the sec-butyl peroxy radical to 550 ppm^{-1} min^{-1}. Although this value lowers the simulated nitrate to nearly half the values reported in the UCR data, we feel the current number used is an upper limit for this particular

TABLE 26. REACTIONS OF BUTANE*

Reaction	Rate constant ($ppm^{-1} min^{-1}$)
$CH_3CH_2CH_2CH_3 + O \xrightarrow{O_2} CH_3CH_2CH(O_2^{\cdot})CH_3 + OH\cdot$	6.4×10^1
$CH_3CH_2CH_2CH_3 + OH\cdot \xrightarrow{O_2} CH_3CH_2CH_2CH_2O_2^{\cdot} + H_2O$	5.74×10^{2}**
$CH_3CH_2CH_2CH_3 + OH\cdot \xrightarrow{O_2} CH_3CH_2CH(O_2^{\cdot})CH_3 + H_2O$	3.44×10^{3}**
$HOCH_2CH_2CH_2C(O)O_2^{\cdot} + NO \xrightarrow{O_2} NO_2 + HOCH_2CH_2CH_2O_2^{\cdot} + CO_2$	3.8×10^3
$HOCH_2CH_2C(O)O_2^{\cdot} + NO \xrightarrow{O_2} NO_2 + HOCH_2CH_2O_2^{\cdot} + CO_2$	3.8×10^3
$CH_3CH_2CH_2C(O)O_2^{\cdot} + NO \xrightarrow{O_2} CH_3CH_2CH_2O_2^{\cdot} + NO_2 + CO_2$	3.8×10^3
$CH_3CH_2C(O)O_2^{\cdot} + NO \xrightarrow{O_2} CH_3CH_2O_2^{\cdot} + NO_2 + CO_2$	3.8×10^3
$HOCH_2CH_2CH_2CH_2O_2^{\cdot} + NO \xrightarrow{O_2} NO_2 + HO_2^{\cdot} + HOCH_2CH_2CH_2CHO$	1.2×10^4
$CH_3CH(O_2^{\cdot})C(O)CH_3 + NO \xrightarrow{O_2} NO_2 + HO_2^{\cdot} + CH_3C(O)C(O)CH_3$	1.2×10^4
$CH_3CH_2CH(O_2^{\cdot})CH_3 + NO \rightarrow NO_2 + CH_3CH_2CH(O\cdot)CH_3$	1.1×10^4
$CH_3CH_2CH(O_2^{\cdot})CH_3 + NO \rightarrow CH_3CH_2CH(ONO_2)CH_3$	5.5×10^2
$CH_3CH_2CH_2CH_2O_2^{\cdot} + NO \rightarrow NO_2 + CH_3CH_2CH_2CH_2O\cdot$	1.1×10^4
$CH_3CH_2CH_2CH_2O_2^{\cdot} + NO \rightarrow CH_3CH_2CH_2CH_2ONO_2$	1×10^3
$HOCH_2CH_2CH_2O_2^{\cdot} + NO \xrightarrow{O_2} NO_2 + HO_2^{\cdot} + HOCH_2CH_2CHO$	1.2×10^4
$HOCH_2CH_2O_2^{\cdot} + NO \xrightarrow{O_2} NO_2 + HO_2^{\cdot} + HOCH_2CHO$	1.2×10^4
$CH_3CH_2CH_2O_2^{\cdot} + NO \rightarrow NO_2 + CH_3CH_2CH_2O\cdot$	1.2×10^4
$CH_3CH_2CH_2O_2^{\cdot} + NO \rightarrow CH_3CH_2CH_2ONO_2$	1×10^2
$CH_3CH_2O_2^{\cdot} + NO \rightarrow NO_2 + CH_3CH_2O\cdot$	1.2×10^4
$CH_3CH_2O_2^{\cdot} + NO \rightarrow CH_3CH_2ONO_2$	1×10^2

TABLE 26 (Continued)

Reaction	Rate constant ($ppm^{-1}min^{-1}$)
$CH_3CH_2CH(O\cdot)CH_3 \xrightarrow{O_2} CH_3CH_2O_2^{\cdot} + CH_3CHO$	$9.2 \times 10^{4,**}$
$CH_3CH_2CH_2CH_2O\cdot \xrightarrow{O_2} HOCH_2CH_2CH_2CH_2O_2^{\cdot}$	$1.6 \times 10^{6\ *,**}$
$CH_3CH_2CH(O\cdot)CH_3 + O_2 \rightarrow CH_3CH_2C(O)CH_3 + HO_2^{\cdot}$	7.1×10^{-1}
$CH_3CH_2CH_2CH_2O\cdot + O_2 \rightarrow CH_3CH_2CH_2CHO + HO_2^{\cdot}$	3.3
$CH_3CH_2CH_2O\cdot + O_2 \rightarrow CH_3CH_2CHO + HO_2^{\cdot}$	3.3
$CH_3CH_2O\cdot + O_2 \rightarrow CH_3CHO + HO_2^{\cdot}$	3.3
$CH_3CH_2CHO + h\nu \xrightarrow{2O_2} CH_3CH_2O_2^{\cdot} + HO_2^{\cdot} + CO$	Experimental*
$CH_3CH_2CH_2CHO + h\nu \xrightarrow{2O_2} CH_3CH_2CH_2O_2^{\cdot} + HO_2^{\cdot} + CO$	Experimental*
$CH_3CH_2CH_2CHO + h\nu \rightarrow CH_3CHO + C_2H_4$	Experimental*
$CH_3CH_2C(O)CH_3 + h\nu \xrightarrow{2O_2} CH_3C(O)O_2^{\cdot} + CH_3CH_2O_2^{\cdot}$	Experimental*
$HOCH_2CHO + h\nu \xrightarrow{2O_2} HCHO + 2HO_2^{\cdot} + CO$	$1 \times 10^{-3*}$
$HOCH_2CH_2CHO + h\nu \xrightarrow{2O_2} HOCH_2CH_2O_2^{\cdot} + HO_2^{\cdot} + CO$	$1 \times 10^{-3*}$
$HOCH_2CH_2CH_2CHO + h\nu \xrightarrow{2O_2} HOCH_2CH_2CH_2O_2^{\cdot} + HO_2^{\cdot} + CO$	Experimental*
$CH_3C(O)C(O)CH_3 + h\nu \xrightarrow{2O_2} 2CH_3C(O)O_2^{\cdot}$	2×10^{-3}
$CH_3CH_2CHO + OH\cdot \xrightarrow{O_2} CH_3CH_2C(O)O_2^{\cdot} + H_2O$	2.4×10^{4}
$CH_3CH_2CH_2CHO + OH\cdot \xrightarrow{O_2} CH_3CH_2CH_2C(O)O_2^{\cdot} + H_2O$	2.4×10^{4}
$CH_3CH_2C(O)CH_3 + OH\cdot \xrightarrow{O_2} CH_3CH(O_2^{\cdot})C(O)CH_3 + H_2O$	4.9×10^{3}
$HOCH_2CH_2CH_2CHO + OH\cdot \xrightarrow{O_2} HOCH_2CH_2CH_2C(O)O_2^{\cdot} + H_2O$	2.2×10^{4}
$HOCH_2CH_2CHO + OH\cdot \xrightarrow{O_2} HOCH_2CH_2C(O)O_2^{\cdot} + H_2O$	2.2×10^{4}

TABLE 26 (Concluded)

Reaction	Rate constant ($ppm^{-1}min^{-1}$)
$HOCH_2CHO + OH\cdot \xrightarrow{O_2} HCHO + HO_2^{\cdot} + CO + H_2O$	2.2×10^4
$HOCH_2CH_2CH_2C(O)O_2^{\cdot} + HO_2^{\cdot} \rightarrow HOCH_2CH_2CH_2C(O)O_2H + O_2$	1.5×10^3
$HOCH_2CH_2C(O)O_2^{\cdot} + HO_2^{\cdot} \rightarrow HOCH_2CH_2C(O)O_2H + O_2$	1.5×10^3
$CH_3CH_2CH_2C(O)O_2^{\cdot} + HO_2^{\cdot} \rightarrow CH_3CH_2CH_2C(O)O_2H + O_2$	1.5×10^3
$CH_3CH_2C(O)O_2^{\cdot} + HO_2^{\cdot} \rightarrow CH_3CH_2C(O)O_2H + O_2$	1.5×10^3
$HOCH_2CH_2CH_2CH_2O_2^{\cdot} + HO_2^{\cdot} \rightarrow HOCH_2CH_2CH_2CH_2O_2H + O_2$	1.5×10^3
$CH_3CH(O_2^{\cdot})C(O)CH_3 + HO_2^{\cdot} \rightarrow CH_3CH(O_2H)C(O)CH_3 + O_2$	1.5×10^3
$CH_3CH_2CH(O_2^{\cdot})CH_3 + HO_2^{\cdot} \rightarrow CH_3CH_2CH(CH_3)O_2H + O_2$	1.5×10^3
$CH_3CH_2CH_2CH_2O_2^{\cdot} + HO_2^{\cdot} \rightarrow CH_3CH_2CH_2CH_2O_2H + O_2$	1.5×10^3
$CH_3CH_2CH_2O_2^{\cdot} + HO_2^{\cdot} \rightarrow CH_3CH_2CH_2O_2H + O_2$	1.5×10^3
$CH_3CH_2O_2^{\cdot} + HO_2^{\cdot} \rightarrow CH_3CH_2O_2H + O_2$	1.5×10^3
$CH_3CH_2CH_2C(O)O_2^{\cdot} + NO_2 \rightarrow CH_3CH_2CH_2C(O)O_2NO_2$	2×10^3
$CH_3CH_2C(O)O_2^{\cdot} + NO_2 \rightarrow CH_3CH_2C(O)O_2NO_2$	2×10^3
$CH_3CH_2C(O)O_2NO_2 \rightarrow NO_2 + CH_3CH_2C(O)O_2^{\cdot}$	2.8×10^{-2}[†]
$CH_3CH_2CH_2C(O)O_2NO_2 \rightarrow NO_2 + CH_3CH_2CH_2C(O)O_2^{\cdot}$	2.8×10^{-2}[†§]
$CH_3CH_2O\cdot + NO_2 \rightarrow CH_3CH_2ONO_2$	1.5×10^4
$CH_3CH_2O\cdot + NO_2 \rightarrow CH_3CHO + HONO$	2.9×10^3
$CH_3CH_2CH_2O\cdot + NO_2 \rightarrow CH_3CH_2CH_2ONO_2$	1.5×10^4
$CH_3CH_2CH_2O\cdot + NO_2 \rightarrow CH_3CH_2CHO + HONO$	2.9×10^3
$CH_3CH_2CH_2CH_2O\cdot + NO_2 \rightarrow CH_3CH_2CH_2CH_2ONO_2$	1.5×10^4
$CH_3CH_2CH_2CH_2O\cdot + NO_2 \rightarrow CH_3CH_2CH_2CHO + HONO$	2.9×10^3
$CH_3CH_2CH(O\cdot)CH_3 + NO_2 \rightarrow CH_3CH_2CH(ONO_2)CH_3$	1.5×10^4
$CH_3CH_2CH(O\cdot)CH_3 + NO_2 \rightarrow CH_3CH_2C(O)CH_3 + HONO$	2.9×10^3

[*] The inorganic, formaldehyde, and acetaldehyde reactions listed earlier must be added to construct the explicit butane mechanism.

[†] Rate constant is min^{-1}.

[§] Activation energy is 12,500K; rate constant is given at 298K.

[**] Activation energy is 8800K; rate constant is given at 298K.

[††] Activation energy is 3900K; rate constant is given at 298K.

[§§] Activation energy is [illegible]; rate constant is given at 298K.

TABLE 27. INITIAL CONDITIONS FOR UCR BUTANE/NO_x EXPERIMENTS

Exp. no.	Temperature (Degrees K)	Initial concentrations					Photolysis constants ($\times 10^4$ min^{-1})*					
		Butane	NO	NO_2	HONO	H_2O	NO_2 →	O_3 → O'D	O_3 → O	HONO →	H_2O_2	FORM→Radicals†
EC-304	303.	4.22	.349	.117	.01	2.7×10^4	.43	5.	134.	1390.	7.	10.
EC-305	303.	4.25	.078	.020	.005	2.73×10^4	.43	5.	134.	1390.	7.	18.
EC-306	303.	6.33	.147	.04	.005	2.5×10^4	.43	10.	135.	1440.	7.	10.
EC-307	304.	6.38	.082	.019	.005	3.0×10^4	.43	10.	135.	1440.	7.	12.
EC-308	289.	4.00	.305	.178	.007	8.8×10^3	.44	10.	138.	1440.	7.	12.
EC-309	312.	4.23	.203	.272	.018	2.3×10^4	.45	10.	141.	1480.	4.6	18.

* Rate constant in min^{-1} for NO_2.

TABLE 28. INITIAL CONDITIONS FOR UNC BUTANE/NO_x EXPERIMENTS

Date	Chamber side	Sky conditions	Beginning time of simulation	Initial concentrations (ppm)					ALD + hν constant
				Butane	NO	NO_2	HONO	H_2O	
10/24/77	Blue	Variable cloudiness	7:16	2.0	.36	.13	.008	1×10^4	1.2
7/21/78	Red	Clear	6:00	1.83	.189	.054	.008	2.4×10^4	1.0*
7/21/78	Blue	Clear	6:00	3.93	.186	.056	.006	2.4×10^4	1.0*
7/22/78	Red	Clear	6:12	2.09	.432	.116	.015	2.4×10^4	1.0*
7/22/78	Blue	Clear	6:12	4.37	.436	.121	.015	2.4×10^4	1.0*
7/27/78	Red	Overcast	6:28	3.37	.189	.077	.017	2.4×10^4	1.0*
7/27/78	Blue	Overcast	6:28	3.30	.385	.124	.024	2.4×10^4	1.0*

* UV data used in computer simulations instead of TSR data.

TABLE 29. UCR BUTANE EXPERIMENTS--SIMULATIONS AND MEASUREMENTS

Exp. No.	Initial $[NO_x]$ (ppm)	Initial NO_2/NO_x ratio	Initial HC/NO_x (ppmC/ppm)	Maximum $[O_3]$ (ppm) Sim.	Maximum $[O_3]$ (ppm) Meas.	Difference in O_3 maxima (percent)	Time to O_3 maximum (minutes) Sim.	Time to O_3 maximum (minutes) Meas.	Difference in times to O_3 maxima (percent)	Maximum $[NO_2]$ (ppm) Sim.	Maximum $[NO_2]$ (ppm) Meas.	Difference in NO_2 maxima (percent)	Time to maximum $[NO_2]$ (minutes) Sim.	Time to maximum $[NO_2]$ (minutes) Meas.	Difference in times to NO_2 maxima (percent)
EC-304	466	.25	36.2	.46	.34	35	>450	>450	--	.24	.22	9	180	180	0.
EC-305	.098	.05	170.0	.45	.39	15	240	300	20	.080	.076	5	50	50	0.
EC-306	.287	.14	88.2	.60	.53	13	360	360	0.	.15	.14	7	100	100	0.
EC-307	.101	.19	252.7	.50	.42	19	280	280	0.	.08	.076	5	50	50	0.
EC-308	.483	.37	33.1	.066	.026	154	>360	>360	--	.21	.17	24	>360	>360	-
EC-309	.475	.57	35.6	.66	.51	29	>360	>360	--	.39	.36	8	60	60	0.

O_3 maxima: average difference = 22 percent; standard deviation = ±9 percent (excluding EC-308).

NO_2 maxima: average difference = 10 percent; standard deviation = ±7 percent.

TABLE 30. UNC BUTANE EXPERIMENTS--SIMULATIONS AND MEASUREMENTS

Date	Chamber side	Initial NO_x (ppm)	Initial NO_2/NO_x ratio	Initial HC/NO_x (ppmC/ppm)	Maximum $[O_3]$ (ppm) Sim.	Maximum $[O_3]$ (ppm) Meas.	Difference in O_3 maxima (percent)	Time to maximum $[O_3]$ Sim.	Time to maximum $[O_3]$ Meas.	Difference in times to O_3 maxima (percent)
10/24/77	Blue	.49	.27	16.3	.012	.002	500.	>400	>400	--
7/21/78	Red	.243	.22	30.1	.78	.75	4	600	600	0.
7/21/78	Blue	.242	.23	65.0	1.04	.92	13	520	540	-4
7/22/78	Red	.548	.21	15.3	.25	.14	79	680	680	0.
7/22/78	Blue	.557	.22	31.4	.80	.75	7	680	680	0.
7/27/78	Red	.266	.29	50.7	.36	.49	-27	>480	>480	0.
7/27/78	Blue	.509	.24	25.9	.20	.23	-13	>480	>480	--

O_3 maxima: average difference = 11 percent; standard deviation = ± 36 percent (excluding run performed on 10/25/77).

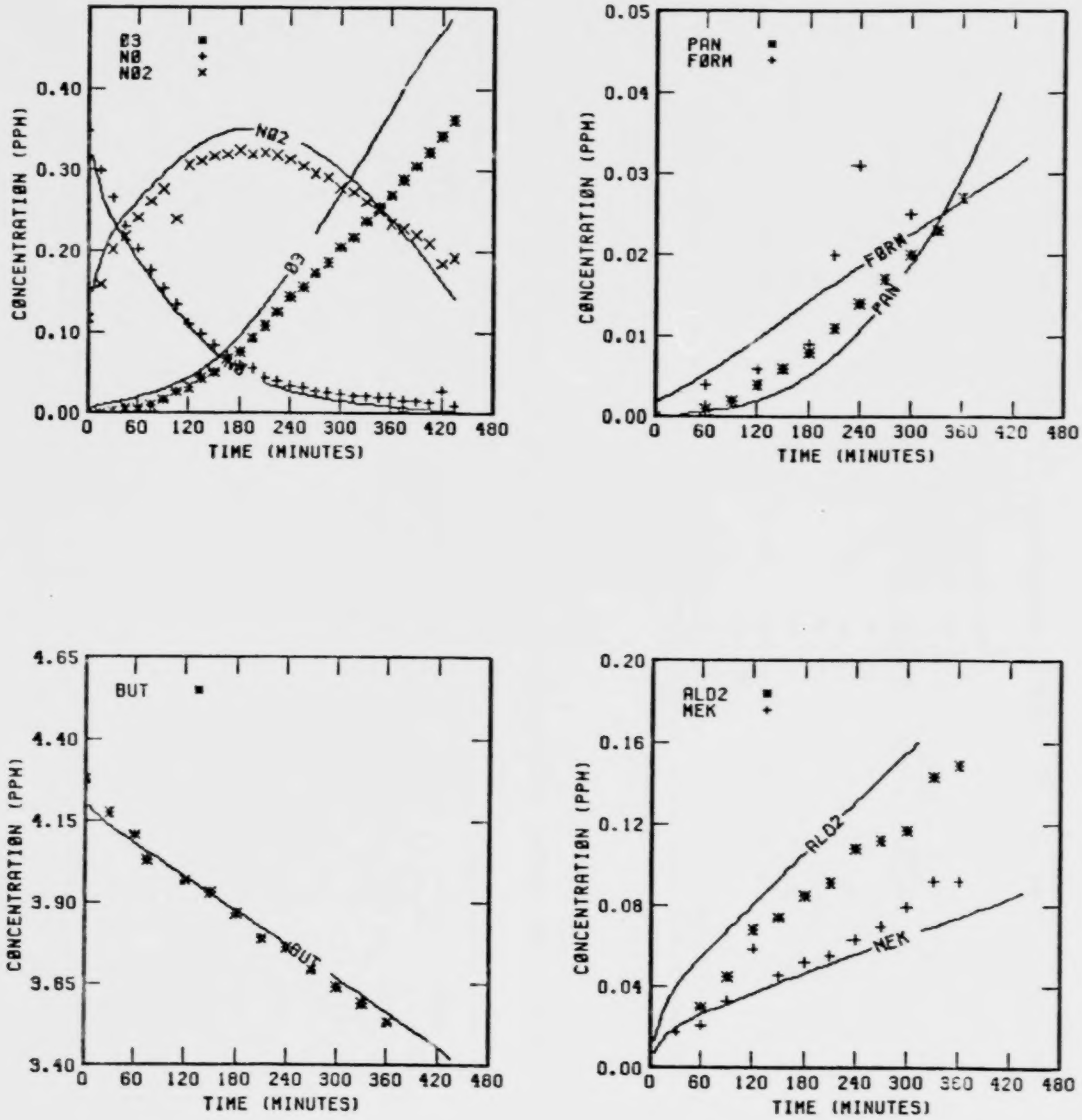

FIGURE 107. SIMULATIØN RESULTS FØR
EC-304

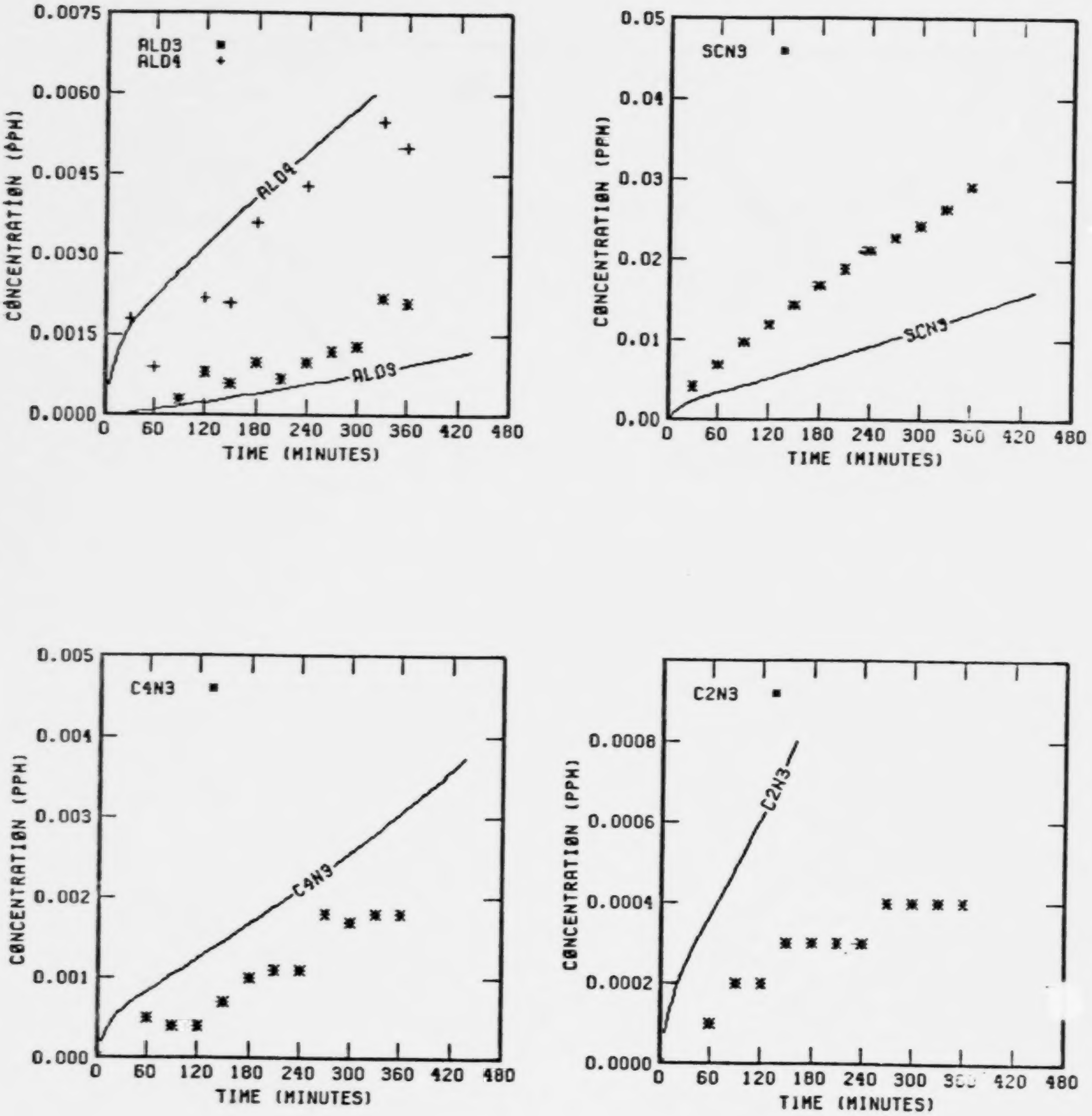

FIGURE 107. (Concluded)

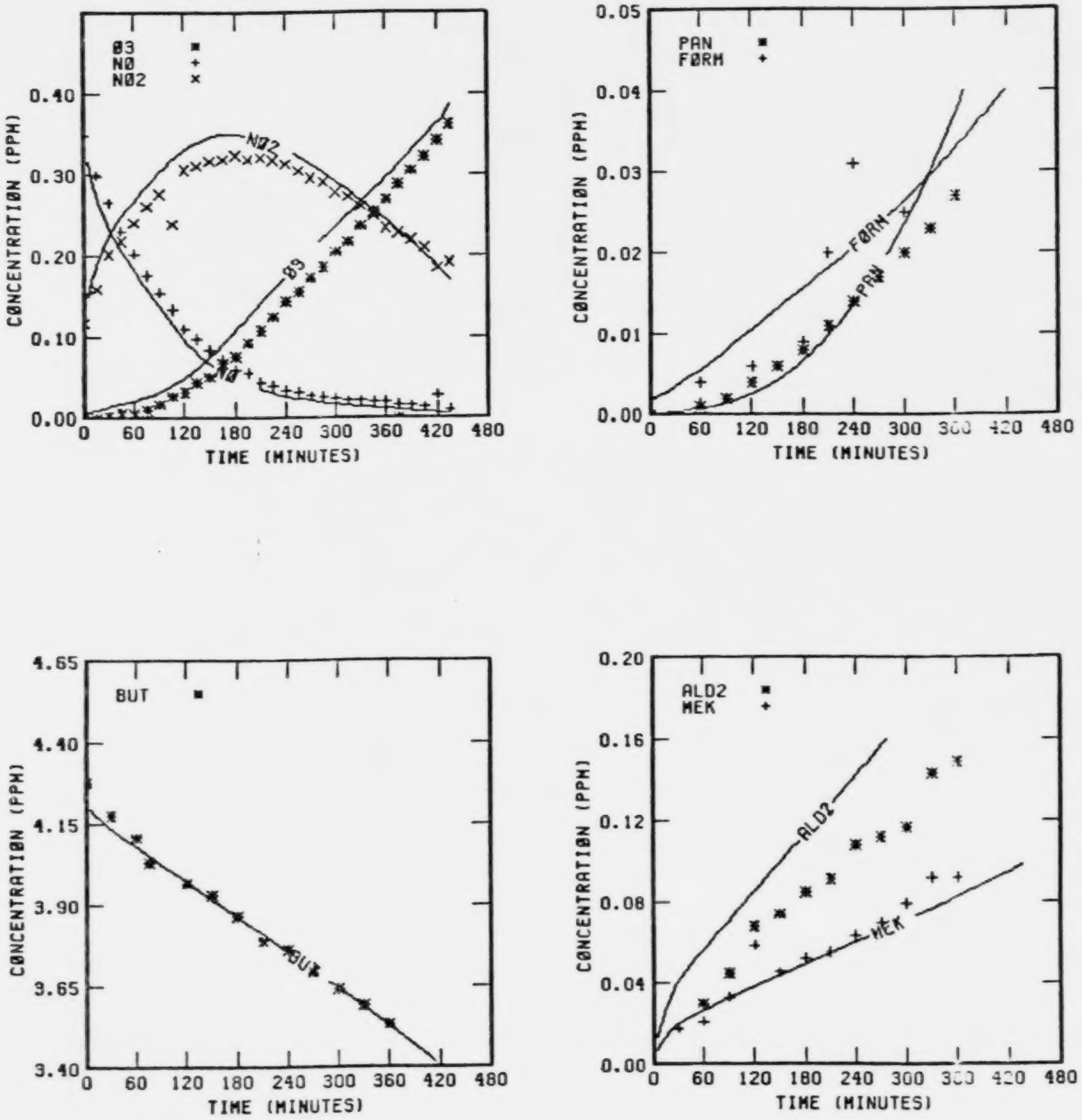

FIGURE 108. SIMULATION RESULTS FOR EC-304 WITH NO$_3$ CONVERSION

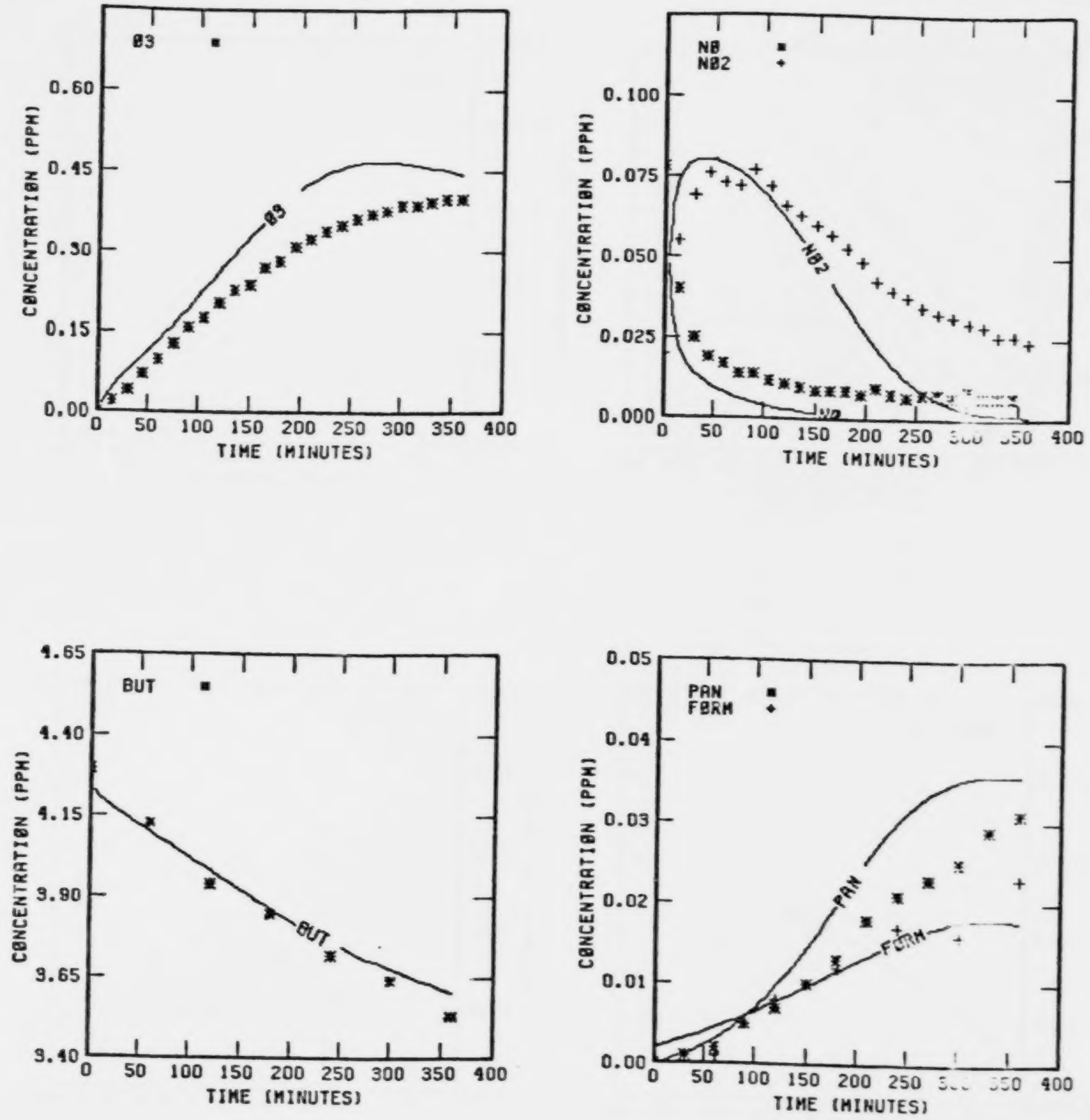

FIGURE 109. SIMULATION RESULTS FOR EC-305

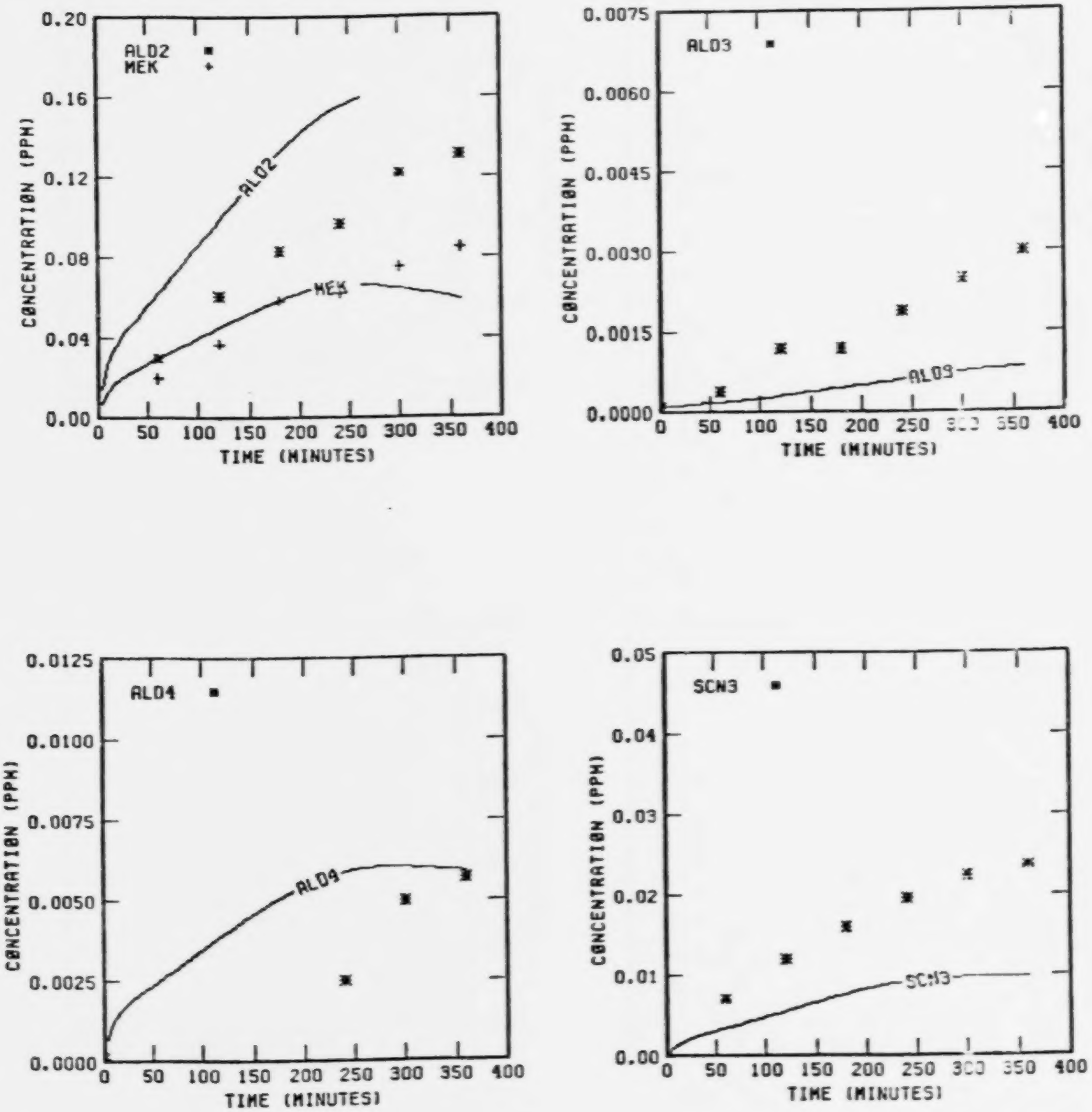

FIGURE 109. (Continued)

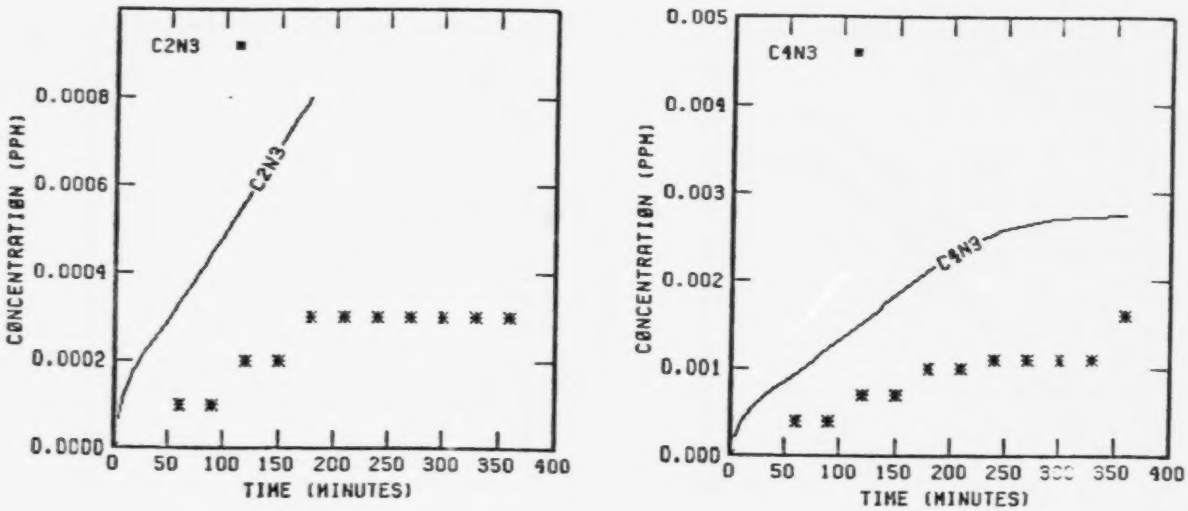

FIGURE 109. (Concluded)

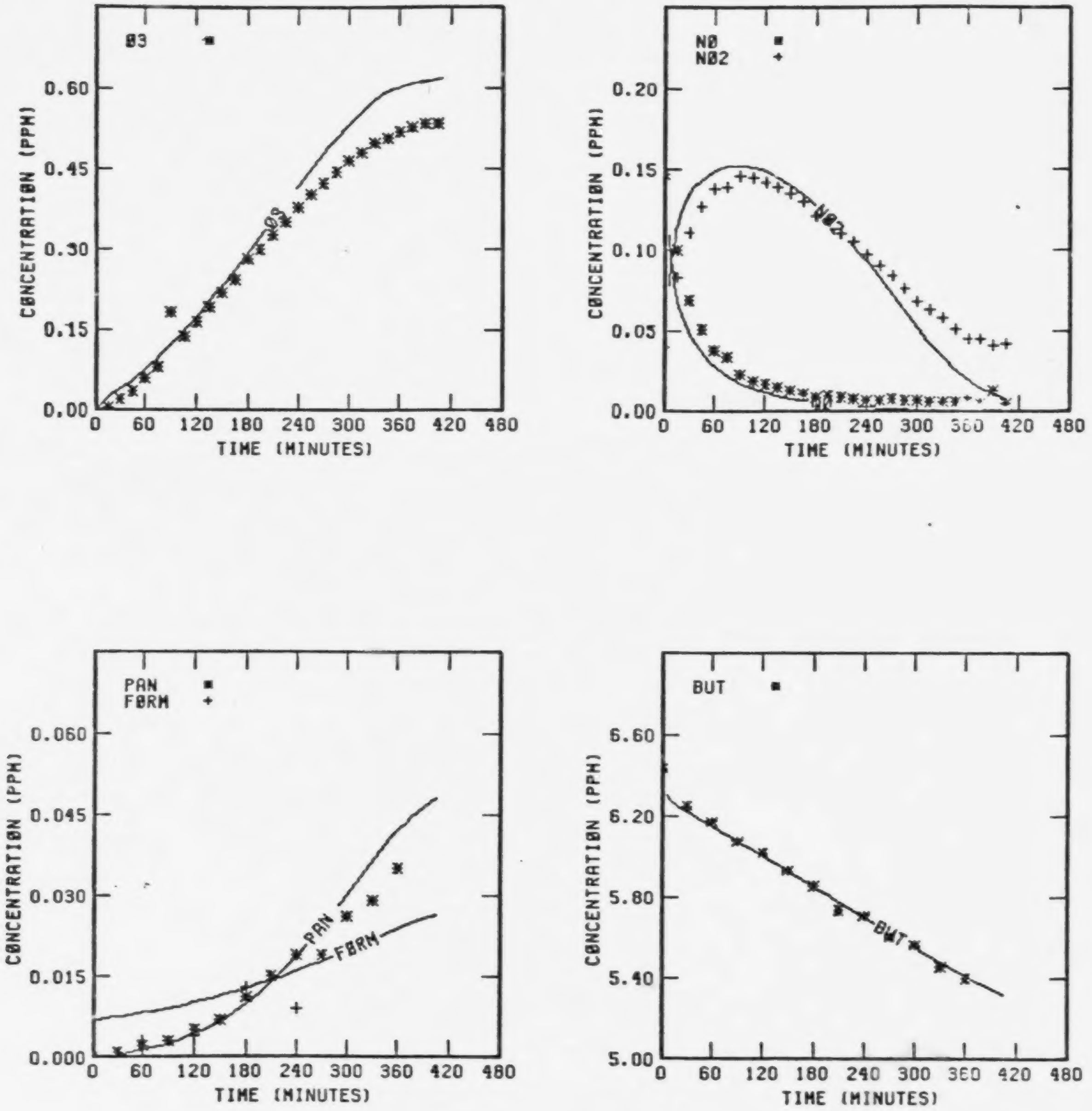

FIGURE 110. SIMULATION RESULTS FOR EC-306

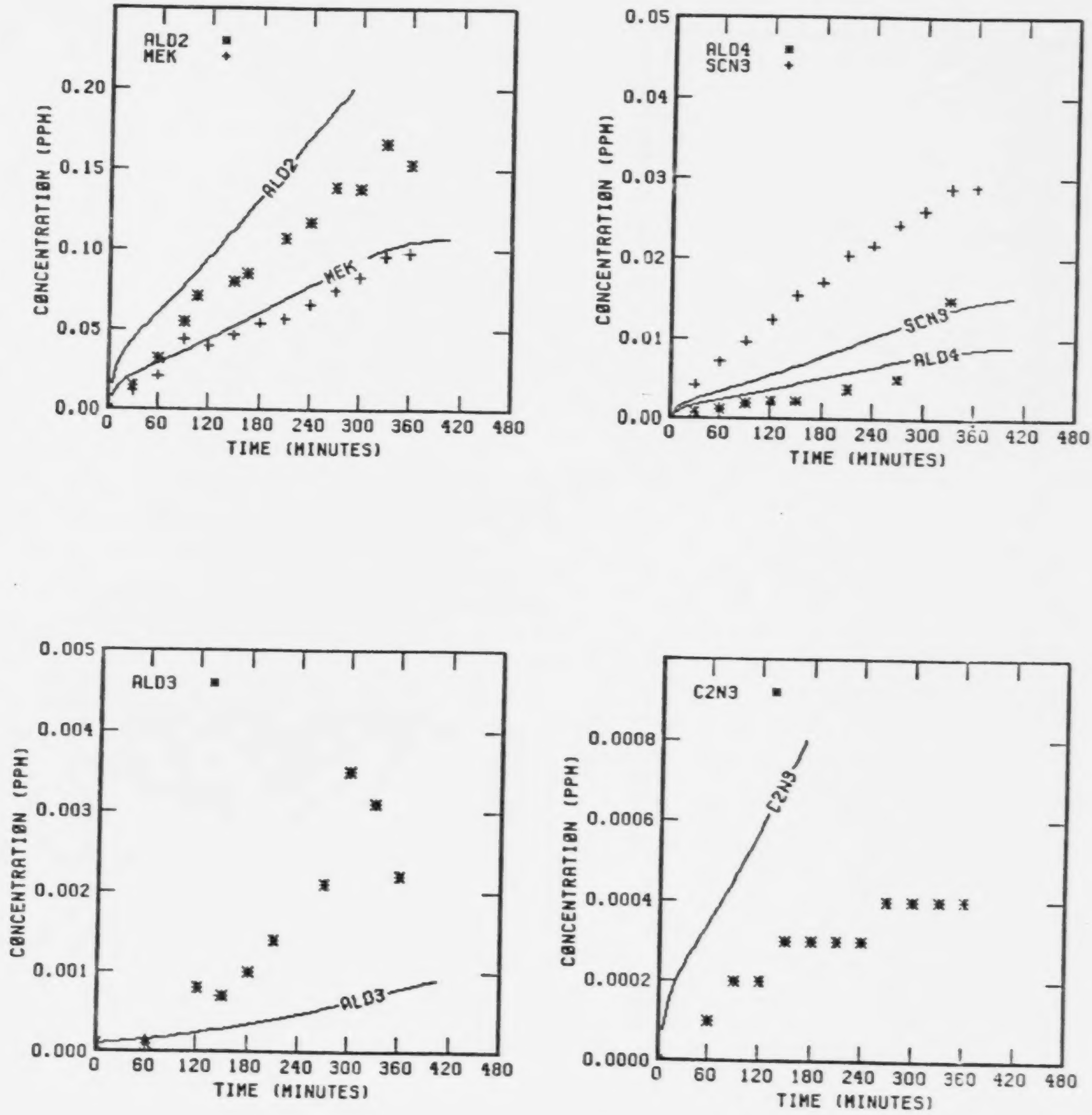

FIGURE 110. (Continued)

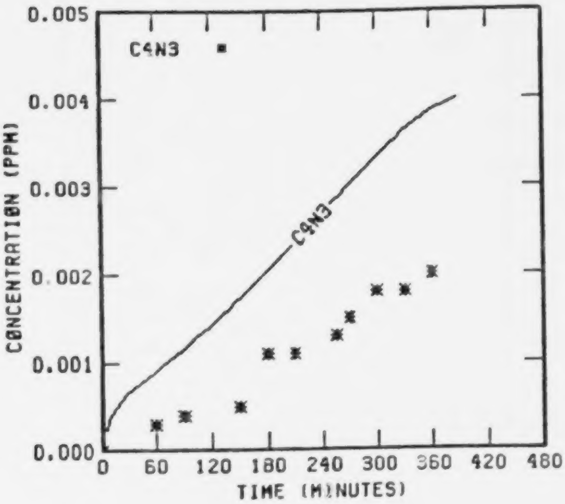

FIGURE 110. (Concluded)

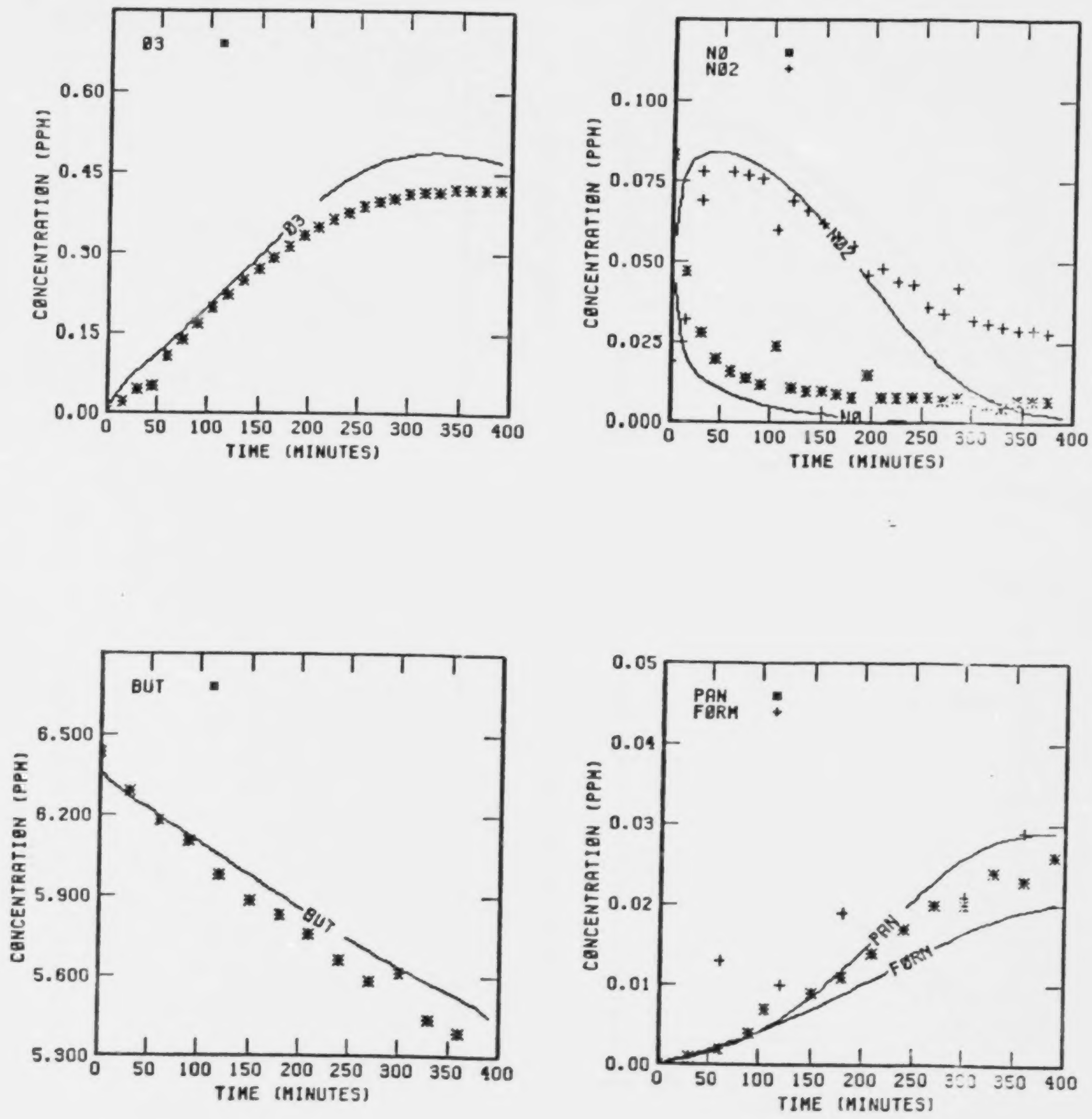

FIGURE 111. SIMULATION RESULTS FOR
EC-307

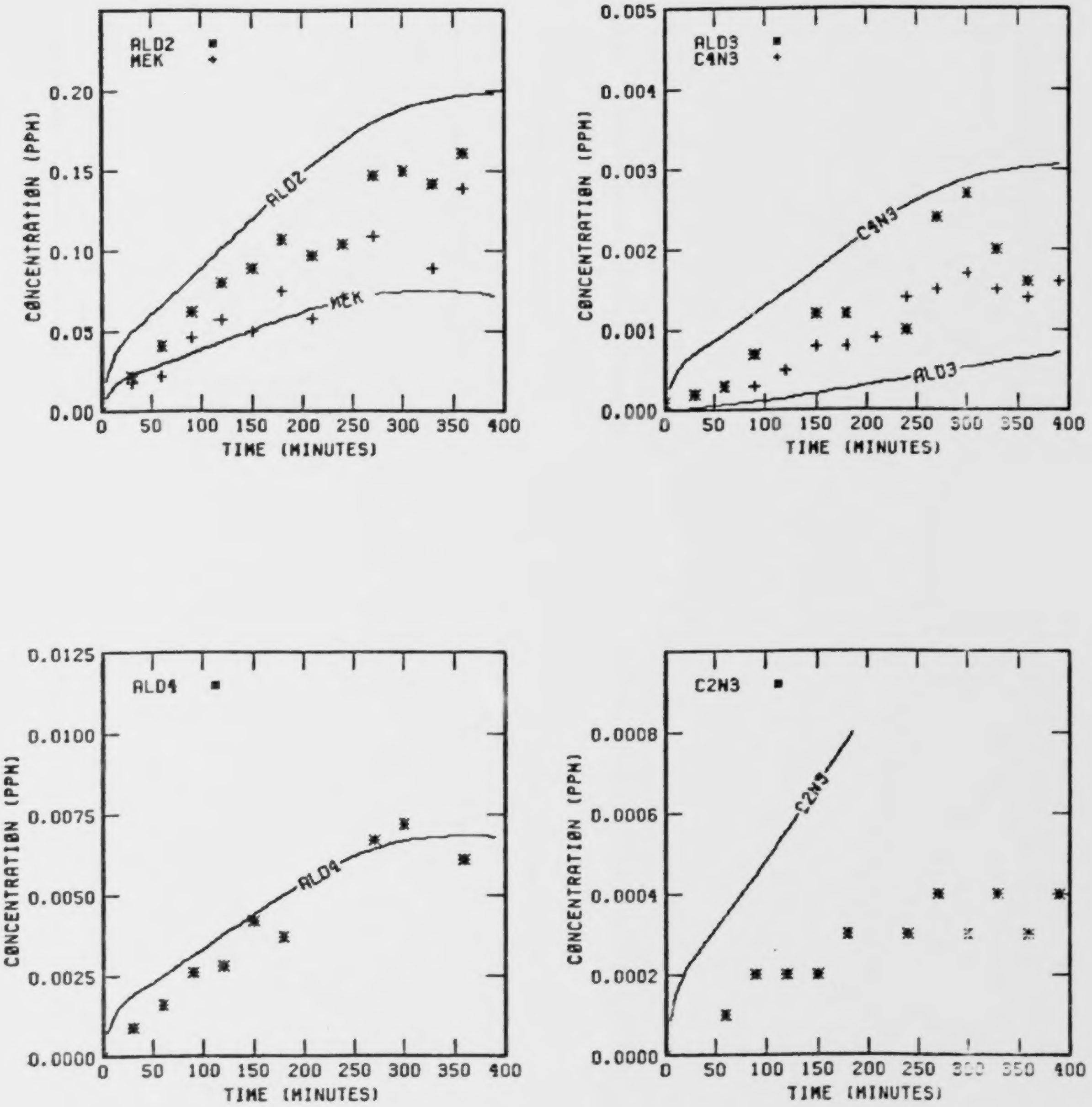

FIGURE 111. (Continued)

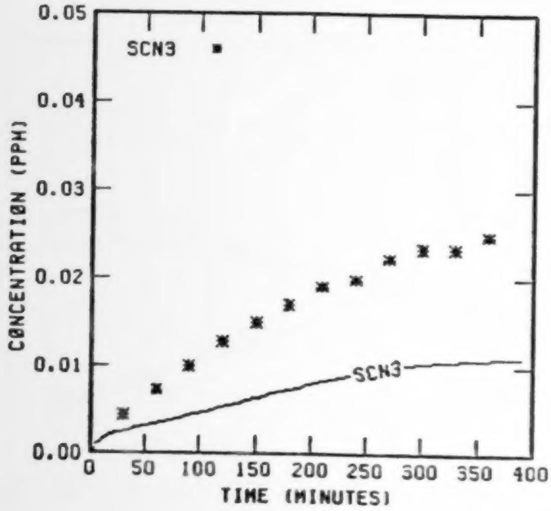

FIGURE 111. (Concluded)

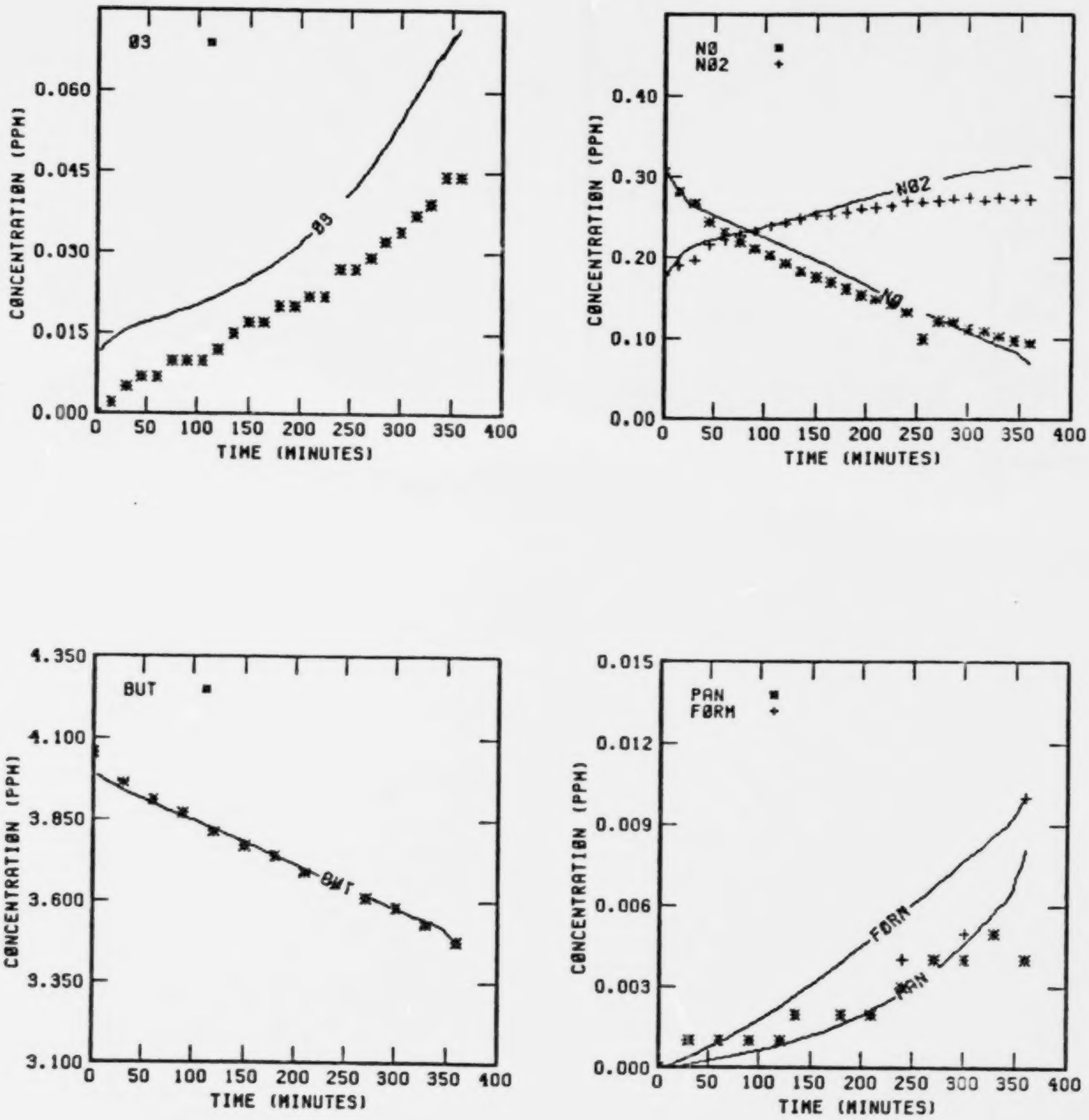

FIGURE 112. SIMULATION RESULTS FOR EC-308

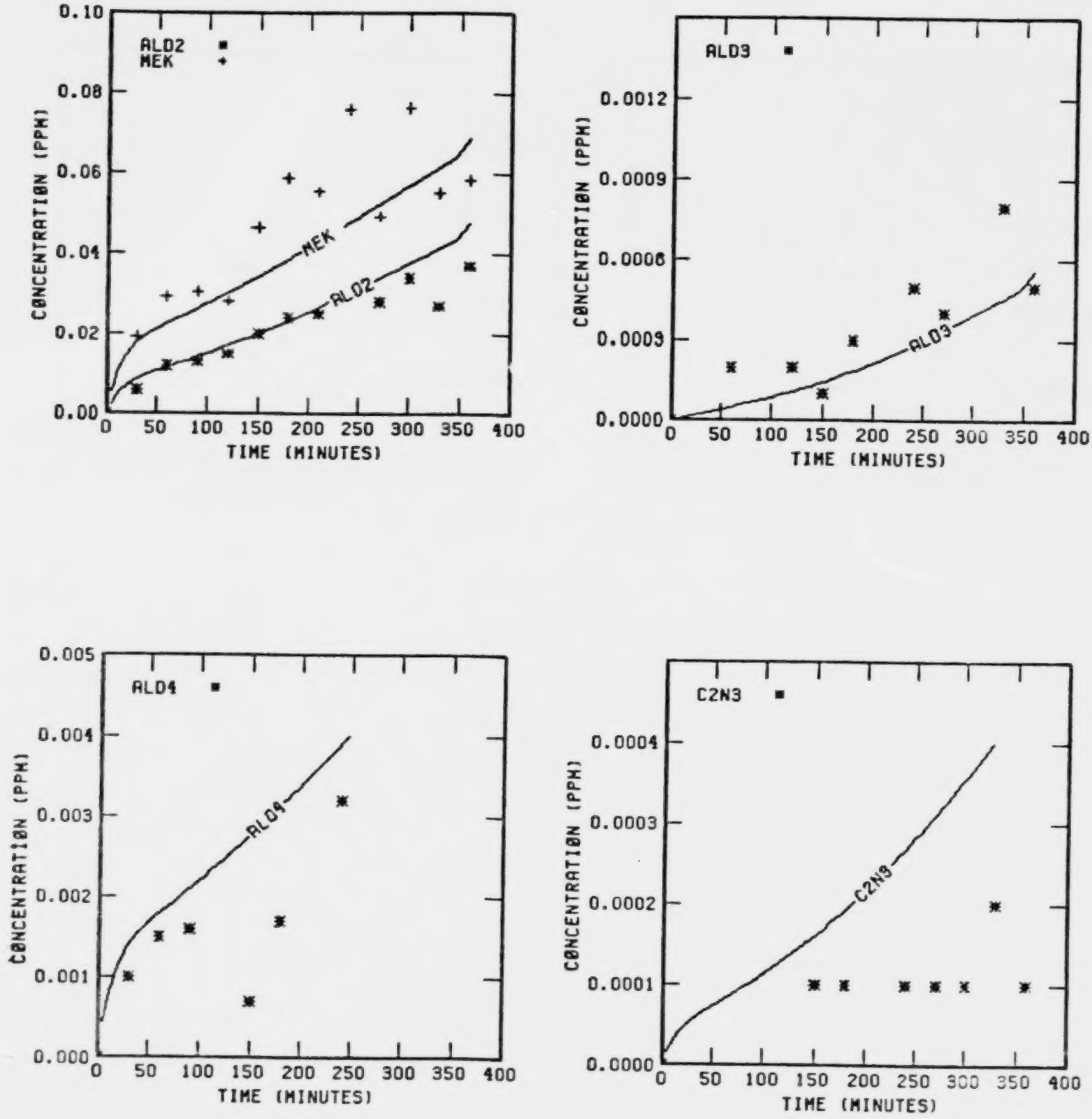

FIGURE 112. (Continued)

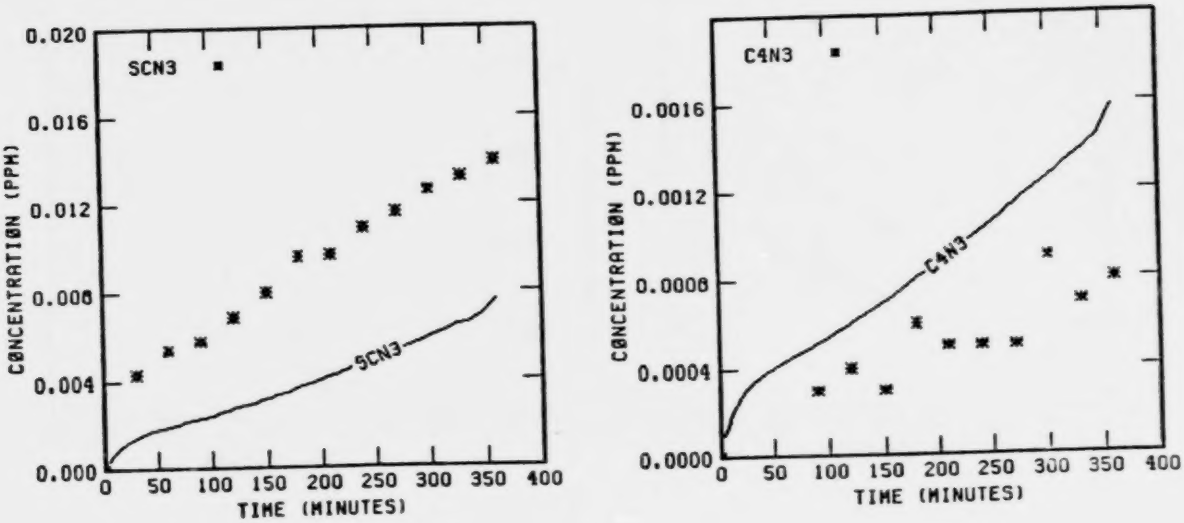

FIGURE 112. (Concluded)

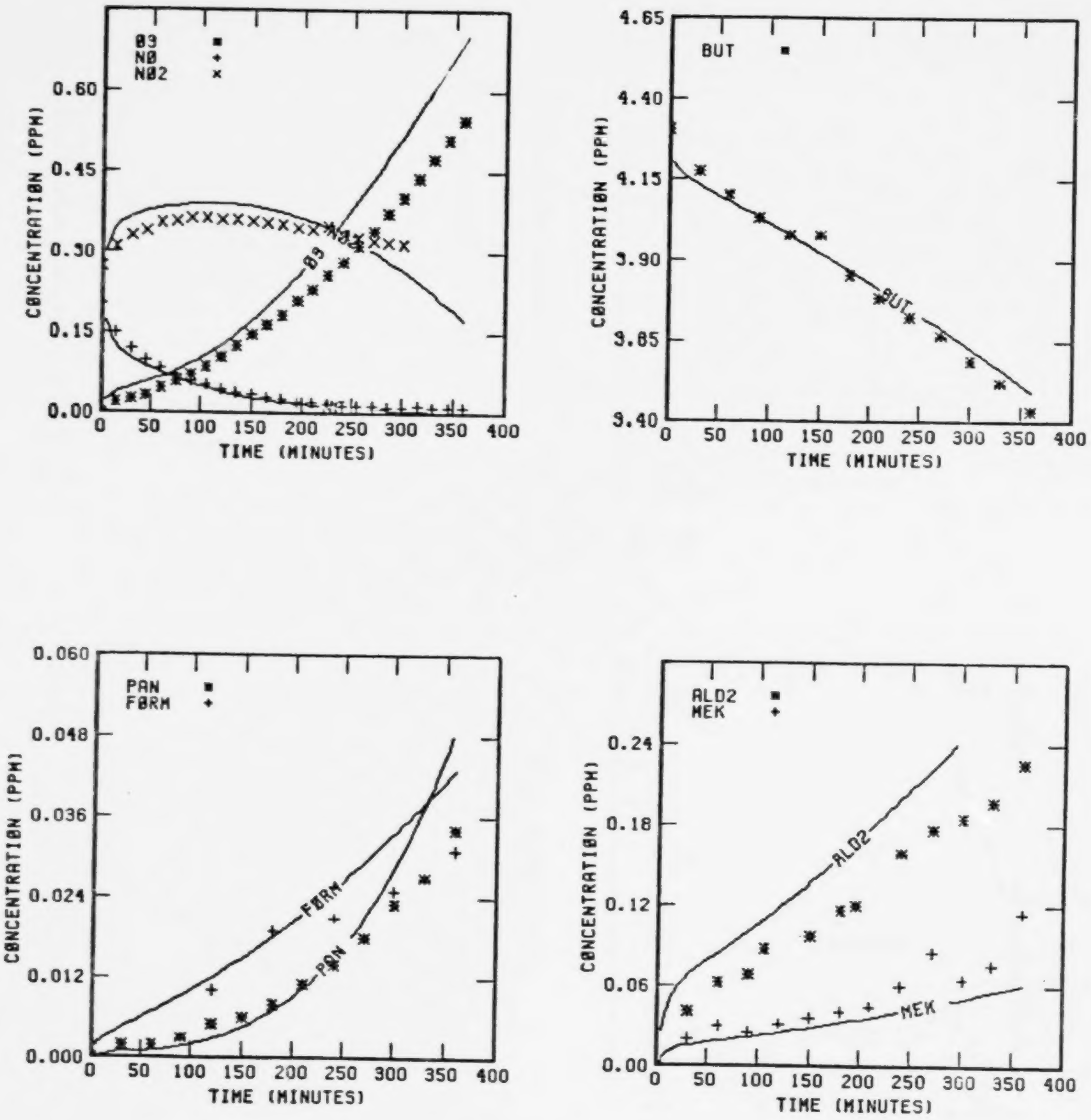

FIGURE 113. SIMULATION RESULTS FOR EC-309

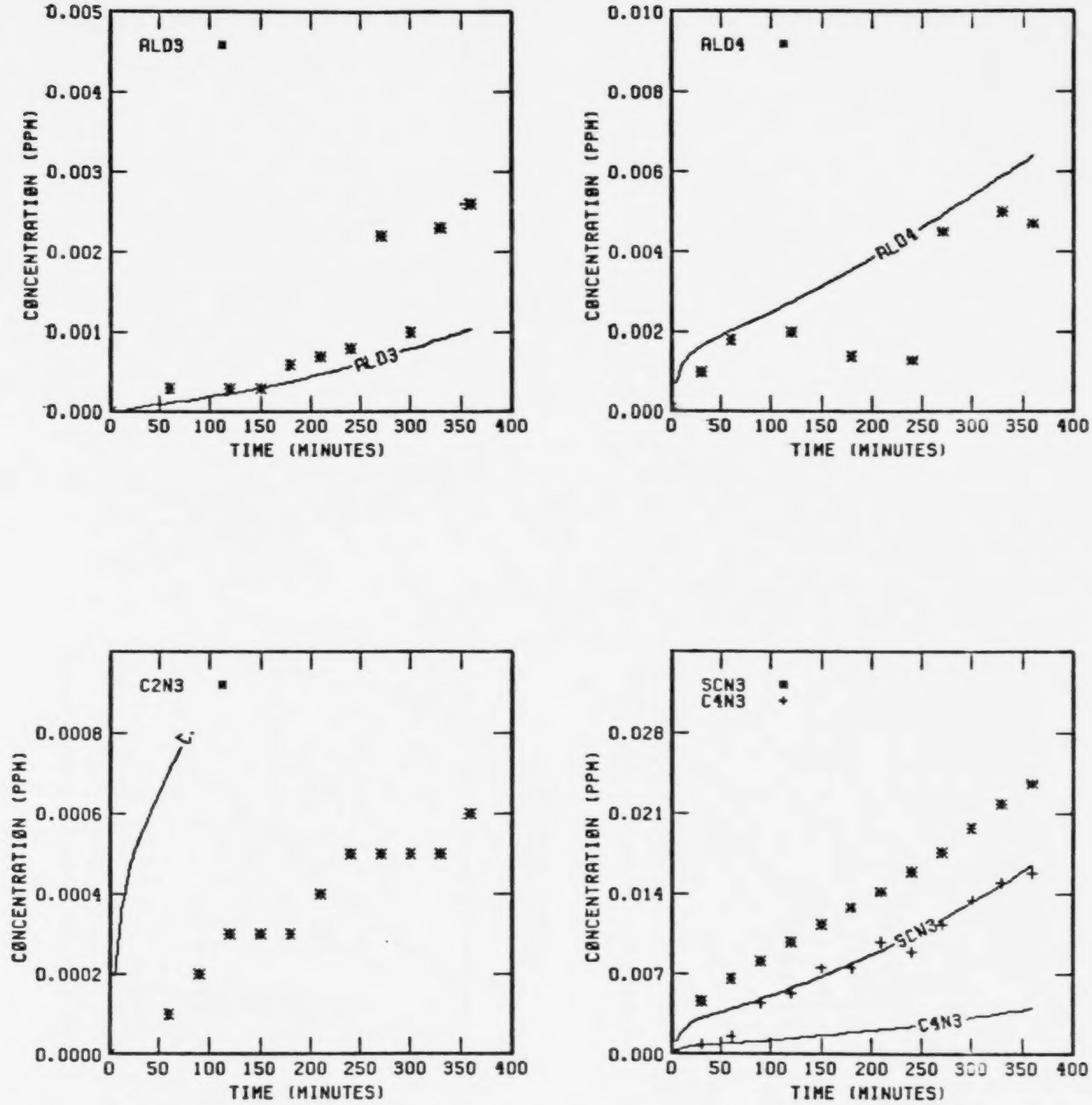

FIGURE 113. (Concluded)

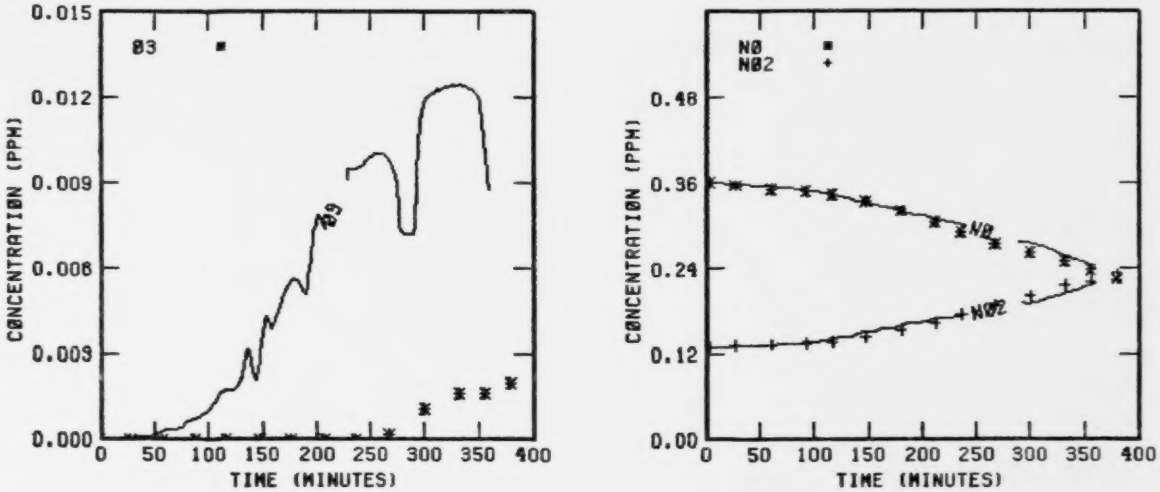

FIGURE 114. SIMULATION RESULTS FOR
UNCB 102477

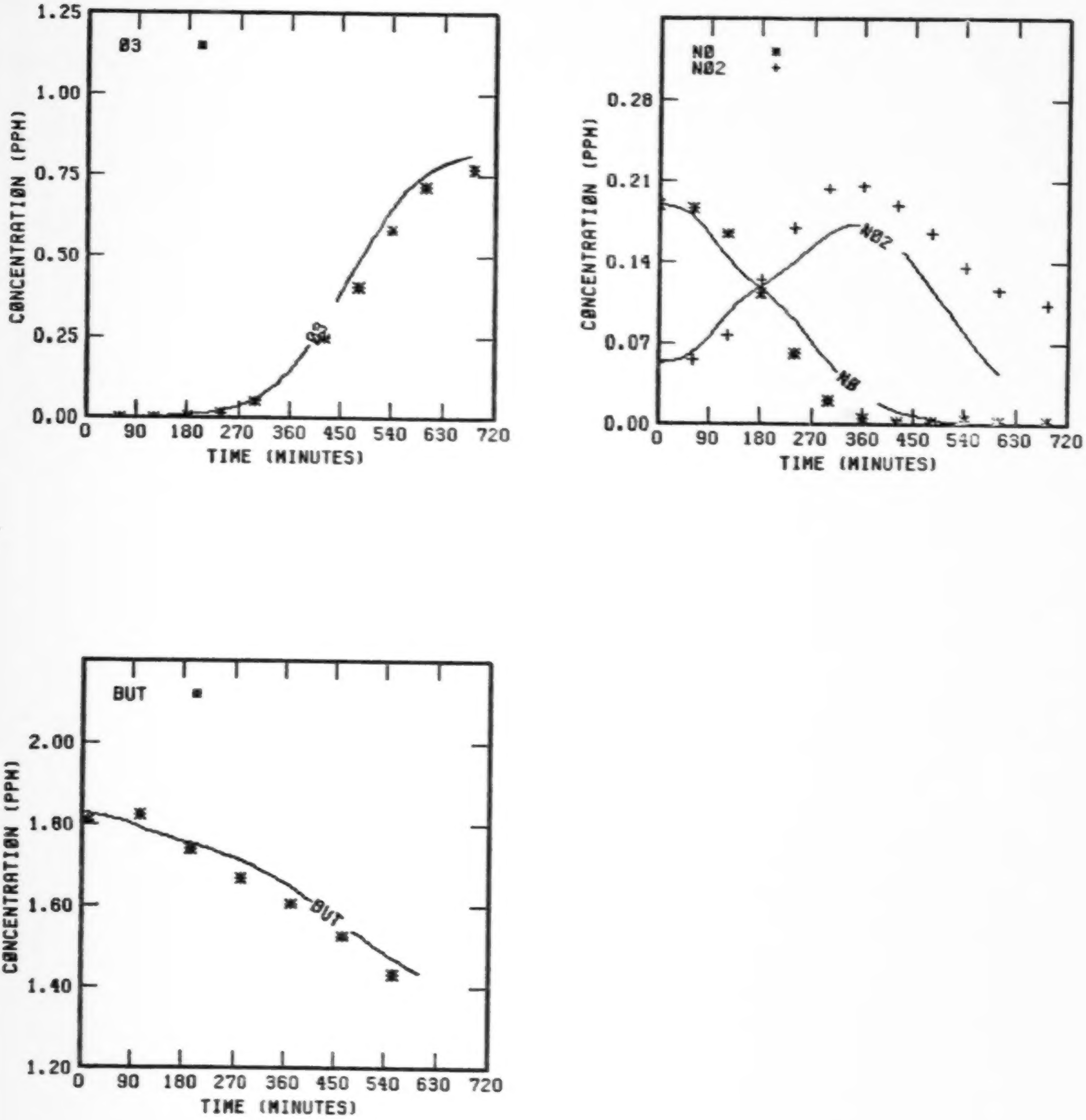

FIGURE 115. SIMULATIØN RESULTS FØR
UNCR 72178

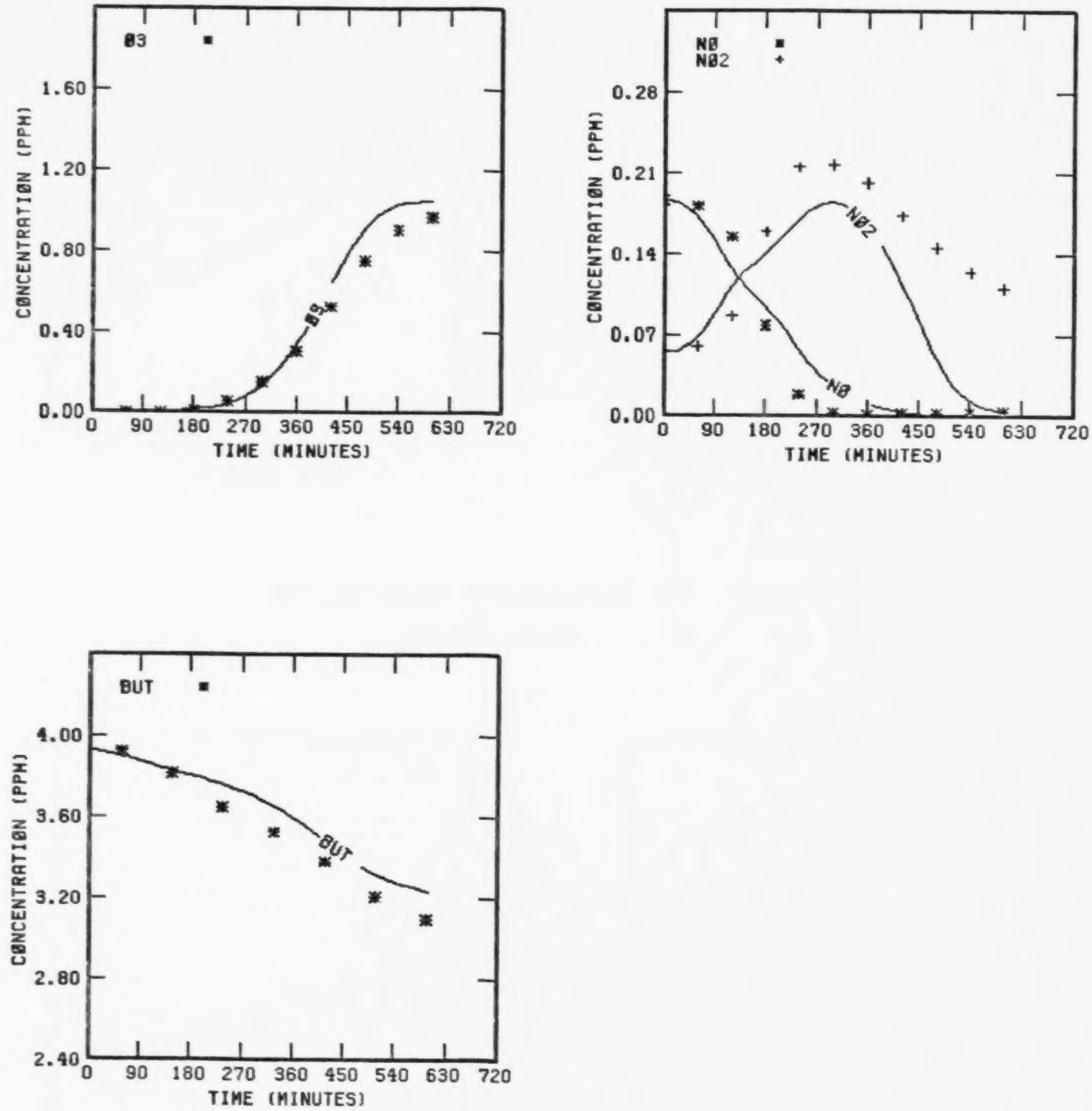

FIGURE 116. SIMULATIØN RESULTS FØR
UNCB 72178

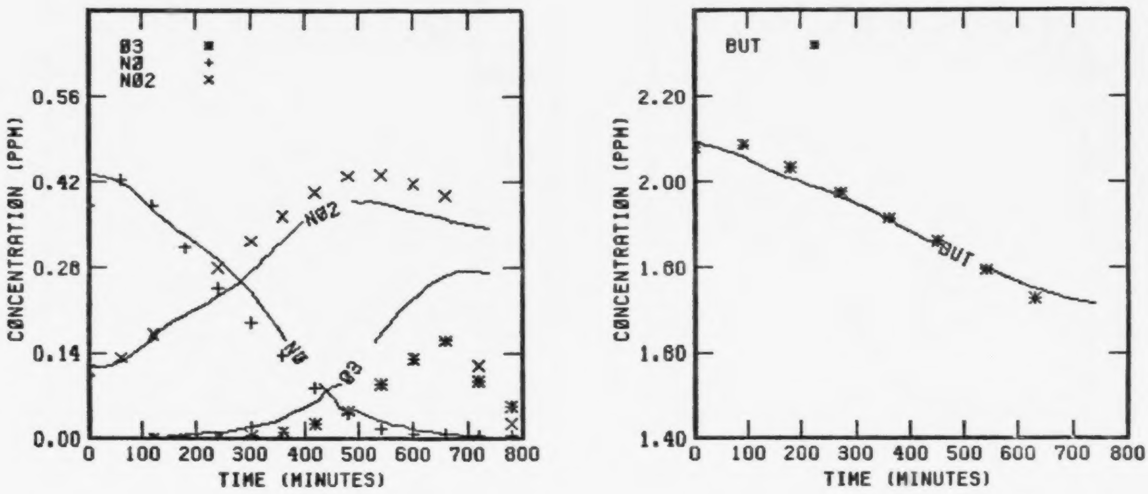

FIGURE 117. SIMULATION RESULTS FOR
UNCR 72278

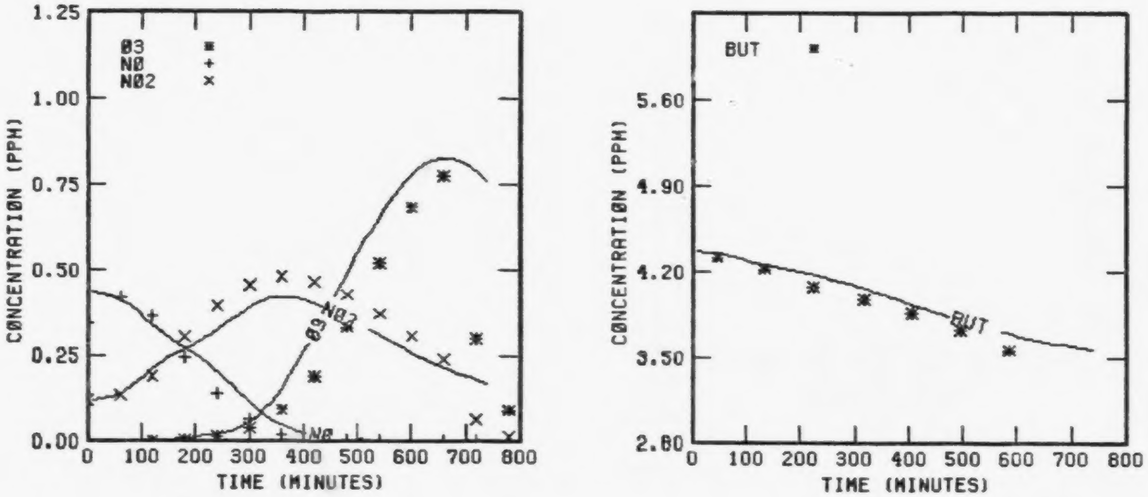

FIGURE 118. SIMULATION RESULTS FOR
UNCB 72278

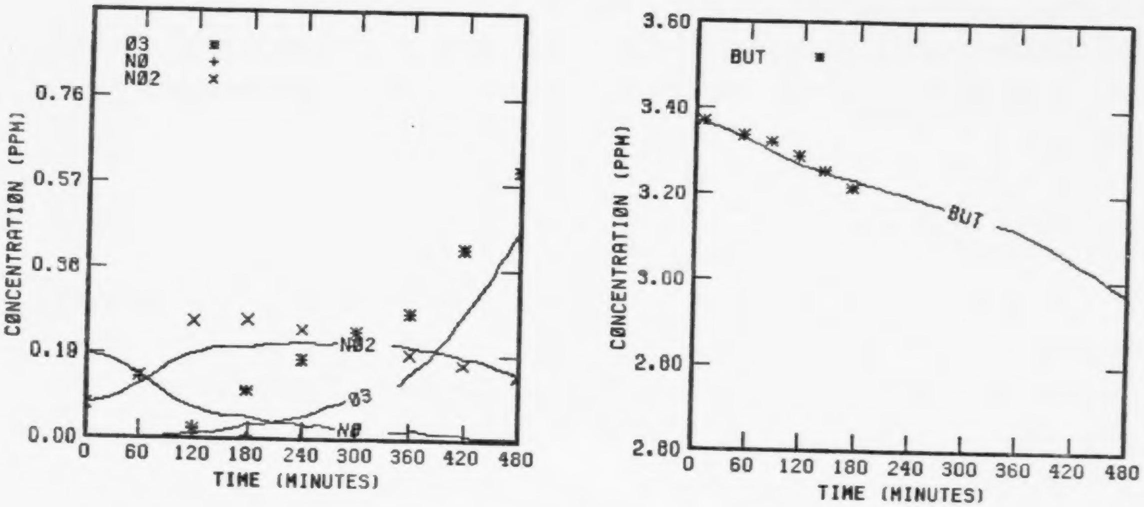

FIGURE 119. SIMULATION RESULTS FOR
UNCR 72778

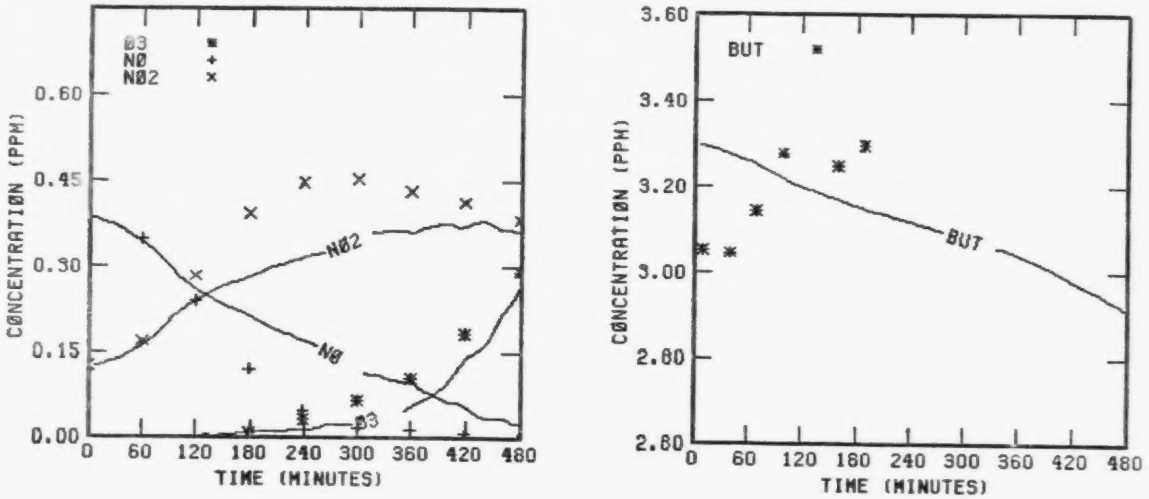

FIGURE 120. SIMULATION RESULTS FOR
UNCB 72778

reaction. Larger numbers produce a decided "kink" in the NO_x profiles near the crossover point in the UNC simulations. Hence we recommend that nitrate data be taken in future UNC experiments to confirm corresponding data received from UCR.

Sec-Butoxyl + O_2

In order to improve the overall product distribution, the reaction rate constant was lowered to half the value used last year. However, we recommend that future butane experiments at UNC include more data on the product of this reaction, methylethylketone (MEK), so that the present distribution can be confirmed.

The set of UCR experiments included a brief study of temperature variation. The changes in product data at these temperatures provided a serendipitous confirmation of a crucial part of the butane mechanism. The main products stemming from butane oxidation are acetaldehyde and MEK. The ratio of these compounds varies from about 0.5 in the low temperature experiment (289K) to about 2.5 in the high temperature experiment (312K). We are encouraged by the agreement between our simulations and the observed changes in this product ratio for two reasons: (1) the activation energy for the decomposition of sec-butoxyl radicals to acetaldehyde is a key factor and the value (8800K) we used appears to be correct (Batt, McCulloch, and Milne, 1975); and (2) the use of rate constants, arbitrarily adjusted by us to provide a close competition between the decomposition reaction and the reaction with oxygen (which forms the MEK) has finally been justified. Estimates and evaluations of the pertinent rate parameters for these two processes have large combined uncertainty factors (Barker et al., 1977); in fact, the combined uncertainty of the ratio could be as high as 100.

The results of the current butane simulations indicate a definite overprediction of ozone. In our interim report (Whitten et al., 1979), we had mentioned a general observation in smog chamber modeling concerning the rate of NO-to-NO_2 conversion. If the hydrocarbon decay is simulated to closely match the observed hydrocarbon decay, the function of any given mechanism is then to provide the intermediate species that convert NO to NO_2, deplete NO_x, and act as sources and sinks for radical balance. We have assumed that a proper conversion rate for NO to NO_2 would automatically generate the correct ozone through the basic, well-established inorganic parts of the chemical mechanism. However, the continuing problem is that an NO-to-NO_2 conversion rate, which may follow experimental observations early in many smog chamber simulations, is often too fast late in the simulation. These butane simulations provide examples of this continuing problem.

Although we have yet to solve this problem, we have attempted to analyze it. First, the observed ozone and NO_x data are not adequate to reconcile the problem. Early in virtually any smog chamber experiment the concentrations of NO and NO_2 are high relative to their concentrations late in the experiment when NO_x has been depleted. The early high NO_x concentrations apparently provide the most reliable NO_x data and the late low concentrations seem to be the least reliable. Previously we discussed a high NO_x (and low formaldehyde) concentration experiment in the UNC chamber regarding the problems with low ozone data taken in the presence of high NO_x concentrations. The possible problem was linked to decay of ozone in the sampling system. The same reasoning explains the ozone data reported for EC-308. We estimate that an eight-second sampling time would lead to the ozone values reported. Hence, there is normally a problem verifying the NO-to-NO_2 conversion rate relationship to ozone formation using observed data.

While preparing for the interim report (Whitten et al., 1979), we considered such reactions as $HO_2 + NO_3$ and $RO_2 + NO_3$, as well as $RO_2 + O_3$. In fact, we included $RO_2 + O_3$ reactions in the propylene mechanism. All of these speculative reactions have the characteristic of reducing the ozone peak without substantial change to the NO-to-NO_2 conversion early in the simulation. In general, the peroxy radicals increase in concentration as the simulation proceeds because their rate of production changes very little yet their destruction is typically determined by reaction with NO, which, of course, is decreasing rapidly.

On the other hand, O_3, PAN, and NO_3 also increase rapidly when NO has been depleted. Hence, a reaction involving one of these three species and/or peroxy radicals appears to be missing from our mechanisms. To demonstrate that a reaction with NO_3 provides a closer simulation to the observed ozone profile for these recent butane experiments, we included a reducing reaction for NO_3 to NO_2 of about 400 min^{-1}. Figure 108 shows that ozone is reduced to near the observed data for EC-304, yet the butane decay, NO_x behavior, and product appearance profiles are essentially unchanged. A reducing species for NO_3 is now under investigation. For an NO_3 reaction with formaldehyde, a value near 10000 $ppm^{-1}min^{-1}$, or for acetaldehyde a value near 2500 $ppm^{-1}min^{-1}$, would produce similar results in these simulations.

The butane decay for UCR runs EC-305 and EC-307 could not be simulated with our current chemistry. Typically, we increase the photolysis constants until the hydrocarbon decay rate is matched. However, these two runs have very high HC/NO_x ratios which lead to rapid NO_x removal, producing, in turn, very low concentrations for NO. The HO_2 reaction with NO restores the OH radicals which, in turn, are responsible for the butane decay. Hence some means of either maintaining NO in the simulation or of restoring OH, other than reaction with NO, must be missing from our mechanism.

SECTION 5

THE TOLUENE MECHANISM

Aromatic compounds form a significant fraction of the reactive hydrocarbons in urban photochemical smog. Our approach to the treatment of aromatics oxidation has involved two activities: (1) the preparation of empirical mechanisms that replicate the behavior of ozone and nitrogen oxide during oxidation, and (2) the explicit modeling of toluene chemistry. During the past year, these two efforts have, to some degree, converged, and our toluene mechanism is reasonably explicit as to the compounds involved; it also reproduces the ozone and NO_x behavior well.

EMPIRICAL FEATURES OF AROMATICS OXIDATION

We have developed a series of empirical kinetic mechanisms to simulate photochemical oxidant production in aromatic hydrocarbon systems (Whitten and Hogo, 1977; Whitten et al., 1979). Our preferred method of mechanism development is first to construct an explicit representation of all major products and reactions in the hydrocarbon decay scheme. From this explicit mechanism, we formulate a condensed mechanism, combining similar radicals, products, and the like into generalized-state variables. It has been difficult to apply this process for aromatic hydrocarbons, since explicit mechanisms that give adequate simulations of hydrocarbon decay, NO_x behavior, and ozone production have been lacking. Thus, we have resorted to the use of empirical mechanisms.

Several observable features differentiate aromatic hydrocarbon photochemistry from that of such compounds as propylene and butane. The most noticeable of these features is the inefficiency of NO-to-NO_2 conversions as compared with the hydrocarbon oxidized. Kopczynski, Kuntz, and Bufalini (1975) reported the ratio of hydrocarbon consumption versus NO oxidized as 1.5 for a paraffin mixture, 2.5 for olefins, and 4.1 for aromatics. Moreover, they noted that the ratio of HC consumption to NO oxidation varied with NO concentration, whereas the olefin and paraffin ratios remained constant. Cox, Derwent, and Williams (private communication, 1979) have obtained similar results in high OH (HONO-driven) hydrocarbon NO_x systems.

In the UCR toluene smog chamber runs analyzed thus far, we have observed a marked decline in the efficiency of NO-to-NO_2 conversions after the NO_2 peak has been reached. This decline in efficiency for aromatic systems appears to be even more pronounced than that observed for olefin and paraffin systems. Our first empirical aromatics mechanism (Whitten and Hogo, 1977) reduced ozone production efficiency by means of an $NO_3^{\cdot}$-aromatics reaction. This reaction was given a rate constant considerably higher than the actual reaction rate of $NO_3^{\cdot}$ with toluene to represent the reaction of the highly unsaturated ring-opened compounds formed in aromatics decomposition. In subsequent mechanisms, we treated the hypothesized compounds more explicitly.

The product of the $NO_3^{\cdot}$ addition to propylene has recently been identified as propylene glycol 1,2 dinitrate (Akimoto et al., 1978). Dinitrates are highly toxic compounds, and their formation in aromatic systems would have important implications in air quality management.

If $NO_3^{\cdot}$ uptake is important in aromatic photochemistry, it may account for another feature of the UCR toluene runs. Estimates of the OH· concentration in UCR smog chamber simulations EC-266 through EC-273 (see Figures 121 through 126) based on toluene decay rates seem inconsistent with the rate of NO_x consumption. More precisely, in these experiments NO_x decay is noticeably greater than can be explained by the observed nitrogen species (PAN, PBN, and so on) and the formation of nitric acid by the reaction of OH· plus NO_2. This nitrogen balance discrepancy is not an obvious feature of the propylene and butane runs that we have examined. We hypothesize that some nitrated organic is being formed. Since any PAN-like compound would tend to register as NO_x (and thus would not appear as a discrepancy)

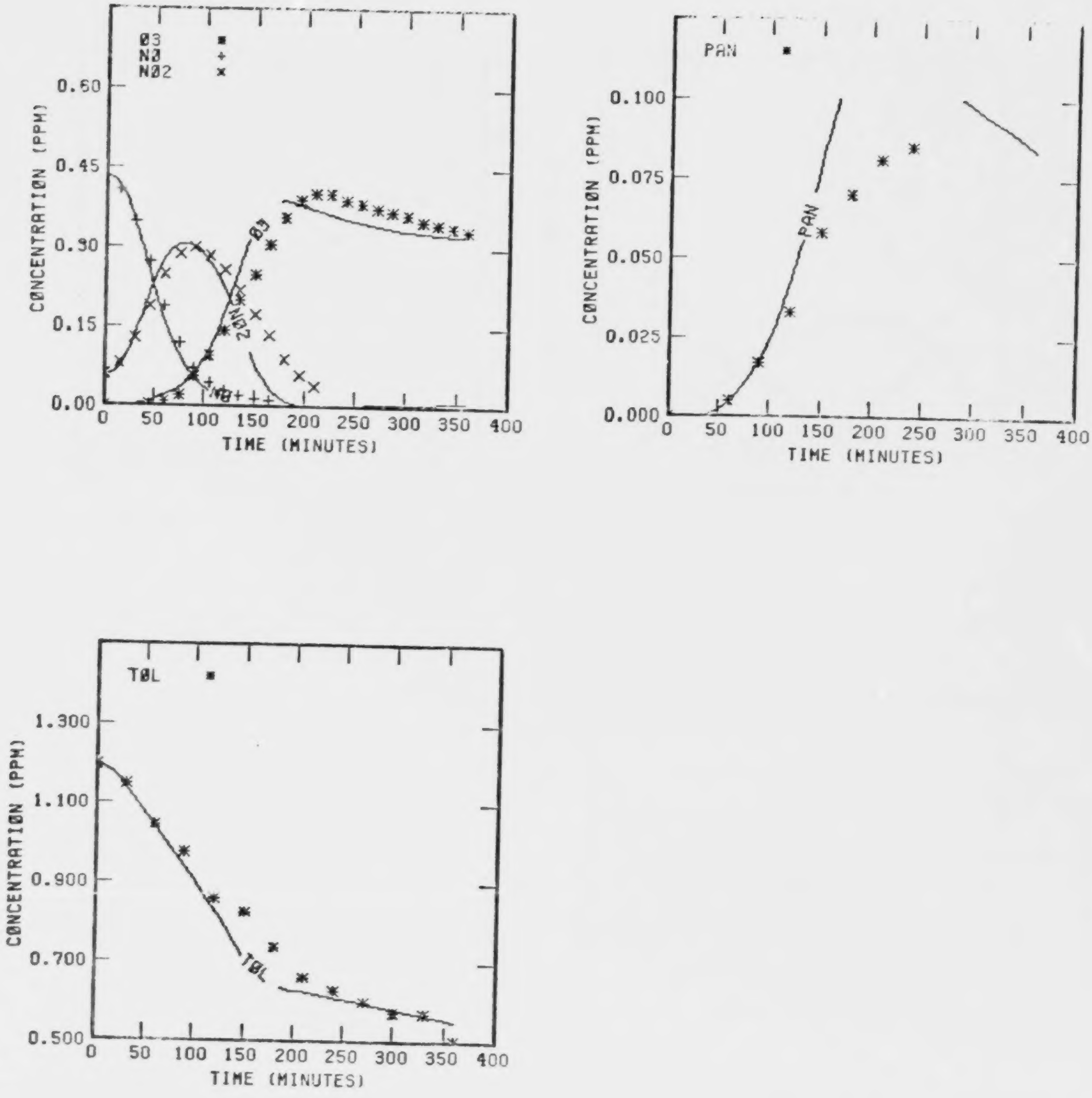

FIGURE 121. SIMULATIØN RESULTS FØR EC-266

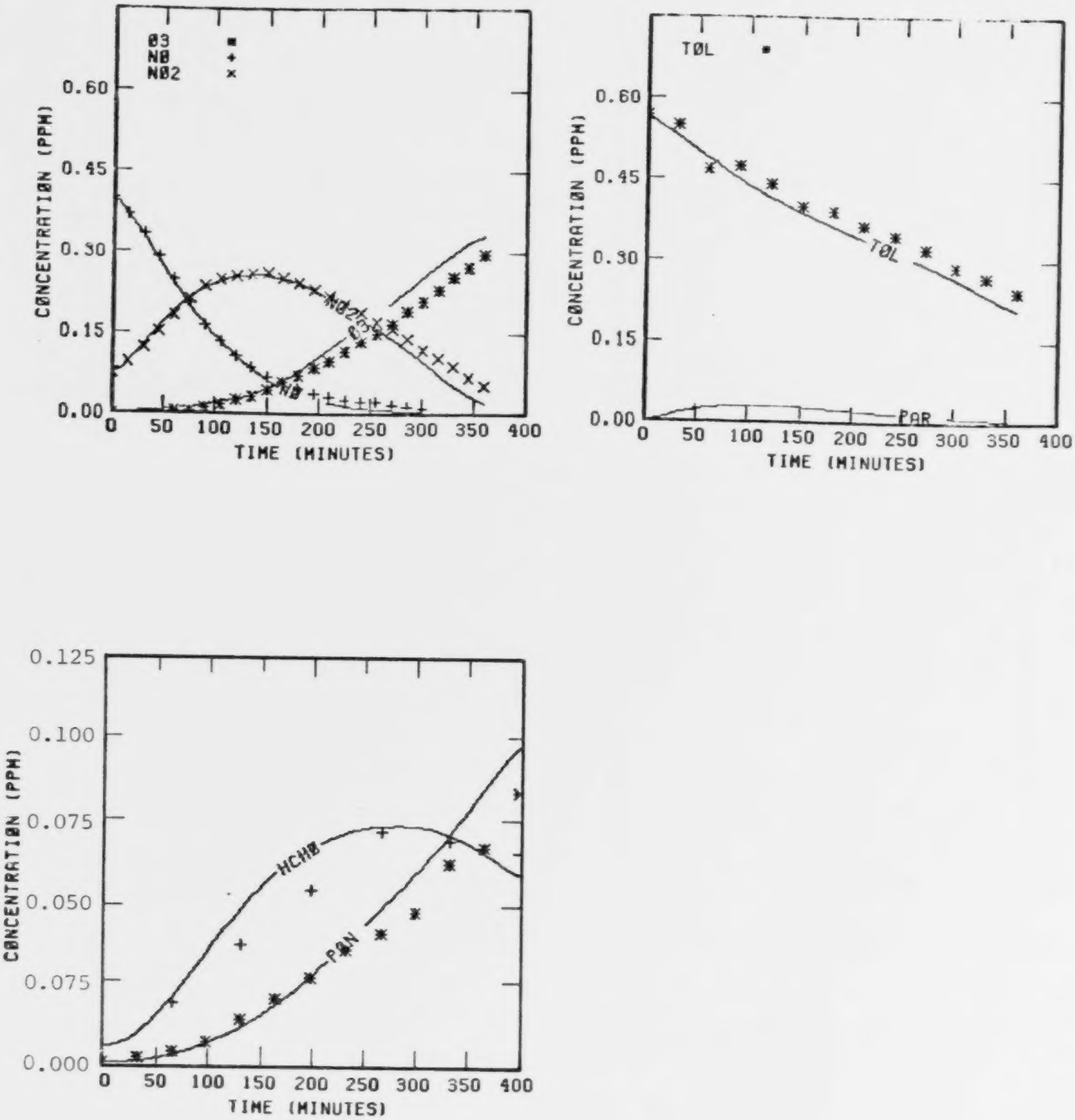

FIGURE 122. SIMULATIØN RESULTS FØR EC-269

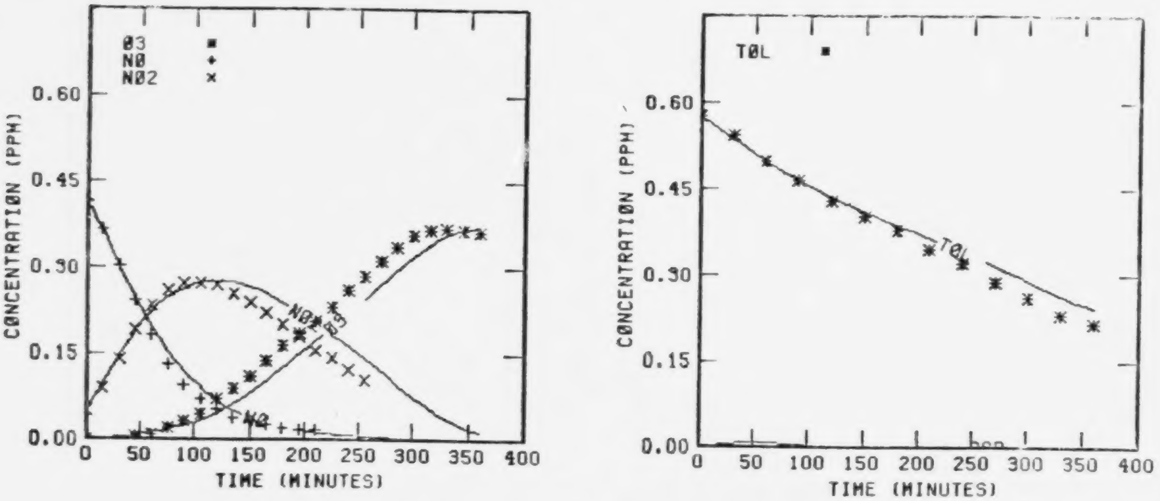

FIGURE 123. SIMULATIØN RESULTS FØR EC-270

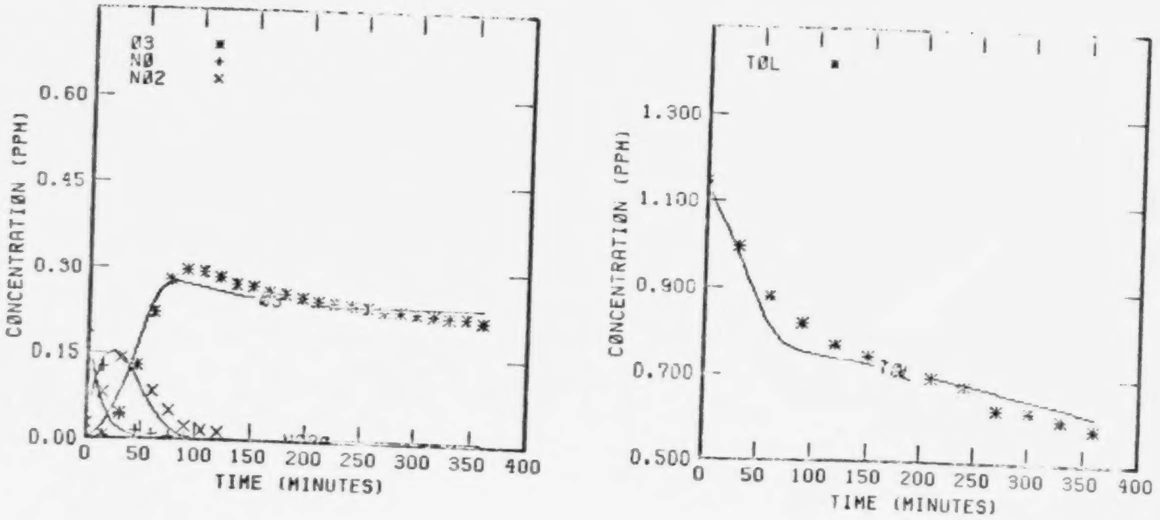

FIGURE 124. SIMULATIØN RESULTS FØR EC-271

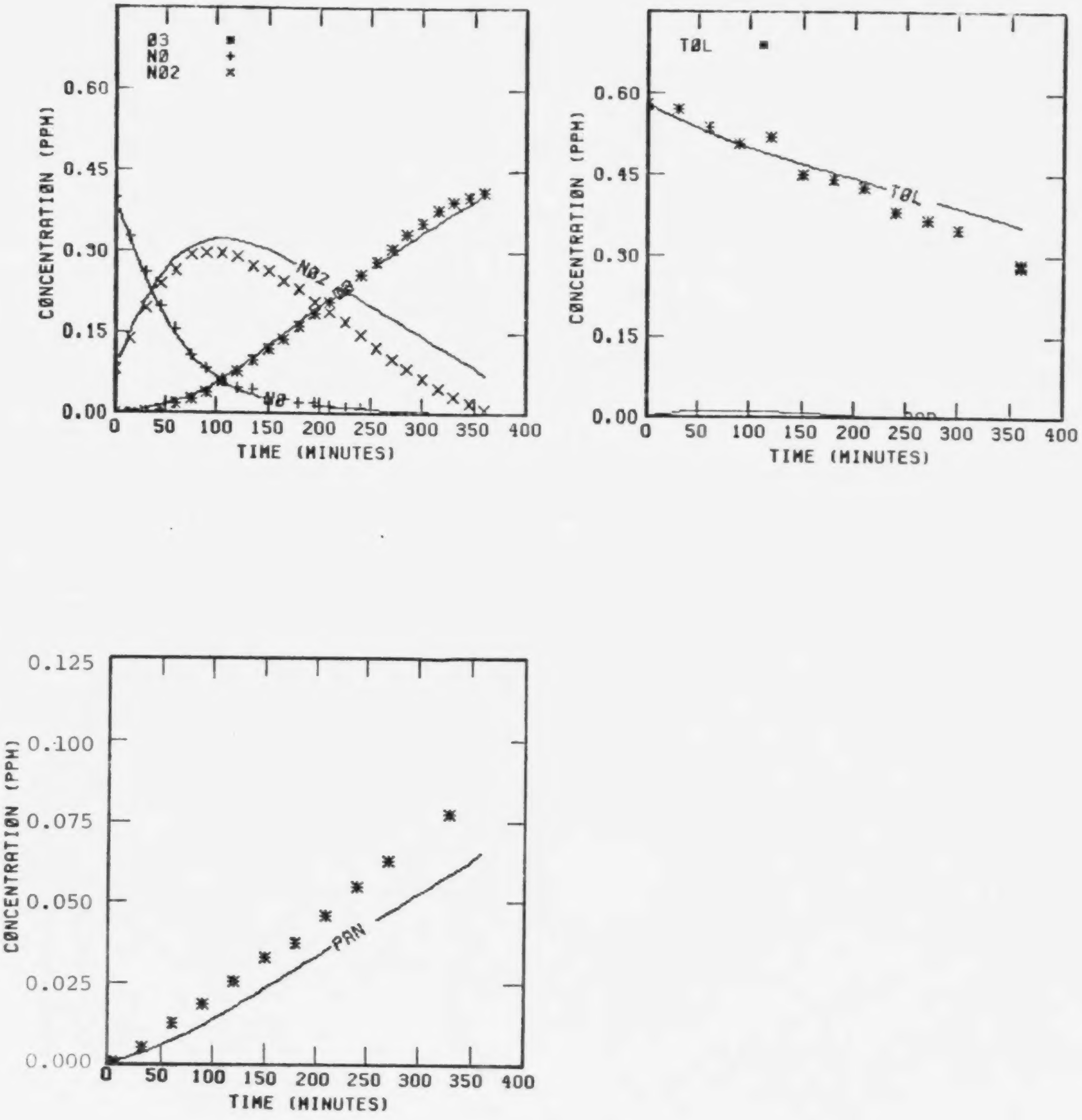

FIGURE 125. SIMULATION RESULTS FOR EC-272

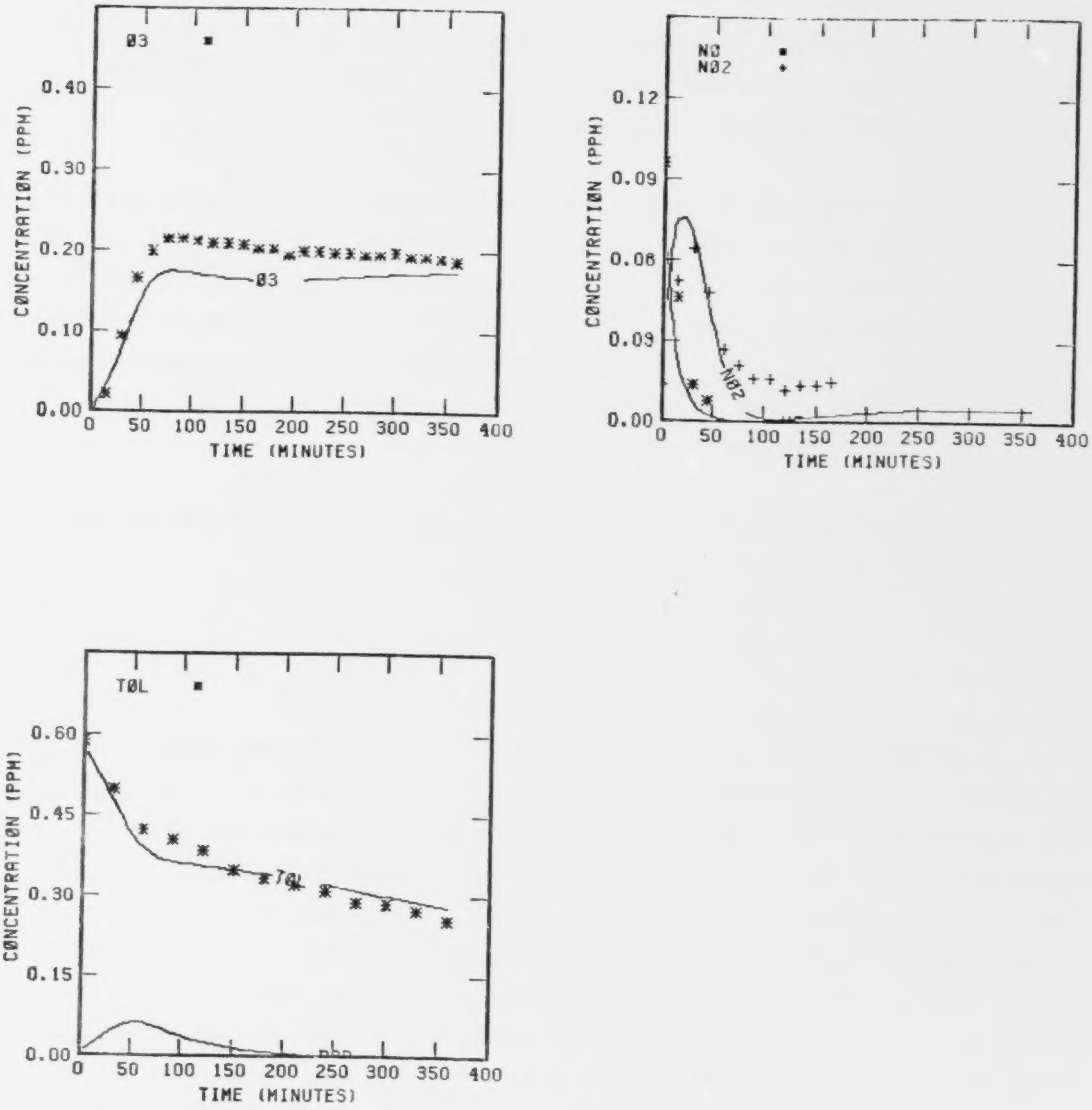

FIGURE 126. SIMULATION RESULTS FOR EC-273

we speculate that perhaps an oxygenated alkyl dinitrate is being formed. Such a compound may be difficult to measure, which might account for the poor nitrogen and carbon balances observed in aromatic systems.

The glyoxal compounds formed in the aromatic ring-opening process photolyze more rapidly than formaldehyde. The radical production rate in toluene systems cannot be explained on the basis of aldehydes alone, and therefore, the additional radicals must come from species peculiar to aromatics systems, such as benzaldehyde and glyoxals. Since the addition of benzaldehyde to a photochemical system actually retards the system (Kuntz, Kopczynski, and Bufalini, 1973), we now believe the glyoxals to be the principal photolytic species.

We refer to the ratio of oxidizing radicals produced by a system to the primary photolysis rate as "Q":

$$Q = \frac{\text{Oxidation}}{\text{Photolysis}} .$$

Factor Q appears to be an important measure of the ozone-forming capacity of the system at high hydrocarbon-to-NO_x (HC/NO_x) ratios. A low Q system should produce less ozone than a high Q system at high HC/NO_x ratios, because the NO_x disappearance rate is faster at high HC/NO_x ratios relative to the O_3 production rate. Since aromatic systems have a demonstrably low oxidizing rate and a high primary photolysis rate, the "Q" for aromatic systems is low. Furthermore, if our hypothesis of dinitrate formation is correct, the difference between the ozone formed at high HC/NO_x ratios by aromatics as compared with olefin-paraffin systems should be even more striking. Accordingly, we designed several experiments to test this hypothesis. The first of these experiments has been carried out and, as predicted, the addition of toluene to a propylene system at high HC/NO_x ratios causes a reduction in peak ozone concentration. We will discuss this experiment in greater detail when we describe our simulations of the UNC outdoor smog chamber results.

THE EXPLICIT PHOTOCHEMISTRY OF AROMATIC COMPOUNDS

The gas phase oxidation of an aromatic hydrocarbon molecule is initiated by a hydroxyl radical. The hydroxyl radical attack may proceed through either addition to the aromatic ring or hydrogen abstraction of side chain groups. In toluene, for example, side chain abstraction gives

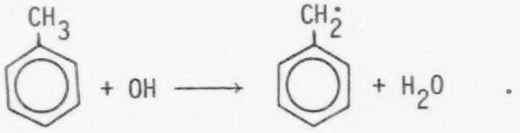
CH3
+ OH
CH2•
+ H2O
.

(8)

The aromatic radical then absorbs oxygen to form a peroxy radical that may, in turn, effect an NO-to-NO_2 conversion and then yield benzaldehyde:

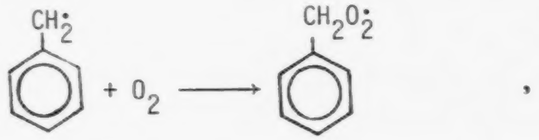
CH2•
+ O2
CH2O2•
,

(9)

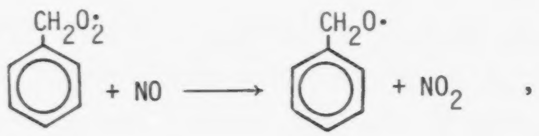
CH2O2•
+ NO
CH2O•
+ NO2
,

(10)

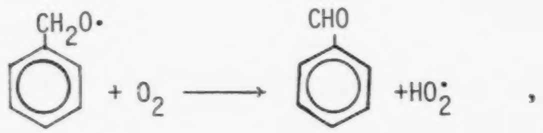
CH2O•
+ O2
CHO
+HO2•
,

(11)

Hydroxyl radical addition to the aromatic ring results in an energy-rich adduct, which becomes stabilized:

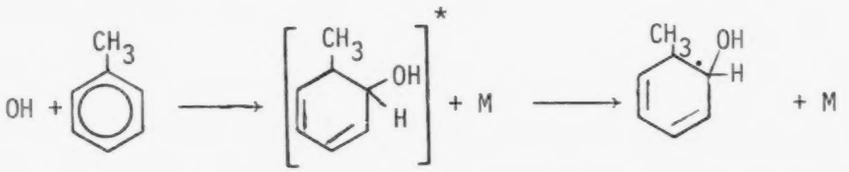
CH3
OH +
CH3
OH
H
*
+ M
CH3
OH
H
+ M

.(12)

According to an analogy with $O(^3P)$ atom reactions, hydroxyl attack at the ortho position will probably predominate (Atkinson et al., 1978).

The thermalized OH-toluene adduct is unstable at temperatures $\geq 380°K$ (Perry, Atkinson, and Pitts, 1977). From extrapolation at high temperatures [where only Reaction (8) is important] to lower temperatures, the ratio of hydroxyl abstraction to addition was estimated by Perry, Atkinson, and Pitts (1977) to be 0.16 (+0.07 or -0.05).

At low pressures (6 to 15 torr), the adduct radical reacts with O_2:

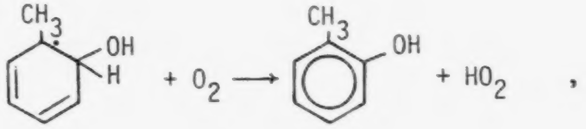

(13)

yielding cresol at a ratio of seven times the yield of benzaldehyde (Hendry, 1978), a rate that agrees with the estimate of Perry, Atkinson, and Pitts (1977).

At higher O_2 pressures, however, the product yield of cresol to benzaldehyde as observed at the UCR chamber and elsewhere (Hoshino, Akimoto, and Okuda, 1978) is closer to 2 to 1. The destruction rate of cresol by OH is too low to explain this discrepancy.

Atkinson et al. (1978) suggest that the OH-toluene adduct radical may react with O_2 to form an oxygenated radical:

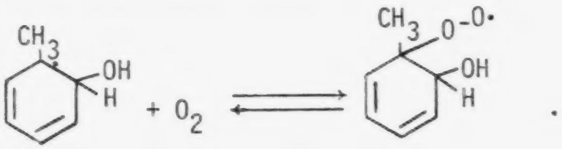

(14)

In the degradation of phenol by gamma-ray-induced hydroxyl in aqueous solution (Sato, Takimoto, and Tsuda, 1978), the secondary reaction with O_2 is immediately followed by ring opening to yield dihydroxymucondialdehyde:

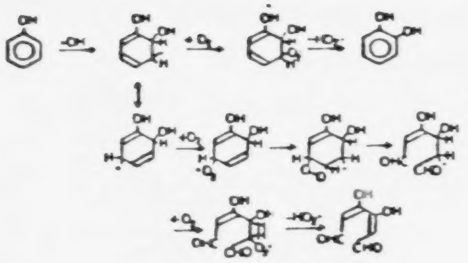

(15)

Consistent with this reaction pathway is the work of Schwartz (1974), who identified ring-opened compounds of six and seven carbon atoms in toluene aerosol.

Smaller ring-opened fragments have also been observed in aromatics-OH systems. Nojima et al. (1974) reported the formation of glyoxal, methylglyoxal, and biacetyl, all of which would have been produced by the cleaving of rings in the photooxidation of benzene, toluene, and xylene. Darnell, Atkinson, and Pitts (1978) have determined that in the NO_x photooxidation of o-xylene, approximately 20 percent of the reaction of OH radicals leads to biacetyl.

Nojima et al. (1974) found that biacetyl production in an o-xylene system was only half as great as methylglyoxal production. However, these experiments were carried out using very high concentrations (1000 ppm) of hydrocarbons. Glyoxal production was observed in all three aromatics systems. For toluene, the principal oxygenated product observed was methylglyoxal.

Takagi et al. (1979) observed the ratio among glyoxal, methylglyoxal, and biacetyl production to be 3.3:0.5:1. These ratios were estimated by Nojima et al. (1974) to be 0.2:2.5:1. Although the variations in these data are large, they suggest that over half of the products of the hydroxyl aromatic reactions are ring cleavage fragments.

The formation of glyoxal compounds might occur with the successive degradation of the ring-opened compound. However, glyoxals seem to form immediately after the initial hydroxyl reaction, suggesting that some fraction of the ring cleavage reaction forms multiple fragments.

One possible pathway involves the oxygenated OH-toluene adduct radical (Atkinson, 1979, private communication):

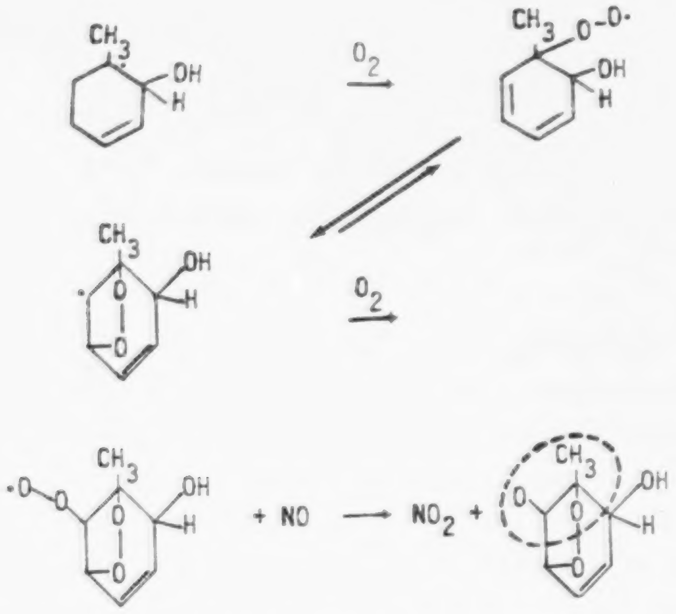

Cleavage then occurs to give methylglyoxal (circled), $HO_2^{\cdot}$, and another ring-opened fragment.

The complementary product to the glyoxals, produced either from further degradation of a ring-opened compound or by cleavage of the ring at multiple points, would be an internally unsaturated dialdehyde (2 butene 1,4 dial for the toluene system):

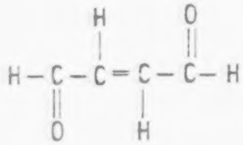

$$\mathrm{H-\underset{\underset{O}{\|}}{C}-\overset{\overset{H}{|}}{C}=\underset{\underset{H}{|}}{C}-\overset{\overset{O}{\|}}{C}-H}$$

The properties of unsaturated dialdehyde compounds such as this (called FOLE in our toluene mechanism), are speculative. These compounds might photolyze; the double bond might react with OH, O_3, or NO_3; the hydrogen atoms might be abstracted to yield peroxyacyl-like radicals, which might form PANs and other compounds. Such compounds might also form aerosols or adhere to the smog chamber walls. The latter effect is likely because dialdehydes have low vapor pressures and high boiling points. Butanedial (succinaldehyde), for example, has a boiling point of 170°C, and hexanedial has a vapor pressure of 3 torr at 90°C (Rappoport, 1967).

The quantum yield for photolysis to radicals for the unsaturated aldehydes is probably low. Acrolein, for example, on absorbing light, tends to form an excited polymerizing molecule rather than decompose (Calvert and Pitts, 1966). The inclusion of a photolysis reaction for the unsaturated dialdehydes would make the simulation mechanism much too reactive.

Reactions involving OH· are probably not important because the number of NO-to-NO_2 conversions would become too large unless some other mechanism exists to reduce the importance of that reaction. The low vapor pressure of these dialdehydes could be responsible for a reduction of any OH· importance. As we have mentioned previously, Schwartz (1974) observed ring-opened compounds in the analysis of toluene aerosols.

Recent measurements (O'Brian, personal communication, 1979) indicate that a substantial fraction of the carbon in toluene oxidation is lost from the gas phase. For unsaturated dialdehydes leaving the gas phase, only a modest first-order loss rate ($\sim 0.05\ min^{-1}$) is necessary to compete with hydroxyl attack and to eliminate the excessive ozone production caused by the hydroxyl reaction.

This reasoning is speculation in support of a specific fact: our simulations of toluene systems work better when the reaction of OH with these secondary oxidation products is eliminated. Therefore, we have eliminated the reaction, noting that the overall behavior is likely to be complex.

The only reactions of the FOLE compounds that are contained in our toluene mechanism are reactions with O_3 and NO_3. We have assumed that the internal double bonds contained in these compounds react with O_3 and NO_3 at rates similar to that of dimethylbutene. These rates are very fast; even if the FOLE compounds are rapidly precipitating from the gas phase, they will tend to react in our simulations with O_3 and NO_3 before they encounter an aerosol particle or a chamber wall.

Fate of Benzaldehyde

Benzaldehyde is a known product of toluene oxidation, accounting for 11 to 23 percent of the overall reaction products (Perry, Atkinson, and Pitts, 1977; Hendry, 1978).

It has long been known that the addition of benzaldehyde to photochemical mixtures tends to retard their photochemical activity (Kuntz, Kopczynski, and Bufalini, 1973). One could explain this effect by suggesting that benzaldehyde is a radical scavenger. However, systems of air, benzaldehyde, and NO_x show increases in NO-to-NO_2 conversions when compared with air systems. Obviously, radical scavenging is balanced by some source of radicals as well.

Hendry (1972) suggests that the rate of decomposition of the benzoyloxy radical is low, allowing it to react with oxides of nitrogen and the reactor wall, thereby serving as a radical sink. This leads to the following reaction sequence (Hendry et al., 1978):

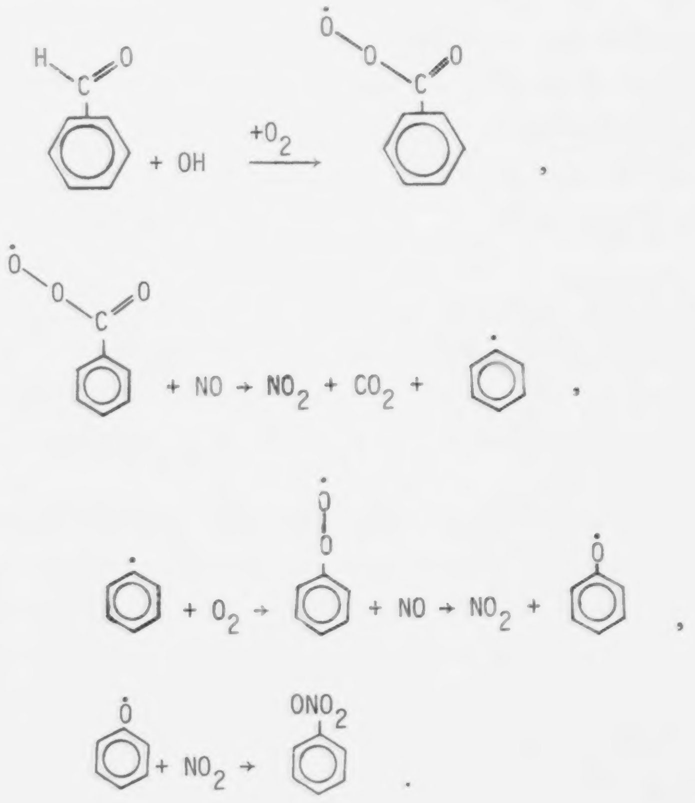

This sequence is primarily a scavenging mechanism: Used alone, it produces too great a retardation of photochemical activity in UCR runs EC-337 and EC-339. Counterbalanced by the scavenging effect is the effect of benzaldehyde photolysis:

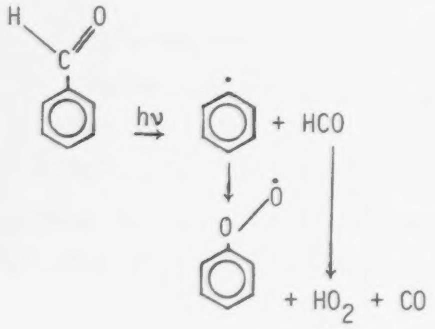

.

We assume that the carbon-phenyl bond is the bond that breaks upon photolysis to reduce the number of NO-to-NO_2 conversions in the photolysis pathway. We have also included a decomposition reaction for the benzoyloxy radical:

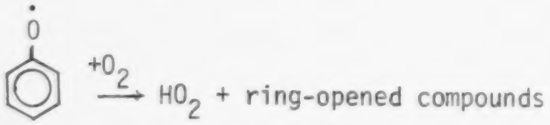

.

This decomposition is assumed to be slow with a pseudo-first-order rate constant of 2.0 min^{-1}.

Photolysis yields for benzaldehyde are not well known. At 313 nm, the quantum yield at room temperature is low. However, a second absorbtion band exists below 310 nm with a very high absorbtion peak (λ max = 282 nm, $\varepsilon = \cong 1600$; Calvert and Pitts, 1966). If benzaldehyde photolysis proves to be unimportant, the decomposition rate of the benzoyloxy radical will have to be increased.

The chemistry of peroxybenzoylnitrate is from Hendry 1972.

Fate of Cresol

Cresol is a reaction product in the toluene system similar in magnitude to that of benzaldehyde (Hoshino, Akimoto, and Okuda, 1978; UCR toluene data). It reacts with OH approximately six times faster than toluene (Perry, Atkinson, and Pitts,1977). The products of this reaction are unknown; we have used dihydroxy toluene as the reaction product.

Although cresol does not react with ozone, there is evidence of a strong reaction with NO_3 (O'Brian, personal communication, 1979). It is possible that cresol is responsible for the NO_3 loss in aromatic systems that we have discussed previously. However, the yield of cresol from toluene oxidation does not seem to be high enough for it to be the principal NO_3 uptake species. The expected product of the NO_3-cresol reaction would be a cresol nitrate.

MASS BALANCE IN THE TOLUENE MECHANISM

The toluene mechanism is given in Table 31. Subsequent to the initial reaction of OH· with toluene, 16 percent of the reacted carbon mass goes to cresol and 11 percent goes to benzaldehyde. Of the remaining 73 percent carbon, 80 percent follows a pathway that leads to ring opening, fracture, and the production of α-dicarbonyls, here assumed to be methyl glyoxal. The complementary product to the methyl glyoxal is labeled FOLE and is assumed to react exclusively with O_3 and $NO_3^{\cdot}$, to form dinitrates. The remaining 20 percent of the ring opening (15 percent overall) goes to a diolefinic compound assumed to react as two FOLE groups.

There is some doubt as to the fate and precise reactions of the compounds grouped as "FOLE." The overall stoichiometry of the toluene oxidation sequence presented here mimics actual toluene oxidation too precisely to be dismissed lightly. If the suggested FOLE reactions do not exist, then they at least emulate reactions that are taking place.

DESCRIPTION OF TOLUENE SIMULATIONS FOR UCR

Initial conditions and photolysis rates for the UCR toluene experiments are given in Table 32 There were minor variations in the solar simulator light intensity during the second series, but we have made no attempt to correct for these effects. Nitrogen dioxide photolysis varied only about 2 percent during the series.

TABLE 31. THE DEVELOPMENTAL TOLUENE MECHANISM

Reactions								Rate Constant	Activation energy
1	NO2			=	NO	O		*	-0.
2	O			=	O3			4.400E+06	-5.100E+02
3	O3	NO		=	NO2			2.660E+01	1.450E+03
4	O	NO2		=	NO			1.340E+04	-0.
5	O3	NO2		=	NO3			4.800E-02	2.450E+03
6	NO3	NO		=	NO2	NO2		2.800E+04	-0.
7	RX†			=	OH			1.300E-01	-0.
8	NO2	OH		=				1.400E+04	-0.
9	O3	OH		=	HO2			1.000E+02	9.400E+02
10	O3	HO2		=	OH			2.400E+02	5.800E+02
11	NO3	NO2	H2O	=				1.560E-03	-0.
12	CO	OH		=	HO2			4.400E+02	-0.
13	HO2	NO		=	OH	NO2		1.200E+04	-0.
14	HO2	HO2		=				7.500E+03	-0.
15	NO	NO		=	NO2	NO2		1.500E-04	-0.
16	PAR	OH		=	MEO2			1.500E+03	-0.
17	PAR	O		=	NEO2	OH		2.000E+01	-0.
19	OLE	OH		=	RAO2			4.200E+04	-0.
20	OLE	O		=	ACO3	MEO2	X	1.400E+03	-0.
21	OLE	O		=	CARB			4.000E+03	-0.
23	OLE	O3		=	CARB	CRIG		8.000E-03	-0.

TABLE 31 (Continued)

Reactions								Rate Constant	Activation energy
24	OLE	O3	=	CARB	MCRG			8.000E-03	-0.
25	ETH	OH	=	RBO2				1.200E+04	-0.
26	ETH	O	=	MEO2	HO2	CO		6.000E+02	-0.
27	ETH	O	=	CARB				6.000E+02	-0.
28	ETH	O3	=	CARB	CRIG			2.400E-03	-0.
29	CARB	OH	=	ACO3	X			8.000E+03§	-0.
30	CARB	OH	=	HO2	CO			1.050E+04§	-0.
31	CARB		=	X	MEO2	HO2		2.000E-04*§	-0.
32	CARB		=	CO	HO2	HO2		1.800E-03*§	-0.
33	CARB		=	CO				3.600E-03*§	-0.
34	MEO2	NO	=	NO2	HCHO	HO2		3.700E+03	-0.
35	MEO2	NO	=	NO2	CARB	HO2		7.300E+03	-0.
36	ACO3	NO	=	NO2	MEO2	CO2		3.800E+03	-0.
37	RBO2	NO	=	NO2	CARB	CARB	HO2	1.200E+04	-0.
38	RBO2	O3	=	HCHO	CARB	HO2		5.000E+00	-0.
39	RAO2	NO	=	NO2	CARB	HCHO	HO2	1.200E+04	-0.
40	RAO2	O3	=	CARB	CARB	HO2		2.000E+04	-0.
41	X	PAR	=					1.000E+05	-0.
42	CRIG	NO	=	NO2	CARB			1.200E+04	-0.
43	CRIG	NO2	=	NO3	CARB			8.000E+03	-0.
44	CRIG	CARB	=	OZD				2.000E+03	-0.

TABLE 31 (Continued)

Reactions									Rate Constant	Activation energy
45	CRIG		=	CO					6.700E+02	-0.
46	CRIG		=						2.400E+02	-0.
47	CRIG		=	HO2	HO2	CO			9.000E+01	-0.
48	MCRG	NO	=	NO2	CARB				1.200E+04	-0.
49	MCRG	NO2	=	NO3	CARB				8.000E+03	-0.
50	MCRG	HCHO	=	OZD					2.000E+03	-0.
51	MCRG		=						1.500E+02	-0.
52	MCRG		=	X	MEO2	CO	OH		3.400E+02	-0.
53	MCRG		=	X	MEO2	HO2			4.250E+02	-0.
54	MCRG		=	HO2	CARB	HO2	X		8.500	-0.
55	MEO2	NO	=	NRAT					1.000E+02	-0.
56	MEO2	O3	=	CARB	HO2				5.000E+00	-0.
57	ACO3	HO2	=						4.000E+03	-0.
58	MEO2	HO2	=						4.000E+03	-0.
61	ACO3	NO2	=	PAN					2.000E+03	-0.
62	PAN		=	ACO3	NO2				2.800E-02	-0.
64	TOL	OH	=	RARO					6.700E+03	-0.
65	TOL	OH	=	CRE	HO2				1.500E+03	-0.
66	TOL	OH	=	BO2					1.000E+03	-0.
67	RARO	NO	=	NO2	HO2	C			1.200E+04	-0.
68	C		=	FOLE	FOLE				2.000E+03	-0.

TABLE 31 (Continued)

Reactions								Rate Constant	Activation energy
70	C		=	GLY	FOLE	PAR		8.000E+03	-0.
71	GLY		=	HO2	CO	ACO3	X	3.600E+01	-0.
73	RARO	O3	=	HO2	AERO			2.000E+01	-0.
74	O3		=					2.200E-04	-0.
75	FOLE	O3	=	AERO				1.500E+00	-0.
76	FOLE	NO3	=	NTO				3.500E+04	-0.
77	NTO	NO	=	DNTR				5.000E+02	-0.
78	BO2	NO	=	BZA	HO2	NO2		1.000E+04	-0.
79	BZA	OH	=	BZO2				2.000E+04	-0.
80	BZO2	NO2	=	PBZN				2.500E+03	-0.
81	BZO2	NO	=	NO2	PHO2			3.700E+03	-0.
85	PBZN		=	BZO2	NO2			2.200E-02	-0.
86	PHO2	NO	=	PHO	NO2			1.000E+04	-0.
87	PHO	NO2	=	PNO3				6.000E+01	-0.
88	BZA		=	HO2	PHO2	CO		2.000E-03*	-0.
89	CRE	OH	=	HO2	DHTL			5.000E+04	-0.
90	CRE	NO3	=	NCR				1.000E+04	-0.
91	PHO		=	HO2	C			2.000E+00	-0.
92	PHO2	HO2	=					4.000E+03	-0.

TABLE 31 (Concluded)

Reactions					Rate Constant	Activation energy
93	OLE	NO3	=	NTO	8.000E+00	-0.
63	H20		=		-4.200E-04	-0.

---

* Photolysis rates in min^{-1}. Photolysis rates are as ratios to K_1 for natural sunlight.

† Fractional splits between carbonyl groups (formaldehyde vs. higher aldehydes) vary when there are coreactants with toluene. The table is for propylene and toluene. Toluene alone is assumed to yield only formaldehyde.

TABLE 32 UCR SIMULATION CONDITIONS

Exp. No.	Initial concentration (ppm)								Photolysis rate constant (min^{-1})			
	NO	NO_2	Tol	HCHO	BZA	Acet	CO	R_x*	NO_2	Mgly	HCHO →Radicals	BZA
EC-266	0.432	0.059	1.196	0.01	0.	0.	0.	0.	0.35	0.0135	3.5×10^{-4}	7.2×10^{-4}
EC-269	0.398	0.074	0.566	0.003	0.	0.	0.	0.005	0.35	0.0135	3.5×10^{-4}	7.2×10^{-4}
EC-270	0.414	0.051	0.576	0.178	0.	0.	0.	0.	0.35	0.0135	3.5×10^{-4}	7.2×10^{-4}
EC-271	0.186	0.029	1.146	0.004	0.	0.	0.	0.008	0.35	0.0135	3.5×10^{-4}	7.2×10^{-4}
EC-272	0.398	0.08	0.58	0.	0.	0.378	0.	0.	0.35	0.0135	3.5×10^{-4}	7.2×10^{-4}
EC-273	0.096	0.014	0.587	0.003	0.	0.	0.	0.008	0.35	0.0135	3.5×10^{-4}	7.2×10^{-4}
EC-327	0.357	0.096	0.573	0.	0.	0.	0.	0.004	0.4	0.015	3.5×10^{-4}	8.0×10^{-4}
EC-336	0.342	0.097	1.008	0.303	0.	0.	0.	0.	0.4	0.015	3.5×10^{-4}	8.0×10^{-4}
EC-337	0.322	0.124	0.959	0.	0.172	0.	0.	0.0025	0.4	0.015	3.5×10^{-4}	8.0×10^{-4}
EC-339	0.341	0.102	0.537	0.	0.187	0.	0.44	0.	0.4	0.015	3.5×10^{-4}	8.0×10^{-4}
EC-340	0.333	0.096	0.537	0.	0.	0.	0.26	0.007	0.4	0.015	3.5×10^{-4}	8.0×10^{-4}

* R_x is an initial radical source having a photolysis rate 1/2 that of HONO (0.03 min^{-1}) to mimic HONO effects.

The only general error seen in these runs is an overprediction of PAN. This is probably caused by our assumption that all of the ∝-dicarbonyls formed are methylglyoxal. If simple glyoxal comprised a significant fraction of the ∝-dicarbonyls, then the production of peroxyacetyl radicals and PAN formation would be reduced.

A comparison of the toluene only runs with those runs having high initial conditions of formaldehyde and acetaldehyde (runs EC-270, EC-271, and EC-336) shows the need for the ∝-dicarbonyls as a radical source. Even if all of the toluene that decays were to go immediately to formaldehyde, the photolysis rate necessary to provide radicals for the toluene runs is twice that needed to fit the formaldehyde-added runs. Clearly, some product having a high photolysis rate is formed from toluene oxidation.

In the later series of experiments, EC-327 through EC-340, analysis of benzaldehyde is begun (see Figures 127 through 131). Runs 337 and 339 contained high initial conditions of benzaldehyde and exhibited the slower chemistry noted previously. Benzaldehyde decay for these runs is slightly underpredicted, and the benzaldehyde peak for the other runs is slightly overpredicted. These factors suggest that the OH· rate constant for benzaldehyde is faster than that used in these simulations or that benzaldehyde photolysis should be faster.

DESCRIPTION OF TOLUENE SIMULATIONS FOR UNC

Initial conditions for the UNC outdoor smog chamber experiments are given in Table 33, and Figures 132 through 139 give the simulation results for these same experiments. Simultaneous experiments involving ethylene and propylene were simulated using the Revised Carbon-Bond Mechanism (CBM-II) given in Table 34. The influence of water on PNA chemistry, discussed in Section 3, was not included in these simulations.

The only modification of the mechanism from experiment to experiment was a change in the fraction of formaldehyde and acetaldehyde used. For ethylene, all aldehydes were assumed to be formaldehyde; for propylene, a 2:1 formaldehyde acetaldehyde ratio was used.

The only noteworthy feature of the 1978 experiments is the very high Rx values required to fit the 91878 runs. The value of 0.06 ppm for Rx is clearly too great to be explained by HONO. Yet without this value, the simulations are greatly retarded, even though the production and decay rates reproduce the data, albeit involving a time lag. One is tempted to consider the possibility that the data were somehow shifted by an hour or two. Otherwise, we have no explanation for this curious feature.

THE PROPYLENE TOLUENE EXPERIMENT (62179)

In order to highlight the NO_x loss, which is one of the most important features of toluene oxidation, we designed an NO_x-limited experiment in which the loss would have an effect upon ozone. As expected, a propylene toluene mix gives a lower ozone peak (20 percent lower) than a propylene-only run, despite a faster initial ozone production rate. Our simulations of these experiments are shown in Figures 140 and 141. (In the 1979 experiment, unlike the 1978 series, PAN data were subtracted from the NO_2 data in order to correct for the known PAN interference.) If our simulations are correct, the increased NO_x loss for the toluene system is equally divided between two mechanisms; one is the loss of NO_3 to organic nitrates as previously described. However, if the NO_3 reactions are removed, some difference still exists (the results are given in Figure 142 with reactions 76 and 90 eliminated). This is because the overall photolysis rate is substantially higher in the toluene-added system, resulting in a higher OH concentration and a higher production rate of nitric acid. The ozone formation rate is enhanced marginally and the ozone peak is reached sooner, though at a lower concentration than in the propylene-only system. This, therefore, is a graphic demonstration of the parameter "Q."

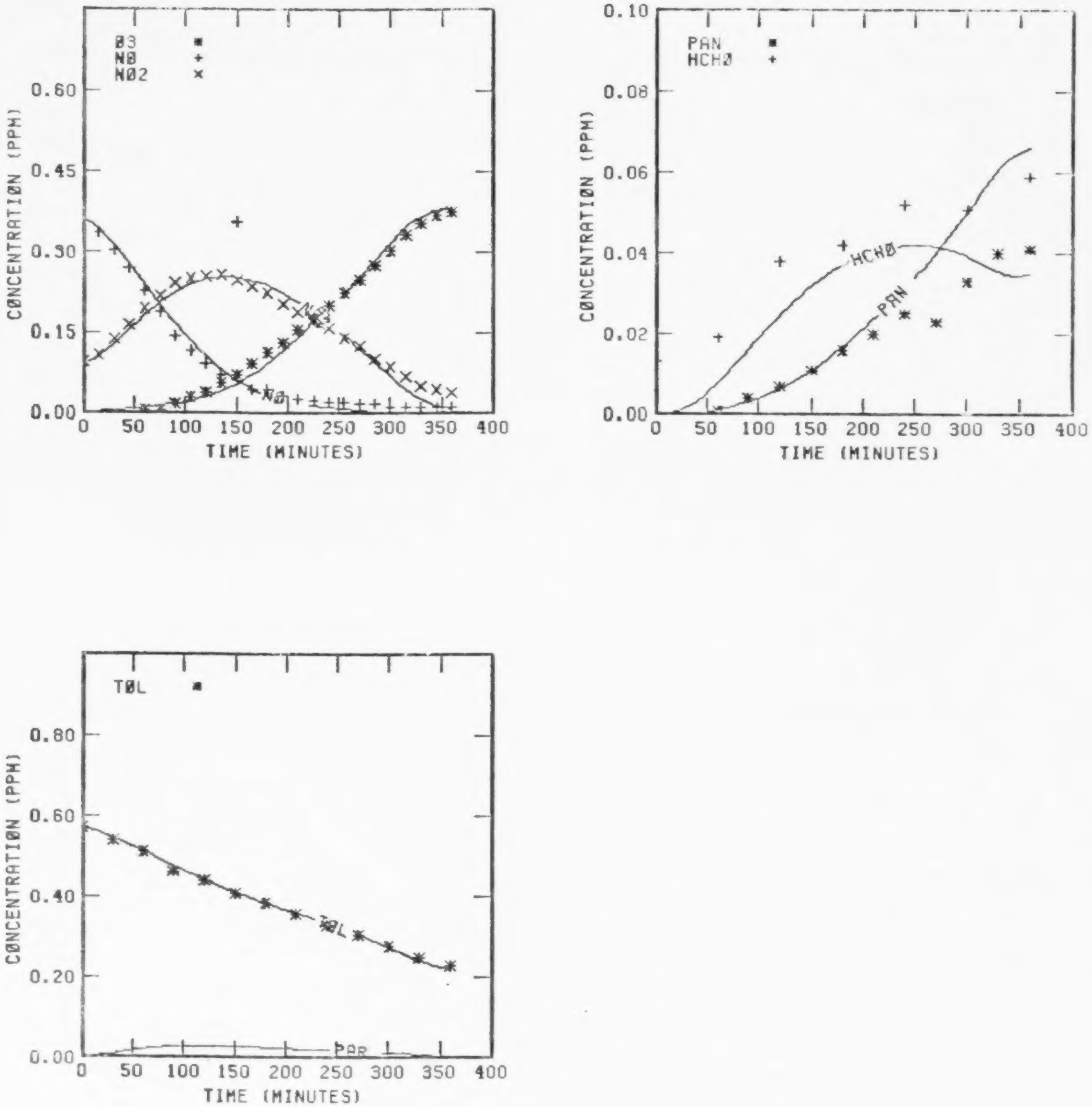

FIGURE 127. SIMULATION RESULTS FOR EC-327

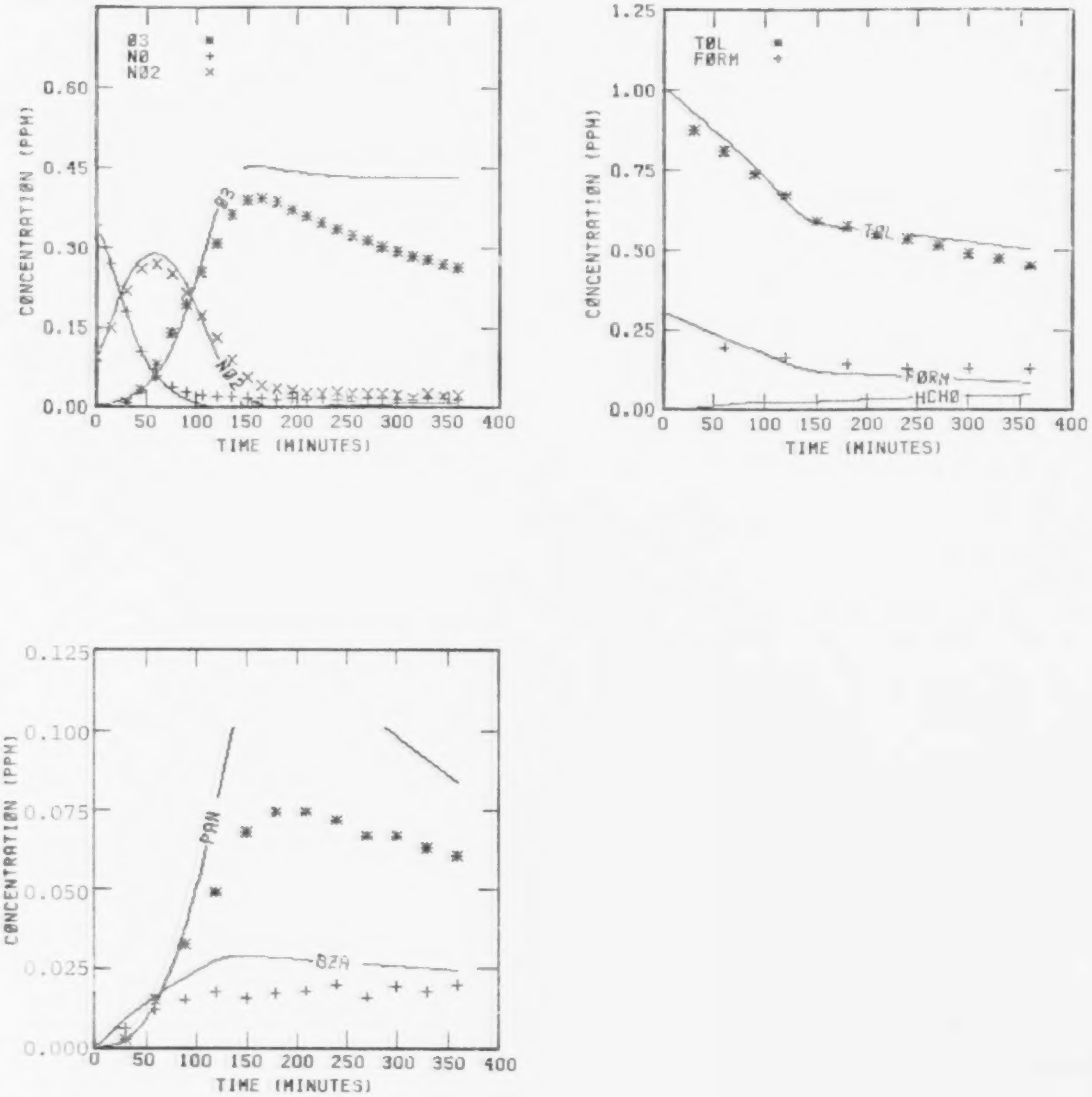

FIGURE 128. SIMULATION RESULTS FOR
EC-336

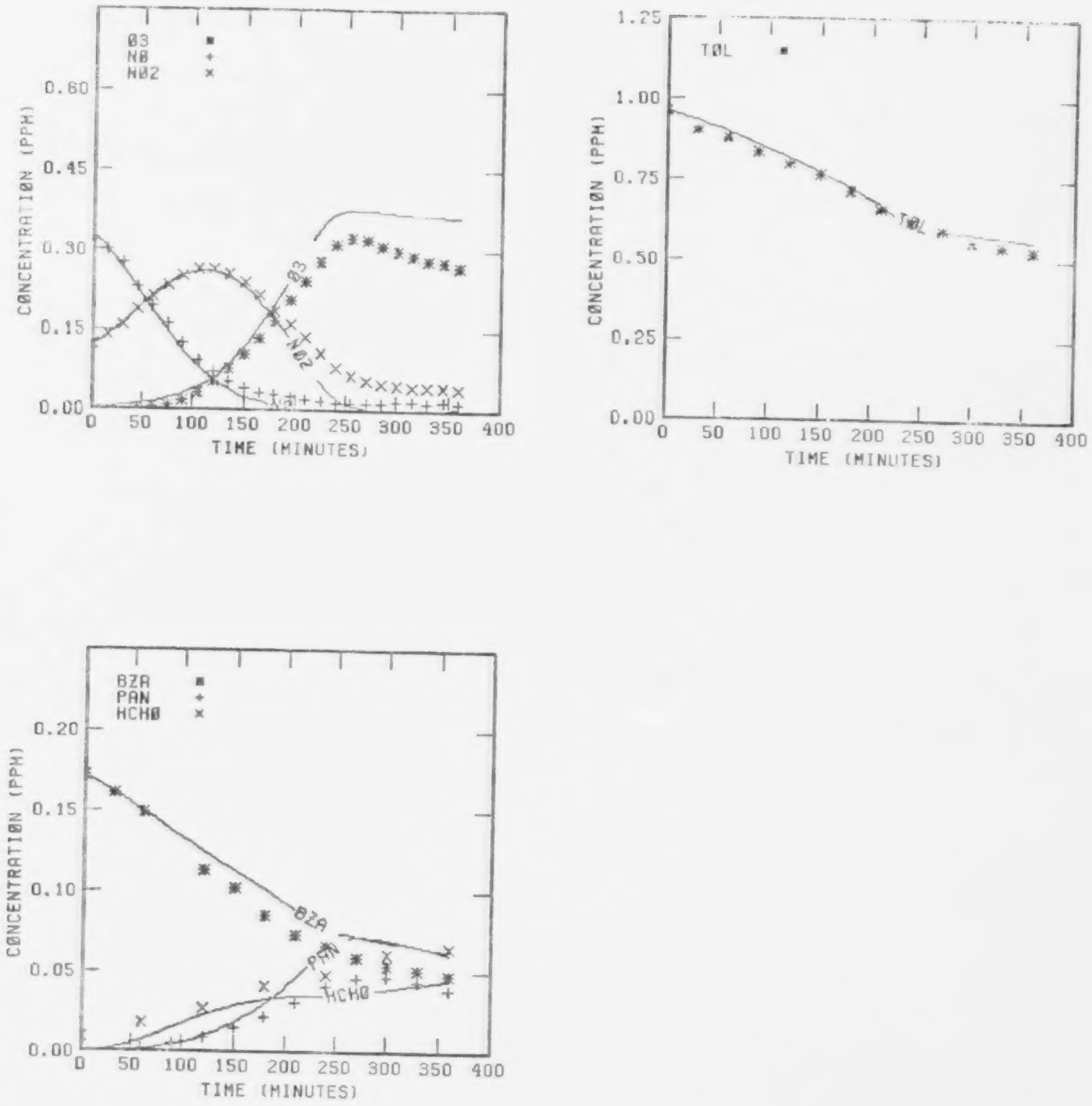

FIGURE 129. SIMULATION RESULTS FOR EC-337

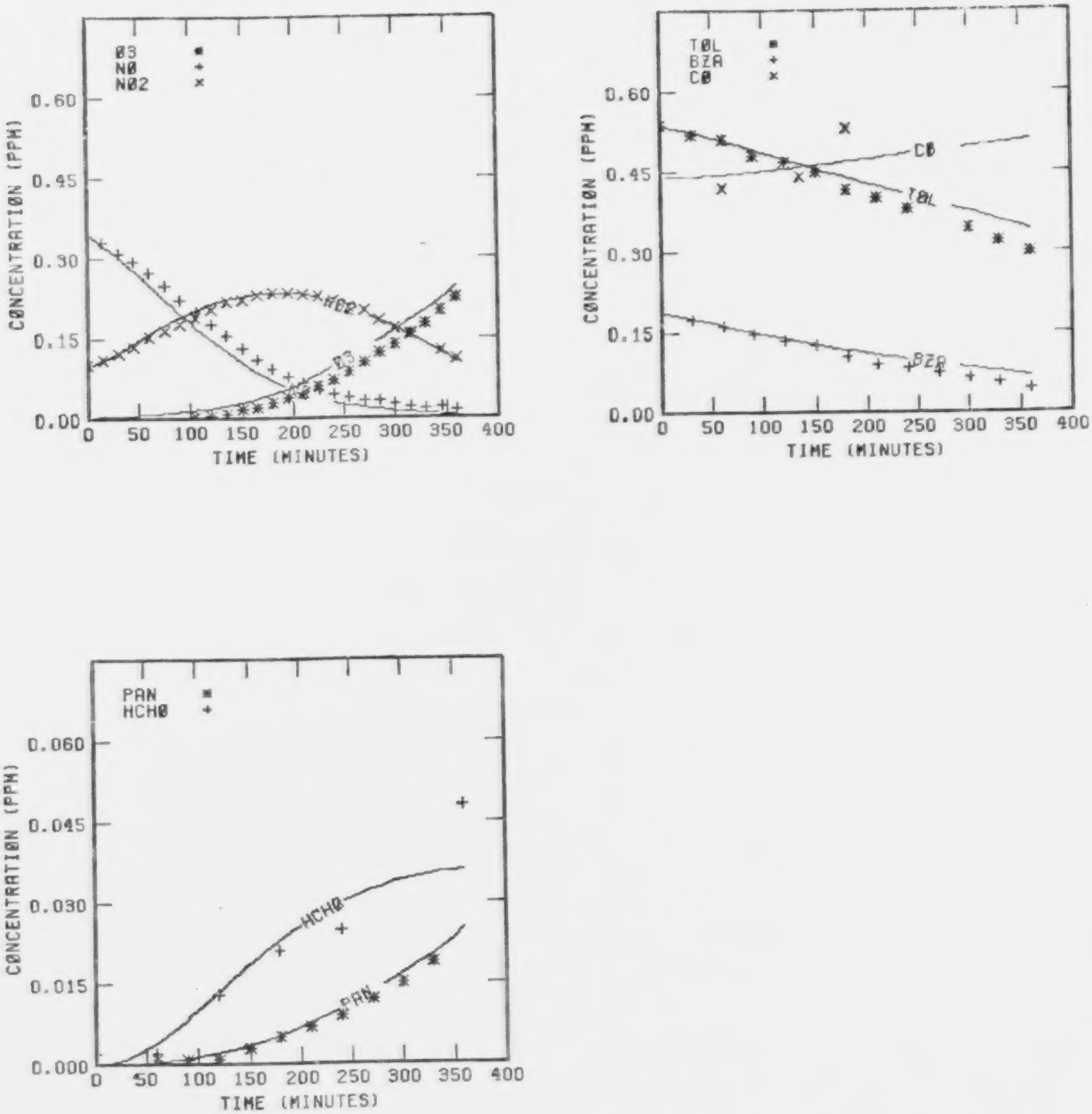

FIGURE 130. SIMULATION RESULTS FOR EC-339

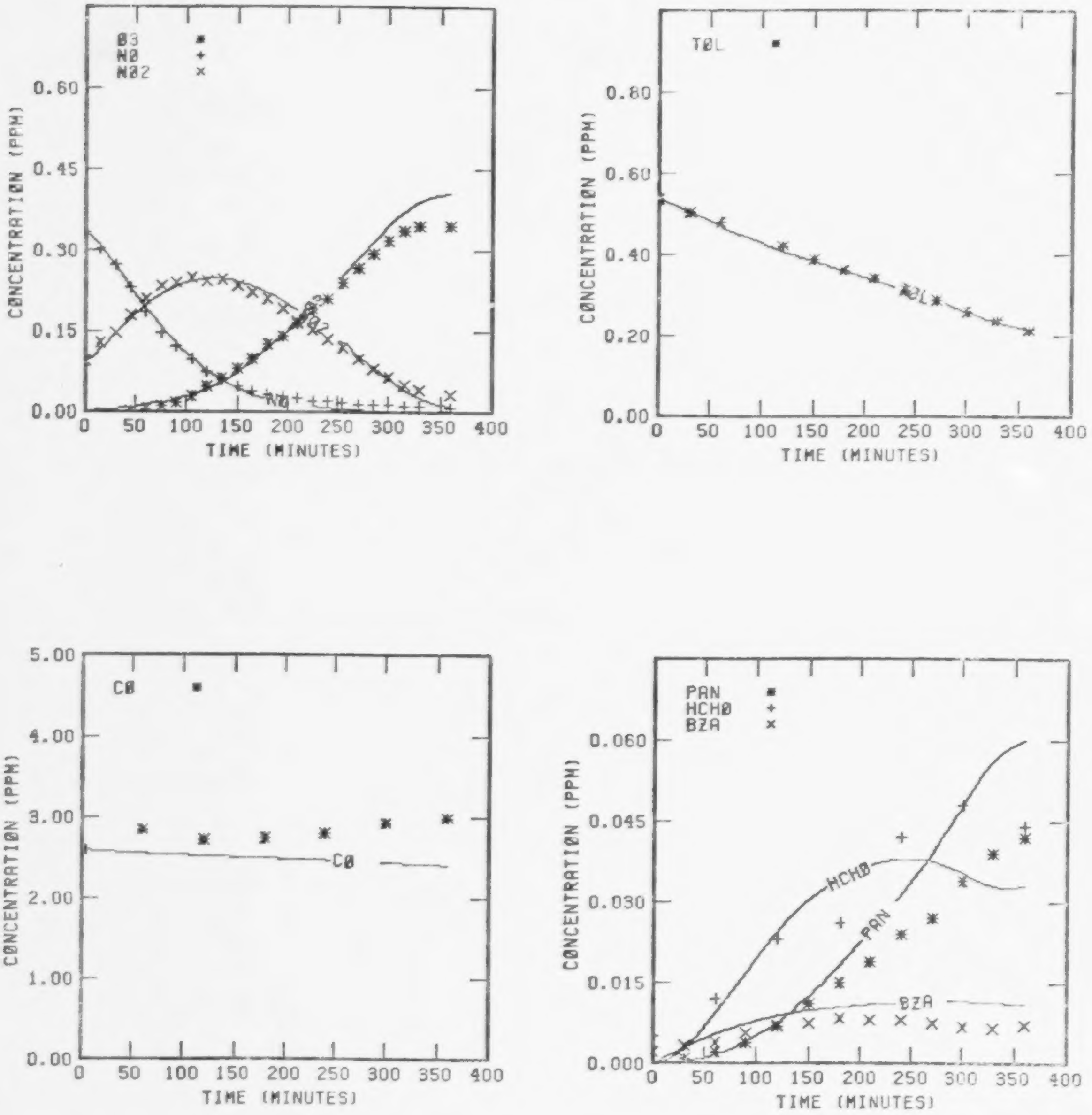

FIGURE 131. SIMULATION RESULTS FOR
EC-340

TABLE 33. UNC SIMULATION CONDITIONS*

Experiment	Initial conditions (ppm)							
	NO	NO_2	TOL	PAR	OLE	ETH	CO	R_x
UNCR 91878(a)	0.4	0.1	0.	0.	0.	1.5	0.32	0.04
UNCB 91878(a)	0.39	0.166	0.6	0.	0.	0.	0.32	0.06
UNCR 91878(b)	0.4	0.1	0.	0.	0.	1.5	0.32	0.01
UNCB 91878(b)	0.39	0.166	0.6	0.	0.	0.	0.32	0.01
UNCR 91478	0.234	0.058	0.319	0.	0.	0.	0.24	0.002
UNCB 91478	0.232	0.062	0.	0.	0.	0.48	0.21	0.007
UNCR 81678	0.		0.	0.51	0.51	0.	0.293	0.004
UNCB 81678	0.606	0.081	0.56	0.	0.	0.	0.293	0.004
UNCR 61379	0.367	0.085	0.	0.93	0.93	0.	--	0.
UNCB 61379	0.36	0.083	0.413	0.91	0.91	0.	--	0.

* Photolysis rates for NO_2 were calculated from TSR and UV data. The ratio of other photolysis to k_1 were methylglyoxal = 0.036; benzaldehyde = 2×10^{-3} formaldehyde to radicals = 2.7×10^{-3}; formaldehyde to stable products = 5.4×10^{-3}; acetaldehyde = 6×10^{-4}.

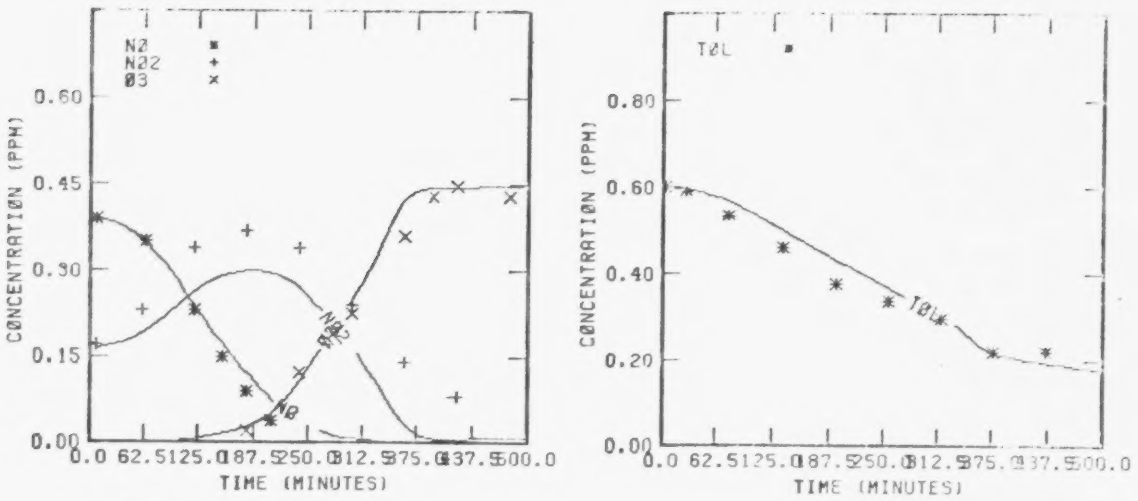

FIGURE 132. SIMULATION RESULTS FOR UNCB TOLUENE--9 18 78

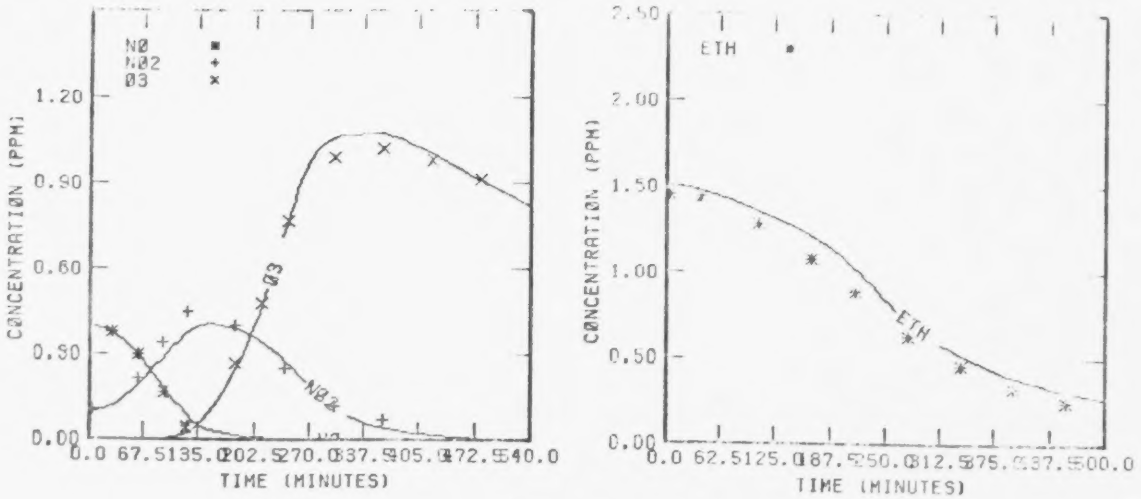

FIGURE 133. SIMULATION RESULTS FOR UNCR ETHYLENE--9 18 78

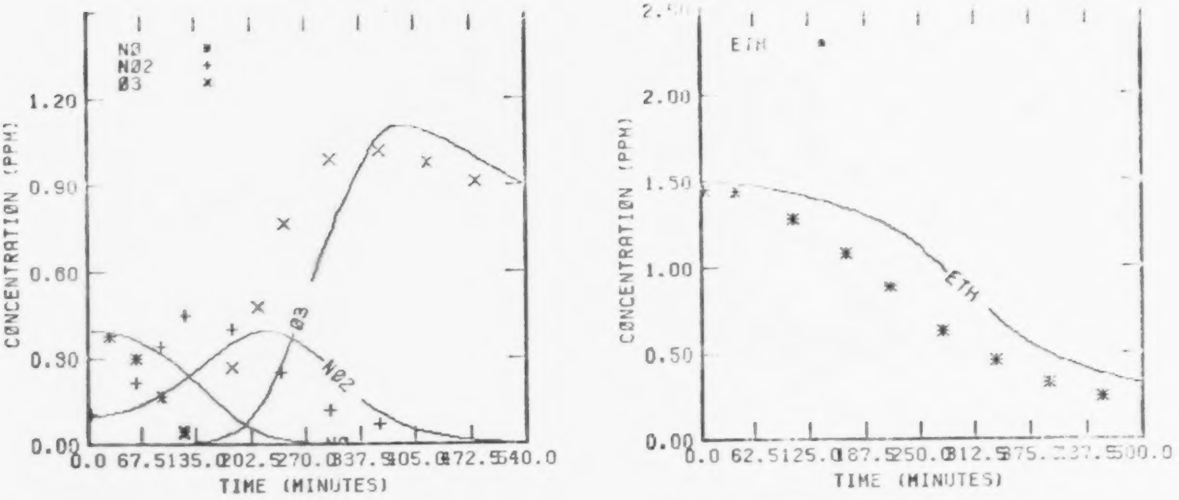

FIGURE 134. SIMULATION RESULTS FOR UNCR ETHYLENE--9 18 78

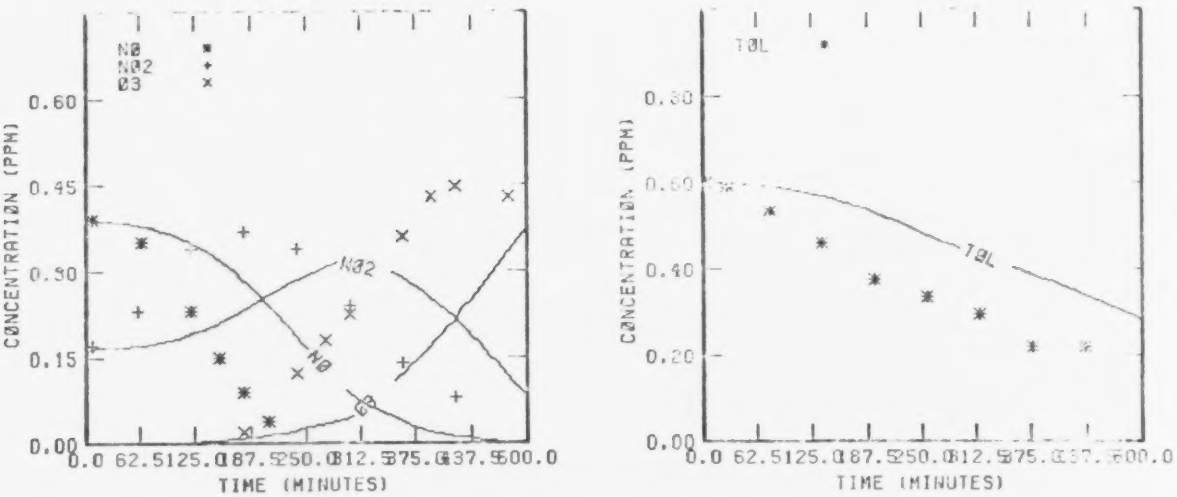

FIGURE 135. SIMULATION RESULTS FOR UNCB TOLUENE--9 18 78

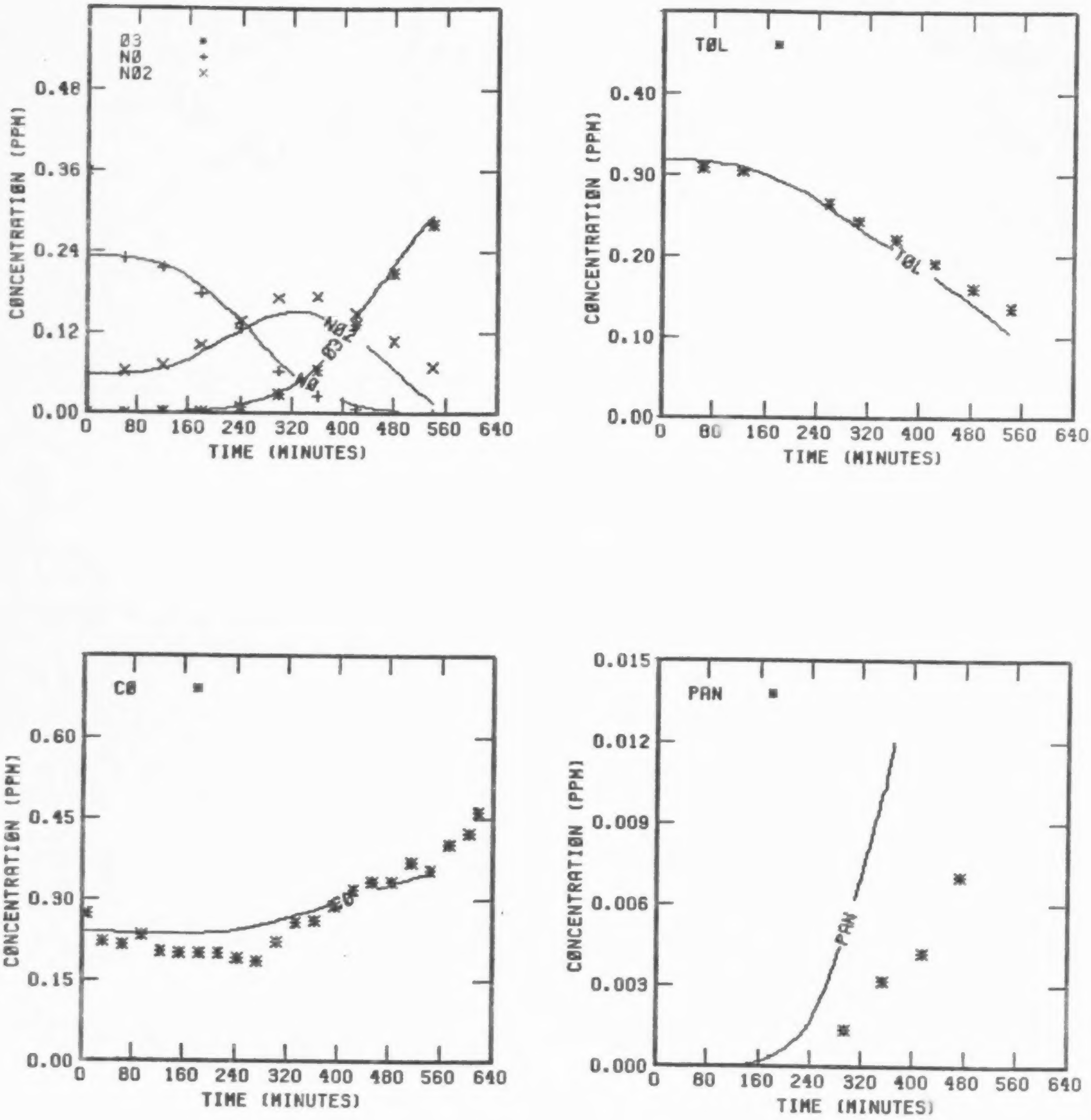

FIGURE 136. SIMULATIØN RESULTS FØR
UNCR 91478

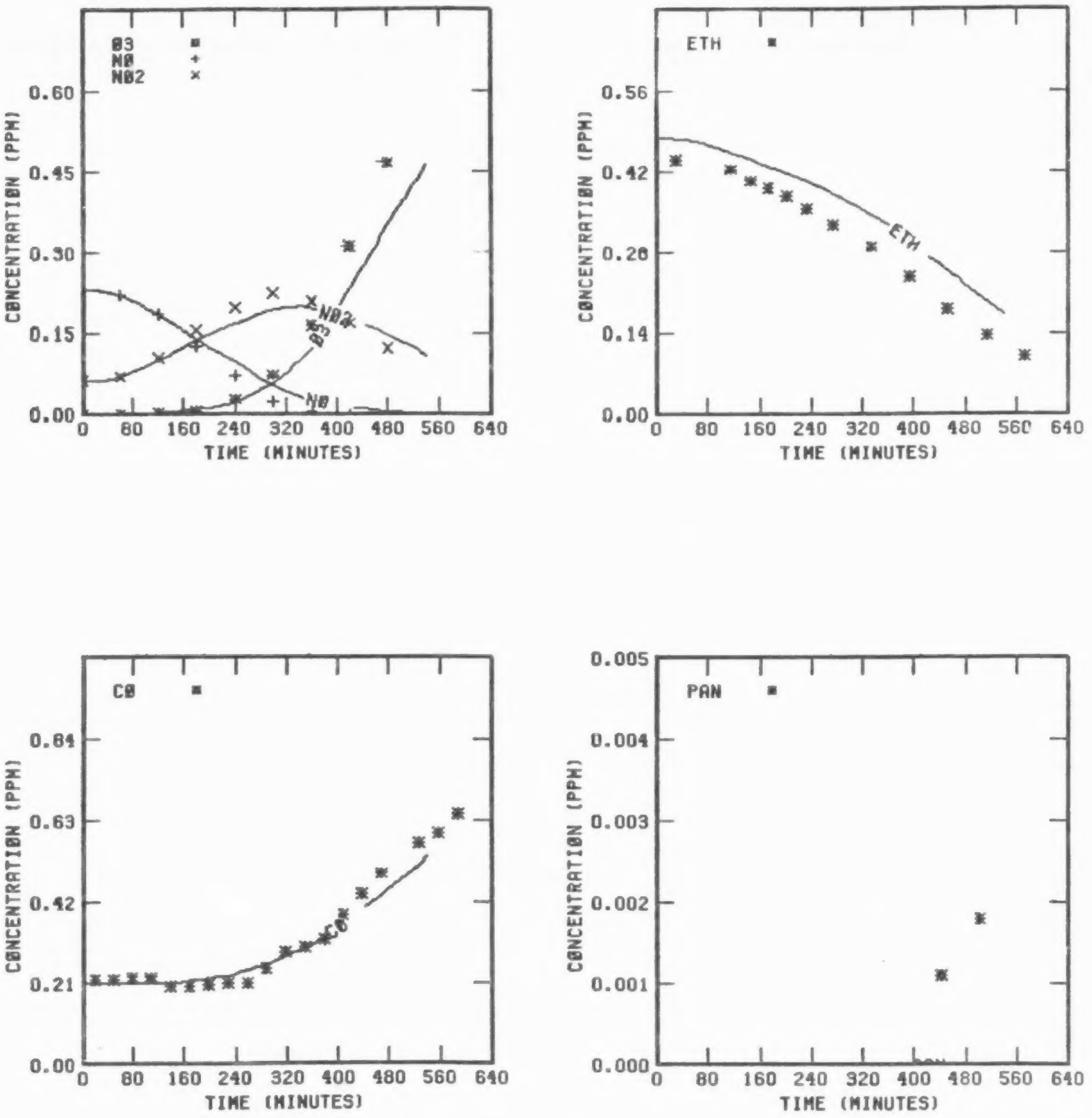

FIGURE 137. SIMULATIØN RESULTS FØR
UNCB 9147B

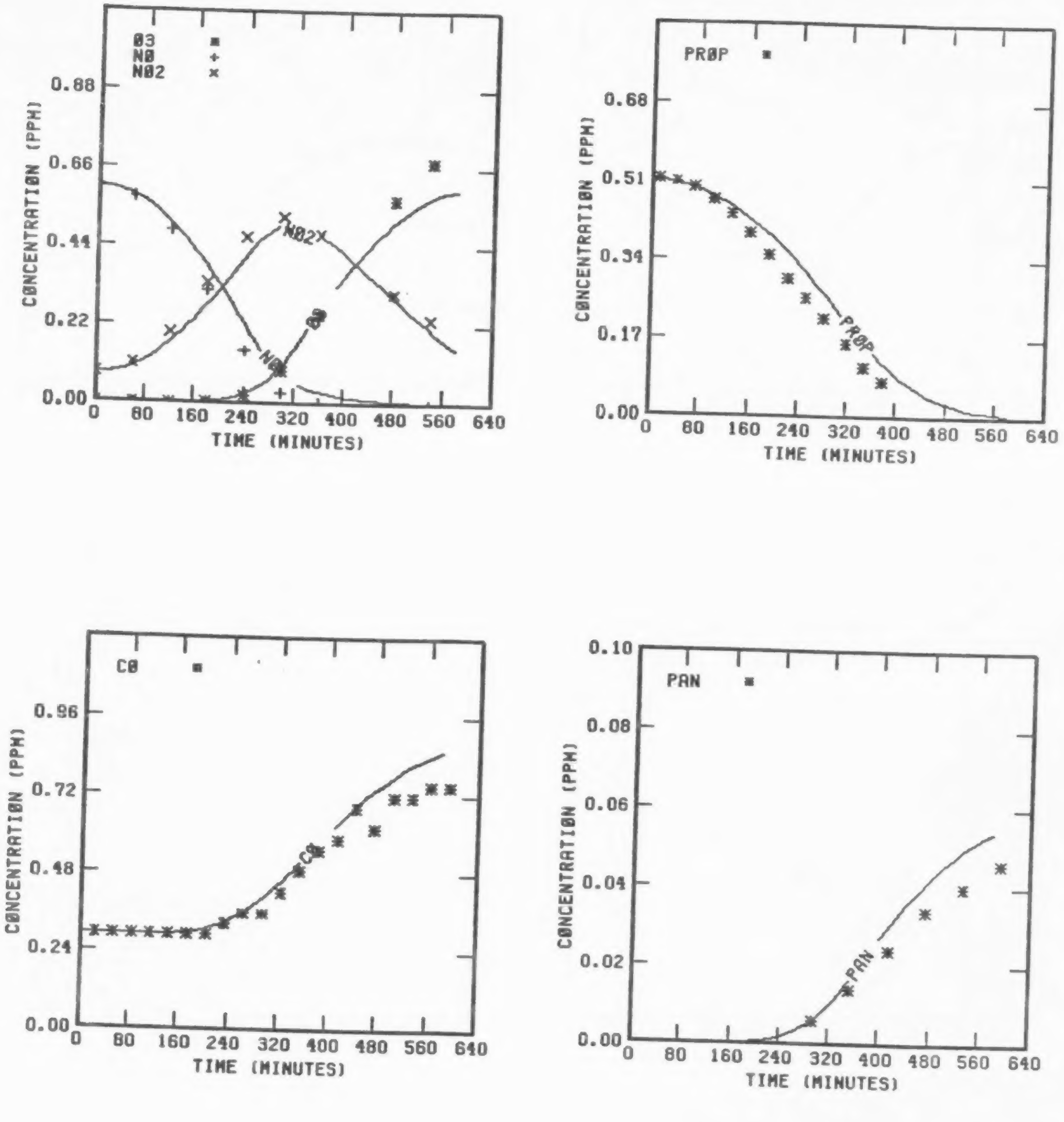

FIGURE 138. SIMULATION RESULTS FOR
UNCR 81678

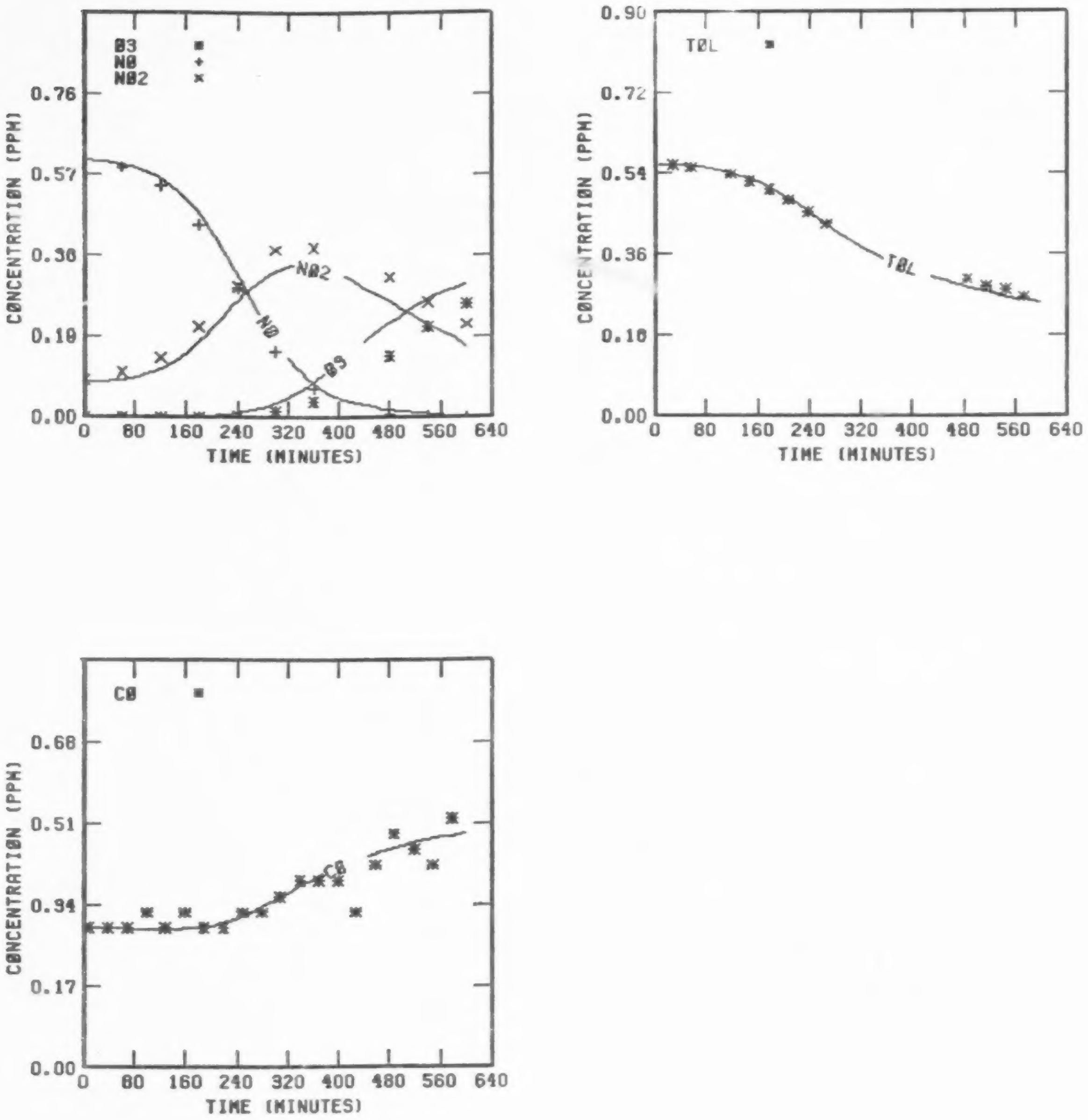

FIGURE 139. SIMULATIØN RESULTS FØR UNCB 81678

TABLE 34. THE CARBON-BOND MECHANISM

Reactions						Rate Constant	Activation energy
1	NO2		=	NO	0	*	-0.
2	0		=	03		4.400 E+06	-5.100E+02
3	03	NO	=	NO2		2.660E+01	1.450E+03
4	0	NO2	=	NO		1.340E+04	-0.
5	03	NO2	=	NO3		4.800E-02	2.450E+03
6	NO3	NO	=	NO2	NO2	2.800E+04	-0.
8	NO2	OH	=			1.400E+04	-0.
9	03	OH	=	HO2		1.000E+02	9.400E+02
10	03	HO2	=	OH		2.400E+00	5.800E+02
12	CO	OH	=	HO2		4.400E+02	-0.
13	HO2	NO	=	OH	NO2	1.200E+04	-0.
14	HO2	HO2	=			7.500E+03	-0.
15	NO	NO	=	NO2	NO2	1.500E-04	-0.
16	PAR	OH	=	MEO2		1.500E+03	-0.
17	PAR	0	=	MEO2	OH	2.000E+01	-0.

(Continued)

TABLE 34 (Continued)

Reactions								Rate Constant	Activation energy
25	ETH	OH	=	RBO2				1.200E+04	-0.
26	ETH	O	=	MEO2	HO2	CO		6.000E+02	-0.
27	ETH	O	=	HCHO				6.000E+02	-0.
28	ETH	O3	=	HCHO	CRIG			2.400E-03	-0.
30	HCHO	OH	=	HO2	CO	X	ACO3	9.500E+03	-0.
29	HCHO	OH	=					9.500E+03	-0.
31	HCHO		=	HO2	HO2	CO		*	-0.
60	HCHO		=	X	MEO2	HO2	CO	*	-0.
32	HCHO		=	CO				*	-0.
35	MEO2	NO	=	NO2	HCHO	HO2		7.300E+03	-0.
36	ACO3	NO	=	NO2	MEO2	CO2		3.800E+03	-0.
37	RBO2	NO	=	NO2	HCHO	HCHO	HO2	1.200E+04	-0.
34	MEO2	NO	=	NO2	HCHO	MEO2	X	3.700E+03	-0.
38	RBO2	O3	=	HCHO	HCHO	HO2		5.000E+00	-0.
19	OLE	OH	=	RAO2				4.200E+04	-0.

(Continued)

TABLE 34 (Continued)

Reactions								Rate Constant	Activation energy
20	OLE	0	=	AC03	ME02	X		1.400E+03	-0.
21	OLE	0	=	HCHO				4.000E+03	-0.
23	OLE	03	=	HCHO	CRIG			8.000E-03	-0.
24	OLE	03	=	HCHO	MCRG			8.000E-03	-0.
39	RA02	NO	=	N02	HCHO	HCHO	H02	1.200E+04	-0.
40	RA02	03	=	HCHO	HCHO	H02		2.000E+04	-0.
48	MCRG	NO	=	N02	HCHO			1.200E+04	-0.
49	MCRG	N02	=	N03	HCHO			8.000E+03	-0.
50	MCRG	HCHO	=	OZD				2.000E+03	-0.
51	MCRG		=					1.500E+02	-0.
52	MCRG		=	X	ME02	CO	OH	3.400E+02	-0.
53	MCRG		=	X	ME02	H02		4.250E+02	-0.
54	MCRG		=	H02	HCHO	H02	X	8.500	-0.
41	X	PAR	=					1.000E+05	-0.
42	CRIG	NO	=	N02	HCHO			1.200E+04	-0.

(Continued)

TABLE 34 (Continued)

Reactions							Rate Constant	Activation energy
43	CRIG	NO2	=	NO3	HCHO		8.000E+03	-0.
44	CRIG	HCHO	=	OZD			2.000E+03	-0.
45	CRIG		=	CO			6.700E+02	-0.
46	CRIG		=				2.400E+02	-0.
47	CRIG		=	HO2	HO2	CO	9.000E+01	-0.
55	MEO2	NO	=	NRAT			5.000E+02	-0.
56	MEO2	O3	=	HCHO	HO2		5.000E+00	-0.
57	ACO3	HO2	=				4.000E+03	-0.
58	MEO2	HO2	=				4.000E+03	-0.
61	ACO3	NO2	=	PAN			2.000E+03	-0.
62	PAN		=	ACO3	NO2		2.800E-02	1.250E+04
63	H2O		=				-4.200E-04	-0.

* Experimental.

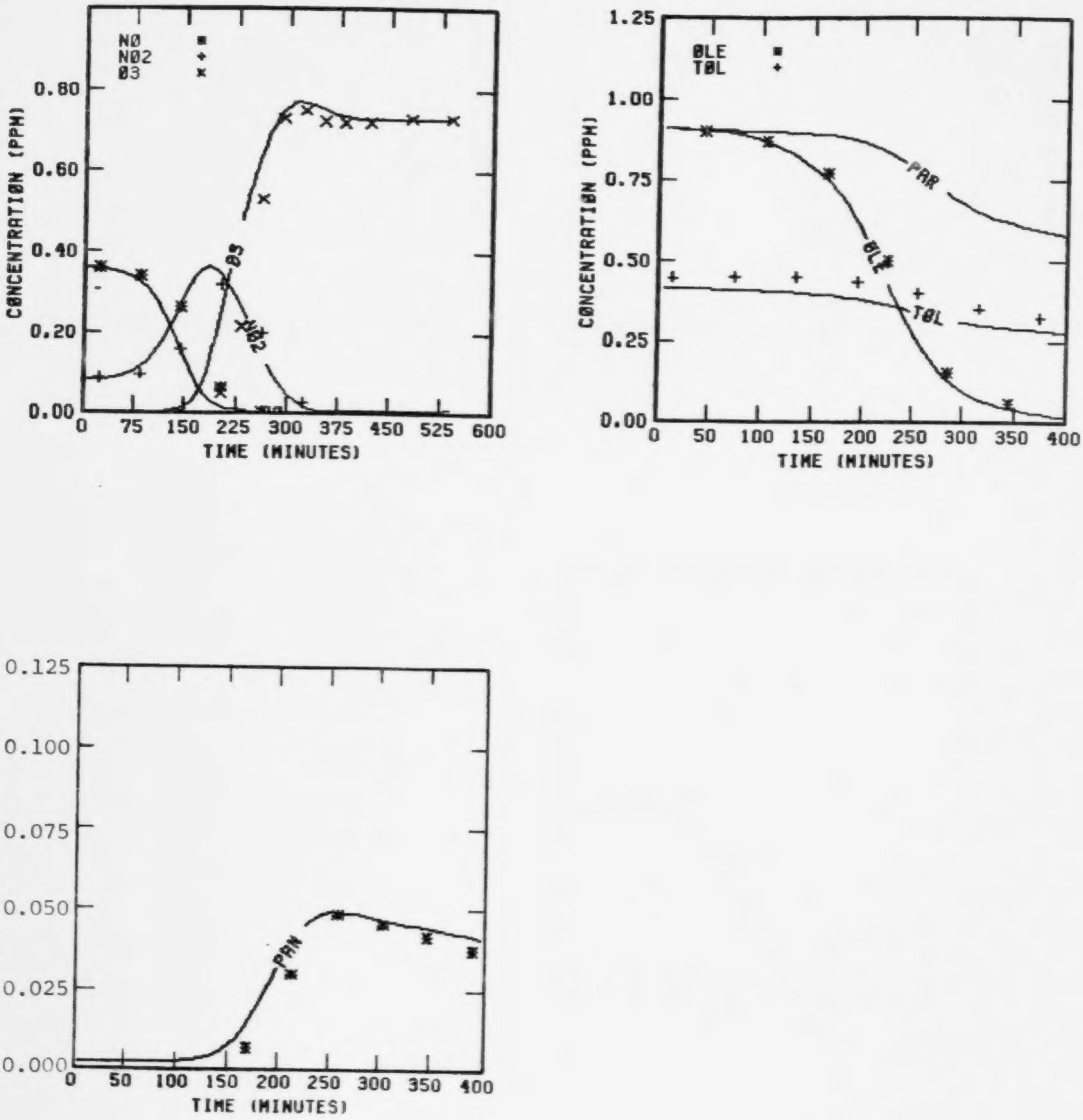

FIGURE 140. SIMULATION RESULTS FOR UNCB TOL-PRO--6 21 79

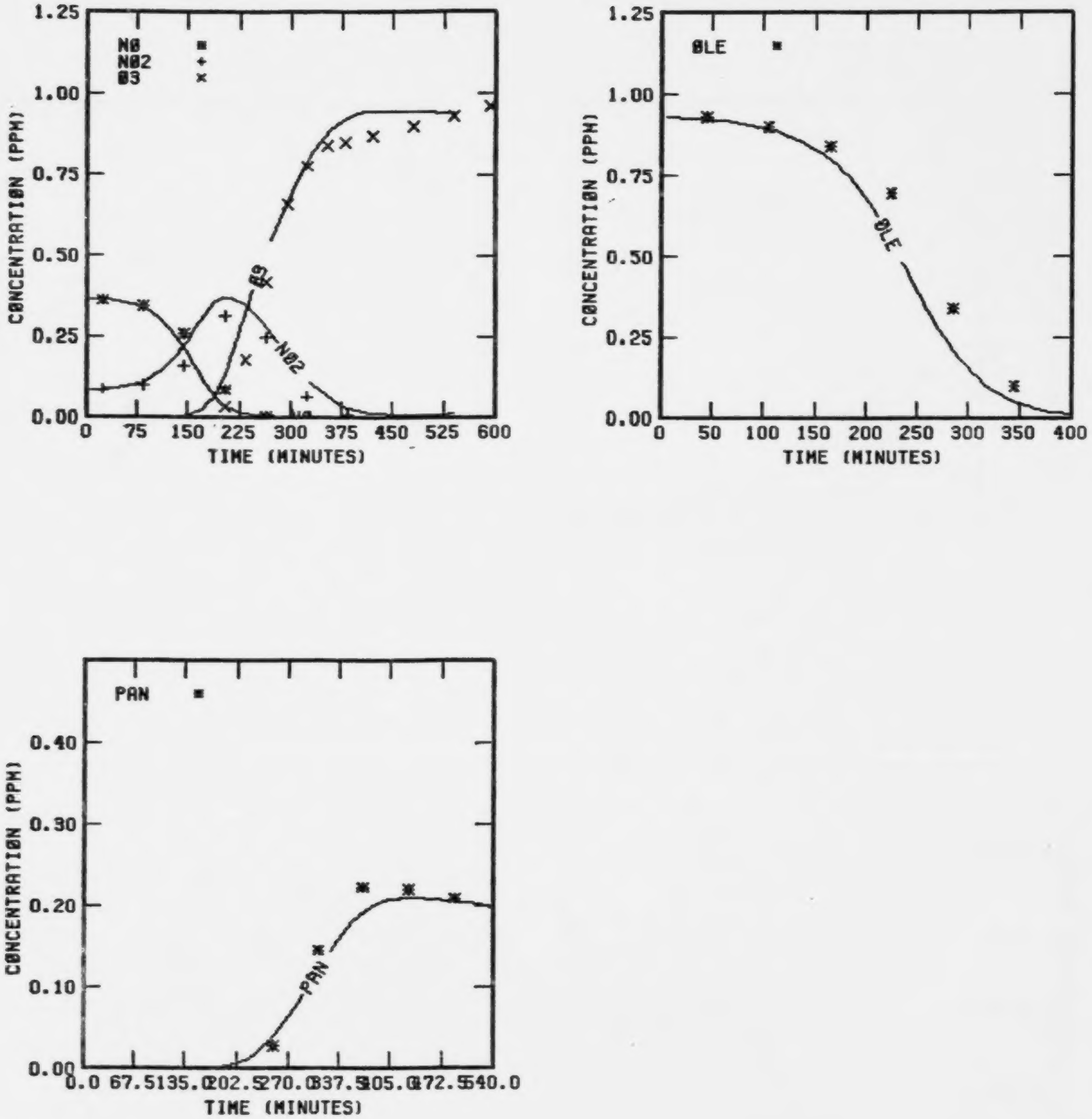

FIGURE 141. SIMULATION RESULTS FOR
UNCR PROPENE
6 21 79

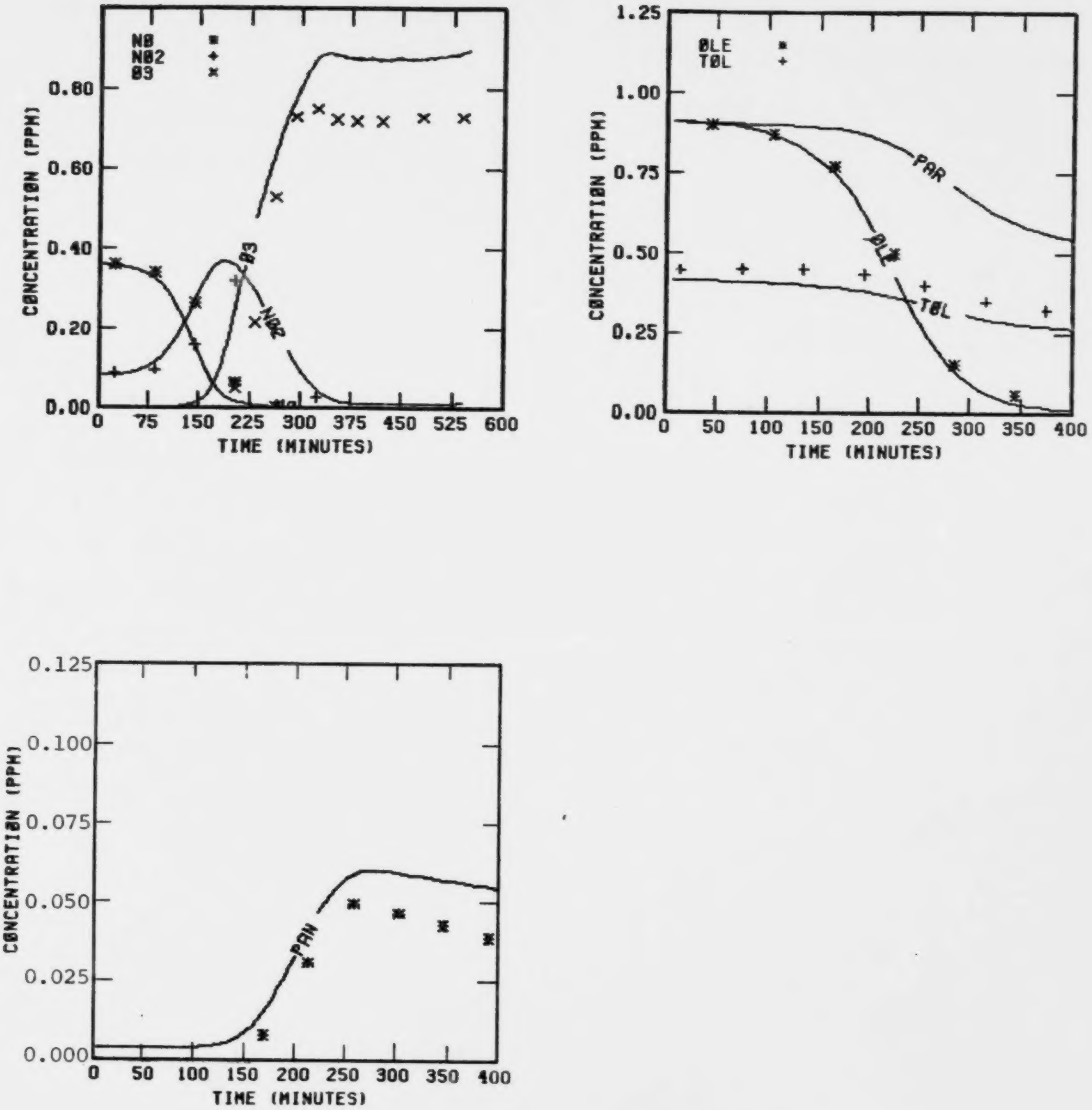

FIGURE 142. SIMULATION RESULTS FOR UNCB TOL-PRO--6 21 79 WITHOUT NO_3 LOSS (REACTIONS 76 AND 90 ELIMINATED)

The toluene-propylene system has a greater photolysis rate and, hence, a lower Q than a propylene-only system. In NO_x-limited circumstances, the ozone peak is lower.

SECTION 6

CARBON-BOND CHEMISTRY

The developments in explicit chemistry, reported in earlier sections, have not been integrated into the Carbon-Bond Mechanism (CBM) because these developments came late in the contract year. Since insufficient time precluded the use of the extensive comparisons with explicit chemistry (as presented in Whitten and Hogo, 1977; Whitten et al., 1979), this section presents only a few simulations with the CBM. Since the report last year, the principal change in the CBM has been a further improvement in the chemistry of aromatics based on the mechanism for toluene described in Section 5 of this report. This section presents a brief review of the differences between the original CBM and its current formulation, CBM-II, along with some simulation results using both versions. A compendium of isopleth diagrams is included to demonstrate the behavior of several species that occur in atmospheric chemistry as a function of the HC and NO_x precursor levels.

COMPARISON OF OLD AND NEW MECHANISMS

The original formulation of the CBM was published in two documents (Whitten and Hogo, 1977; Whitten, Hogo, and Killus, 1979). Table 35 presents the version of the old CBM used in the present study. The interim report of last year (Whitten et al., 1979) presents an extensively revised version of the CBM (CBM-II). Shortly after publication of that report some minor improvements were added to the aromatics chemistry, bringing the mechanism to the level shown in Table 36. Both versions of the CBM have been used in several atmospheric studies. The present comparison study suggests that either version appears to reproduce smog chamber experiments, though the newer version is more scientifically relevant; the atmospheric studies previously performed using the old CBM are probably still valid from the standpoint of the chemistry.

TABLE 35. THE ORIGINAL FORMULATION OF THE CARBON-BOND MECHANISM

Reaction	Rate constant[*] (ppm^{-1} min^{-1})
$NO_2 + h\nu \rightarrow NO + O\cdot$	3×10^{-1}[†]
$O\cdot + O_2 (+ M) \rightarrow O_3 (+ M)$	2.08×10^{-5}
$O_3 + NO \rightarrow NO_2 + O_2$	25.2
$O\cdot + NO_2 \rightarrow NO + O_2$	1.34×10^4
$O_3 + NO_2 \rightarrow NO_3 + O_2$	5×10^{-2}
$NO_3 + NO \rightarrow NO_2 + NO_2$	1.3×10^4
$NO_3 + NO_2 + H_2O \rightarrow 2HNO_3$	1.66×10^{-3}[§]
$NO + NO_2 + H_2O \rightarrow 2HNO_2$	2.2×10^{-9}[§]
$HNO_2 + h\nu \rightarrow NO + OH$	3×10^{-2}[†]
$NO_2 + OH\cdot \rightarrow HNO_3$	9×10^3
$NO + OH\cdot \rightarrow HNO_2$	9×10^3
$CO + OH\cdot \rightarrow CO_2 + HO_2$	2.06×10^2
$OLE + OH\cdot \xrightarrow{O_2} HCHO + CH_3O_2$	3.8×10^4
$PAR + OH\cdot \xrightarrow{O_2} CH_3O_2 + H_2O$	1.3×10^3
$ARO + OH\cdot \xrightarrow{O_2} HCHO + CH_3O_2$	8×10^3
$OLE + O\cdot \xrightarrow{2O_2} HC(O)O_2\cdot + CH_3O_2$	5.3×10^3
$PAR + O\cdot \xrightarrow{O_2} CH_3O_2^{\cdot} + OH\cdot$	20
$ARO + O\cdot \xrightarrow{2O_2} HC(O)O_2 + CH_3O_2$	37
$OLE + O_3 \xrightarrow{O_2} HC(O)O_2 + HCHO + OH\cdot$	0.01

(continued)

TABLE 35 (Concluded)

Reaction	Rate constant (ppm^{-1} min^{-1})
$ARO + O_3 \xrightarrow{O_2} HC(O)O_2 + HCHO + OH\cdot$	0.002
$OLE + O_3 \rightarrow$ ozonide	0.005
$HCHO + h\nu \xrightarrow{2O_2} HC(O)O_2 + HO_2$	4×10^{-4}†
$HCHO + h\nu \rightarrow CO + H_2$	4×10^{-4}†
$HCHO + OH\cdot \xrightarrow{O_2} HC(O)O_2 + H_2O$	1×10^4
$HO_2 + NO \rightarrow OH\cdot + NO_2$	2×10^3
$CH_3O_2 + NO \rightarrow NO_2 + HCHO + HO_2$	2×10^3
$HC(O)O_2 + NO \rightarrow NO_2 + CO_2 + HO_2$	2×10^3
$H_2O_2 + h\nu \rightarrow OH\cdot + OH\cdot$	6.6×10^{-4}†
$HO_2 + HO_2 \rightarrow H_2O_2 + O_2$	4×10^3
$CH_3O_2 + HO_2 \rightarrow H_3COOH + O_2$	4×10^3
$HC(O)O_2^{\cdot} + HO_2 \rightarrow HC(O)OOH + O_2$	1×10^4
$HC(O)O_2 + NO_2 \rightarrow PAN$	50
$PAN \rightarrow HC(O)O_2^{\cdot} + NO_2$	0.02†
$ARO + NO_3 \rightarrow$ Products	1.1
$HO_2 + NO_2 \rightarrow HNO_2$	20.

---

* Rate/constants are modified for the computer simulations of UCR smog chamber experiments.

† Units of min^{-1}.

§ Units of $ppm^{-2}min^{-1}$.

TABLE 36. THE NEW CARBON-BOND MECHANISM (CBM-II)

Reaction	Rate constant at 298K* ($ppm^{-1} min^{-1}$)	Activation energy (K)
$NO_2 + h\nu \rightarrow NO + O$	Experimental**	--
$O + O_2 + M \rightarrow O_3 + M$	2.1×10^{-5}†	--
$O_3 + NO \rightarrow NO_2 + O_2$	23.9	1,450
$O_3 + NO_2 \rightarrow NO_3 + O_2$	4.8×10^{-2}	2,450
$O + NO_2 \rightarrow NO + O_2$	1.34×10^{4}	--
$O_3 + OH \rightarrow HO_2 + O_2$	7.7×10^{1}	1,000
$O_3 + HO_2 \rightarrow OH + 2O_2$	5.0	1,525
$NO_2 + OH \rightarrow HNO_3$	1.4×10^{4}	--
$CO + OH \xrightarrow{O_2} HO_2 + CO_2$	4.4×10^{2}	--
$NO + NO + O_2 \rightarrow 2NO_2$	7.1×10^{-10}†	--
$NO_3 + NO \rightarrow 2NO_2$	2.8×10^{4}	--
$NO_3 + NO_2 + H_2O \rightarrow 2HNO_3$	$311 \times k(N_2O_5 + H_2O)$***	-10,600
$HO_2 + NO \rightarrow NO_2 + OH$	1.2×10^{4}	--
$HO_2 + HO_2 \rightarrow$	1.5×10^{4}	--
$PAR + O \rightarrow MEO_2 + OH$	2×10^{1}	--
$PAR + OH \rightarrow MEO_2$	1.5×10^{3}	--
$OLE + O \rightarrow MEO_2 + ACO_3 + X$	2.7×10^{3}	--
$OLE + O \rightarrow CARB$	2.7×10^{3}	--
$OLE + OH \rightarrow RAO_2$	4.2×10^{4}	--
$OLE + O_3 \rightarrow CARB + CRIG$	8×10^{-3}	--
$OLE + O_3 \rightarrow CARB + MCRG$	8×10^{-3}	--
$ETH + O \rightarrow MEO_2 + HO_2 + CO$	6×10^{2}	--
$ETH + O \rightarrow CARB$	6×10^{2}	--

TABLE 36 (Continued)

Reaction	Rate constant at 298K ($ppm^{-1} min^{-1}$)	Activation energy (K)
$ETH + OH \rightarrow RBO_2$	1.2×10^4	--
$ETH + O_3 \rightarrow CARB + CRIG$	2.4×10^{-3}	
$ACO_3 + NO \rightarrow NO_2 + MEO_2 + CO_2$	3.8×10^3	--
$RBO_2 + NO \rightarrow NO_2 + 2\ CARB + HO_2$	1.2×10^4	--
$RAO_2 + NO \rightarrow NO_2 + 2\ CARB + HO_2$	1.2×10^4	--
$MEO_2 + NO \rightarrow NO_2 + CARB + MEO_2 + X$	$(1.2 \times 10^4)(A-1)/A^{**}$	--
$MEO_2 + NO \rightarrow NO_2 + CARB + HO_2$	$(1.2 \times 10^4)/A^{**}$	--
$MEO_2 + NO \rightarrow$ Nitrate	5×10^2	--
$RBO_2 + O_3 \rightarrow 2\ CARB + HO_2$	5.0	--
$RAO_2 + O_3 \rightarrow 2\ CARB + HO_2$	2×10^2	--
$MEO_2 + O_3 \rightarrow CARB + HO_2$	5.0	--
$CARB + OH \rightarrow \alpha(HO_2 + CO) + (1 - \alpha)(ACO_3 + X)$	$(2.4 - \alpha) \times 10^4$	--
$CARB + h\nu \rightarrow CO$	$\alpha k_f^{*\dagger\dagger}$	--
$CARB + h\nu \rightarrow (1 + \alpha)HO_2 + (1 - \alpha)(MEO_2 + X) + CO$	$\left(\frac{\alpha + 1}{2}\right)k_f^{*\dagger\dagger}$	--
$X + PAR \rightarrow$	1×10^5	--
$ACO_3 + NO_2 \rightarrow PAN$	2×10^3	--
$PAN \rightarrow ACO_3 + NO_2$	$2.8 \times 10^{-2\dagger}$	12,500
$ACO_3 + HO_2 \rightarrow$	4×10^3	--
$MEO_2 + HO_2 \rightarrow$	4×10^3	--
$CRIG + NO \rightarrow NO_2 + CARB$	1.2×10^4	--
$CRIG + NO_2 \rightarrow NO_3 + CARB$	8×10^3	--
$CRIG + CARB \rightarrow$ Ozonide	2×10^3	--
$MCRG + NO \rightarrow NO_2 + CARB$	1.2×10^4	--
$MCRG + NO_2 \rightarrow NO_3 + CARB$	8×10^3	--

TABLE 36 (Concluded)

MCRG + CARB → Ozonide	2×10^3	--
CRIG → CO	6.7×10^{2}†	--
CRIG → Stable Products	2.4×10^{2}†	--
CRIG → $2HO_2 + CO_2$	9×10^{1}†	--
MCRG → Stable Products	1.5×10^{2}†	--
MCRG → MEO_2 + OH + CO	3.4×10^{2}†	--
MCRG → $MEO_2 + HO_2 + CO_2$	4.25×10^{2}†	--
MCRG → CARB + $2HO_2$ + CO	8.5×10^{1}†	--
ARO + OH → ARPI + ARPI + ARPI + HO_2	6×10^3	--
ARO + OH → HO_2 + GLY + X	1.6×10^3	--
ARO + OH → OH + GLY + W	1.5×10^4	--
W + CARB →	1.0×10^5	--
ARPI + NO → NO + CARB + PAR	30	--
ARPI + NO → NO_2 + AEROSOL	15	--
ARPI + NO_3 → CARB + CARB	3.5×10^4	--
ARPI + O_3 → Aerosol	0.6	--
GLY + OH → HO_2 + ARPI + ARPI + ARPI + CO	10^4	--
GLY → $MeO_2 + HO_2$ + ARPI + ARPI + ARPI	K_{GLY}§§	--

---

* The rate constants shown are as used to model eleven experiments at UCR that used mixes of seven hydrocarbons. For that study the default values, $\alpha = 0.5$ and $A = 1.3$, were used.

† Units of min^{-1}.

§ Units of $ppm^{-2}min^{-1}$.

** A = A is the average number of $RO_2^{\cdot}$-type radicals generated from a hydrocarbon between attack by OH· and generation of $HO_2^{\cdot}$

†† α is the fraction of total aldehydes that represents formaldehyde and ketones. k_f is the carbonyl photolysis rate constant.

§§ $K_{GLY} = 0.036 \times k_{(HO_2 + h\nu)}$

*** $k_{(N_2O_5 + H_2O)} = 5 \times 10^{-6}\ ppm^{-1}min^{-1}$ for UCR simulations.

The main features that distinguish the two versions of the CBM are briefly explained in the following discussion.

- Aromatics Chemistry. Approximately one year ago, a semi-empirical aromatics mechanism was constructed to simulate the hydrocarbon decay, NO-to-NO_2 conversion, NO_x decay to nitrates, PAN formation, and ozone formation seen in a series of smog chamber experiments involving either nitrogen oxides and pure aromatics or NO_x and mixtures of hydrocarbons containing aromatics. This mechanism has been incorporated into the SAI Airshed Model.

  During the past year, we have been studying the fundamental chemistry involving aromatics that has emerged from recent laboratory kinetics studies. The CBM-II mechanism in Table 36 reflects our present thinking on the fundamental chemistry of aromatics, yet is still compatible with the SAI Airshed Mechanism, requiring only a modification of rate constants and a relabeling of the aromatic photolytic species as GLY (glyoxals). Approximately 73% of the oxidation pathway leads to glyoxal photolysis in both the CBM-II mechanism and the toluene developmental mechanism. Cresol and benzaldehyde are neglected as unimportant in the CBM-II mechanism. The overall rate constant for OH oxidation of aromatics is taken to be an average of toluene and xylenes. The aromatics mechanism in the CBM may be said to have evolved to the state of being primarily a condensed mechanism of known fundamental chemistry.

- PAN Chemistry. In the old CBM, the peroxyformyl radical ($HCO_3^{\cdot}$) was used to generate PAN formation via reaction with NO_2 using an empirical rate constant. In the CBM-II, the $HCO_3^{\cdot}$ has been eliminated, and a new species representing peroxyacyl radicals ($ACO_3^{\cdot}$) is now used. $ACO_3^{\cdot}$ is formed from the hydroxyl radical ($OH^{\cdot}$) attack on carbonyl compounds (surrogate CARB). The amount of ACO$_3^\cdot$ formation is proportional to 1-α, which represents the higher aldehydes. Hence, PAN chemistry itself uses no empirical rate constants. Furthermore, the use of α in the new CBM has been carefully conceived to ensure that ozone production is rather insensitive, yet PAN production is sensitive, to the choice of α. In the old CBM and in other mechanisms such as the well-known Hecht, Seinfeld, and Dodge (HSD) mechanism, the parameter that governs PAN formation significantly affects ozone production--if too much PAN is simulated by the mechanism, then O_3 will be low and vice versa. CBM-II eliminates this problem. A poor choice for α should only produce incorrect PAN simulations.

- Organic Nitrates. The CBM-II incorporates recent discoveries concerning the formation of these compounds. Darnell et al. (1976) have found that RO_2-type radicals having large R groups can form organic nitrates via reaction with NO. The aromatics chemistry also leads to nitrate formation. Unfortunately, at present,the rate constant for RO_2 plus NO leading to nitrate is empirically adjusted to provide proper organic nitrate levels in the UCR smog chamber experiments used to validate the new mechanism. Until smog chamber data are available for a large variety of individual compounds and a variety of mixtures, this rate constant cannot be determined from the reactivity of the hydrocarbon mix.

- Large Paraffin Chemistry. Carter et al. (1976) have shown that a cyclic intermediate could allow large RO radicals to isomerize in air to $HORO_2$ radicals. The explicit mechanisms for butane and 2,3-dimethylbutane show that, subsequent to attack by hydroxyl radicals, on the average, more than one RO_2 intermediate form prior to the production of an $HO_2^\cdot$ radical. The cyclic isomerization reaction accounts for some of this effect, and decomposition reactions for large RO radicals account for the rest. In CBM-II, this complex chemistry is treated through a parameter, A, which is determined from the average number of RO_2 intermediates between hydroxyl attack on paraffins and generation of HO_2, which occurs in explicit mechanisms via the O_2 abstraction of RO intermediates.

- Ozone Olefin Chemistry. CBM-II treats the diradical intermediates that, according to recent studies conducted by NBS, Ford, and EPA, are formed during these reactions. Although these intermediates--sometimes referred to as Criegee intermediates--are known to react unimolecularly or in combination with NO, NO_2, aldehydes, and SO_2, the relative rates between these various possibilities are not yet known.

- Activation of Single Bonds. CBM-II accounts for the formation of RO_2 radicals from the chemistry of carbonyl compounds other than formaldehyde. In order to maintain carbon mass balance, a special species, x, is used that removes a carbon group from the single bonded surrogate, PAR, whenever an extra carbon group is generated. For example, if the surrogate carbonyl species were to represent pure acetaldehyde ($\alpha = 0$), hydroxyl attack would produce $ACO_3^{\cdot}$. However, the surrogate, $ACO_3^{\cdot}$, in the new CBM has two carbon atoms and the precursor, CARB, has but one carbon atom, so an x is formed along with $ACO_3^{\cdot}$. Then, a fast reaction in the CBM-II between PAR and x immediately removes one PAR from the system, thereby accounting for the extra carbon generated in the $ACO_3^{\cdot}$ radical.

- Elimination of HONO. As shown in Whitten et al. (1979), this compound is rapidly photolyzed and re-formed in a "do nothing" cycle in the atmosphere. These reactions lead to an average steady-state value that is very small. Modeling studies at SAI have confirmed that the elimination of this species leads to trivial differences in computer smog simulations.

> Explicit Treatment of the Olefin Hydroxyl Addition Product. The explicit chemistry of hydroxyl attack on olefins leads to the formation of two aldehydes from the initial addition product, which in air is a $HORO_2$ radical. The old CBM treated this radical as a typical RO_2 radical that produces but one aldehyde; the extra aldehyde was added along with the RO_2 as a product in the initial OH reaction. However, the present version of the CBM-II includes a special reaction of the $HORO_2$ addition product with O_3. Hence, the explicit treatment allows the formation of two aldehydes from the $HORO_2$ or reaction with O_3. The O_3 reaction is still under investigation, and future versions of the CBM may not require this reaction.

In addition to these changes, the use of carbon bond chemistry has been improved and can be applied to either version of the CBM. In one study it was found that the concentration-weighted root-mean-square method of averaging the hydrocarbon rate constants produced the best overall performance of the CBM in a series of simulations of smog chamber experiments using mixtures of hydrocarbons. A related study showed that internal olefins could be simulated as two carbonyls per double bond. Thus, the CBM can treat three levels of reactivity for olefins: Ethylene is treated as a separate species, terminal olefins are treated by the surrogate double-bond species OLE, and the highly reactive internal olefins are treated as two CARBs per olefin bond.

Performance of the CBM-II should not differ significantly from the old CBM, according to the tests on several smog chamber experiments reported below. However, the new mechanism incorporates an extensive range of recent information on smog chemistry. One notable difference has been a prediction, using the new chemistry, that the addition of aromatics to a mixture of olefins and paraffins at high hydrocarbon-to-NO_x ratios would suppress ozone formation. A recent experiment at the outdoor chamber at UNC has confirmed this prediction as shown in Section 5.

To represent the performance of both the old and new versions of the CBM, we have included two sets of results from simulations of 11 smog chamber experiments. Figures 143 through 164 compare the observed data with the computed simulations for each version of the CBM. Tables 37, 38, and 39 present the initial conditions.

Ozone formation is determined by the conversion of NO to NO_2, which in turn is determined from the decay of the hydrocarbons. The decay rate of the hydrocarbons is primarily a function of the hydroxyl radical level that is, in turn, determined by a balance between radical sources and sinks. The sink reactions in the old CBM are not controllable, but the organic nitrate formation from RO_2 and NO in the CBM-II should be adjusted within a factor of 2 from the default value of 500 ppm if nitrate data are available. The major adjustments in these simulations were of the carbonyl photolysis rate, but these adjustments were within the range of uncertainty of the artificial light source used.

Before judging the ozone performance of any mechanism, the hydrocarbon decay and NO_x conversion and loss rates should be correctly simulated. The basic function of a properly assembled mechanism is then the correct maintenance of radicals in generating ozone and nitrates.

Table 40 presents statistical evidence, based on the mechanisms of Tables 35 and 36, demonstrating the ability of both versions of the CBM to simulate ozone. Bias for both versions is slightly high, as indicated by the positive mean errors. CBM-II shows only +3 ppb, or +2.8 percent, on an average relative to the observed data. Although both versions show an average absolute error of about ±0.06 ppm, the newer version appears to show a better relative error of ±18 percent, compared to ±26 percent for the older CBM. This difference is visually manifested in the simulation results figures; the older version seems to produce ozone peaks with a noticeable bulge.

SIMULATION RESULTS OF UCR EXPERIMENTS USING THE ORIGINAL CARBON-BOND MECHANISM

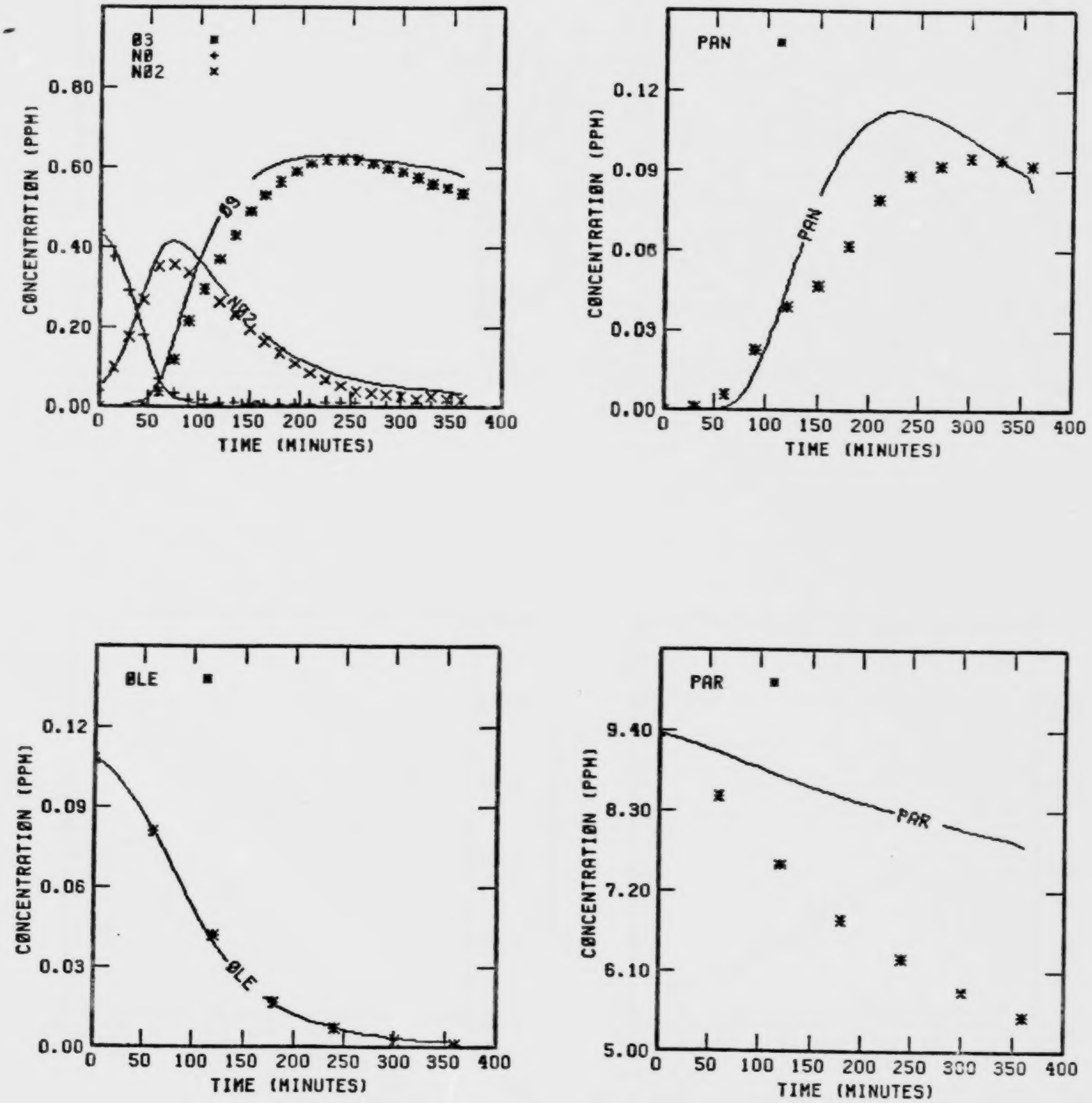

FIGURE 143. SIMULATION RESULTS FOR EC-231

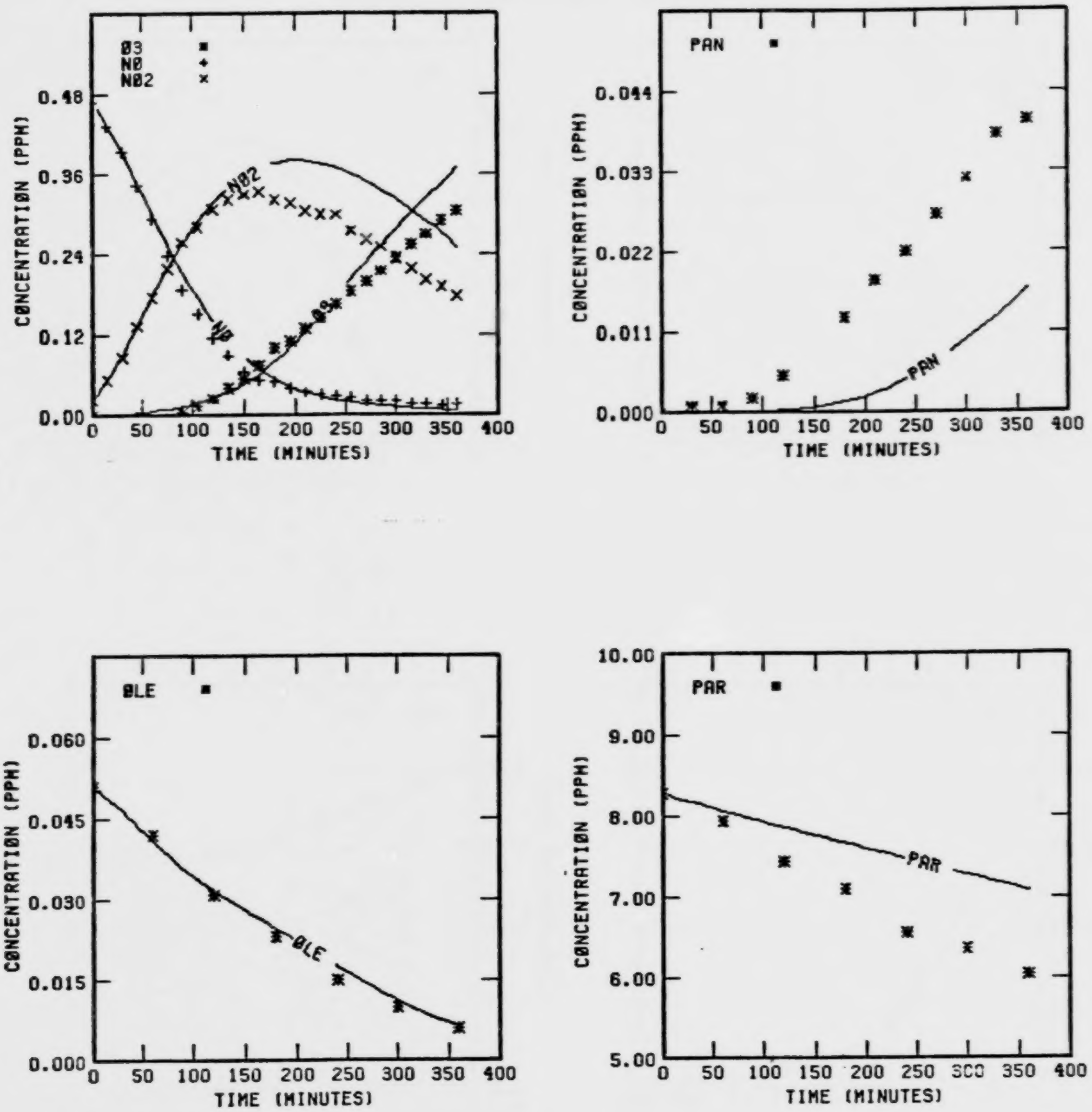

FIGURE 144. SIMULATION RESULTS FOR
EC-232

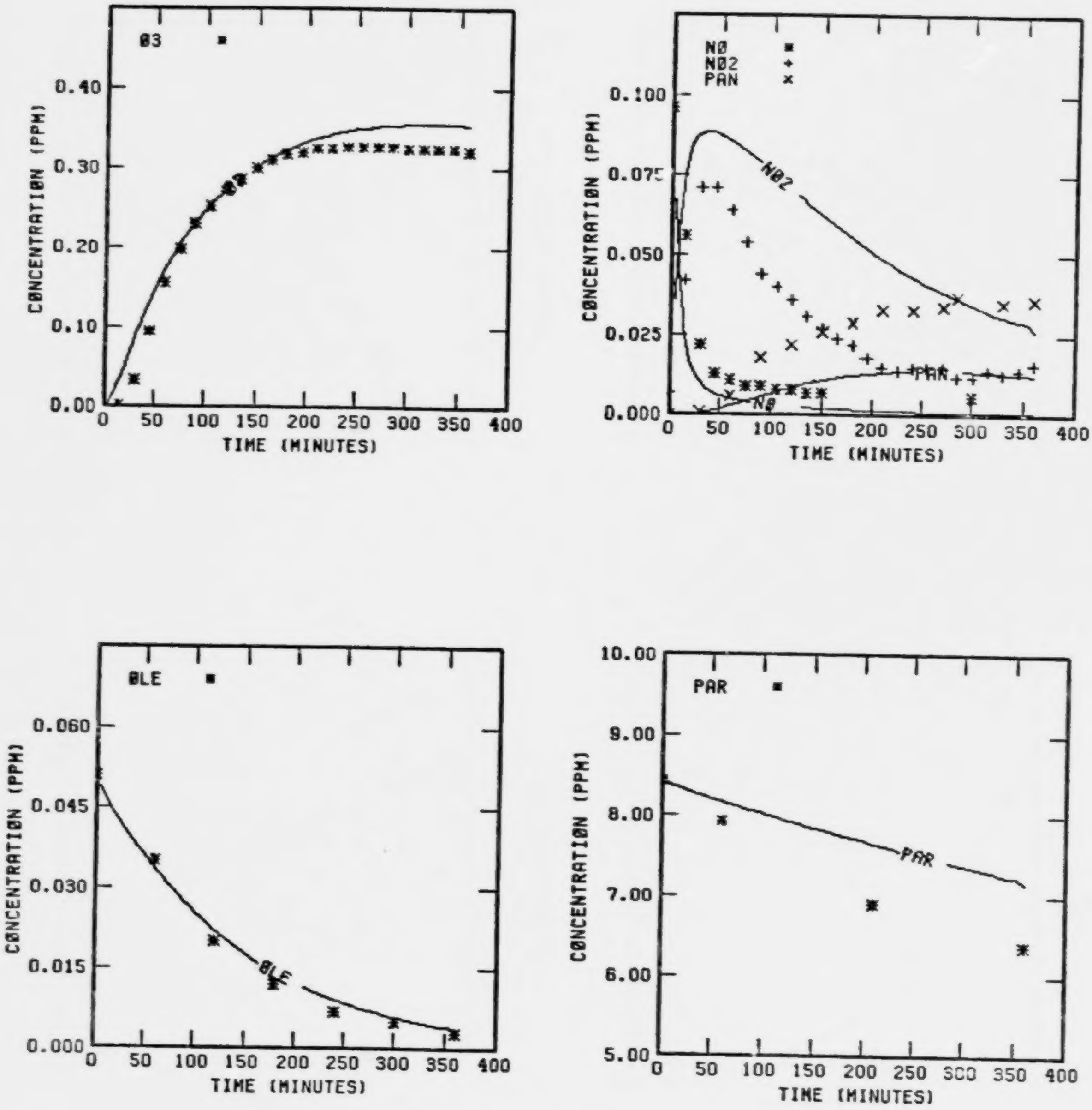

FIGURE 145. SIMULATIØN RESULTS FØR
EC-233

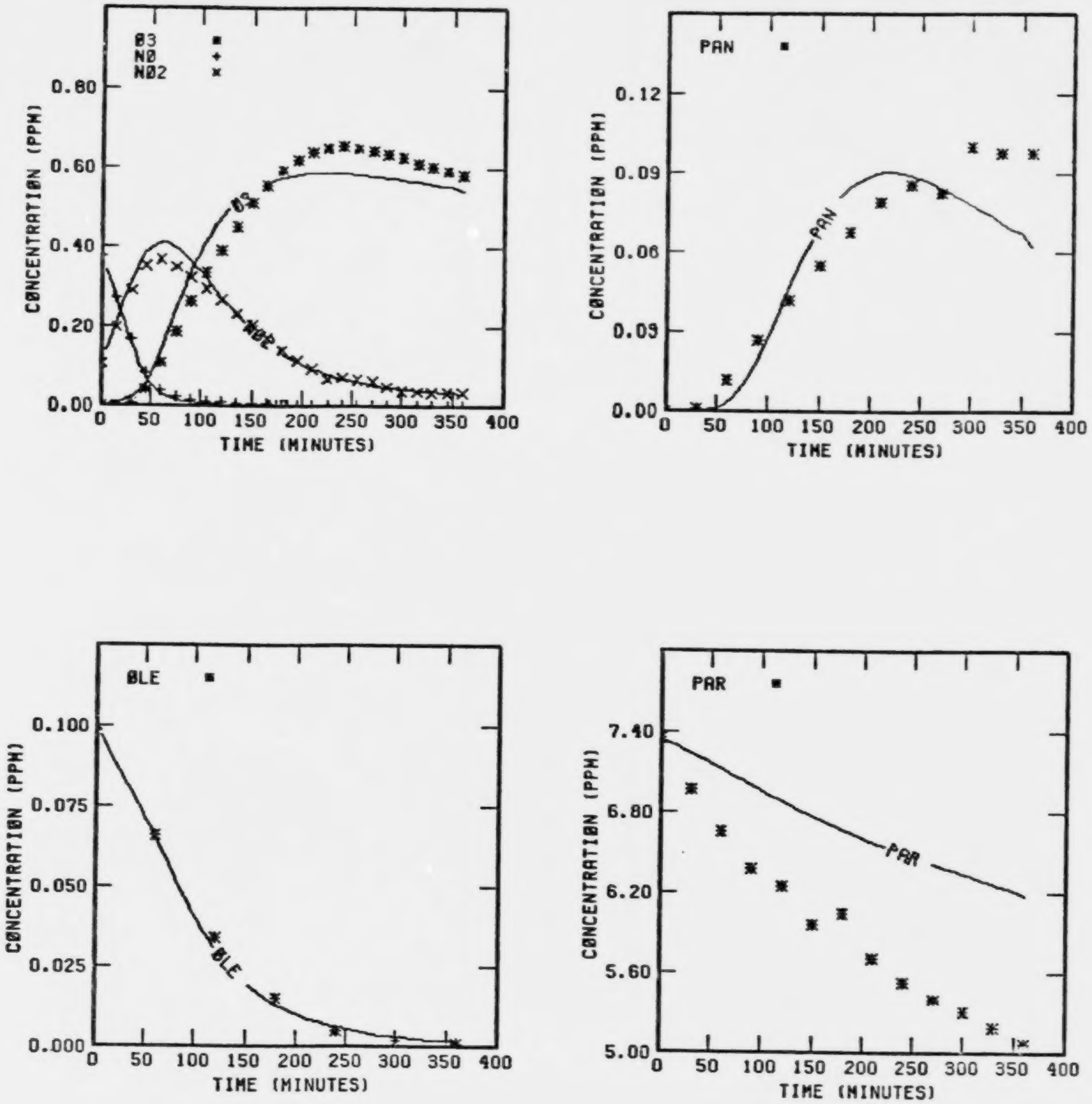

FIGURE 146. SIMULATION RESULTS FOR EC-237

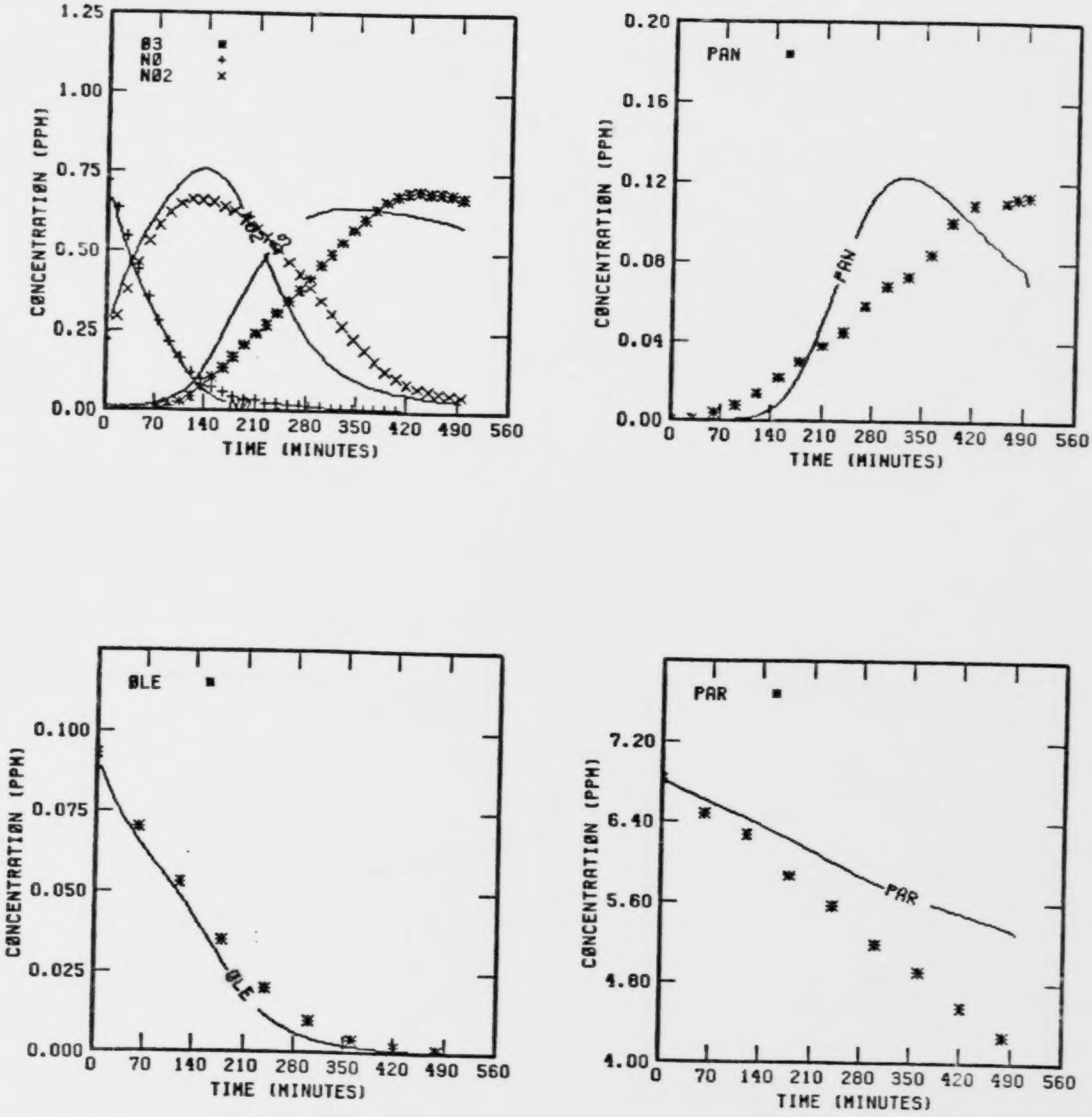

FIGURE 147. SIMULATION RESULTS FOR
EC-238

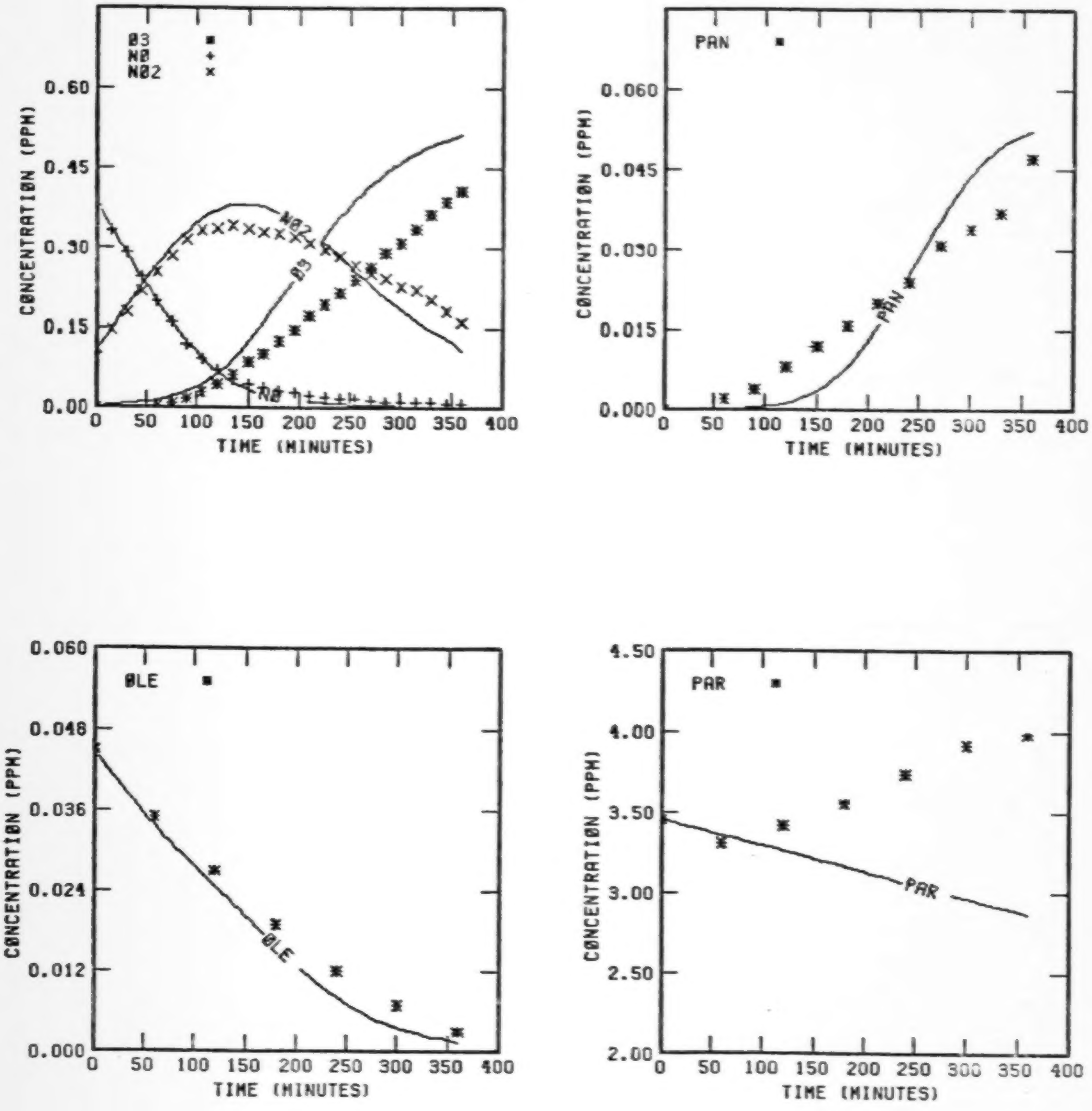

FIGURE 148. SIMULATIØN RESULTS FØR EC-241

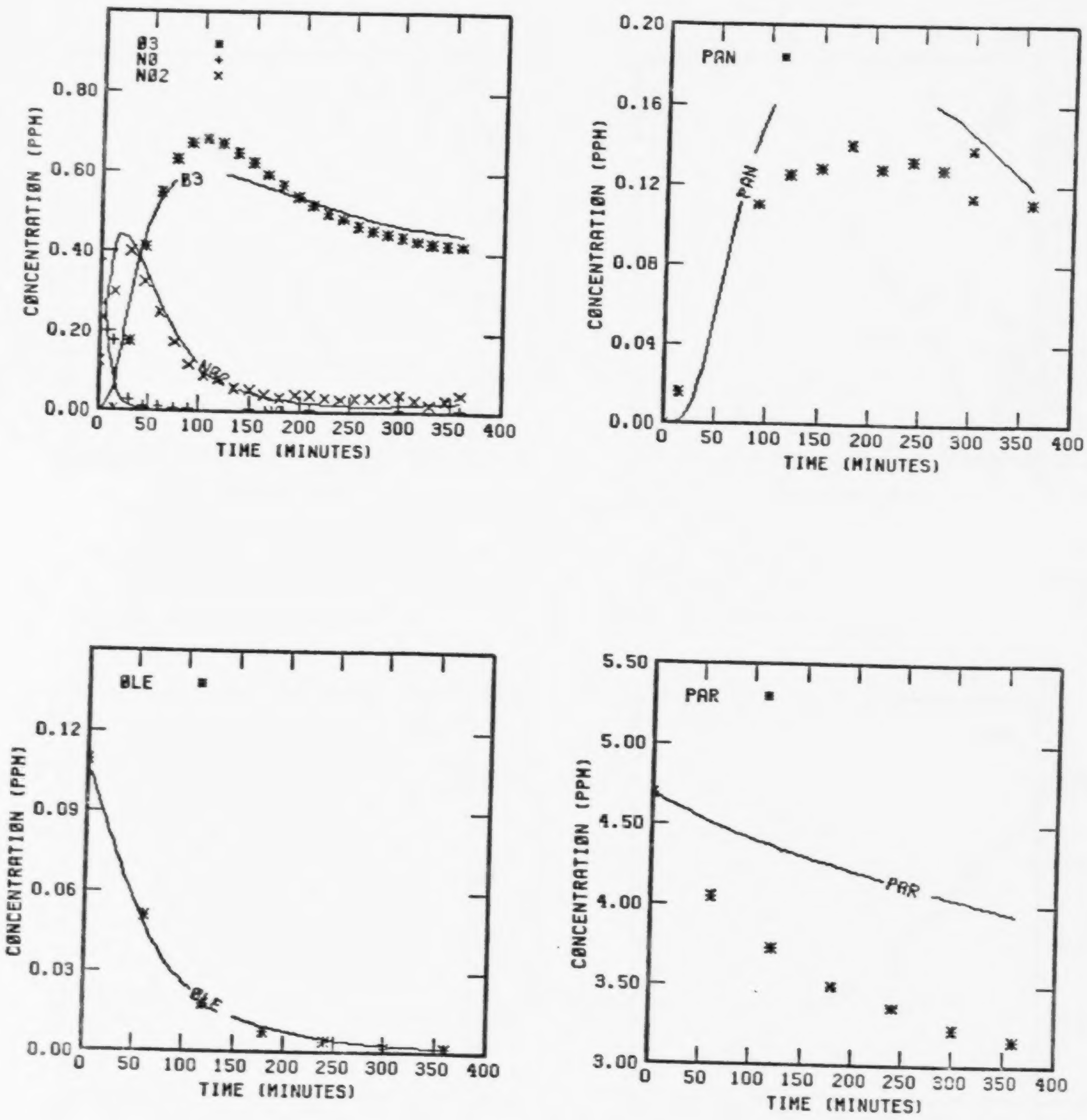

FIGURE 149. SIMULATION RESULTS FOR EC-242

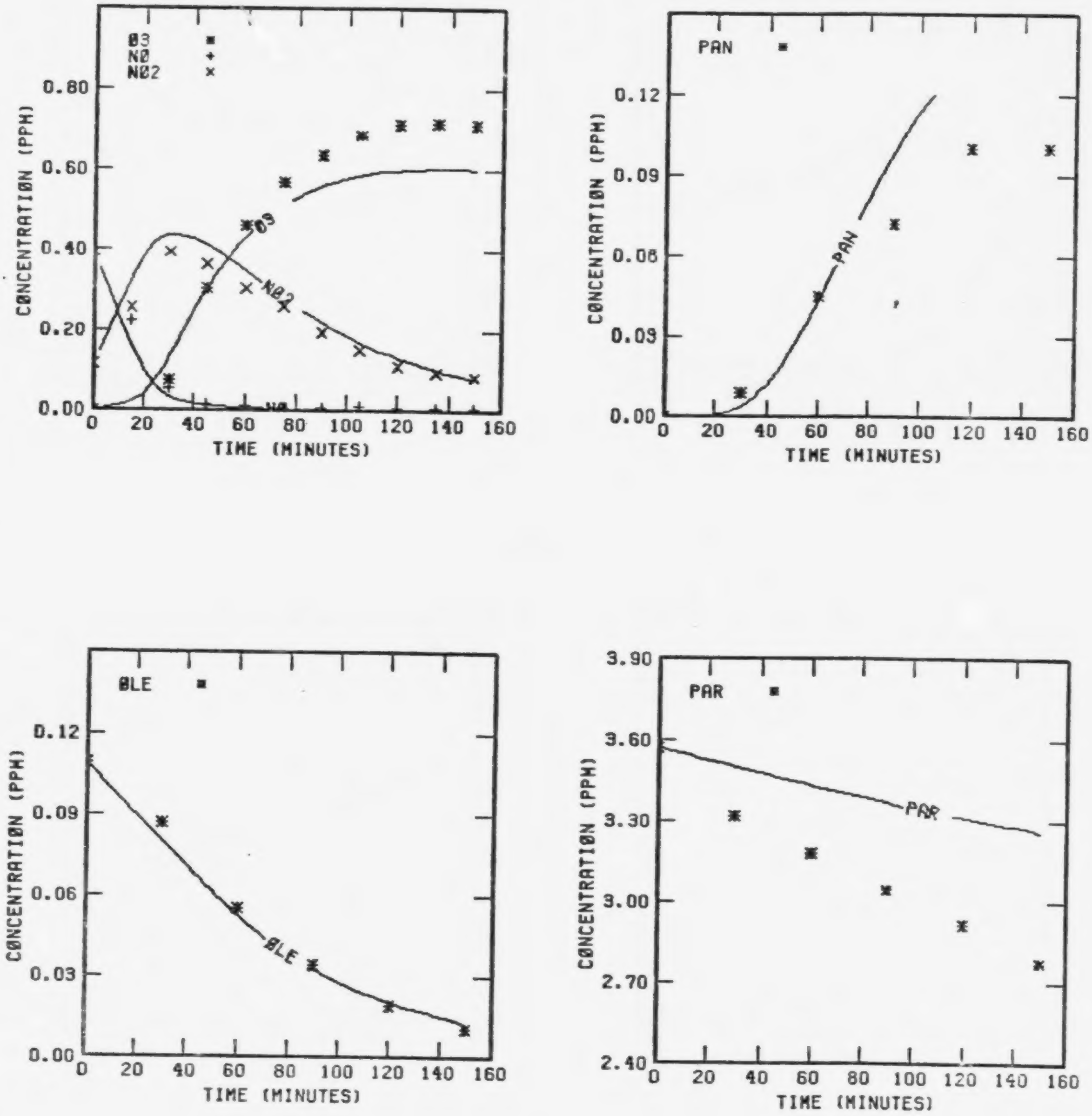

FIGURE 150. SIMULATIØN RESULTS FØR
EC-243

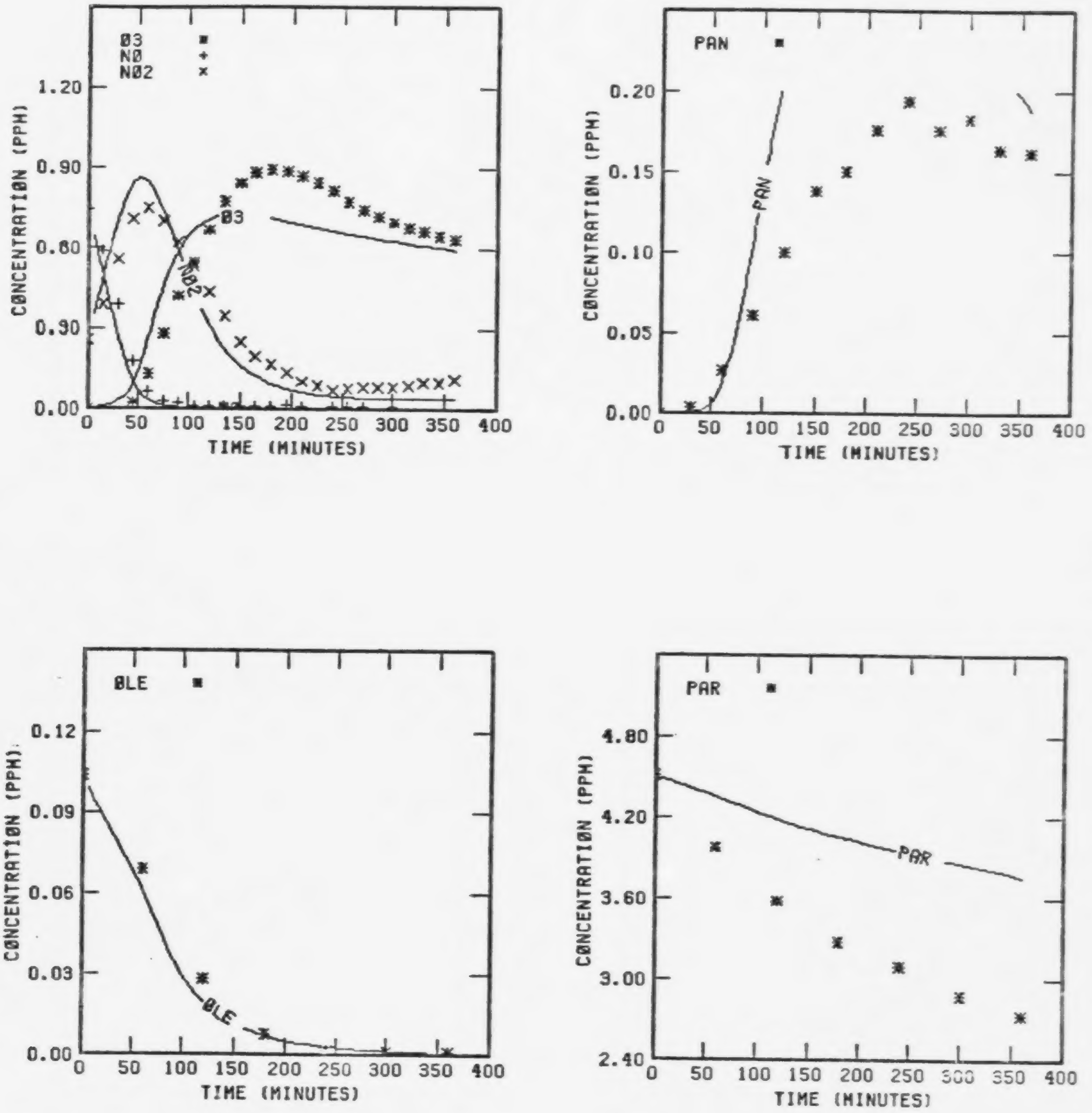

FIGURE 151. SIMULATION RESULTS FOR
EC-245

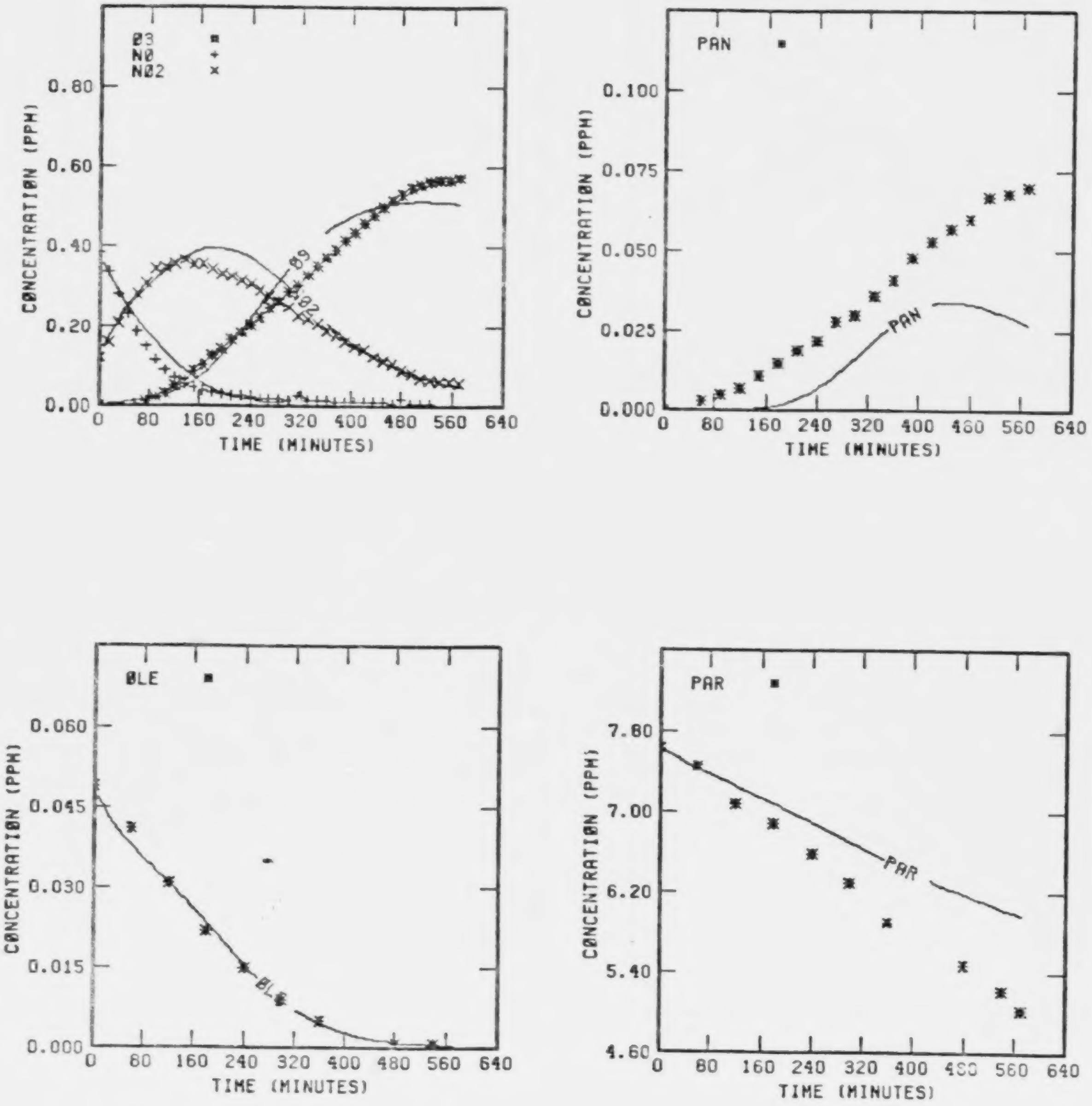

FIGURE 152. SIMULATION RESULTS FOR
EC-246

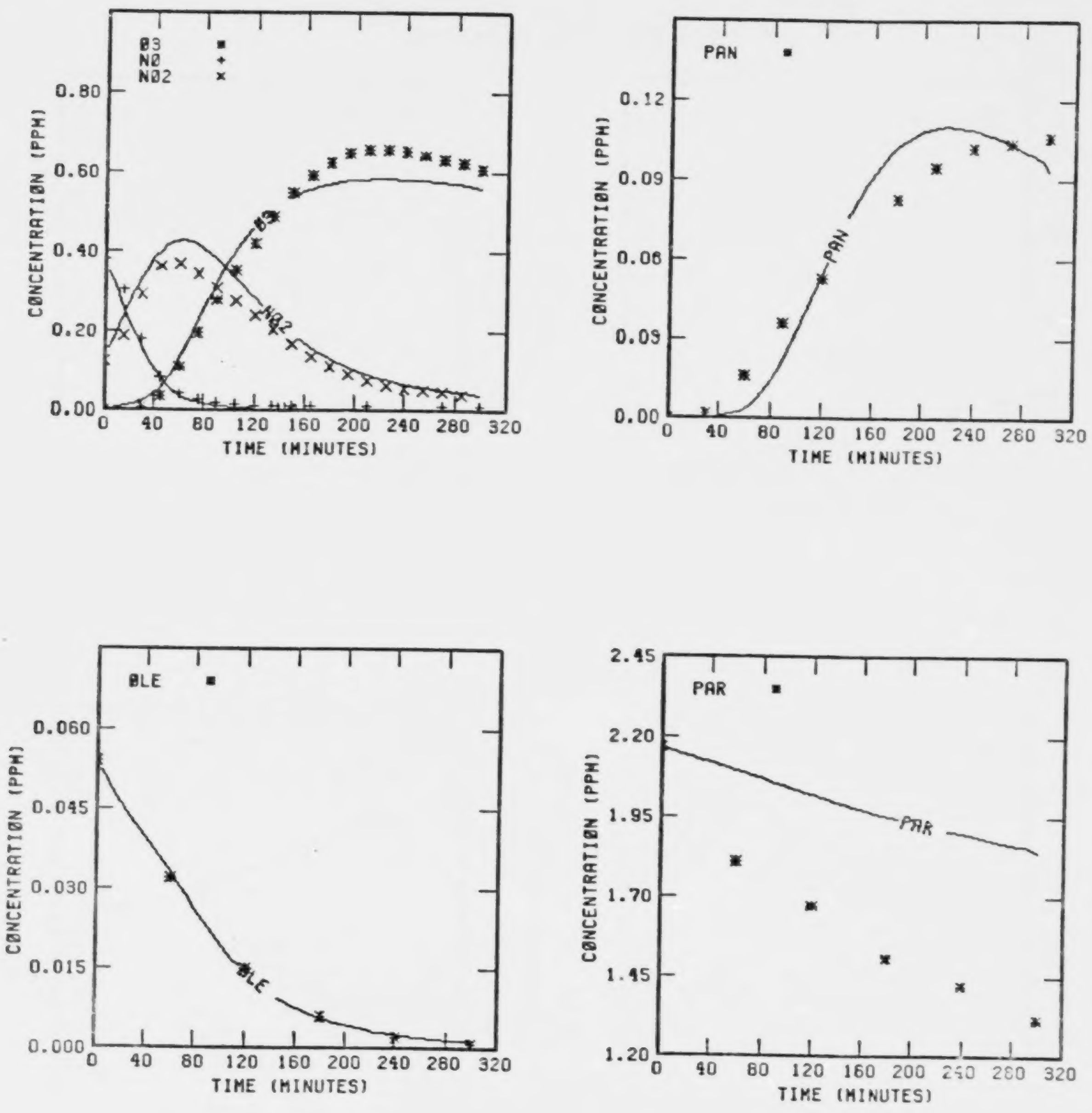

FIGURE 153. SIMULATION RESULTS FOR
EC-247

SIMULATION RESULTS OF UCR EXPERIMENTS USING
THE NEW CARBON-BOND MECHANISM

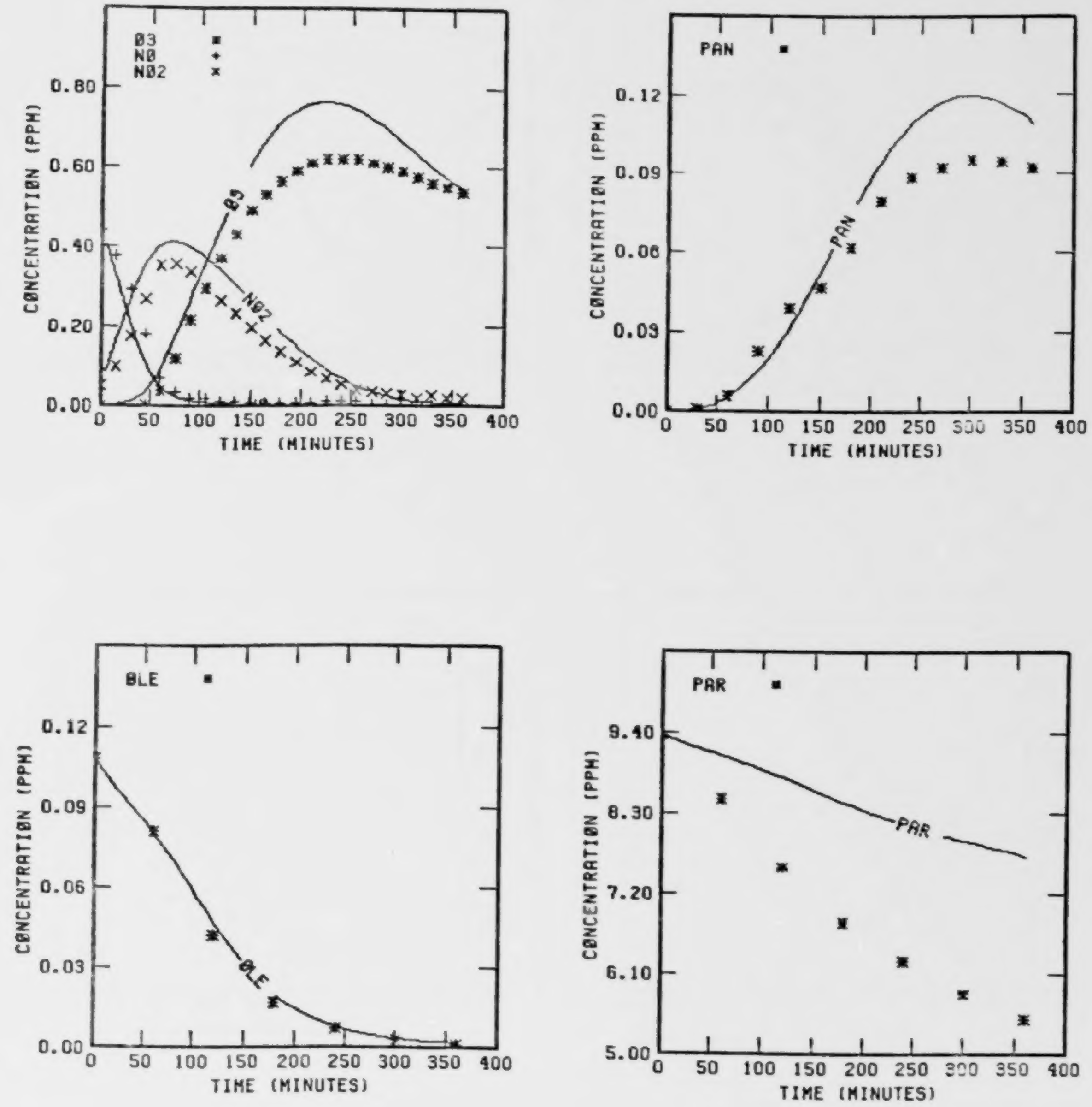

FIGURE 154. SIMULATION RESULTS FOR
EC-231

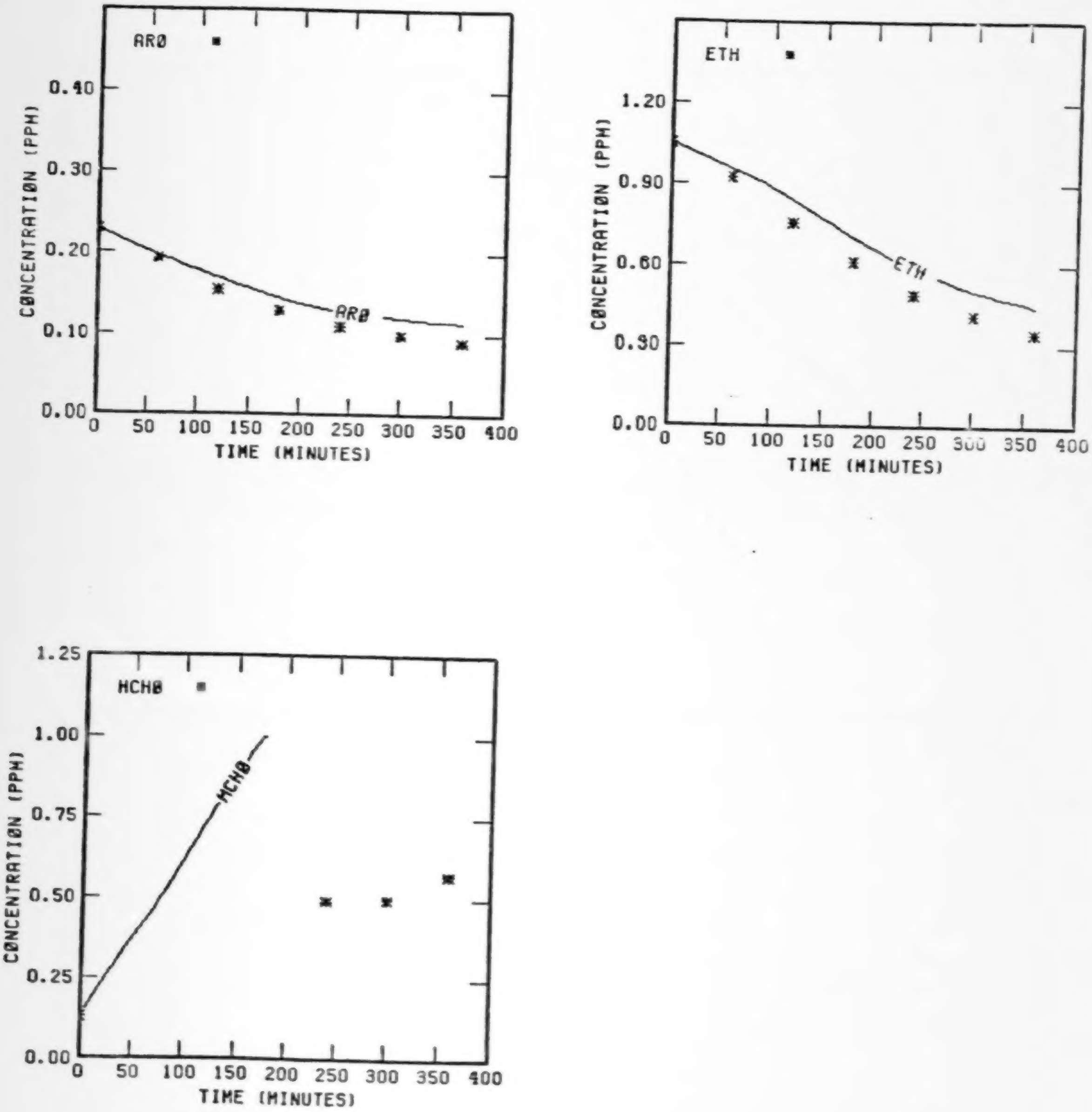

FIGURE 154. (Concluded)

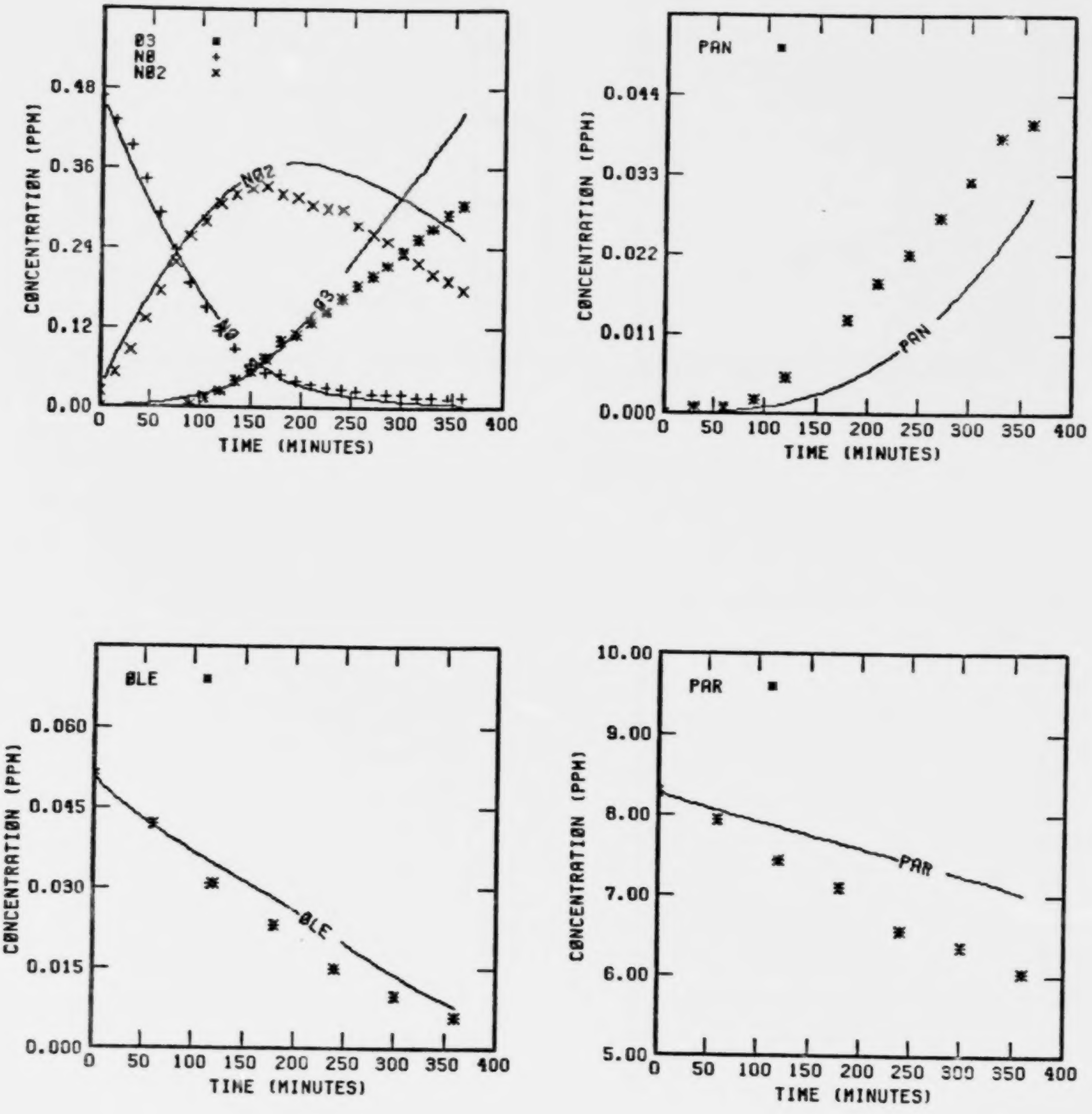

FIGURE 155. SIMULATIØN RESULTS FØR EC-232

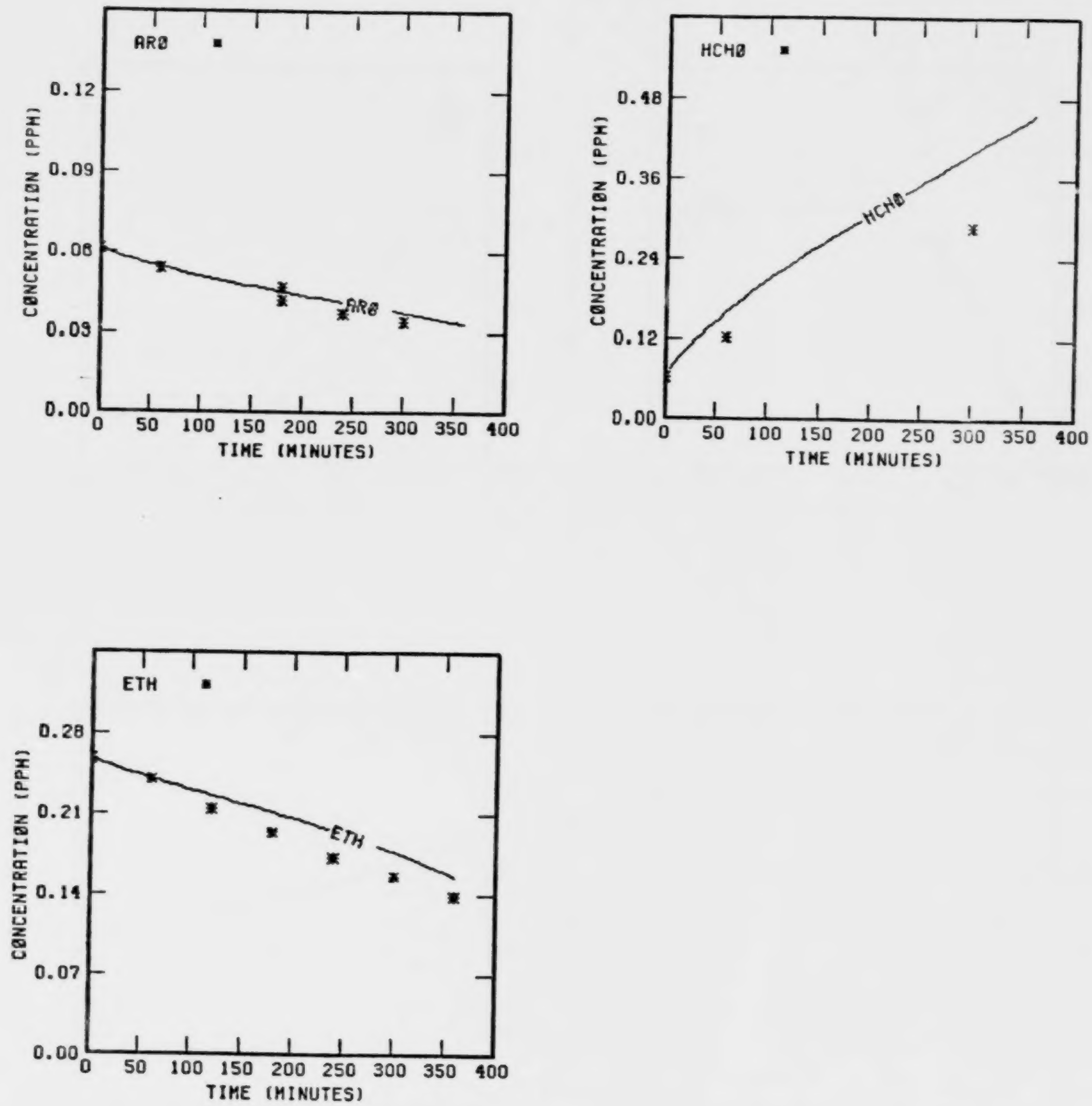

FIGURE 155. (Concluded)

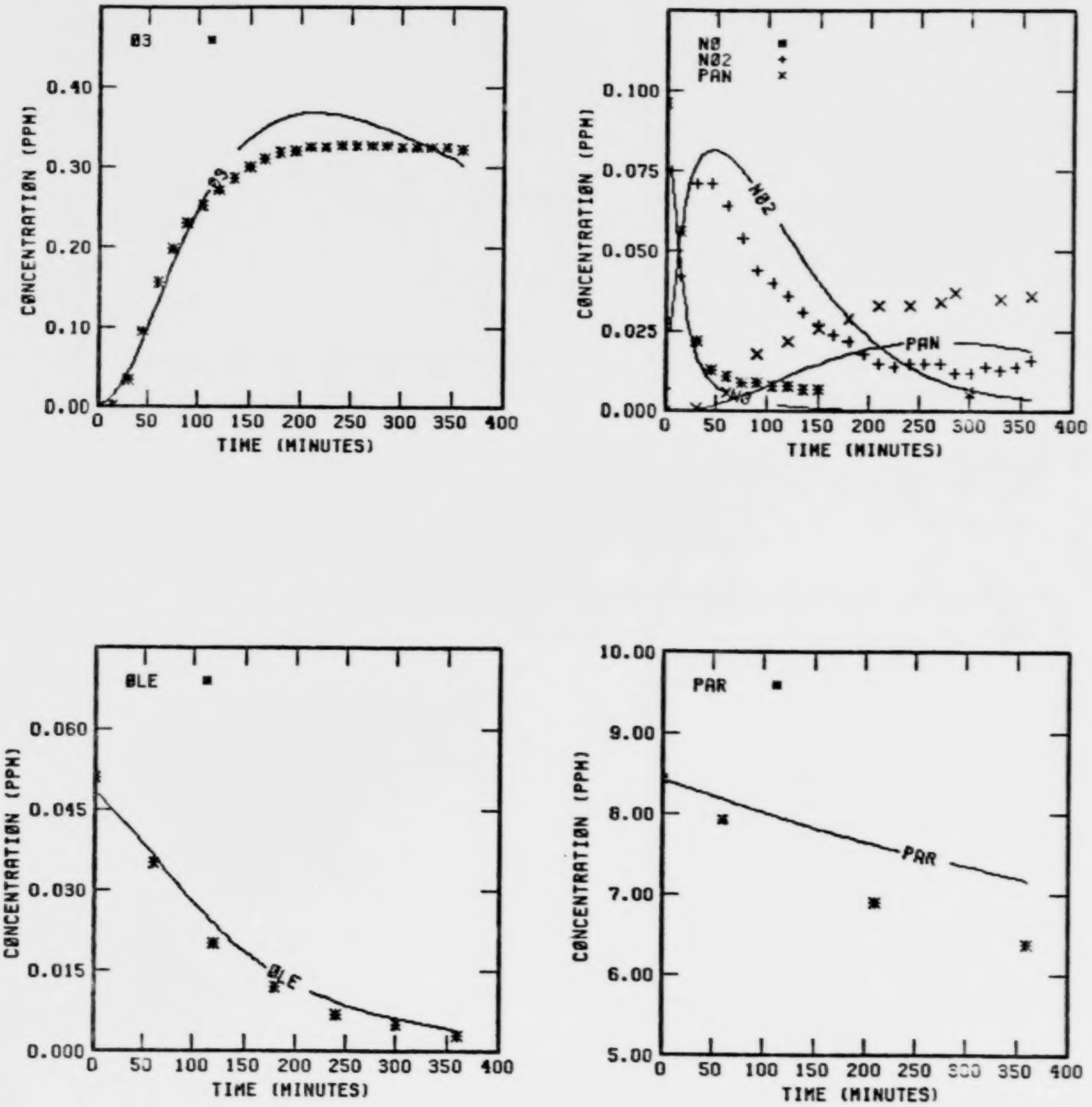

FIGURE 156. SIMULATION RESULTS FOR EC-233

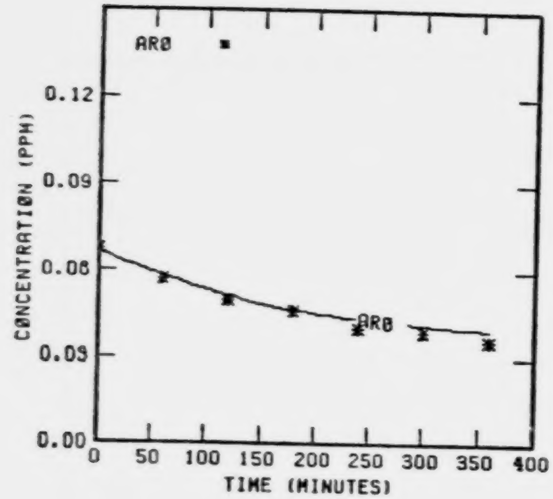

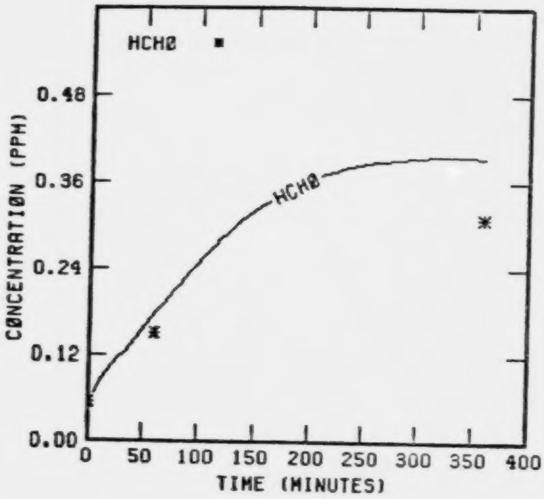

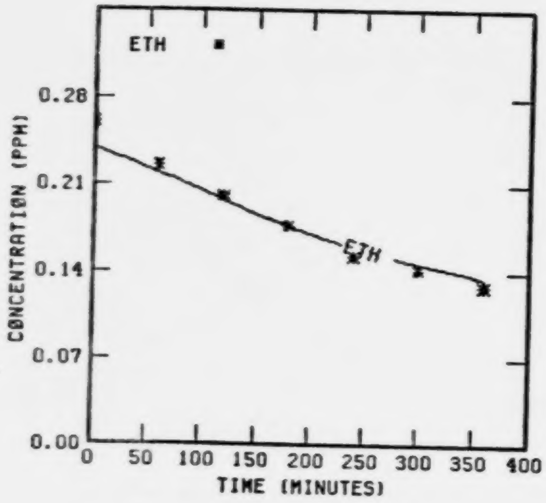

FIGURE 156. (Concluded)

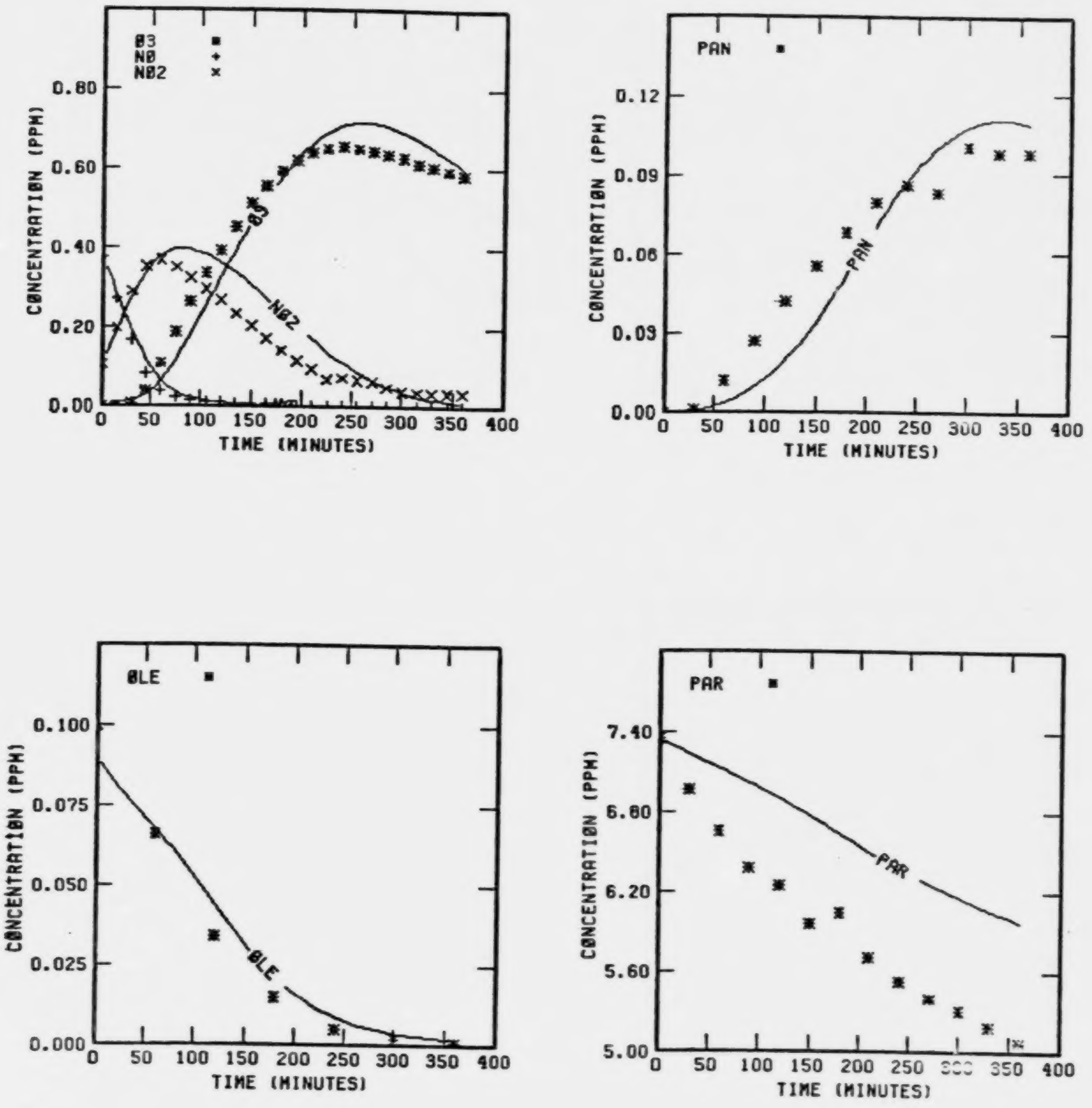

FIGURE 157. SIMULATIØN RESULTS FØR
EC-237

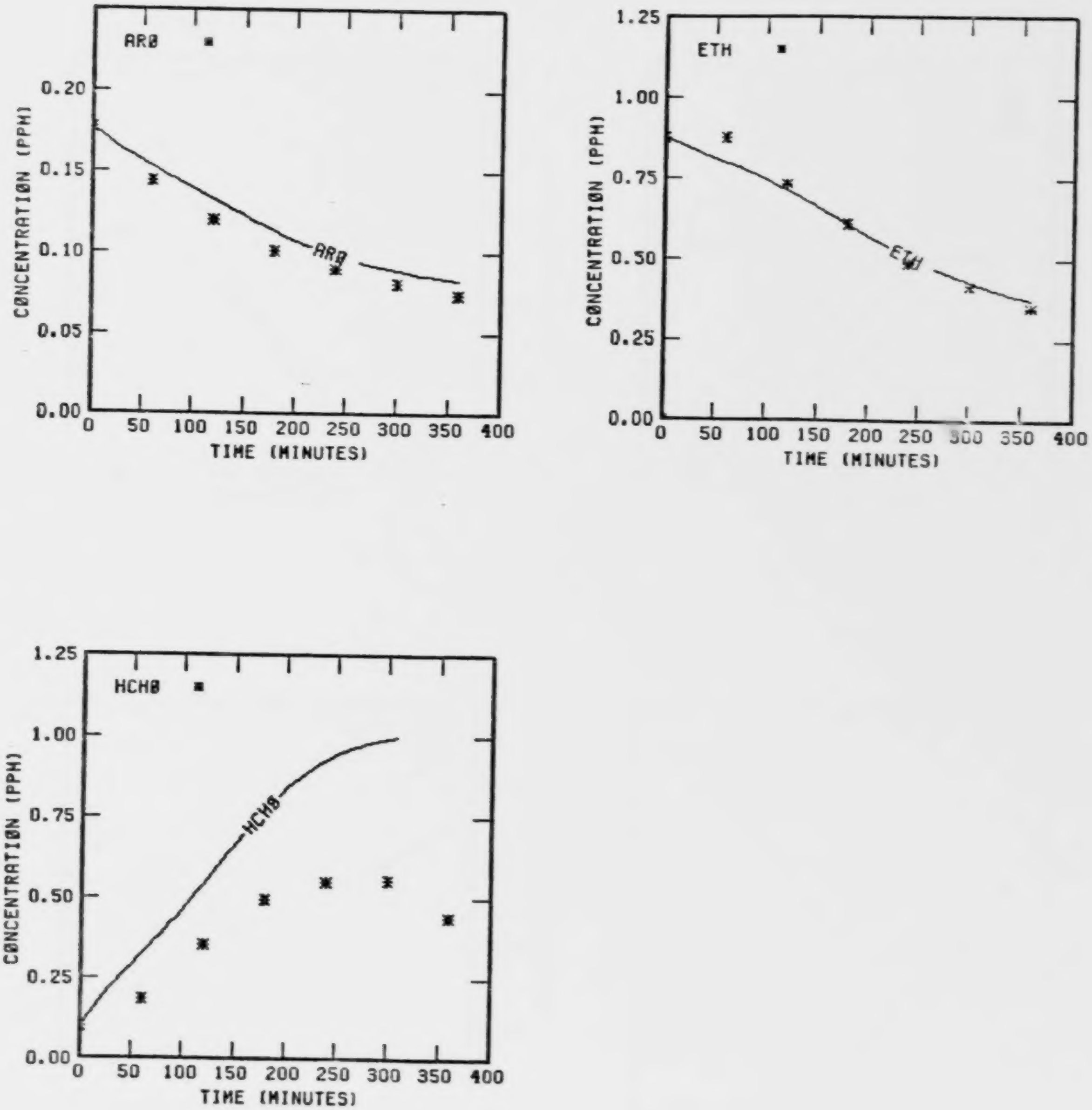

FIGURE 157. (Concluded)

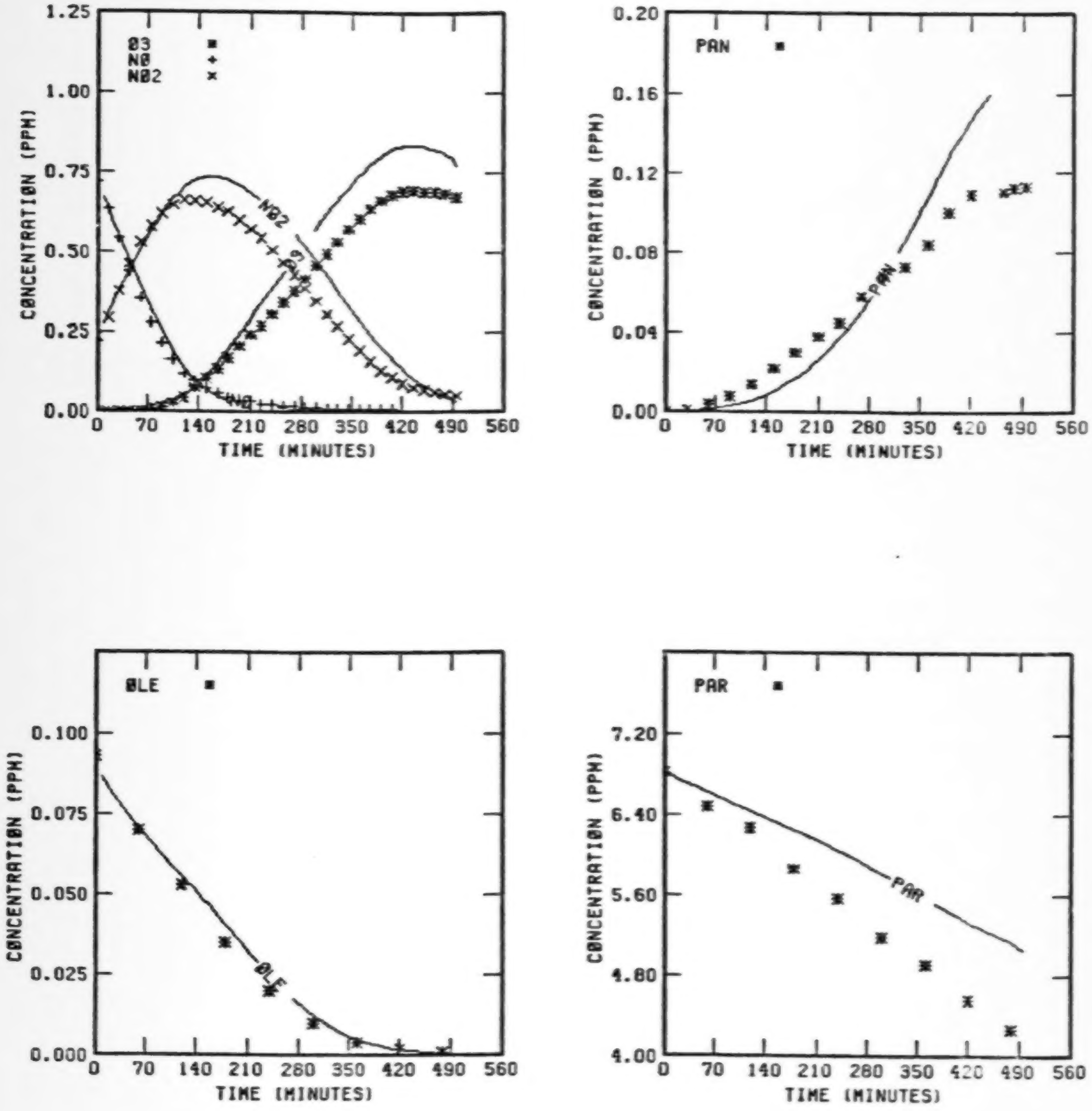

FIGURE 158. SIMULATION RESULTS FOR EC-238

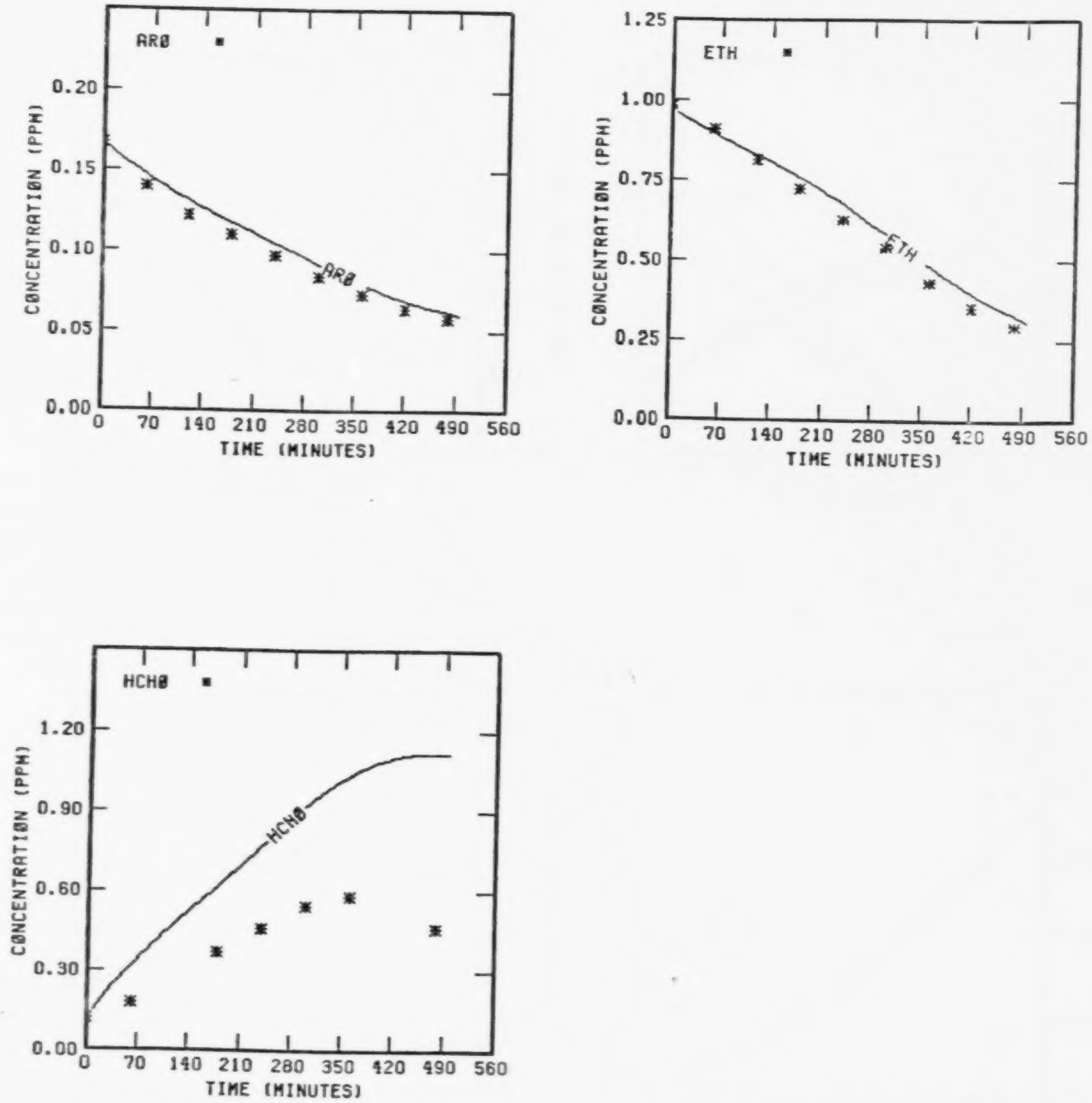

FIGURE 158. (Concluded)

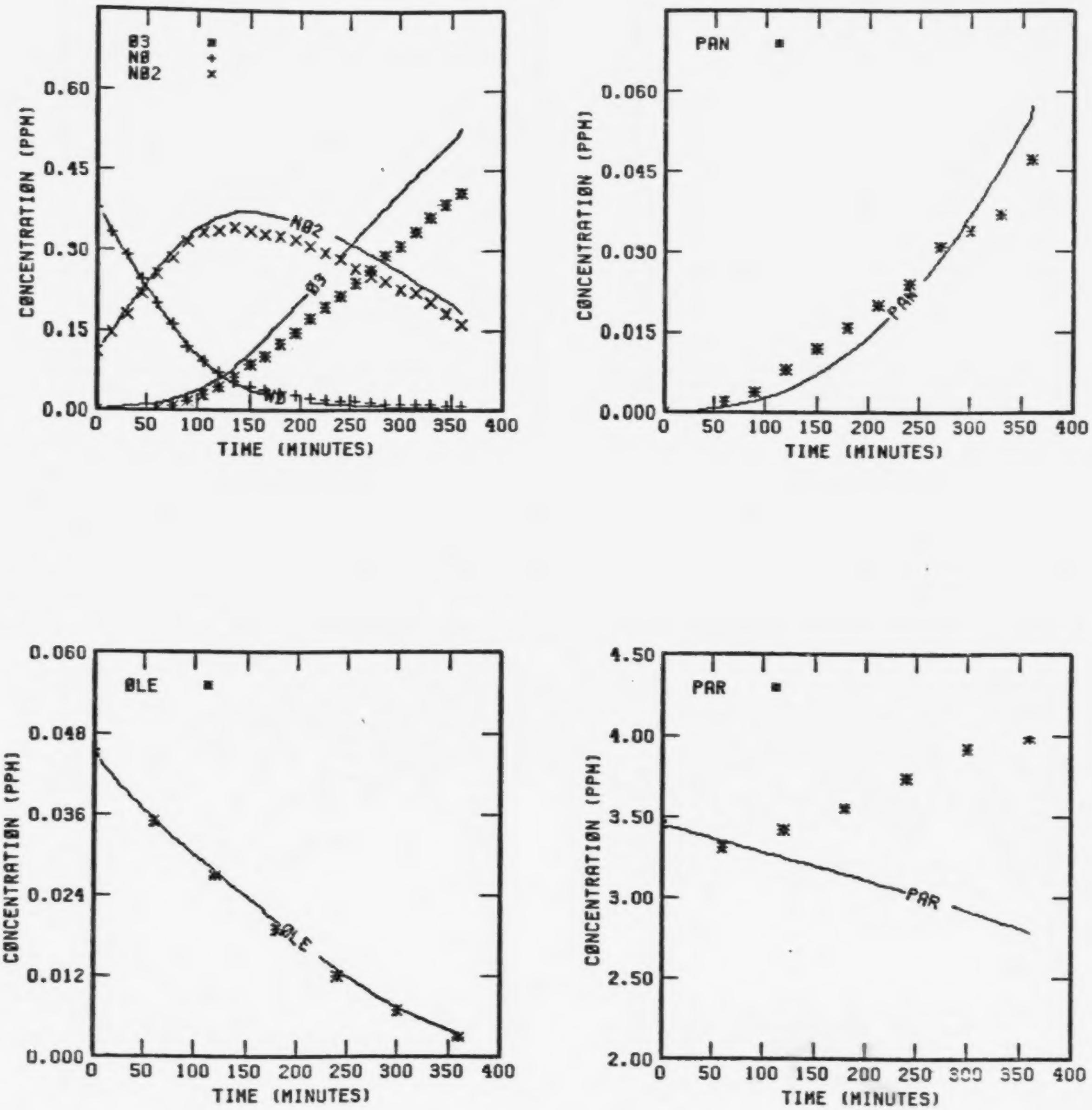

FIGURE 159. SIMULATION RESULTS FOR
EC-241

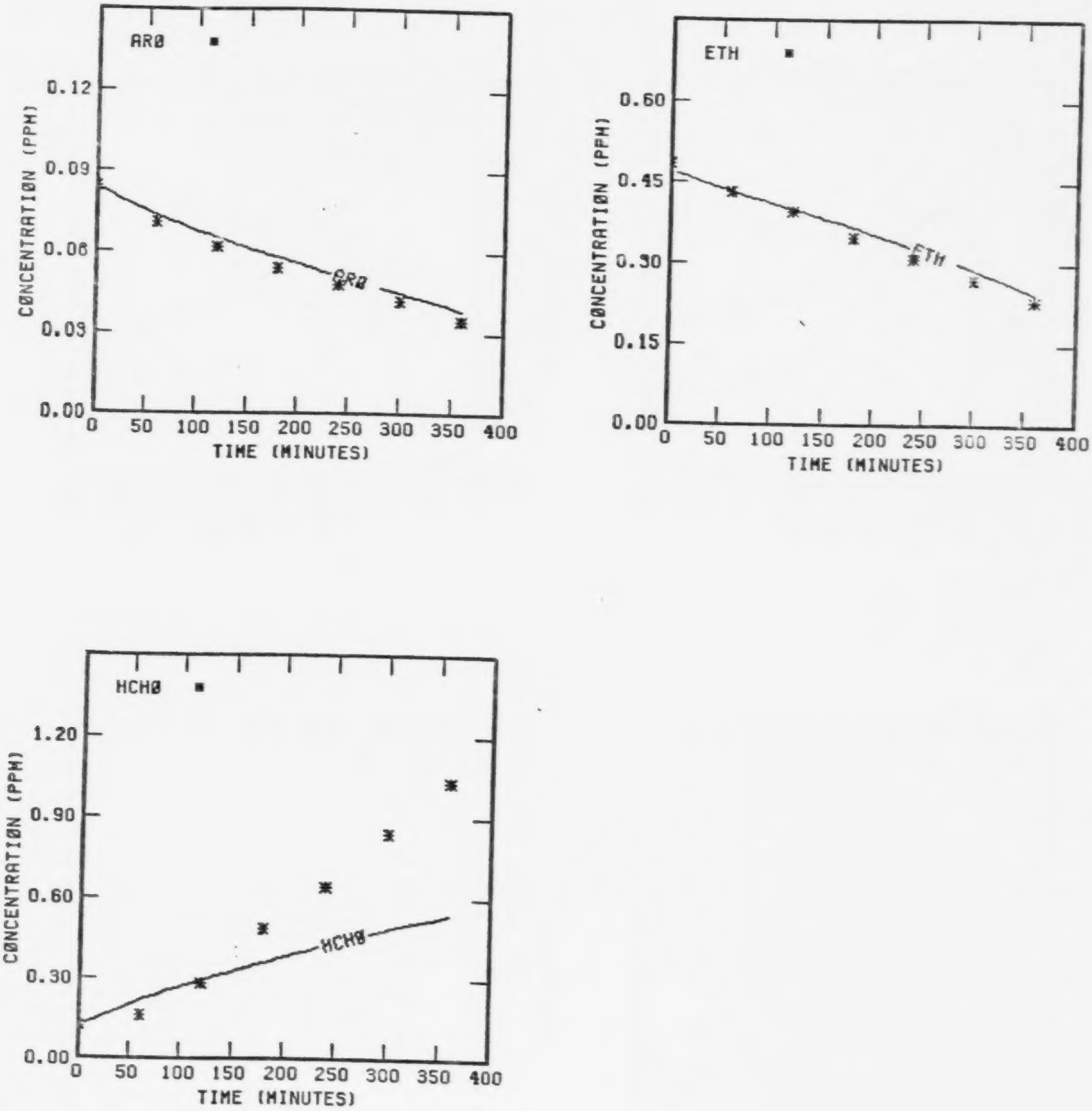

FIGURE 159. (Concluded)

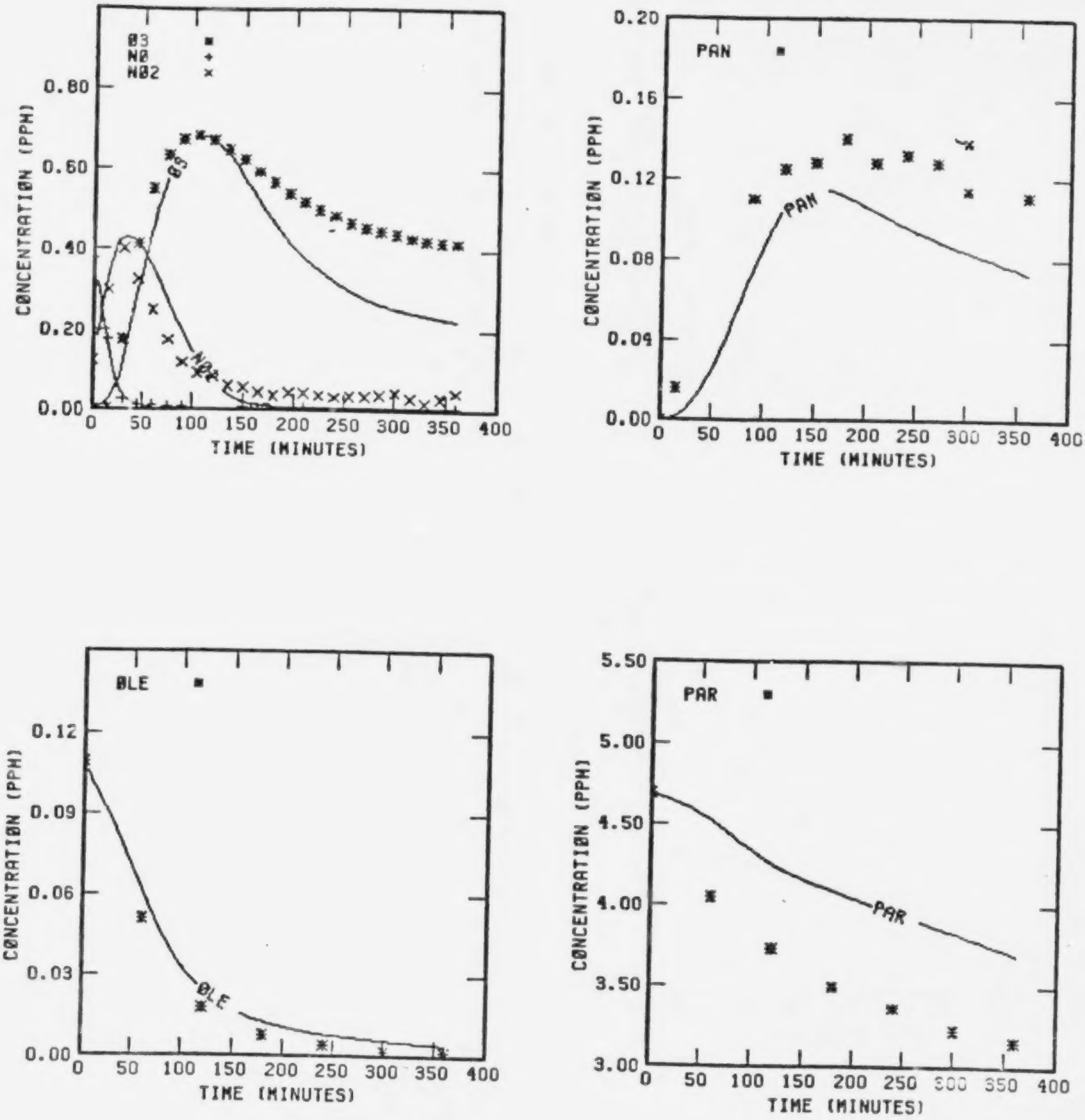

FIGURE 160. SIMULATION RESULTS FOR EC-242

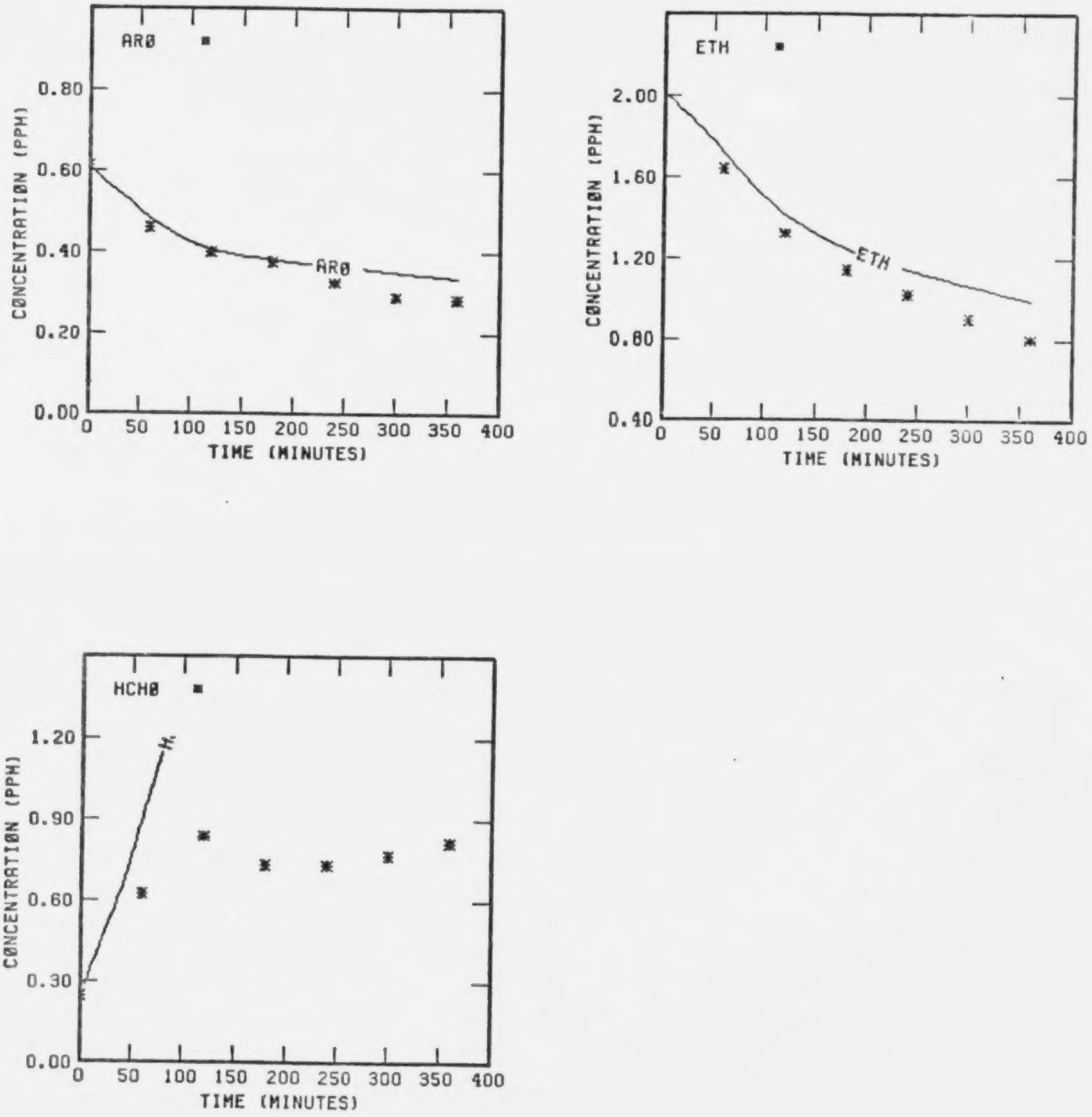

FIGURE 160. (Concluded)

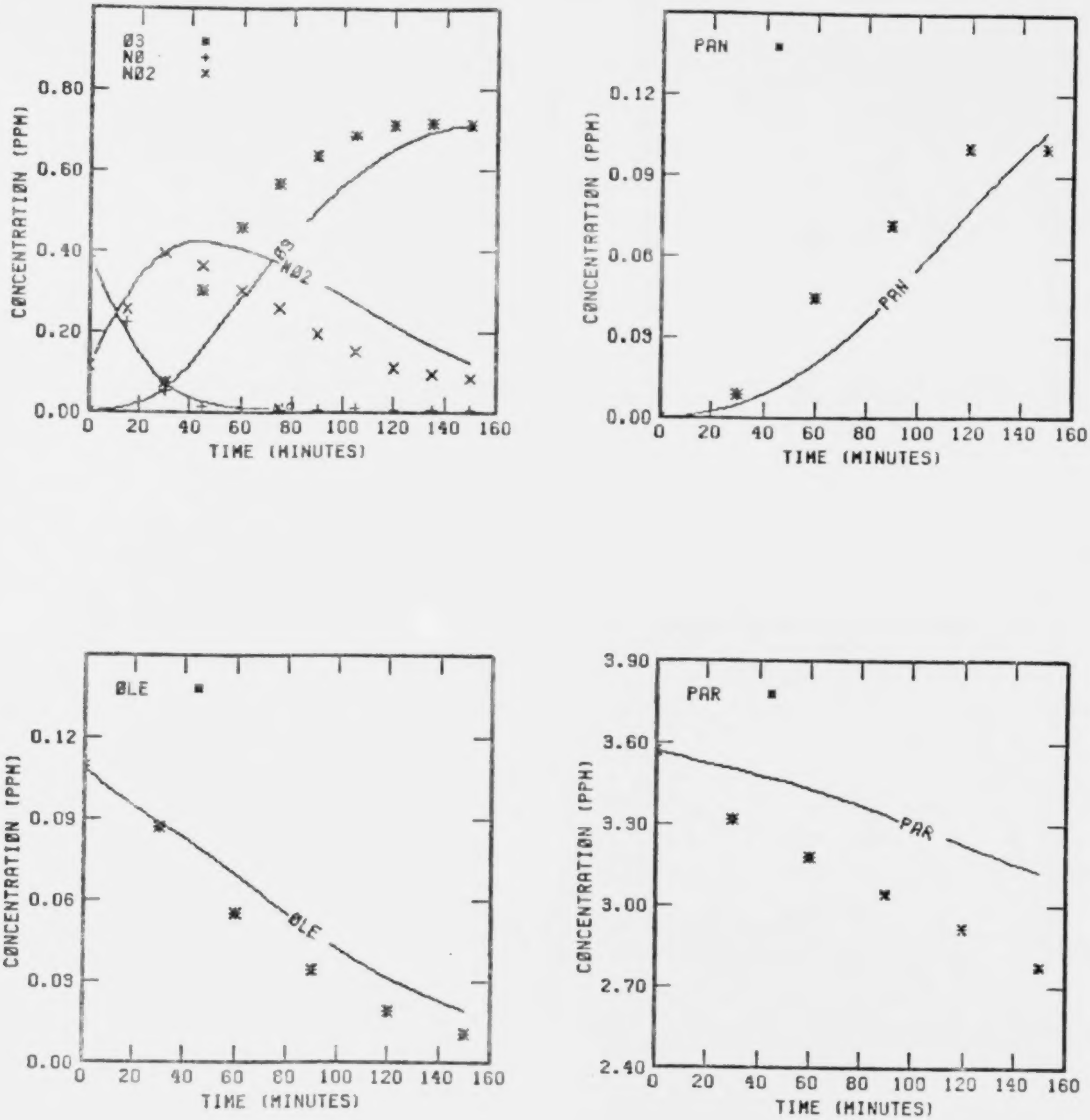

FIGURE 161. SIMULATIØN RESULTS FØR EC-243

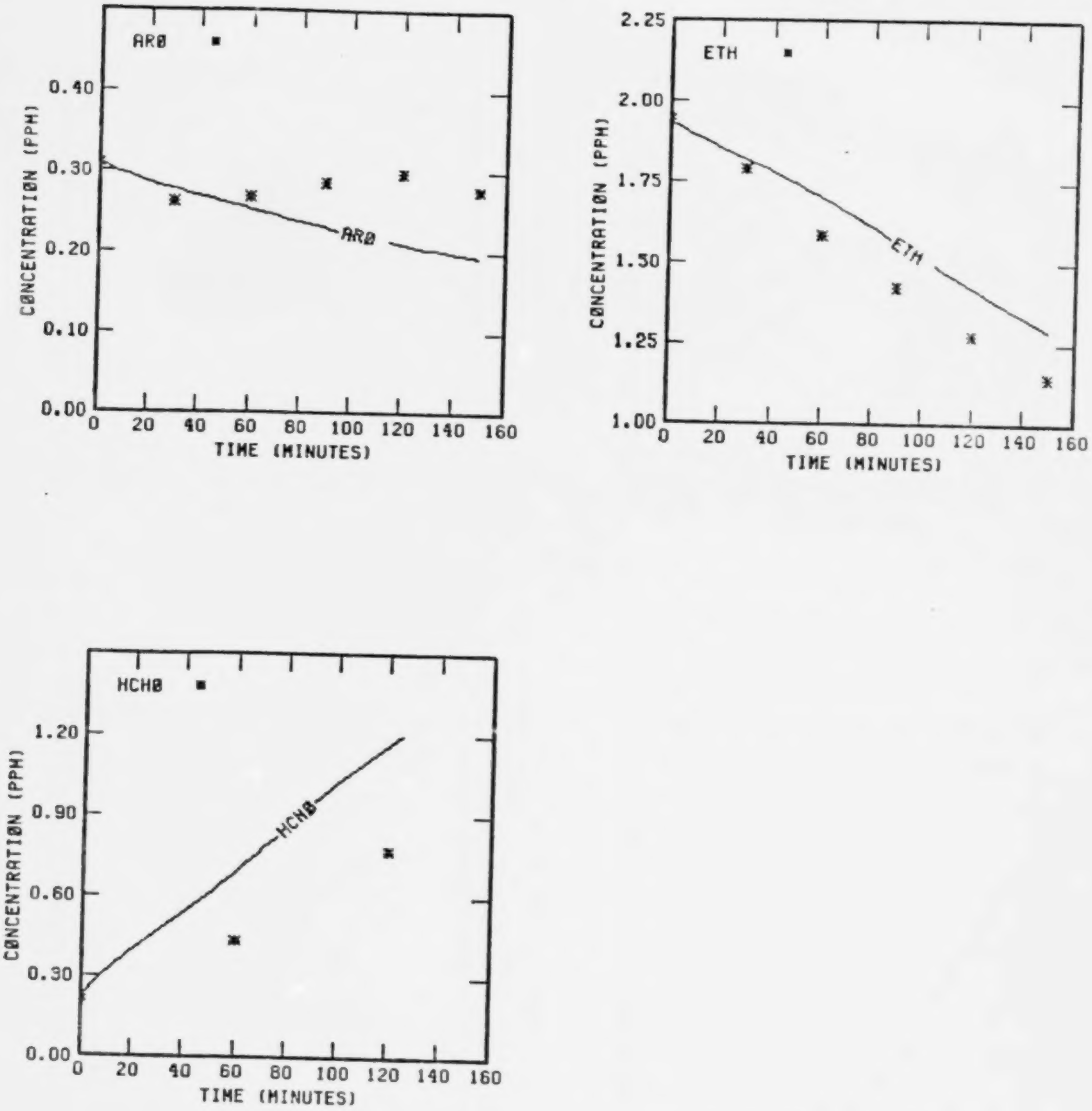

FIGURE 161. (Concluded)

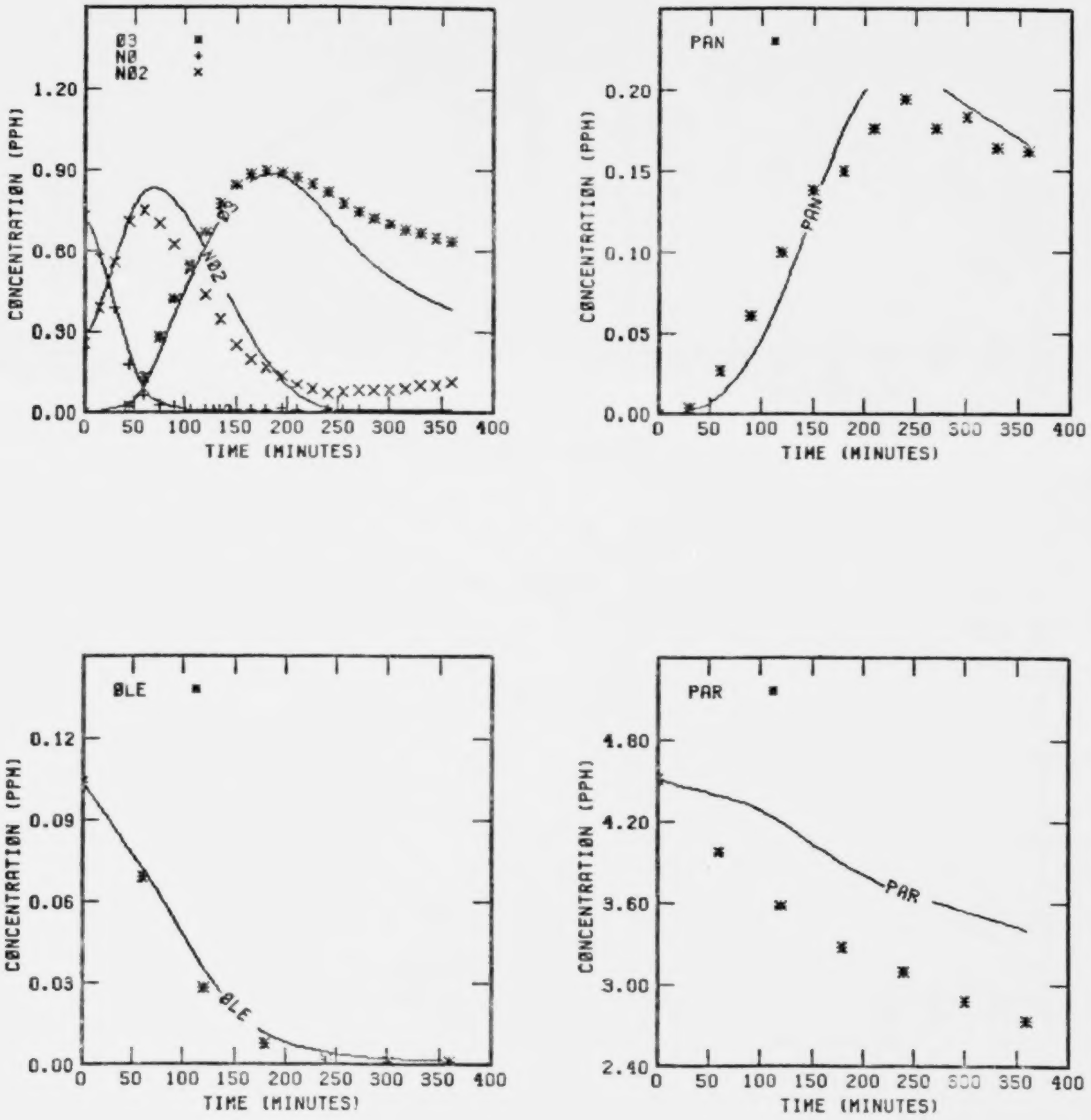

FIGURE 162. SIMULATION RESULTS FOR
EC-245

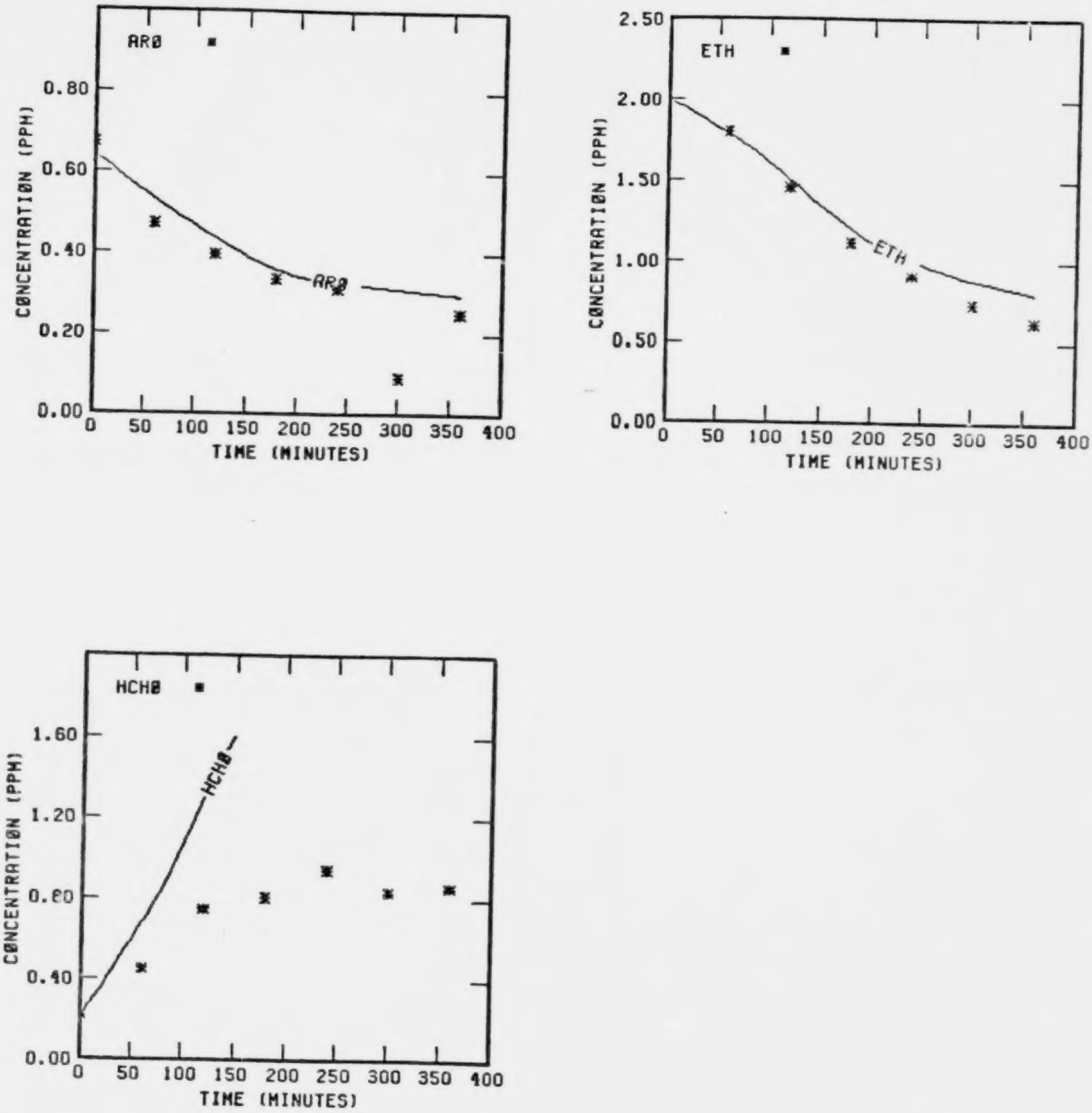

FIGURE 162. (Concluded)

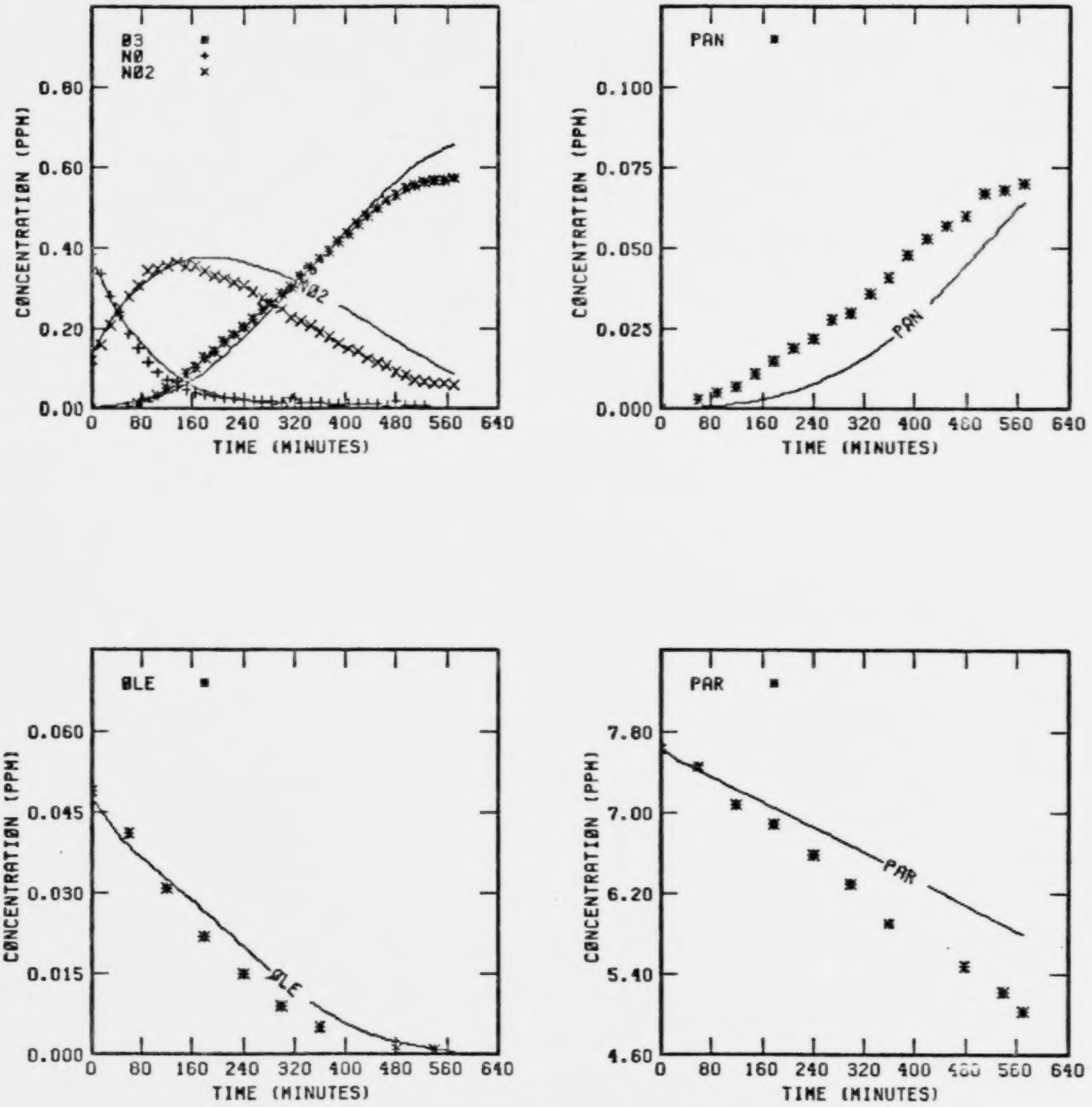

FIGURE 163. SIMULATION RESULTS FOR
EC-246

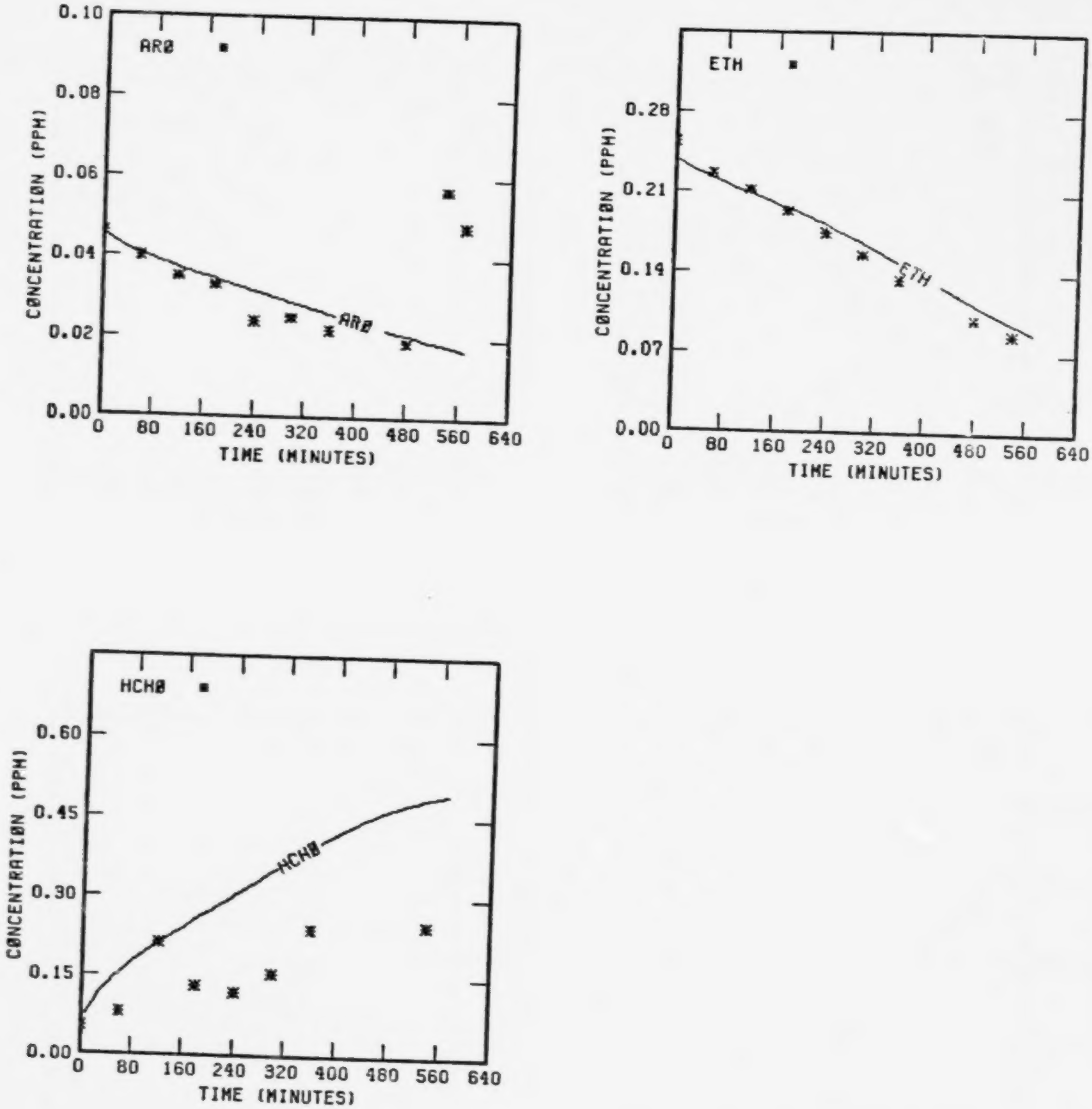

FIGURE 163. (Concluded)

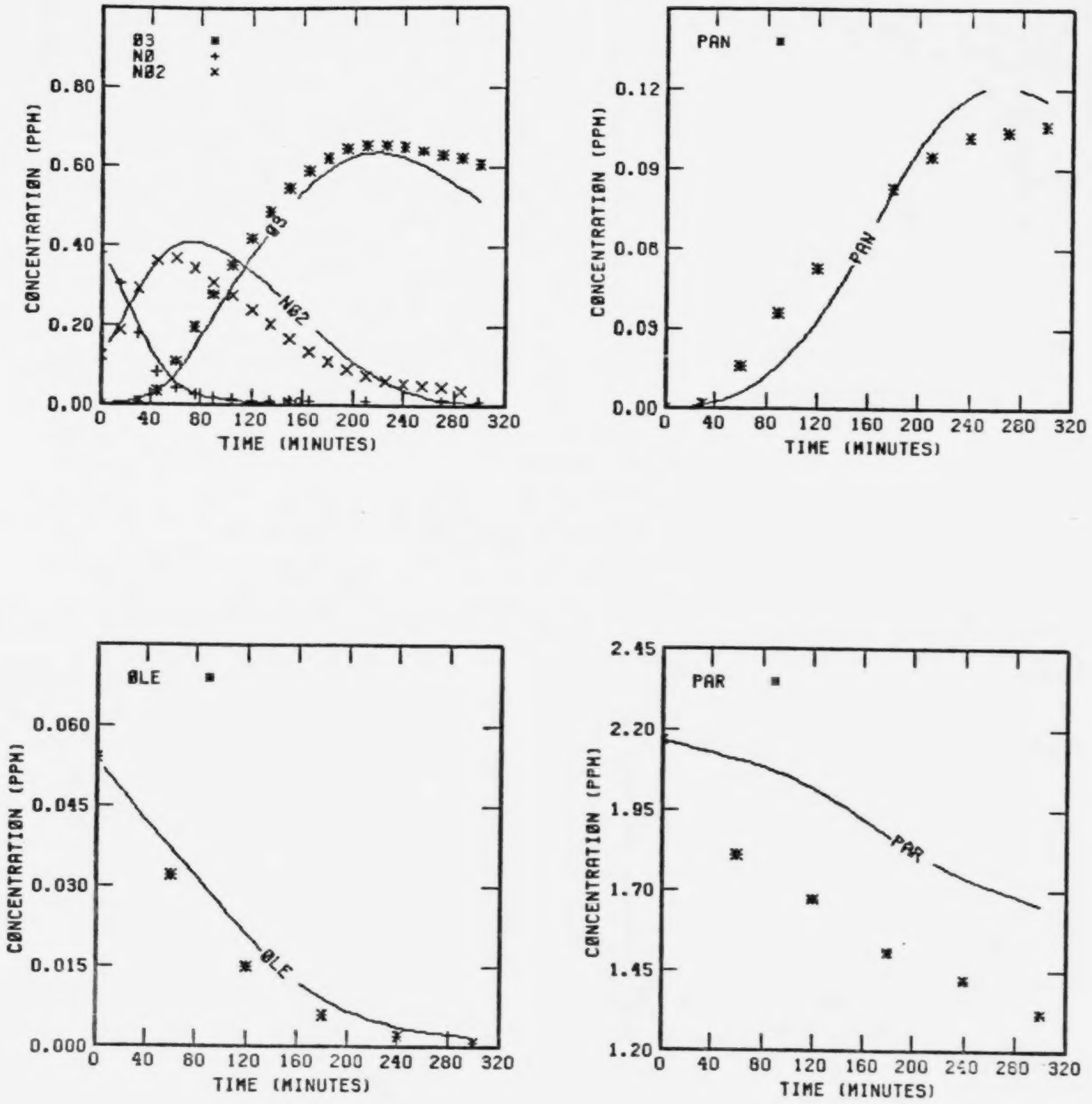

FIGURE 164. SIMULATIØN RESULTS FØR EC-247

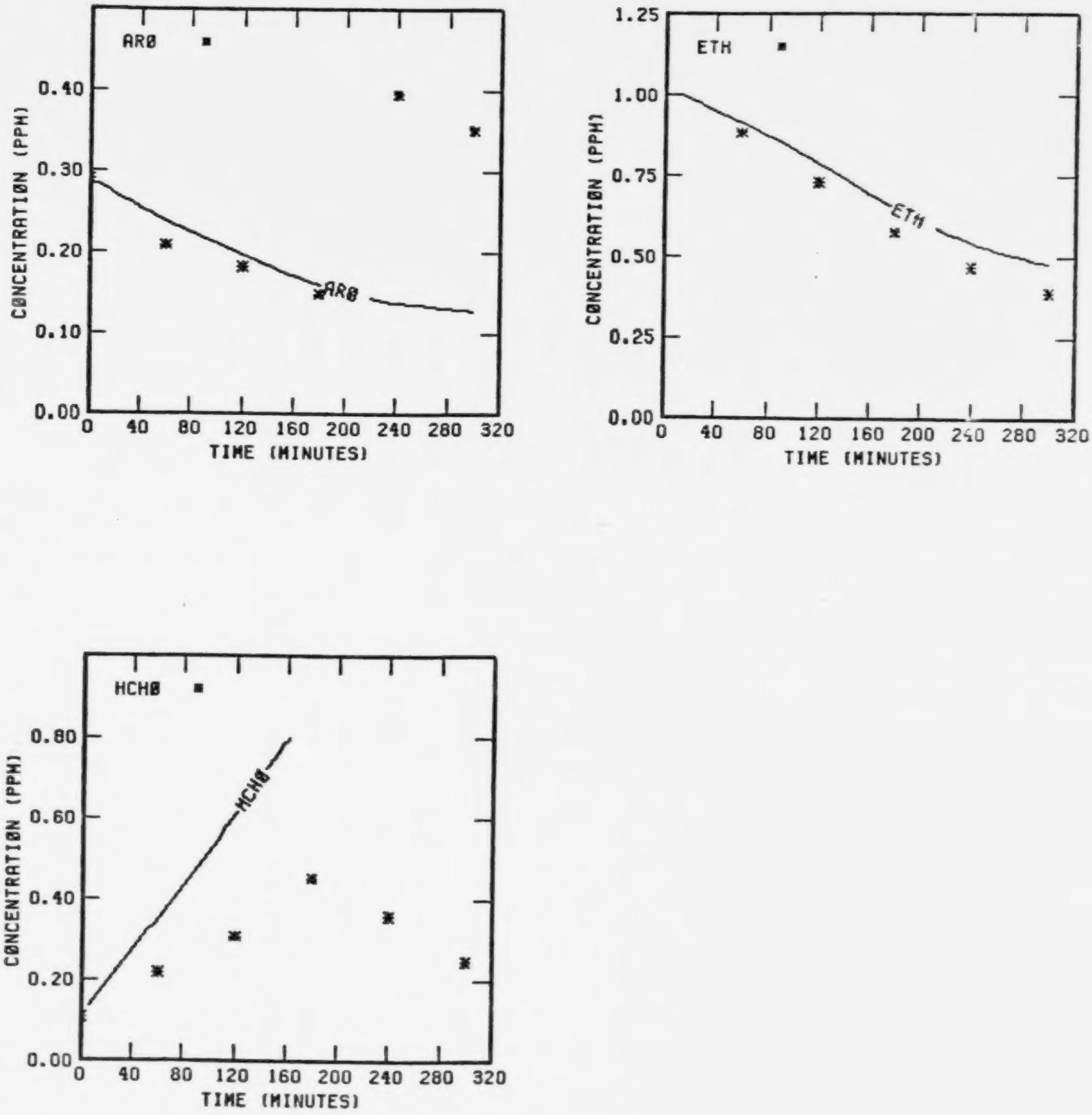

FIGURE 164. (Concluded)

TABLE 37. INITIAL CONDITIONS FOR THE SEVEN-HYDROCARBON/NO_x EXPERIMENTS

	Initial concentration (ppm)									
Run number	NO	NO_2	Ethylene	Propylene	Butane	t-2-Butene	2,3-Dimethylbutane	Toluene	m-Xylene	Initial HC/NO_x (ppmC/ppm)
EC-231	0.44	0.052	1.051	0.108	1.13	0.055	0.715	0.121	0.108	26.8
EC-232	0.469	0.024	0.258	0.051	1.102	0.026	0.612	0.032	0.029	18.9
EC-233	0.096	0.007	0.260	0.051	1.085	0.025	0.648	0.034	0.033	92.2
EC-237	0.377	0.106	0.875	0.100	1.025	0.050	0.463	0.086	0.091	21.7
EC-238	0.718	0.234	0.982	0.093	0.966	0.047	0.420	0.083	0.084	10.6
EC-241	0.379	0.110	0.484	0.045	0.464	0.024	0.211	0.04	0.044	10.1
EC-242	0.377	0.125	2.014	0.109	0.558	0.108	0.203	0.306	0.306	25.5
EC-243	0.386	0.114	1.939	0.109	0.568	0.110	0.084	0.155	0.154	19.4
EC-245	0.743	0.259	2.055	0.104	0.534	0.102	0.185	0.321	0.317	13.0
EC-246	0.386	0.122	0.253	0.049	1.058	0.026	0.538	0.023	0.023	16.9
EC-247	0.38	0.125	1.025	0.054	0.273	0.053	0.080	0.145	0.145	12.2

TABLE 38. NORMALIZED INITIAL CONDITIONS FOR THE SEVEN-HYDROCARBON/NO_x EXPERIMENTS (ppmC) USED FOR CARBON-BOND I

Run number	Total HC (ppmC)	Mixture	Initial conditions (percent of total HC)					Photolysis rate constant (min^{-1})			
			1-Olefins*	Paraffins†	Aromatics§	Carbonyls**	HNO_2††	k_1	$HNO_2+h\nu$	$H_2O_2+h\nu$	$ALD+h\nu$
EC-231	13.187	B	1.64	71.02	26.36	0.98	0.000	0.3	0.087	6.6×10^{-4}	8×10^{-4}
EC-232	9.323	A	1.10	88.77	9.46	0.67	0.002	0.3	0.087	6.6×10^{-4}	8×10^{-4}
EC-233	9.5	A	1.07	88.65	9.70	0.58	0.002	0.3	0.087	6.6×10^{-4}	8×10^{-4}
EC-237	10.463	B	1.91	70.25	26.87	0.97	0.006	0.3	0.087	6.6×10^{-4}	8×10^{-4}
EC-238	10.094	B	1.84	67.59	29.38	1.19	0.017	0.3	0.087	6.6×10^{-4}	8×10^{-4}
EC-241	5.141	B	1.75	67.22	28.64	2.39	0.004	0.3	0.087	6.6×10^{-4}	8×10^{-4}
EC-242	12.855	C	1.70	36.51	59.89	1.90	0.011	0.3	0.087	6.6×10^{-4}	8×10^{-4}
EC-243	9.743	C	2.24	36.65	58.83	2.28	0.009	0.3	0.087	6.6×10^{-4}	8×10^{-4}
EC-245	12.875	C	1.62	35.02	61.65	1.71	0.017	0.3	0.087	6.6×10^{-4}	8×10^{-4}
EC-246	8.566	A	1.14	89.11	9.13	0.62	0.007	0.3	0.087	6.6×10^{-4}	8×10^{-4}
EC-247	6.174	C	1.74	35.10	61.39	1.77	0.010	0.3	0.087	6.6×10^{-4}	8×10^{-4}

* Propylene only.

† Butane, 2,3-dimethylbutane, and all single-bonded carbon atoms from the olefins, aromatics, and carbonyls.

§ Toluene and m-Xylene, and ethylene.

** All aldehydes and internal olefin (trans-2-butene).

†† In ppm.

§§ One-half to stable products.

TABLE 39. NORMALIZED INITIAL CONDITIONS FOR THE SEVEN-HYDROCARBON/NO_x EXPERIMENTS (ppmC) USED FOR CBM-II

			Initial conditions (percent of total HC)						Photolysis rate constant (min^{-1})			
Run number	Total HC (ppmC)	Mixture	1-Olefins*	Paraffins†	Aromatics§	Ethylene	Carbonyls**	RX††	k_1	RX+hν	ALD+hν§§	BZA+hν
EC-231	13.187	B	1.64	71.02	10.42	15.94	0.98	0.000	0.3	0.03	8.1×10^{-4}	0.011
EC-232	9.323	A	1.10	88.77	3.93	5.53	0.67	0.003	0.3	0.03	8.1×10^{-4}	0.011
EC-233	9.5	A	1.07	88.65	4.23	5.47	0.58	0.004	0.3	0.03	8.1×10^{-4}	0.011
EC-237	10.463	B	1.91	70.25	10.15	16.72	0.97	0.004	0.3	0.03	8.1×10^{-4}	0.011
EC-238	10.094	B	1.84	67.59	9.93	19.45	1.19	0.007	0.3	0.03	8.1×10^{-4}	0.011
EC-241	5.141	B	1.75	67.22	9.80	18.84	2.39	0.001	0.3	0.03	8.1×10^{-4}	0.011
EC-242	12.855	C	1.70	36.51	28.56	31.33	1.90	0.002	0.3	0.03	8.1×10^{-4}	0.011
EC-243	9.743	C	2.24	36.65	19.02	39.81	2.28	0.004	0.3	0.03	8.1×10^{-4}	0.011
EC-245	12.875	C	1.62	35.02	29.73	31.92	1.71	0.001	0.3	0.03	8.1×10^{-4}	0.011
EC-246	8.566	A	1.14	89.11	3.23	5.90	0.62	0.012	0.3	0.03	8.1×10^{-4}	0.011
EC-247	6.174	C	1.74	35.10	28.19	33.20	1.77	0.003	0.3	0.03	8.1×10^{-4}	0.011

* Propylene only.

† Butane, 2,3-dimethylbutane, and all single-bonded carbon atoms from the olefins, aromatics, and carbonyls.

§ Toluene and m-Xylene.

** All aldehydes and internal olefin (trans-2-butene).

†† In ppm.

§§ One-third to stable products.

TABLE 40. STATISTICAL ANALYSIS OF THE ORIGINAL CBM AND CBM-II OZONE PREDICTIONS COMPARED WITH MEASURED DATA

	RMS error (ppm)	Mean error (ppm)	Relative mean error	Mean absolute error (ppm)	Relative mean absolute error	Correlation coefficient
CBM-II	0.0854	0.0032	0.0277	0.0650	0.1819	0.9306
Original CBM	0.0839	0.0160	0.1790	0.0596	0.2605	0.9321

A COMPENDIUM OF ISOPLETH DIAGRAMS

As part of our analysis of the behavior of the CBM, we have prepared a series of isopleth diagrams showing the formation of various smog constituents as predicted by the CBM. The species included are:

> Ozone
> PAN
> NO_2
> HNO_3
> $NO_3^{\bullet}$
> Carbonyls
> $HO_2^{\bullet}$
> H_2O_2
> OH
> Organic Nitrates.

The hydrocarbon mixture used in these isopleths consisted of the following carbon fractions: 0.034 ethylene, 0.25 aromatic, 0.034 olefinic, 0.65 parafinic, 0.034 carbonyl (i.e., these fractions are the amount of carbon in each bond category). This hydrocarbon split represents an average automobile emissions mixture combining both evaporative (40 percent) and exhaust emissions (60 percent) (Killus et al., 1977). The mixture has been normalized to remove unreactive hydrocarbons.

Standard OZIPP (or EKMA) conditions were used except that aldehyde photolysis to stable products was changed to 0.35 of the nominal program value in order to make it consistent with the values that we have been using for the UNC outdoor chamber (Whitten and Hogo, 1978).

Ozone

The Carbon-Bond Mechanism (Figure 165) is somewhat more reactive than the mechanism used by Dodge (1977) in the Empirical Kinetic Modeling Approach (EKMA) (Figure 166). However, when used on a propylene-butane mix (Figure 167), the shape of the curves are similar. The inclusion of the aromatic mechanism alters the shape of the Carbon Bond isopleth diagrams for the automobile hydrocarbon mix.

PAN

The PAN isopleths (Figure 168) are interesting for several reasons. They are similar in shape to the ozone isopleths, yet the region of maximum efficiency is broader and shifted slightly to the higher HC/NO_x ratios. The PAN isopleths resemble the ozone isopleths of a propylene butane mix (Figure 167) more closely than they resemble ozone from our simulated automobile emissions. This suggests that the aromatics mechanism in some fashion distorts the ozone chemistry while PAN chemistry is left unperturbed.

If we plot ozone formation as a function of increasing precursor concentration at the HC/NO_x ratio of maximum production efficiency, we obtain a curve similar to the Appendix J rollback curve (Figure 169). Ozone production efficiency declines at higher precursor concentration levels, while PAN production efficiency increases at higher concentration levels (Figure 169), indicating that pollution control measures work more effectively on PAN than on ozone.

NO_2

The isopleths of peak NO_2 concentration (Figure 170) show an almost linear dependence on NO_x. Only at very low HC/NO_x ratios (HC/NO_x $<$ 2) is the NO_2

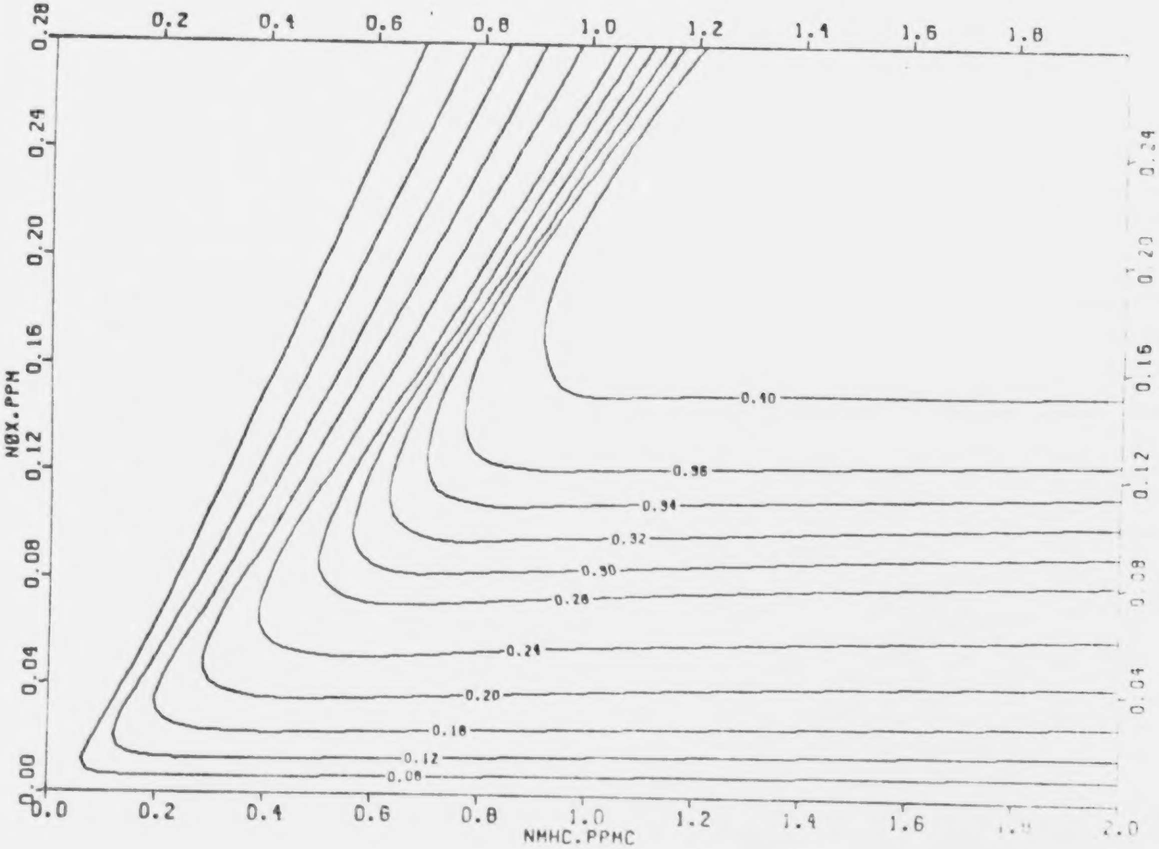

FIGURE 165. STANDARD OZONE ISOPLETH CONDITIONS

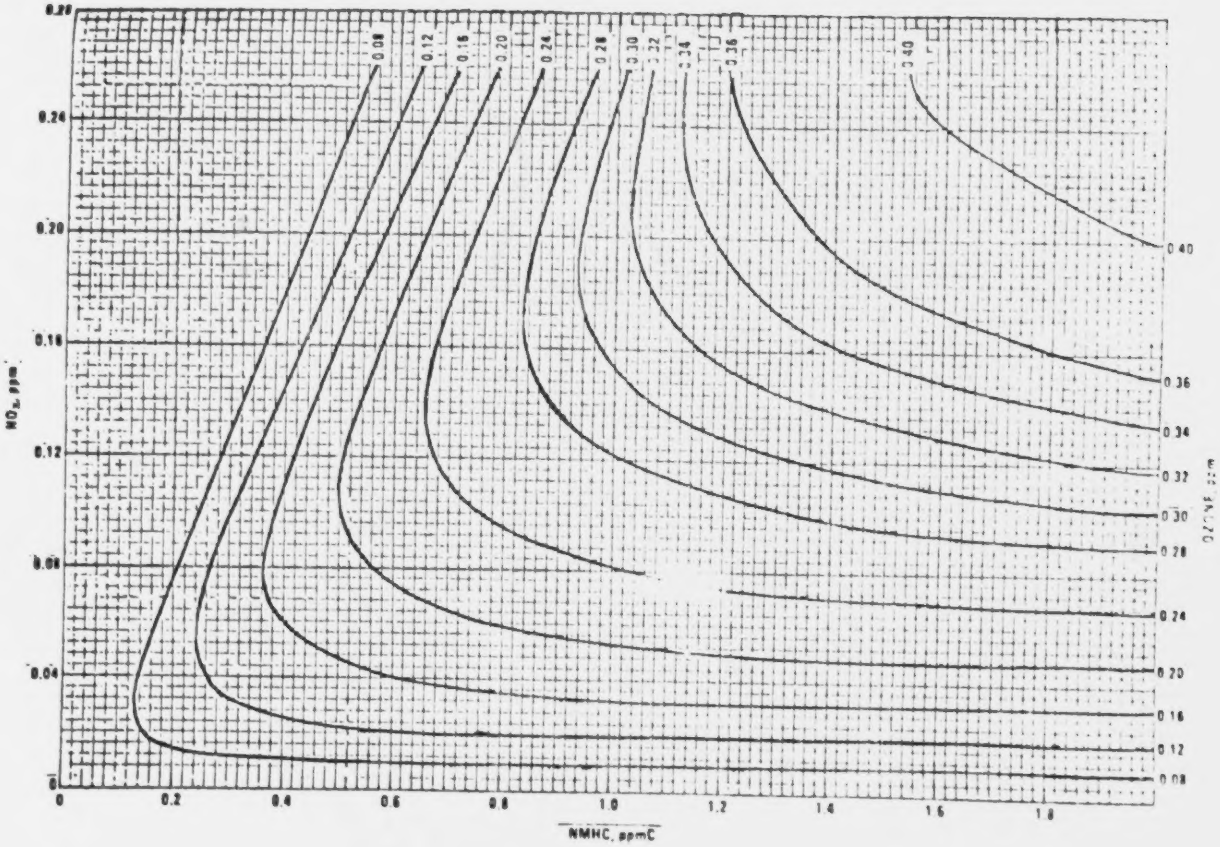

FIGURE 166. OZONE ISOPLETH USED IN EKMA

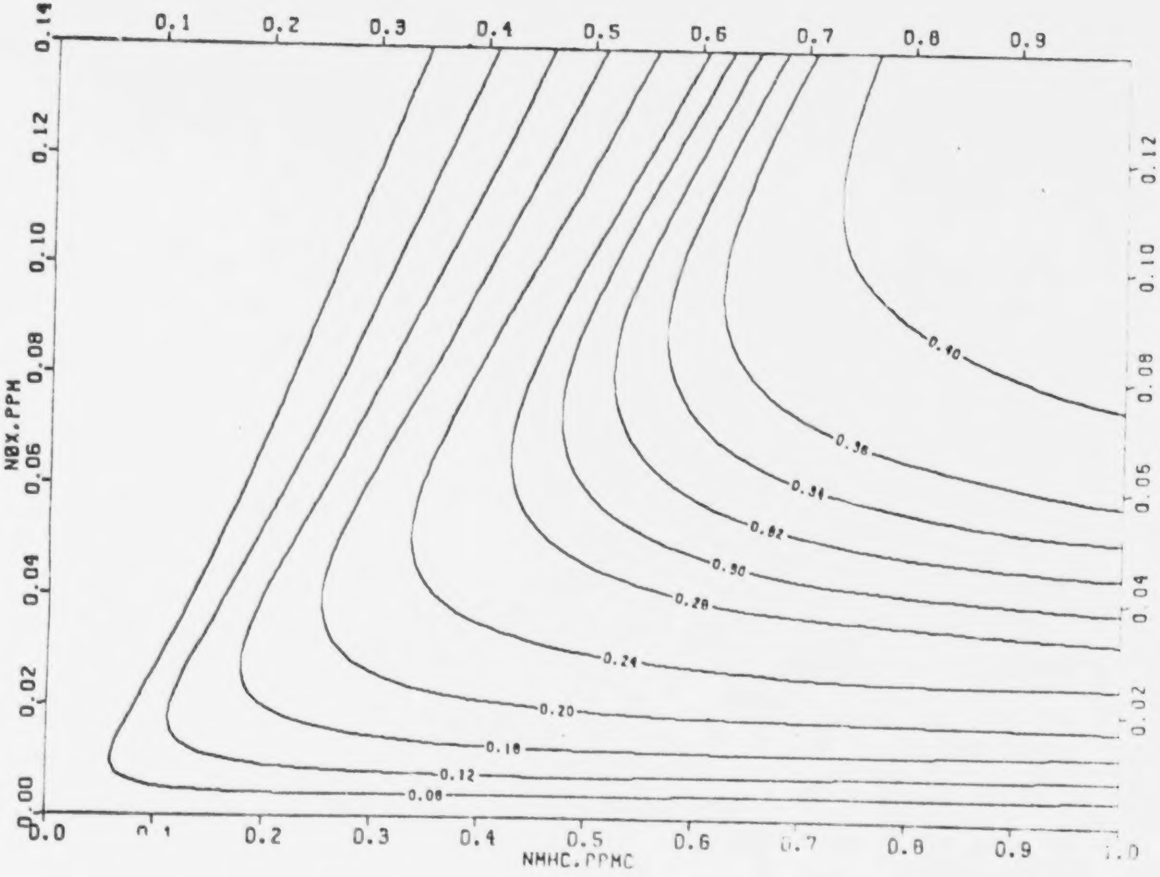

FIGURE 167. OZONE PRODUCED BY A 10/90 PROPYLENE BUTANE MIX

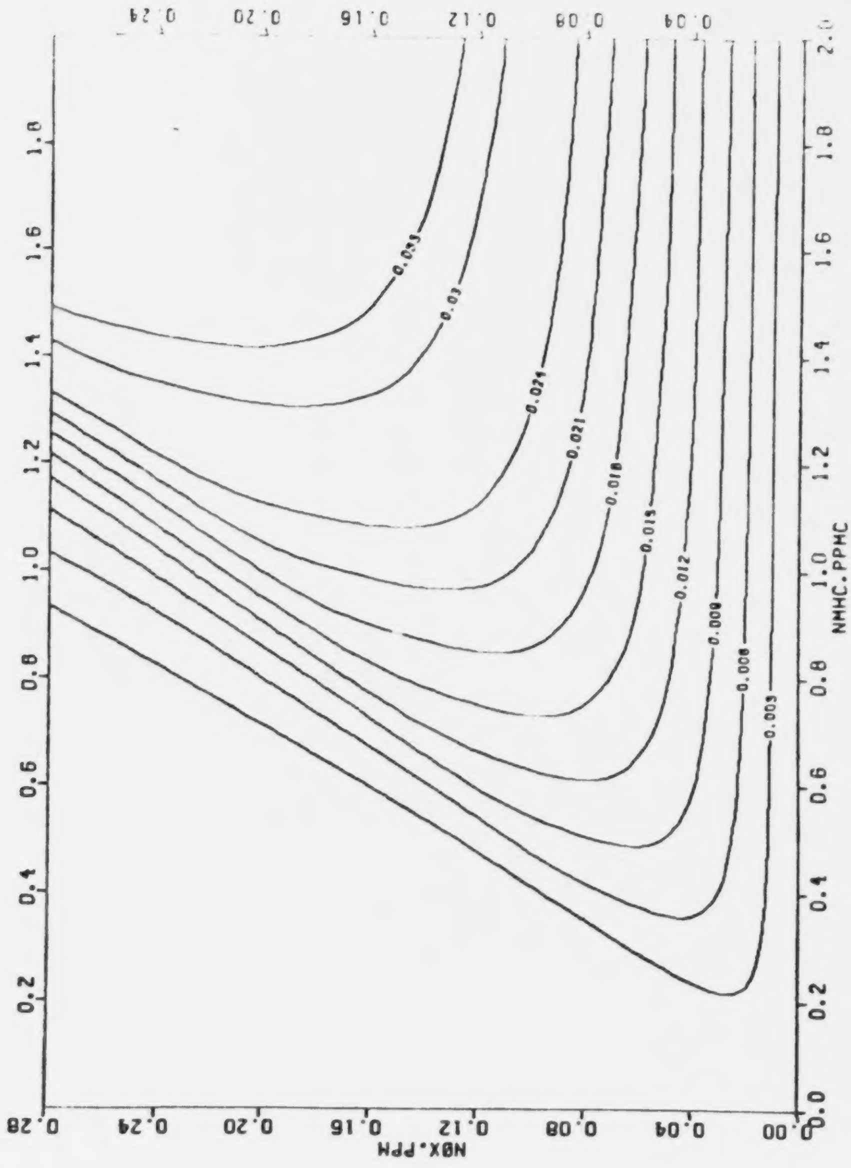

FIGURE 168. PAN ISOPLETH

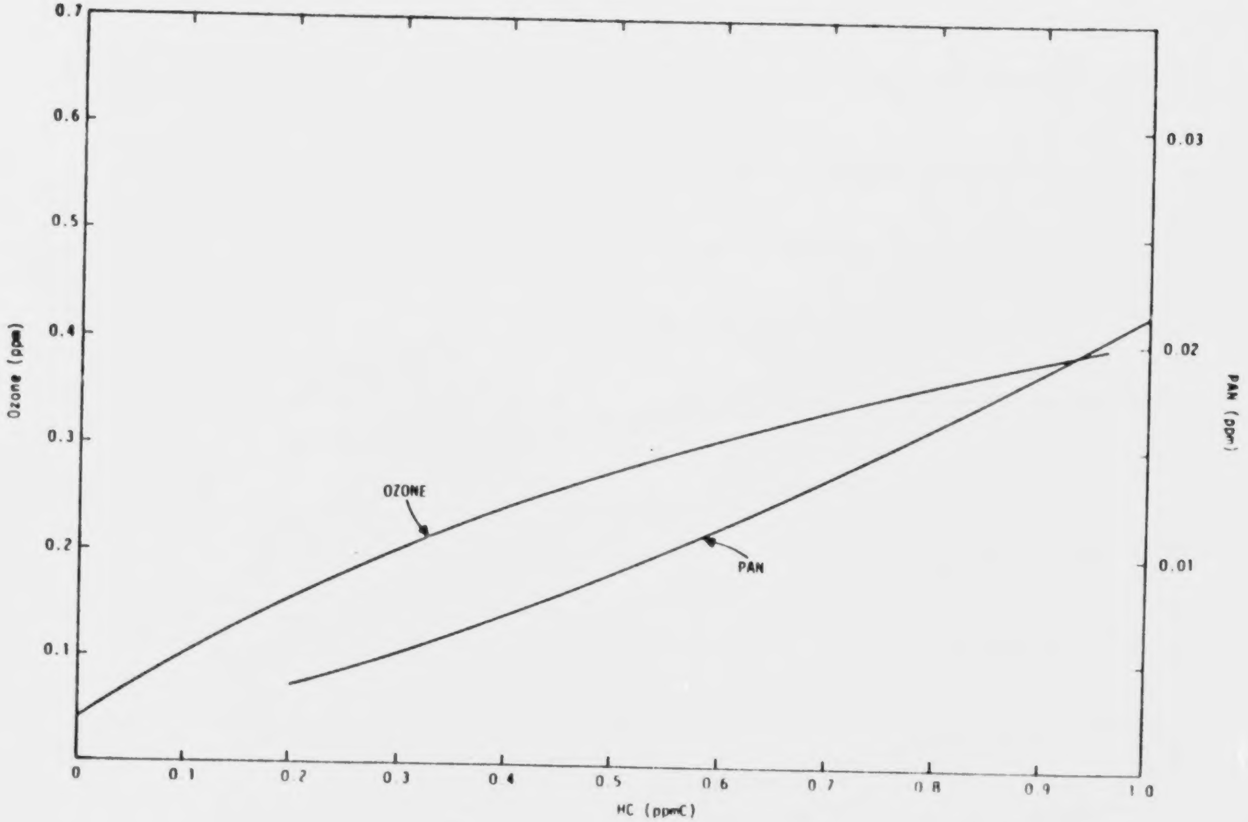

FIGURE 169. OZONE AND PAN AT HC/NO_x = 6.7

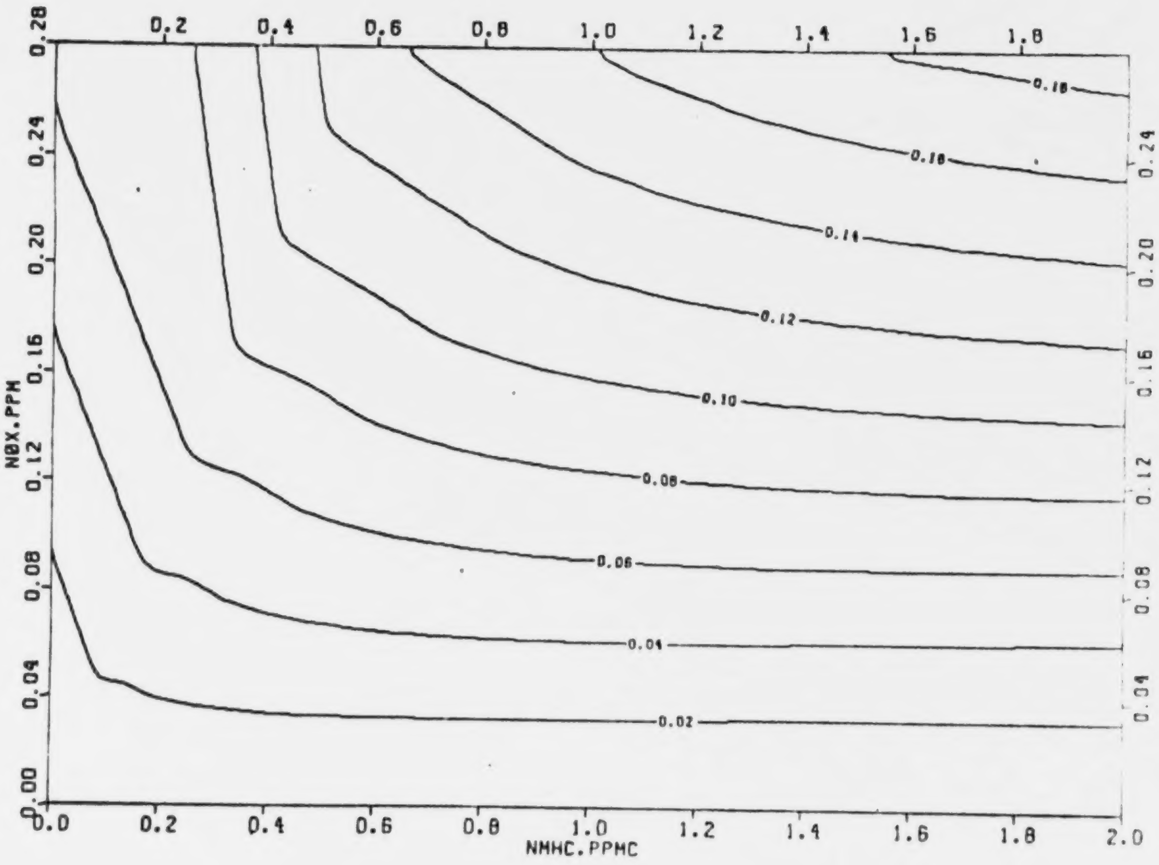

FIGURE 170. NO_2 ISOPLETH

peak not reached. The NO_2 recovery is surprisingly low, only about 60 percent of total NO_x. Dilution is responsible for some of this NO_x loss, but the majority seems to be in the form of organic nitrate, which is discussed below.

HNO_3

Nitric acid isopleths (Figure 171) show few surprises. Their linear relation to NO_x is nearly identical to the NO_2 isopleths, although most nitric acid is formed after the NO_2 peak. The bend in the HNO_3 isopleths occurs at slightly lower HC/NO_x ratios than the ozone bend. Below this ratio, nitric acid appears to be completely hydrocarbon limited.

NO_3

The NO_3 isopleth diagram (Figure 172) is very similar to ozone isopleths. However, NO_3 is destroyed rapidly at high NO_x concentrations by the reaction with NO and at high hydrocarbon concentrations by the reactions with aromatics intermediates. Thus, the NO_3 isopleths bend sharply away from both axes.

Aldehydes

The aldehyde isopleths (Figure 173) show the effects of two factors. Because aldehydes are emitted directly, they form a fractional part of the hydrocarbons and the isopleths tend to run parallel to the hydrocarbon axis at the lowest HC/NO_x ratios where the chemistry is slow. Aldehydes are also efficiently produced at high HC/NO_x ratios. It appears that aldehydes can reach a maximum of 10 percent of the initial hydrocarbon concentration, or roughly twice the emissions rate.

HO_2 and H_2O_2

HO_2 concentration (Figure 174) is maximized at very high HC/NO_x ratios. Hydrogen peroxide formation (formed by $HO_2^{\cdot}$ - $HO_2^{\cdot}$ reaction) peaks at a somewhat smaller HC/NO_x ratio. Hydrogen peroxide isopleths (Figure 175) look very similar to reported isopleths for aerosol formation (Miller and

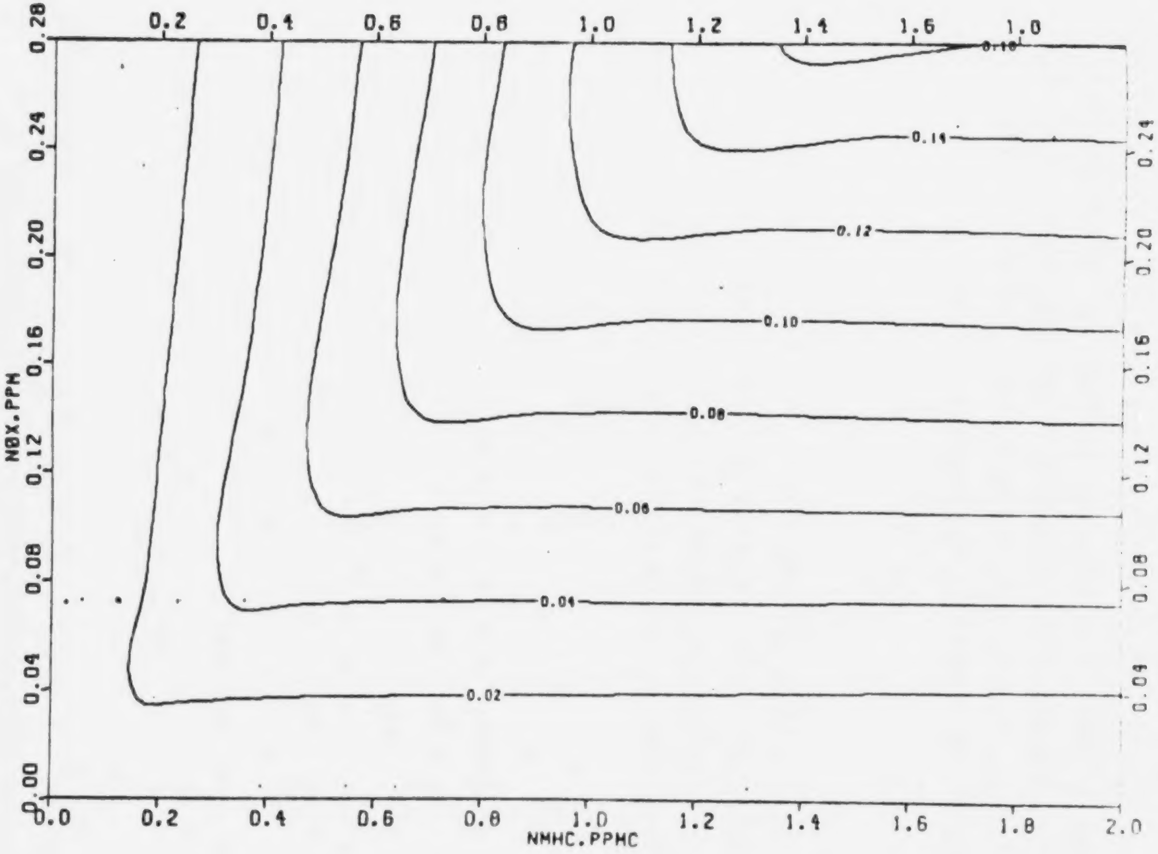

FIGURE 171. HNO_3 ISOPLETH

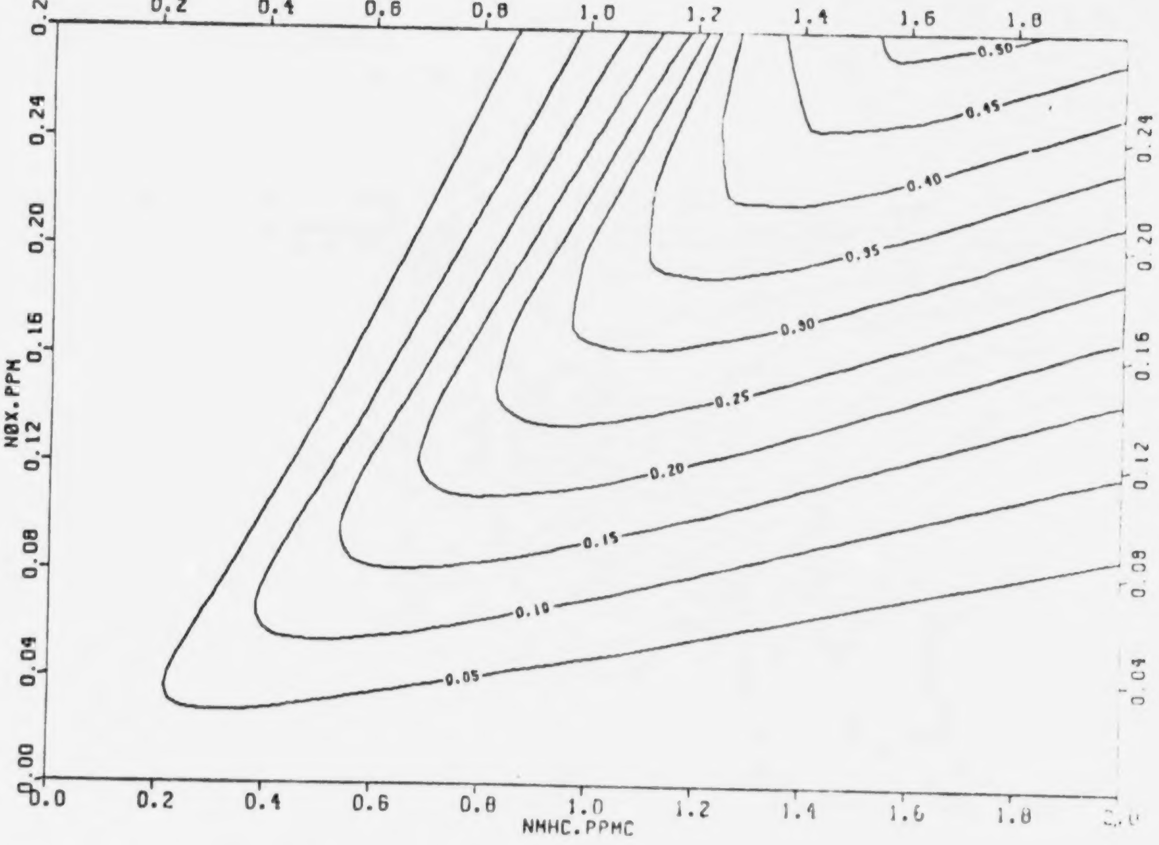

FIGURE 172. NO_3 ISOPLETH (10000 X PPM)

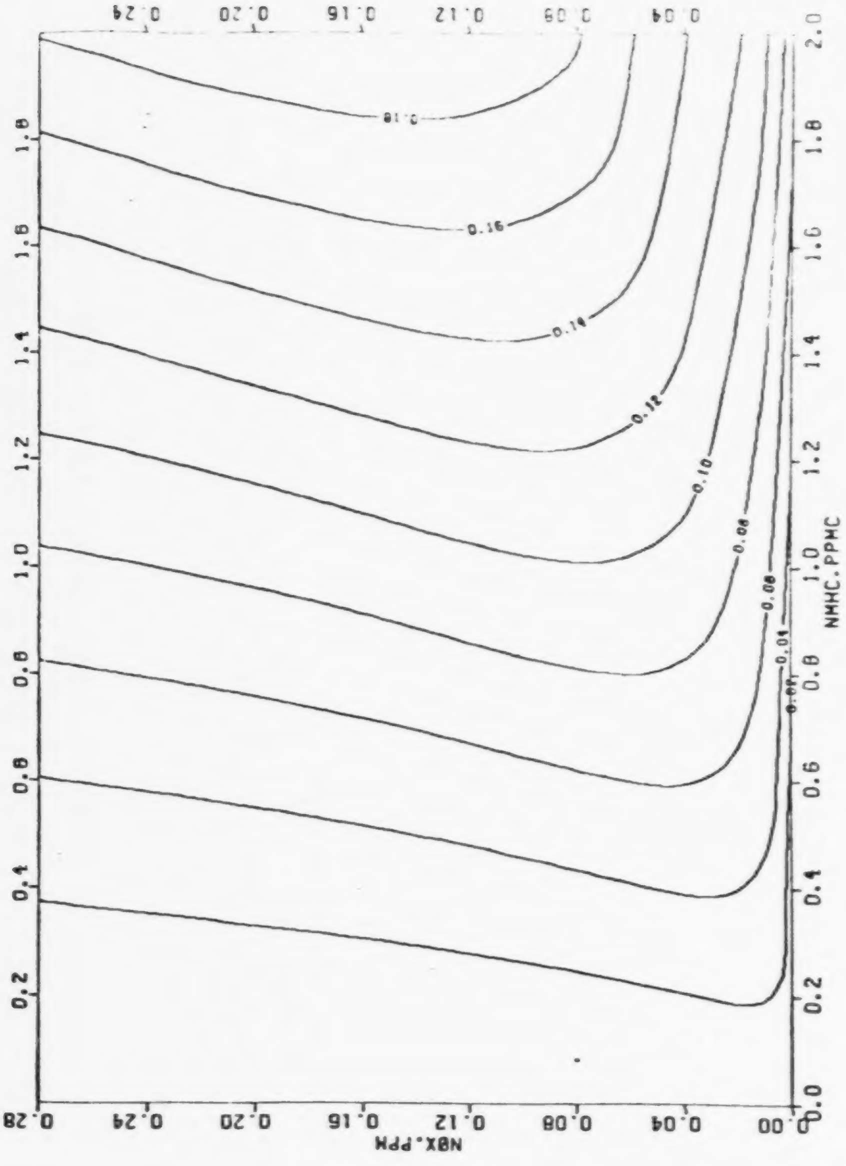

FIGURE 173. HCHO ISOPLETH

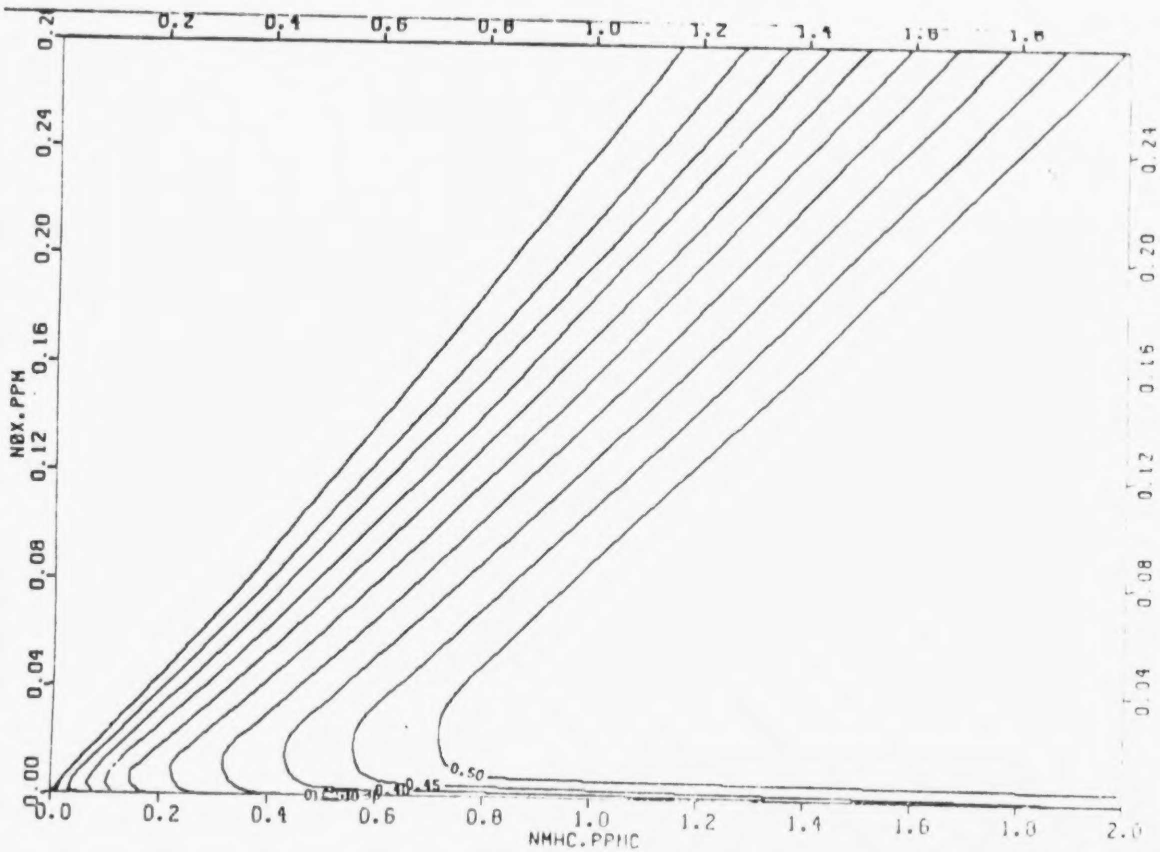

FIGURE 174. HO_2 ISOPLETH (10000 X PPM)

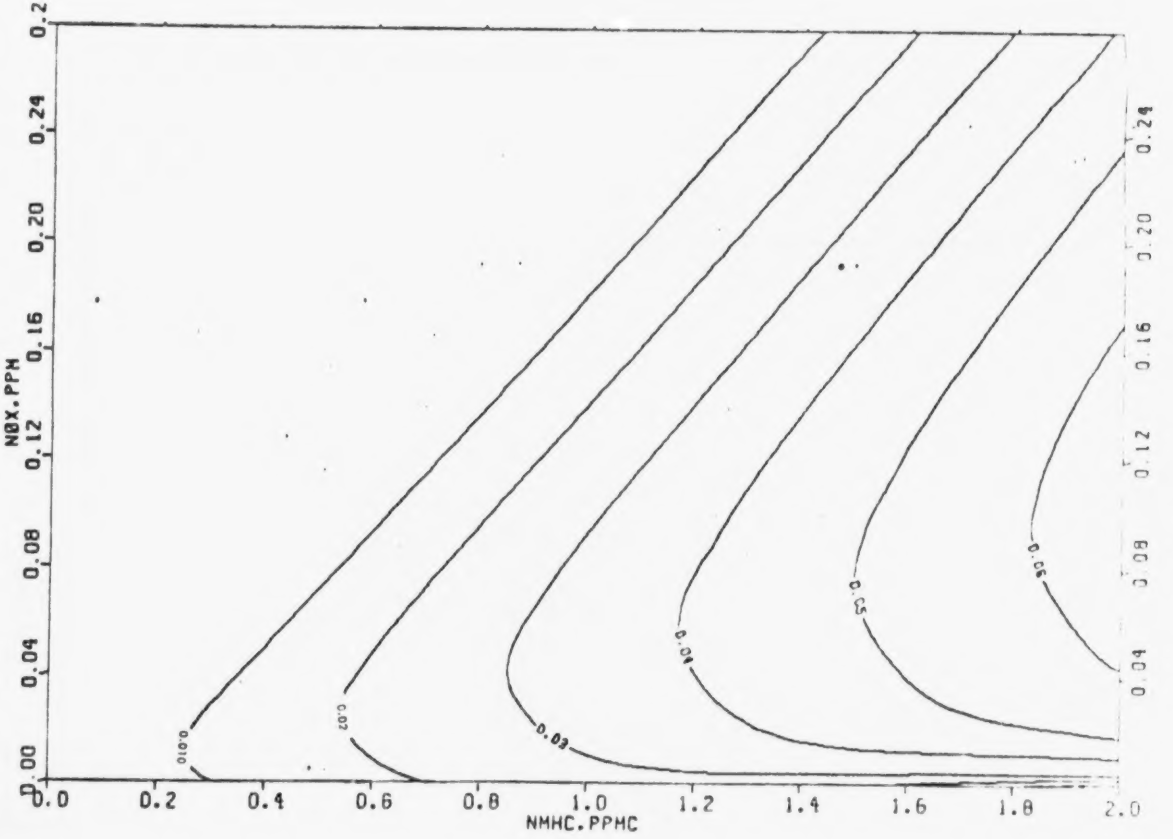

FIGURE 175. H_2O_2 ISOPLETH

Joseph, 1977). Wu, Bogard, and Brock (1978) have suggested that some particulate formation is the result of ozonides that react with other ozonides to form polymeric aerosols. Such a reaction sequence could well resemble hydrogen peroxide formation.

OH·

Isopleths of 10-hour average OH· concentrations (Figure 176) seem to depend almost solely on the HC/NO_x ratio, and have little to do with precursor concentration. This is in keeping with elementary steady state analysis. To a first approximation, at low HC/NO_x ratios, OH depends on the ratio of aldehyde photolysis to NO_2 concentration. At high HC/NO_x ratios, hydrogen peroxide formation removes HO_2 from the system before OH is reformed.

Organic Nitrates

Isopleths were generated for the ratio of organic nitrate production to total nitrate (the remainder being HNO_3) after 10 hours (Figure 177). Organic nitrates are produced in the CBM in roughly equal amounts from two sources: the $RO_2^{\bullet}$ reaction with NO and the reaction of NO_3 with an aromatics intermediate. Smog chamber experiments with large paraffins or aromatics are predicted by the new CBM to produce organic nitrates at high HC/NO_x ratios. Future experiments will be needed to confirm this prediction.

This set of isopleth diagrams can be used to assess the chemical reactivity of chemistry secondary to ozone chemistry, such as SO_2 conversion to sulfate. The OH· diagram indicates that if OH was responsible for the major fraction of sulfate production then HC and NO_x control strategies aimed at reducing sulfate would not be effective at constant HC/NO_x ratios even though ozone and PAN would be reduced.

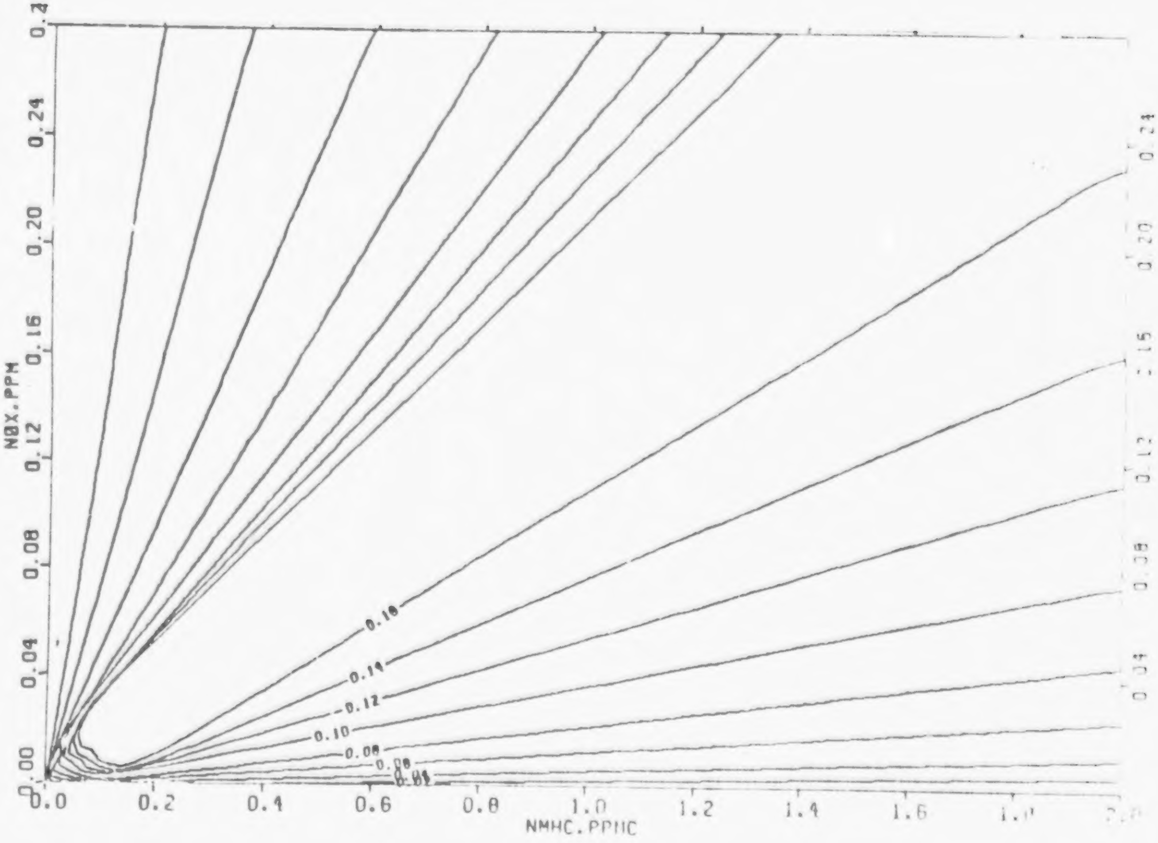

FIGURE 176. OH ISOPLETH (1 X 10^6 X PPM)

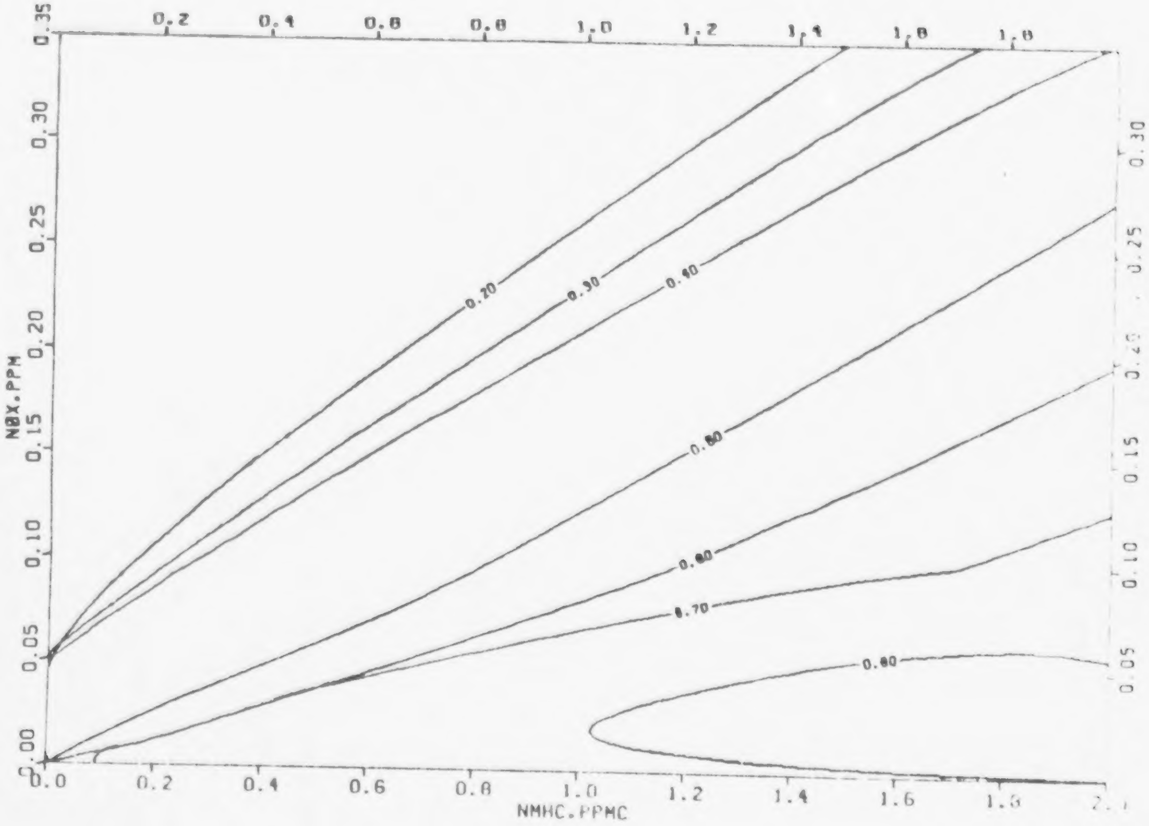

FIGURE 177. RATIO OF ORGANIC NITRATE TO TOTAL NITRATE AFTER 10 HOURS

REFERENCES

Akimoto, H., et al. (1978), "Formation of Propylene Glycol 1,2-Dinitrate in the Photooxidation of a Propylene-Nitrogen Oxides-Air System," *J. Environ. Sci. Health*, Vol. 9, pp. 677-686.

Atkinson, R., et al. (1978) "Kinetics and Mechanism of the Reactions of the Hydroxyl Radical with Organic Compound in the Gas Phase," to be published in *Advances in Photochemistry*.

Barker, J. R., et al. (1977), "Measurement of Rate Constants of Importance in Smog," EPA-600/3-77-110, Environmental Protection Agency, Research Triangle Park, North Carolina.

Batt, L., R. D. McCulloch, and R. T. Milne (1975), "Thermochemical and Kinetic Studies of Alkyl Nitrites (RONO) - D(RO-NO), the Reactions between RO· and NO, and the Decomposition of RO·," *Int. J. Chem. Kinetics*, Symposium No. 1, pp. 441-461.

Busse, A.D. (1971), "Attributes of the Earth-Sun Relationship," Internal Memorandum, Meteorology and Assessment Division, NOAA/EPA, Research Triangle Park, North Carolina.

Calvert, J. G., and J. N. Pitts, Jr. (1966), *Photochemistry* (John Wiley & Sons, New York, New York).

Carter, W. P. L., et al. (1976), "Evidence fo Alkoxy Radical Isomerization in C_4-C_5 Alkanes in NO_x-Air Systems," Extended Abstracts, 12th Informal Conference on Photochemistry, National Bureau of Standards, Washington, D.C., pp. N4-1 to N4-5.

Cox, R. A., and K. Patrick (1979), "Kinetics at the Reaction of the HO_2 + NO_2 (+M) $\rightleftarrows$ HO_2NO_2 Using Molecular Modulation Spectrometry, " *Int. J. Chem. Kinetics*, Vol. 11, pp. 635-648.

Darnell, K. R., R. Atkinson, and J. N. Pitts, Jr. (1979), "Observation of Biacetyl from the Reaction of OH Radicals with o-Xylene: Evidence for Ring Cleavage," submitted for publication to *J. Phys. Chem.*

Darnell, K. R., et al. (1976), "Importance of RO_2 + NO in Alkyl Nitrate Formation from C_4-C_6 Alkane Photooxidation Under Simulated Atmospheric Conditions," *J. Phys. Chem.*, Vol. 80, pp. 1948-1950.

Demerjian, K. L., K. L. Schere, and J. T. Peterson (1979), "Theoretical Estimates of Actinic (Spherically Integrated) Flux and Photolytic Rate Constants of Atmospheric Species in the Lower Troposphere," in *Advances in Environmental Science and Technology*, Vol. 9 (Wiley Interscience, New York, New York, in press).

DeMore, W. B. (1979), "Reaction of HO_2 with O_3 and the Effect of Water Vapor on HO_2 Kinetics," *J. Phys. Chem.*, Vol. 83, pp. 1113-1118.

DeMore, W. B., et al. (1979), "Chemical Kinetic and Photochemical Data for Use in Stratospheric Modelling, Evaluation No. 2, JPL Publication 79-27., Jet Propulsion Laboratory, California Institute of Technology, Pasadena, California.

Dodge, M. C. (1977), "Effect of Selected Parameters on Predictions of a Photochemical Model," EPA-600-3-77-048, U.S. Environmental Protection Agency, Research Triangle Park, North Carolina.

Graham, R. A., A. M. Winer, and J. N. Pitts, Jr. (1978), "Pressure and Temperature Dependence of the Unimolecular Decomposition of HO_2NO_2," *J. Chem. Phys.*, Vol. 68, pp. 4505-4510.

Hamilton, E. J., Jr., and R. R. Lii (1977), "The Dependence on H_2O and on NH_3 of the Kinetics of the Self-Reaction of HO_2 in the Gas-Phase Formation of $HO_2 \cdot H_2O$ and $HO_2 \cdot NH_3$ Complexes," Int. J. Chem. Kinetics, Vol. 9, pp. 875-885.

Hamilton, E. J., Jr., and C. A.Naleway (1976), "Theoretical Calculation of Strong Complex Formation by the HO_2 Radical: $HO_2 \cdot H_2O$ and $HO_2 \cdot NH_3$," J. Phys. Chem., Vol. 80, pp. 2037-2040.

Hampson, R. F., Jr., and D. Garvin (1978), "Reaction Rate and Photochemical Data for Atmospheric Chemistry-1977," NBS Special Publication 513, National Bureau of Standards, Washington, D.C.

Hendry, D. G. (1978), "Reactions of Aromatic Compounds in the Atmosphere," Conference on Chemical Kinetic Data Needs for Modeling the Lower Troposphere, 15-17 May 1978, Reston, Virginia.

Hendry, D. G., et al. (1978), "Computer Modeling of Simulated Photochemical Smog," EPA-600/3-78-059, Environmental Protection Agency, Research Triangle Park, North Carolina.

Hendry, D. G. (1972), private communication, to Kuntz, Kopczynski, and Baffalini.

Hoshino, M., H. Akimoto, and M. Okuda (1978), "Photochemical Oxidation of Benzene, Toluene, and Ethylbenzene Initiated by OH Radicals in the Gas Phase," Bull. Chem. Soc. Jpn., Vol. 51, pp. 718-724.

Jeffries, H., D. Fox, and R. Kamens (1976), "Outdoor Smog Chamber Studies: Light Effects Relative to Indoor Chambers," Environ. Sci. Technol., Vol. 10, pp. 1006-1011.

Killus, J. P., et al. (1977), "Continued Research in Mesoscale Air Pollution Simulation Modeling: Volume V--Refinements in Numerical Analysis, Transport, Chemistry, and Pollutant Removal," Report No.

EF77-142 to Environmental Protection Agency, Contract No. 68-02-1237, Systems Applications, Incorporated.

Kopczynski, S. L., R. L. Kuntz, and J. S. Bufalini (1975), "Reactivities of Complex Hydrocarbon Mixtures," Environ. Sci. Technol., Vol. 9, No. 7, p. 649.

Kuntz, R. L., S. L. Kopczynski, and J. J. Bufalini (1973), "Photochemical Reactivity of Benzaldehyde-NO_x and Benzaldehyde-Hydrocarbon-NO_x Mixtures," Environ. Sci. Technol., Vol. 7, No. 13, pp. 1119-1123.

Levine, S. Z. et al. (1977), "The Kinetics and Mechanism of the HO_2-NO_2 Reactions; The Significance of Peroxynitric Acid Formation in Photochemical Smog," Chem. Phys. Letters, Vol. 48, p. 528.

Miller, D. F., and D. W. Joseph (1977), "Smog Chamber Studies on Photochemical Aerosol-Precursor Relationships," EPA-600/3-77-080, Environmental Sciences Review Laboratory, Environmental Protection Agency, Research Triangle Park, North Carolina.

Nojima, K., et al. (1974), "The Formation of Glyoxals by the Photochemical Reaction of Aromatic Hydrocarbons in the Presence of Nitrogen Monoxide," Chemosphere, Vol. 5, pp. 247-252.

Perry, R. A., R. Atkinson, and J. N. Pitts, Jr. (1977), "Kinetics and Mechanism of the Gas Phase Reaction of OH Radicals with Aromatics Hydrocarbons over the Temperature Range 296-473K," J. Phys. Chem., Vol. 81, pp. 296-304.

Rappoport, Z. (1967), Handbook of Tables for Organic Compound Identification, Third Edition (CRC Press, Cleveland, Ohio).

Sato, K., K. Takimoto, and S. Tsuda (1978), "Degradation of Aqueous Phenol Solution by Gamma Irradiation," Environ. Sci. Tech., Vol. 12, p. 1043.

Schere, K. L., and K. L. Demerjian (1977), "Calculation of Selected Photolytic Rate Constants Over a Diurnal Range, A Computer Algorithm," EPA-600/4-77-015, Environmental Protection Agency, Research Triangle Park, North Carolina.

Schwartz, W. (1974), "Chemical Characterization of Model Aerosols," EPA-650/3-74-011, Chemistry and Physics Laboratory, Environmental Protection Agency, Research Triangle Park, North Carolina.

Takagi, H., et al. (1979), "Photooxidation of o-xylene in the NO-H_2O-AIR Systems," submitted for publication to J. Phys. Chem.

Whitten , G. Z., and H. Hogo (1978), "User's Manual for Kinetics Mode and Ozone Isopleth Plotting Package," EPA-600/8-78-014a, U.S. Environmental Protection Agency, Research Triangle Park, North Carolina.

Whitten, G. Z., and H. Hogo (1977), "Mathematical Modeling of Simulated Photochemical Smog," EPA-600/3-77-001, Systems Applications, Incorporated, San Rafael, California.

Whitten, G. Z., H. Hogo, and J. P. Killus (1979), "The Carbon-Bond Mechanism--A Condensed Kinetic Mechanism for Photochemical Smog," Systems Applications, Incorporated, San Rafael, California, submitted for publication to Environ. Sci. Technol.

Whitten, G. Z., et al. (1979), "Modeling of Simulated Photochemical Smog with Kinetic Mechanisms, Vol. I: Interim Report," EPA-600/3-79-001a, Systems Applications, Incorporated, San Rafael, California.

Whitten, G. Z., et al. (1978), "Modeling of Simulated Photochemical Smog with Kinetic Mechanisms," Draft Interim Report - August, 1978, Systems Applications, Incorporated, San Rafael, California.

Wu, M. S., J. M. Bogard, and J. R. Brock (1978), "Particle Formation in the Ozone-Propylene Reaction," J. Environ. Sci. Health, A13(8), pp. 571-584.

ADDENDUM

CORRECTIONS TO 1977 and 1978 UNC PAN DATA

Subsequent to submission of this report, corrections to the 1977 and 1978 UNC PAN data were transmitted to SAI. During 1977 and 1978 UNC used three different PAN calibration procedures. The following corrections serve to make the 1977 and 1978 PAN data set consistent with the 1979 data set. These resulted from a comprehensive study of the calibration techniques that had been used.

RUN DATE	PAN CONCENTRATION TO BE MULTIPLIED BY
7/18/77	0.73
10/24/77	0.61
11/12/77	0.63
11/20/77	0.63
12/26/77	0.85
2/27/78	1.0
3/31/78	0.58
6/16/78	0.72
6/30/78	0.63
7/01/78	0.72
7/24/78	0.84
7/30/78	1.0
8/05/78	1.55
8/08/78	1.3
8/15/78	1.55
8/16/78	1.55
8/17/78	1.0
8/21/78	1.5
8/24/78	1.5
9/14/78	1.5
9/15/78	1.5
9/18/78	1.5
9/19/78	1.5
10/02/78	1.5
10/03/78	1.5
10/12/78	1.28
10/13/78	1.5
10/17/78	1.5
10/18/78	1.5
10/20/78	1.51
10/21/78	1.34
10/22/78	1.30
10/25/78	1.25
10/29/78	1.21
11/07/78	1.0